SEISMIC BEHAVIOR & COMPUTER MODELING OF LOW-RISE STEEL FRAME STRUCTURES

by

Mark S. Bakhtavar

B.Sc., Sharif University of Technology, 1991

A THESIS SUBMITTED IN PARTIAL FULFILLMENT OF

THE REQUIREMENTS FOR THE DEGREE OF

MASTER OF APPLIED SCIENCE

in

THE FACULTY OF GRADUATE STUDIES

Department of Civil Engineering

We accept this thesis as conforming

to the required standard

THE UNIVERSITY OF BRITISH COLUMBIA

July, 2000

ABSTRACT

Recorded motion of structures during recent earthquakes provide valuable information on the performance of various types of the buildings under seismic loading. This information can be used to evaluate the accuracy of structural analysis techniques and the efficiency of the current design methods.

The objective of the first part of this study was to extract as much information as possible from the recorded motion of 11 well instrumented low-rise steel frame buildings in California, which experienced the 1987 Whittier, 1989 Loma Prieta, 1992 Landers and 1994 Northridge Earthquakes. The results showed that, in most cases, the periods of the buildings were significantly higher that those estimated by the code empirical formulae. Three of the buildings which had fundamental periods of greater than 1.0 second (with six to seven stories), behaved in a way that is usually expected from high-rise buildings.

The second part of this research included computer modeling of one of the above mentioned structures, the Burbank 6-story office building, and comparing the anticipated response of the building using various analysis methods to the actual response, measured during the Whittier and Northridge earthquakes. The results indicated that proper modeling of the structure for a dynamic time-history analysis may predict the seismic response of the structures very accurately.

A comparative study was performed to evaluate the accuracy and the efficiency of the various analysis techniques.

At the end, Non-Linear Time-History Analysis was used to predict the performance of the Burbank 6-story office building, under higher levels of ground motion.

TABLE OF CONTENTS

LIST OF TABLES

LIST OF FIGURES

ACKNOWLEDGEMENTS

I would like to thank my supervisor Dr. Carlos E. Ventura for introducing me to the project, guiding me in selecting and using the proper techniques and his valuable comments throughout the project.

I would also like to thank Professor Donald E. Anderson for his valuable lessons during the course of "Earthquake Resistant Structures".

Financial support for this project was provided in part by the Steel Structures Educational Foundation.

To my brother who inspired me in becoming an engineer

Chapter 1 INTRODUCTION

1.1 General Remarks

Building codes provide guidelines for designing structures in seismically active regions. These guidelines include defining a design level of seismic loading based on an estimated natural period of the building and a simplified approximate method for distributing the loads along the height of the structure. There are several complex factors that control the response of the structures to a given ground motion, such as the three dimensional nature of loading and response, coupling between modes in different directions, the effect of higher modes, nonlinear behaviour of the structure and its ductility.

All of the above mentioned factors have been considered in developing the simplified methods suggested by seismic design codes. However, there is still need for more research on the behaviour of the structures in earthquakes to evaluate the efficiency of the simplified methods and the accuracy of more sophisticated methods of analysis such as nonlinear static, spectral dynamic, linear and nonlinear time history analysis.

Due to this need, several buildings in California have been thoroughly instrumented by the California Strong Motion Program (CSMIP) and the United States Geological Survey (USGS). The buildings include series of instruments that measure the motion at selected locations of the structure. The instruments have recorded the motions during recent severe earthquakes. In this research, the recorded motions of 11 low-rise (two to seven story) steel frame structures were used to evaluate the behavior of this type of buildings under seismic loading.

1.2 Objectives

The main objective of this study is to gain a better understanding of the behaviour of low-rise steel frame buildings during earthquakes by:

1. Conducting a detailed study of the recorded response of 11 low-rise steel frame buildings during recent earthquakes,
2. Determining the natural vibration frequencies and mode shapes of the buildings based on the recorded data,
3. Comparing the measured fundamental vibration period of the buildings to that estimated utilizing code formulae,
4. Developing a refined structural model of one of the buildings for dynamic time-history analysis and comparing the results to the recorded data.
5. Studying the nonlinear response of the structural model when subjected to higher levels of ground motion.
6. Comparing the results of various analysis techniques.

1.3 Scope of Work

Throughout the course of this project the following work was done to achieve the above mentioned objectives.

1. A review of signal processing and system identification techniques was conducted to set up a procedure for determining the vibration properties of the buildings using the strong motion data.
2. Vibration properties of the first two or three modes in each of the three lateral directions (X

and Y translational and rotational) were estimated. These properties included natural frequencies, mode shapes, damping values and modal amplification factors.

3. The recorded motions of buildings at the locations of the installed accelerometers were processed to separate the translational and rotational components of the motion. These data were used to obtain a better estimate of the translational and rotational response properties.
4. For each building, the properties of the recorded ground motions and the structural response were presented in the form of a series of graphs and tables.
5. A nonlinear structural model of a six story building in Burbank was developed and dynamic time-history analyses were performed using the ground accelerations recorded during the 1987 Whittier and 1994 Northridge earthquakes.
6. The structural model was refined so that the results of the time-history analyses matched the recorded data.
7. The structural model was analyzed using various linear elastic analysis methods such as: Spectral dynamic analysis (using true response spectrum and code recommended design response spectra) and equivalent static analysis. The results were compared to those of linear elastic time-history analyses.
8. Nonlinear dynamic time history analyses were performed using two and three times the ground accelerations recorded during the 1994 Northridge earthquake.
9. A nonlinear elastic (push-over) analysis was performed and the results were compared to those of the nonlinear time-history analysis.

Chapter 2 BACKGROUND OF THE PROJECT

2.1 Strong Motion Data

The California Strong Motion Instrumentation Program **(CSMIP)** and the United States Geological Survey **(USGS)** have installed an extensive array of instruments to measure the motion of a large number of buildings, bridges, dams, and free field vibrations during earthquakes. Many of these instruments have recorded the motions of several earthquakes that have happened in recent years, thus providing an extensive database of valuable information for earthquake engineering research.

2.2 Previous Work

The strong motion data have been used to study the behaviour of a large number of structures of various types in recent years. Only a limited portion of this work, however, has focused on low-rise steel frame buildings. A brief review of some of the previous research on the behaviour of this type of structures is described in the following paragraphs.

Pardoen (1989) studied the recorded response of three instrumented buildings. This included the study of the response of a four story steel frame hospital building in Palm Springs during the Palm Springs earthquake of 1986.

A detailed study was conducted by Shen and Astaneh (1990) on the behaviour of the Burbank 6-story office building during the Whittier earthquake. The study included system identification using the Whittier earthquake records and linear elastic dynamic time-history analysis of a refined model of the structure. They concluded that proper modeling of connections and floor diaphragms can lead to accurate predictions of the response. They also concluded that code procedures (at the time of the study) predict a period that usually is significantly smaller than the actual period of the steel structures similar to the one studied in that research.

Fenves (1990) studied the behavior a four story (steel frame) hospital in San Francisco during the 1984 Morgan Hill and 1989 Loma Prieta earthquakes and a six story hospital in Sylmar during the 1987 Whittier earthquake. The Sylmar building had a cruciform shape in plan with concrete shear walls in the lower two stories and steel frames in the upper four stories. The two buildings were selected for their irregular features. A mathematical model of the San Francisco four story hospital was developed for linear dynamic analysis. Close correlation between the measured and analytical response was obtained when mass eccentricity was included (which created coupled modal response as apparent in the recorded response).

McClure (1991) used a three dimensional model of a two story (steel frame) office building in Oakland to evaluate its response during the Loma Prieta earthquake. The structural model was validated by the periods obtained from forced vibration measurements. Time-history and response spectrum methods were used in the analyses. The displacements obtained from the time-history analyses were very close to those obtained from strong motion records. Peak accelerations of 0.65 g, 0.39 g, and 0.26 g, were observed at the roof, second floor and, ground, respectively during the Loma Prieta earthquake.According to the time-history analyses, however, the maximum base shear was 14% of the weight of the building.

De la Llera and Chopra (1991 and 1992) studied the response of three nominally symmetric-plan buildings to evaluate the code accidental torsional provisions. Two of these buildings were low-rise steel frame buildings (a three story office building in Richmond and a three story office building in San Jose). The recorded response of these buildings during the 1989 Loma Prieta earthquake was studied. Three-dimensional models of the buildings were prepared and static analyses were performed at many time instants. The results demonstrated that the accidental torsion specified by the Uniform Building Code (UBC) is adequate in representing the torsion in the recorded motions of these three buildings.

Cole et al. (1992) developed a database of fundamental periods of 64 buildings to investigate the efficiency of code period formulas. Only regular buildings contemplated by the 1991 Uniform Building Code were included in the study. The following low-rise steel moment frame buildings were included in the study: 1) Burbank 6-story office building, 2) Palm Springs 4-story hospital, 3) Richmond 3-story office building, 4) San Bernardino 3-story office building, 5) San Jose 3-story office building, 6) San Francisco 4-story hospital.

Huang et al. (1993) studied the recorded motion of four base-isolated buildings during the 1992 Landers earthquake. Three of these were steel braced frame buildings including: 1) Rancho Cucamonga 4-story Law and Justice Center, 2) Los Angeles 2-story fire control building, 3) Los Angeles 7-story University hospital. The peak accelerations measured at the foundation level of the buildings were between 0.04 g and 0.11 g. For each building the drifts between roof and the base of the superstructure and the deformation of the isolators were derived from the strong motion data. The results showed that the two story building responded almost like a rigid superstructure over isolators and had negligible drift in the superstructure. The drifts in the superstructures of the other three buildings were considerable. The deformation of the isolators for these four buildings ranged from 0.8 to 1.6 cm.

Shakal et al. (1994) studied the strong motion data recorded in several buildings during the 1994 Northridge earthquake. The buildings included the following low-rise steel frame buildings: the Burbank 6-story office building, the Sylmar 6-story hospital and, the Los Angeles 7-story University hospital (base-isolated). The study included a preliminary interpretation of the recorded response of the buildings in terms of the natural vibration periods, peak accelerations, displacements and the response spectra of the recorded ground motions.

Nagarajaiah and Xiahong (1995) studied the response of the Los Angeles 2-story fire control building and the Los Angeles 7-story University hospital (both base-isolated) during the 1994 Northridge earthquake. The study included system identification, nonlinear analytical modeling, interpretation of structural behaviour during the Northridge earthquake , and evaluation of the effectiveness of seismic isolation. The study concluded that 1) the 7-story University hospital performed very well and the seismic isolation was effective in reducing the response, 2) the 2-story fire control building also performed well. Accidental pounding, however, reduced the effectiveness of seismic isolation (due to lack of sufficient free movement at the seismic isolation gap), 3) the analysis techniques used in the study predicted the response of the base-isolated buildings accurately.

De la Llera and Chopra (1995) studied the behaviour of eight instrumented buildings during the 1994 Northridge earthquake to evaluate the UBC seismic design provisions. This study included the following steel frame buildings: 1) Burbank 6-story office building, 2) Los Angeles 2-story fire control building (base-isolated), 3) Los Angeles 3-story commercial building, 4) Los Angeles 6-story office building, 5) Los Angeles 7-story University hospital (base-isolated), 6) Sylmar 6-story hospital. The study included system identification utilizing signal processing techniques, and comparison of the recorded data with the results of linear and nonlinear dynamic time history analyses. The results were used to discuss issues such as instrumentation, building modeling, ductility of the structures and the performance of the perimeter frame systems. They concluded that thorough instrumentation of all floors of the buildings is not economically feasible. As a result, the records of the instrumented floors must be used to predict the motions of the un-instrumented floors by system identification and/or record interpretation. A degree of uncertainty exists in the accuracy of the structural models that are prepared based on conventional methods. The study showed that the level of uncertainty is highly correlated with the complexity of the structure. The use of inelastic models for the buildings that are designed to experience substantial inelastic behaviour was highly recommended. The study concluded that perimeter frame systems violate the redundancy requirement for ductile behaviour in the structure. Perimeter frame systems also have a serious deficiency in their inelastic behaviour.

Naeim (1996) conducted an elaborate study of the performance of 20 instrumented buildings during the 1994 Northridge earthquake. This study included the following low-rise steel frame buildings: 1) Sylmar 6-story hospital 2) Los Angeles 3-story commercial building, 3) Burbank 6-story building, 4) Los Angeles 6-story office building. The research included inspection of the buildings, damage assessment, and performance evaluation. The forces, displacements, and dynamic characteristics were obtained from the strong motion data and were compared with those suggested by building codes. Some of the results of the study include: 1) Building code estimates are consistently less than observed periods. 2) In most cases, the base shears obtained from interpretation of the recorded data were larger than the base shears they had apparently been designed for, i.e. in most cases the buildings performed much better than they were expected to by routine design analysis techniques. 3) The ratio of the base shears to design code base shears did not correlate very well with the extent of damage observed. However, the overall drift ratios correlated rather well. 4) The drift ratios were significantly less than what would have been expected from ordinary design analysis techniques. 5) Evaluation of the deformed shape at the time of maximum lateral displacements showed that, at that instant, the deformed shape is almost always similar to the first mode of vibration. In most cases, however, maximum forces and maximum displacements were not concurrent, and except for the short buildings, the distribution of the forces at the time of maximum base shear were radically different from lateral force profile obtained from code suggested static procedure. 6) Except for the buildings with structural damage, the period of the building according to the recorded data did not elongate significantly. When elongation occurred, the period returned to the vicinity of the initial value towards the end of the ground motion. 7) For several buildings, torsion contributed significantly to the seismic response.

Goel and Chopra (1997) investigated the empirical formulae for estimating the periods of moment-resisting frame buildings. They studied the fundamental periods of a large number of structures, including six steel frame buildings with two to six stories, which were obtained from analyzing the strong motion data. The measured periods were used to improve the period formulae suggested by the building codes. It was concluded that the code formula for steel moment resisting frame buildings leads to shorter values than measured periods, with the margin between the two being much larger than for concrete moment frame buildings. The research showed that the intensity of ground shaking has little influence in elongating the period. In steel frame buildings, the period elongates slightly due to stronger shaking but less than that for reinforced concrete buildings.

2.3 Demand for Further Studies

In many of the previous studies, the extent of the research was to determine the periods of the first one or two translational modes of vibration in each direction, acceleration amplifications, displacements and inter-story drift ratios. Structural models of some of the buildings were analyzed using linear static or dynamic methods in most cases. Nonlinear analysis for these buildings was rarely performed.

This project was inspired by the need for a better understanding of the behaviour of structures (in particular, low-rise steel frame structures) during earthquakes and the effectiveness of the various analysis techniques currently available for seismic design of structures. This can be accomplished through more detailed analysis of the recorded data, investigating the higher modes of vibrations of the buildings using system identification techniques, and a comparative study of the results from various analysis techniques.

2.4 Selection of the Buildings

The criteria for selecting the buildings from the strong motion data archives for this study were:

- Steel moment resisting or braced frames for lateral load resisting system,
- Seven or fewer stories,
- Preferably recorded peak ground accelerations (PGA) of greater than 0.2 g.

Eleven buildings were selected for this study. The peak ground accelerations measured at the foundations of the selected buildings were within 0.06 g to 0.37 g. Description of the buildings and the layout of the recording instrumentation are presented in Chapter 4.

This research includes data processing of two base-isolated structures. The Los Angeles 2-story fire control building and the Los Angeles 7-story University hospital were chosen for this purpose.

2.5 Earthquakes Considered in this Study

The strong motion data used in this research was selected from the database of the recorded motions of the following four earthquakes:

1) **Northridge** earthquake of January 17, 1994

Hypocenter: 34.215 ^{o} N, 118.538 ^{o} W

Depth: 18 km

Magnitude: 6.7

2) **Landers** earthquake of June 28, 1992

Hypocenter: 34.217 ^{o} N, 116.433 ^{o} W

Depth: 9 km

Magnitude: 7.5

3) Santa Cruz Mountains **(Loma Prieta)** earthquake of October 17, 1989

Hypocenter: 37.037 ^{o} N, 121.883 ^{o} W

Depth: 18 km

Magnitude: 7.1

4) **Whittier** earthquake of October 1, 1987

Hypocenter: 34.062 ^{o} N, 116.433 ^{o} W

Depth: 9 km

Magnitude: 7.5

Chapter 3 REVIEW OF SYSTEM IDENTIFICATION TECHNIQUES USED IN THE PROJECT

3.1 Natural Vibration Frequencies

One of the main objectives of this project was to determine the natural frequencies and mode shapes of the buildings using the strong motion data. To achieve this, the concept of resonance was used.

We know from structural dynamics that the response of a vibrating system to harmonic loading is harmonic and the amplitude of the response depends on the ratio of the rotational frequency of the loading (ω) to the natural frequency of the system (ω_n). The response is at a maximum when the frequency of excitation is equal to the natural frequency of the system. This is known as the resonance condition. This means that if we have a plot of response versus the frequency of the loading, the peak of the graph will correspond to the natural frequency of the system (Figure 3.1). In the resonance condition the response has a 90^o phase lag with respect to the excitation. For practical purposes this property can be used as a tool to verify that the peak of the plot truly indicates a natural frequency (see Figure 3.1).

Ground motion during an earthquake is not harmonic, so the strong motion data cannot be used directly to determine the natural frequencies. To solve this problem, the **Fourier Transform** of the time history of ground motion and the response of the system are used.

The Fourier Transform is a mathematical tool used to represent a time variable function as the summation of a series of sinusoidal functions with different frequencies. A plot of these amplitudes vs. frequency is called a **Fourier Spectrum**. Processing the data using their Fourier Spectra is usually called **Frequency Domain Analysis**. After calculating the Fourier Spectra of the input (ground motion) and the output (response of the system), a plot of the ratio of output to input vs. frequency can be prepared. This is called **Frequency Response Function (FRF).** The FRF is a measure of amplification of the motion by the vibrating system, and it can be used to determine the natural frequencies by locating the peaks of the FRF plot.

This procedure should be carried out with caution, because not every maximum point on a FRF plot indicates a natural frequency and there are several factors which induce errors in this procedure. The sources of errors will be discussed in Section 3.4.

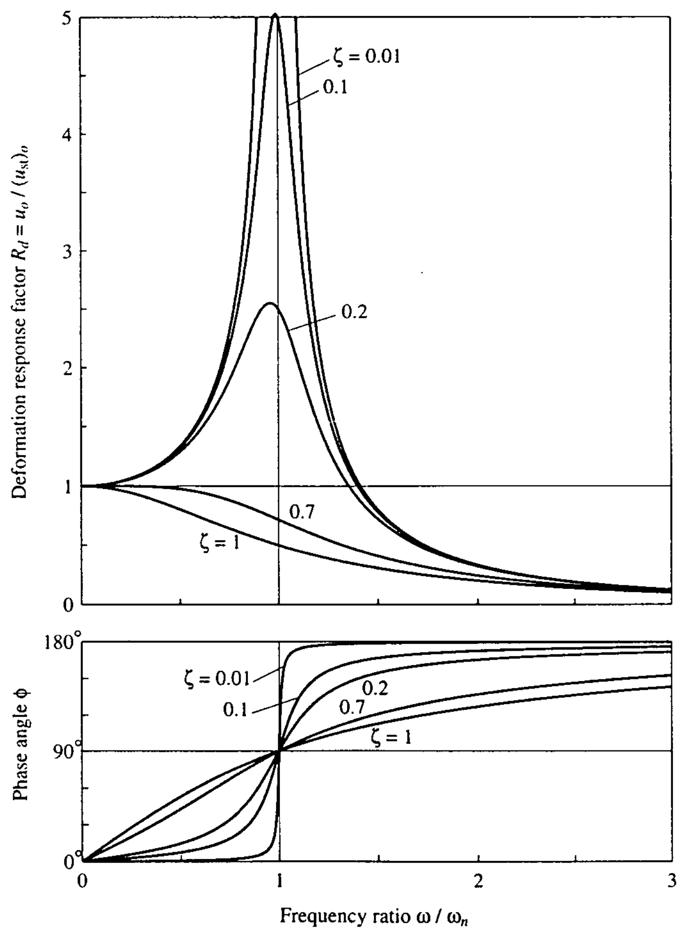

Figure 3.1 Displacement Response factor and phase angle for a damped system excited by harmonic force (after Chopra, 1995).

3.2 Mode Shapes

After finding a natural frequency, a deformed shape of the building can be plotted according to the amplitudes of FRF's at the natural frequency. This will be a good approximation of the corresponding mode shape. If the plotted shape resembles one of the expected mode shapes of the structure, it may confirm that the calculated frequency is a true natural frequency of the system.

3.3 Estimating Damping

The method used to estimate damping is based on the concept of Half Power Band Width.

On the frequency response curve, if ω_a and ω_b are frequencies on two sides of the resonant frequency where the amplitude is $2^{(-1/2)}$ of the resonant amplitude (Figure 3.2), the damping value can be calculated using the following equation:

$$\frac{\omega_a - \omega_b}{2.\omega_n} = 2 \cdot \zeta$$ (Equation 3.3.1)

This method was used in this study to estimate the modal damping values.

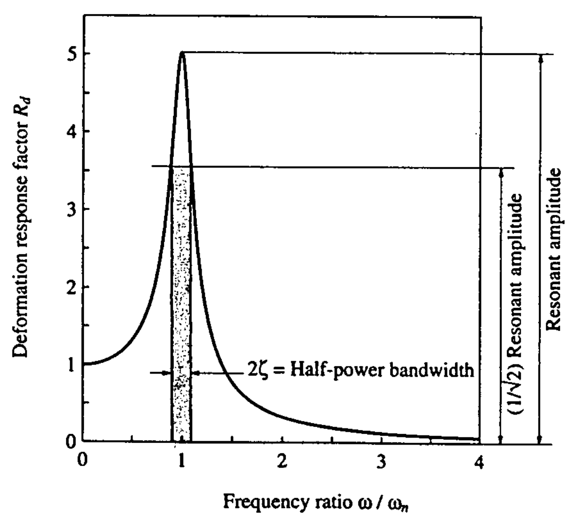

Figure 3.2 Definition of half-power bandwidth (After Chopra, 1995).

3.4 Sources of Error and Reliability of the Results

There were several factors that seemed to induce errors in the results of the system identification and data processing in this research and influence the reliability of the results. This section includes a brief review of the important issues that seem to be a source of error in this project. These sources of error are as follows.

1. The measuring instruments have a certain level of accuracy and their sensitivity is not necessarily the same for all frequencies. There is also a measure of electronic noise being recorded by the instrumentation.

2. The original recorded data usually are not usable directly. The data are usually undergone a series of signal processing stages to be filtered (removing the frequencies that are lower or higher than certain values which could only indicate noise not meaningful data) and base-line corrected. A more realistic data are retrieved from the original data.

Although this process improves the accuracy of the data, a measure of noise and error still remains in them. Also some of the information may deteriorate or altered during this process.

3. The concept of Fourier Transform has been mathematically proven to be correct for periodic functions with infinite time window length. Applying this technique to strong motion data, which are transient (non-periodic with limited time domain) includes a measure of error. This is called Leakage (see ME'Scope, Operating manual, 1998, Appendix note # 1).

To minimize leakage, the data are usually multiplied by a function which takes a value of zero at the beginning and at the end, and is one in the middle, so that the product will be zero at the beginning and the end, and it will have characteristics closer to a periodic function. Experience shows that a sinusoidal function which is commonly known as the **Hanning window** is one of the most efficient windows to be used in this type of analysis. Using Hanning window results in more accuracy in frequencies, but increases the error in the amplitudes. This may be one of the main reasons that the estimated damping values using the Half-Power Bandwidth method were not as reliable as the estimated natural frequencies.

4. The FRF's of strong motion data usually contain several sharp peaks, which may not represent meaningful information. This usually happens when, at a data point, the denominator of the FRF is close to zero. In such cases a small error in the value of the Fourier Spectrum can result in a large error in the FRF. To overcome this, an averaging technique is usually used. The original data are broken into a series of shorter data blocks which have a length of order of 2^n (see Section 3.5) and are overlapped by 50 to 90 percent. The Fourier Transform is applied to these blocks and the average of the results are used as the final FRF. This makes the FRF smoother and decreases the random error. Figure 3.3 shows an example of two time-history records measured in an actual earthquake (Record A as Input and Record B as Output). Figures 3.4 and 3.5 show Fourier Spectra of A & B, and the Frequency Response Function (B/A) which are calculated with averaging. Figure 3.6 shows the FRF obtained without averaging.

It can be observed from Figure 3.6 that the FRF calculated without averaging is not providing a realistic representation of the behaviour of the system.

5. The results for the higher modes typically include a higher level error. This is due to the fact that the response has a higher amplitude in the frequency range closer to the fundamental mode, the signal to noise ratio is larger in this range and the results are more reliable for lower modes. On the other hand, the signal to noise ratio decreases in higher frequencies so that, beyond a certain limit, the data become meaningless and determining the higher natural frequencies becomes impossible.

As an example, Figure 3.4 shows that the amplitudes of records A and B are close to zero for the frequencies above 15 Hz. This shows that the large amplitude of the FRF at this frequency range (Figure 3.5) is not a true representation of the behavior of the system since it is the result of a zero-over-zero condition.

6. The buildings have distributed mass in all the elements which result in local vibration modes, which may be present in the computed FRF.

7. Flexibility of the diaphragms and nonlinear behaviour of the structures may also induce a measure of error in the system identification results.

8. When the location of a sensor is close to a nodal point of one of the higher modes of vibration (which theoretically has zero displacement at that mode), the corresponding FRF will not show any amplification of motion at the frequency of that mode of vibration. This may cause confusion in interpreting the results. In such cases FRF's corresponding to other floors can be used to determine the natural frequency.

3.5 Program "ME'scope"

A signal processing program called **ME'scope** (ME'Scope Operating Manual, 1998) was used in the first part of this research to evaluate the vibration properties of the buildings selected for data analysis. ME'scope calculates the Fourier spectra using the Fast Fourier Transform **(FFT)** technique. This is a numerical method to efficiently calculate the Fourier Transform of a time variable function. To use the FFT efficiently, the number of data points in time domain should be a power of 2, i.e. $N=2^n$. Frequency resolution of the results depends on the total time length of the data T=N.dt (where N is the number of data points)

$$\Delta f = 1 / N.\Delta t \qquad \text{(Equation 3.5.1)}$$

and the maximum frequency depends on the time increment (Δt)

$$f_{max} = 1 / 2.\Delta t \qquad \text{(Equation 3.5.2)}$$

Since the number of data points in practical experiments is not of the order of 2^n, only a portion of data can be used in each FFT calculation. The user has the option of using the averaging technique explained in item 5 of Section 3.4. This results in smoother FFT and FRF plots and the results are usually more reliable. The number of segments used in this averaging process can be increased by reducing the length of the segments but the trade-off will be a reduction in frequency resolution.

The program uses FRF functions to evaluate the natural frequencies and damping values of the system as explained in Sections 3.1 and 3.3. Since the FRF's do not have a smooth shape like the response function shown in Figure 3.1, a curve fitting technique is used by ME'scope to improve the results. The user can optimize the curve fitting results by visually inspecting the FRF plot and selecting a narrower band of the FRF where a natural frequency seems to exist. Multi Input Multi Output (**MIMO**) analysis allows the user to define a series of data as input (ground motion data in this case) and a set of output data (motions of the upper floors) resulting in a matrix of FRF's rather than a single function. The user has the option of selecting some of the FRF functions and conducting the curve fitting process. For example, to determine the natural periods in the X direction, only FRF's with input and outputs in that direction may be used. The results for frequencies and damping are the average of the values obtained from all the selected FRF's. The magnitude of each FRF at a natural frequency indicates the corresponding component of the natural mode shape of the building at that frequency.

ME'scope also has the option of drawing a structure as a combination of nodes, lines, and surfaces. The user can animate the motion of the structure in both time and frequency domains.

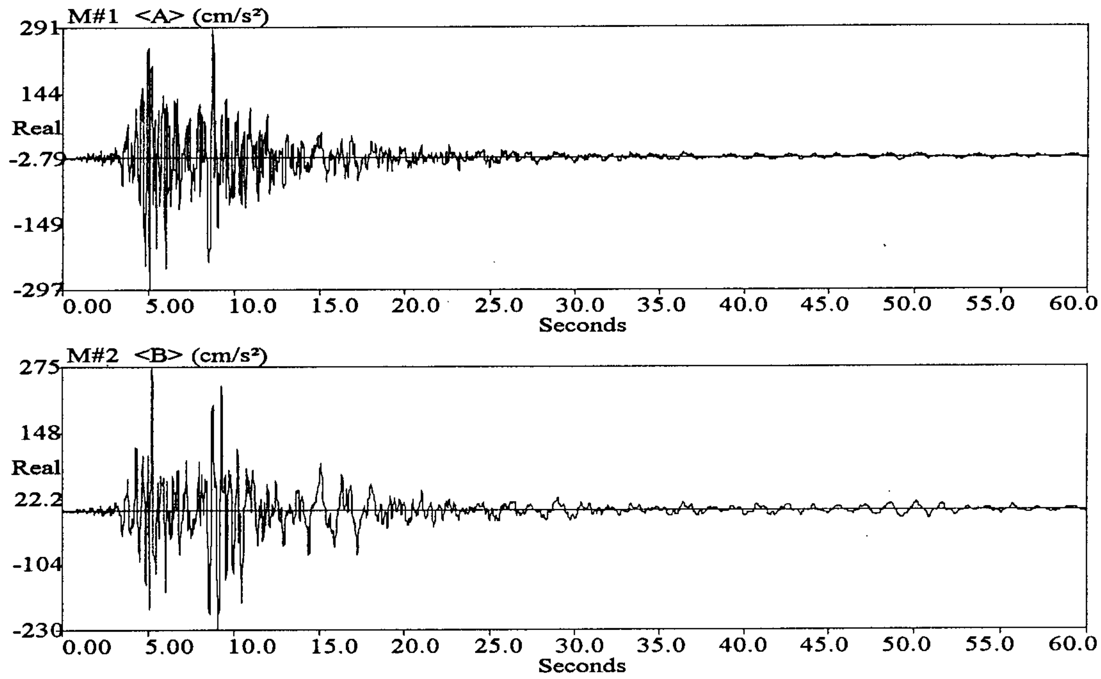

Figure 3.3 Example of recorded time-histories, Record length T = 60sec, $\Delta t = 0.02$sec, N = 3000.

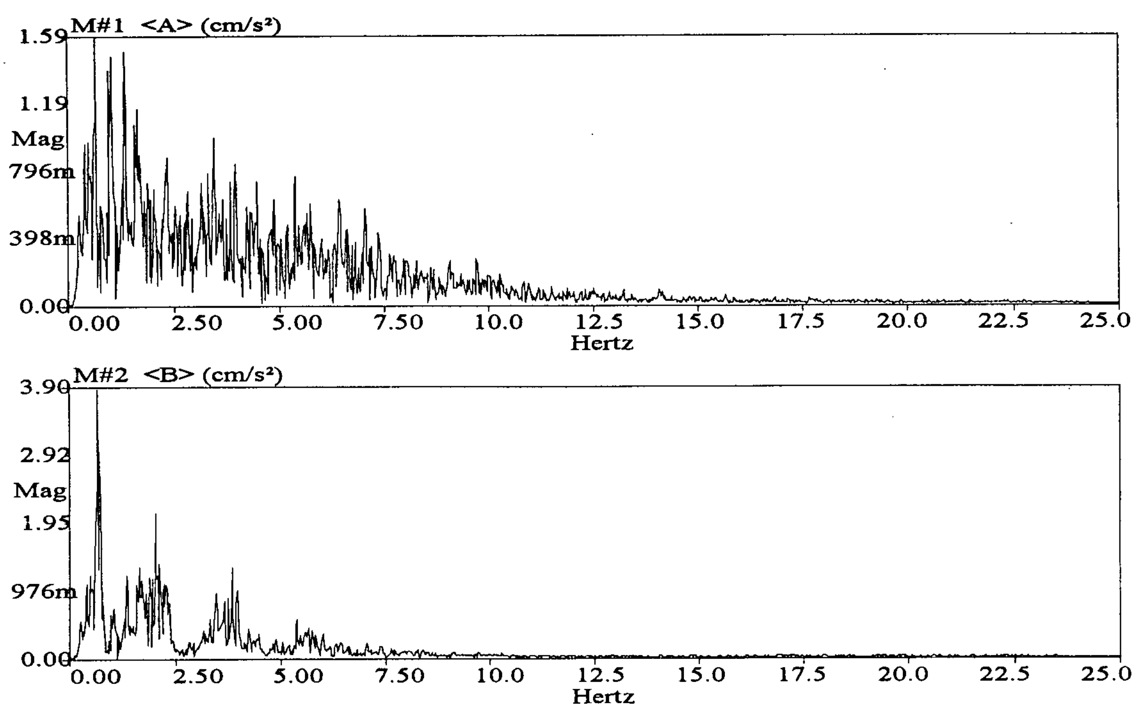

Figure 3.4 Fourier Spectra of example Records A & B computed using a Hanning window, a block size N= 2048, 5 averages and 88% segment overlap.

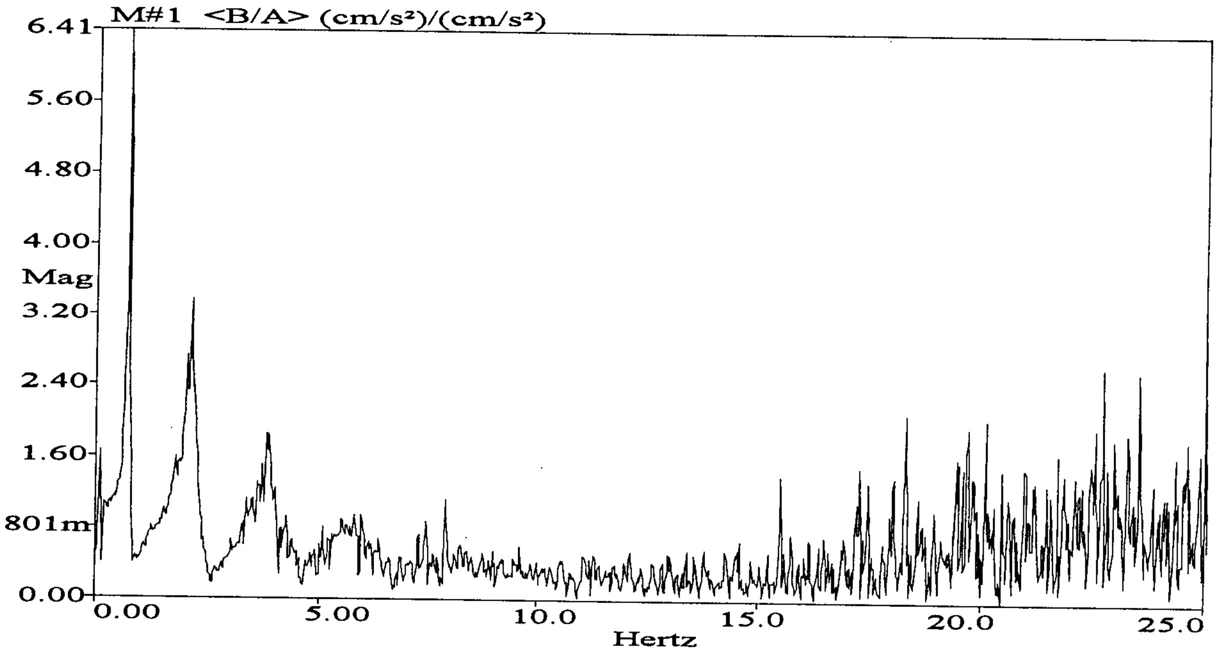

Figure 3.5 Example of Frequency Response Function (B / A) calculated with 5 averages.

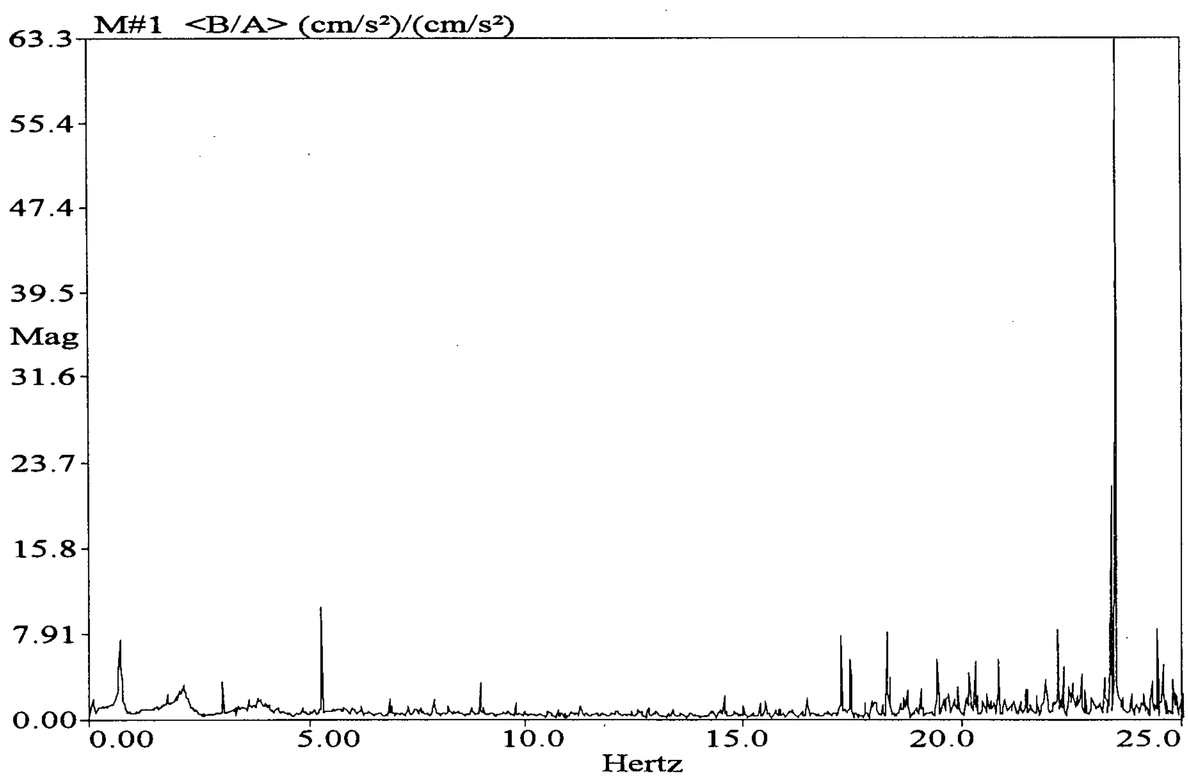

Figure 3.6 Example of Frequency Response Function (B / A) calculated without averaging.

3.6 Verification of the Results of ME'scope

To investigate the accuracy of the results of ME'scope, a series of artificial records were processed with ME'scope to evaluate the natural frequencies, mode shapes and damping values of a linear elastic structural model. The response data for this model was generated utilizing the program **SAP90** (SAP90 Users Manual, 1989). The model is a 6-story 3-D rigid frame and its mass and stiffness properties were selected so that its fundamental natural frequency was close to that of the Burbank 6-story office building, which was considered in this study. The model had 2.5-5.0% mass eccentricity at each floor to create some degree of coupling between modes in different directions. The actual ground motion recorded at this building during the Northridge earthquake was used for a linear time history analysis of the model. The response time histories of the second, third and roof levels were used in ME'scope to determine vibration properties of the system. Due to limitations of the version of SAP90 used in this project, no rotational ground motion was considered in the analysis.

A damping value of 5% was applied to all modes. The SAP90 model is shown in Figure 3.7 and Figure 3.8 shows an example of FRF's calculated using the output time-histories of the dynamic analysis. This represents the true response of a linear multi-degree of freedom system to dynamic loading. A comparison of the vibration properties of the model and the values estimated by ME'scope is presented in Table 3.1. The results show that if an accurate set of records are used, ME'scope can estimate all the natural frequencies of a linear system with an error of less than 1 percent. However, the estimated damping values were not as accurate. The results showed that the error in estimated damping values varied randomly. This suggests that the reliability of the damping values estimated from strong motion data in this research is questionable.

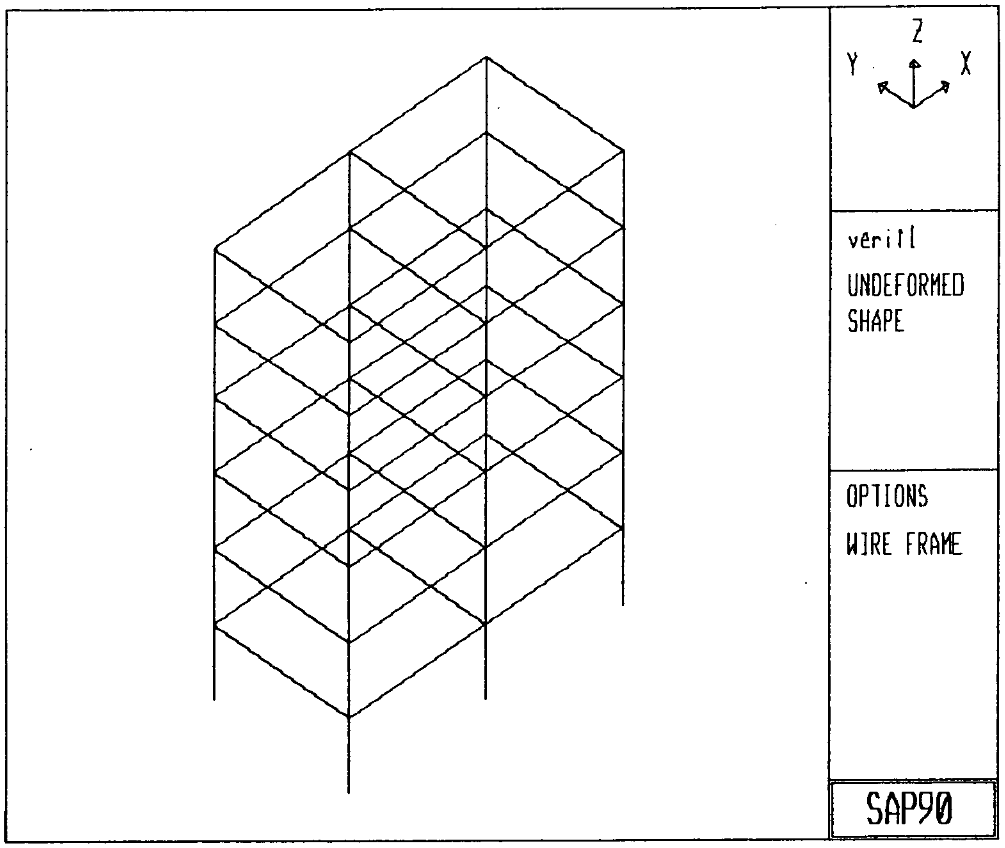

Figure 3.7 The **SAP90** model used to verify the accuracy of the results of ME'scope.

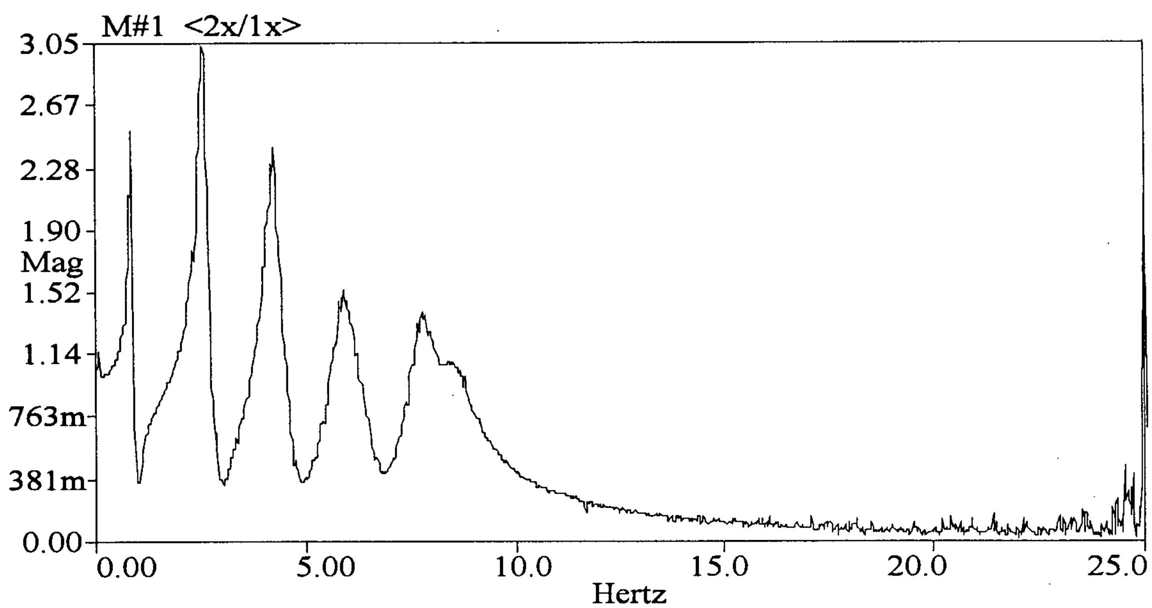

Figure 3.8 An example of the FRF's calculated from the time histories generated by **SAP90**.

Table 3.1 Comparison of the vibration properties of the SAP90 model and the values estimated based on the output time histories using the ME'scope.

Properties of the **SAP90** model				Values estimated by **ME'scope**	
Mode number	Modal direction	Period (sec)	Frequency (Hz)	Estimated frequency (Hz)	Estimated damping (%)
1	Y(1)	1.263	0.792	0.798	4.59
2	X(1)	1.157	0.864	0.861	3.27
3	ROT(1)	0.782	1.279	1.278	3.05
4	Y(2)	0.461	2.169	2.178	4.33
5	X(2)	0.391	2.557	2.563	4.10
6	ROT(2)	0.288	3.467	3.369	0.68
7	Y(3)	0.255	3.927	3.949	4.02
8	X(3)	0.237	4.226	4.239	3.87
9	Y(4)	0.192	5.211	5.213	3.32
10	X(4)	0.170	5.887	5.822	4.40
11	ROT(3)	0.162	6.188	6.015	3.20
12	Y(5)	0.145	6.900	6.907	4.35
13	X(5)	0.129	7.741	7.735	3.08
14	ROT(4)	0.119	8.407	7.897	5.08
15	-	0.116	8.624	8.508	2.03
16	-	0.113	8.850	8.768	3.68
17	-	0.092	10.819	10.793	3.10
18	-	0.0757	13.2152	13.184	0.13
Note: The SAP90 model had a damping value of 5.00 % for all modes.					

3.7 Three-Dimensional Animation of the Mode Shapes

To visualize the mode shapes, simple prismatic structural models have been prepared as described in Section 3.5. The X and Y displacements of the corners of the models were required for animation. Since these data were not measured directly, the recorded data were used to generate the required data based on the assumption that all floors behave as rigid diaphragms and the displacements are small. ME'scope uses interpolated displacements for the floors that have no assigned data. So when investigating the mode shapes presented in the following chapters, it is important to take into account that only some of the floors represent actual data.

3.8 Introducing the Concept of "Spectral Response Function"

As explained in the previous sections, the FRF's of actual data contain several sharp peaks close to each other which may make it difficult to identify the natural frequencies. For this reason the author was looking for another function with similar properties to the FRF but with smoother curves and better distinguished peaks. For this purpose, the author developed a plot of the ratio of response spectrum of output data to that of the input motion versus frequency. This function will be referred to as Spectral Response Function **(SRF)** in this study.

The advantage of the SRF plots to FRF's is that when the Fourier spectrum of an acceleration record shows a very low or very high amplitude for a certain frequency (compared to the amplitude of the adjacent points), the response spectrum, which is governed by the overall properties of the acceleration record does not show a sudden and sharp change in the amplitude of the response. Therefore the SRF plots are smoother and reflect the overall properties of the recorded data and, in some cases, make it easier to identify a peak, which indicates a natural frequency.

The SRF plots appear to give reliable results for the lower modes of vibration, which have a relatively higher amplification factor. In this study the SRF's were used to verify the results obtained using ME'scope.

The programs used to calculate the response spectra were:

a) NONLIN, developed by Charney A. Finley, Ph.D., P.E., Advanced Structural Concepts, Incorporated, under a contract with the Federal Emergency Management Agency (FEMA)

b) SPECEQ, programmed by N.C. Nigam & P.C. Jennings, California Institute of Technology, Pasadena, California, modified by C.E. Ventura (1992), University of British Columbia, Vancouver, British Columbia

To compare the SRF's and FRF's, the Spectral Response Functions were calculated from the zero damping and 1% damping response spectra of the same input and output time histories that were used to obtain the Frequency Response Function of Figure 3.8. These SRF plots are presented in Figure 3.9.

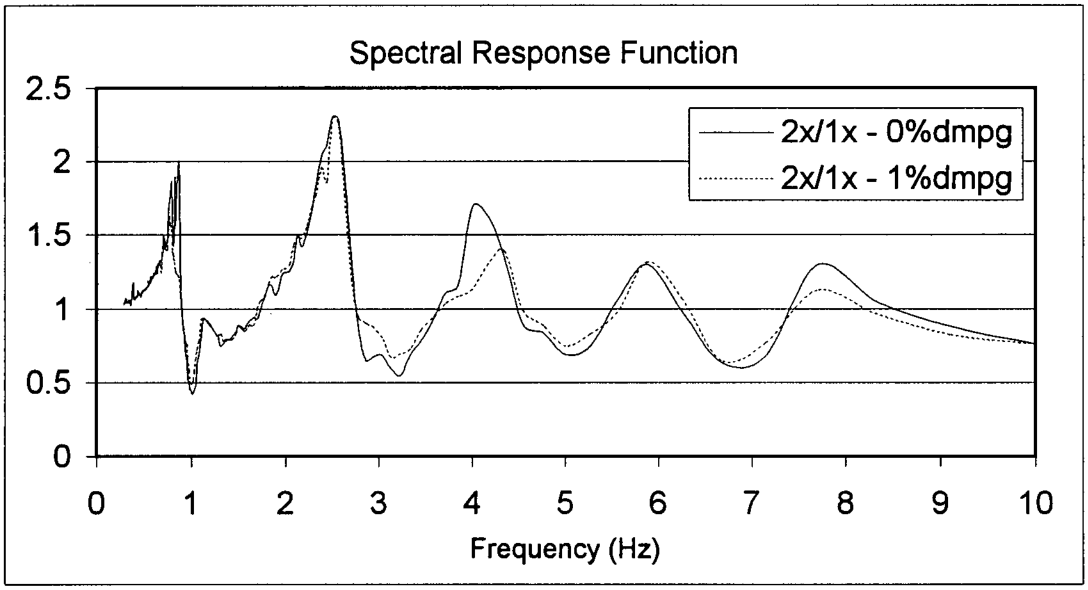

Figure 3.9 An example Spectral Response Function obtained from 0 % and 1 % damping response spectra.

Chapter 4 DESCRIPTION OF THE BUILDINGS UNDER STUDY

4.1 General

This chapter includes the description of the buildings under study, their location, and figures showing their shape, major dimensions, and the layout of the accelerometers installed on the buildings to record their motion during earthquakes.

The arrows in the figures represent the direction of the sensors. The dots represent the sensors measuring the accelerations in the direction perpendicular to the plane of the paper.

Table 4.1 shows a list of these buildings. A summary of general information on the buildings is presented in Table 4.2.

The location of the buildings and the epicenter of the earthquakes are shown in Figure 4.1.

Sections 4.2 to 4.12 describe each building in more detail.

Table 4.1 List of buildings under study.

Building	CSMIP Station #	Earthquake studied
1) Burbank, 6-Story Office Building	24370	Whittier Northridge
2) San Bernardino 5-Story Hospital	23634	Northridge
3) Pasadena 6-Story Office Building	24541	Northridge
4) San Jose 3-Story Office Building	57562	Loma Prieta
5) San Francisco 4-Story Hospital	58261	Loma Prieta
6) Berkeley 2-Story Hospital	58496	Loma Prieta
7) Richmond 3-Story Office Building	58506	Loma Prieta
8) Redlands 7-Story Commercial Building	23481	Landers
9) San Bernardino 3-Story Office Building	23516	Landers
10) Los Angeles 2-Story Fire Control Building	24580	Northridge
11) Los Angeles 7-Story University Hospital	24605	Northridge

Table 4.2 General description of the buildings under study.

Building	Plan Shape	Major dimensions (m)			Lateral Load Resisting System
		E-W	N-S	height	
1) Burbank, 6-story office bldg.	Square	36.6	36.6	25.2	Perimeter moment resisting frames
2) San Bernardino 5-story hptl.	L-Shape	45.7	55.2	21.0	Moment resisting frames
3) Pasadena 6-story office bldg.	Rectan-gular	35.7	38.1	25.0	Moment resisting frames
4) San Jose 3-story office bldg.	Rectan-gular	76.2	28.3	15.1	Moment resisting frames
5) San Francisco 4-story hptl.	Rectan-gular	35.7	66.8	16.0	Moment resisting frames (concrete walls at first floor)
6) Berkeley 2-story hptl.	Rectan-gular	43.0	35.7	7.7	Eccentrically braced frames
7) Richmond 3-story office bldg.	Rectan-gular	24.4	50.3	13.4	Perimeter moment resisting frames
8) Redlands 7-story bldg.	Rectan-gular	42.7	28.3	28.8	Perimeter moment resisting frames
9) San Bernardino 3-story bldg.	Rectan-gular	40.2	43.9	12.6	Perimeter moment resisting frames
10) LA 2-story fire cntrl bldg.	Rectan-gular	25.6	57.3	9.8	Perimeter braced (chevron) frames **(Base Isolated)**
11) LA 7-story University hptl.	S-shape	77.1	92.4	35.7	Diagonally braced perimeter frames **(Base Isolated)**

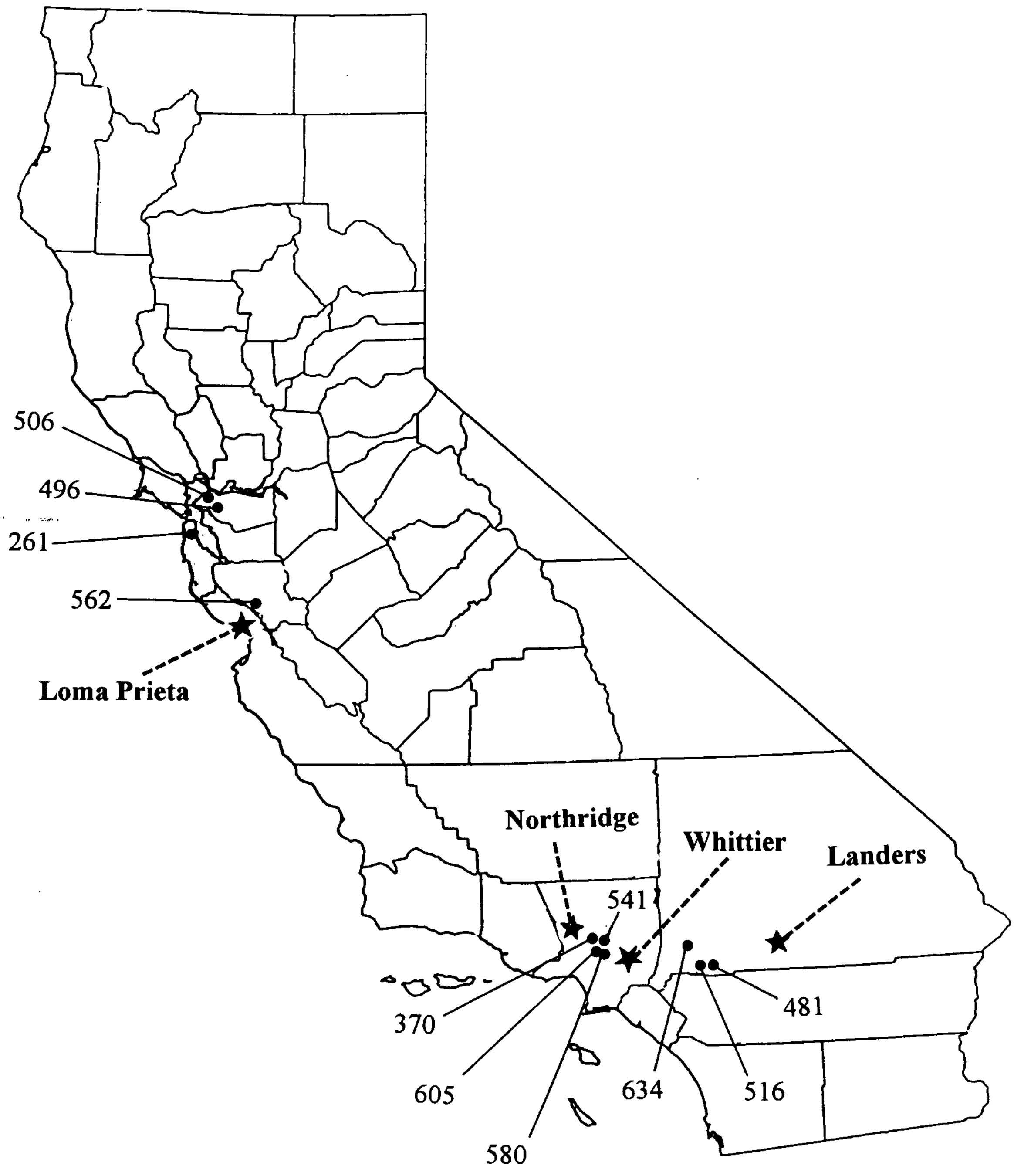

Figure 4.1 Location of the buildings and the epicenter of the earthquakes.

Note: The numbers represent the last 3 digits of CSMIP station numbers. * indicates the location of the earthquakes.

4.2 Burbank, 6-Story Office Building

Building Description:

Location: Burbank, CA

Zip Code: 91502

Coordinates: 34.185 ^{o}N, 118.308 ^{o}W

CSMIP Station number: 24370

Earthquake records studied: Northridge (1994), Whittier (1987)

Height & Number of Stories above ground: 25.2m (82.5ft), 6 stories

Plan Shape: Rectangular

Typical floor plan dimensions: N-S direction: 36.6m (120ft), E-W direction: 36.6m (120ft)

Vertical force resisting system: Steel beams & columns, 3 1/4" concrete slab over metal deck

Lateral force resisting system: Perimeter Moment Resisting Steel Frames

Design/Construction date: 1976/1977

Foundation type: Concrete Caissons (approx. 9.8m deep)

Number of stories below ground: 0

Site Geology: Alluvium

Epicentral distance: 22km W

est of bldg. (Northridge EQ)

26km South-East of bldg. (Whittier EQ)

Note: The above information was obtained from "Shakal et al., 1987"

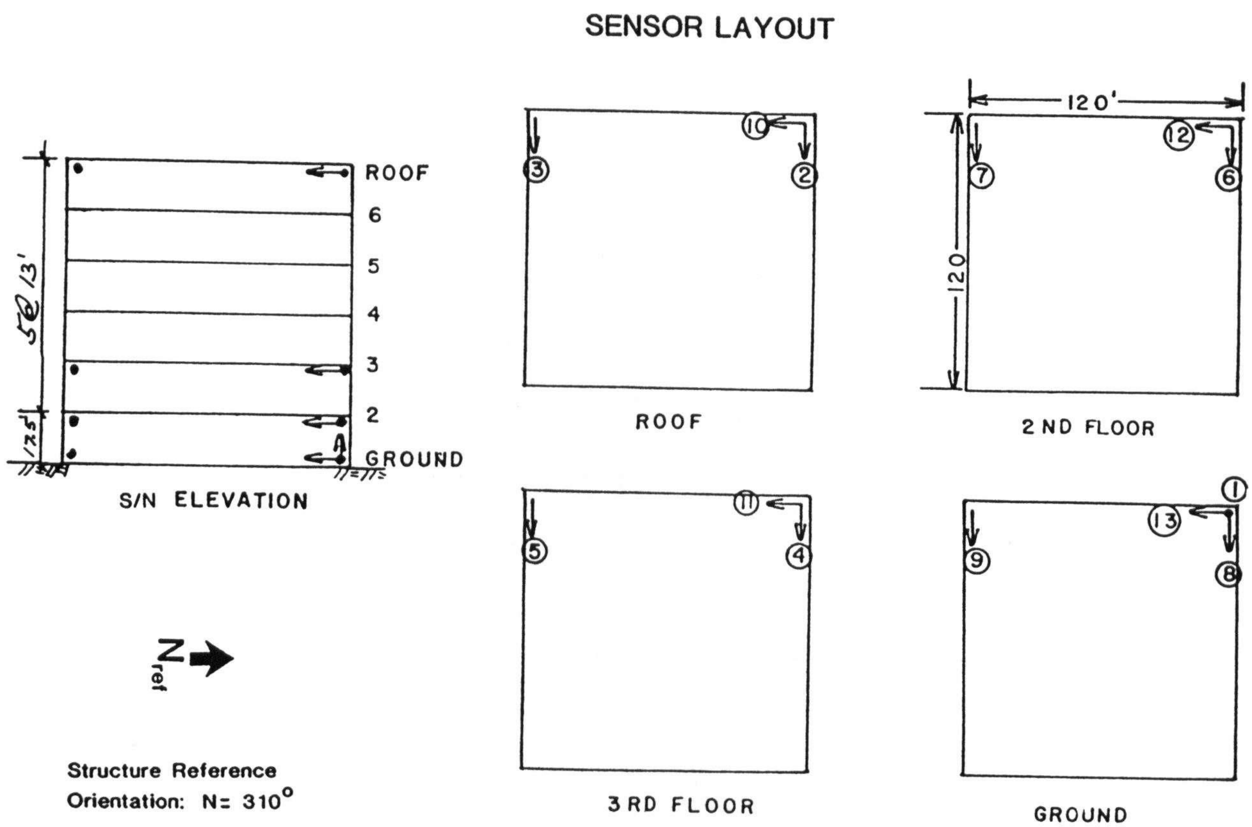

Figure 4.2 Overview of Burbank 6-Story Building and Sensor layout, (After Shakal, et al., 1987)

4.3 San Bernardino 5-Story Hospital

Building Description:

Location: San Bernardino, CA

Zip Code: ---

Coordinates: 34.132 ° N, 117.321 ° W

CSMIP Station number: 23634

Earthquake record studied: Northridge (1994)

Height & Number of Stories above ground: 21m (69ft), 5 stories

Plan Shape: L-shape

Typical floor plan dimensions: N-S direction: 55.2m (181ft), E-W direction: 45.7m (150ft)

Vertical force resisting system: Steel beams & columns

Lateral force resisting system: Moment Resisting Steel Frames

Design/Construction date: 1986/---

Foundation type: Concrete piles

Number of stories below ground: 0

Site Geology: Deep Alluvium

Epicentral distance: 113km West of building

Note: The above information was obtained from "Shakal et al., 1994"

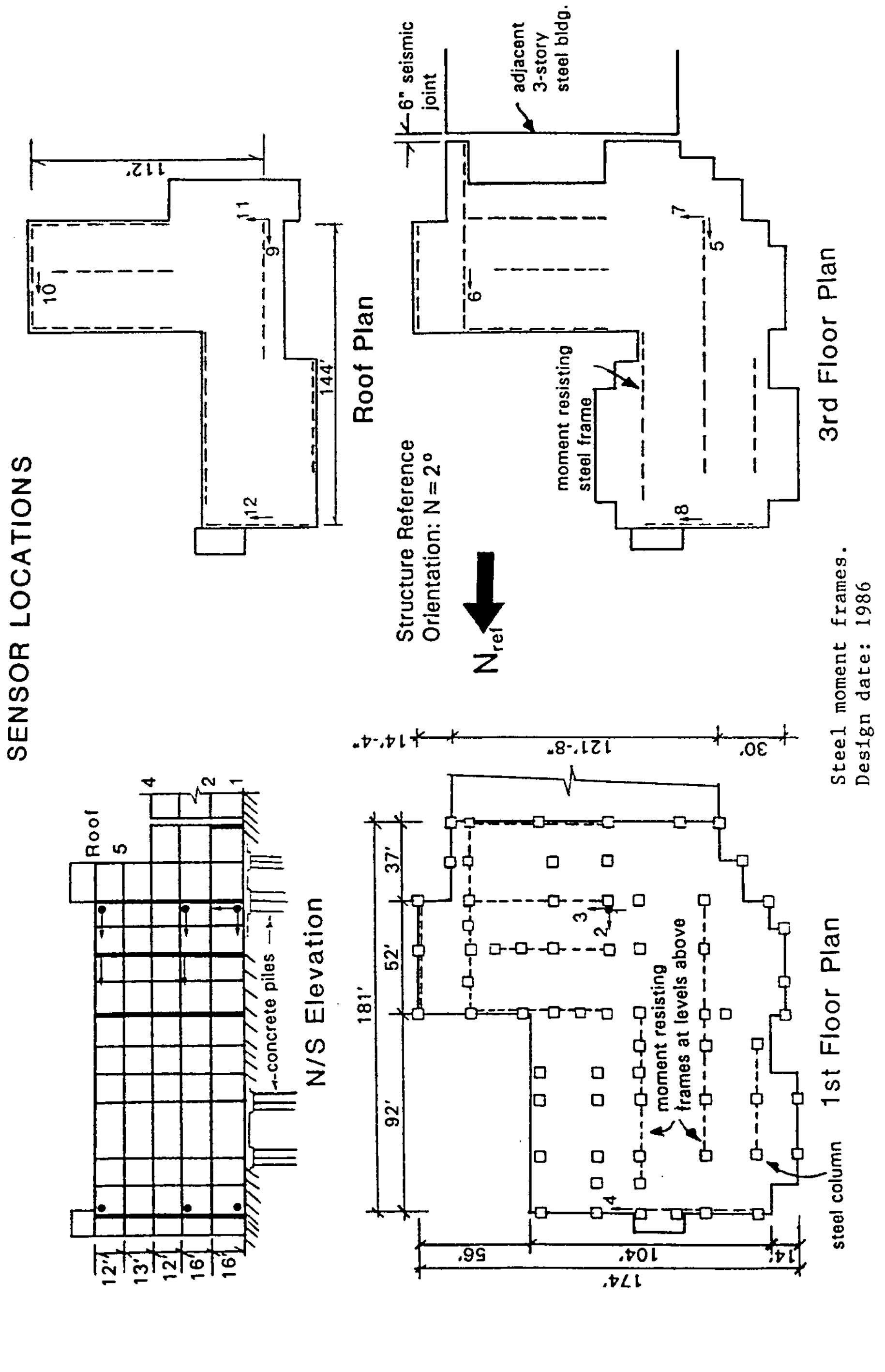

Figure 4.3 Overview of San Bernardino 5-Story Hospital and Sensor layout, (After Shakal, et al., 1994)

4.4 Pasadena 6-Story Office Building

Building Description:

Location: Pasadena, CA

Zip Code: ---

Coordinates: 34.146 $^{\circ}$N, 118.147 $^{\circ}$W

CSMIP Station number: 24541

Earthquake record studied: Northridge (1994)

Height & Number of Stories above ground: 25m (82ft), 6 stories + attic

Plan Shape: Rectangular

Typical floor plan dimensions: N-S direction: 38.1m (125ft), E-W direction: 35.7m (117ft)

Vertical force resisting system: Steel beams & columns

Lateral force resisting system: Steel frames with URM infill walls

Design/Construction date: 1906/---

Foundation type: ---

Number of stories below ground: 1

Site Geology: Deep Alluvium

Epicentral distance: 37km West of the building

Note: The above information was obtained from “Shakal et al., 1994”

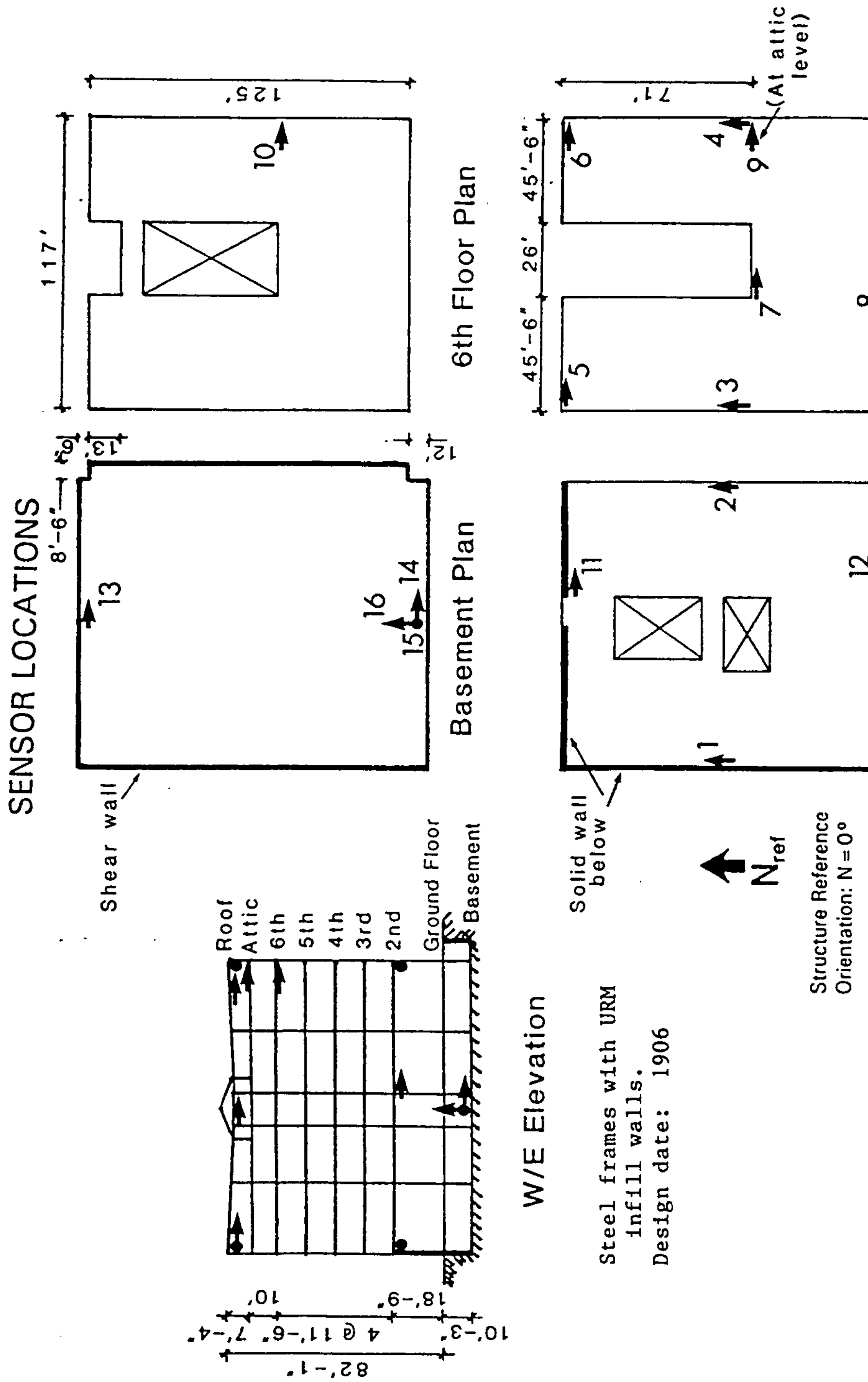

Figure 4.4 Overview of Pasadena 6-Story Office Building and Sensor layout, (After Shakal, et al., 1994)

4.5 San Jose 3-Story Office Building

Building Description:

Location: Santa Teresa Hills, San Jose, CA

Zip Code: ---

Coordinates: 37.212 ^{o} N, 121.803 ^{o} W

CSMIP Station number: 57562

Earthquake record studied: Loma Prieta (1989)

Height & Number of Stories above ground: 15.1m (49.5ft), 3 stories

Plan Shape: Rectangular

Typical floor plan dimensions: N-S direction: 28.3m (92.7ft), E-W direction: 76.2m (250ft)

Vertical force resisting system: Concrete slab on steel deck supported by steel frame

Lateral force resisting system: Moment resistant steel frames with exterior cladding

Design/Construction date: 1983/1984

Foundation type: Spread footing

Number of stories below ground: 0

Site Geology: Alluvium over serpentine

Epicentral distance: 21km South-West of the building

Note: The above information was obtained from "Shakal et al., 1989"

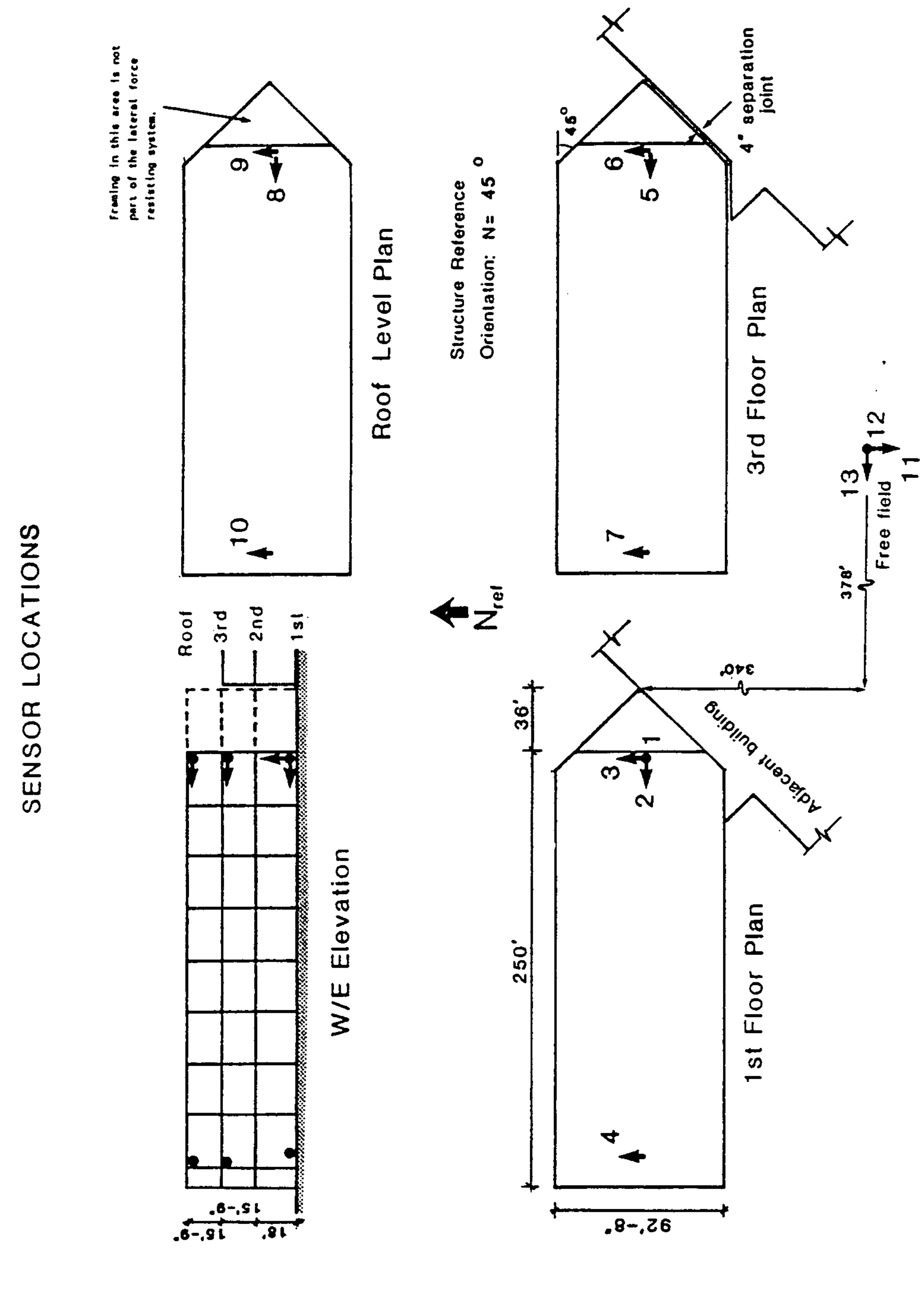

Figure 4.5 Overview of San Jose 3-Story Office Building and Sensor layout, (After Shakal, et al., 1989)

4.6 San Francisco 4-Story Hospital

Building Description:

Location: San Francisco, CA

Zip Code: ---

Coordinates: 37.66 ° N, 122.439 ° W

CSMIP Station number: 58261

Earthquake record studied: Loma Prieta (1989)

Height & Number of Stories above ground: 16m (52.5ft), 4 stories

Plan Shape: Rectangular

Typical floor plan dimensions: N-S direction: 66.8m (219ft), E-W direction: 35.7m (117ft)

Vertical force resisting system: 3.5" light-weight concrete fill over metal deck supported by steel frame

Lateral force resisting system: Moment-resistant steel frames (Concrete shear walls at 1st floor)

Design/Construction date: 1972/1973-75

Foundation type: Piles (15 - 21m deep); 8" concrete slab on grade

Number of stories below ground: 0

Site Geology: Fill over Sandstone

Epicentral distance: 85km South-East of the building

Note: The above information was obtained from "Shakal et al., 1989"

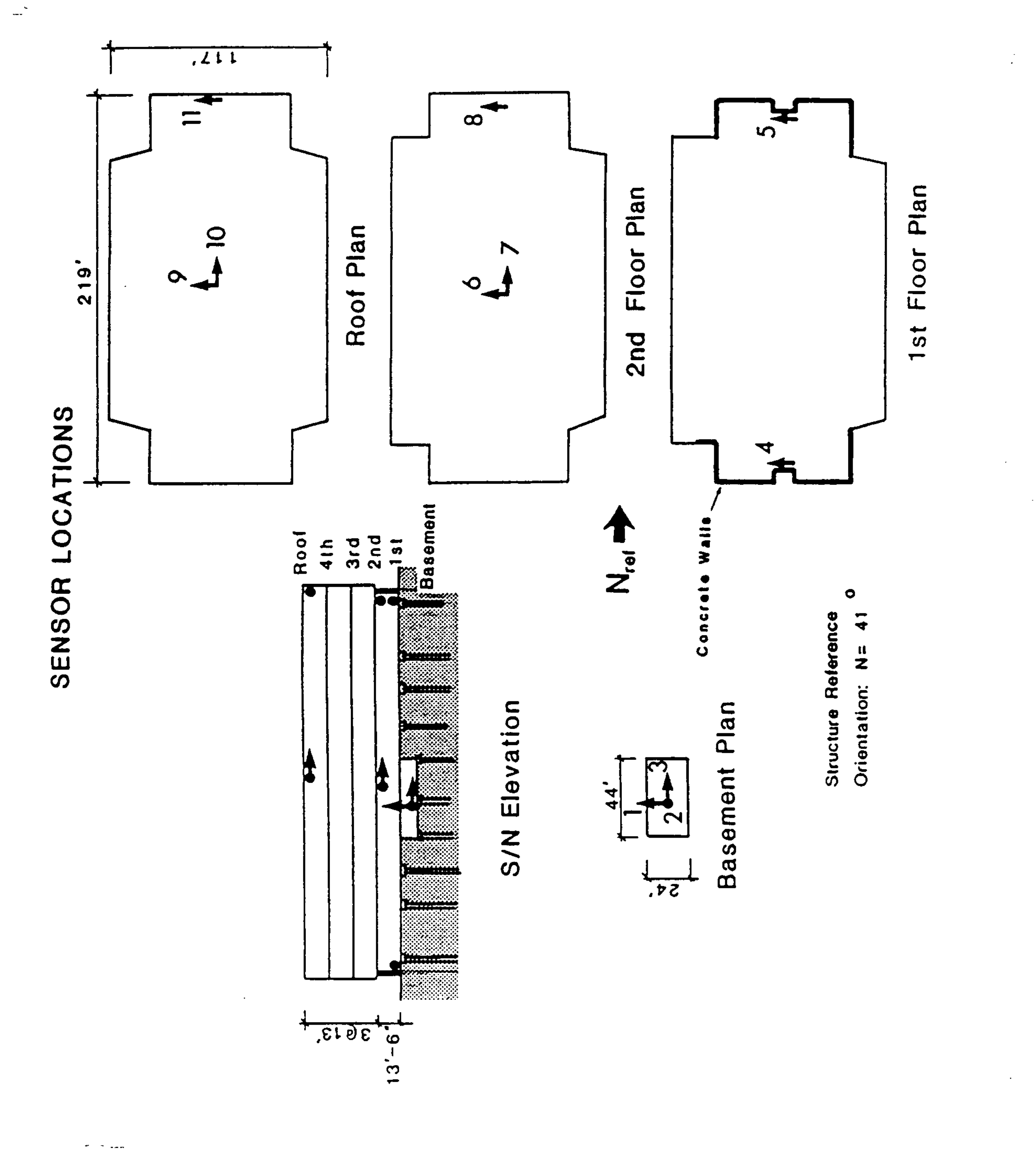

Figure 4.6 Overview of San Francisco 4-Story Hospital and Sensor layout, (After Shakal, et al., 1989)

4.7 Berkeley 2-Story Hospital

Building Description:

Location: Berkeley, CA

Zip Code: ---

Coordinates: 37.855 °N, 122.256 °W

CSMIP Station number: 58496

Earthquake record studied: Loma Prieta (1989)

Height & Number of Stories above ground: 7.7m (25.2ft), 2 stories

Plan Shape: Rectangular

Typical floor plan dimensions: N-S direction: 35.7m (117ft), E-W direction: 43m (141ft)

Vertical force resisting system: Steel frames

Lateral force resisting system: Eccentrically braced Steel frames

Design/Construction date: 1984/---

Foundation type:---

Number of stories below ground: 1

Site Geology: Alluvium

Epicentral distance: 97km South of the building

Note: The above information was obtained from "Shakal et al., 1989"

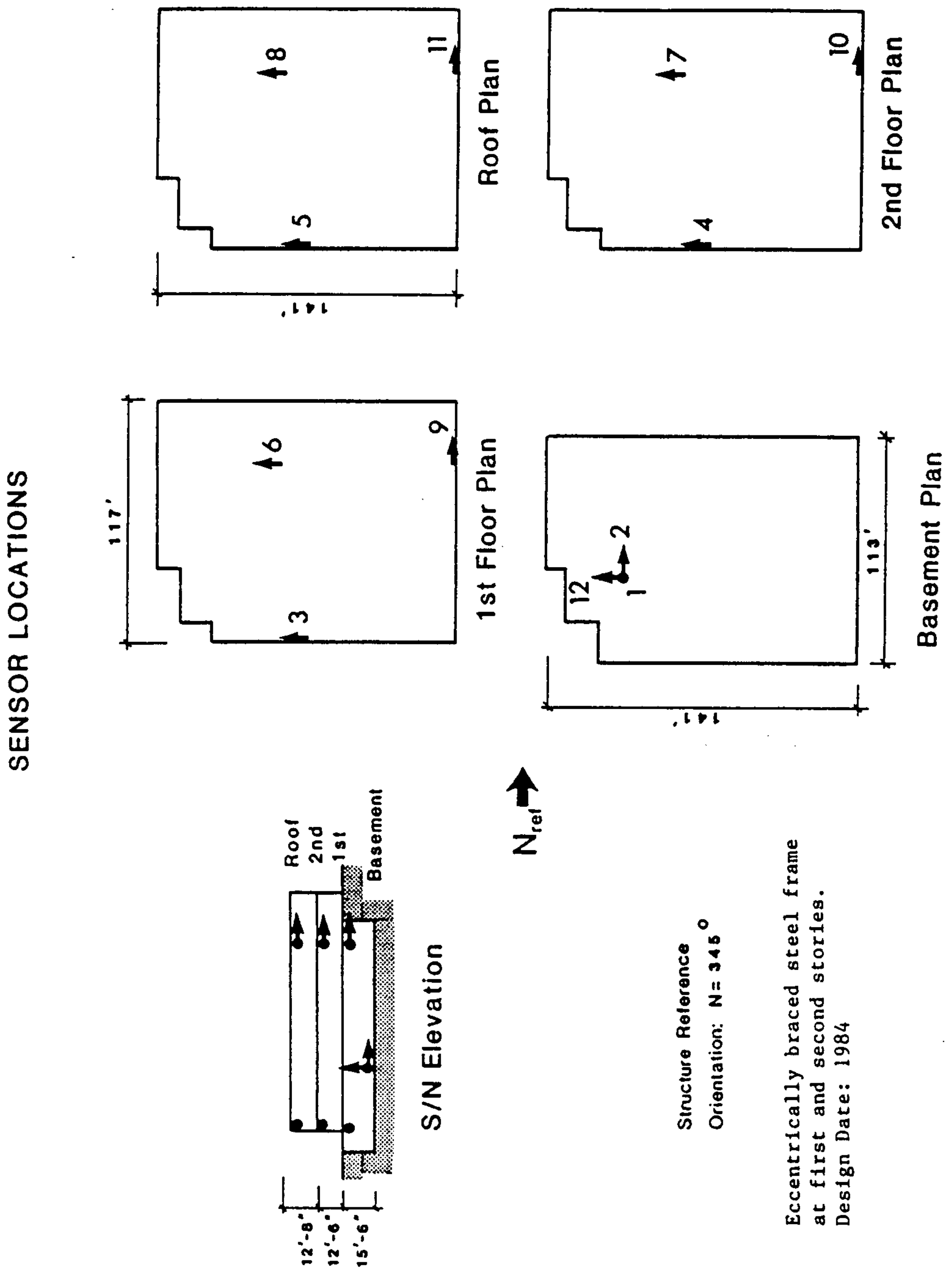

Figure 4.7 Overview of Berkeley 2-Story Hospital and Sensor layout, (After Shakal, et al., 1989)

4.8 Richmond 3-Story Office Building

Building Description:

Location: Richmond, CA

Zip Code: ---

Coordinates: 37.979 ° N, 122.329 ° W

CSMIP Station number: 58506

Earthquake record studied: Loma Prieta (1989)

Height & Number of Stories above ground: 13.4m (44.1ft), 3 stories

Plan Shape: Rectangular

Typical floor plan dimensions: N-S direction: 50.3m (165ft), E-W direction: 24.4m (80ft)

Vertical force resisting system: Steel frames with concrete slab over steel decking

Lateral force resisting system: Perimeter Moment-Resistant Steel Frames

Design/Construction date: 1984/1985

Foundation type: Concrete pile caps at each column (Precast-Prestressed piles) - Grade beams

Number of stories below ground: 0

Site Geology: Approx. 15 meter of fill

Epicentral distance: 112km South of the building

Note: The above information was obtained from "Shakal et al., 1989"

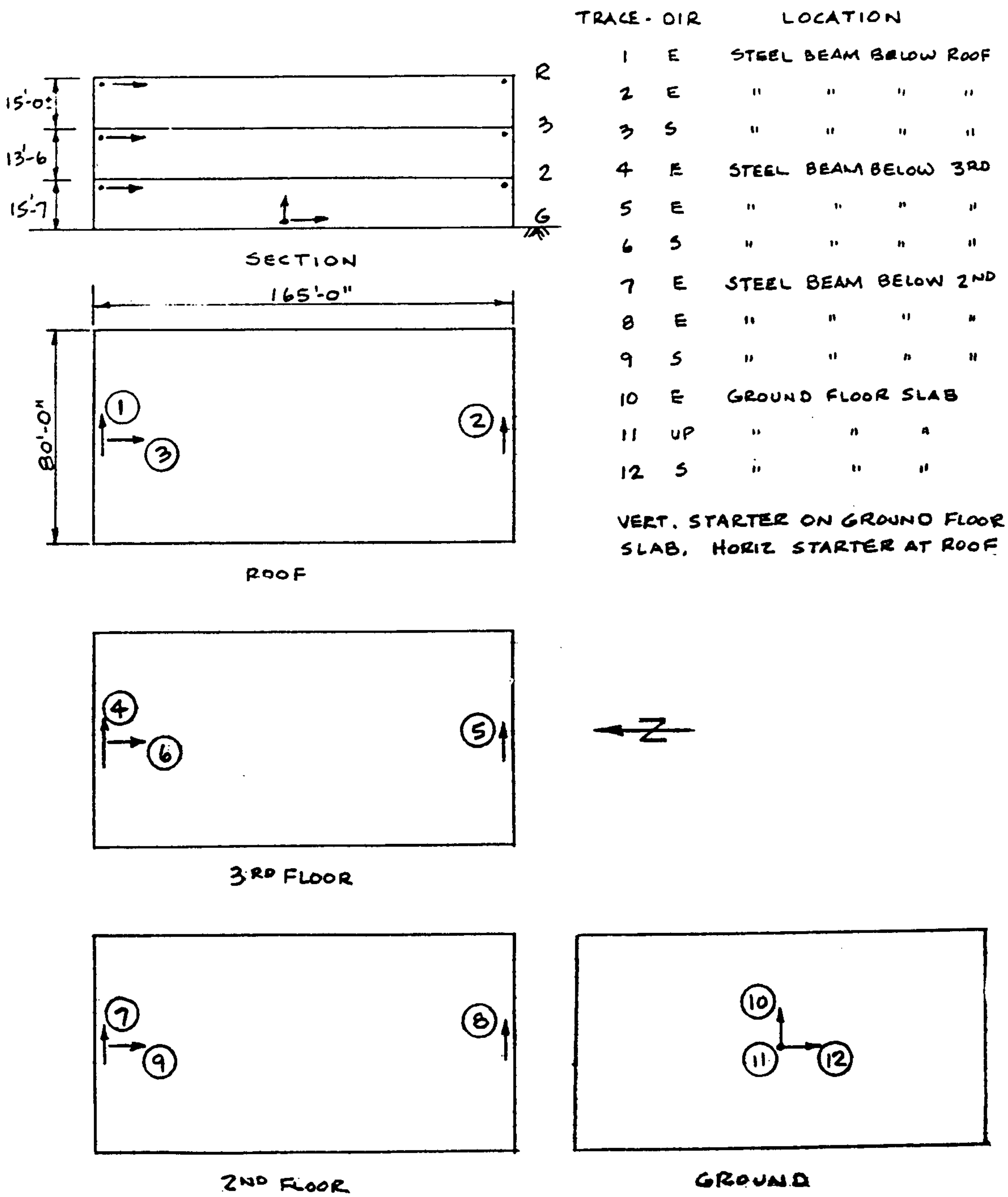

Figure 4.8 Overview of Richmond 3-Story Office Building and Sensor layout, (After Shakal, et al., 1989)

4.9 Redlands 7-Story Commercial Building

Building Description:

Location: Redlands, CA

Zip Code: ---

Coordinates: 34.056 ^{o} N, 117.178 ^{o} W

CSMIP Station number: 23481

Earthquake record studied: Landers (1992)

Height & Number of Stories above ground: 28.8m (94.4ft), 7 stories

Plan Shape: Rectangular

Typical floor plan dimensions: N-S direction: 28.3m (93ft), E-W direction: 42.7m (140ft)

Vertical force resisting system: Concrete encased Steel columns

Lateral force resisting system: Perimeter Moment-Resistant Steel Frames

Design/Construction date: 1988/---

Foundation type: ---

Number of stories below ground: 1

Site Geology: Alluvium

Epicentral distance: 72km East of the building

Note: The above information was obtained from "Shakal et al., 1992"

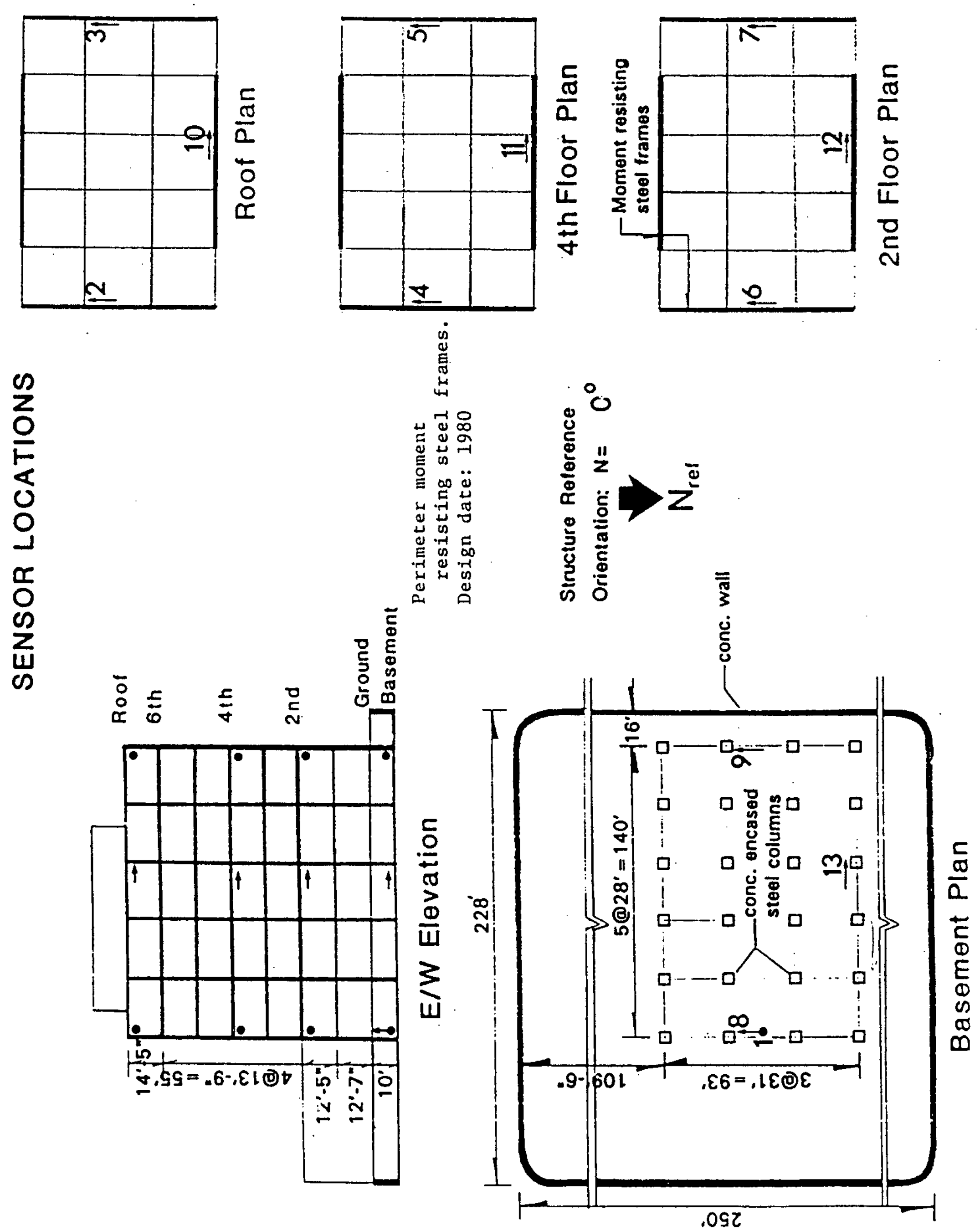

Figure 4.9 Overview of Redlands 7-Story Commercial Building and Sensor layout, (After Shakal, et al., 1992)

4.10 San Bernardino 3-Story Office Building

Building Description:

Location: San Bernardino, CA

Zip Code: ---

Coordinates: 34.056 ^{o} N, 117.289 ^{o} W

CSMIP Station number: 23516

Earthquake record studied: Landers (1992)

Height & Number of Stories above ground: 12.6m (41.3ft), 3 stories

Plan Shape: Rectangular

Typical floor plan dimensions: N-S direction: 43.9m (144ft), E-W direction: 40.2m (132ft)

Vertical force resisting system: Steel frames

Lateral force resisting system: Perimeter Moment-Resistant Steel Frames

Design/Construction date: 1983/---

Foundation type: ---

Number of stories below ground: 0

Site Geology: Deep Alluvium

Epicentral distance: 83km East of the building

Note: The above information was obtained from "Shakal et al., 1992"

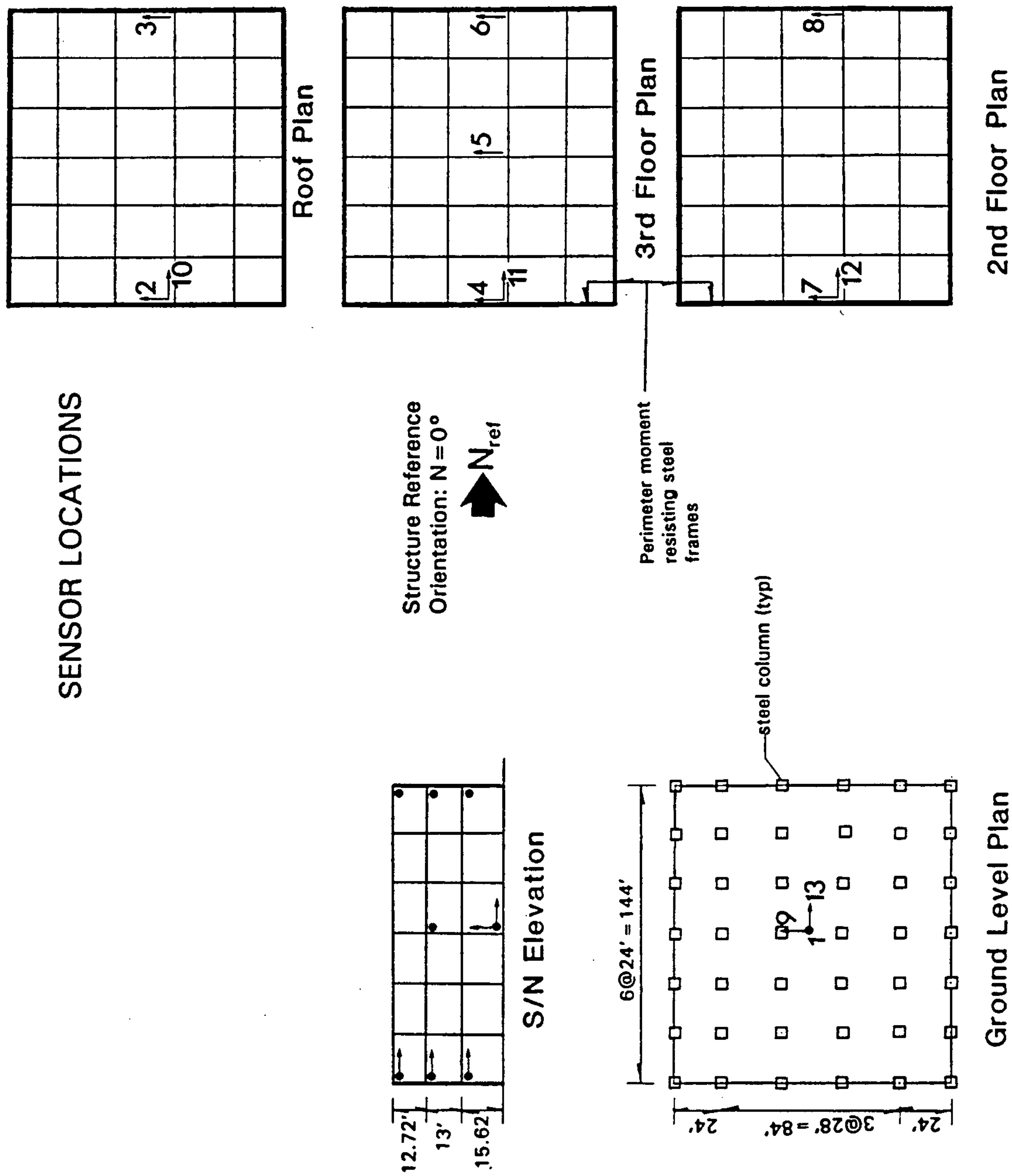

Figure 4.10 Overview of San Bernardino 3-Story Office Building and Sensor layout, (After Shakal, et al., 1992)

4.11 Los Angeles 2-Story Fire Command Control Building (Base-Isolated)

Building Description:

Location: Los Angeles, CA

Zip Code: 90063

Coordinates: 34.053 °N, 118.171 °W

CSMIP Station number: 24580

Earthquake record studied: Northridge (1994)

Height & Number of Stories above ground: 9.8m (32ft), 2 stories

Plan Shape: Rectangular

Typical floor plan dimensions: N-S direction: 57.3m (188ft), E-W direction: 25.6m (84ft)

Vertical force resisting system: Steel vented roof decking and steel decking with 3-4" concrete fill supported by steel frames and rubber bearings

Lateral force resisting system: Perimeter braced (Chevron) steel frames isolated by elastomeric bearings (under all 32 columns)

Design/Construction date: 1988/1989-90

Foundation type: Spread footings

Number of stories below ground: 0

Site Geology: Rock Sedimentary

Epicentral distance: 38km North-West of the building

Note: The above information was obtained from "Shakal et al., 1994"

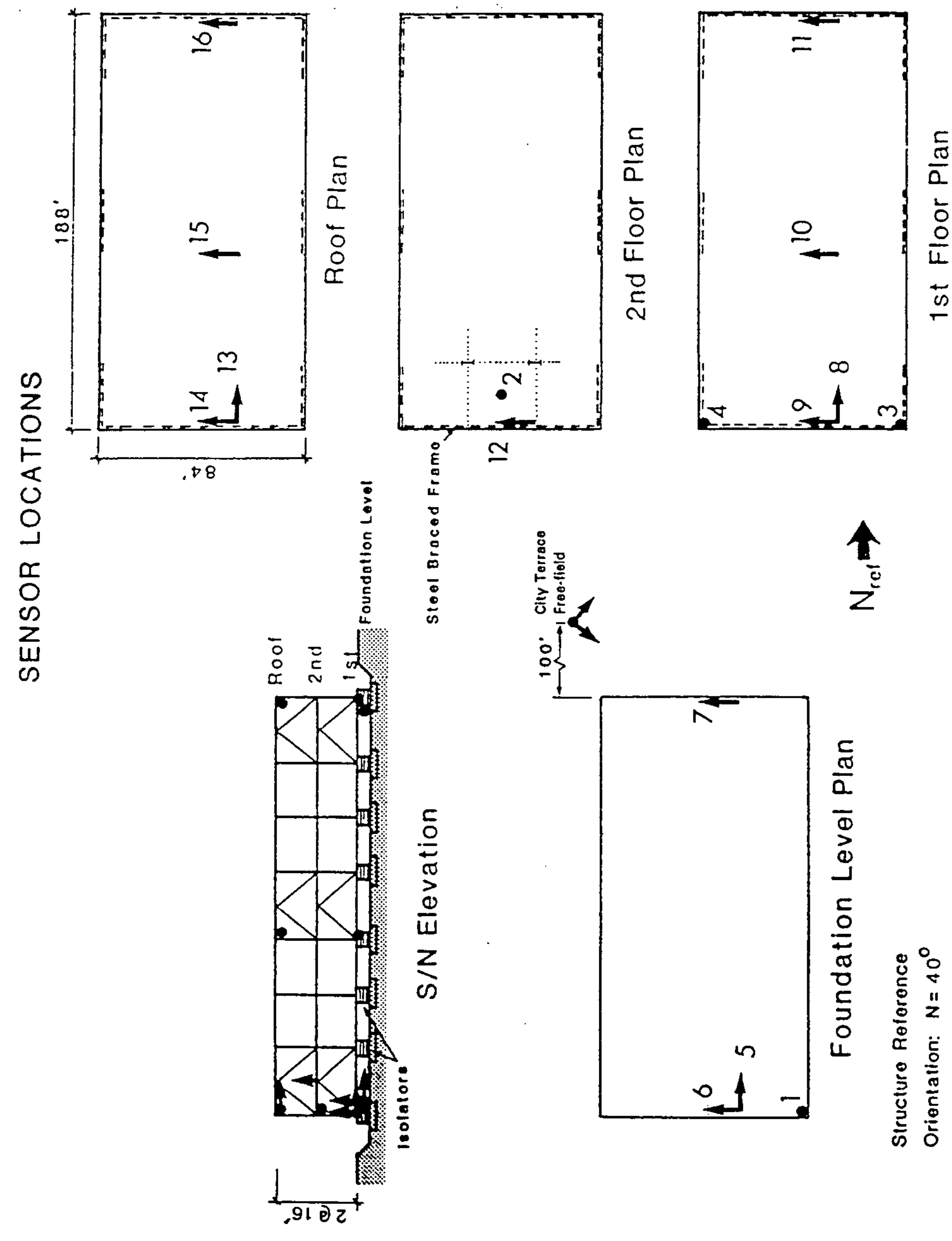

Figure 4.11 Overview of LA 2-Story Fire Control Building and Sensor layout, (After Shakal, et al., 1994)

4.12 Los Angeles 7-Story University Hospital (Base-Isolated)

Building Description:

Location: Los Angeles, CA

Zip Code: 90033

Coordinates: 34.062 ° N, 118.198 ° W

CSMIP Station number: 24605

Earthquake record studied: Northridge (1994)

Height & Number of Stories above ground: 31.1m (102ft), 7 stories

Height & Number of Stories above isolated base: 35.7m (117ft), 8stories

Plan Shape: S-shape

Typical floor plan dimensions: N-S direction: 92.4m (303ft), E-W direction: 77.1m (253ft)

Vertical force resisting system: Concrete slabs over steel deck supported by steel frames and rubber isolators

Lateral force resisting system: Diagonally braced perimeter steel frames isolated by lead-rubber and elastomeric isolators

Design/Construction date: 1988/1989-91

Foundation type: Continuous Spread footings under perimeter isolators and spread footings under interior isolators

Site Geology: Rock Sedimentary

Epicentral distance: 36km North-West of the building

Note: The above information was obtained from "Shakal et al., 1994"

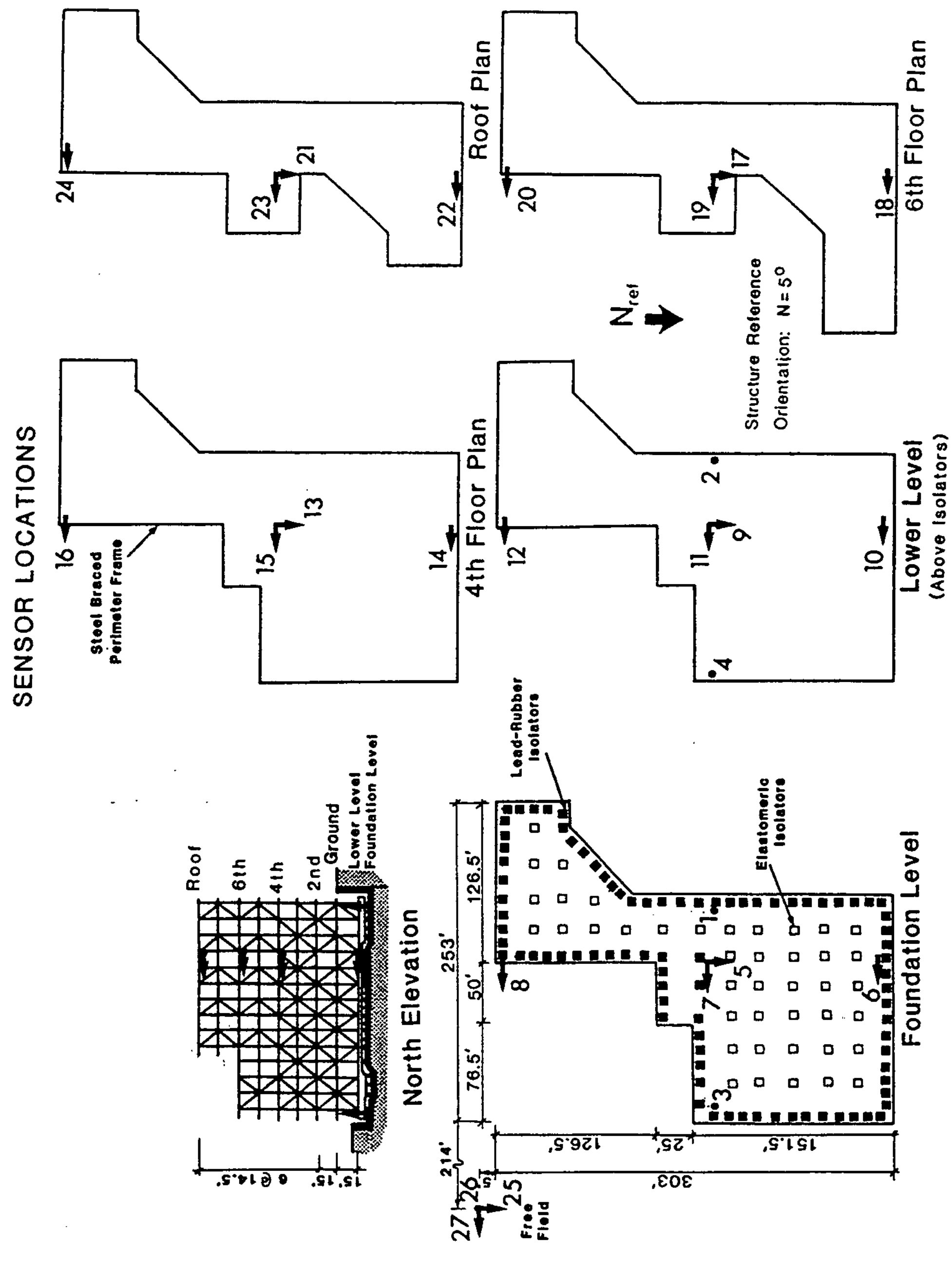

Figure 4.12 Overview of LA 7-Story University Hospital and Sensor layout, (After Shakal, et al., 1994)

Chapter 5 DETAILED STUDY OF THE RECORDED RESPONSE OF THE BUILDINGS

5.1 General

The information obtained by processing the strong motion data recorded at each of the buildings is presented by a series of graphs and tables in Sections 5.2 to 5.11 of this chapter. These results will be discussed in Chapter 6.

Sections 5.2 to 5.11 include the following:

1. Time-history of the accelerations recorded at the base of the buildings, which show the magnitude and the duration of the ground motions.
2. Pseudo acceleration response spectra of the ground motions, which show the expected level of seismically induced loads on the buildings, given their natural periods.
3. Relative displacement response spectra, which indicate the expected level of displacements in the buildings.
4. The Fourier spectra of the ground motion time histories are presented in a normalized form to show the frequency content of the ground vibrations.
5. The response of the buildings to the ground motions are presented as time-histories of absolute accelerations and relative displacements of the upper floors.
6. Rotational motions are computed as half the difference between the translations (or accelerations) of the two ends of each building. The summation of the translation at the center of the building and the rotation (as presented in this report) will result in the measured translation at the end of the building. The calculation of the rotational motions presented in the figures

is explained for each building in the beginning of the sections 5.2 to 5.12. The rotational data presented in the figures have the same units as the translational data.

7. Plots of orthogonal (X vs. Y) displacements (floor orbital motion) show the magnitude and direction of the displacements at the center of each floor.
8. Plots of absolute accelerations vs. relative displacements represent an estimate of the hysteretic behaviour of the buildings.
9. Frequency response functions of the recorded accelerations show a measure of the acceleration amplification vs. frequency. These plots are used to determine the natural frequencies as explained in Chapter 3. The better distinguished and more relevant peaks on the FRF plots provide a higher level of accuracy in the estimation of the natural frequencies.
10. Spectral Response Functions are used to verify the results obtained from FRF's.
11. Tables of acceleration amplification factors associated with the potential modes are used to compare the amplification factors of the various modes. These values provide information that is similar to the modal participation factors in dynamic analysis. Note that in some cases two frequencies were associated with a single potential mode where there were two very close peaks on a FRF, or the peaks of the FRF's of two different floors corresponding the same potential mode did not occur at the same frequency. These cases represent a limitation of the accuracy of the system identification method.
12. The value of the Spectral Response Functions are presented for comparison with those of the FRF's.

5.2 Burbank 6-Story Office Building

5.2a Whittier Earthquake Records

Properties of the Strong Motion Data

Record Length: 40 sec

Time interval: 0.02 sec

No. of data points for each channel: 2000

Usable frequency range: 0.5 Hz to 23.0 Hz

Assuming a rigid diaphragm at each floor, the accelerations, velocities and displacements at the center of the building in three directions, E-W (or X-directions), N-S (or Y-directions) and rotation about vertical axis (or R-component) at levels 1, 2, 3 and 7 (roof) were obtained by manipulating the recorded data of channels 1 to 13 as follows:

1X = (Chan9 + Chan8)/2 , 1Y = -Chan13 + (Chan9-Chan8)/2 , 1R = (Chan9-Chan8)/2

2X = (Chan7 + Chan6)/2 , 2Y = -Chan12 + (Chan7-Chan6)/2 , 2R = (Chan7-Chan6)/2

3X = (Chan5 + Chan4)/2 , 3Y = -Chan11 + (Chan5-Chan4)/2 , 3R = (Chan5-Chan4)/2

7X = (Chan3 + Chan2)/2 , 7Y = -Chan10 + (Chan3-Chan2)/2 , 7R = (Chan3-Chan2)/2

A similar procedure was used to infer data for the corners of the buildings (assuming that diaphragms are rigid and the displacements are small). These data were used to animate a 3-D representation of the buildings in order to evaluate the mode shapes.

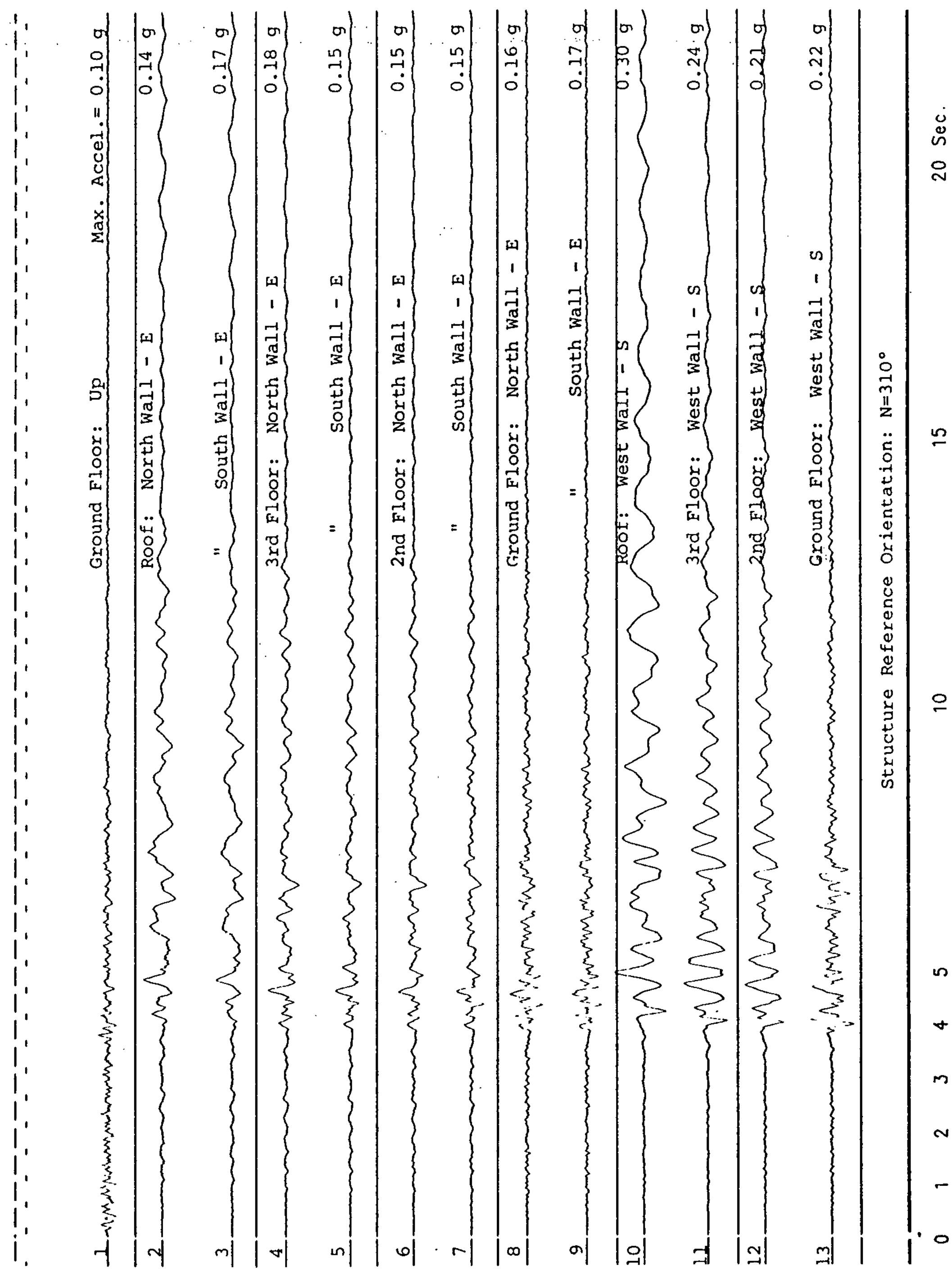

Figure 5.2a.1 Accelerations recorded at the Burbank 6-story bldg., during the 1987 Whittier Earthquake (After Shakal, et al., 1987)

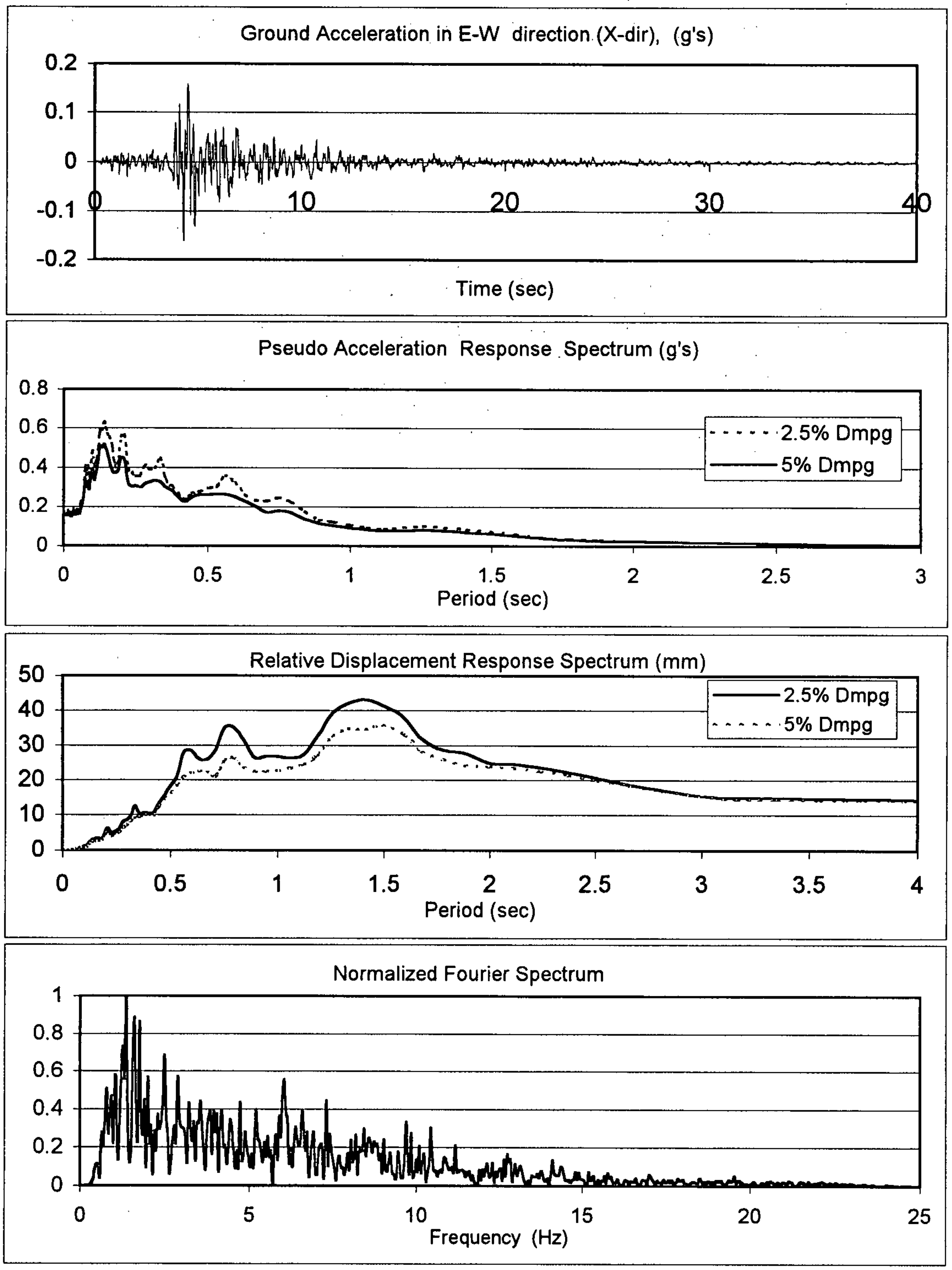

Figure 5.2a.2 Time-history and spectral characteristics of E-W (X) component of the ground motion recorded at the Burbank 6-story bldg., during the 1978 Whittier EQ.

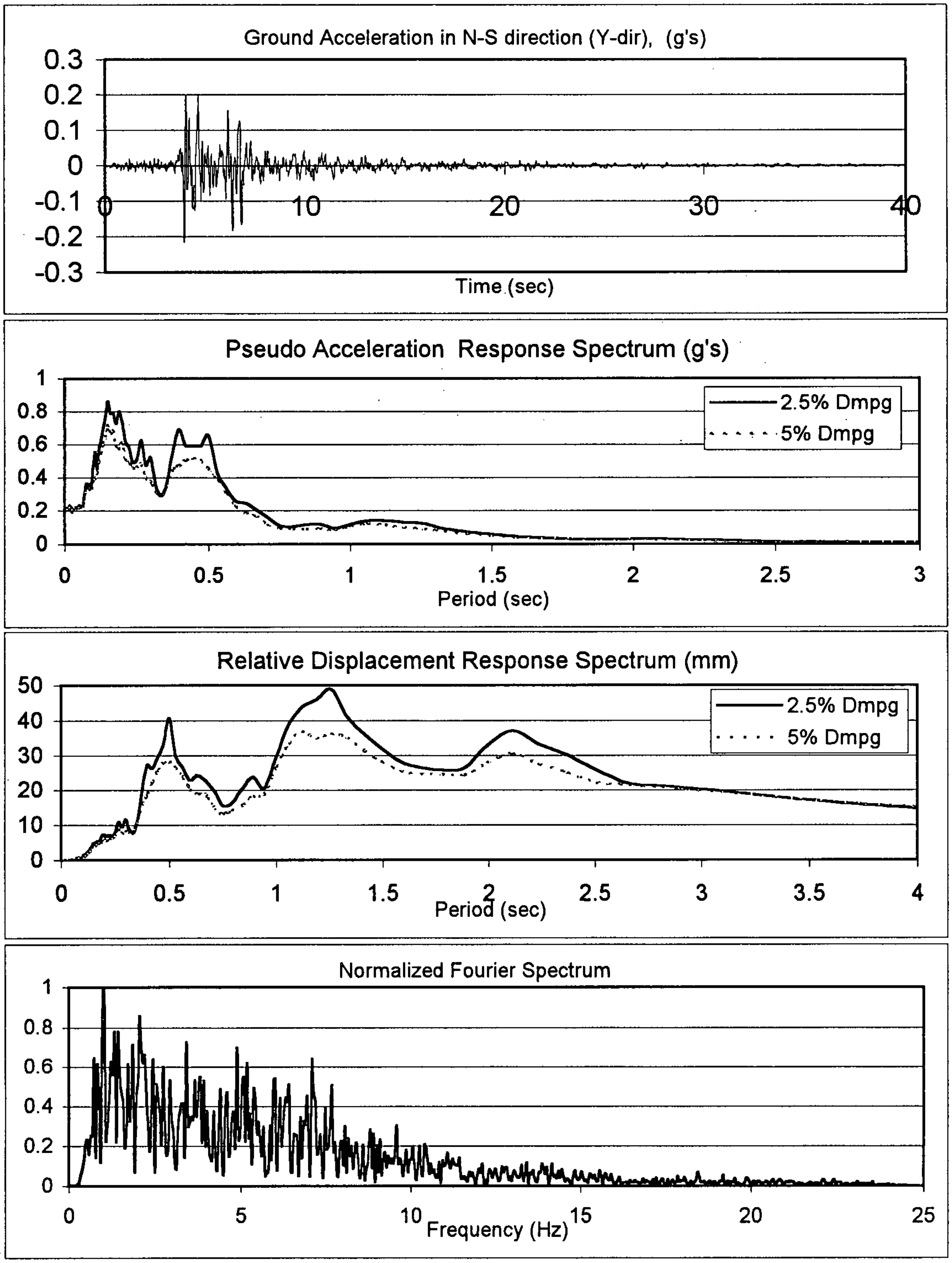

Figure 5.2a.3 Time-history and spectral characteristics of N-S (Y) component of the ground motion recorded at the Burbank 6-story bldg., during the 1978 Whittier EQ.

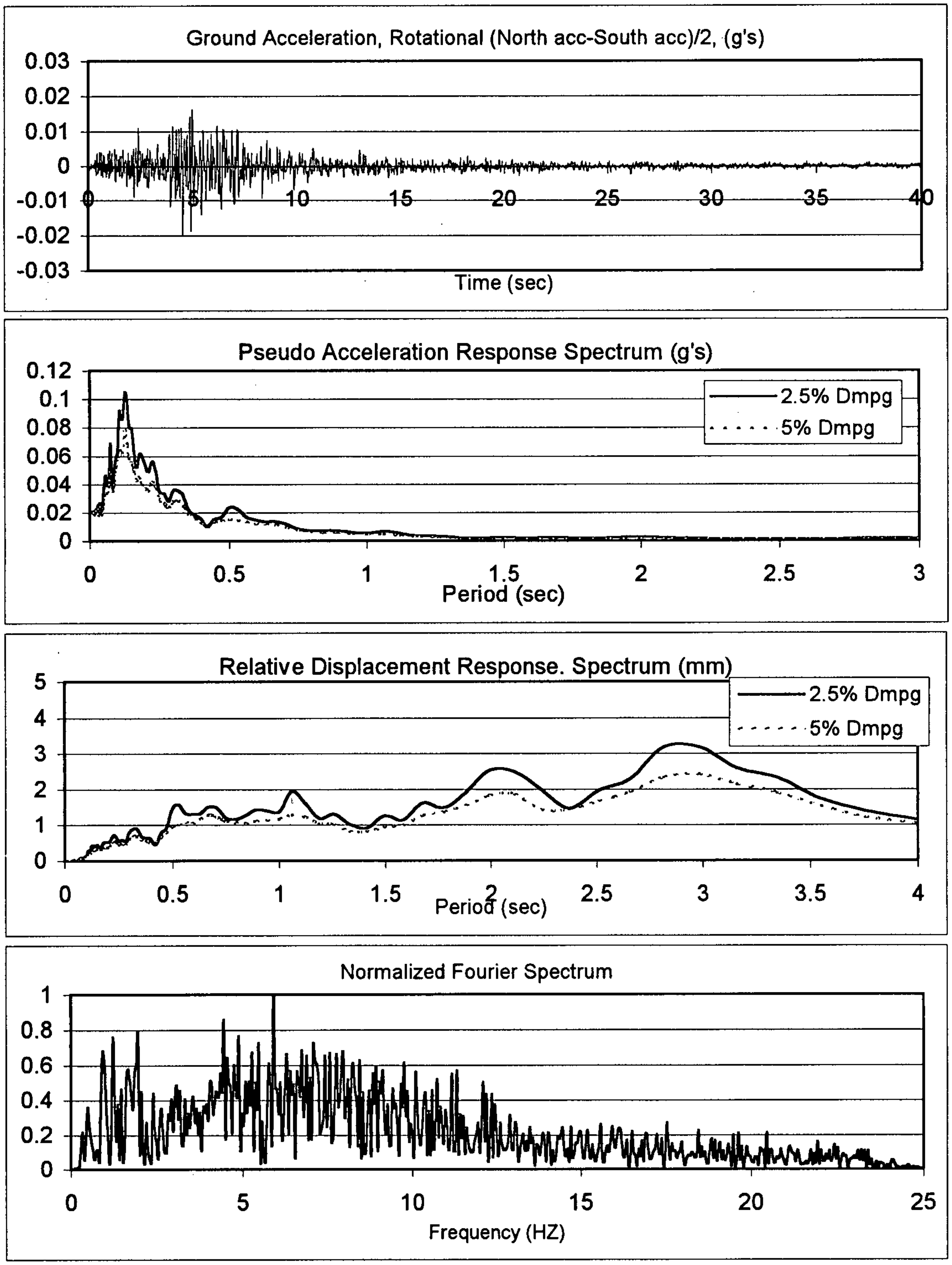

Figure 5.2a.4 Time-history and spectral characteristics of rotational (R) component of the ground motion recorded at the Burbank 6-story bldg., during the 1978 Whittier EQ.

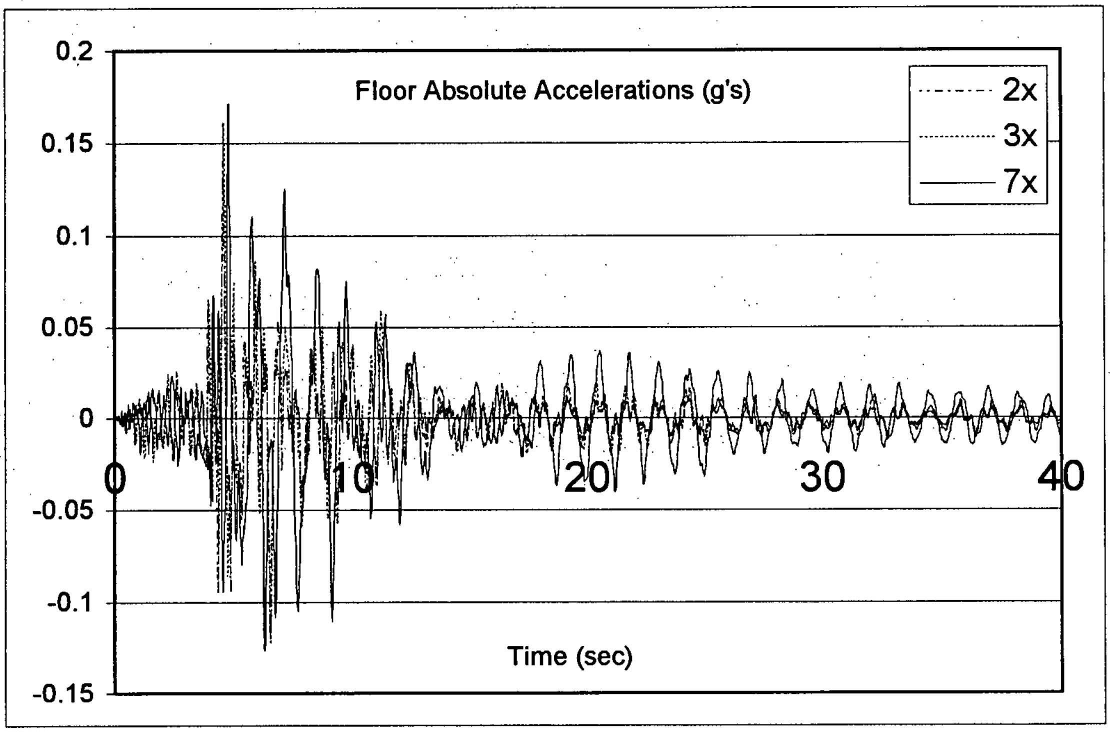

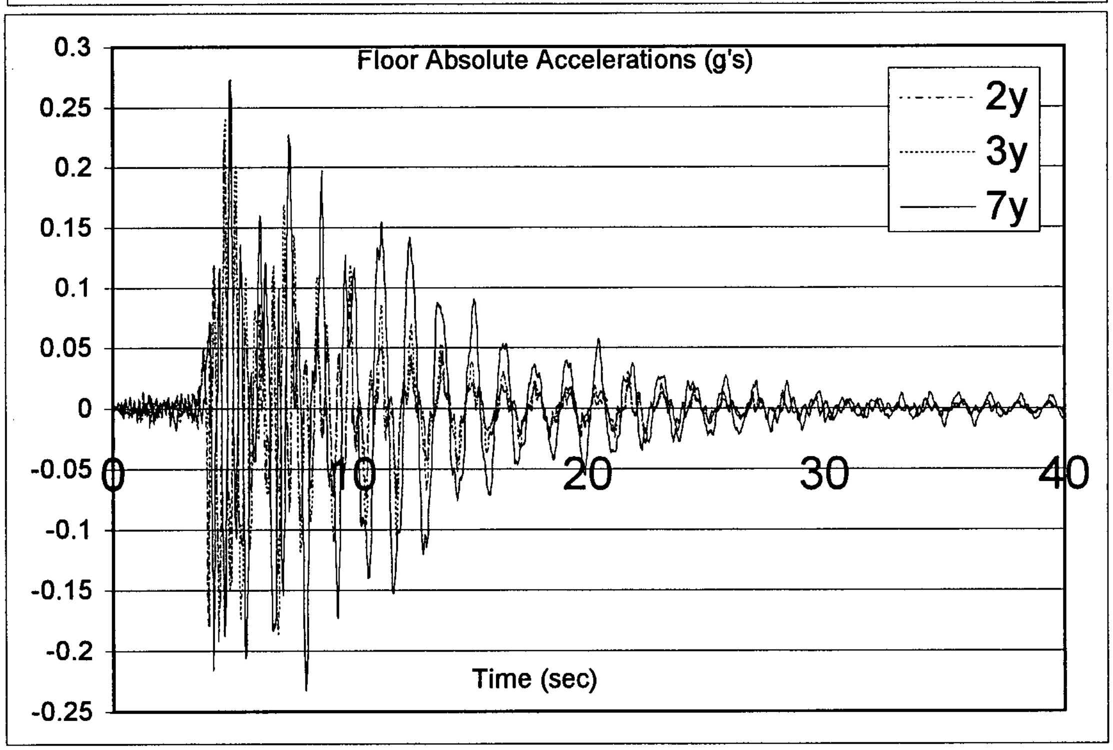

Figure 5.2a.5 E-W (X-direction) & N-S (Y-direction) absolute accelerations of the instrumented upper floors of the Burbank 6-story bldg., during the 1987 Whittier EQ.

Note: See Appendix A for individual plots of the absolute accelerations.

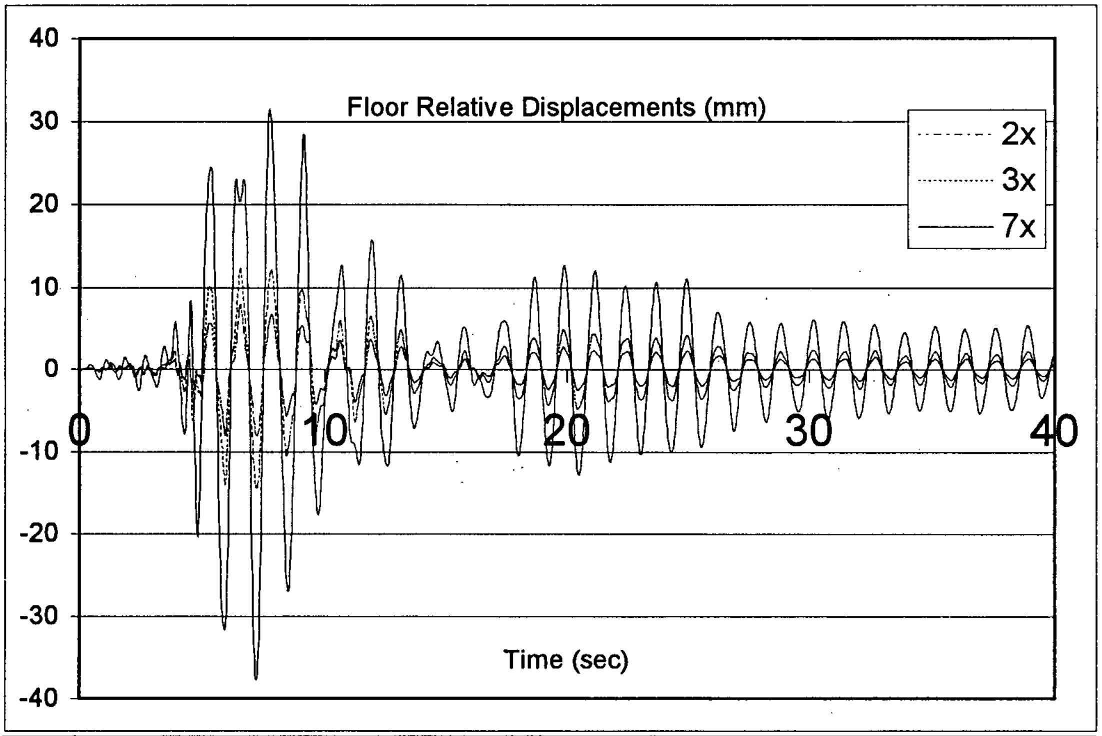

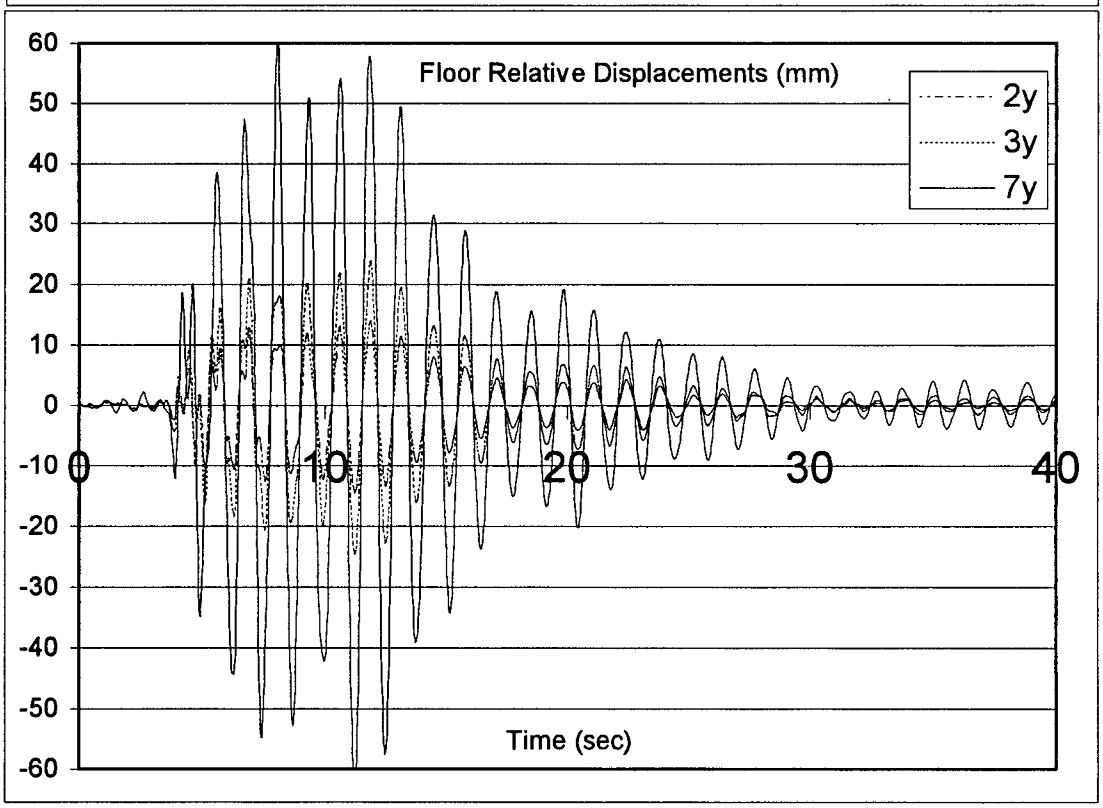

Figure 5.2a.6 E-W (X-direction) & N-S (Y-direction) relative displacements of the instrumented upper floors of the Burbank 6-story bldg., during the 1987 Whittier EQ.

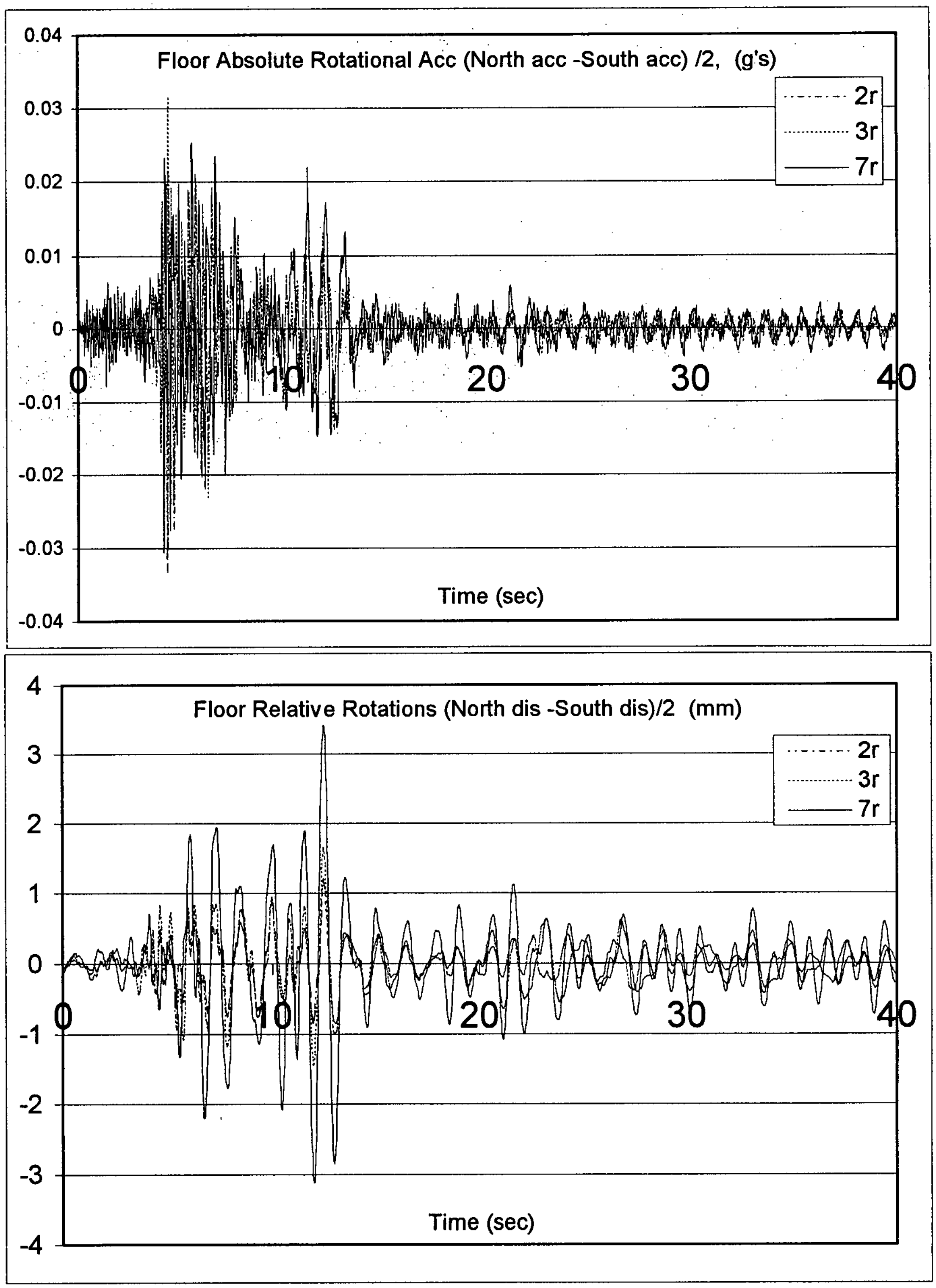

Figure 5.2a.7 Torsional response of the instrumented upper floors of the Burbank 6-story bldg., during 1987 Whittier EQ. (See section 5.1 for explanation on obtaining the rotational data.)

Absolute Displ. **Relative Displ.**

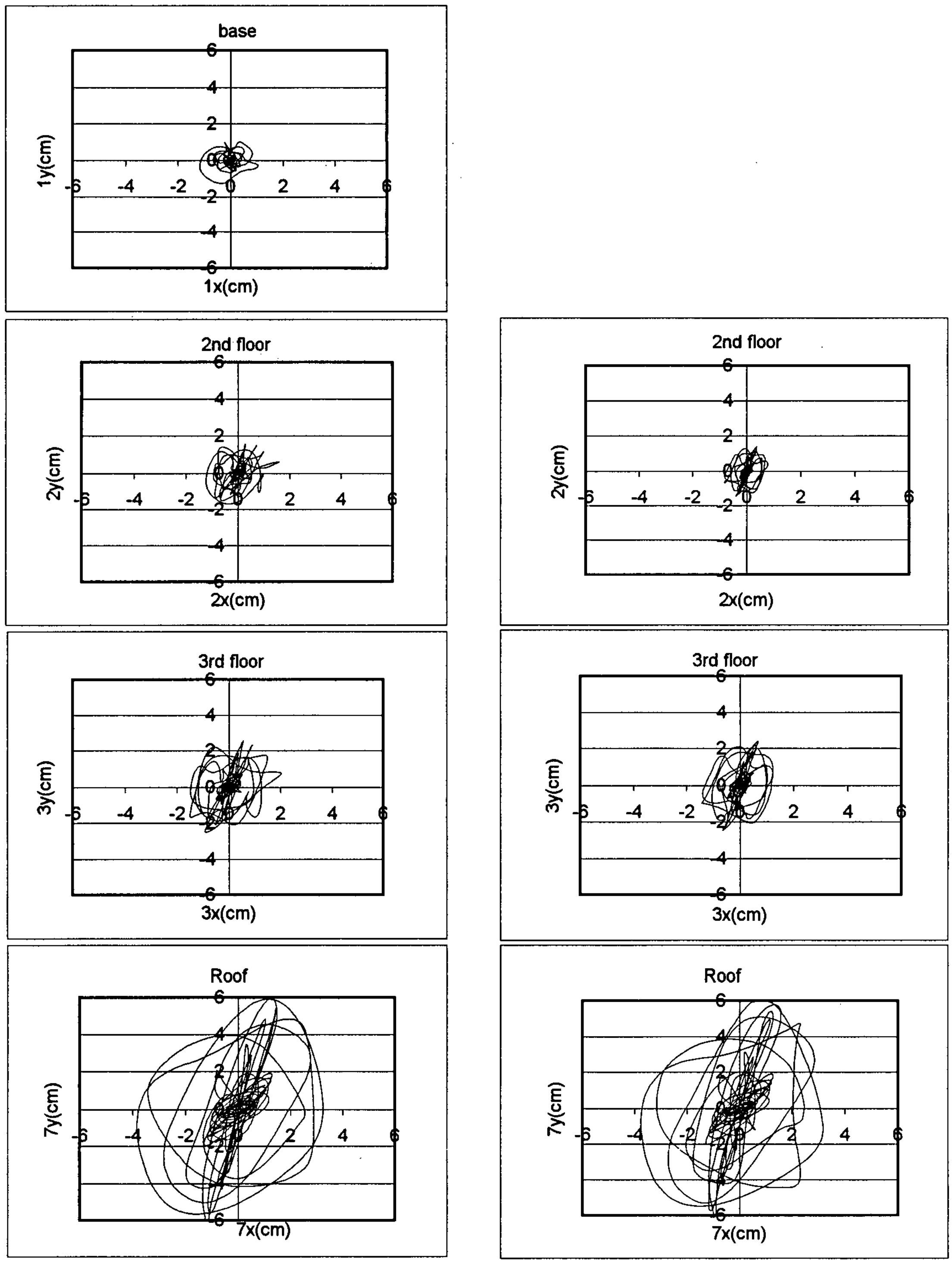

Figure 5.2a.8 Orbital displacements at the center of the instrumented floors of the Burbank 6-story bldg., during the 1987 Whittier EQ.

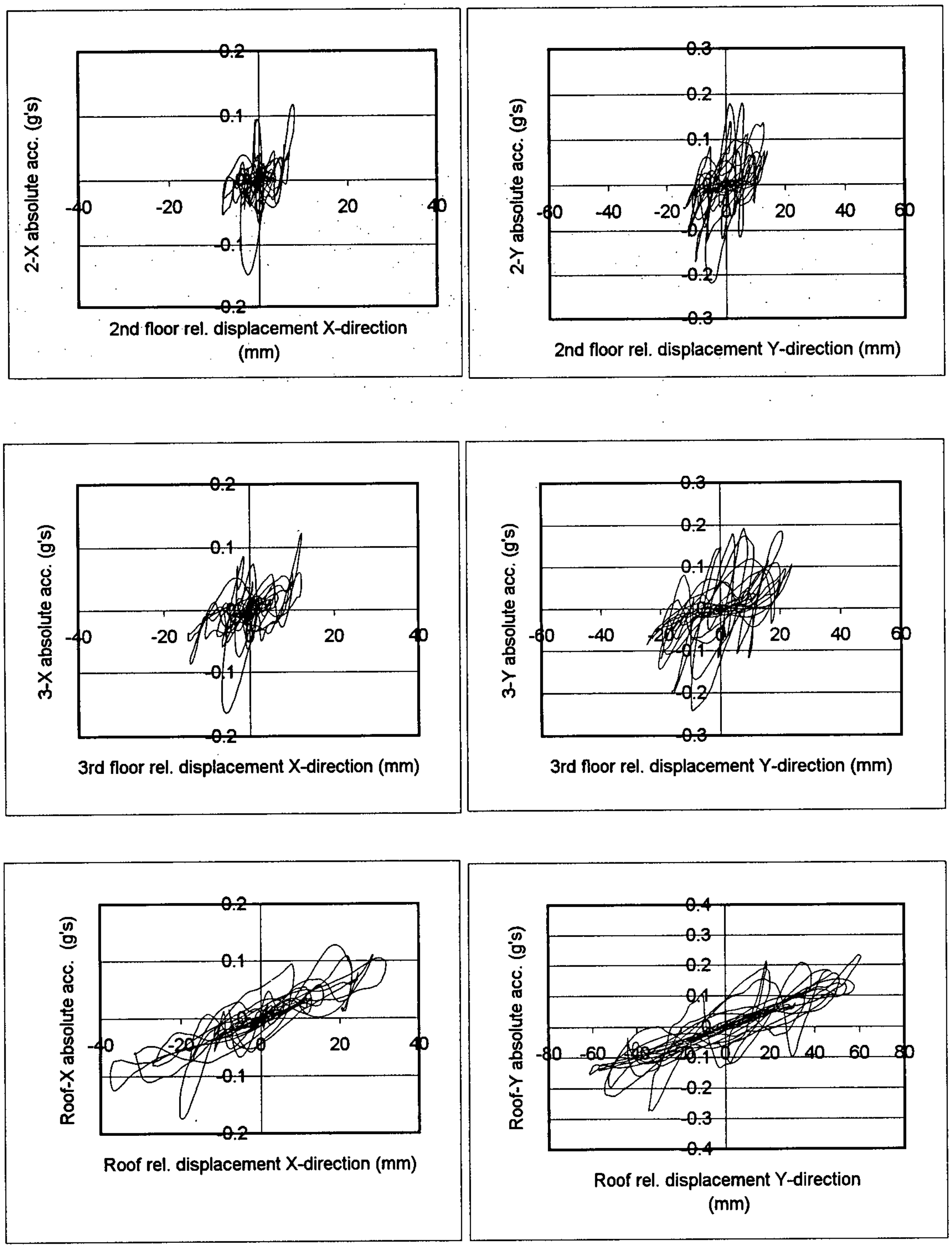

Figure 5.2a.9 Representation of Hysteretic behaviour at the instrumented floors of the Burbank 6-story bldg., during the 1987 Whittier EQ.

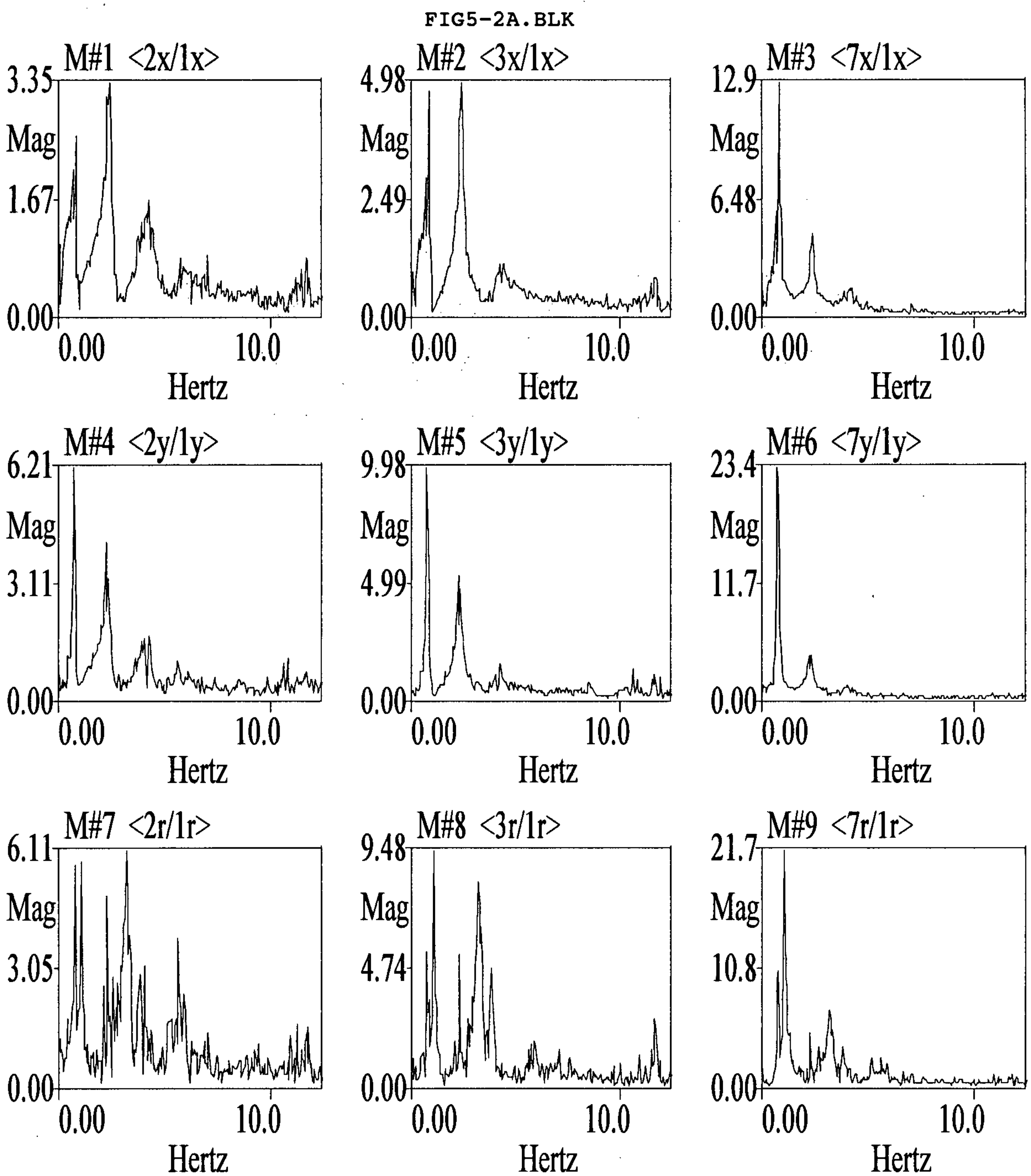

Figure 5.2a.10 Frequency Response Functions of the instrumented floors of the Burbank 6-Story Bldg., obtained from the 1987 Whittier EQ records.

Note: The FRF's are computed by ME'scope using a Hanning window, a block size N=1024, 10 averages and 89% segment overlap.

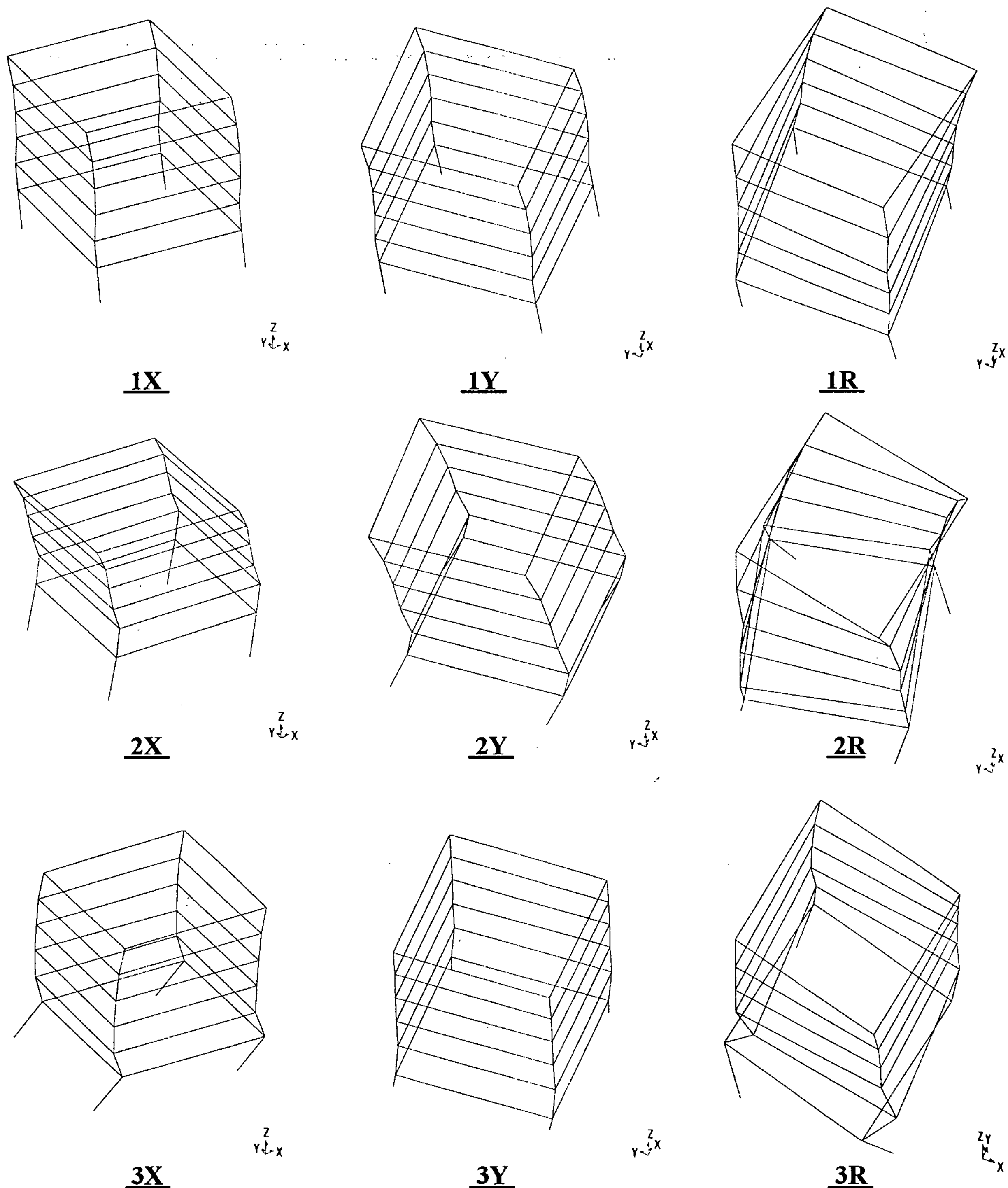

Figure 5.2a.11 Mode shapes of the Burbank 6-story bldg., obtained from the 1987 Whittier EQ records.

Note: The displacements of levels 2,3 and 7 (roof) are obtained from measured data. Displacements of the other floors are based on ME'scope's interpolation algorithm.

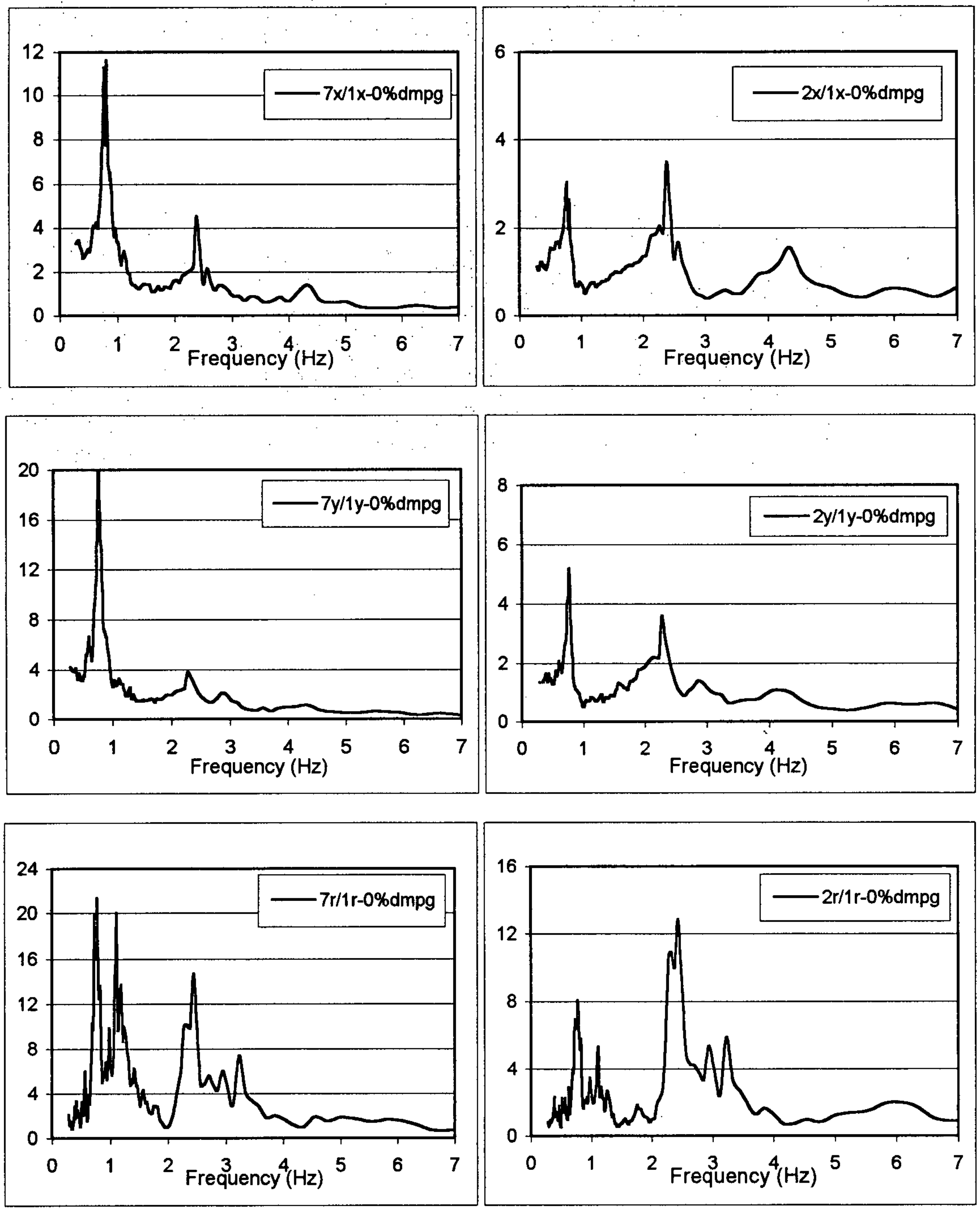

Figure 5.2a.12 Spectral Response Functions of the Burbank 6-story bldg., obtained from the 1987 Whittier EQ records.

Table 5.2a.1 Results of Frequency Response Functions for the Burbank 6-story bldg., obtained from the 1987 Whittier EQ records.

X-direction				
Potential Mode #	Frequency (Hz)	Amplification Factor (2X/1X)	Amplification Factor (3X/1X)	Amplification Factor (7X/1X)
1	0.82	2.58	4.80	13.0
2a	2.34	3.03	4.27	3.81
2b	2.39	3.35	4.99	4.58
3	4.25	1.67	1.13	1.60
Damping Ratio estimated by ME'scope for mode 1X: **4.54%**				
Y-direction				
Potential Mode #	Frequency (Hz)	Amplification Factor (2Y/1Y)	Amplification Factor (3Y/1Y)	Amplification Factor (7Y/1Y)
1a	0.73	6.22	9.99	23.4
1b	0.78	4.19	7.83	22.2
2a	2.25	4.20	5.31	4.43
2b	2.29	2.38	3.19	3.11
3a	4.05	1.66	0.94	1.42
3b	4.25	1.72	1.51	1.06
Damping Ratio estimated by ME'scope for mode 1Y: **3.00%**				
R-direction				
Potential Mode #	Frequency (Hz)	Amplification Factor (2R/1R)	Amplification Factor (3R/1R)	Amplification Factor (7R/1R)
1	1.08	5.80	9.49	21.8
2	3.17	6.11	8.29	7.08
3a	5.62	3.85	1.48	2.68
3b	5.91	1.95	1.55	1.51
Damping Ratio estimated by ME'scope for mode 1R: **1.66%**				

Table 5.2a.2 Results of Spectral Response Functions for the Burbank 6-story bldg., obtained from the 1987 Whittier EQ records.

X-direction				
Potential Mode #	Frequency (Hz)	SRF 0% damping (2X/1X)	SRF 0% damping (3X/1X)	SRF 0% damping (7X/1X)
1a	0.77	3.05	4.83	11.3
1b	0.80	2.65	4.52	11.6
2	2.38	3.50	5.08	4.51
3	4.35	1.55	1.12	1.40
Y-direction				
Potential Mode #	Frequency (Hz)	SRF 0% damping (2Y/1Y)	SRF 0% damping (3Y/1Y)	SRF 0% damping (7Y/1Y)
1	0.77	5.17	8.45	21.4
2	2.27	3.56	4.64	3.78
3a	4.17	1.08	0.96	1.01
3b	4.35	0.99	0.91	1.14
R-direction				
Potential Mode #	Frequency (Hz)	SRF 0% damping (2R/1R)	SRF 0% damping (3R/1R)	SRF 0% damping (7R/1R)
1	1.11	5.33	8.70	20.0
2	3.23	5.88	8.71	7.44
3a	5.88	1.98	1.56	1.66
3b	6.25	1.86	1.59	1.32

Burbank 6-Story Office Building

5.2b Northridge Earthquake Records

Properties of the Strong Motion Data

Record Length: 60 sec

Time interval: 0.02 sec

No. of data points for each channel: 3000

Usable frequency range: 0.2 Hz to 23.0 Hz

Manipulating the data to obtain the motion of the center of the building in the 3 directions, E-W (or X-directions) , N-S (or Y-directions) and rotation about vertical axis (or R-component) :

1X = (Chan9 + Chan8)/2 , 1Y = -Chan13 + (Chan9-Chan8)/2 , 1R = (Chan9-Chan8)/2

2X = (Chan7 + Chan6)/2 , 2Y = -Chan12 + (Chan7-Chan6)/2 , 2R = (Chan7-Chan6)/2

7X = (Chan3 + Chan2)/2 , 7Y = -Chan10 + (Chan3-Chan2)/2 , 7R = (Chan3-Chan2)/2

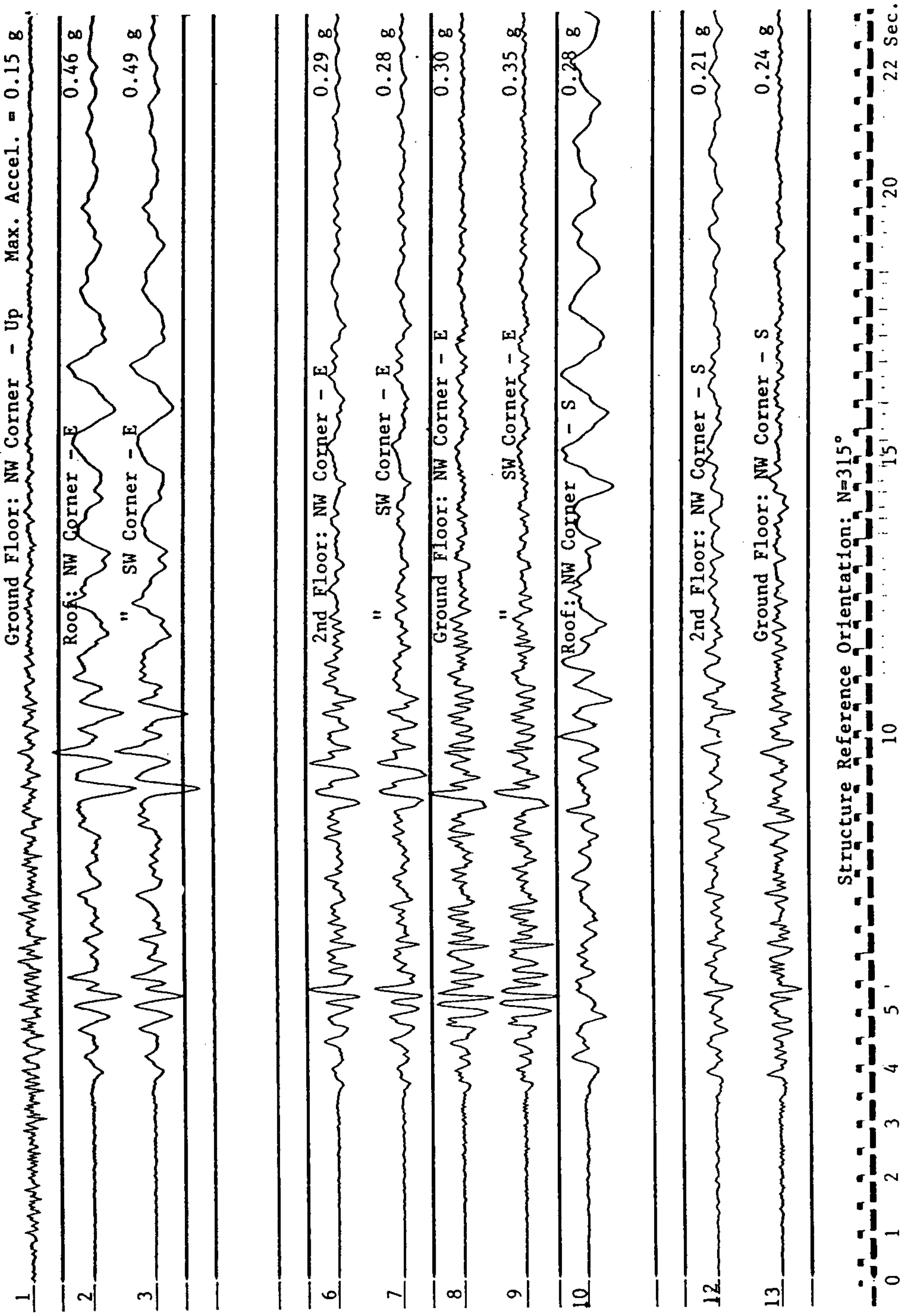

Figure 5.2b.1 Accelerations recorded at the Burbank 6-story bldg., during the 1994 Northridge EQ. (After Shakal, et al., 1994)

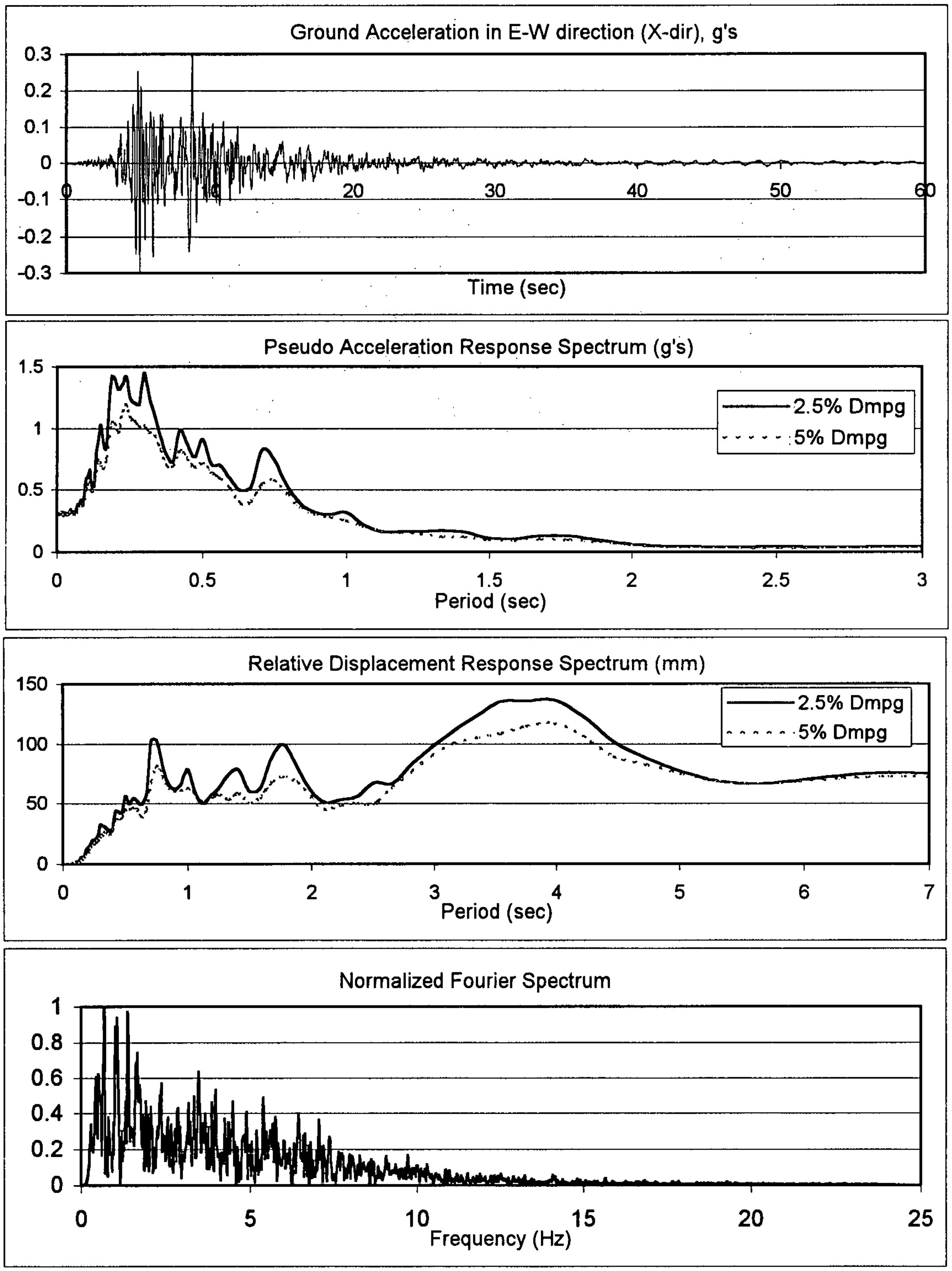

Figure 5.2b.2 Time-history and spectral characteristics of E-W (X) component of the ground motion recorded at the Burbank 6-story bldg., during the 1994 Northridge EQ.

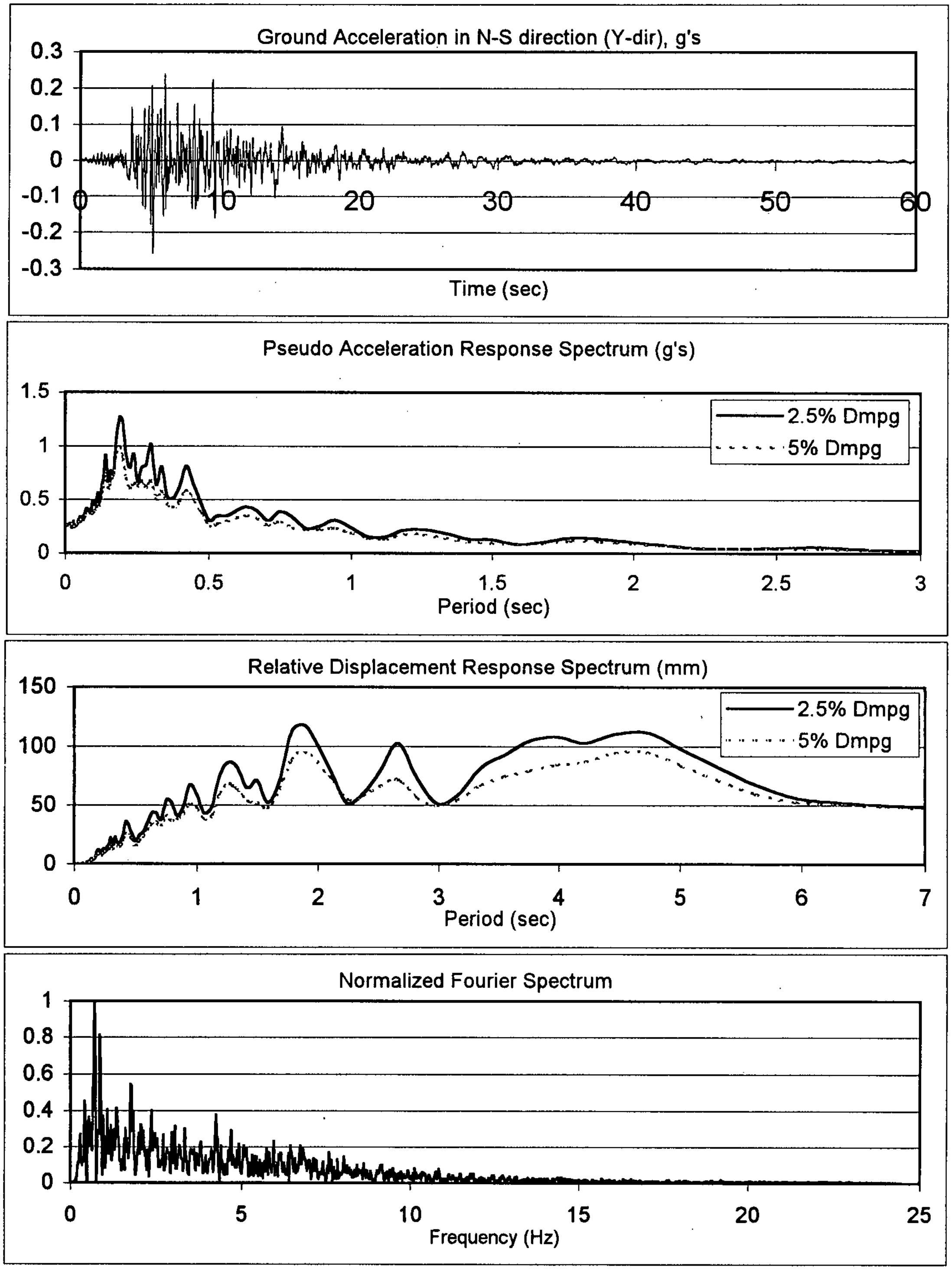

Figure 5.2b.3 Time-history and spectral characteristics of N-S (Y) component of the ground motion recorded at the Burbank 6-story bldg., during the 1994 Northridge EQ.

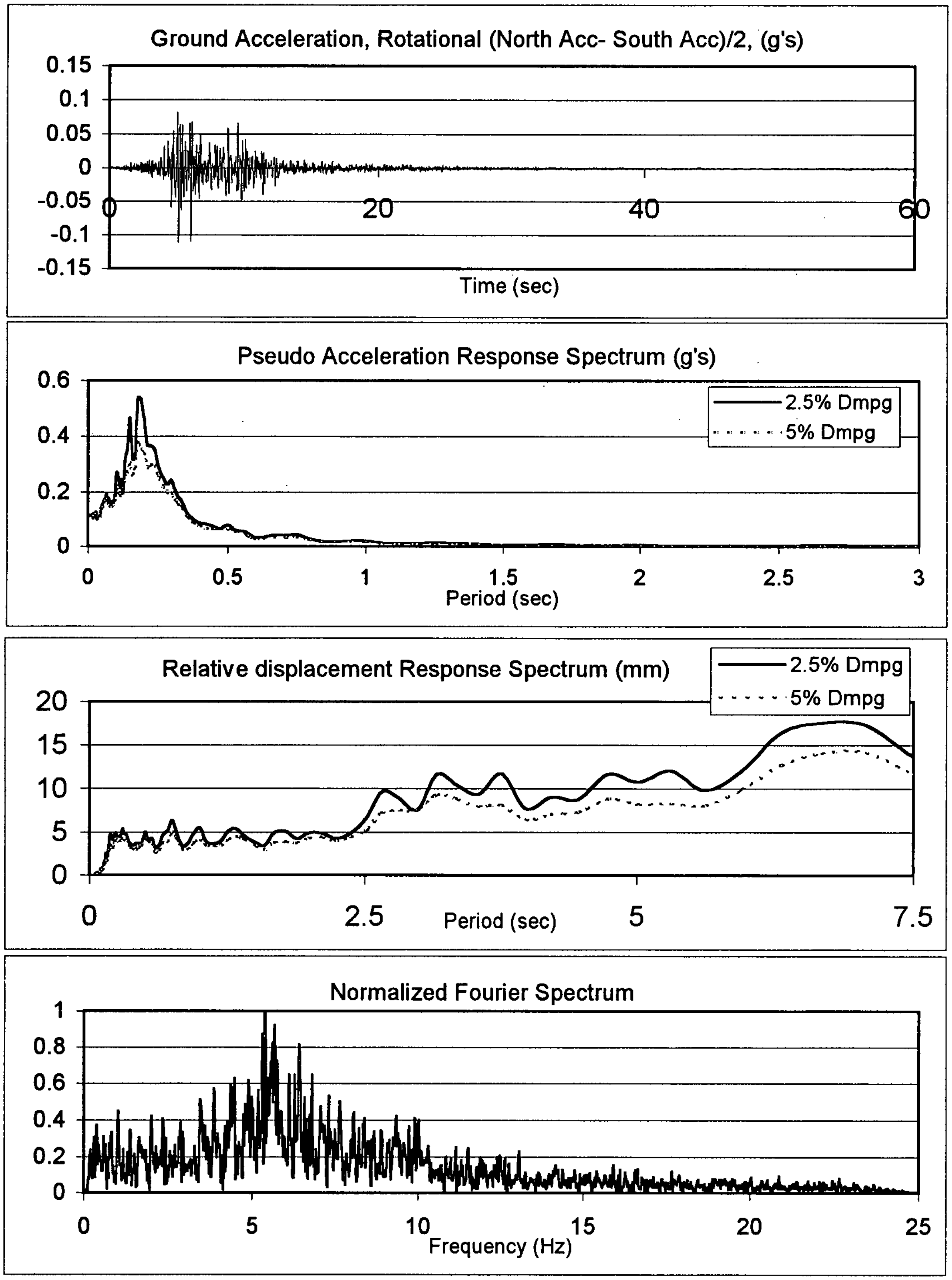

Figure 5.2b.4 Time-history and spectral characteristics of rotational (R) component of the ground motion recorded at the Burbank 6-story bldg., during the 1994 Northridge EQ.

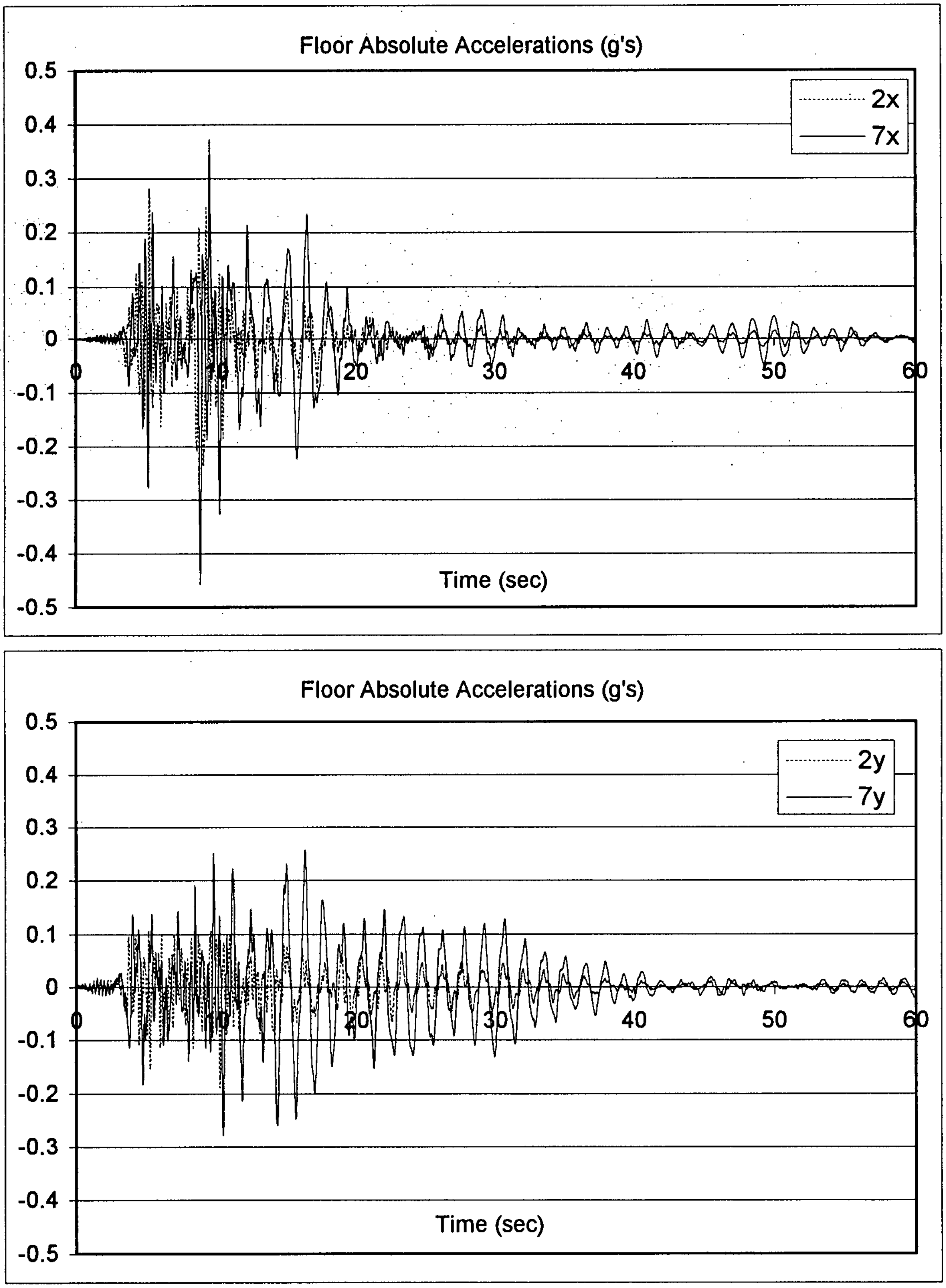

Figure 5.2b.5 E-W (X-direction) & N-S (Y-direction) absolute accelerations of the instrumented upper floors of the Burbank 6-story bldg., during the 1994 Northridge EQ.

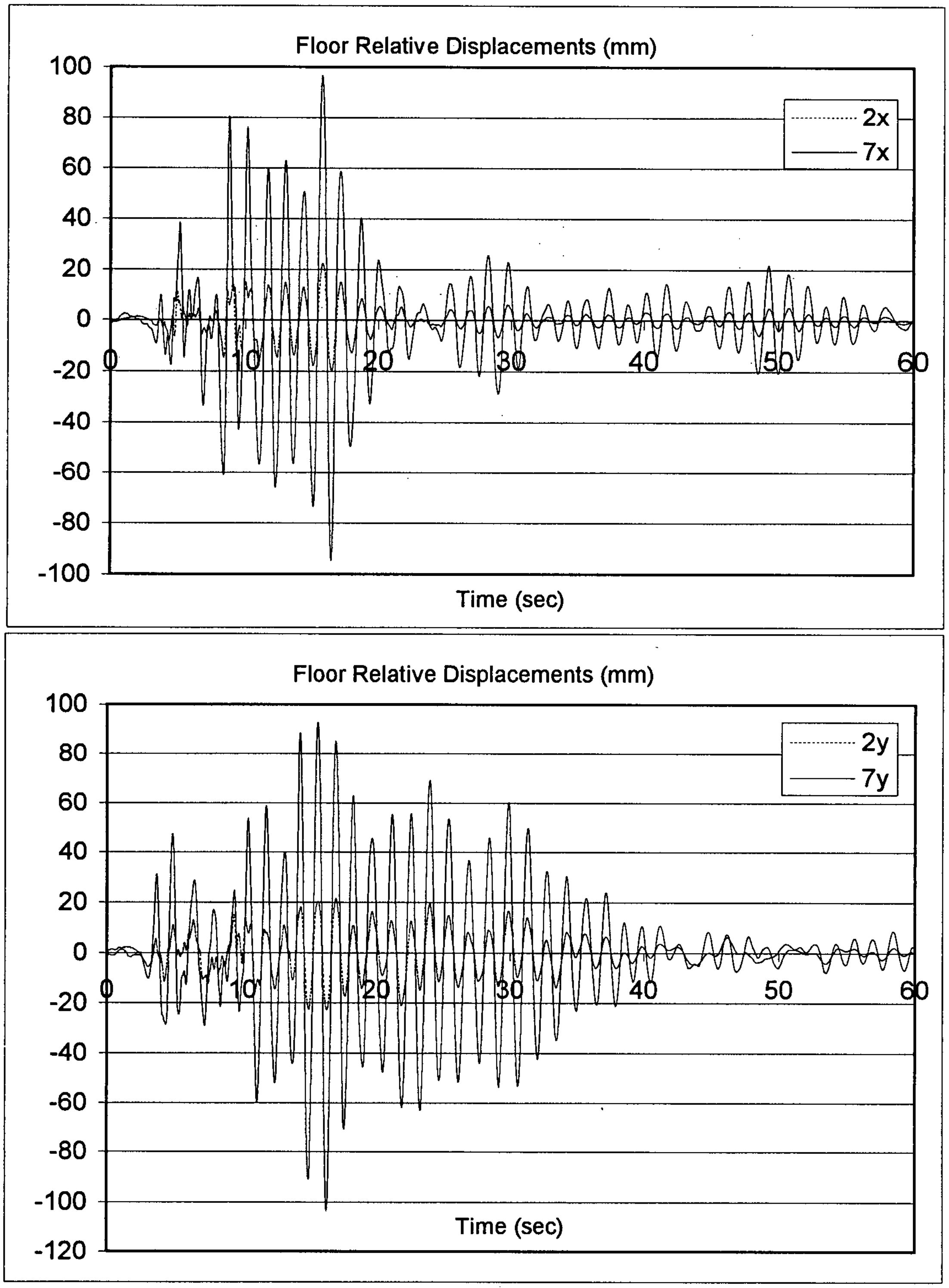

Figure 5.2b.6 E-W (X-direction) & N-S (Y-direction) relative displacements of the instrumented upper floors of the Burbank 6-story bldg., during the 1994 Northridge EQ.

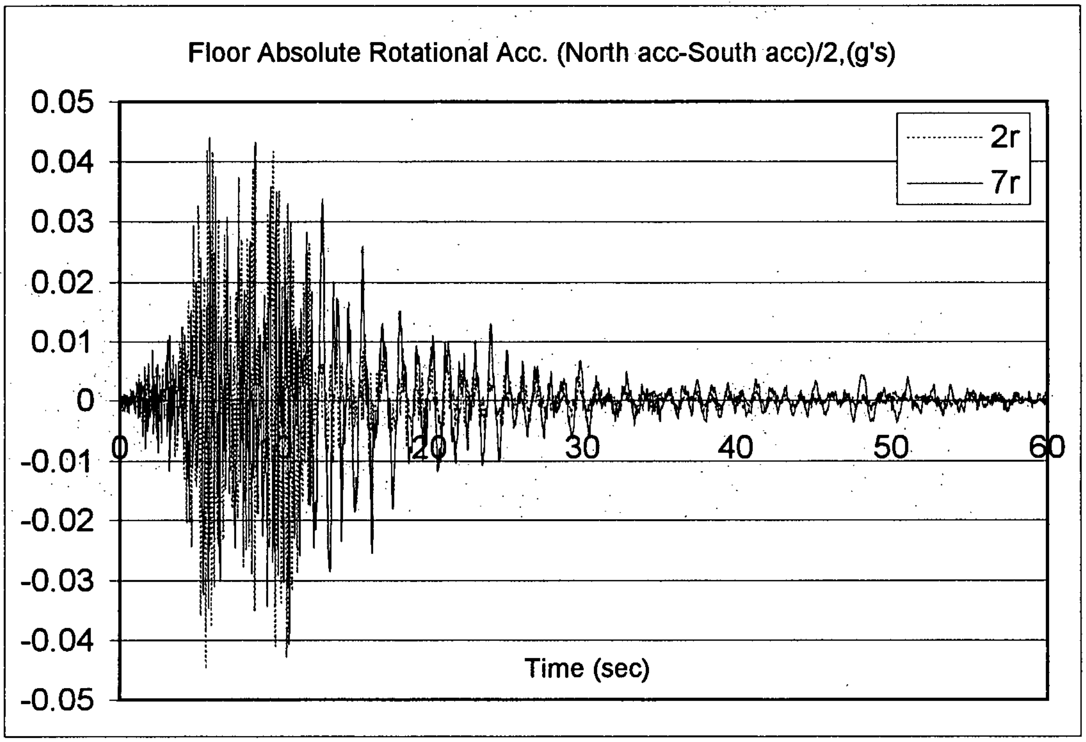

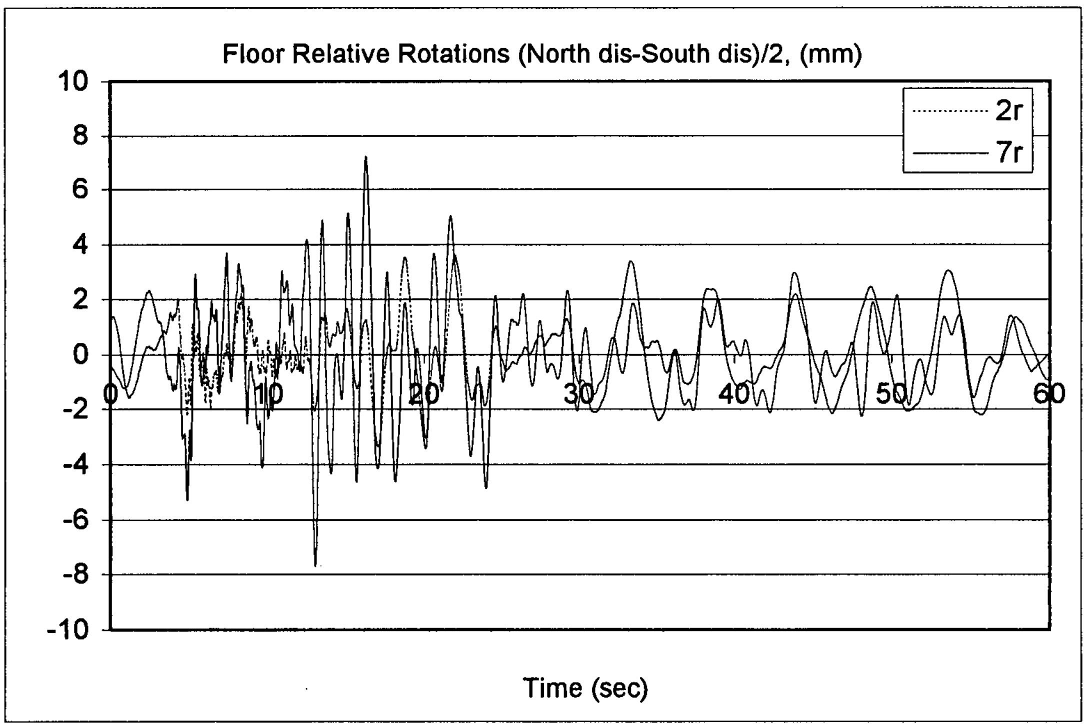

Figure 5.2b.7 Torsional response of the instrumented upper floors of the Burbank 6-story bldg., during the 1994 Northridge EQ.

Absolute Displ. Relative Displ.

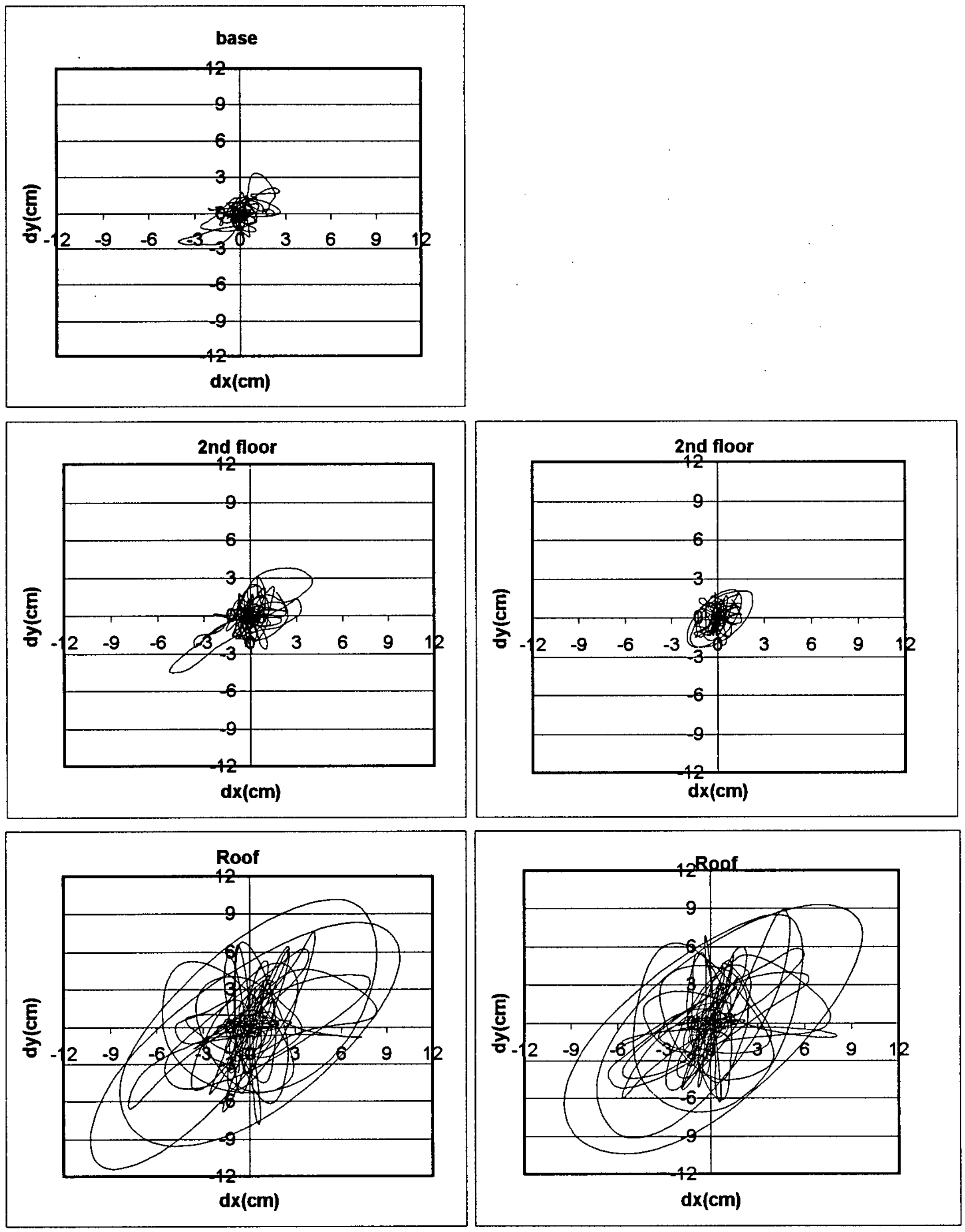

Figure 5.2b.8 Orbital displacements at the center of the instrumented floors of the Burbank 6-story bldg., during the 1994 Northridge EQ.

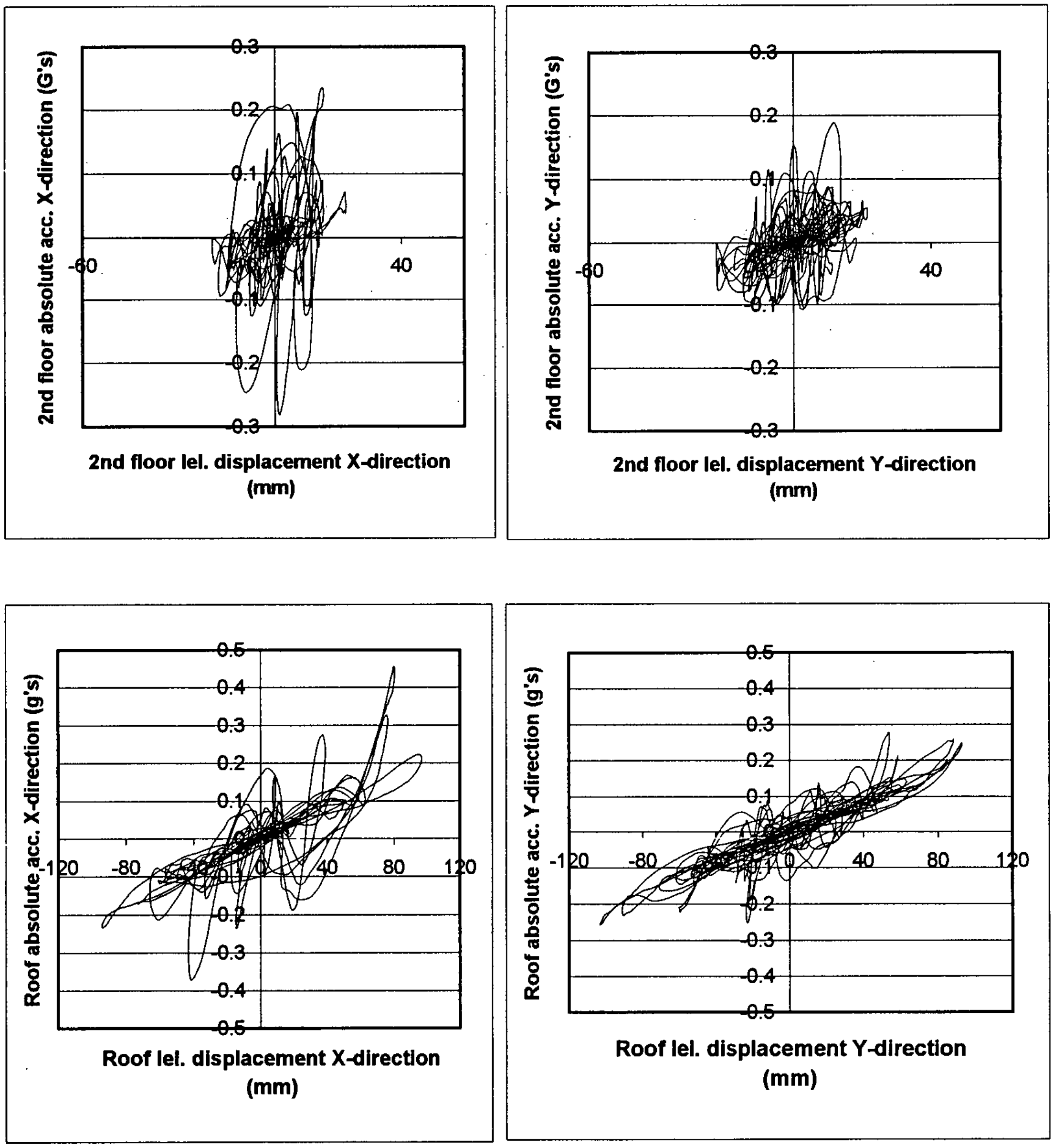

Figure 5.2b.9 Representation of hysteretic behaviour at the instrumented floors of the Burbank 6-story bldg., during the 1994 Northridge EQ.

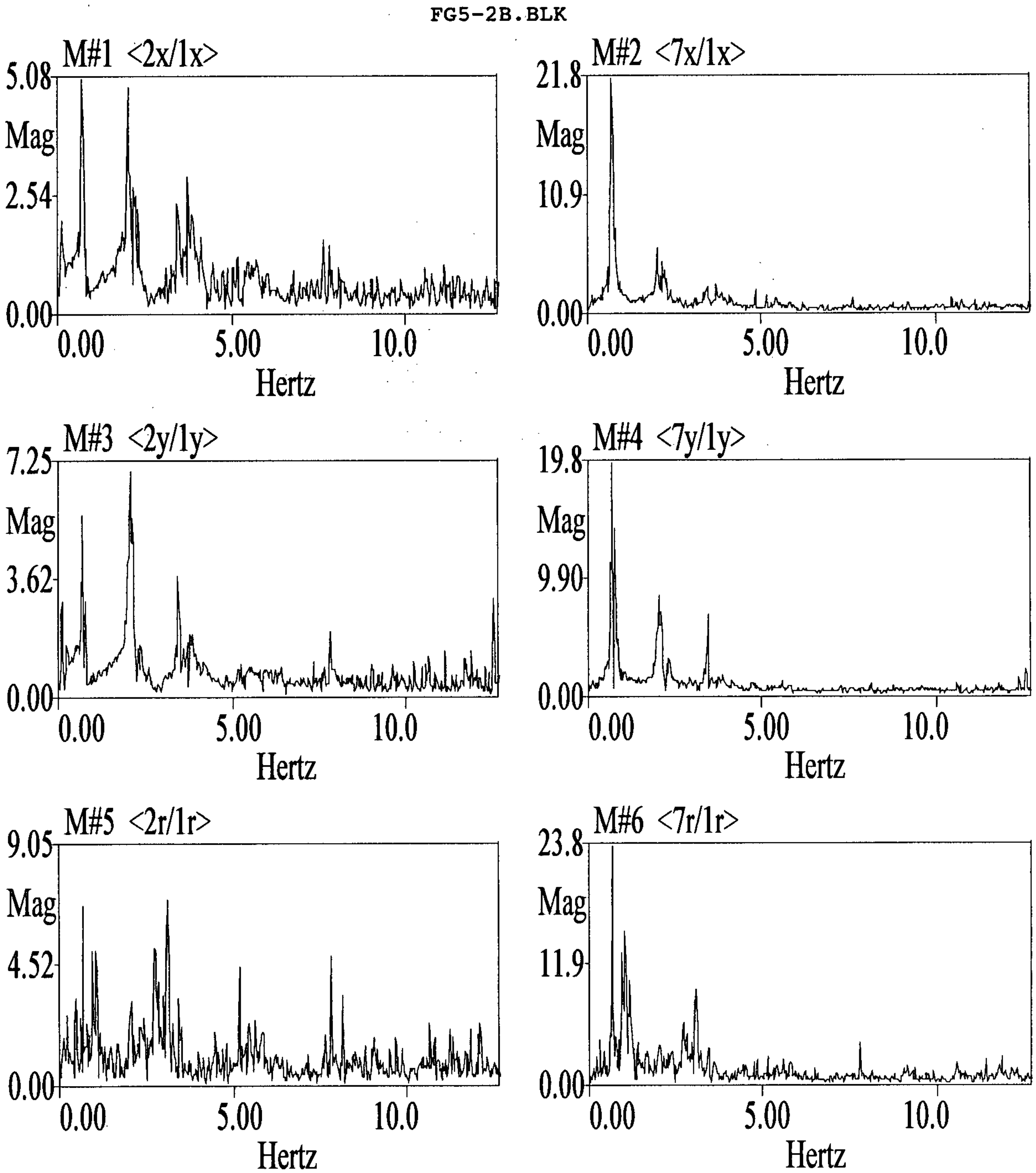

Figure 5.2b.10 Frequency Response Functions of the instrumented floors of the Burbank 6-story bldg., obtained from the 1994 Northridge EQ records.

Note: The FRF's are computed by ME'scope using a Hanning window, a block size N=2048, 5 averages and 88% segment overlap.

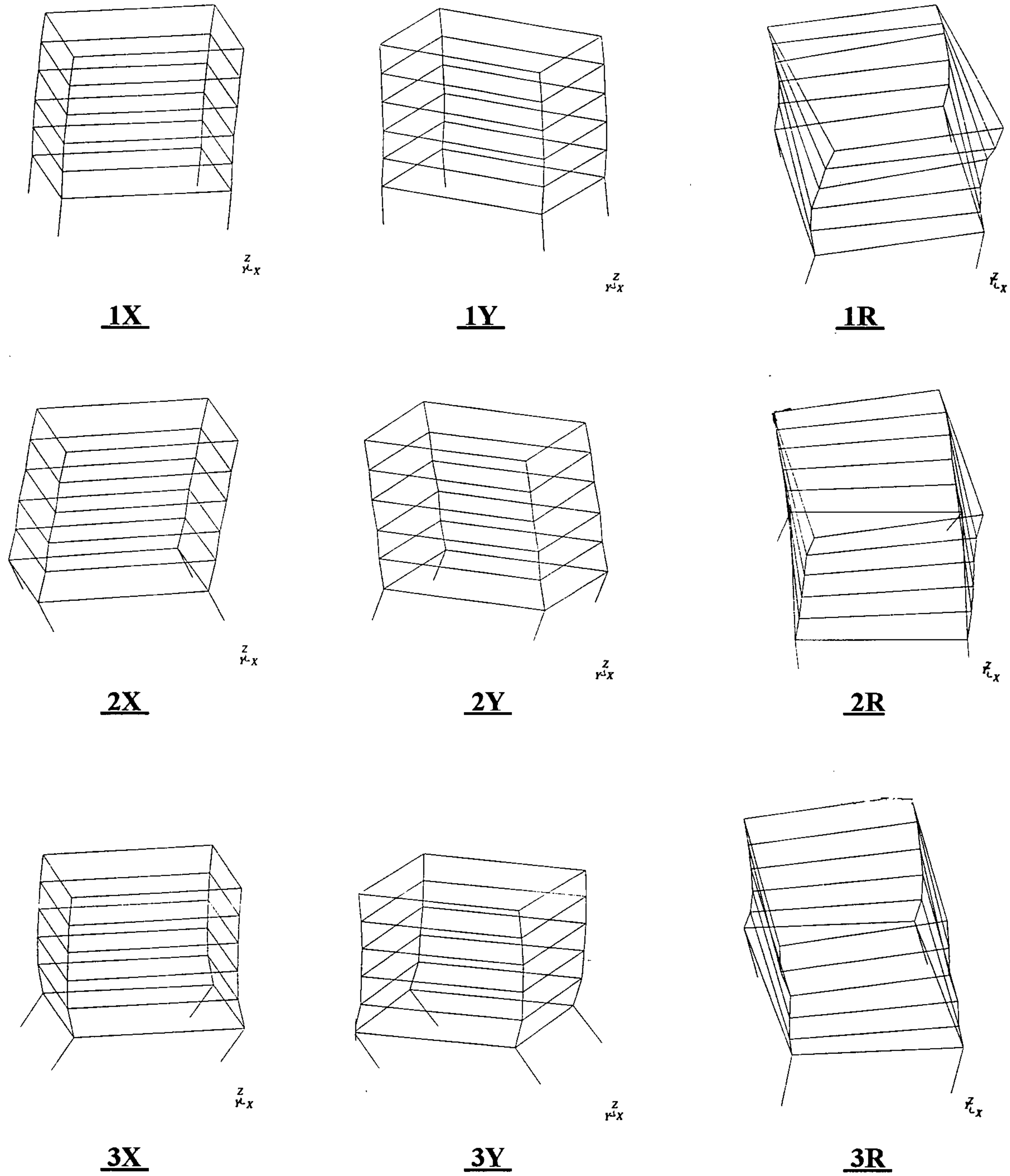

Figure 5.2b.11 Mode shapes of the Burbank 6-story bldg., obtained from the 1994 Northridge EQ records.

Note: The displacements of levels 2 and 7 (roof) are obtained from measured data. Displacements of the other floors are based on ME'scope's interpolation algorithm.

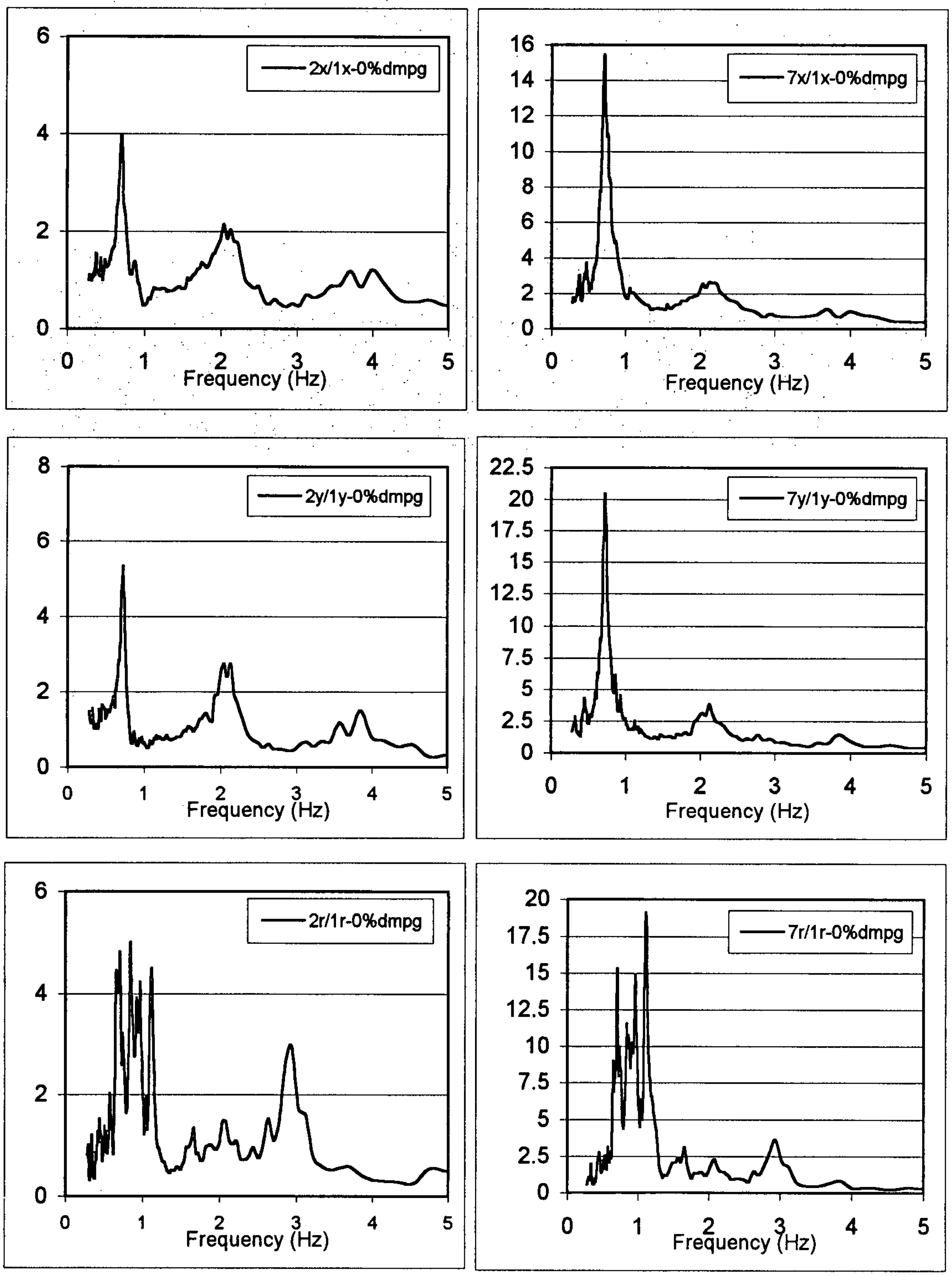

Figure 5.2a.12 Spectral Response Functions of the Burbank 6-story bldg., obtained from the 1994 Northridge EQ records.

Table 5.2b.1 Results of Frequency Response Functions for the Burbank 6-story bldg., obtained from the 1994 Northridge EQ records

X-direction				
Potential Mode #	Frequency (Hz)	Amplification Factor (2X/1X)	Amplification Factor (3X/1X)	Amplification Factor (7X/1X)
1	0.71	5.09	-	21.9
2	2.00	4.89	-	6.03
3	3.71	3.00	-	3.71
4	4.86	0.98	-	1.96
Damping Ratio estimated by ME'scope for mode 1X: **3.28%**				
Y-direction				
Potential Mode #	Frequency (Hz)	Amplification Factor (2Y/1Y)	Amplification Factor (3Y/1Y)	Amplification Factor (7Y/1Y)
1	0.71	5.60	-	19.8
2	2.05	6.99	-	8.42
3	3.42	3.70	-	6.74
Damping Ratio estimated by ME'scope for mode 1Y: **2.00%**				
R-direction				
Potential Mode #	Frequency (Hz)	Amplification Factor (2R/1R)	Amplification Factor (3R/1R)	Amplification Factor (7R/1R)
1	1.09	5.06	-	15.3
2	3.10	7.00	-	9.30
3	5.15	4.41	-	2.42
Damping Ratio estimated by ME'scope for mode 1R: **1.10%**				

Table 5.2b.2 Results of Spectral Response Functions for the Burbank 6-story bldg., obtained from the 1994 Northridge EQ records.

X-direction				
Potential Mode #	Frequency (Hz)	SRF 0% damping (2X/1X)	SRF 0% damping (3X/1X)	SRF 0% damping (7X/1X)
1	0.714	3.84	-	15.4
2	2.04	2.14	-	2.55
3	3.70	1.20	-	1.15
Y-direction				
Potential Mode #	Frequency (Hz)	SRF 0% damping (2Y/1Y)	SRF 0% damping (3Y/1Y)	SRF 0% damping (7Y/1Y)
1	0.72	5.34	-	20.4
2	2.13	2.74	-	3.84
3	3.85	1.50	-	1.45
R-direction				
Potential Mode #	Frequency (Hz)	SRF 0% damping (2R/1R)	SRF 0% damping (3R/1R)	SRF 0% damping (7R/1R)
1	1.11	4.5	-	19.1
2	2.94	2.97	-	3.68
3	5.88	1.05	-	0.83

Table 5.2.3 Estimated natural frequencies (and periods) of the Burbank 6-story bldg. based on the results of FRF results, SRF results and visual inspection of the three dimensional mode shapes obtained from analysis of 1987 Whittier and 1994 Northridge EQ data.

WHITTIER EARTHQUAKE DATA						
	X-Direction (E-W)		Y-Direction (E-W)		Rotation	
	Frequency (Hz)	Period (S)	Frequency (Hz)	Period (S)	Frequency (Hz)	Period (S)
Model	0.80	1.25	0.76	1.32	1.10	0.91
Mode 2	2.37	0.42	2.27	0.44	3.20	0.31
Mode 3	4.30	0.23	4.20	0.24	5.70	0.18
NORTHRIDGE EARTHQUAKE DATA						
	X-Direction (E-W)		Y-Direction (E-W)		Rotation	
	Frequency (Hz)	Period (S)	Frequency (Hz)	Period (S)	Frequency (Hz)	Period (S)
Mode 1	0.71	1.41	0.71	1.41	1.10	0.91
Mode 2	2.02	0.50	2.05	0.49	3.05	0.33
Mode 3	3.70	0.27	3.65	0.27	5.40	0.19
Mode 4	4.86	0.21	-	-	-	-

Fundamental Period according to **NBCC 1995**:

T = 0.1 N ==> **T** = 0.60 sec

$\mathbf{T = 0.085\ (h_n)^{3/4}} = 0.085\ (25.15\text{m})^{3/4} = 0.96$ sec

Fundamental Period according to **UBC 1997**:

$\mathbf{T = 0.035\ (h_n)^{3/4}} = 0.035\ (82.5\text{ ft})^{3/4} = 0.96$ sec

5.3 San Bernardino 5-Story Hospital

Properties of the Strong Motion Data:

Record Length: 100 sec

Time interval: 0.01 sec

No. of data points for each channel: 10001

Usable frequency range: 0.3 Hz to 46.0 Hz

Manipulating the data to obtain the motion of the center of the building in the 3 directions, E-W (or X-directions) , N-S (or Y-directions) and rotation about vertical axis (or R-component) :

1X = (2 .Chan3 + Chan4)/3 , 1Y = Chan2 , 1R = (Chan3-Chan4)/2

3X = (2 .Chan7+Chan8)/3 , 3Y = (2 .Chan5+ Chan6)/3

3R = {[(Chan7-Chan8)/2] + [(Chan6-Chan5)/2] .(140/110) }/ 2

6X = (2 .Chan7+Chan8)/3 , 6Y = (2 .Chan5+ Chan6)/3

6R = {[(Chan7-Chan8)/2] + [(Chan6-Chan5)/2] .(140/110) }/ 2

Note: Rotation of level 3 could be obtained both from the difference of channels 7 & 8 and channels 5 & 6. The average of the two values are used in this study as shown above. This also applies to level 6 data.

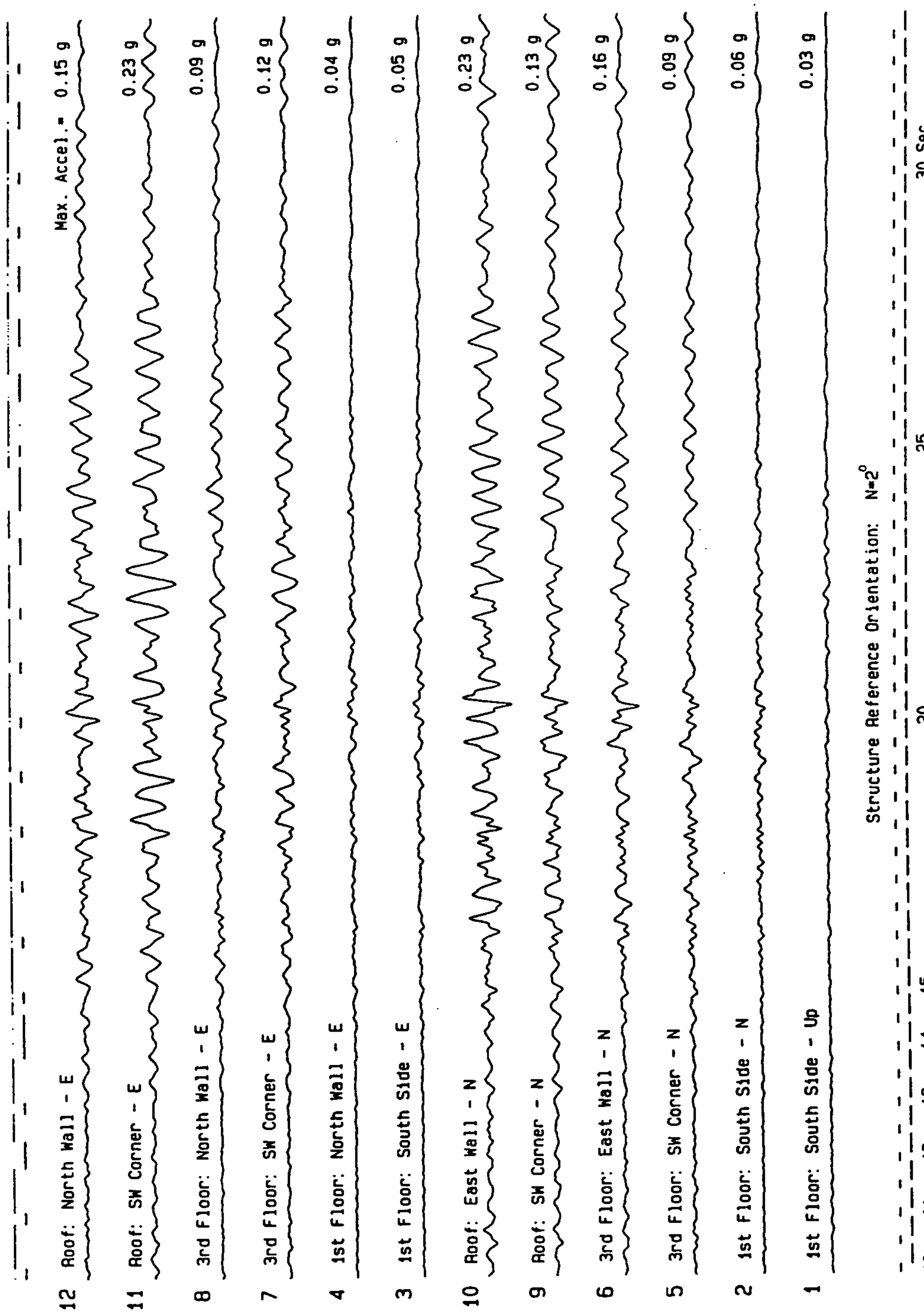

Figure 5.3.1 Accelerations recorded at the San Bernardino 5-story hospital during the 1994 Northridge Earthquake. (After Shakal, et al., 1994)

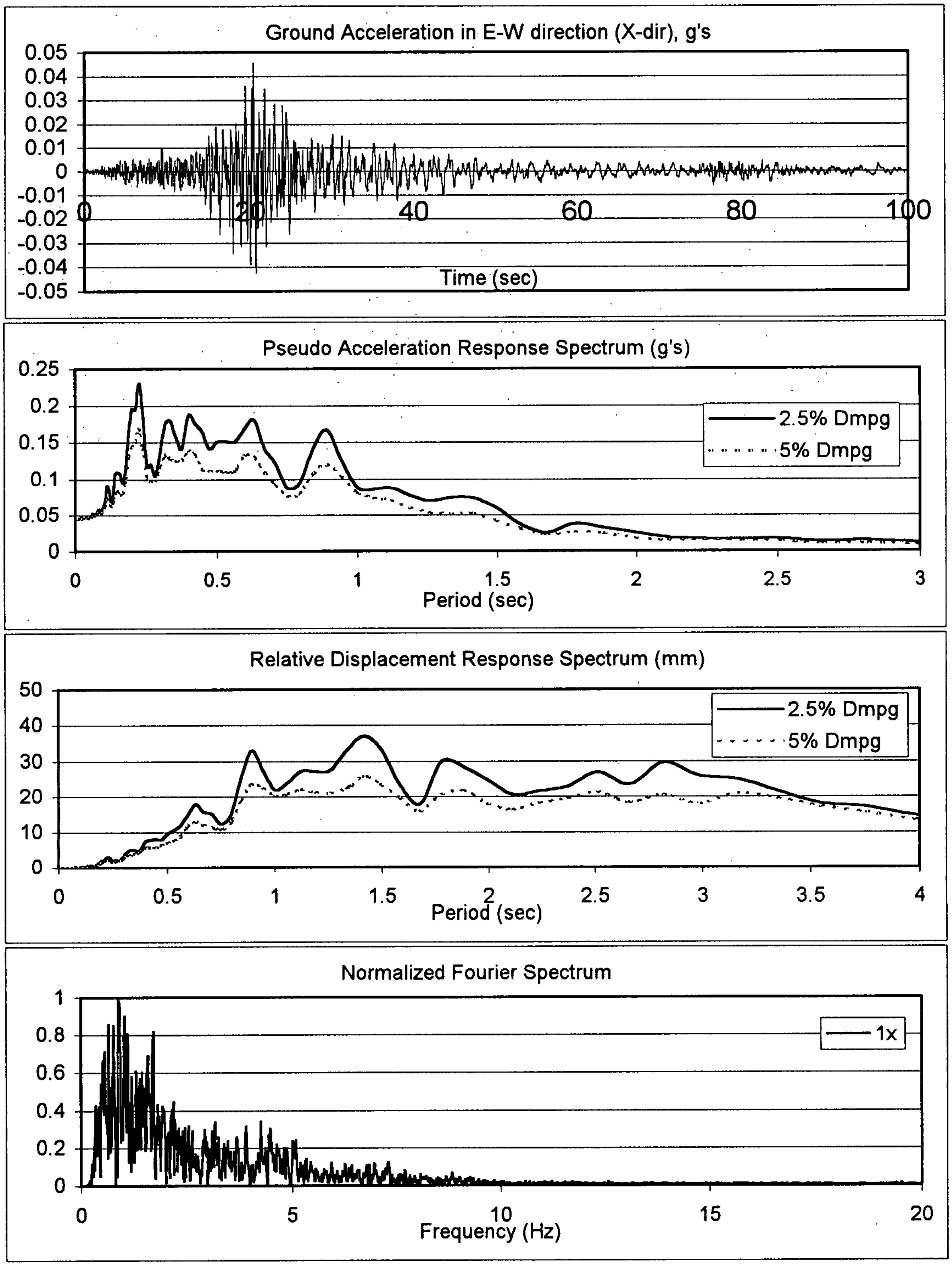

Figure 5.3.2 Ground motion properties, E-W (X-direction), San Bernardino 5-story hospital, Northridge EQ.

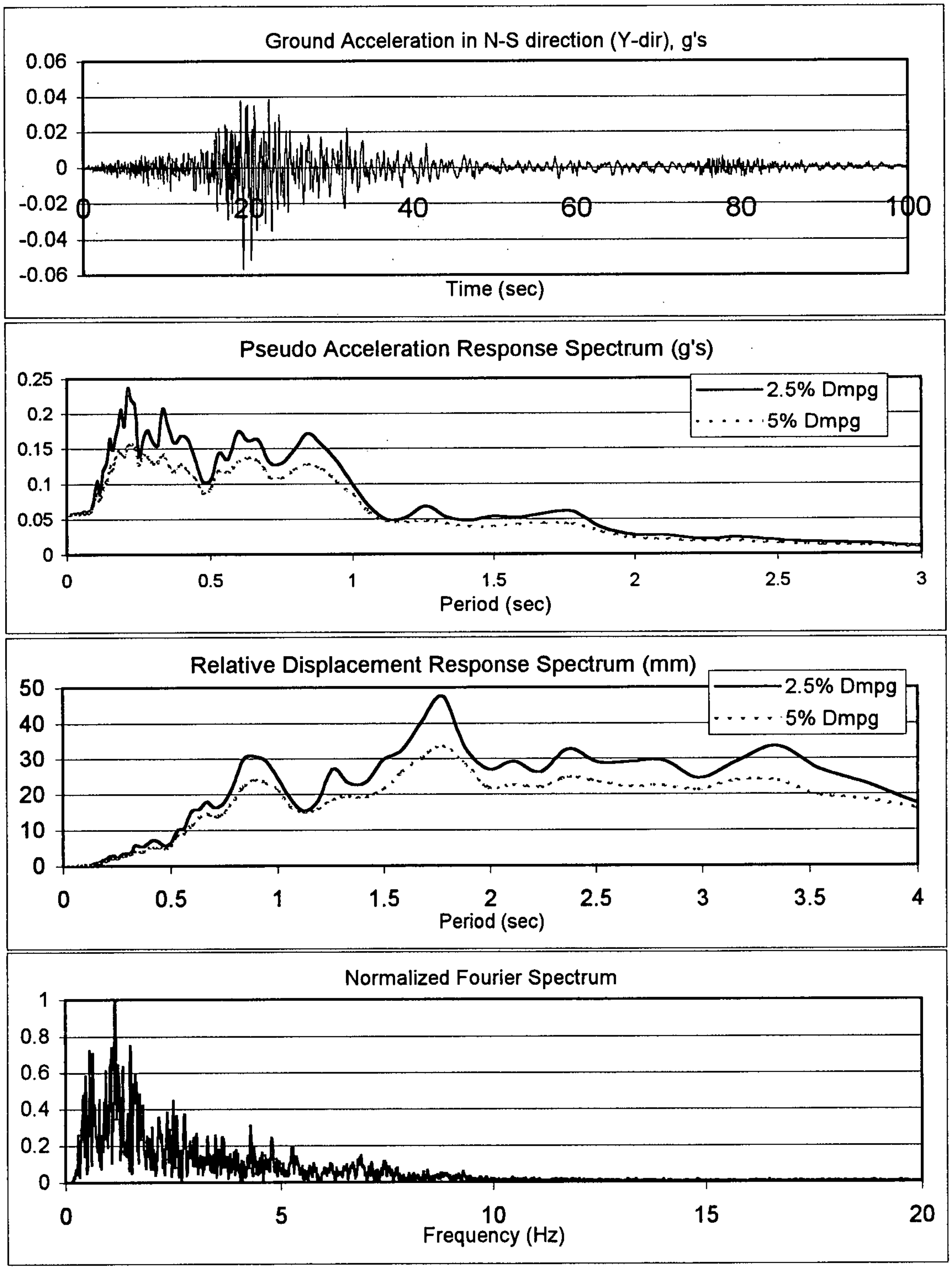

Figure 5.3.3 Time-history and spectral characteristics of N-S (Y) component of the ground motion recorded at the San Bernardino 5-story hospital during the 1994 Northridge EQ.

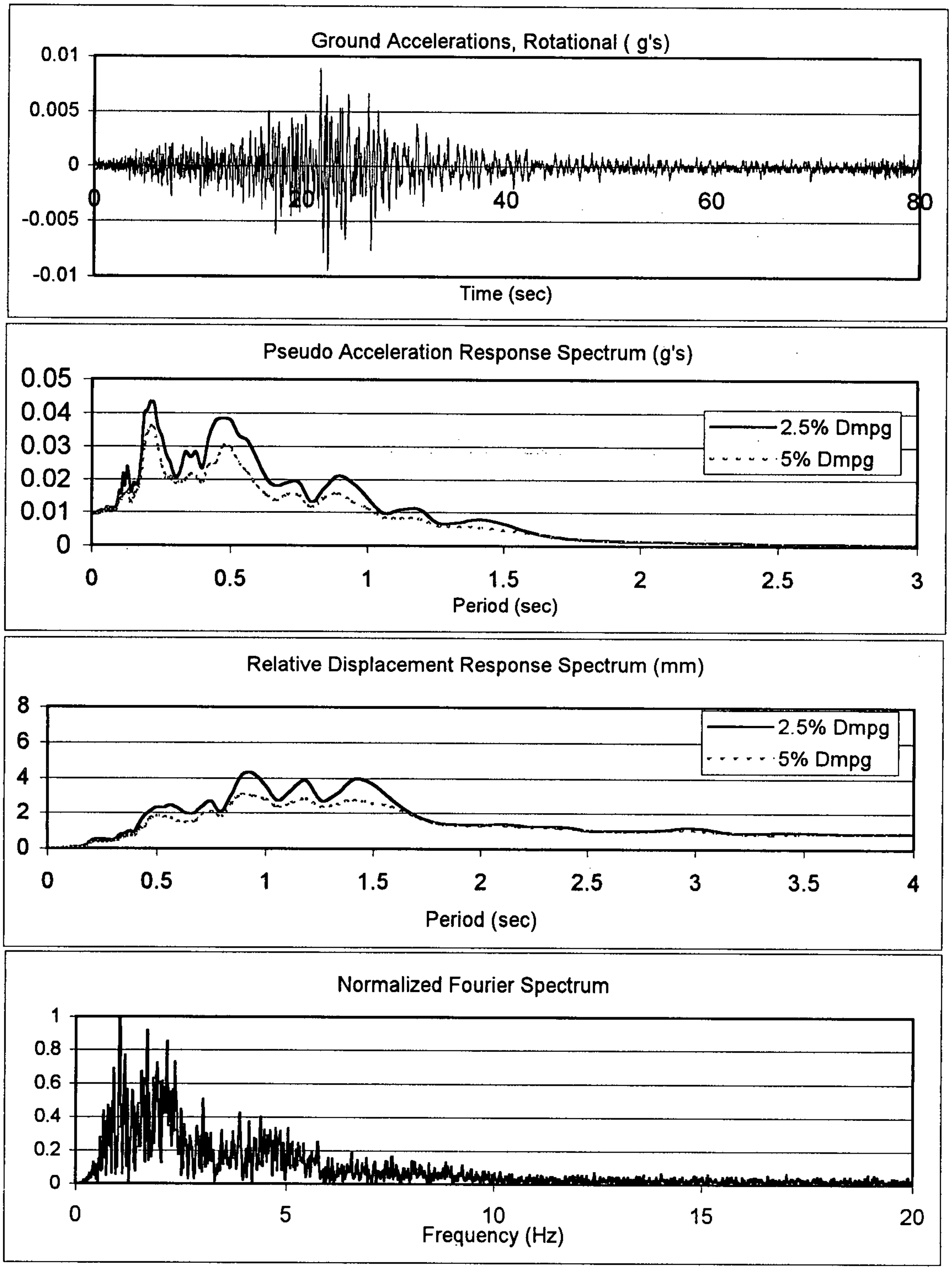

Figure 5.3.4 Time-history and spectral characteristics of rotational (R) component of the ground motion recorded at the San Bernardino 5-story hospital during the 1994 Northridge EQ.

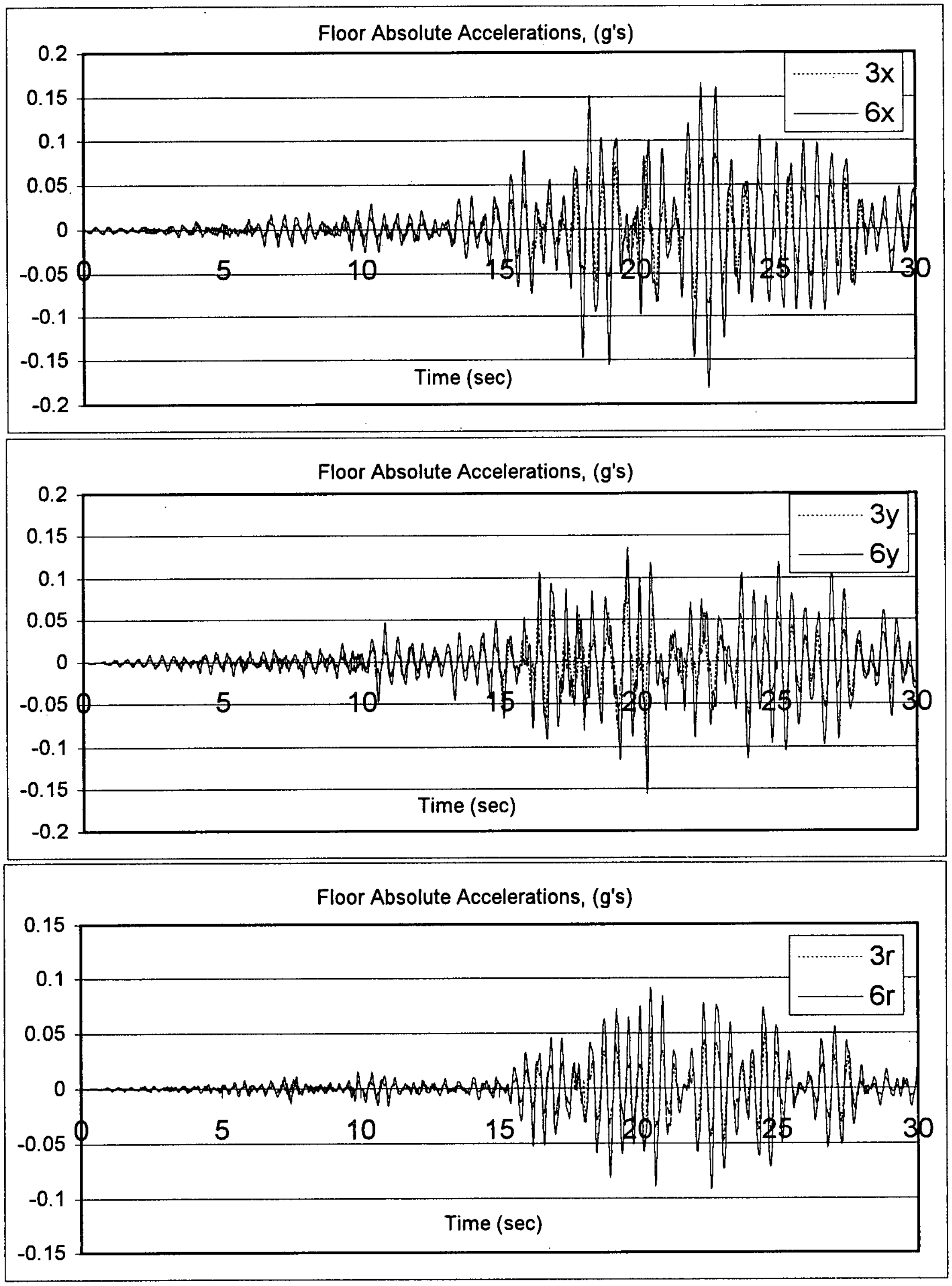

Figure 5.3.5 Absolute accelerations of the instrumented upper floors of the San Bernardino 5-story hospital during the 1994 Northridge EQ.

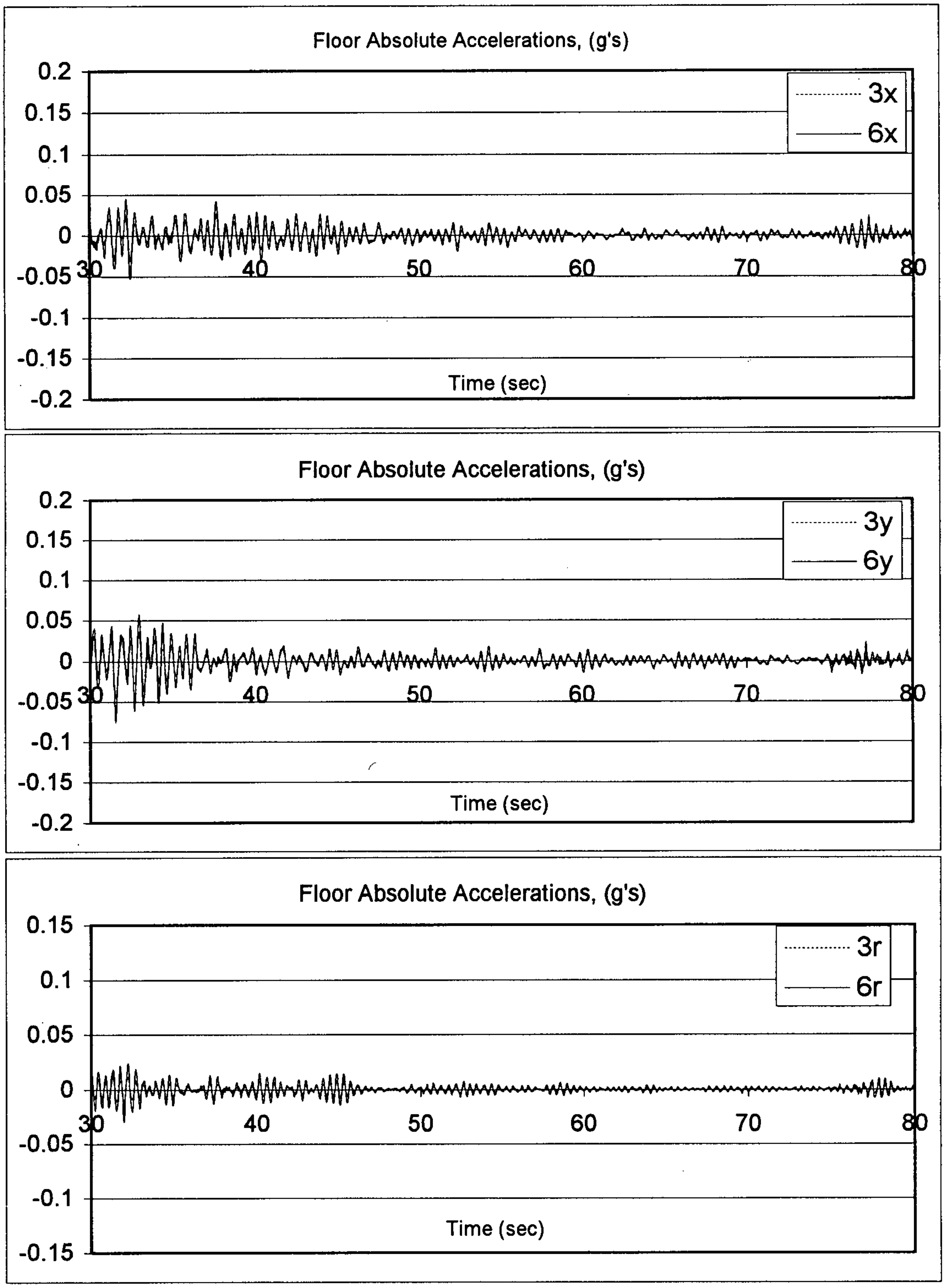

Figure 5.3.5 Cont'd

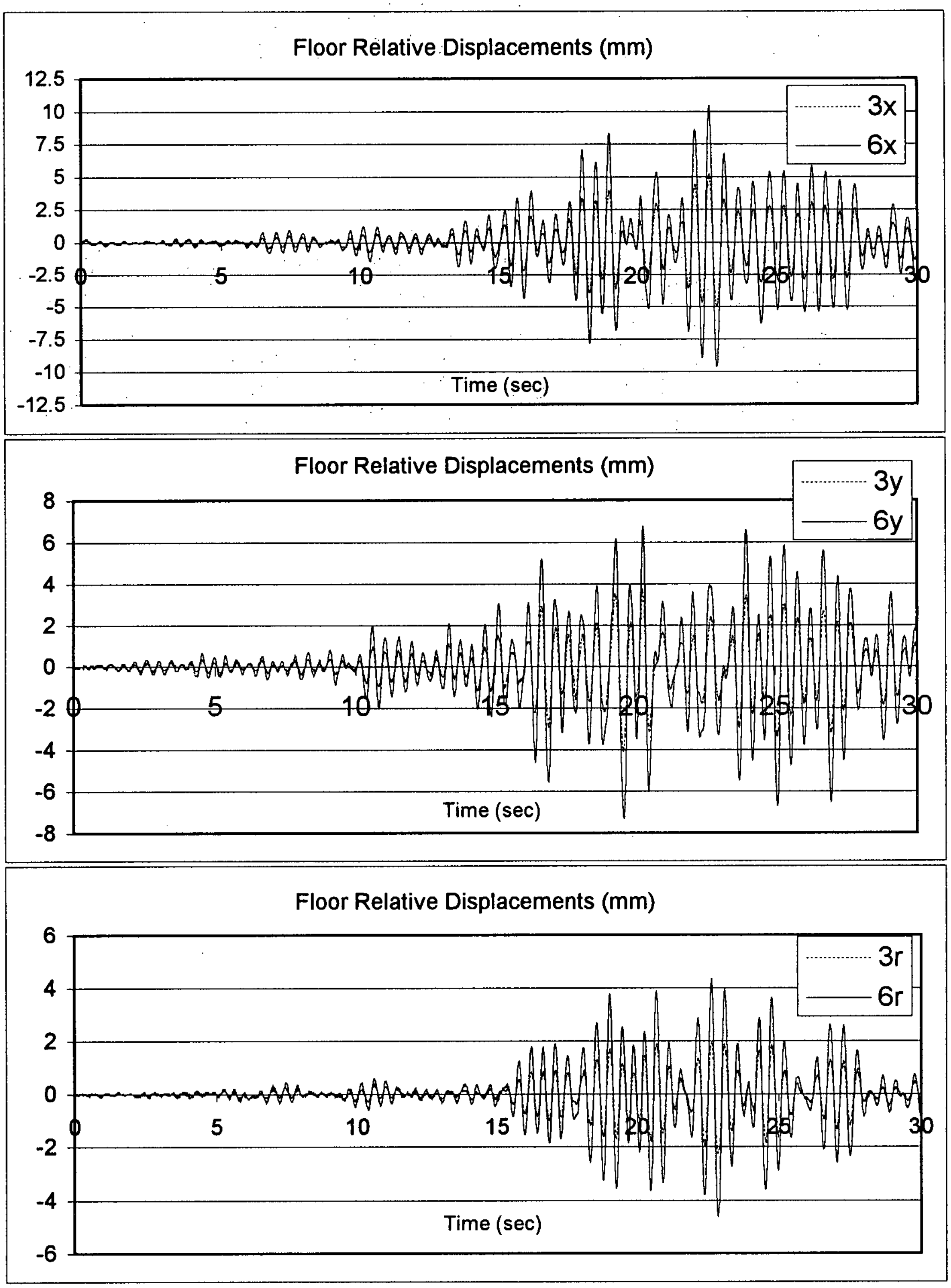

Figure 5.3.6 Relative displacements of the instrumented upper floors of the San Bernardino 5-story hospital during the 1994 Northridg EQ.

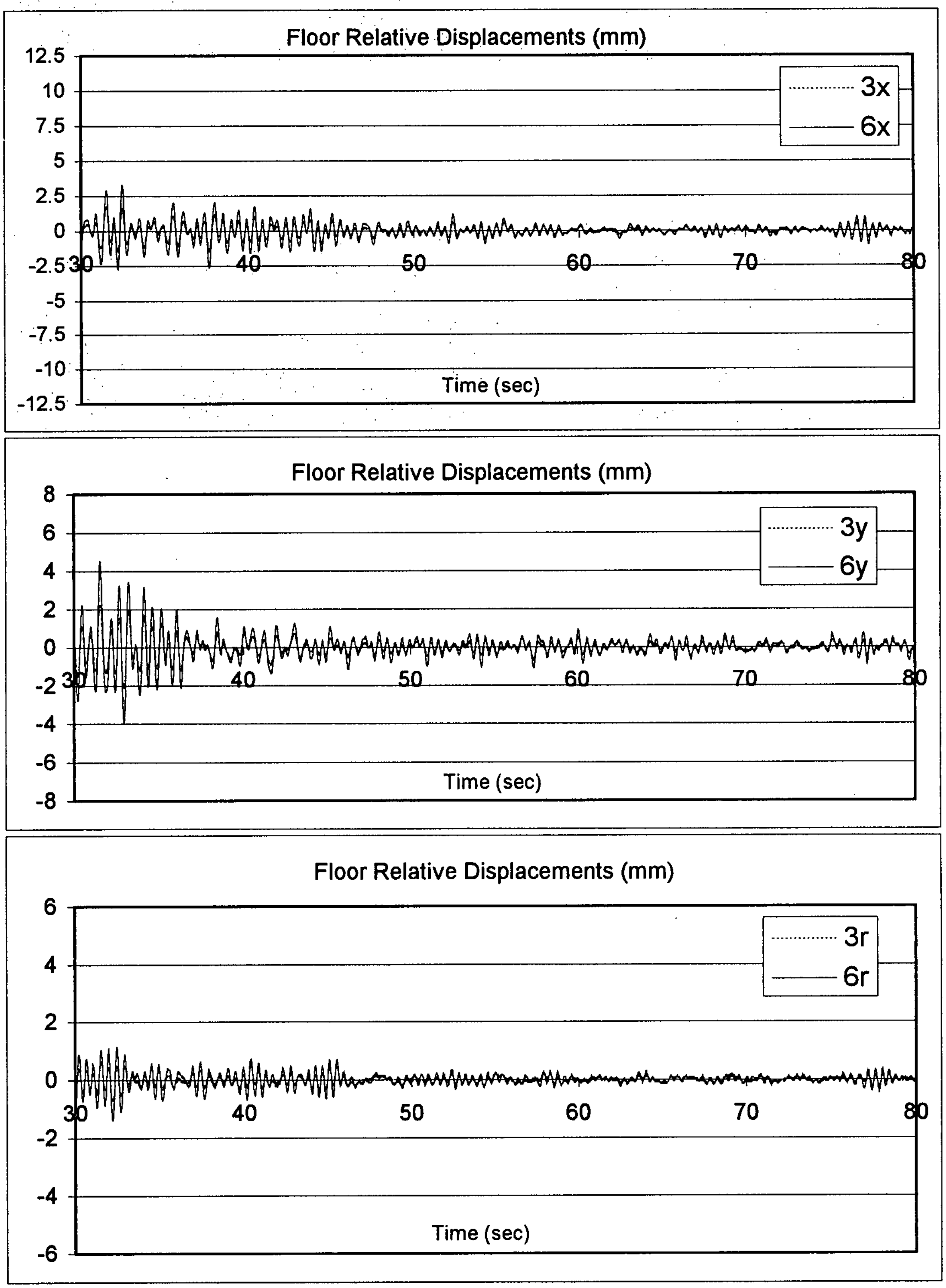

Figure 5.3.6 Cont'd

Absolute Displ. **Relative Displ.**

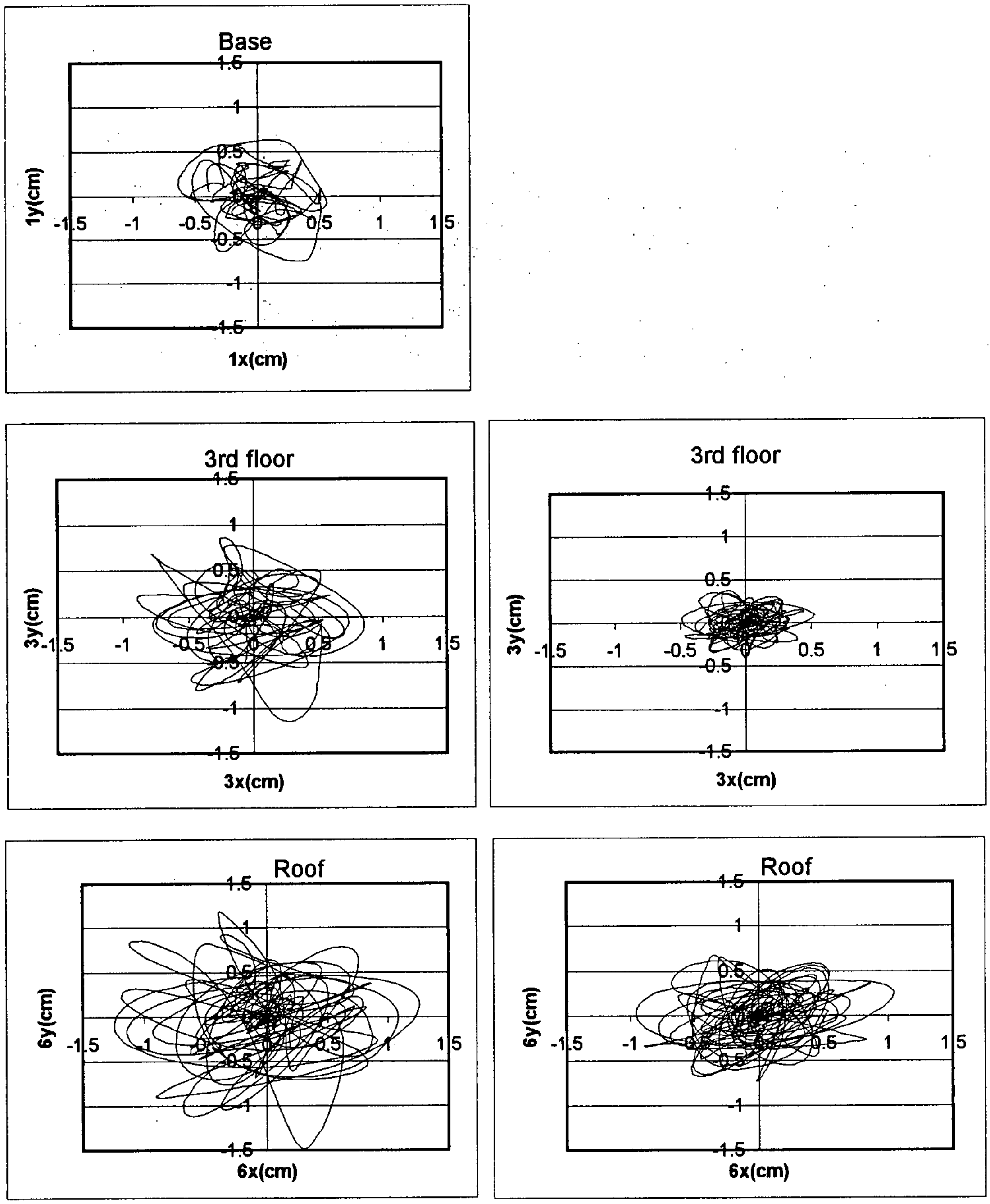

Figure 5.3.7 Orbital displacements at the center of the instrumented floors of the San Bernardino 5-story hospital during the 1994 Northridge EQ.

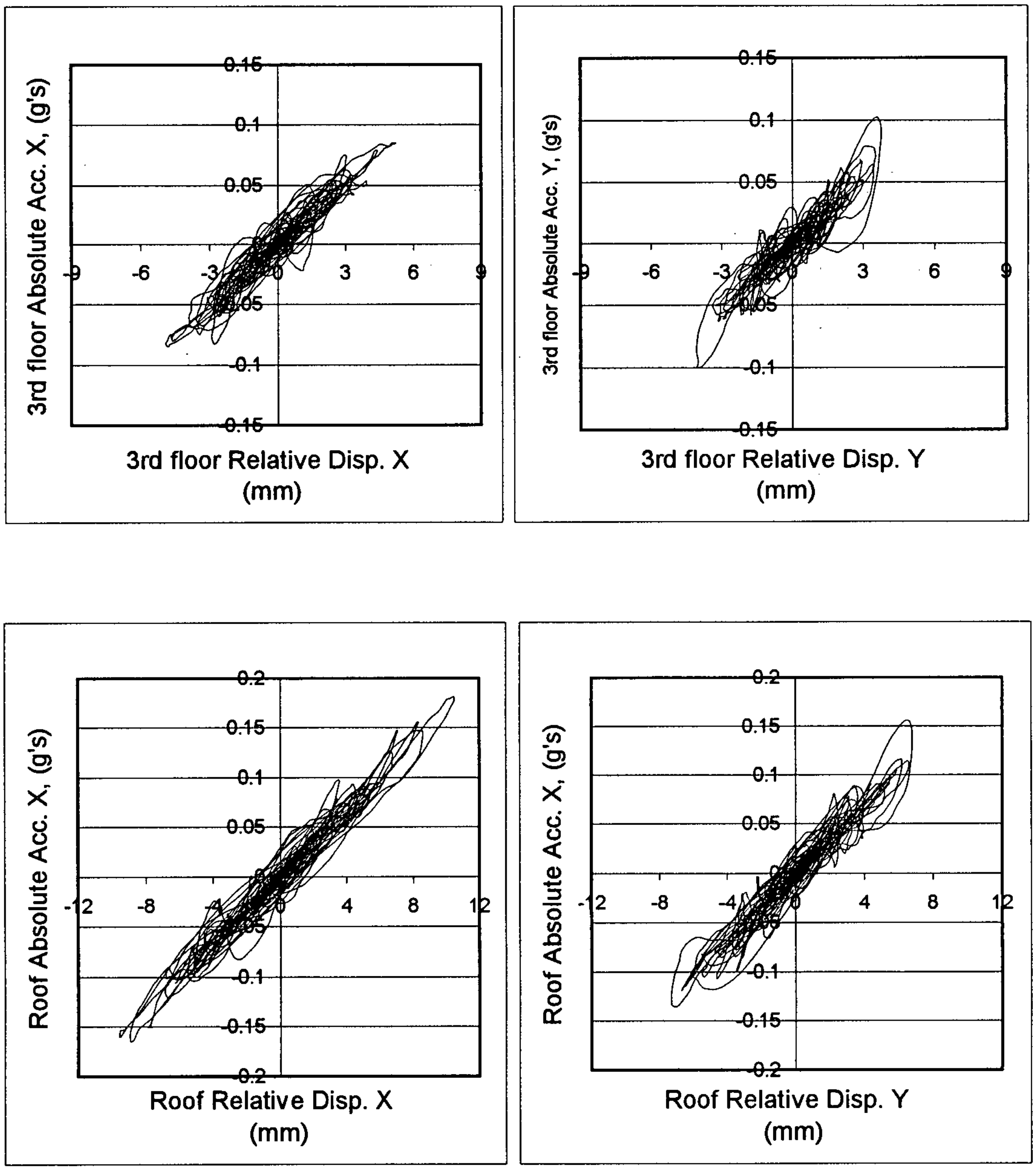

Figure 5.3.8 Representation of hysteretic behaviour at the instrumented floors of the San Bernardino 5-story hospital during the 1994 Northridge EQ.

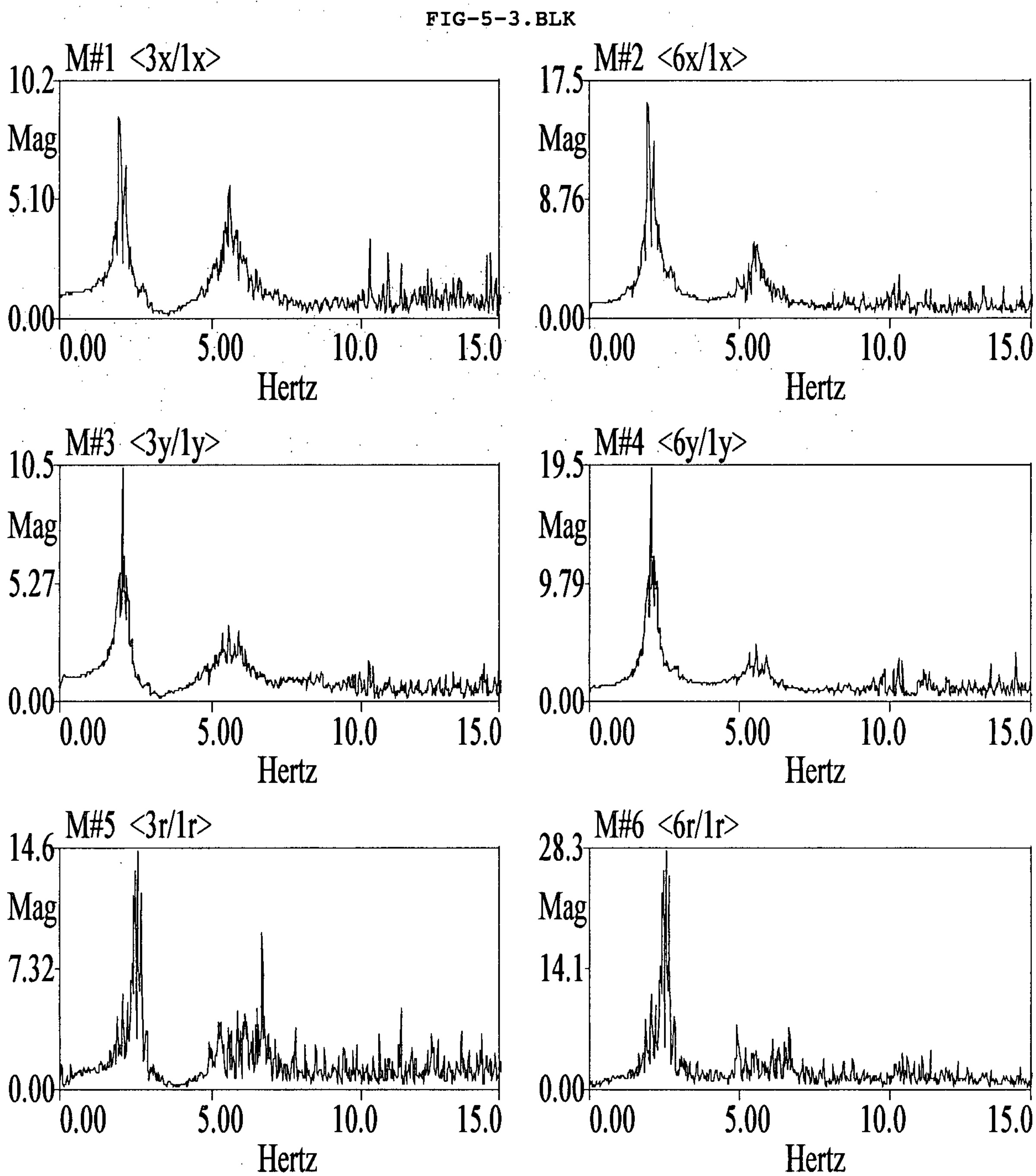

Figure 5.3.9 Frequency Response Functions of the instrumented floors of the San Bernardino 5-story hospital, obtained from the 1994 Northridge EQ records.

Note: The FRF's are computed by ME'scope using a Hanning window, a block size N=4096, 10 averages and 89% segment overlap.

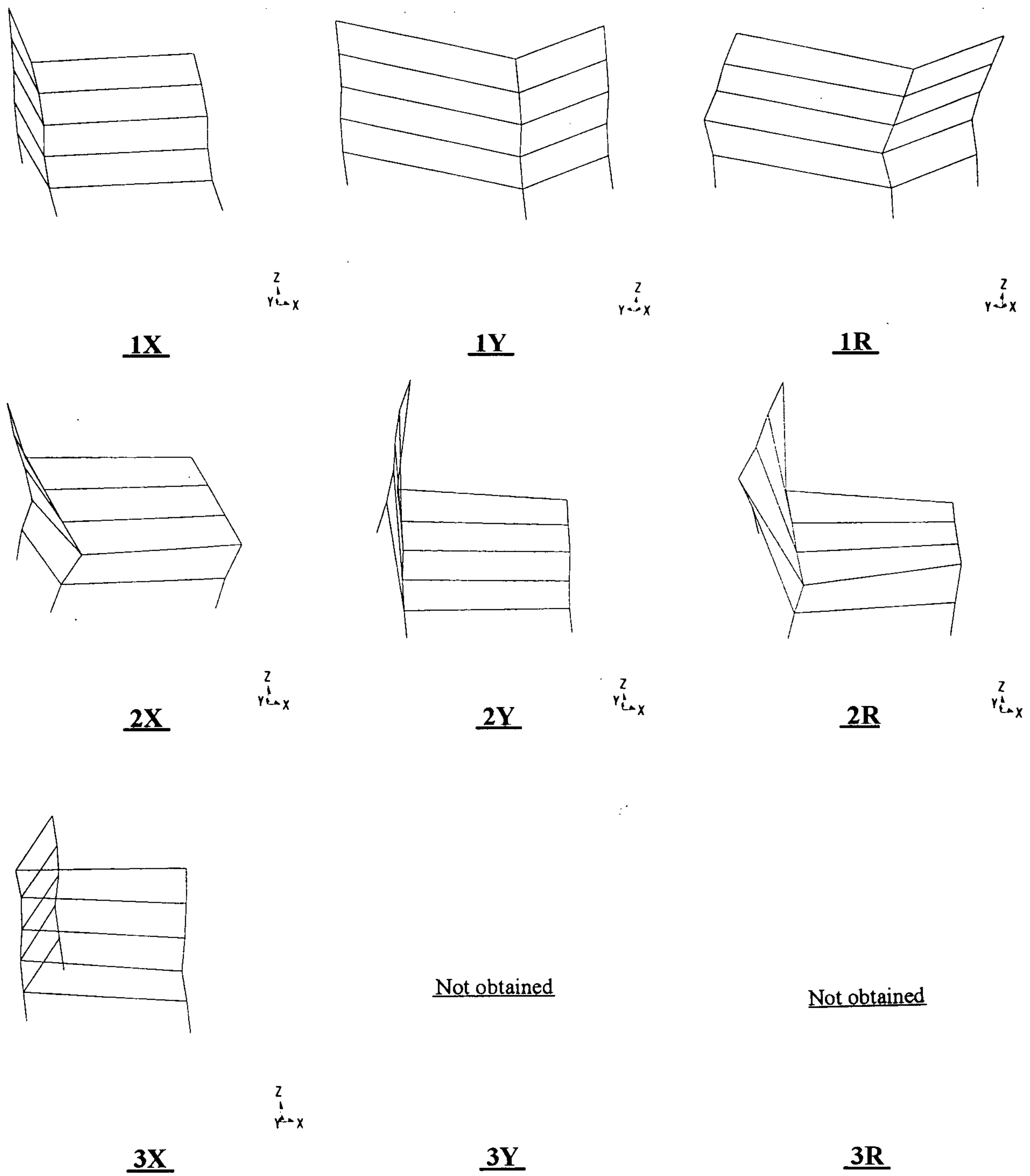

Figure 5.3.10 Mode shapes of (L-shape presentation of) the San Bernardino 5-story hospital, obtained from the 1994 Northridge EQ records.

Note: The displacements of levels 3 and 6 (roof) are obtained from measured data. Displacements of the other floors are based on ME'scope's interpolation algorithm.

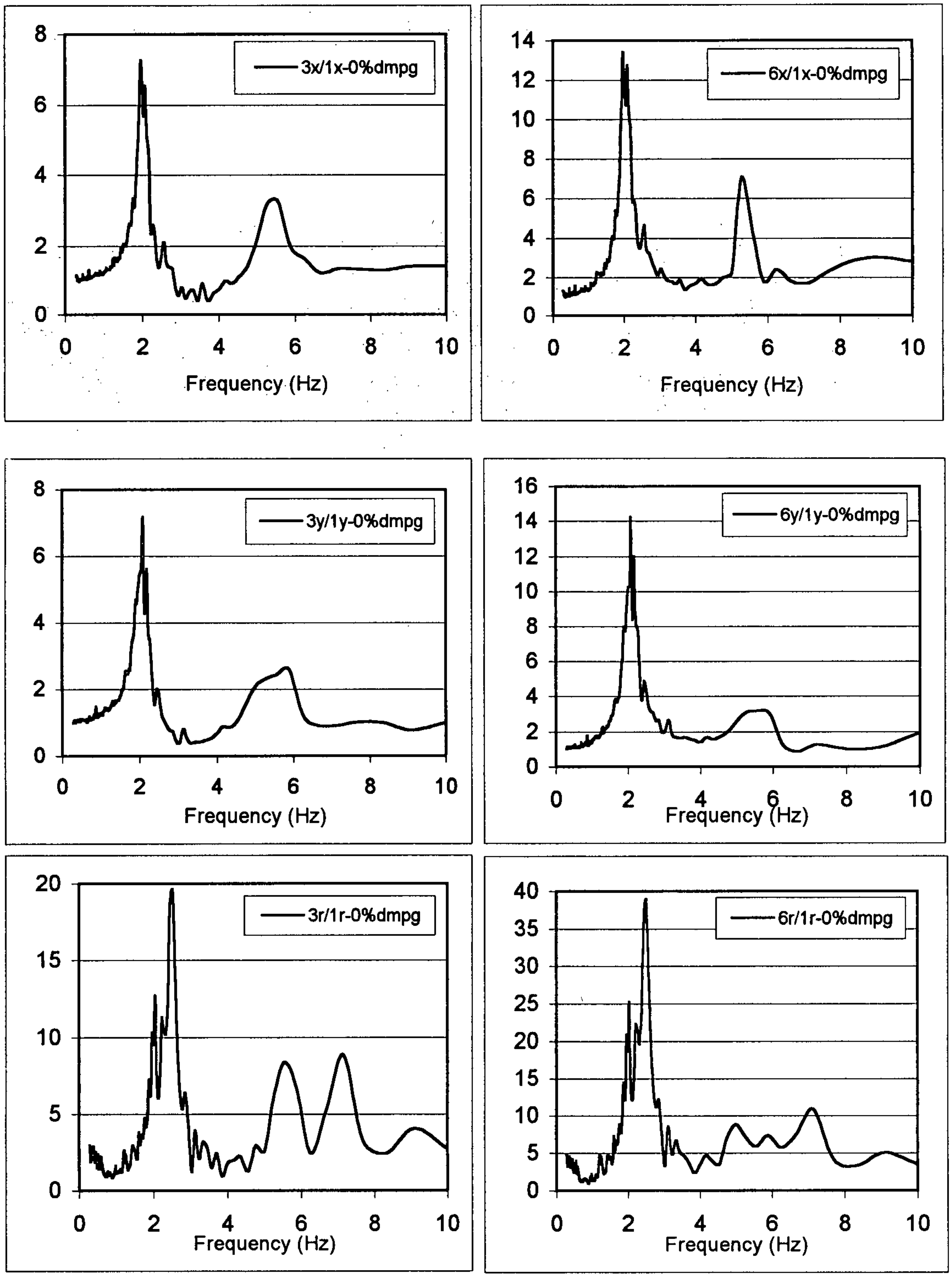

Figure 5.3.11 Spectral Response Functions of the San Bernardino 5-story hospital, obtained from the 1994 Northridge EQ records.

Table 5.3.1 Results of Frequency Response Functions for the San Bernardino 5-story hospital, obtained from the 1994 Northridge EQ records

X-direction			
Potential Mode #	Frequency (Hz)	Amplification Factor (3X/1X)	Amplification Factor (6X/1X)
1	1.98	8.80	16.1
2	5.51	3.84	5.68
3	10.25	3.37	3.16
Damping Ratio estimated by ME'scope for mode 1X: **3.30%**			
Y-direction			
Potential Mode #	Frequency (Hz)	Amplification Factor (3Y/1Y)	Amplification Factor (6Y/1Y)
1	2.08	10.5	19.6
2	5.57	3.42	4.60
3	10.37	1.56	3.25
Damping Ratio estimated by ME'scope for mode 1Y: **2.80%**			
R-direction			
Potential Mode #	Frequency (Hz)	Amplification Factor (3R/1R)	Amplification Factor (6R/1R)
1	2.56	14.6	28.3
2	6.67	9.64	7.03
3a	11.2	4.91	4.51
3b	13.33	3.52	0.84
Damping Ratio estimated by ME'scope for mode 1R: **1.00%**			

Table 5.3.2 Results of Spectral Response Functions for the San Bernardino 5-story hospital, obtained from the 1994 Northridge EQ records.

X-direction			
Potential Mode #	Frequency (Hz)	SRF 0% damping (3X/1X)	SRF 0% damping (6X/1X)
1	1.96	7.26	13.4
2	5.26	3.19	7.03
3	9.10	3.03	1.41
Y-direction			
Potential Mode #	Frequency (Hz)	SRF 0% damping (3Y/1Y)	SRF 0% damping (6Y/1Y)
1	2.08	7.14	14.2
2	5.88	2.58	3.07
3	-	-	-
R-direction			
Potential Mode #	Frequency (Hz)	SRF 0% damping (3R/1R)	SRF 0% damping (6R/1R)
1	2.50	19.6	38.9
2	7.10	8.0	10.9
3	-	-	-

Table 5.3.3 Estimated natural frequencies (and periods) of the San Bernardino 5-story hospital based on the results of FRF results, SRF results and visual inspection of the three dimensional mode shapes obtained from analysis of 1994 Northridge EQ data.

NORTHRIDGE EARTHQUAKE DATA						
	X-Direction (E-W)		Y-Direction (E-W)		Rotation	
	Frequency (Hz)	Period (S)	Frequency (Hz)	Period (S)	Frequency (Hz)	Period (S)
Mode1	2.00	0.50	2.10	0.48	2.50	0.4
Mode 2	5.50	0.18	5.60	0.18	7.00	0.14
Mode 3	10.1	0.10	10.4	0.10	12.5	0.08

*** Spectral values at the natural periods in the ground motion response spectra and the response time-histories suggest that the 1st mode dominated the structural response.**

Fundamental Period according to **NBCC 1995**:

$\mathbf{T = 0.1\ N} \Longrightarrow \mathbf{T} = 0.50$ sec

$\mathbf{T = 0.085\ (h_n)^{3/4}} = 0.085\ (21.03\text{m})^{3/4} = 0.84$ sec

Fundamental Period according to **UBC 1997**:

$\mathbf{T = 0.035\ (h_n)^{3/4}} = 0.035\ (69\ \text{ft})^{3/4} = 0.84$ sec

5.4 Pasadena 6-Story Office Building

Properties of the Strong Motion Data:

Record Length: 60sec

Time interval: 0.02 sec

No. of data points for each channel: 3000

Usable frequency range: 0.24 Hz to 23.0 Hz

Manipulating the data to obtain the motion of the center of the building in the 3 directions, E-W (or X-directions) , N-S (or Y-directions) and rotation about vertical axis (or R-component):

1X = (Chan14+ Chan13)/2 , 1Y = Chan16 , 1R = (Chan14-Chan13)/2

2X = (Chan12+ Chan11)/2 , 2Y = (Chan2+Chan1)/2 ,

2R = {[(Chan12-Chan11)/2] + [(Chan2-Chan1)/2].(125/117)}/2

8X = (Chan8+ Chan6)/2 , 8Y = (Chan4+Chan3)/2 ,

8R = {[(Chan8-Chan7)/2] .(125/54) + [(Chan4-Chan3)/2] .(125/117) }/2

8X(modified) = Chan7 -{ [(8R) .(2/125)] . (8.5) }

Note: Rotation of level 2 could be obtained both from the difference of channels 12& 11 and channels 1& 2. The average of the two values are used in this study as shown above. Similar idea has been applied to level 8 (roof).

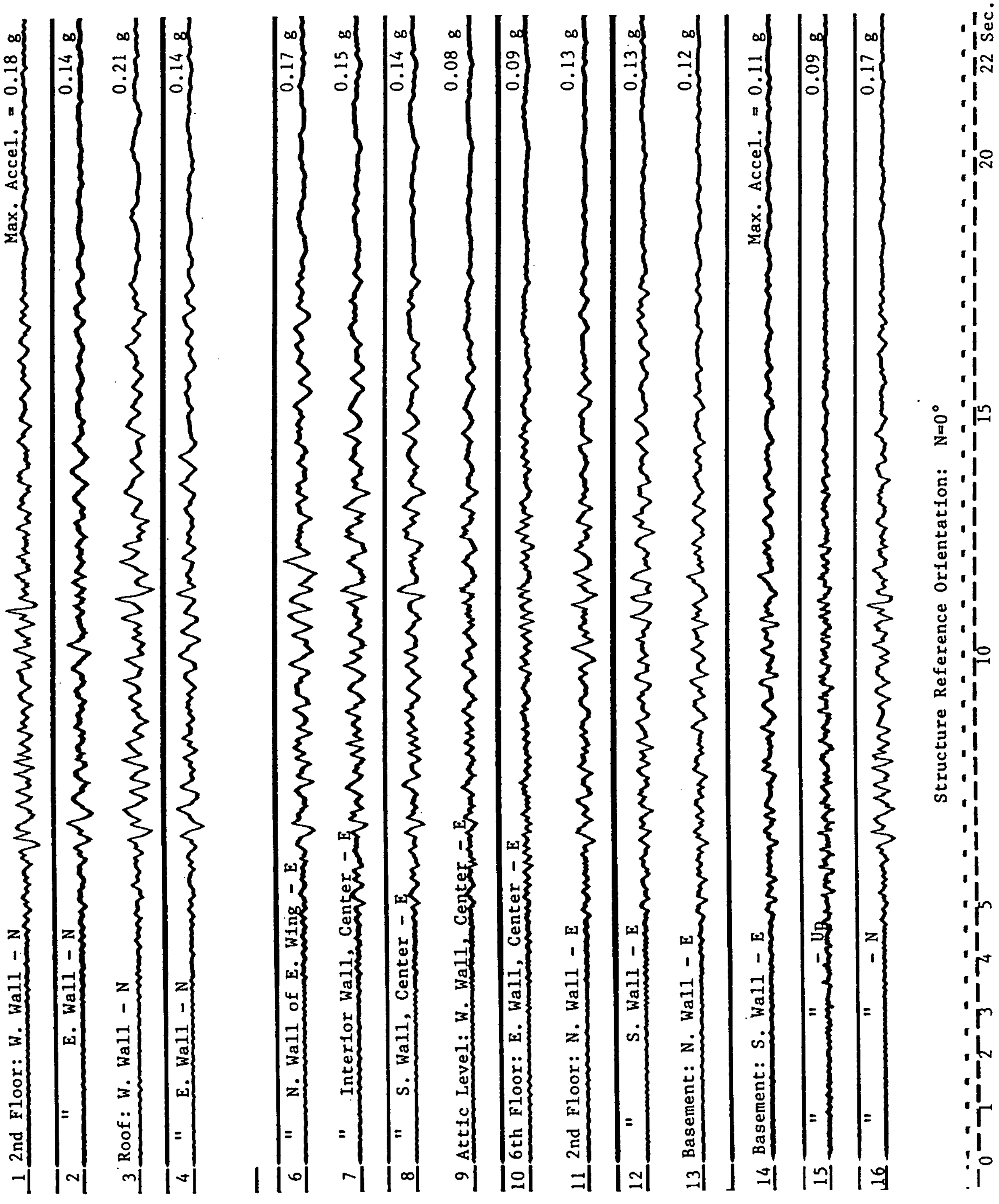

Figure 5.4.1 Accelerations recorded at the Pasadena 6-story office building during the 1994 Northridge Earthquake, (After Shakal, et al., 1994)

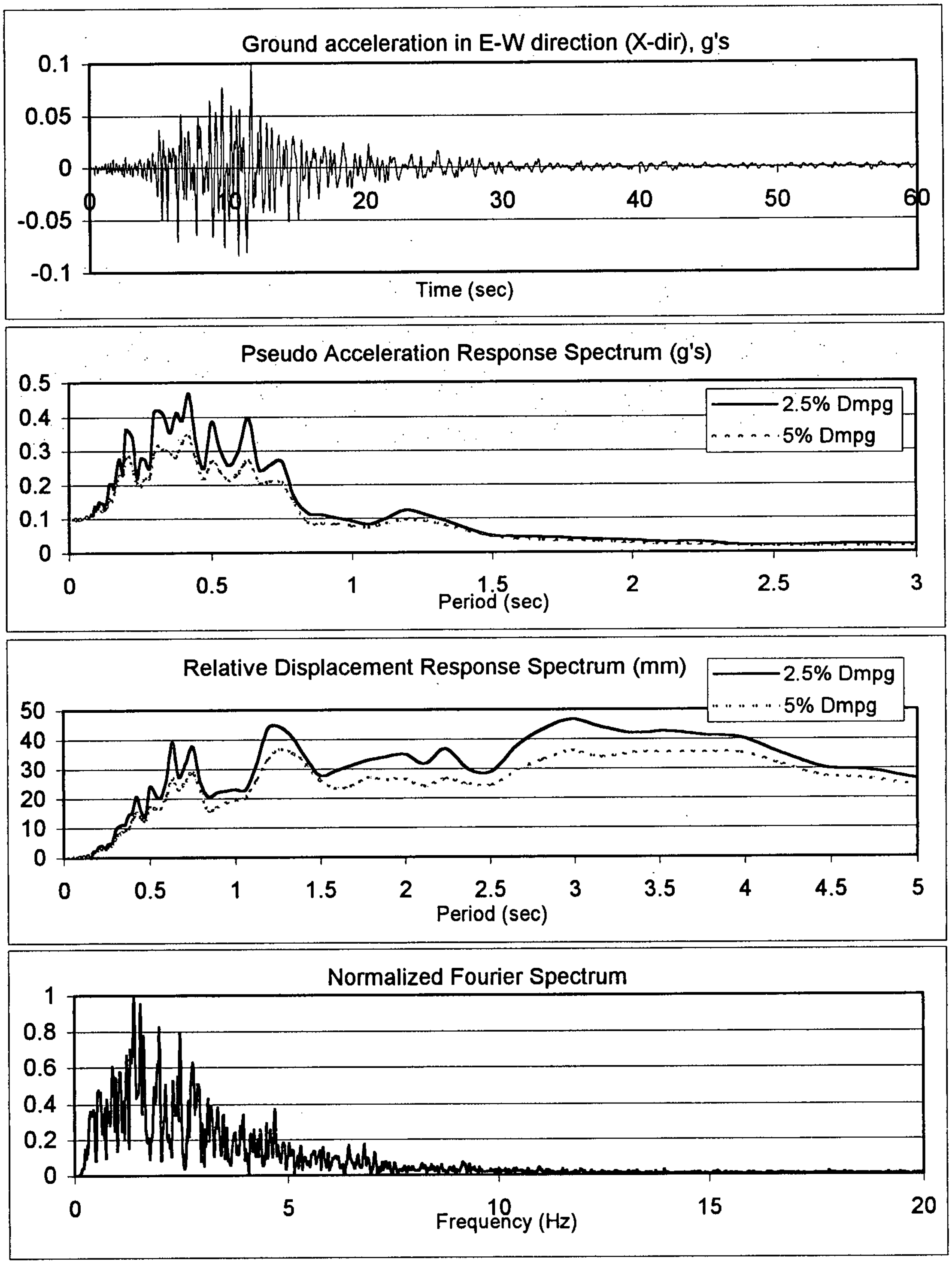

Figure 5.4.2 Time-history and spectral characteristics of E-W (X) component of the ground motion recorded at the Pasadena 6-story office bldg. during the 1994 Northridge EQ.

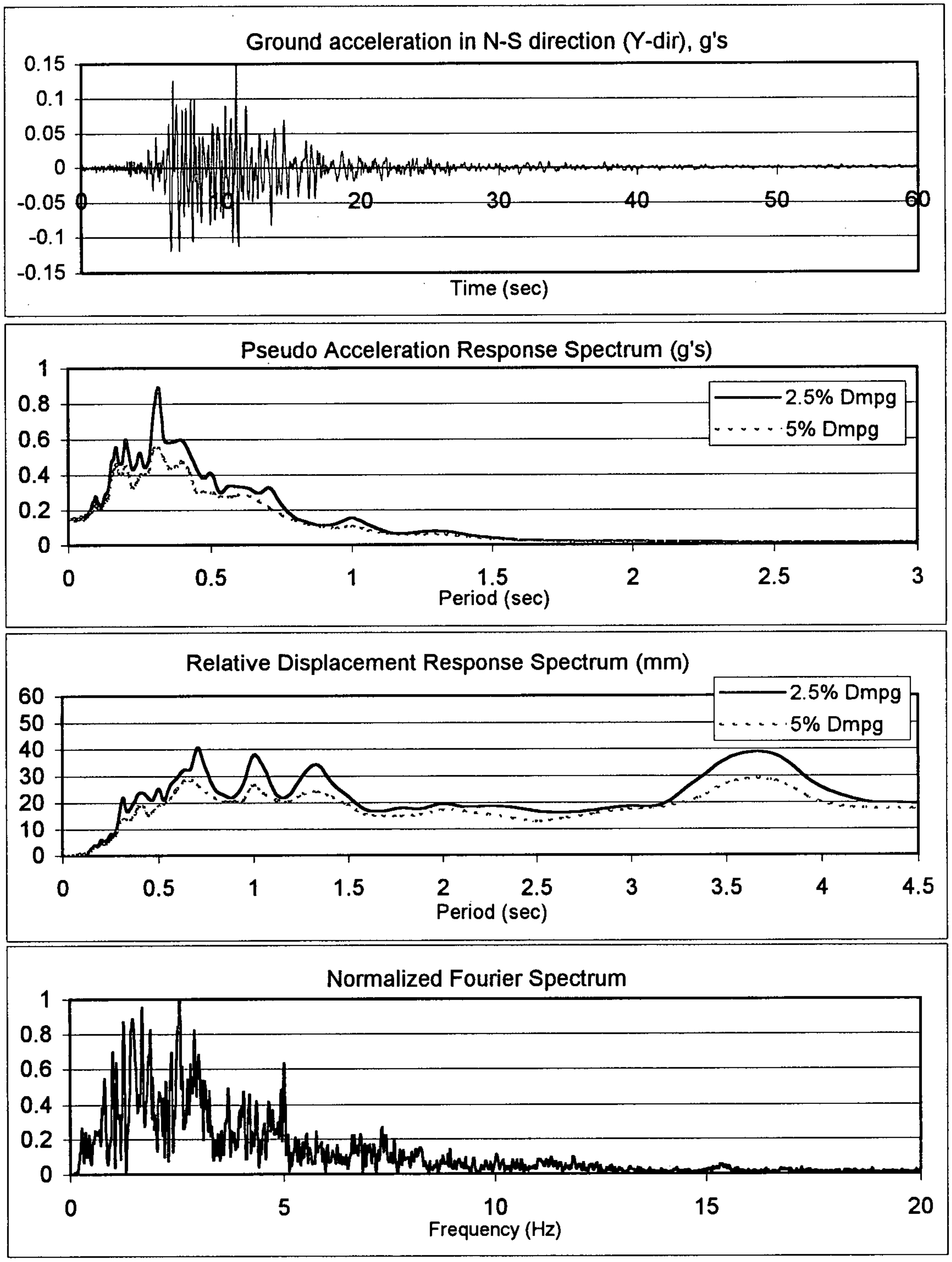

Figure 5.4.3 Time-history and spectral characteristics of N-S (Y) component of the ground motion recorded at the Pasadena 6-story office bldg. during the 1994 Northridge EQ.

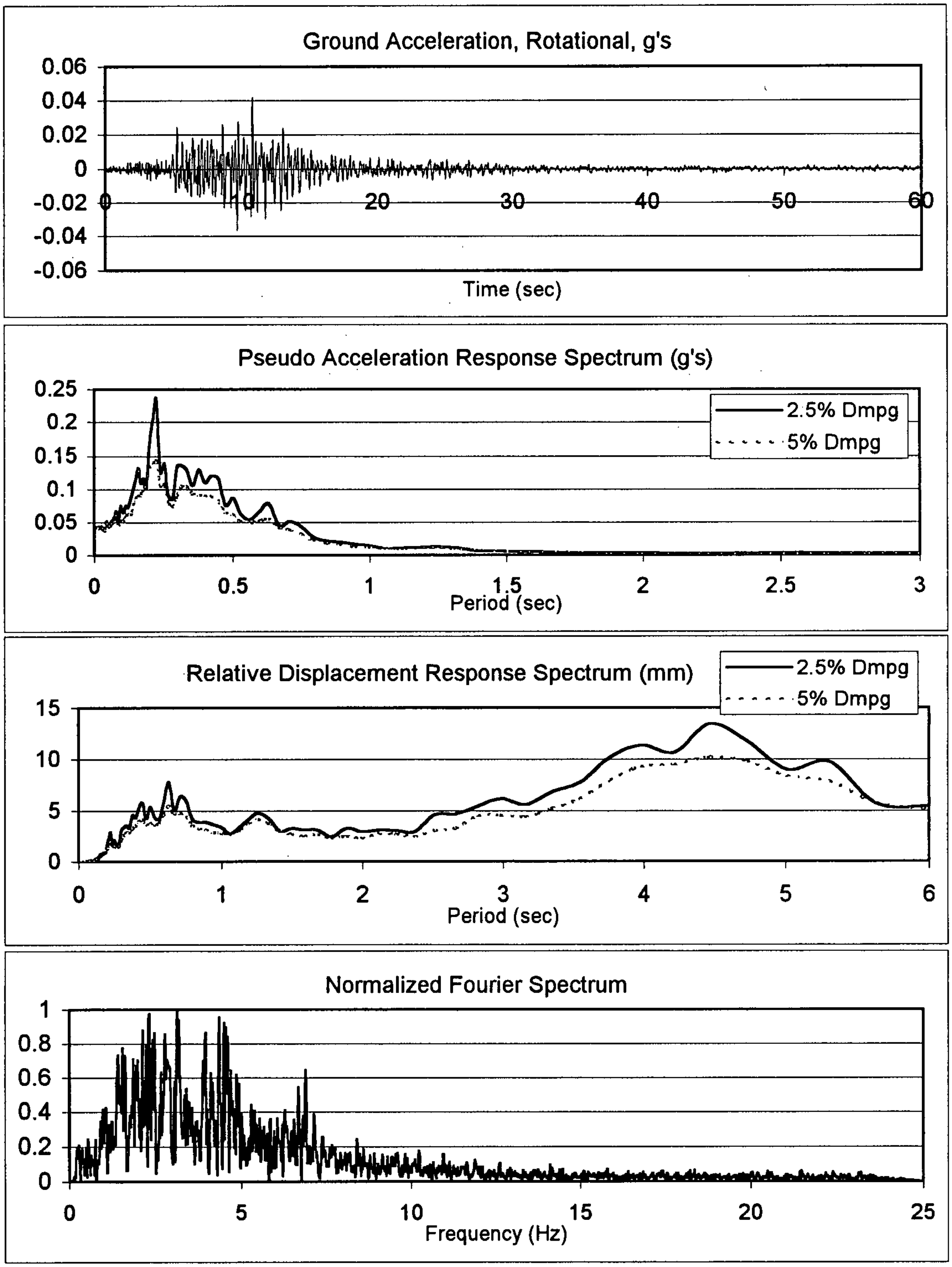

Figure 5.4.4 Time-history and spectral characteristics of rotational (R) component of the ground motion recorded at the Pasadena 6-story office bldg. during the 1994 Northridge EQ.

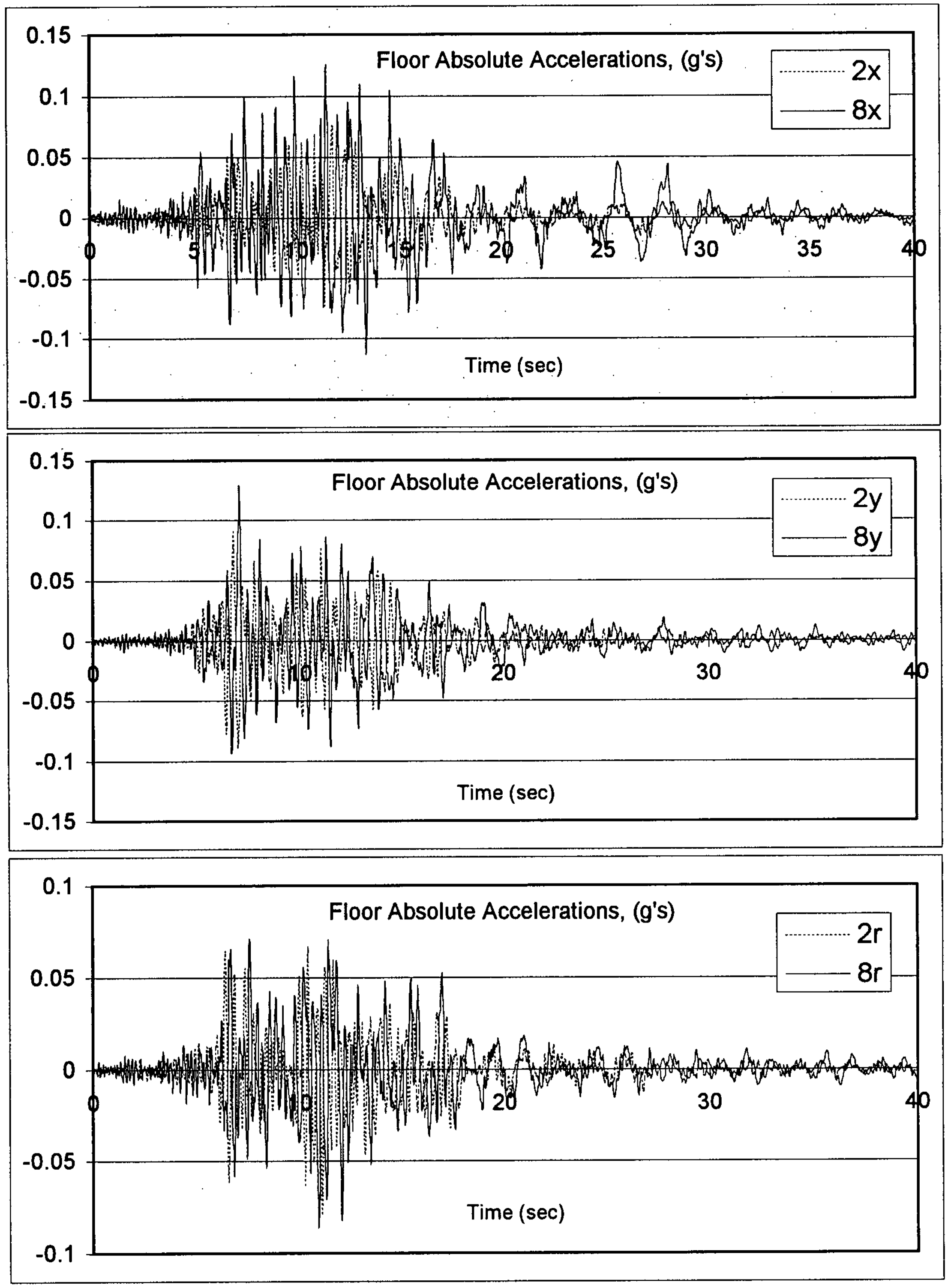

Figure 5.4.5 Absolute accelerations of the instrumented upper floors of the Pasadena 6-story office bldg., during the 1994 Northridge EQ.

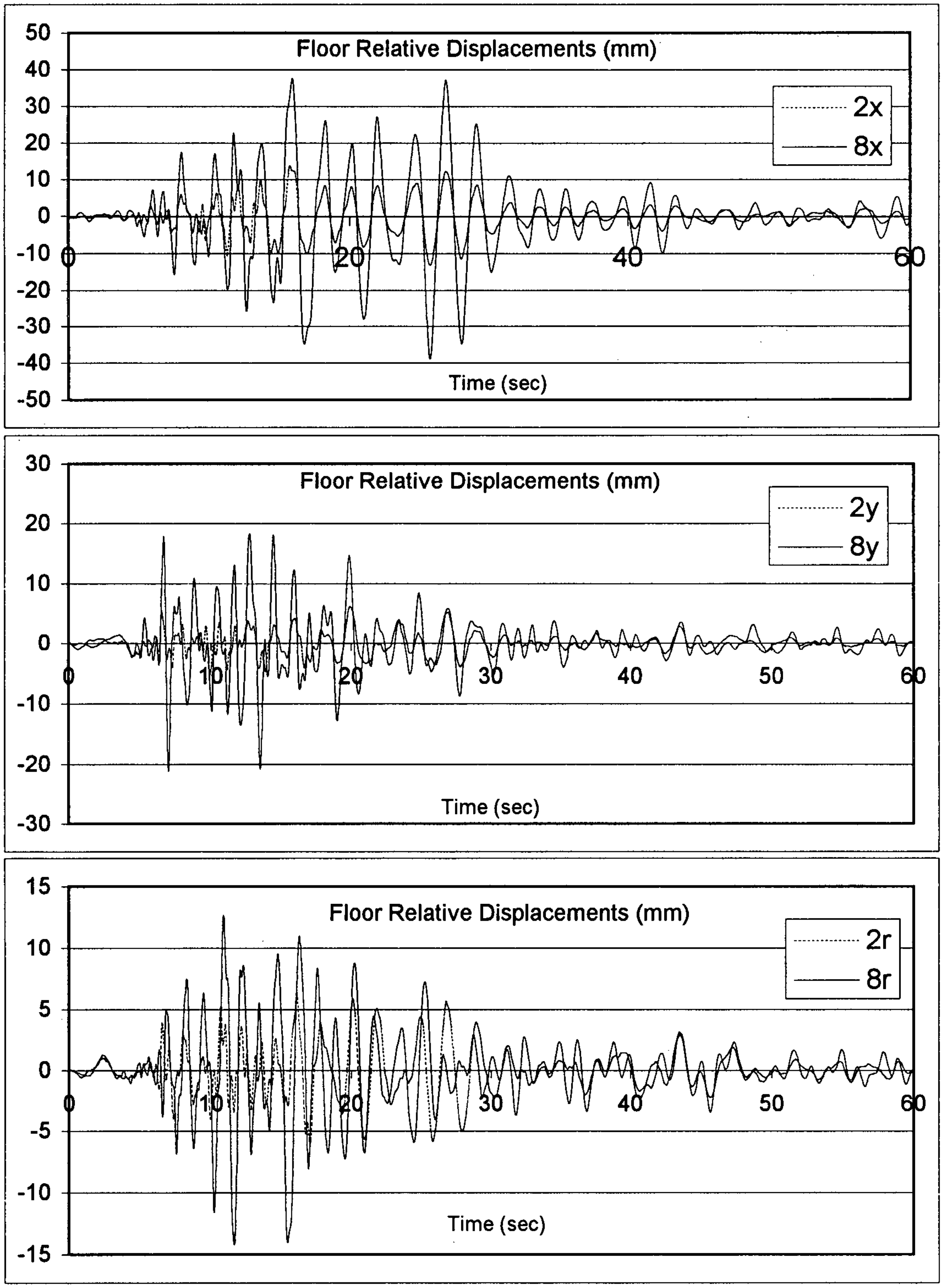

Figure 5.4.6 Relative displacements of the instrumented upper floors of the Pasadena 6-story office bldg. during the 1994 Northridge EQ.

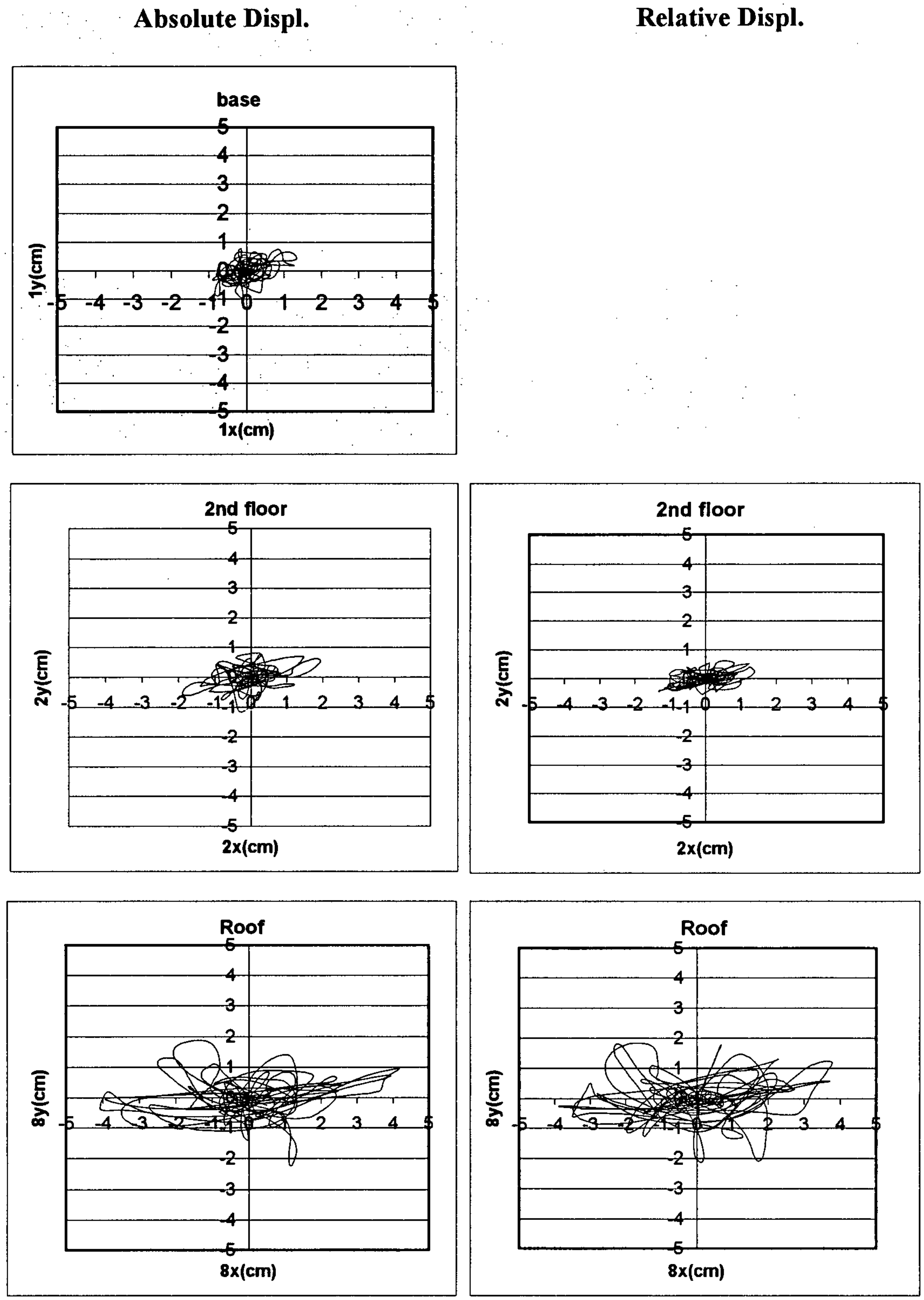

Figure 5.4.7 Orbital displacements at the center of the instrumented floors of the Pasadena 6-story office bldg. during the 1994 Northridge EQ.

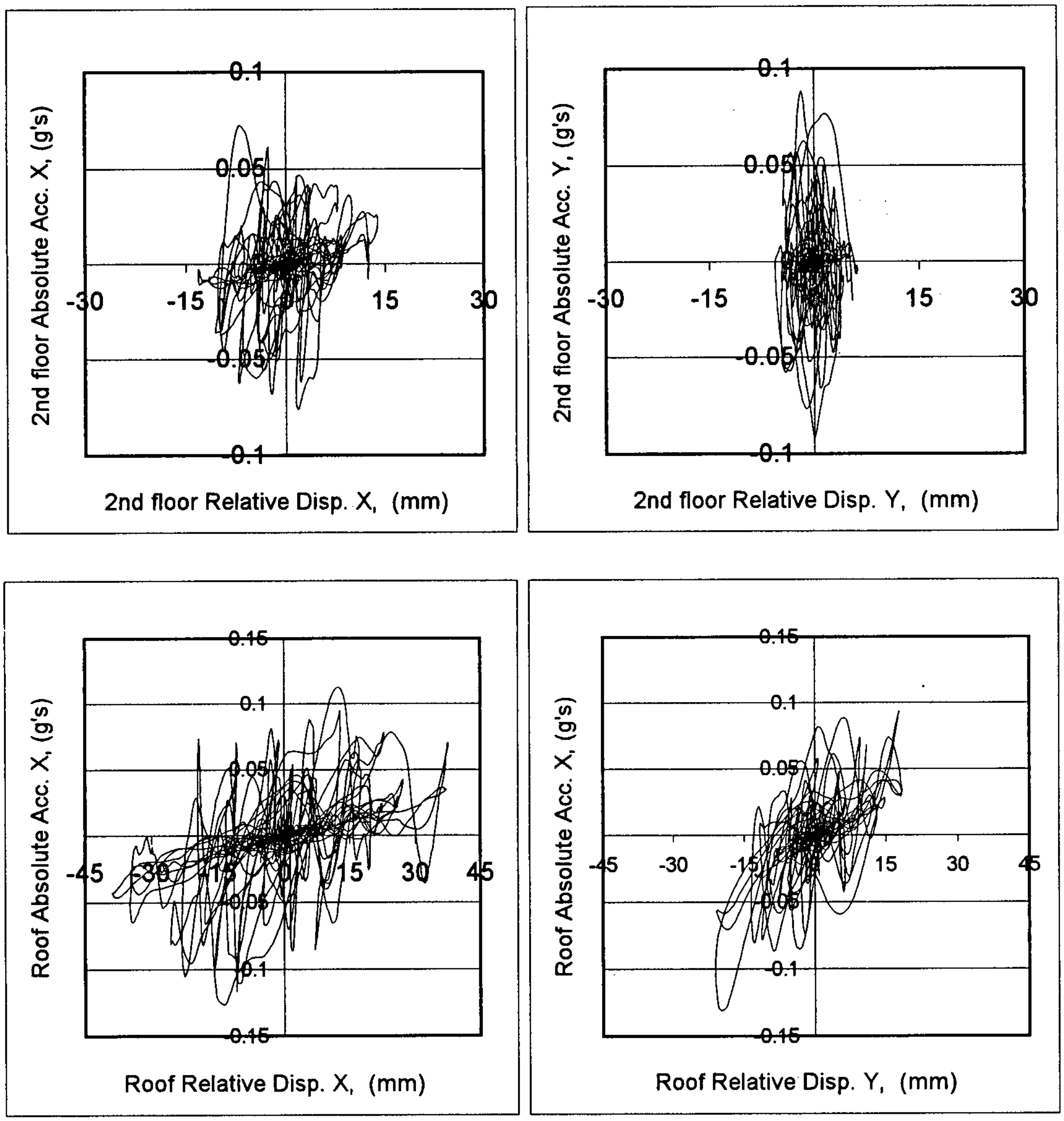

Figure 5.4.8 Representation of hysteretic behaviour at the instrumented floors of the Pasadena 6-story office bldg., during the 1994 Northridge EQ.

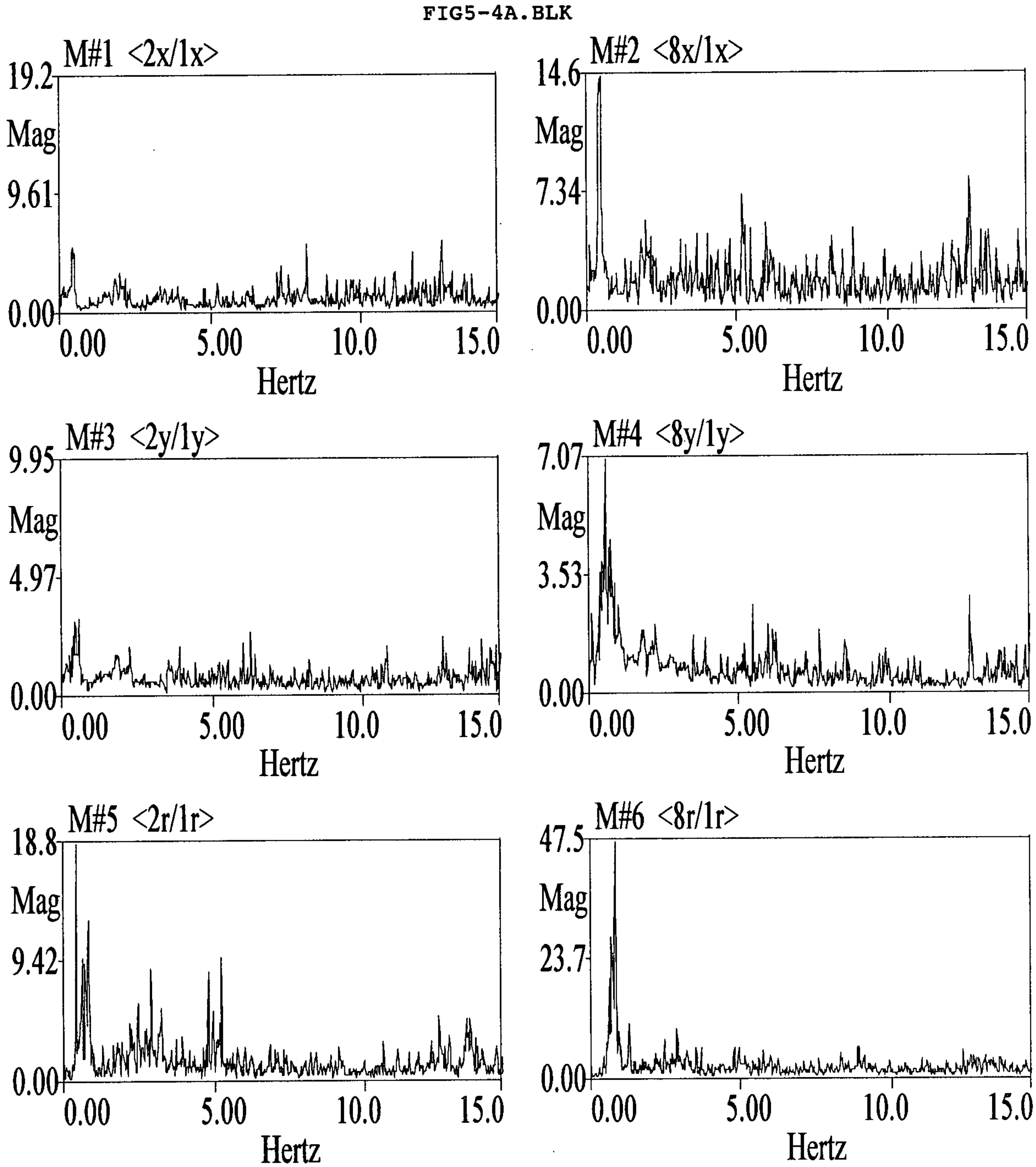

Figure 5.4.9a Frequency Response Functions of the instrumented floors of the Pasadena 6-story office bldg., obtained from the 1994 Northridge EQ Records. (With 5 averages).

Note: The FRF's are computed by ME'scope using a Hanning window, a block size N=2048 and 88% segment overlap.

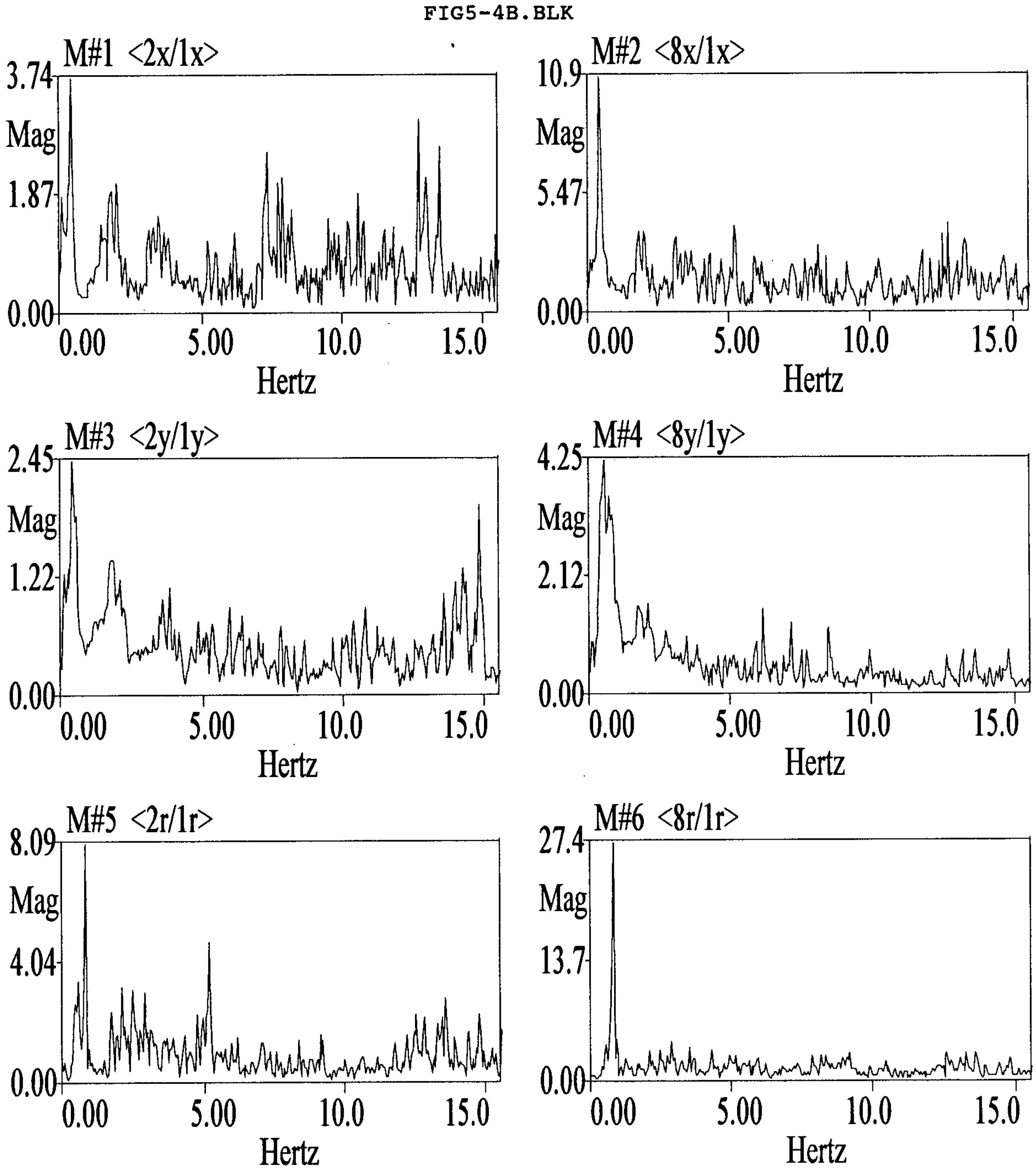

Figure 5.4.9b Frequency Response Functions of the instrumented floors of the Pasadena 6-story office bldg., obtained from the 1994 Northridge EQ records. (With 20 averages).

Note: The FRF's are computed by ME'scope using a Hanning window, a block size N=1024 and 90% segment overlap.

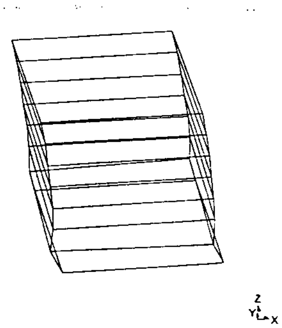

1X

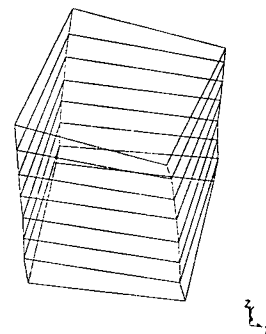

1R

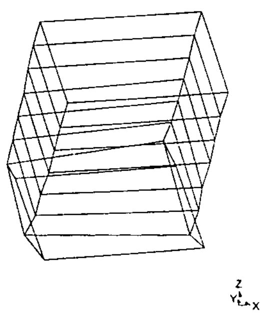

2X

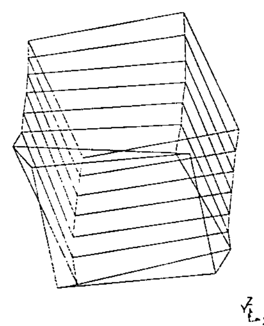

2R

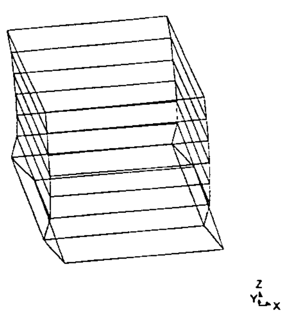

3X

Not obtained

3R

Figure 5.4.10 Mode shapes of the Pasadena 6-story office bldg., obtained from the 1994 Northridge EQ records.

Note: The displacements of levels 2 and 8 are obtained from measured data. Displacements of the other floors are based on ME'scope's interpolation algorithm.

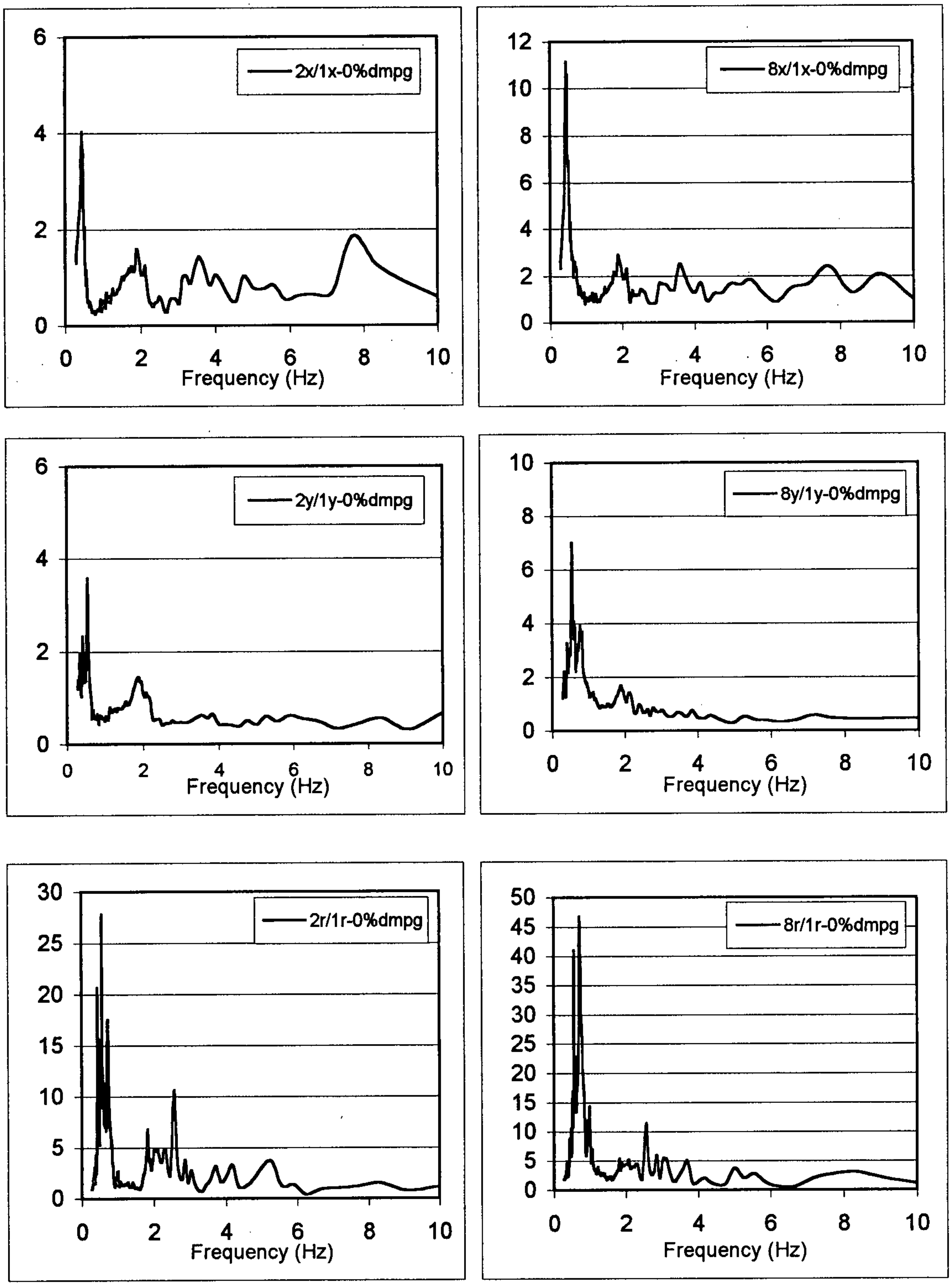

Figure 5.4.11 Spectral Response Functions of the Pasadena 6-story office bldg., obtained from the 1994 Northridge EQ records.

Table 5.4.1 Results of Frequency Response Functions for the San Bernardino 5-story hospital, obtained from the 1994 Northridge EQ records

X-direction			
Potential Mode #	Frequency (Hz)	Amplification Factor (2X/1X)	Amplification Factor (8X/1X)
1	0.45	5.32	14.7
2	1.81	2.82	4.42
3	3.32	2.00	4.09
Damping Ratio estimated by ME'scope for mode 1X: **3.90%**			
Y-direction			
Potential Mode #	Frequency (Hz)	Amplification Factor (2Y/1Y)	Amplification Factor (8Y/1Y)
1	0.59	3.22	7.08
2	2.22	2.07	2.00
3	3.89	1.96	1.62
Damping Ratio estimated by ME'scope for mode 1Y: **3.40%**			
R-direction			
Potential Mode #	Frequency (Hz)	Amplification Factor (2R/1R)	Amplification Factor (8R/1R)
1	0.84	12.85	47.6
2	2.47	6.01	7.32
3a	4.8	8.46	5.65
3b	5.2	9.75	1.43
Damping Ratio estimated by ME'scope for mode 1R: **2.00%**			

Table 5.4.2 Results of Spectral Response Functions for the San Bernardino 5-story hospital, obtained from the 1994 Northridge EQ records.

X-direction			
Potential Mode #	Frequency (Hz)	SRF 0% damping (2X/1X)	SRF 0% damping (8X/1X)
1	0.45	4.0	11.1
2	1.89	1.6	2.9
3	3.57	1.4	2.5
Y-direction			
Potential Mode #	Frequency (Hz)	SRF 0% damping (2Y/1Y)	SRF 0% damping (8Y/1Y)
1	0.55	3.6	7.0
2	2.13	1.1	1.4
3	-	-	-
R-direction			
Potential Mode #	Frequency (Hz)	SRF 0% damping (2R/1R)	SRF 0% damping (8R/1R)
1	0.72	17.6	46.2
2	2.56	10.5	11.5
3	-	-	-

Table 5.4.3 Estimated natural frequencies (and periods) of the Pasadena 6-story office building based on the results of FRF results, SRF results and visual inspection of the three dimensional mode shapes obtained from analysis of 1994 Northridge EQ data.

NORTHRIDGE EARTHQUAKE DATA						
	X-Direction (E-W)		Y-Direction (E-W)		Rotation	
	Frequency (Hz)	Period (S)	Frequency (Hz)	Period (S)	Frequency (Hz)	Period (S)
Mode1	0.45	2.22	0.58	1.72	0.82	1.22
Mode 2	1.85	0.54	2.20	0.45	2.50	0.40
Mode 3	3.40	0.29	3.9	0.26	-	-

*** Spectral values at the natural periods in the ground motion response spectra and the response time-histories suggest that the 2nd & 3rd modes had a significant contribution in the structural response.**

Fundamental Period according to **NBCC 1995**:

$\mathbf{T = 0.1\ N} \Longrightarrow \mathbf{T} = 0.70$ sec

$\mathbf{T = 0.085\ (h_n)^{3/4}} = 0.085\ (25.0\text{m})^{3/4} = 0.95$ sec

Fundamental Period according to **UBC 1997**:

$\mathbf{T = 0.035\ (h_n)^{3/4}} = 0.035\ (82\text{ ft})^{3/4} = 0.95$ sec

5.5 San Jose 3-Story Office Building

Properties of the Strong Motion Data:

Record Length: 50 sec

Time interval: 0.02 sec

No. of data points for each channel: 2500

Usable frequency range: 0.16 Hz to 23.0 Hz

Manipulating the data to obtain the motion of the center of the building in the 3 directions, E-W (or X-directions) , N-S (or Y-directions) and rotation about vertical axis (or R-component):

1X = - Chan2 , 1Y = (Chan3 + Chan4)/2 , 1R = (Chan3-Chan4)/2

3X = - Chan5 , 3Y = (Chan6 + Chan7)/2 , 3R = (Chan6-Chan7)/2

4X = - Chan8 , 4Y = (Chan9 + Chan10)/2 , 4R = (Chan9-Chan10)/2

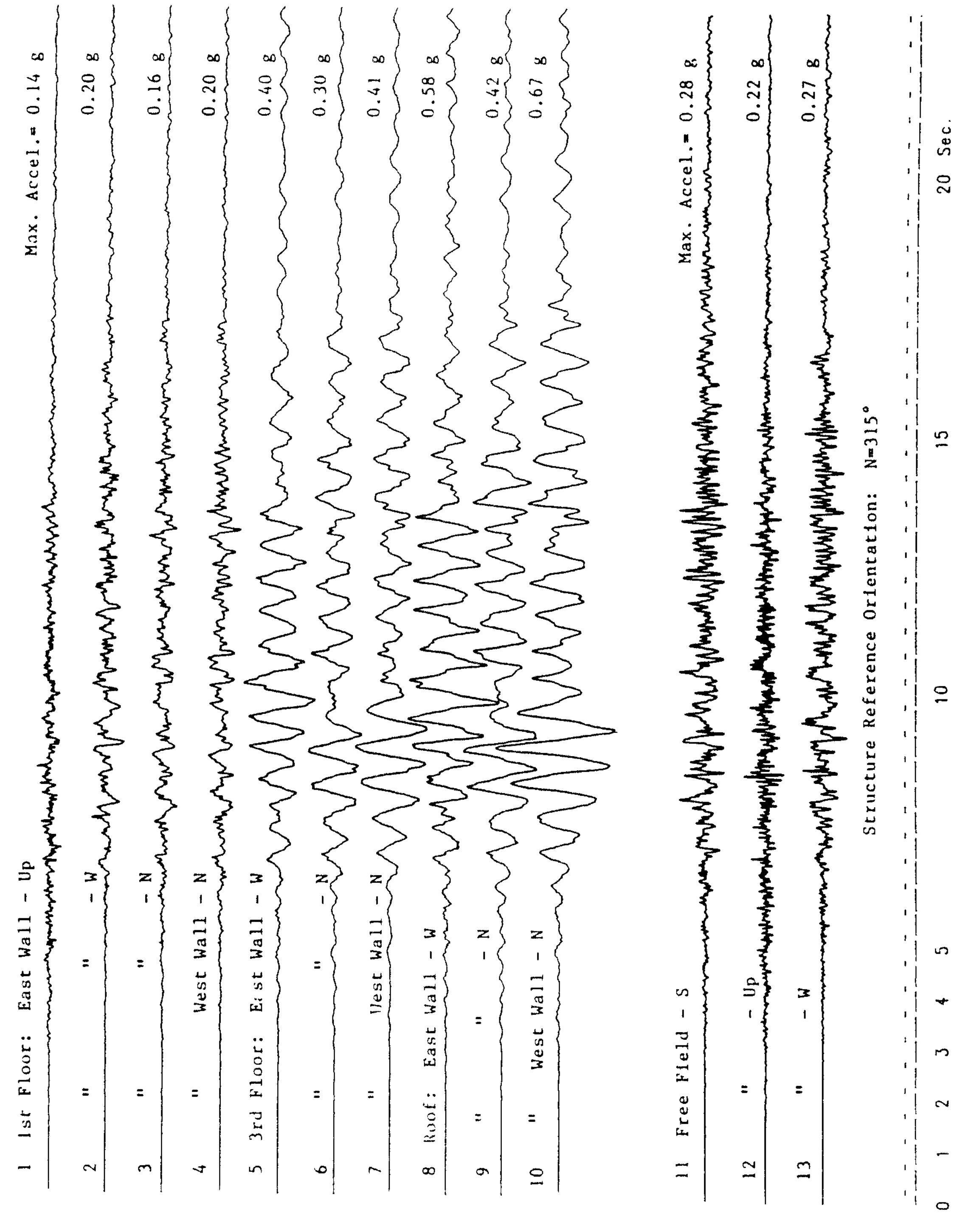

Figure 5.5.1 Accelerations recorded at the San Jose 3-story office building during the 1989 Loma Prieta EQ. (After Shakal, et al., 1989)

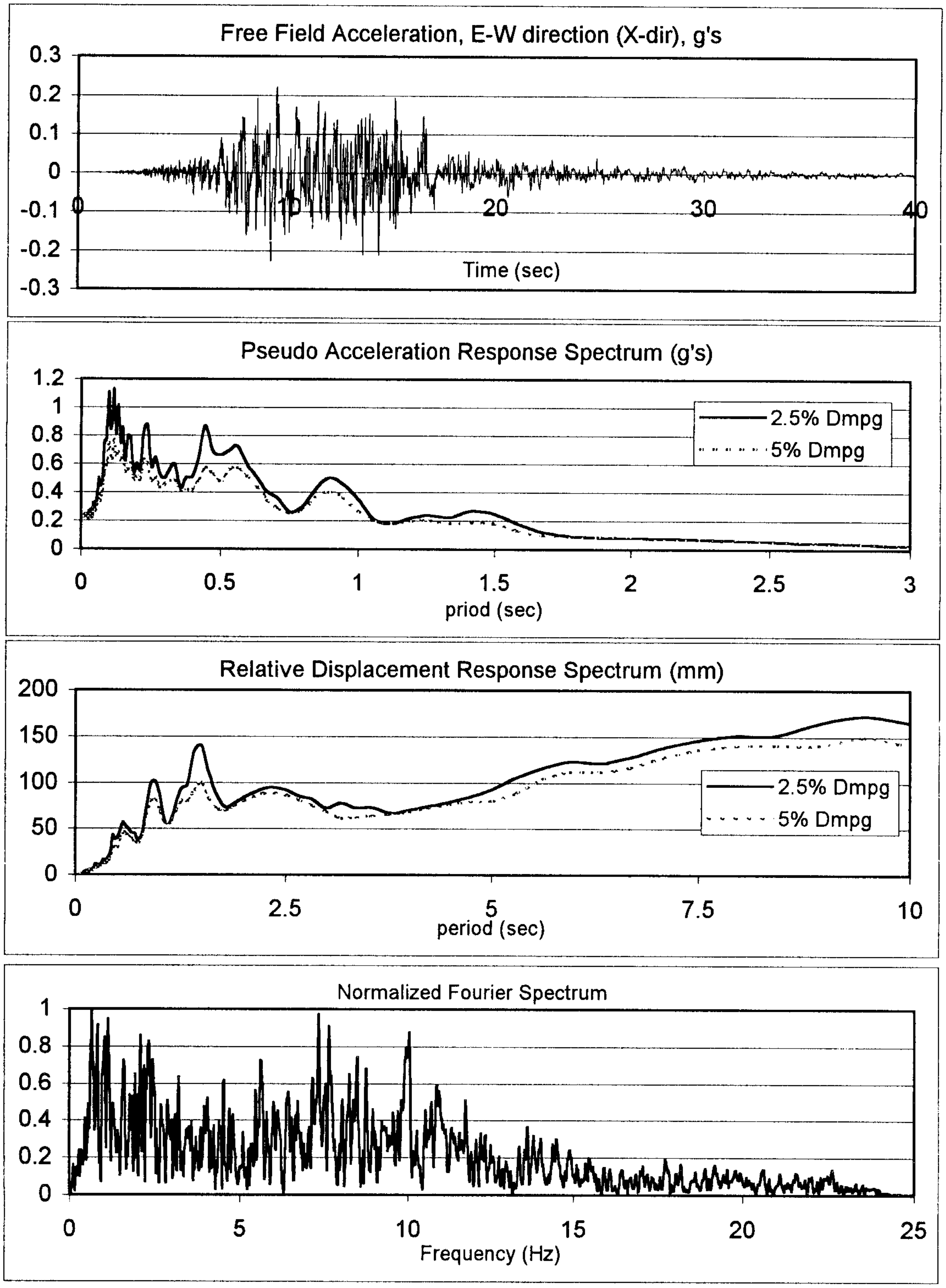

Figure 5.5.2 Time-history and spectral characteristics of E-W (X) component of the free field motion recorded at the San Jose 3-story office bldg., during the 1989 Loma Prieta EQ.

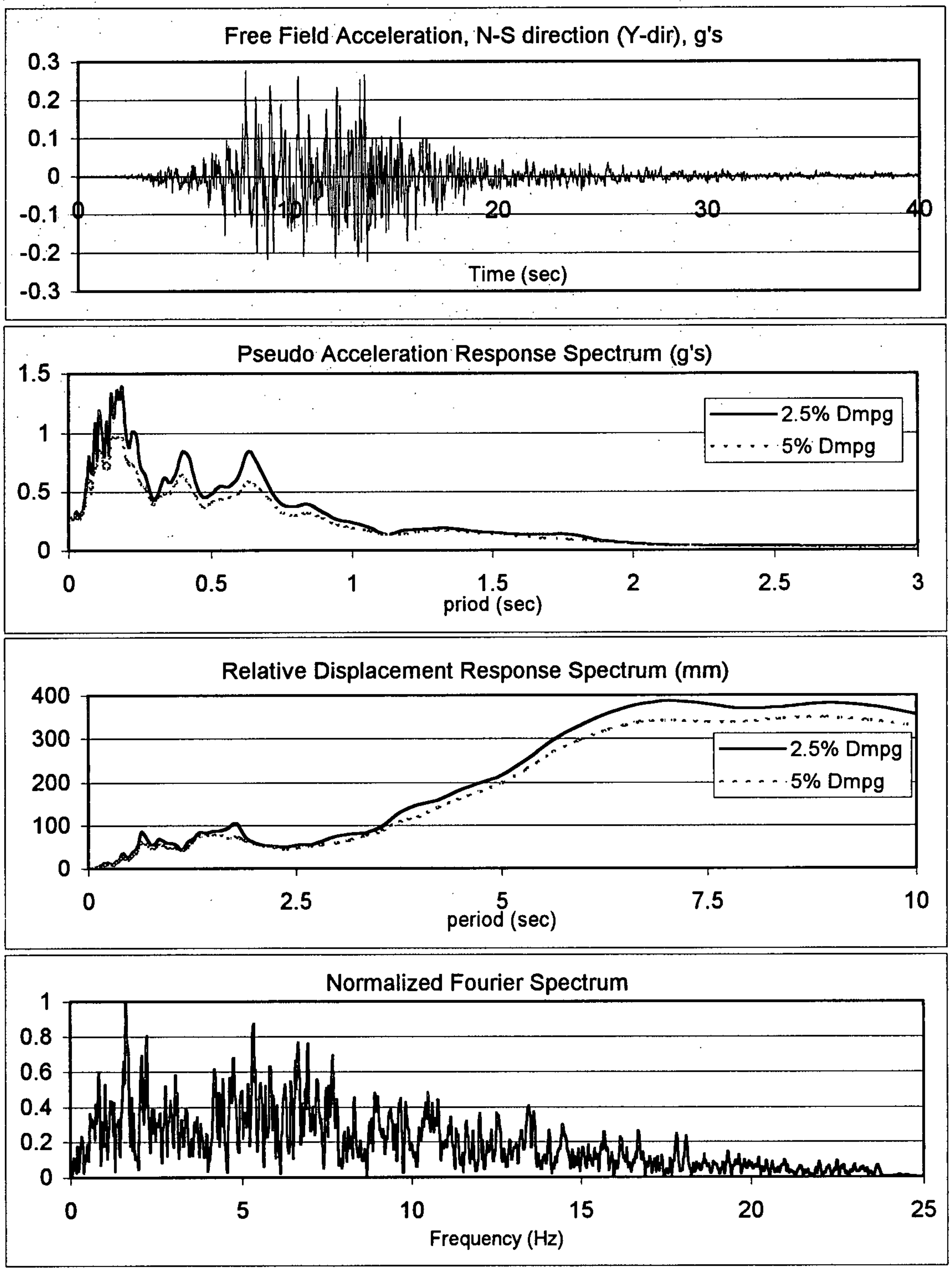

Figure 5.5.3 Time-history and spectral characteristics of N-S (Y) component of the free field motion recorded at the San Jose 3-story office bldg., during the 1989 Loma Prieta EQ.

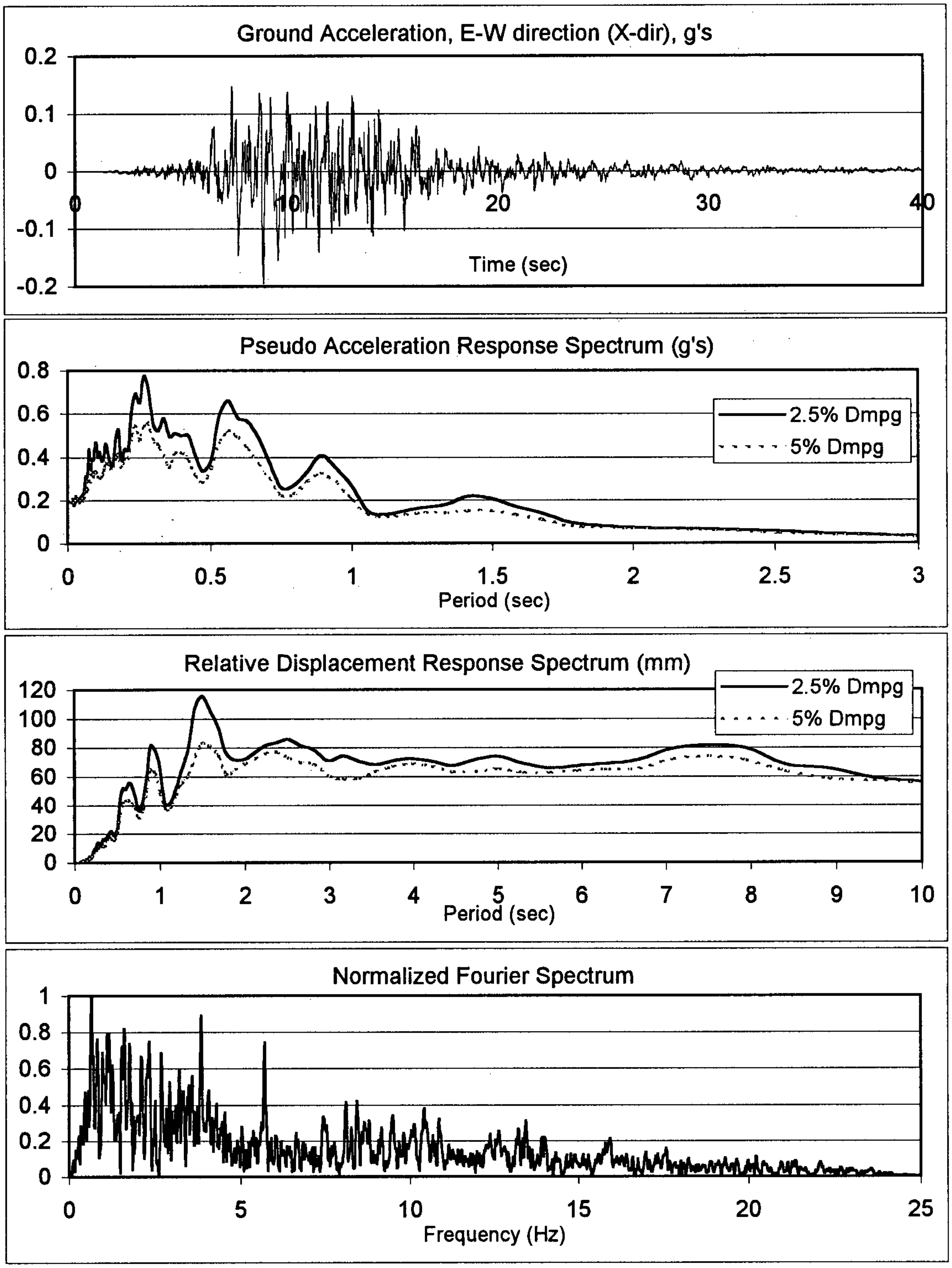

Figure 5.5.4 Time-history and spectral characteristics of E-W (X) component of the ground motion recorded at the San Jose 3-story office bldg., during the 1989 Loma Prieta EQ.

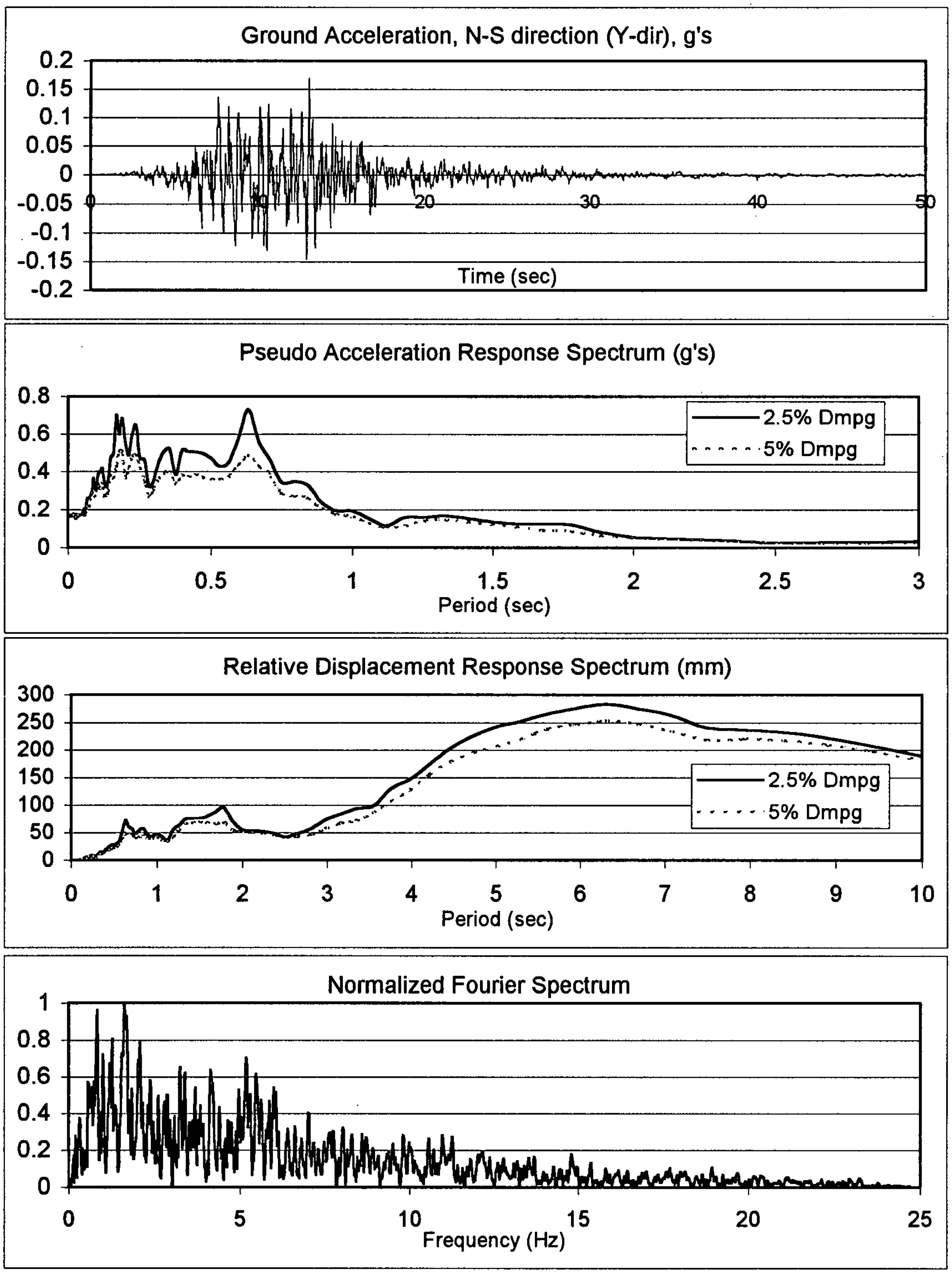

Figure 5.5.5 Time-history and spectral characteristics of N-S (Y) component of the ground motion recorded at the San Jose 3-story office bldg., during the 1989 Loma Prieta EQ.

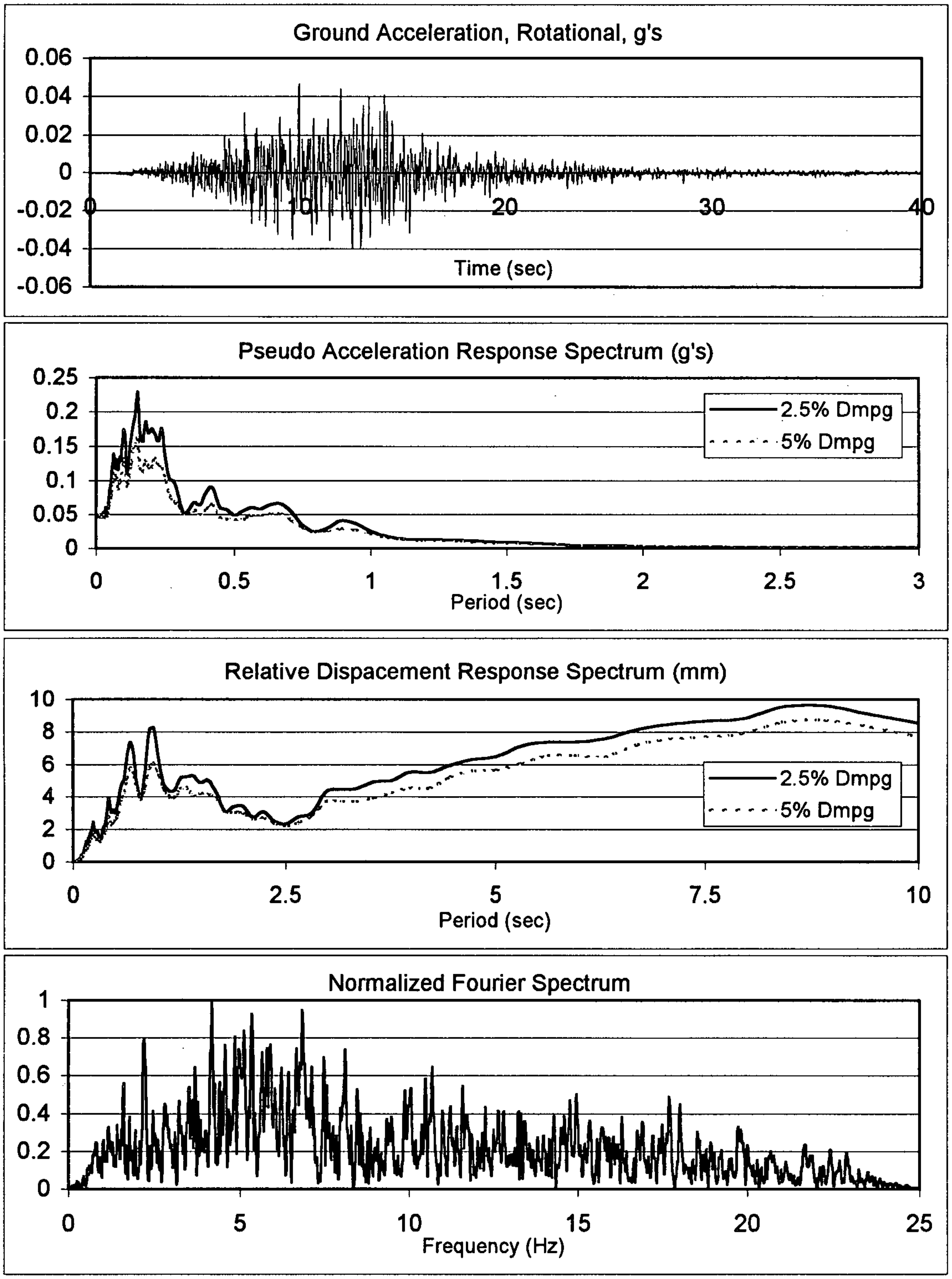

Figure 5.5.6 Time-history and spectral characteristics of rotational (R) component of the ground motion recorded at the San Jose 3-story office bldg., during the 1989 Loma Prieta EQ.

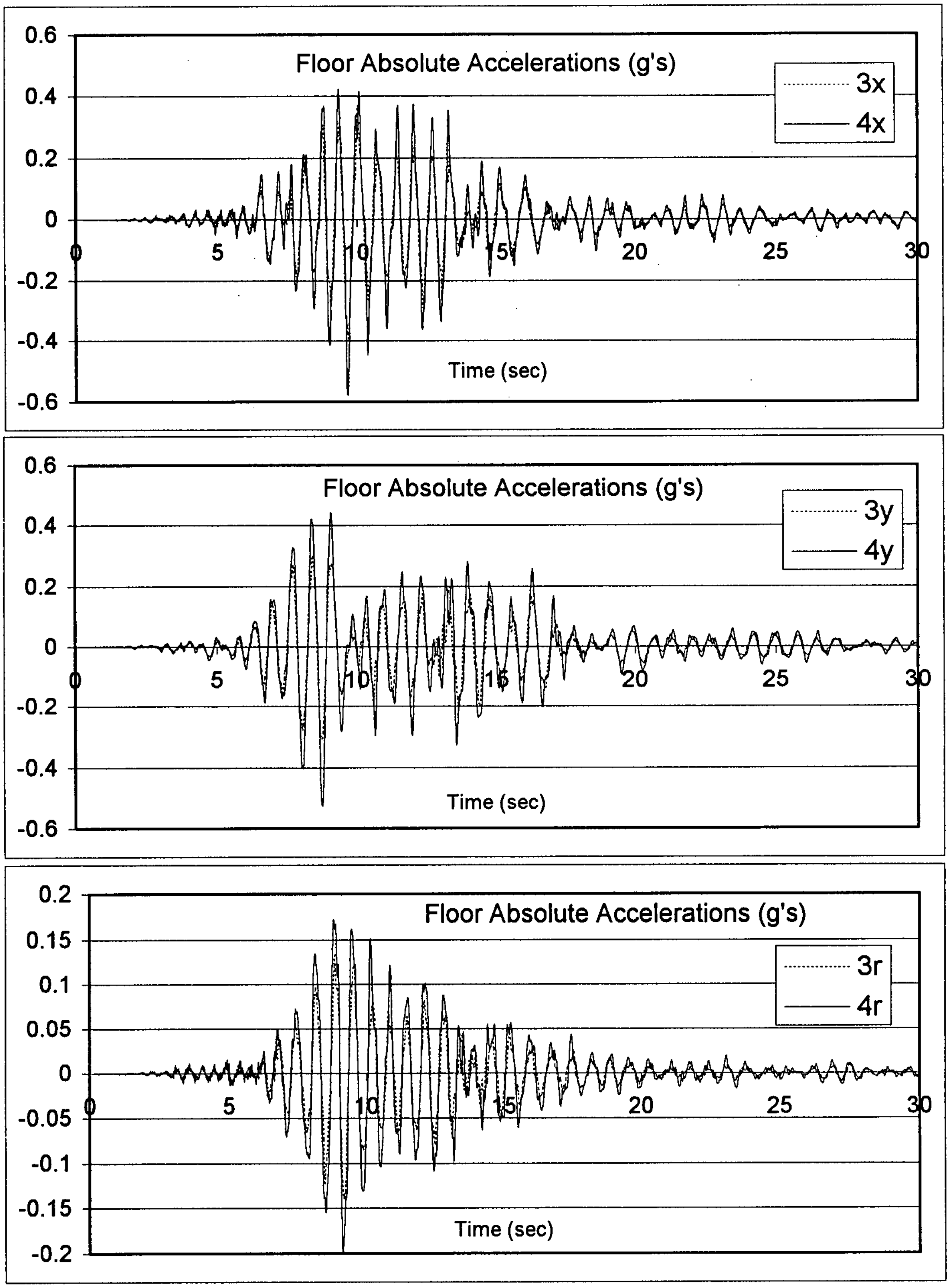

Figure 5.5.7 Absolute accelerations of the instrumented upper floors of the San Jose 3-story office bldg., during the 1989 Loma Prieta EQ.

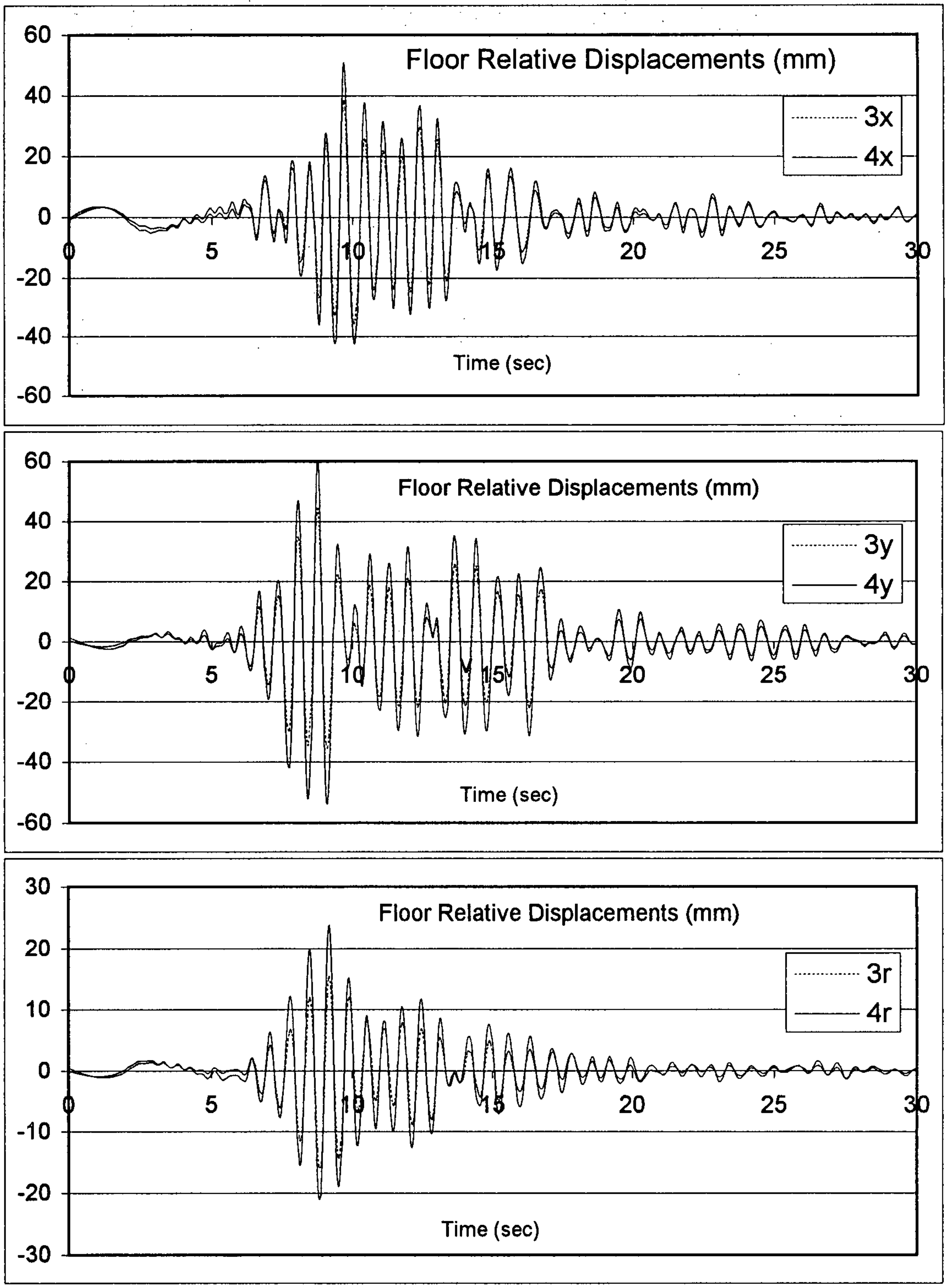

Figure 5.5.8 Relative displacements of the instrumented upper floors of the San Jose 3-story office bldg., during the 1989 Loma Prieta EQ.

Absolute Displ. **Relative Displ.**

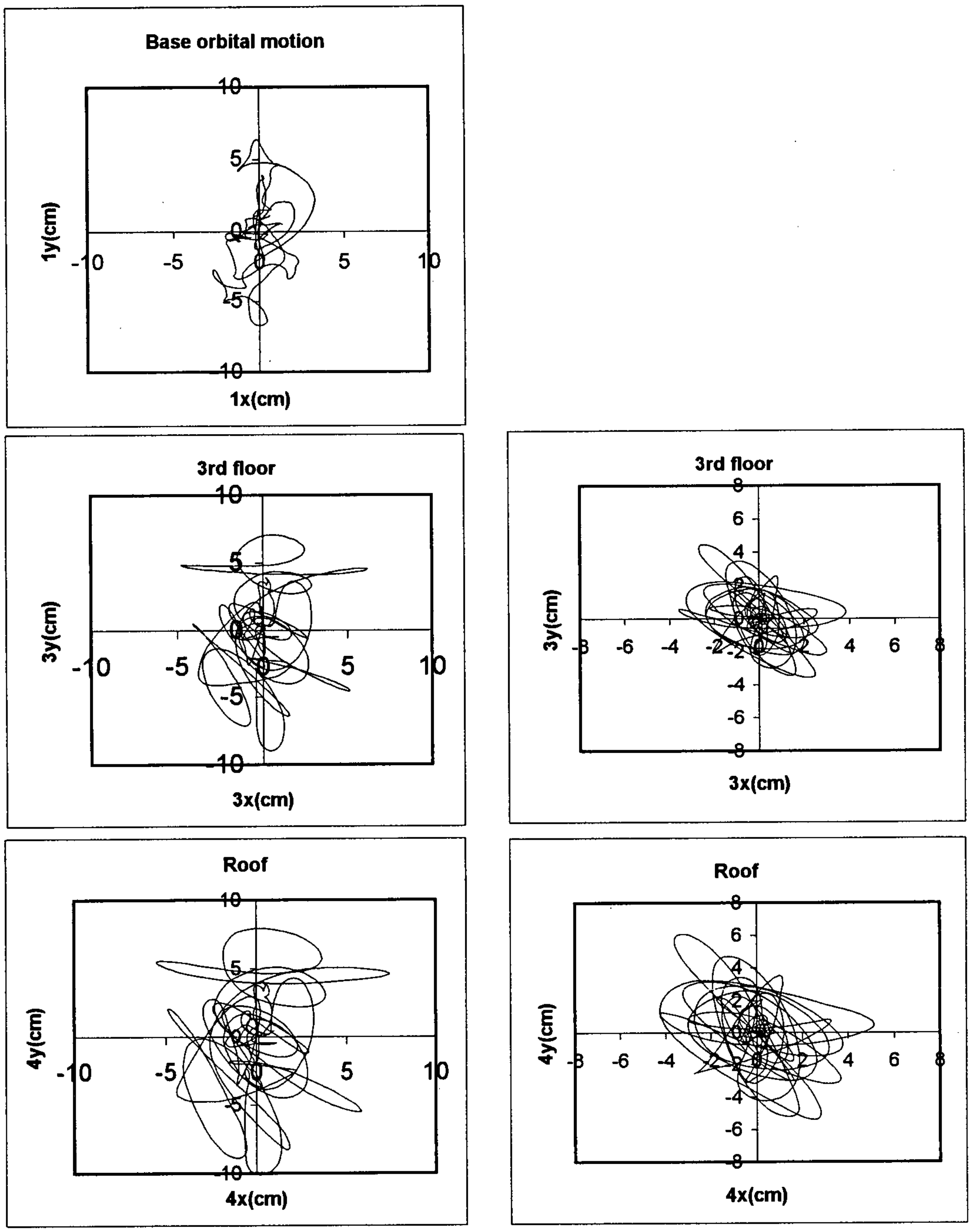

Figure 5.5.9 Orbital displacements at the center of the instrumented floors of the San Jose 3-story office bldg., during the 1989 Loma Prieta EQ.

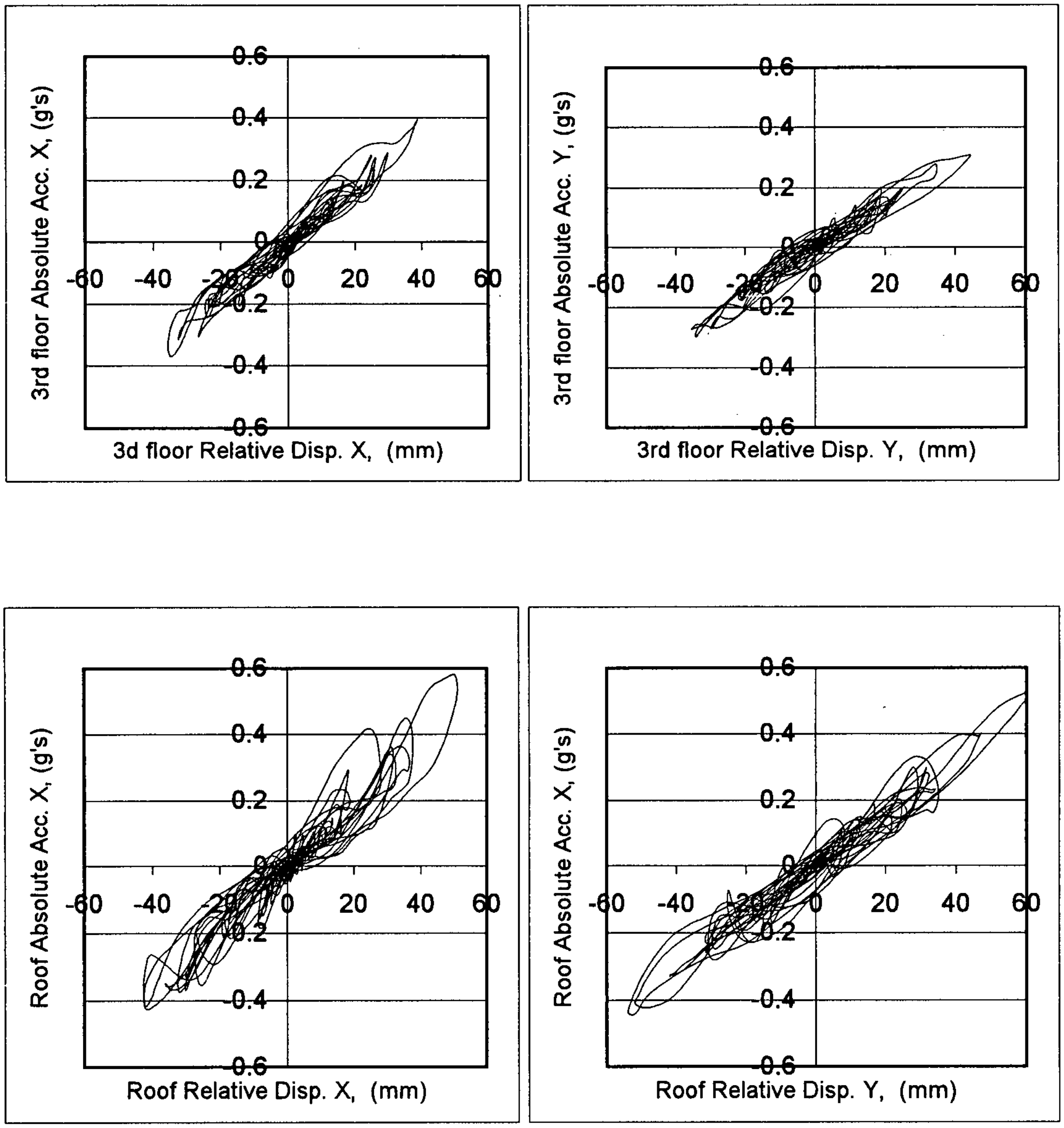

Figure 5.5.10 Representation of hysteretic behaviour at the instrumented floors of the San Jose 3-story office bldg., during the 1989 Loma Prieta EQ.

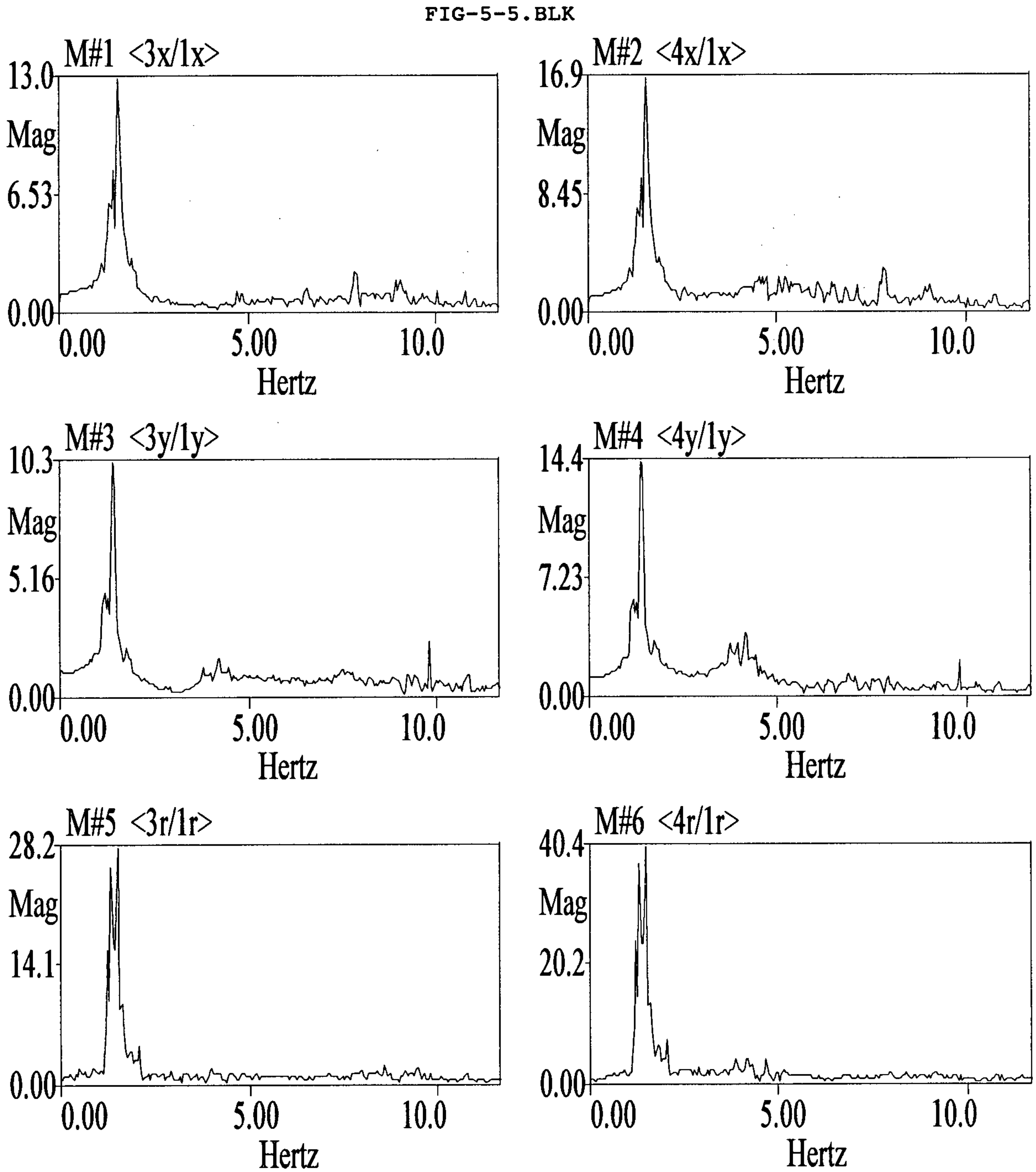

Figure 5.5.11 Frequency Response Functions of the instrumented floors of the San Jose 3-story office bldg., obtained from the 1989 Loma Prieta EQ records.

Note: The FRF's are computed by ME'scope using a Hanning window, a block size N=2048, 3 averages and 89% segment overlap.

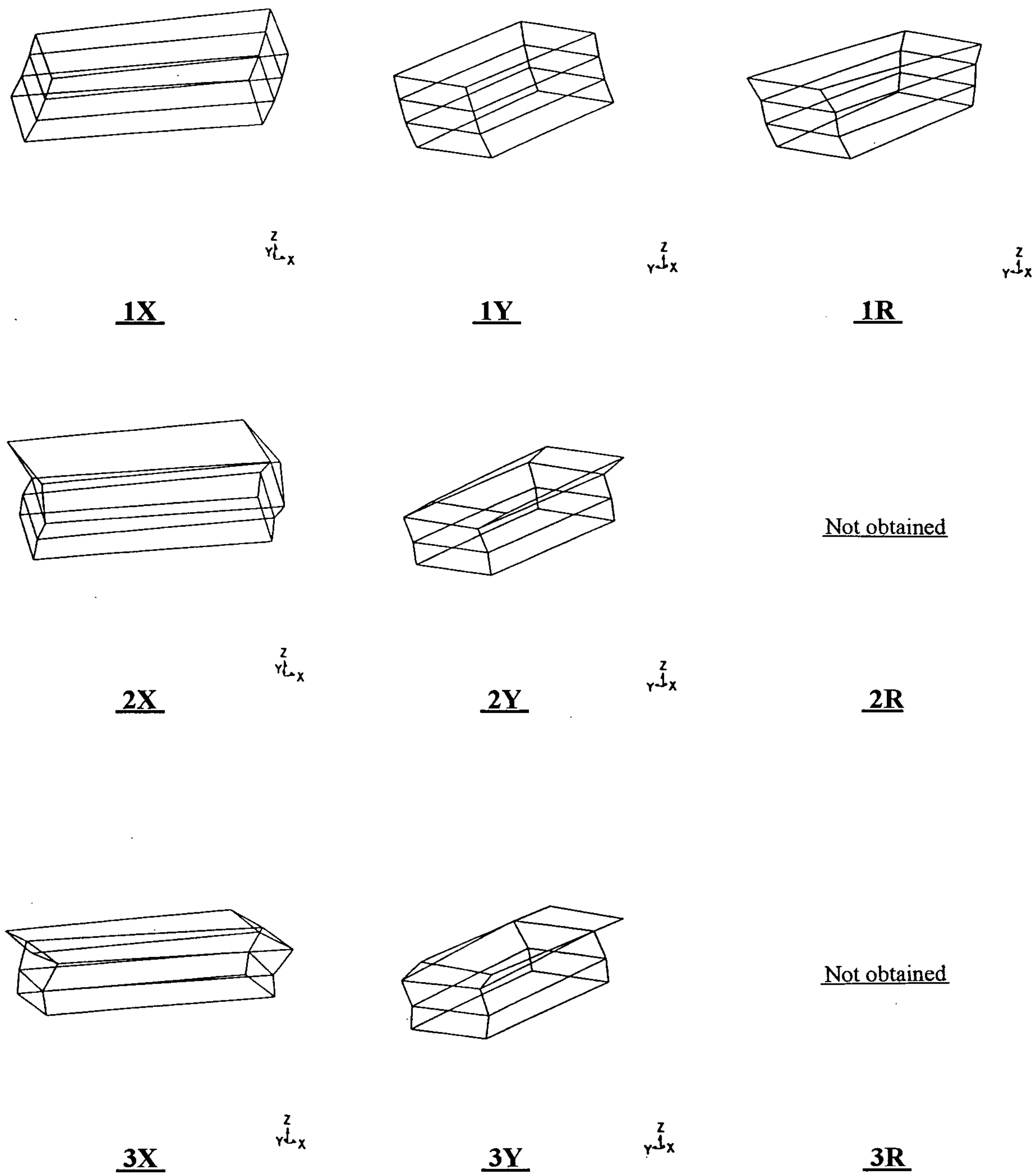

Figure 5.5.12 Mode shapes of the San Jose 3-story office bldg., obtained from the 1989 Loma Prieta EQ records.

Note: The displacements of levels 3 and 4 (roof) are obtained from measured data. Displacements of the other floors are based on ME'scope's interpolation algorithm.

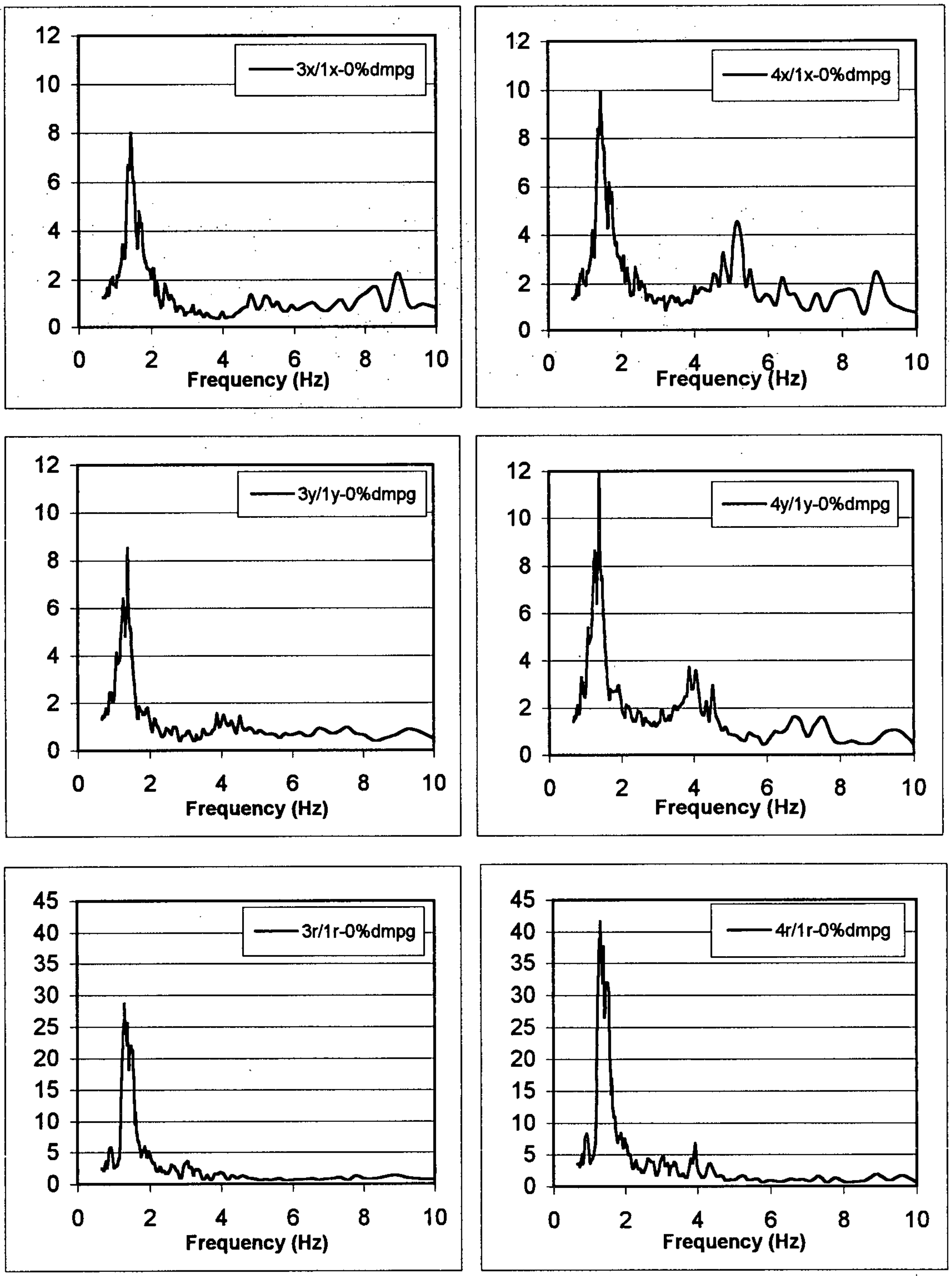

Figure 5.5.13 Spectral Response Functions of the San Jose 3-story office bldg., obtained from the 1989 Loma Prieta EQ records.

Table 5.5.1 Results of Frequency Response Functions for the San Jose 3-story office bldg., obtained from the 1989 Loma Prieta EQ records

X-direction			
Potential Mode #	Frequency (Hz)	Amplification Factor (3X/1X)	Amplification Factor (4X/1X)
1	1.562	13.1	16.9
2	4.69	1.12	2.51
3	7.81	2.16	3.10
Damping Ratio estimated by ME'scope for mode 1X: **4.70%**			
Y-direction			
Potential Mode #	Frequency (Hz)	Amplification Factor (3Y/1Y)	Amplification Factor (4Y/1Y)
1	1.37	10.3	14.5
2	4.15	1.64	3.74
3	6.68	0.67	1.27
Damping Ratio estimated by ME'scope for mode 1Y: **2.10%**			
R-direction			
Potential Mode #	Frequency (Hz)	Amplification Factor (3R/1R)	Amplification Factor (4R/1R)
1	2.05	4.45	7.07
2	-	-	-
Damping Ratio estimated by ME'scope for mode 1R: **0.40%**			

Table 5.5.2 Results of Spectral Response Functions for the San Jose 3-story office bldg., obtained from the 1989 Loma Prieta EQ records.

X-direction			
Potential Mode #	Frequency (Hz)	SRF 0% damping (3X/1X)	SRF 0% damping (4X/1X)
1	1.453	8.02	9.93
2	5.17	1.31	4.55
3	-	-	-

Y-direction			
Potential Mode #	Frequency (Hz)	SRF 0% damping (3Y/1Y)	SRF 0% damping (4Y/1Y)
1	1.39	8.5	12.0
2	4.06	1.5	3.60
3a	6.73	0.9	1.60
3b	7.55	1.0	1.60

Note: The SRF's did not provide usable information for torsional modes.

Table 5.5.3 Estimated natural frequencies (and periods) of the San Jose 3-story office bldg. based on the results of FRF results, SRF results and visual inspection of the three dimensional mode shapes obtained from analysis of 1989 Loma Prieta EQ data.

LOMA PRIETA EARTHQUAKE DATA						
	X-Direction (E-W)		Y-Direction (E-W)		Rotation	
	Frequency (Hz)	Period (S)	Frequency (Hz)	Period (S)	Frequency (Hz)	Period (S)
Mode1	1.56	0.64	1.37	0.73	2.05	0.49
Mode 2	4.80	0.21	4.15	0.24	-	-
Mode 3	7.80	0.13	6.70	0.15	-	-

*** Spectral values at the natural periods in the ground motion response spectra and the response time-histories suggest that the 1st mode dominated the structural response.**

Fundamental Period according to **NBCC 1995**:

$\mathbf{T = 0.1\ N} \Longrightarrow \mathbf{T} = 0.30$ sec

$\mathbf{T = 0.085\ (h_n)^{3/4}} = 0.085\ (15.09\text{m})^{3/4} = 0.65$ sec

Fundamental Period according to **UBC 1997**:

$\mathbf{T = 0.035\ (h_n)^{3/4}} = 0.035\ (49.5\ \text{ft})^{3/4} = 0.65$ sec

5.6 San Francisco 4-Story Hospital

Properties of the Strong Motion Data:

Record Length: 40 sec

Time interval: 0.02 sec

No. of data points for each channel: 2000

Usable frequency range: 0.16 Hz to 23.0 Hz

Manipulating the data to obtain the motion of the center of the building in the 3 directions, E-W (or X-directions) , N-S (or Y-directions) and rotation about vertical axis (or R-component):

0X = - Chan1 , 0Y = Chan3

1X = - (Chan5 + Chan4)/2 , 1R = (Chan5-Chan4)/2

2X = - Chan6 , 2Y = Chan7 , 2R = (Chan8-Chan6)

5X = - Chan9 , 5Y = Chan10 , 5R = (Chan11-Chan9)

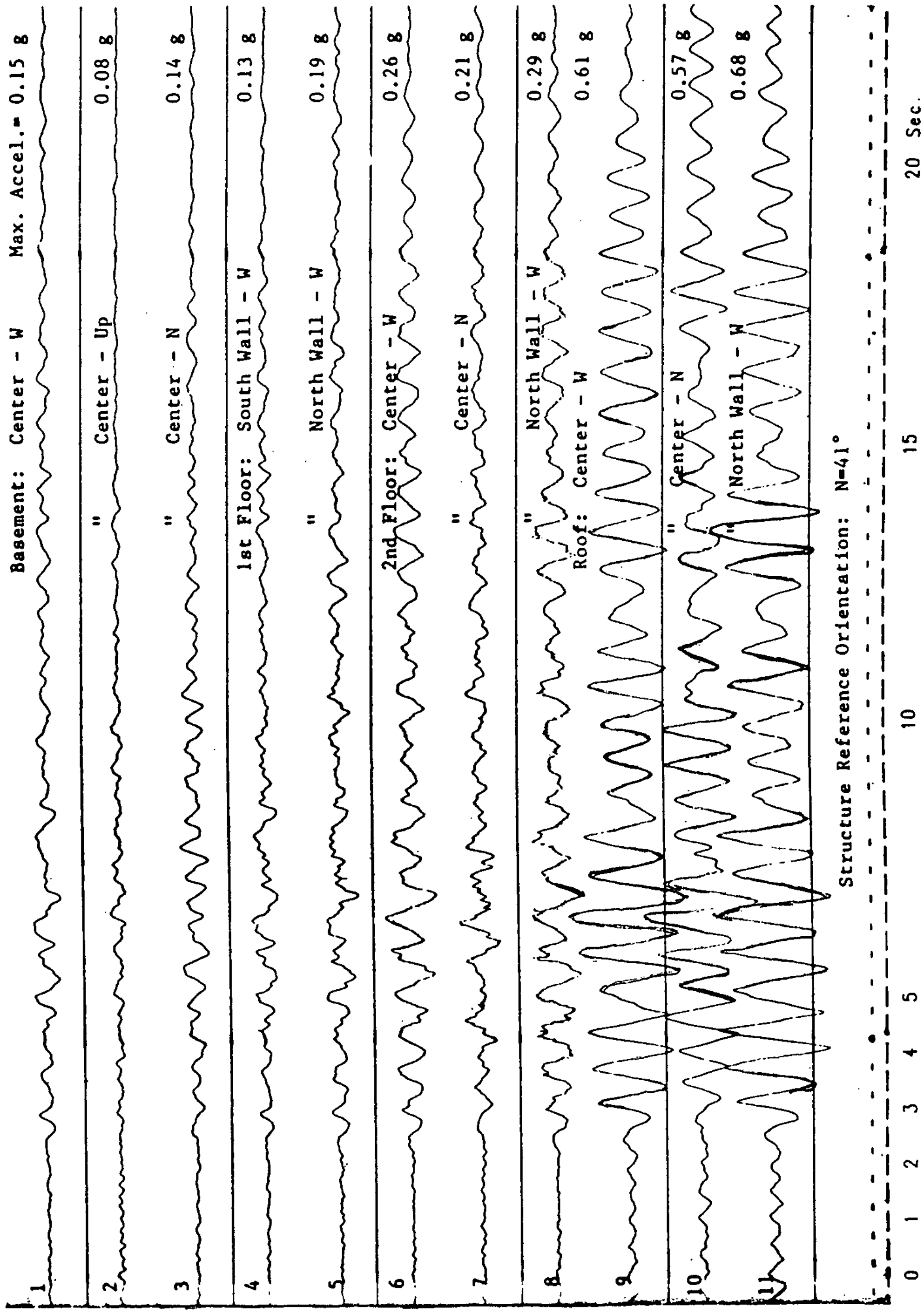

Figure 5.6.1 Accelerations recorded at the San Francisco 4-story hospital during the 1989 Loma Prieta EQ. (After Shakal, et al., 1989)

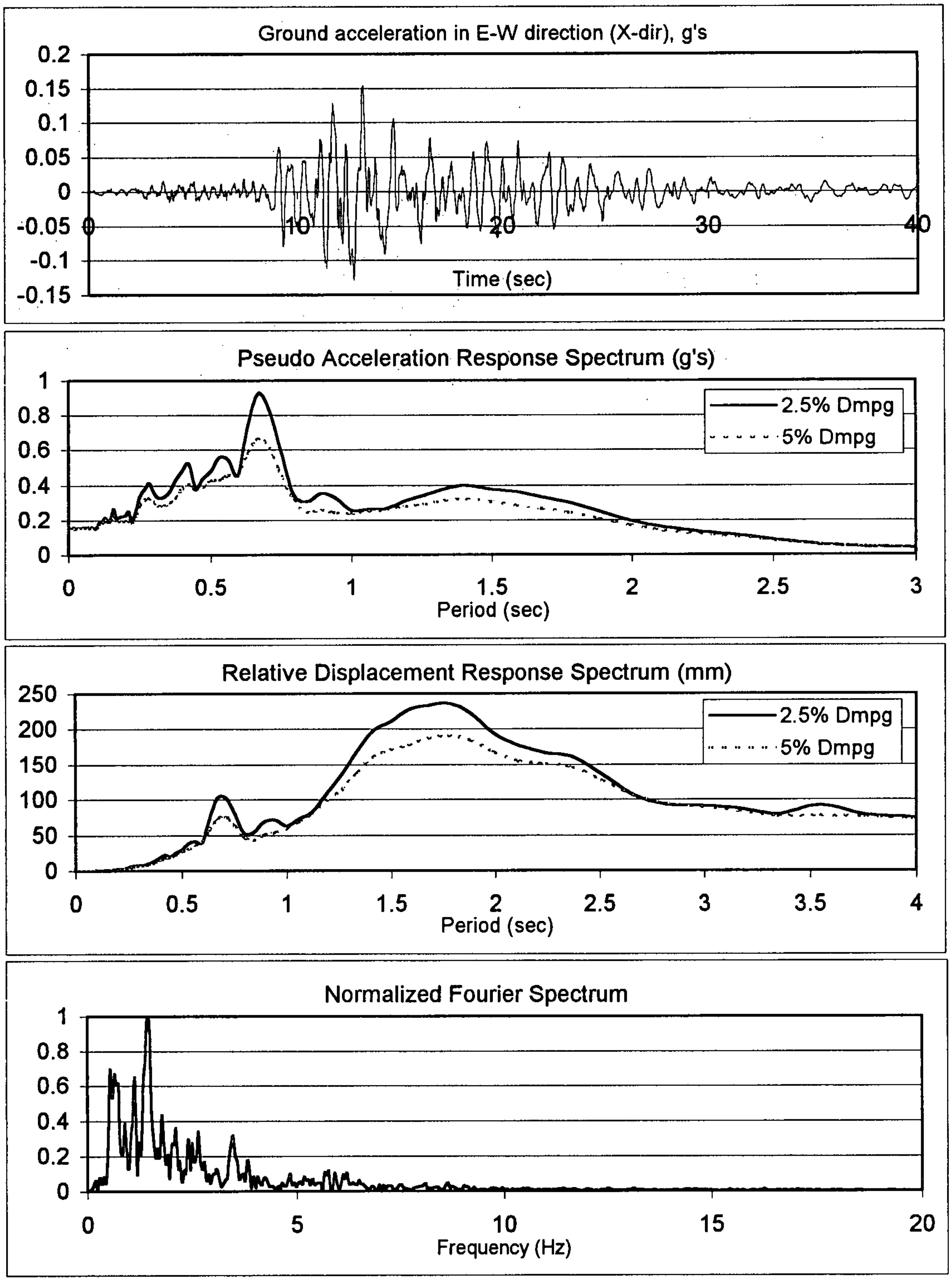

Figure 5.6.2 Time-history and spectral characteristics of E-W (X) component of the ground motion recorded at the San Francisco 4-story hospital, during the 1989 Loma Prieta EQ.

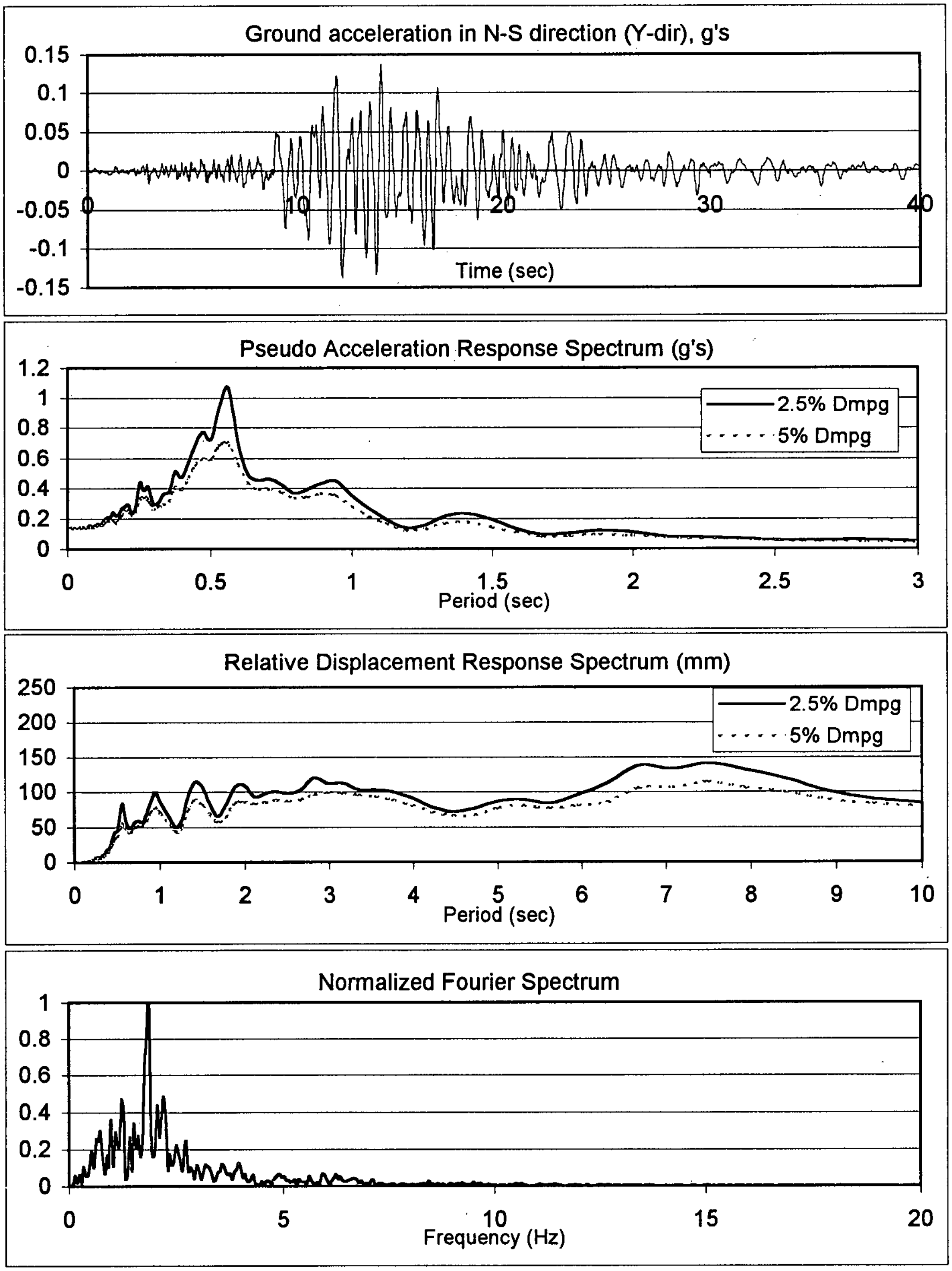

Figure 5.6.3 Time-history and spectral characteristics of N-S (Y) component of the ground motion recorded at the San Francisco 4-story hospital, during the 1989 Loma Prieta EQ.

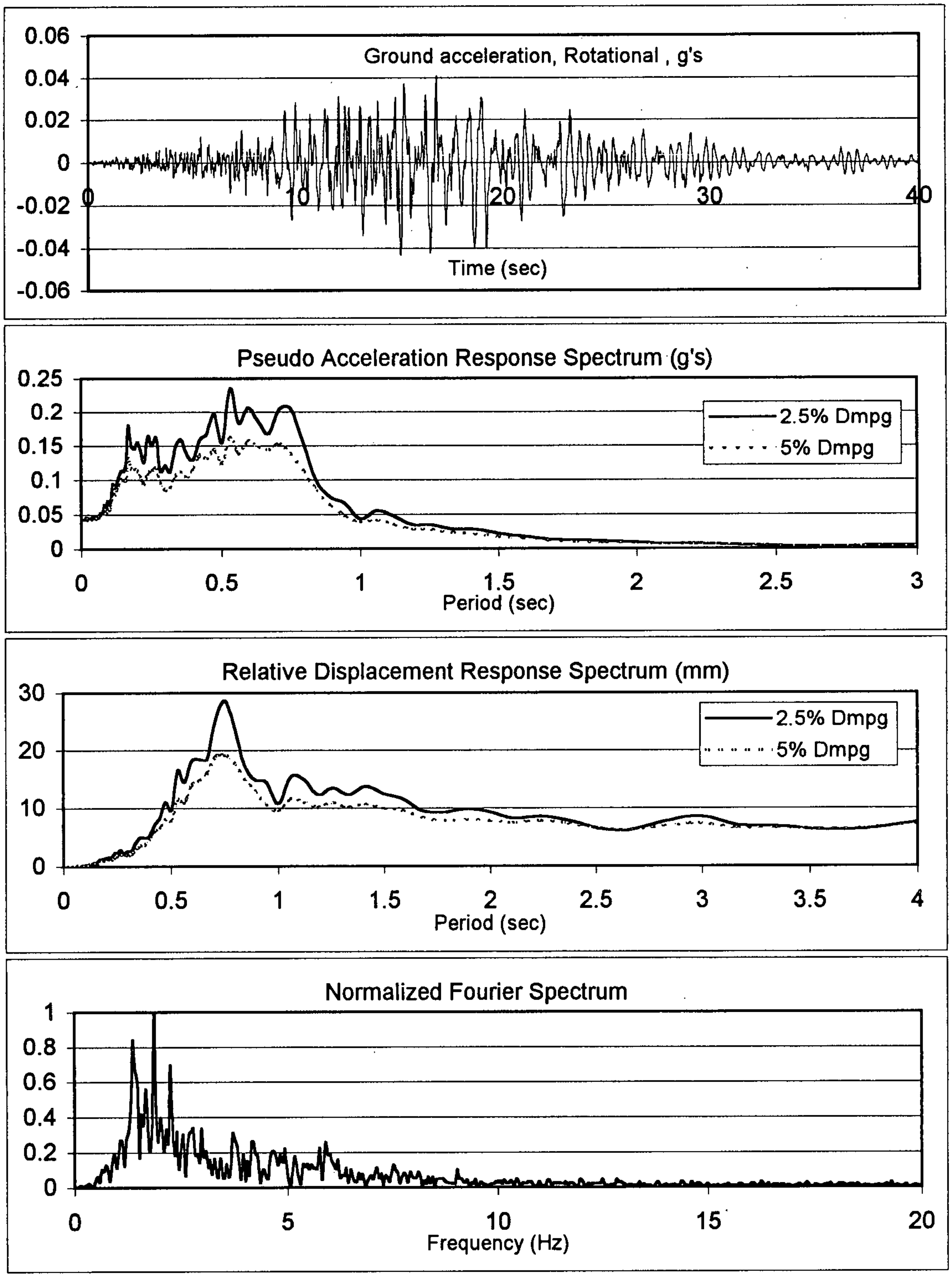

Figure 5.6.4 Time-history and spectral characteristics of rotational (R) component of the ground motion recorded at the San Francisco 4-story hospital, during the 1989 Loma Prieta EQ

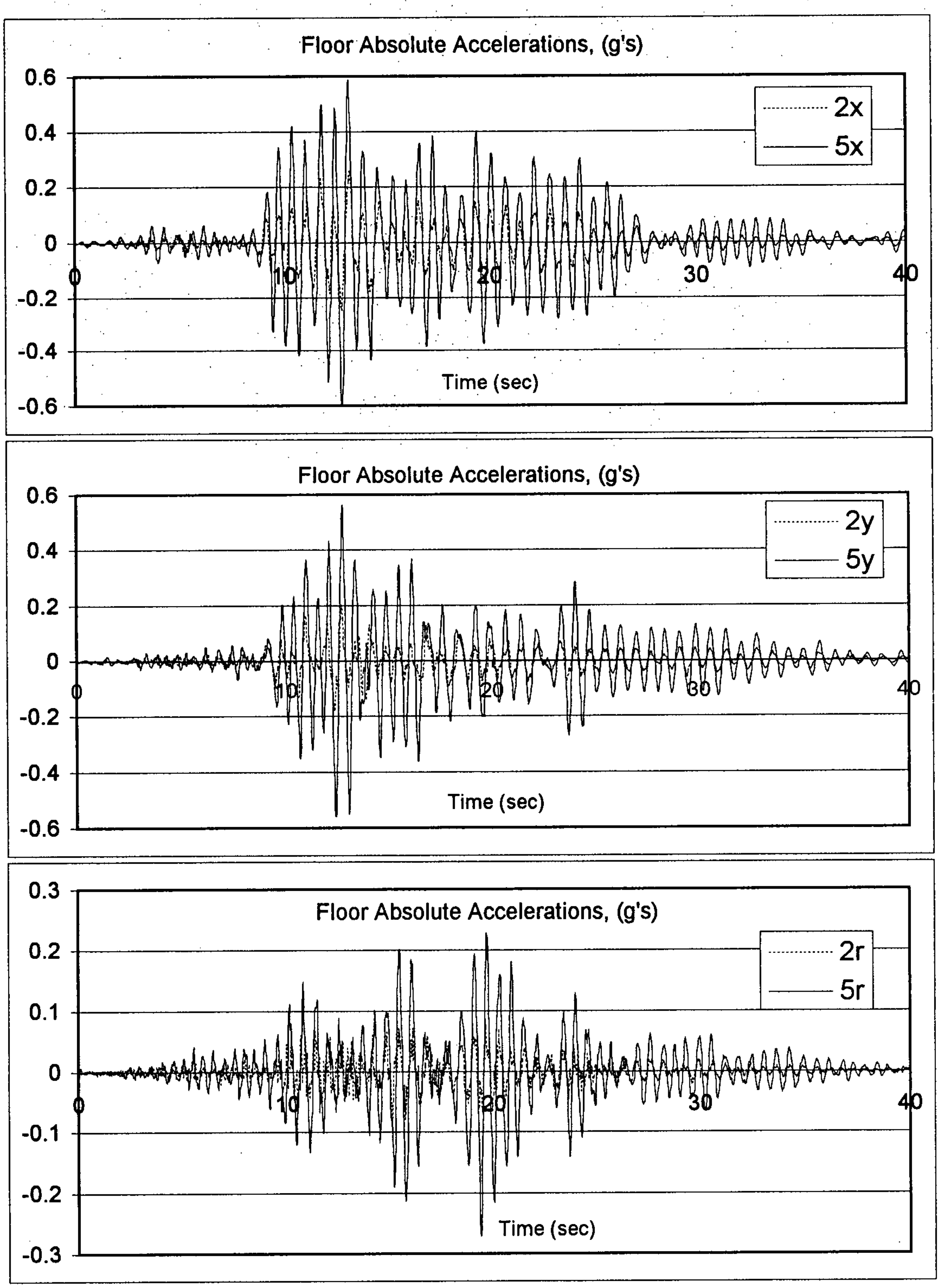

Figure 5.6.5 Absolute accelerations of the instrumented upper floors of the San Francisco 4-story hospital, during the 1989 Loma Prieta EQ.

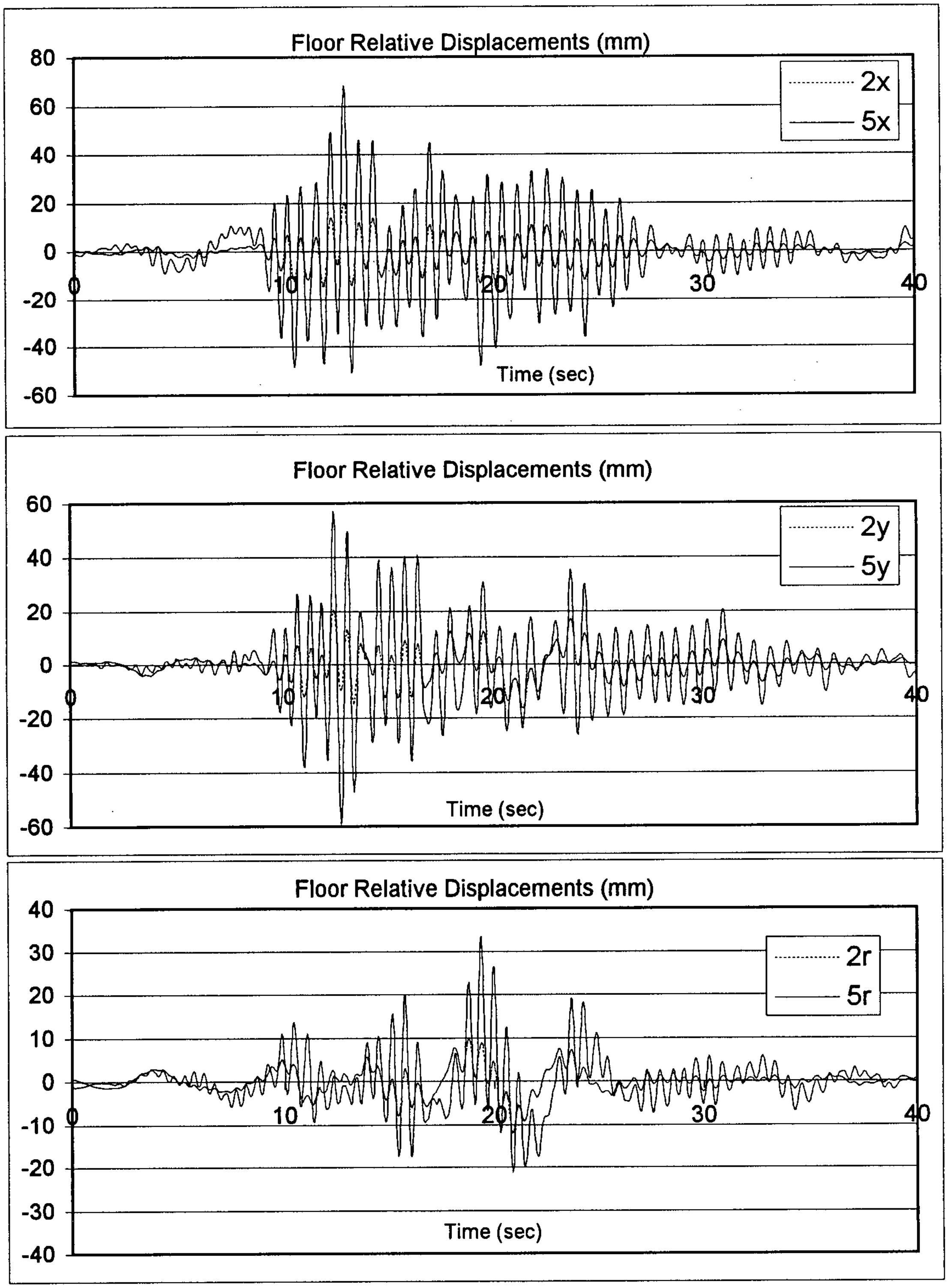

Figure 5.6.6 Relative displacements of the instrumented upper floors of the San Francisco 4-story hospital, during the 1989 Loma Prieta EQ.

Absolute Displ. **Relative Displ.**

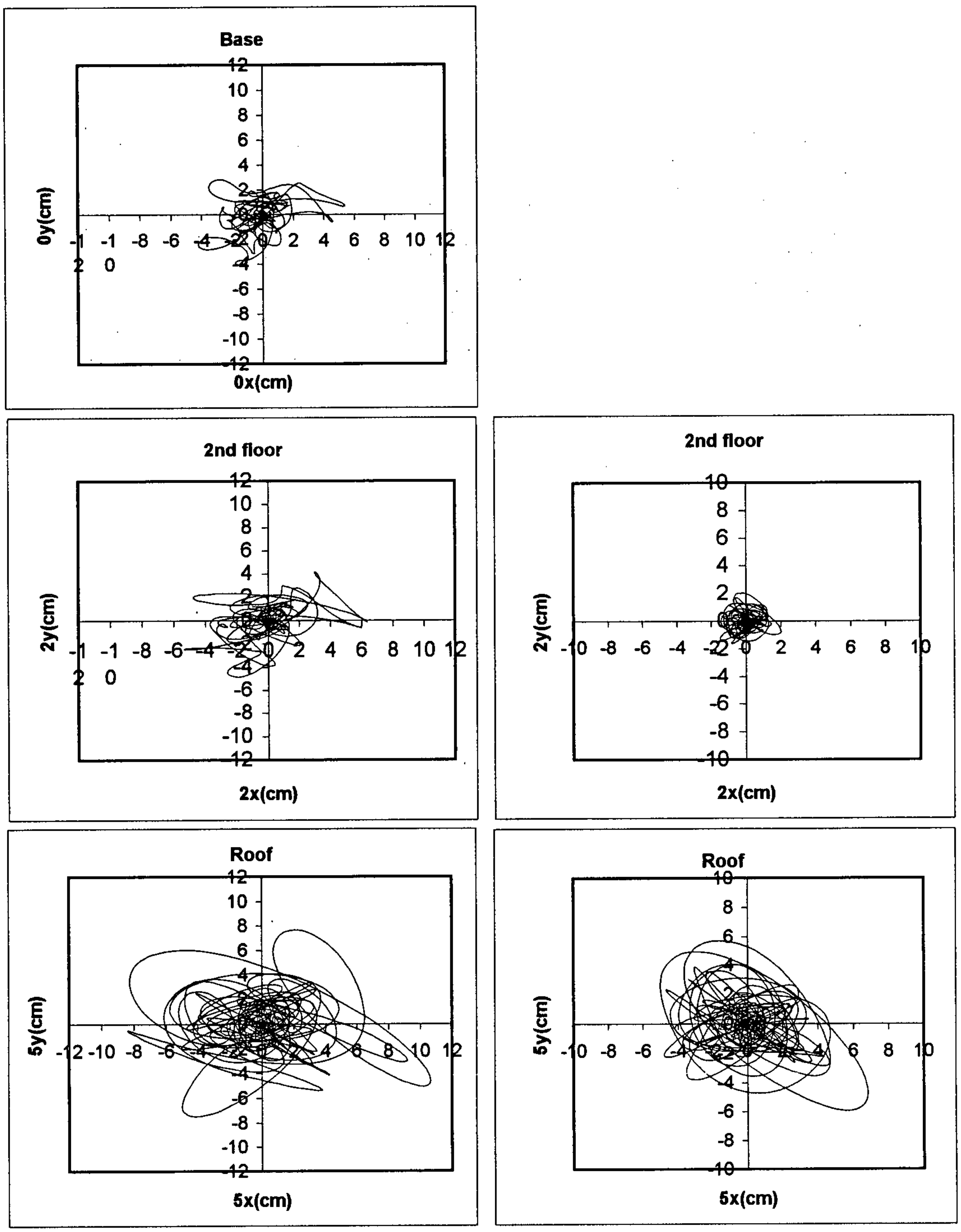

Figure 5.6.7 Orbital displacements at the center of the instrumented floors of the San Francisco 4-story hospital, during the 1989 Loma Prieta EQ.

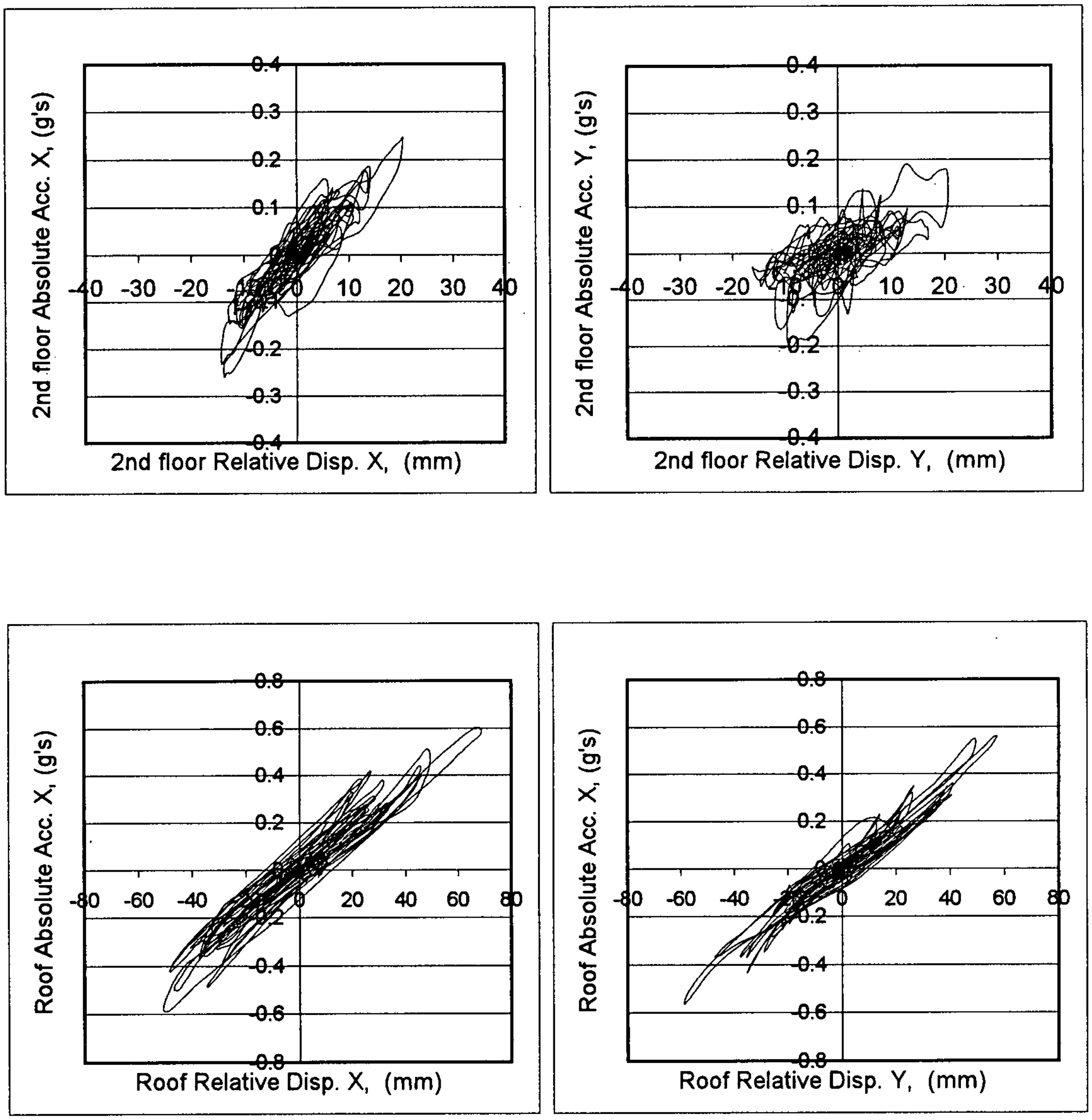

Figure 5.6.8 Representation of hysteretic behaviour at the instrumented floors of the San Francisco 4-story hospital, during the 1989 Loma Prieta EQ.

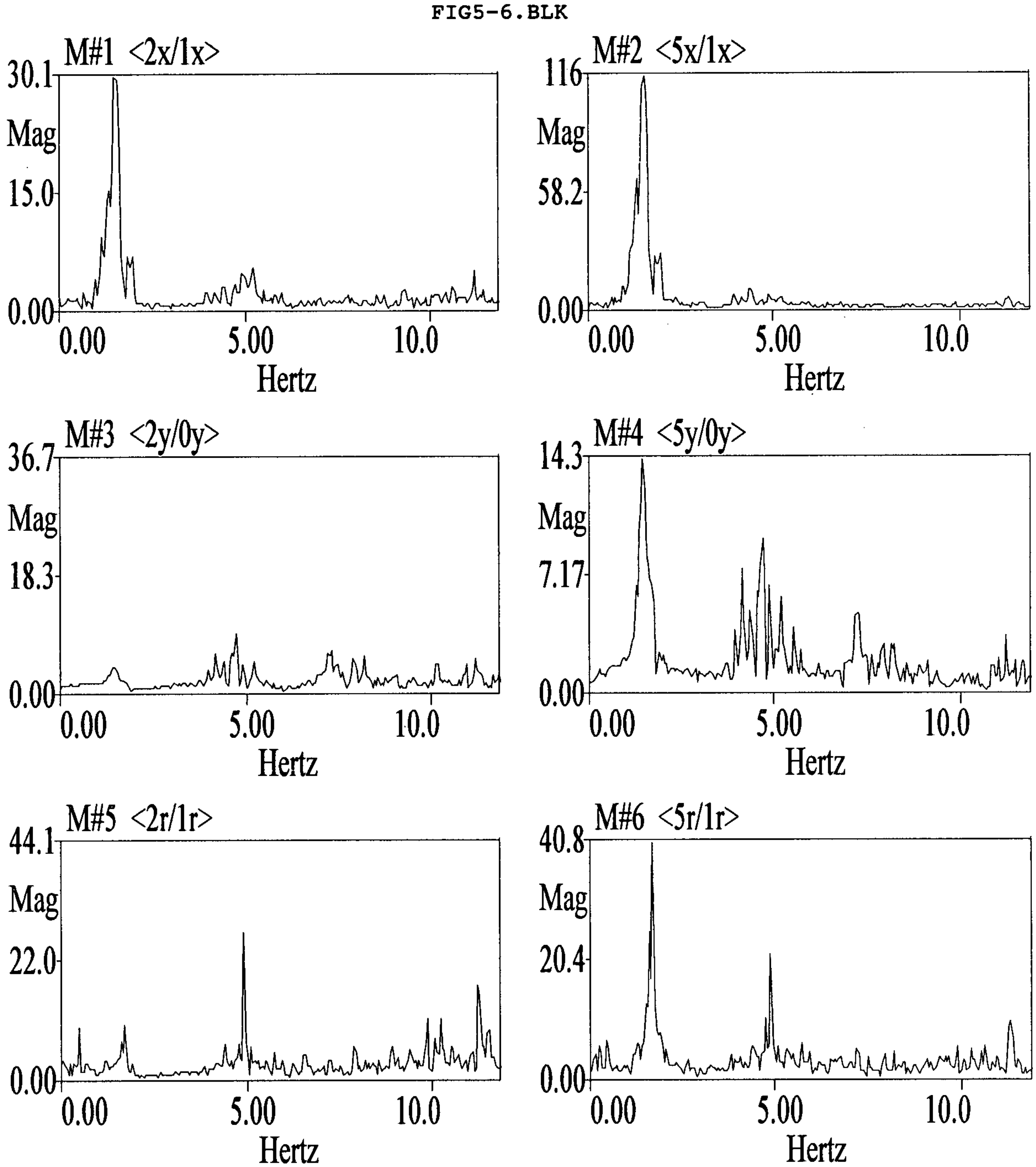

Figure 5.6.9 Frequency Response Functions of the instrumented floors of the San Francisco 4-story hospital, obtained from the 1989 Loma Prieta EQ records.

Note: The FRF's are computed by ME'scope using a Hanning window, a block size N=1024, 10 averages and 89% segment overlap.

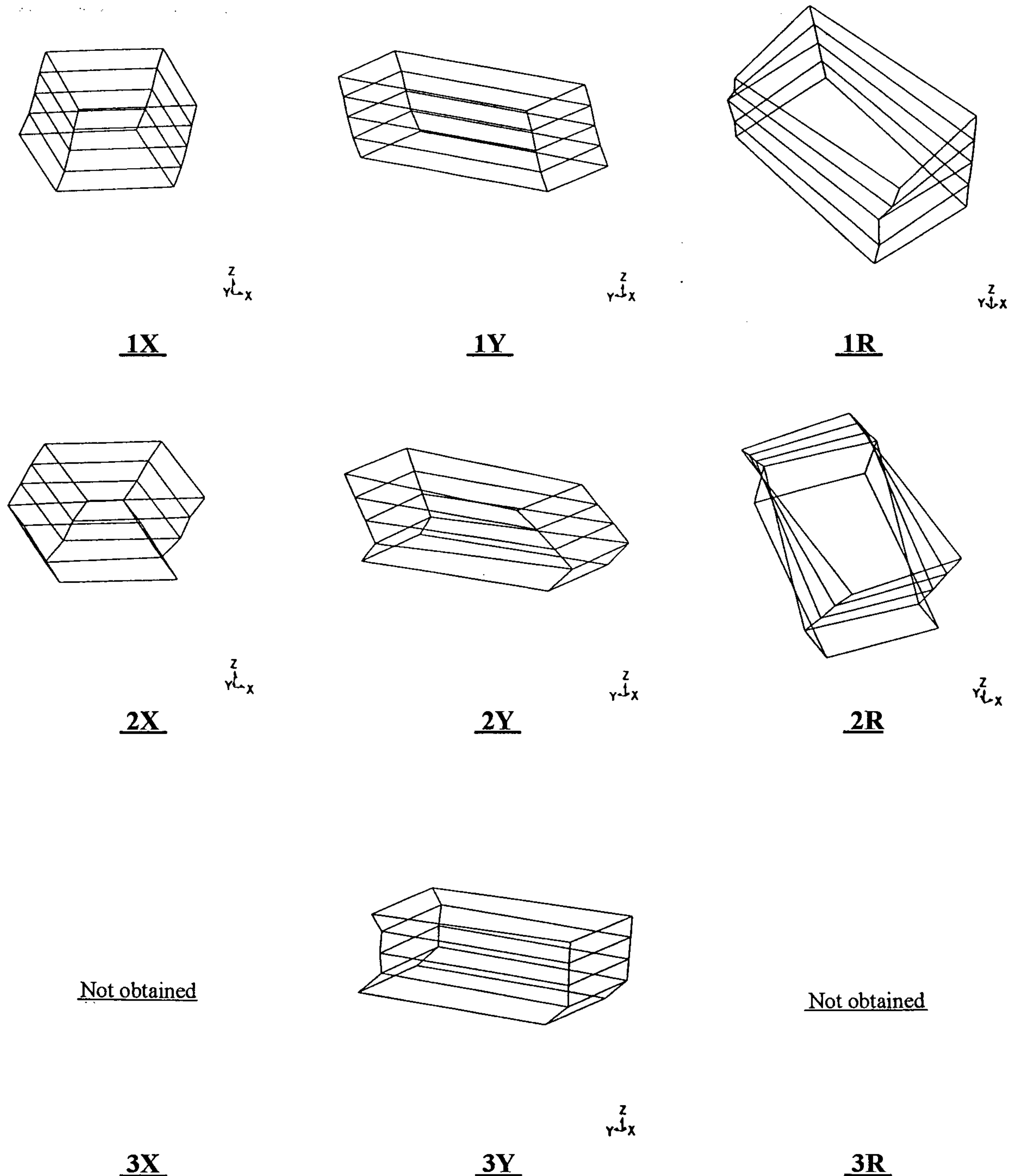

Figure 5.6.10 Mode shapes of the San Francisco 4-story hospital, obtained from the 1989 Loma Prieta EQ records.

Note: The displacements of levels 2 and 5 (roof) are obtained from measured data. Displacements of the other floors are based on ME'scope's interpolation algorithm.

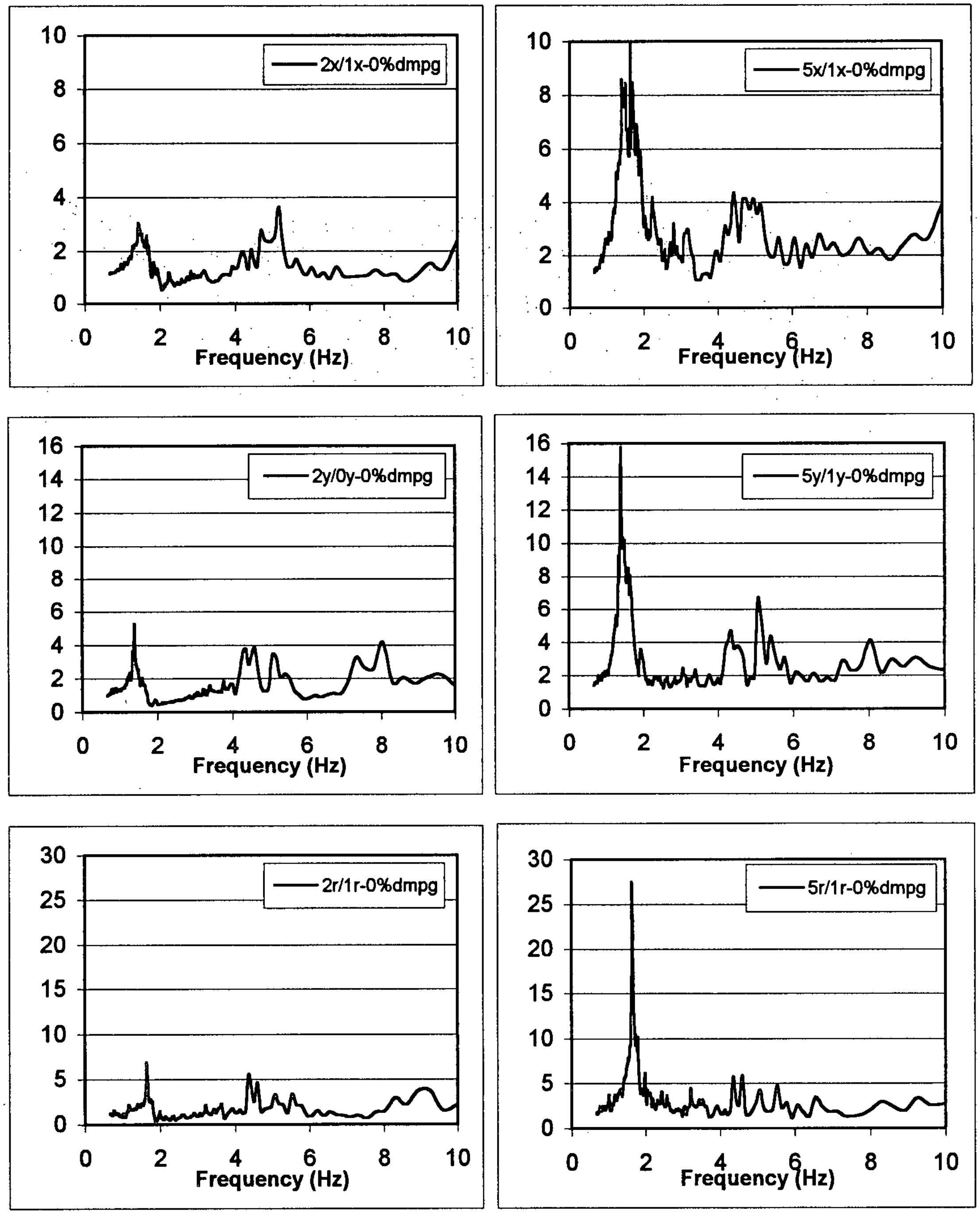

Figure 5.6.11 Spectral Response Functions of the San Francisco 4-story hospital, obtained from the 1989 Loma Prieta EQ records.

Table 5.6.1 Results of Frequency Response Functions for the San Francisco 4-story hospital, obtained from the 1989 Loma Prieta EQ records.

X-direction			
Potential Mode #	Frequency (Hz)	Amplification Factor (2X/1X)	Amplification Factor (5X/1X)
1	1.46	30.13	110.4
2	4.39	3.02	9.68
3	-	-	-
Damping Ratio estimated by ME'scope for mode 1X: **1.20%**			
Y-direction			
Potential Mode #	Frequency (Hz)	Amplification Factor (2Y/0Y)	Amplification Factor (5Y/0Y)
1	1.42	3.98	14.3
2	4.15	6.04	7.60
3	7.23	5.89	4.75
Damping Ratio estimated by ME'scope for mode 1Y: **0.07%**			
R-direction			
Potential Mode #	Frequency (Hz)	Amplification Factor (2R/1R)	Amplification Factor (5R/1R)
1	1.72	10.11	40.9
2	4.89	27.5	21.2
Damping Ratio estimated by ME'scope for mode 1R: **0.47%**			

Table 5.6.2 Results of Spectral Response Functions for the San Francisco 4-story hospital, obtained from the 1989 Loma Prieta EQ records.

X-direction			
Potential Mode #	Frequency (Hz)	SRF 0% damping (2X/1X)	SRF 0% damping (5X/1X)
1a	1.41	3.05	8.56
1b	1.65	2.58	10.0
2a	4.97	2.34	4.14
2b	5.17	3.64	3.9
Y-direction			
Potential Mode #	Frequency (Hz)	SRF 0% damping (2Y/0Y)	SRF 0% damping (5Y/0Y)
1	1.40	5.07	15.7
2a	4.51	3.39	3.77
2b	5.07	3.43	6.55
3	8.04	4.18	4.13
R-direction			
Potential Mode #	Frequency (Hz)	SRF 0% damping (2R/1R)	SRF 0% damping (5R/1R)
1	1.64	6.82	27.4

Table 5.6.3 Estimated natural frequencies (and periods) of the San Francisco 4-story hospital, based on the results of FRF results, SRF results and visual inspection of the three dimensional mode shapes obtained from analysis of 1989 Loma Prieta EQ data.

LOMA PRIETA EARTHQUAKE DATA						
	X-Direction (E-W)		Y-Direction (E-W)		Rotation	
	Frequency (Hz)	Period (S)	Frequency (Hz)	Period (S)	Frequency (Hz)	Period (S)
Model	1.50	0.67	1.42	0.70	1.70	0.59
Mode 2	4.40	0.23	4.20	0.24	5.00	0.20
Mode 3	-	-	7.20	0.14	-	-

*** Spectral values at the natural periods in the ground motion response spectra and the response time-histories suggest that the 1st mode dominated the structural response.**

Fundamental Period according to **NBCC 1995**:

$\mathbf{T = 0.1\ N} \Longrightarrow \mathbf{T} = 0.40$ sec

$\mathbf{T = 0.085\ (h_n)^{3/4}} = 0.085\ (16.0\text{m})^{3/4} = 0.68$ sec

Fundamental Period according to **UBC 1997**:

$\mathbf{T = 0.035\ (h_n)^{3/4}} = 0.035\ (52.5\ \text{ft})^{3/4} = 0.68$ sec

5.7 Berkeley 2-Story Hospital

Properties of the Strong Motion Data:

Record Length: 40 sec

Time interval: 0.02 sec

No. of data points for each channel: 2000

Usable frequency range: 0.24 Hz to 23.0 Hz

Manipulating the data to obtain the motion of the center of the building in the 3 directions, E-W (or X-directions), N-S (or Y-directions) and rotation about vertical axis (or R-component):

1X = - (Chan3 + 2 . Chan6)/3 , 1Y = Chan9 - {[(Chan6-Chan3)/2] .(70/87)}

1R = [(Chan6-Chan3)/2] .(117/87)

2X = - (Chan4 + 2 . Chan7)/3 , 2Y = Chan10 - {[(Chan7-Chan4)/2] .(70/87)}

2R = [(Chan7-Chan4)/2] .(117/87)

3X = - (Chan5 + 2 . Chan8)/3 , 3Y = Chan11 - {[(Chan8-Chan5)/2] .(70/87)}

3R = [(Chan8-Chan5)/2] .(117/87)

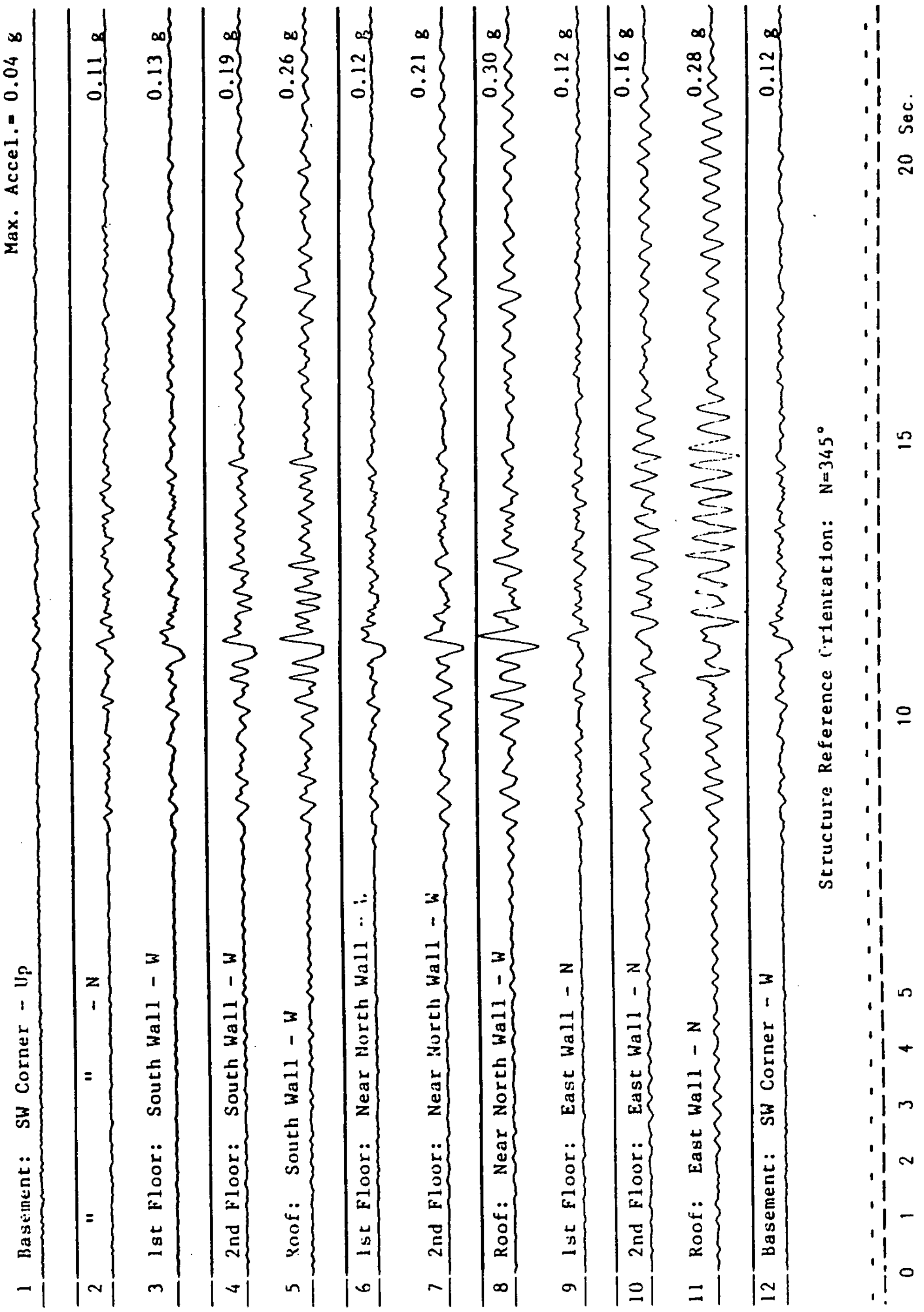

Figure 5.7.1 Accelerations recorded at the Berkeley 2-story hospital during the 1989 Loma Prieta EQ. (After Shakal, et al., 1989)

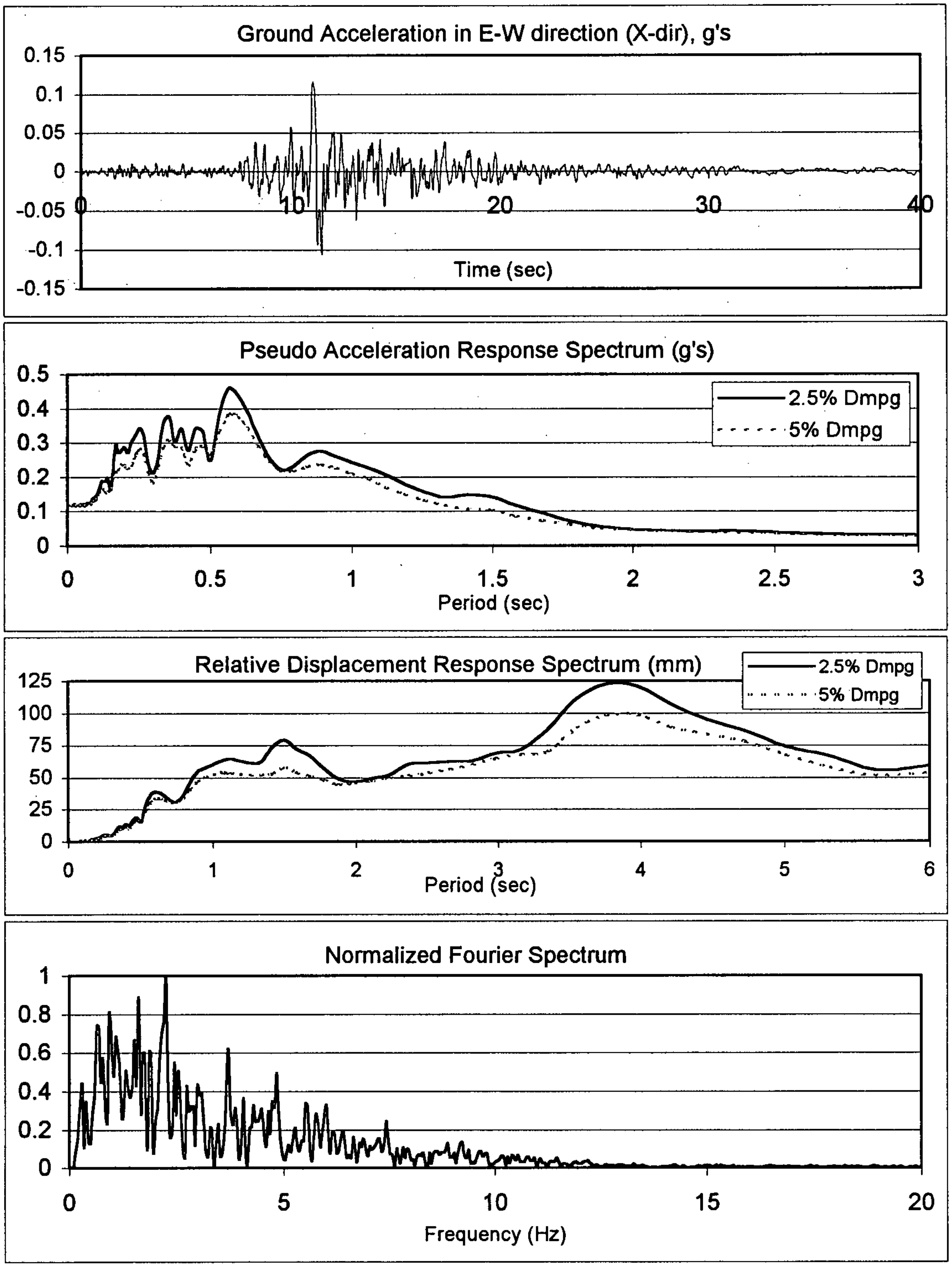

Figure 5.7.2 Time-history and spectral characteristics of E-W (X) component of the ground motion recorded at the Berkeley 2-story hospital, during the 1989 Loma Prieta EQ.

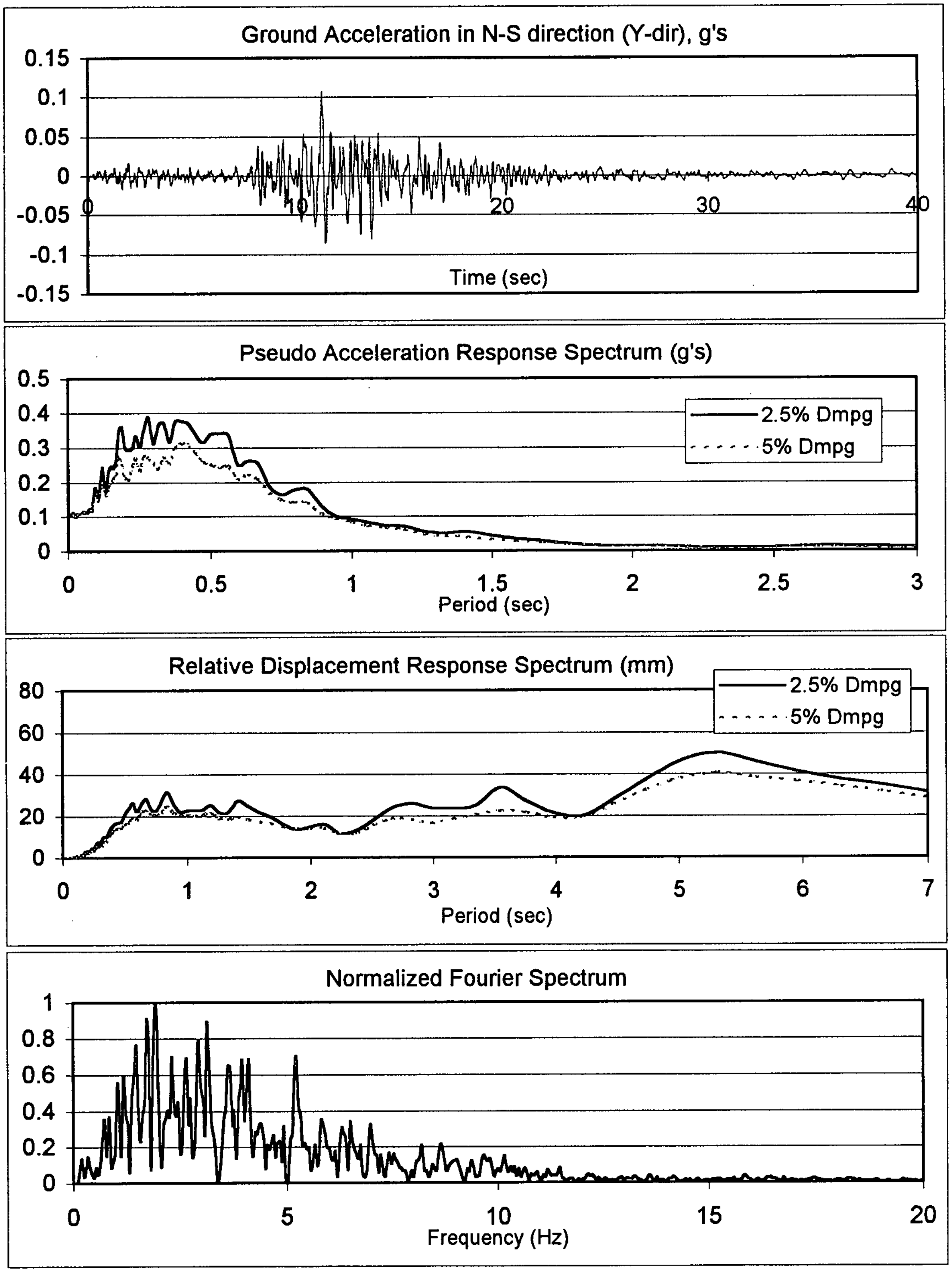

Figure 5.7.3 Time-history and spectral characteristics of N-S (Y) component of the ground motion recorded at the Berkeley 2-story hospital, during the 1989 Loma Prieta EQ.

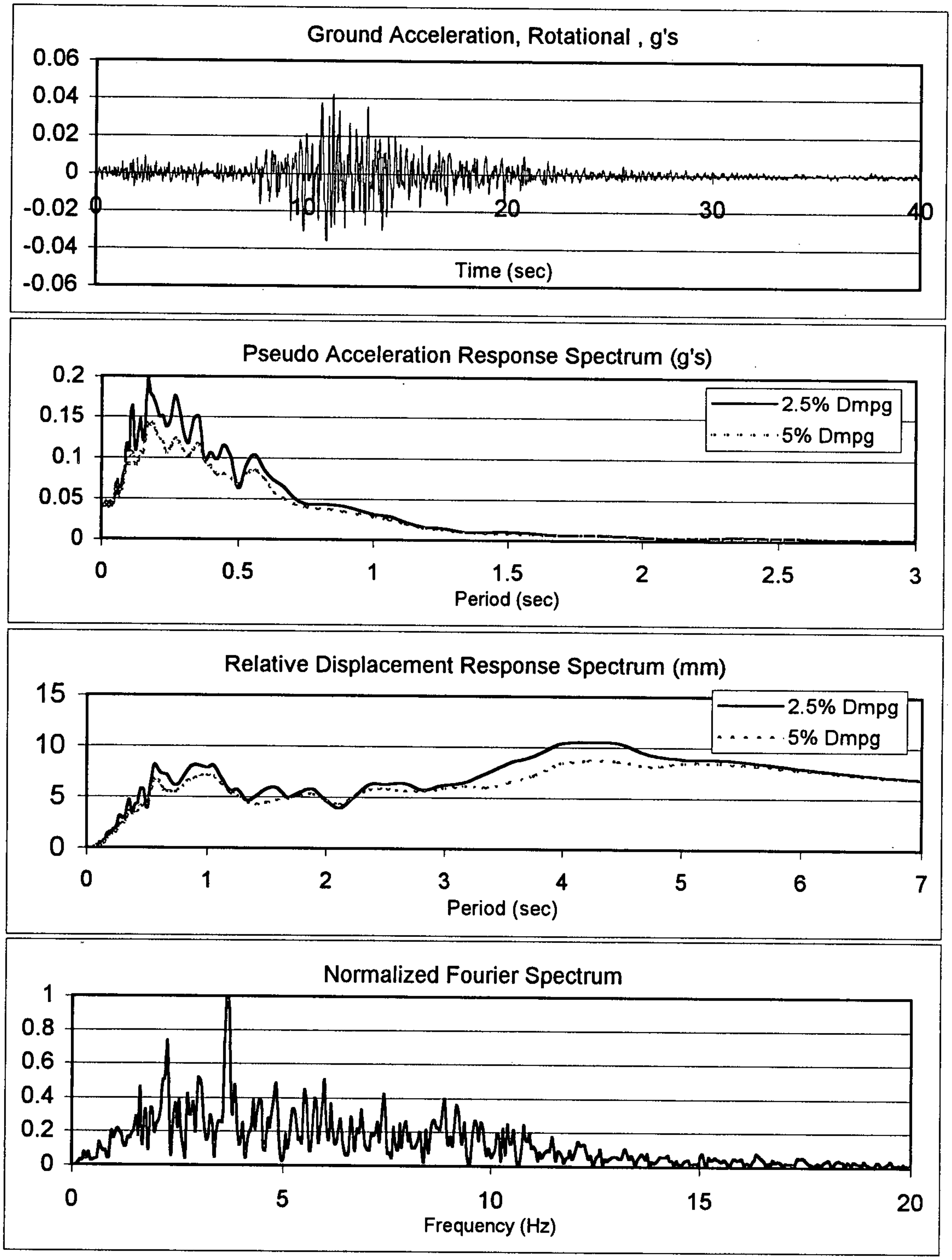

Figure 5.7.4 Time-history and spectral characteristics of rotational (R) component of the ground motion recorded at the Berkeley 2-story hospital, during the 1989 Loma Prieta EQ.

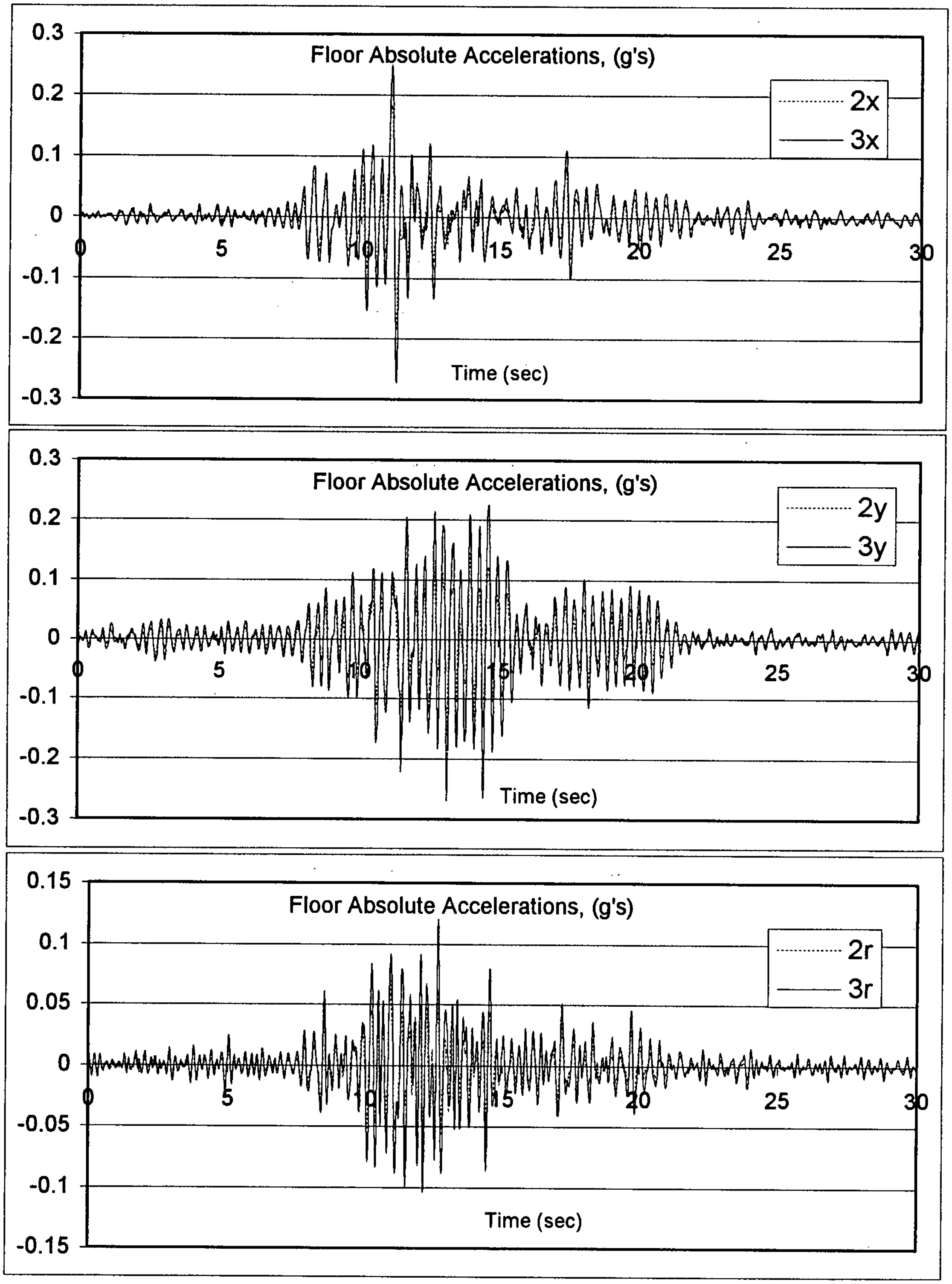

Figure 5.7.5 Absolute accelerations of the upper floors of the Berkeley 2-story hospital, during the 1989 Loma Prieta EQ.

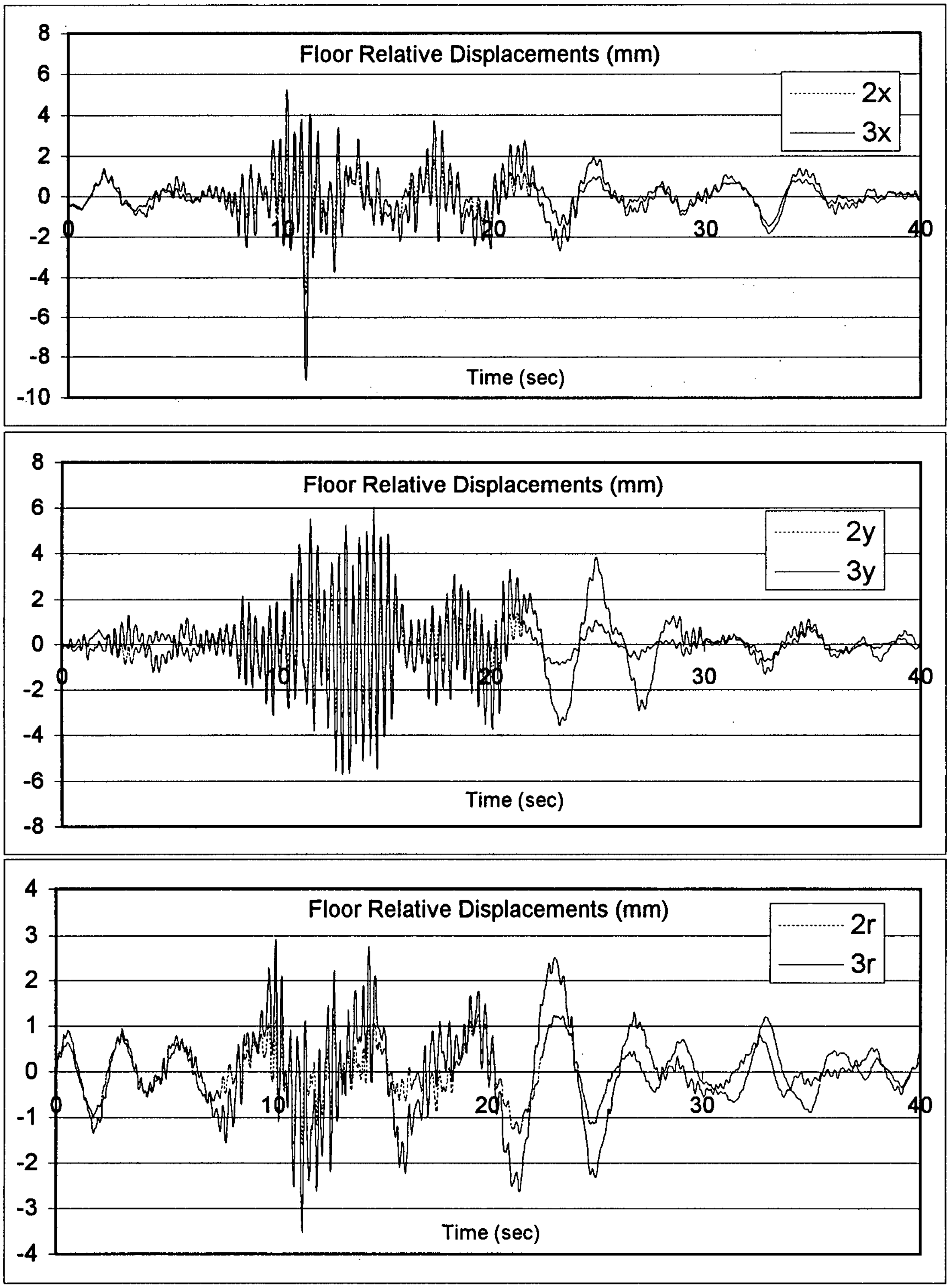

Figure 5.7.6 Relative displacements of the upper floors of the Berkeley 2-story hospital, during the 1989 Loma Prieta EQ.

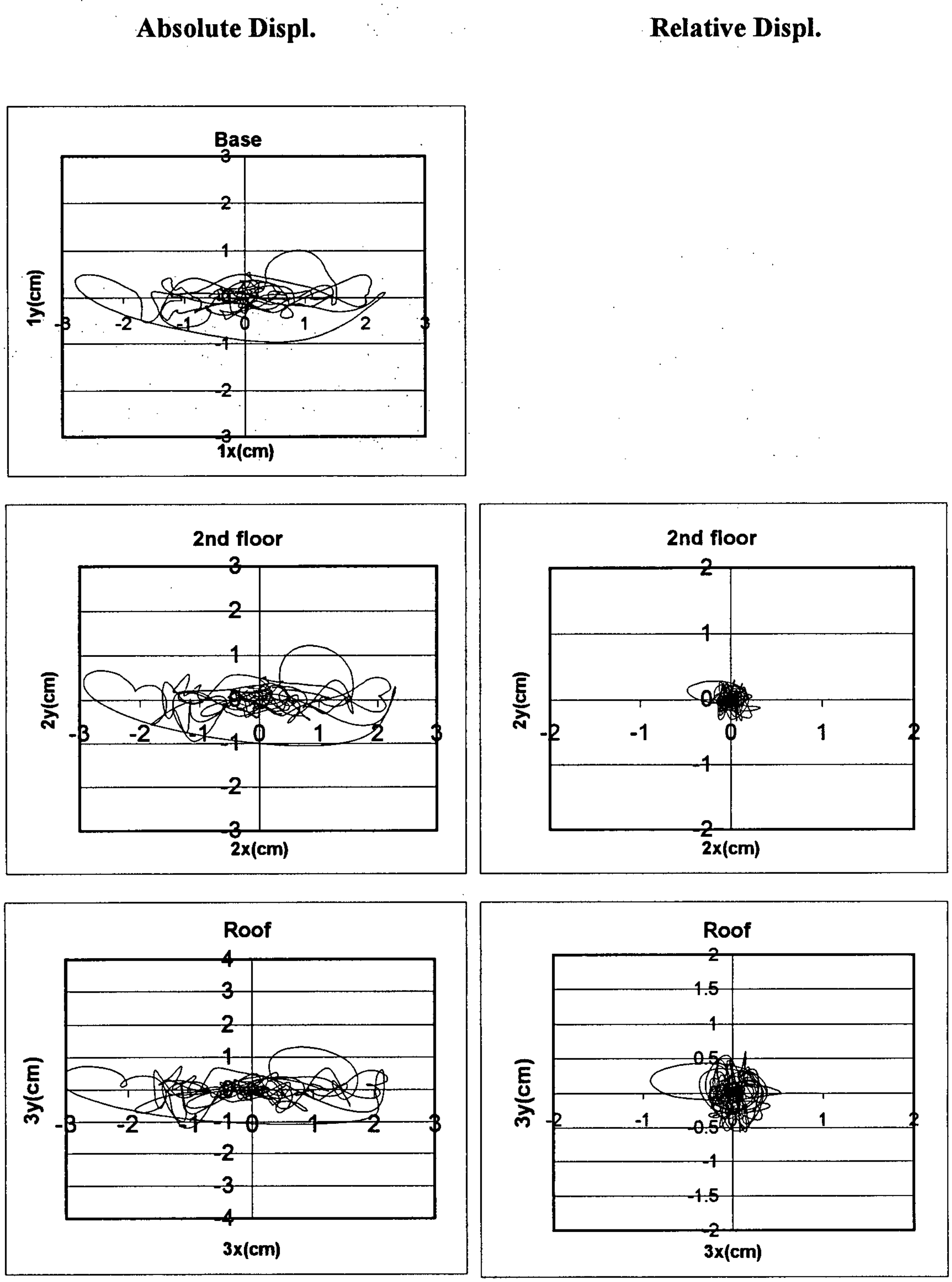

Figure 5.7.7 Orbital displacements at the center of the floors of the Berkeley 2-story hospital, during the 1989 Loma Prieta EQ.

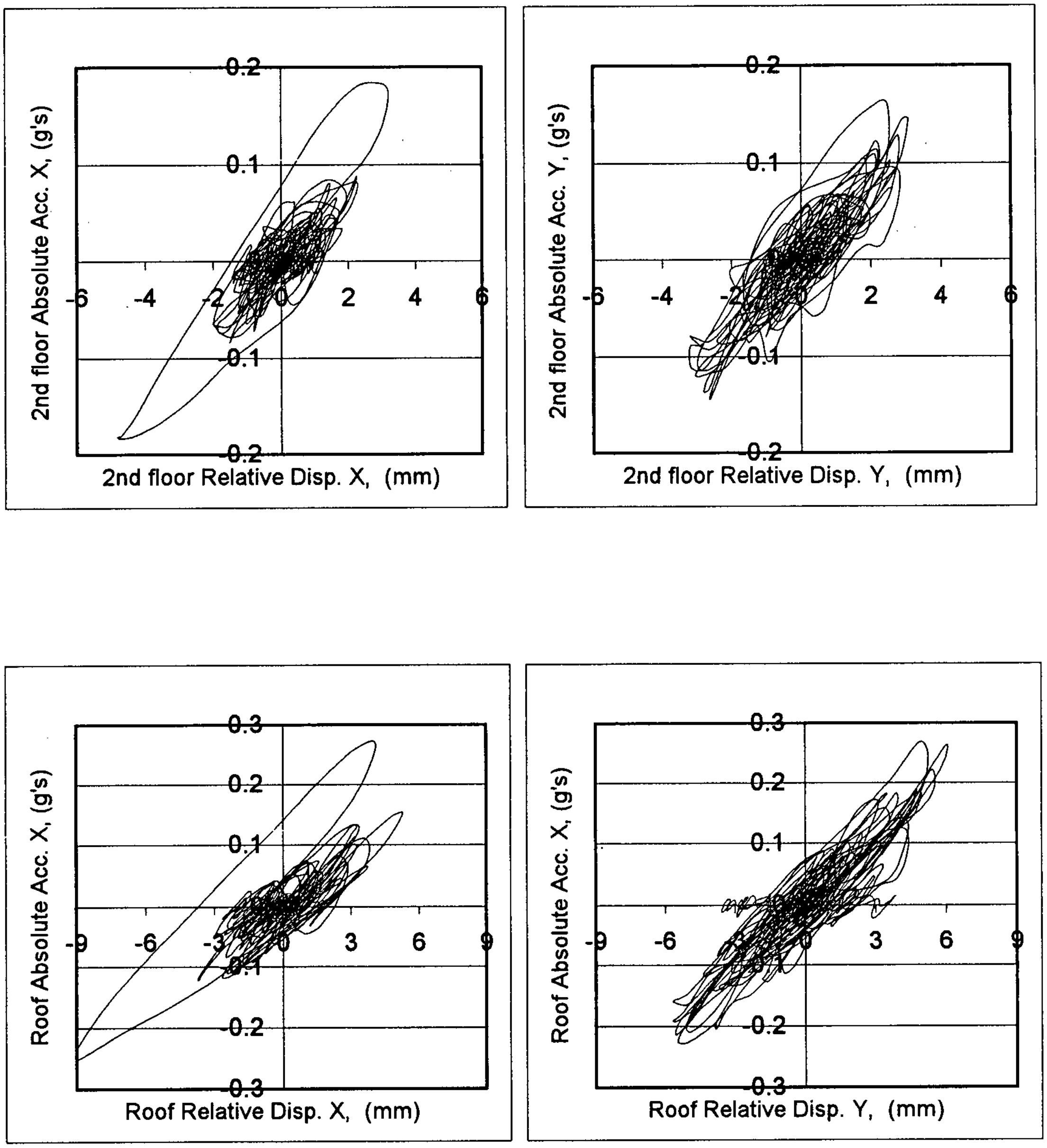

Figure 5.7.8 Representation of hysteretic behaviour at the instrumented floors of the Berkeley 2-story hospital, during the 1989 Loma Prieta EQ.

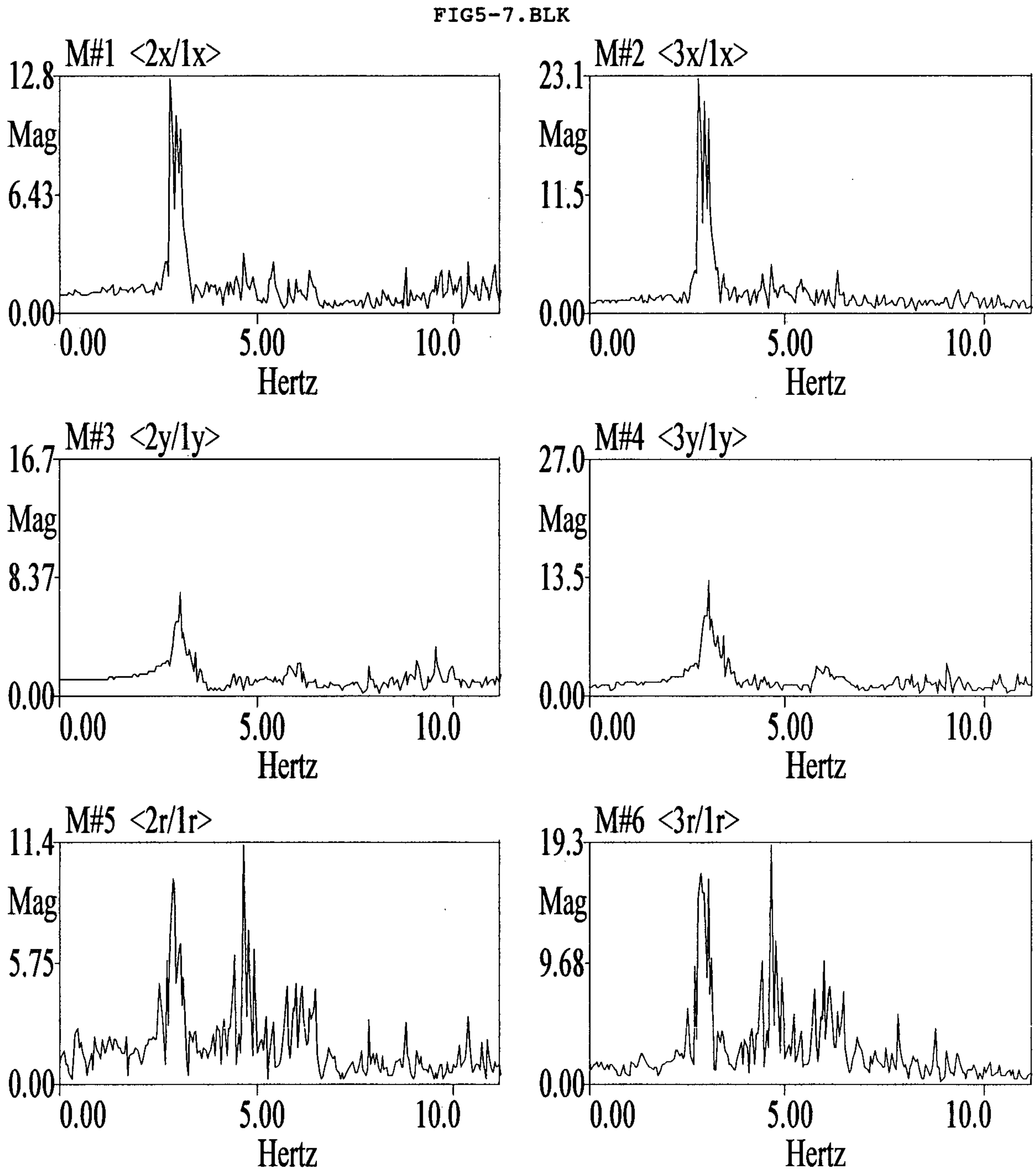

Figure 5.7.9 Frequency Response Functions of the Berkeley 2-story hospital, obtained from the 1989 Loma Prieta EQ records.

Note: The FRF's are computed by ME'scope using a Hanning window, a block size N=1024, 10 averages and 89% segment overlap.

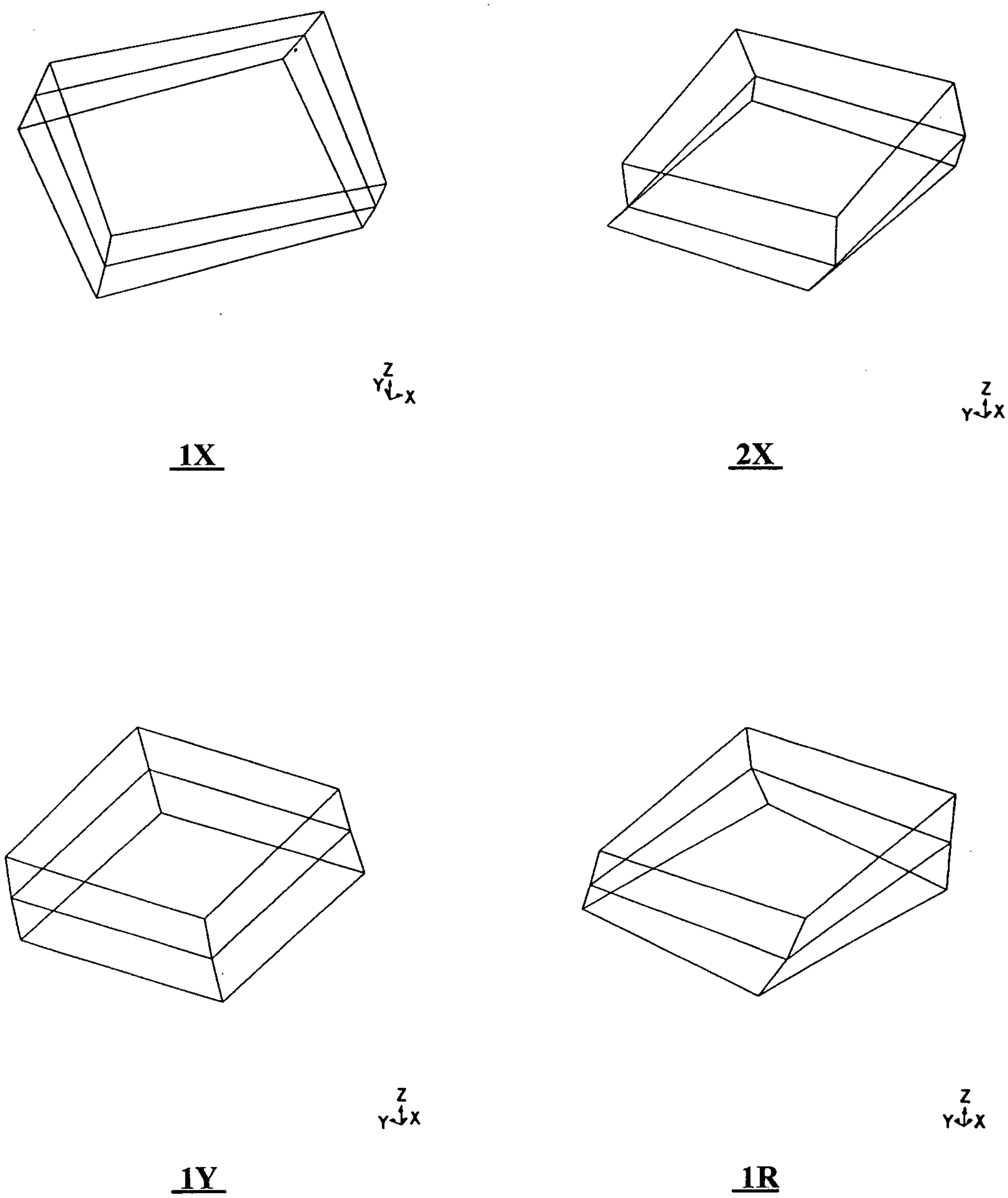

Figure 5.7.10 Mode shapes of the Berkeley 2-story hospital, obtained from the 1989 Loma Prieta EQ records.

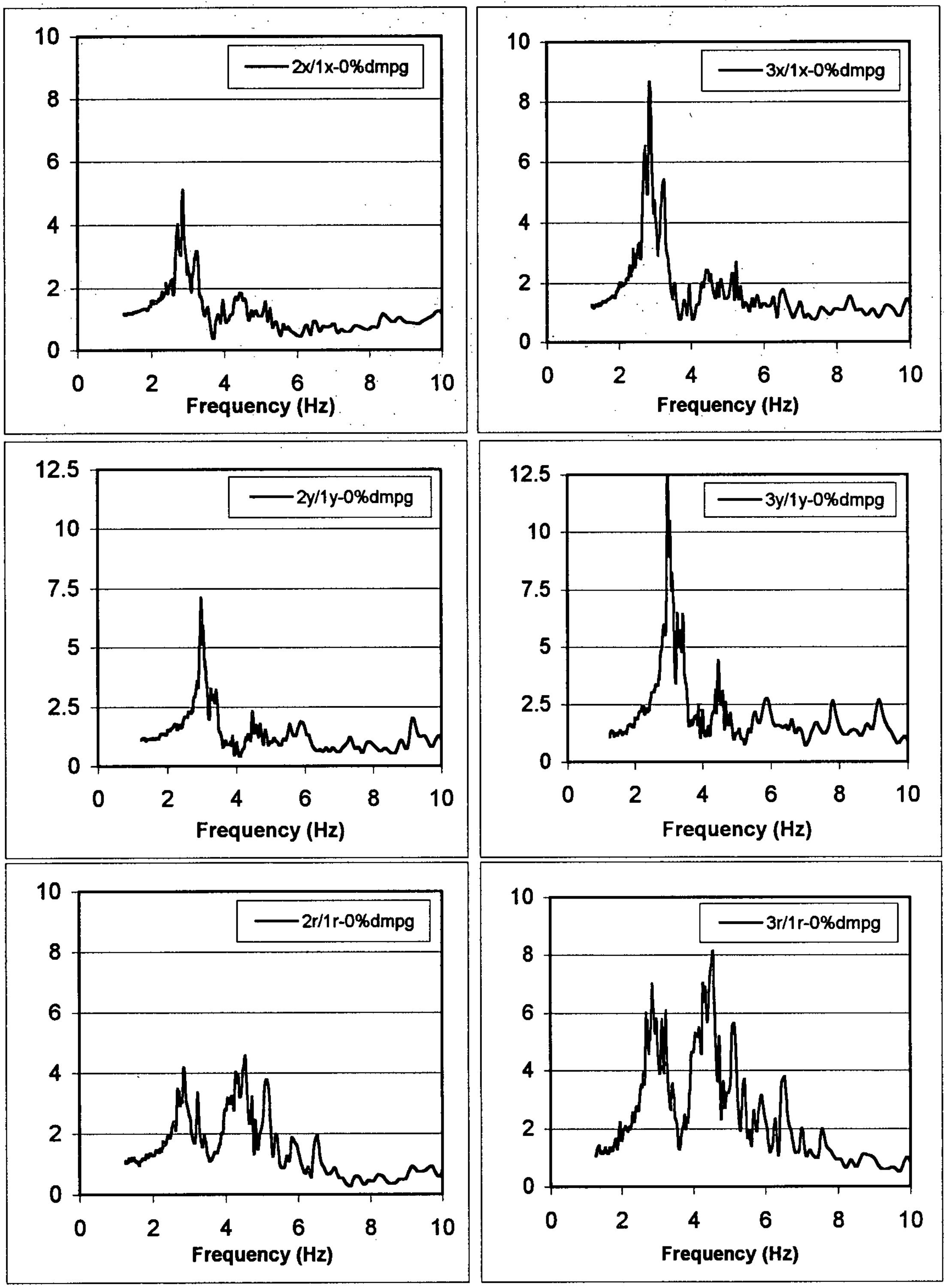

Figure 5.7.11 Spectral Response Functions of the Berkeley 2-story hospital, obtained from the 1989 Loma Prieta EQ records.

Table 5.7.1 Results of Spectral Response Functions for the Berkeley 2-story hospital, obtained from the 1989 Loma Prieta EQ records.

Mode #	Frequency (Hz)	Amplification Factor (2nd floor / base)	Amplification Factor (3rd floor / base)
1X	2.86	12.9	23.1
1Y	3.00	7.33	13.2
1R	4.55	11.5	19.4

Table 5.7.2 Estimated natural frequencies (and periods) of the Berkeley 2-story hospital, based on the results of FRF results and visual inspection of the three dimensional mode shapes obtained from analysis of 1989 Loma Prieta EQ data.

1

Mode #	Frequency (Hz)	Period (sec)	Amplification Factor (2nd floor / base)	Amplification Factor (3rd floor / base)	Damping ratio
1X	2.88	0.35	12.9	23.1	0.81%
1Y	3.07	0.33	7.33	13.2	0.66%
1R	4.63	0.22	11.5	19.4	0.75%

*** Spectral values at the natural periods in the ground motion response spectra and the response time-histories suggest that the 1st mode dominated the structural response.**

Fundamental Period according to **NBCC 1995**:

$\mathbf{T = 0.1\ N} \Longrightarrow \mathbf{T} = 0.20$ sec

$\mathbf{T = 0.09\ h_n / (D_s)^{1/2}} = 0.09 \times (7.67\text{ m}) / (18.30\text{ m})^{1/2} = 0.16$ sec (for both directions)

Fundamental Period according to **UBC 1997**:

$\mathbf{T = 0.020\ (h_n)^{3/4}} = 0.020\ (25.17\text{ ft})^{3/4} = 0.23$ sec

5.8 Richmond 3-Story Office Building

Properties of the Strong Motion Data:

Record Length: 80 sec

Time interval: 0.02 sec

No. of data points for each channel: 4000

Usable frequency range: 0.2 Hz to 23.0 Hz

Manipulating the data to obtain the motion of the center of the building in the 3 directions, E-W (or X-directions), N-S (or Y-directions) and rotation about vertical axis (or R-component):

1X = Chan10 , 1Y = - Chan12

2X = (Chan8+Chan7)/2 , 2Y = -Chan9 , 2R = (Chan8-Chan7)/2

3X = (Chan5+Chan4)/2 , 3Y = -Chan6 , 3R = (Chan5-Chan4)/2

4X = (Chan2+Chan1)/2 , 4Y = -Chan3 , 4R = (Chan2-Chan1)/2

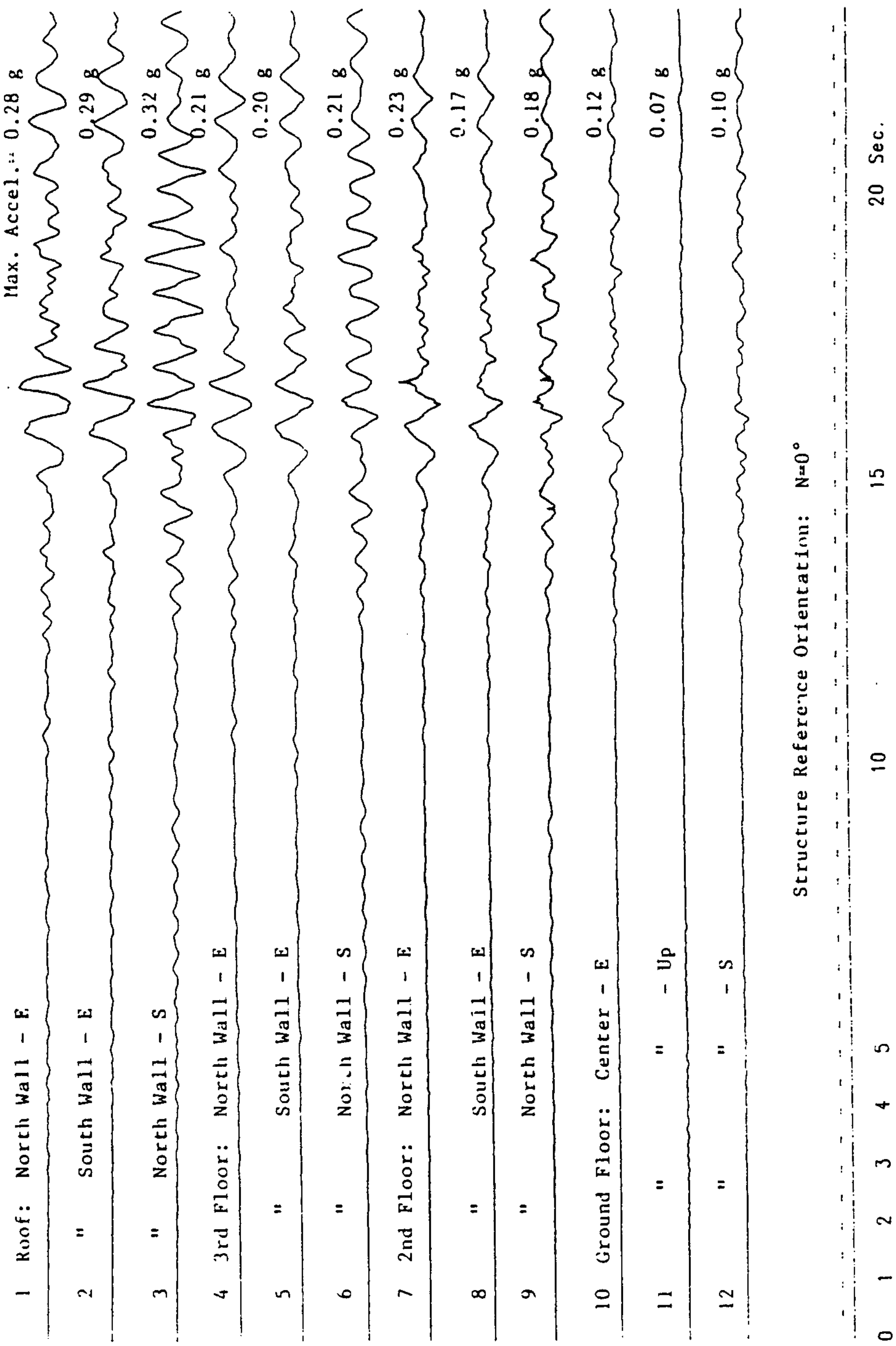

Figure 5.8.1 Accelerations recorded at the Richmond 3-story office building, during the 1989 Loma Prieta EQ. (After Shakal, et al., 1989)

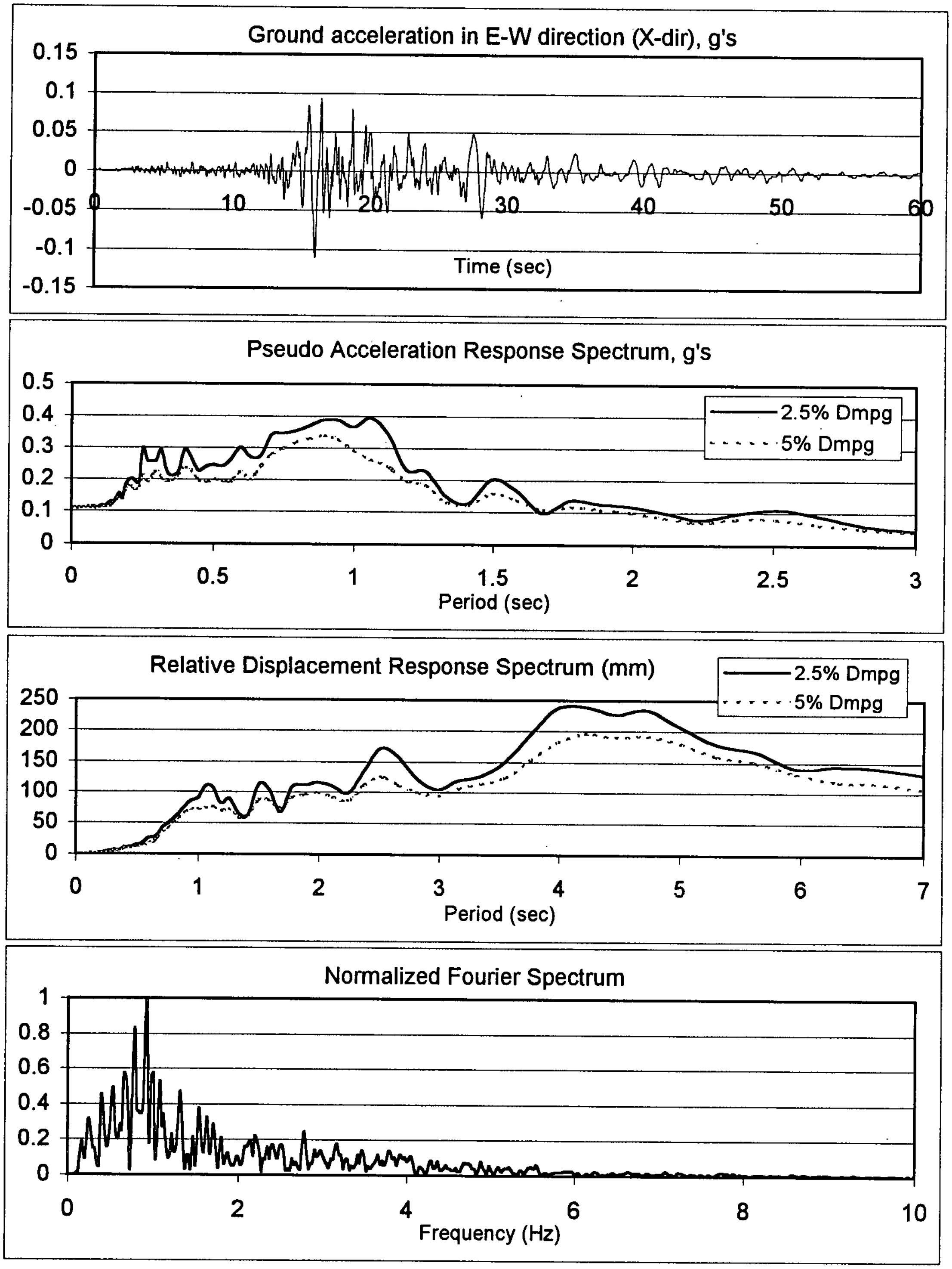

Figure 5.8.2 Time-history and spectral characteristics of E-W (X) component of the ground motion recorded at the Richmond 3-story office building, during the 1989 Loma Prieta EQ.

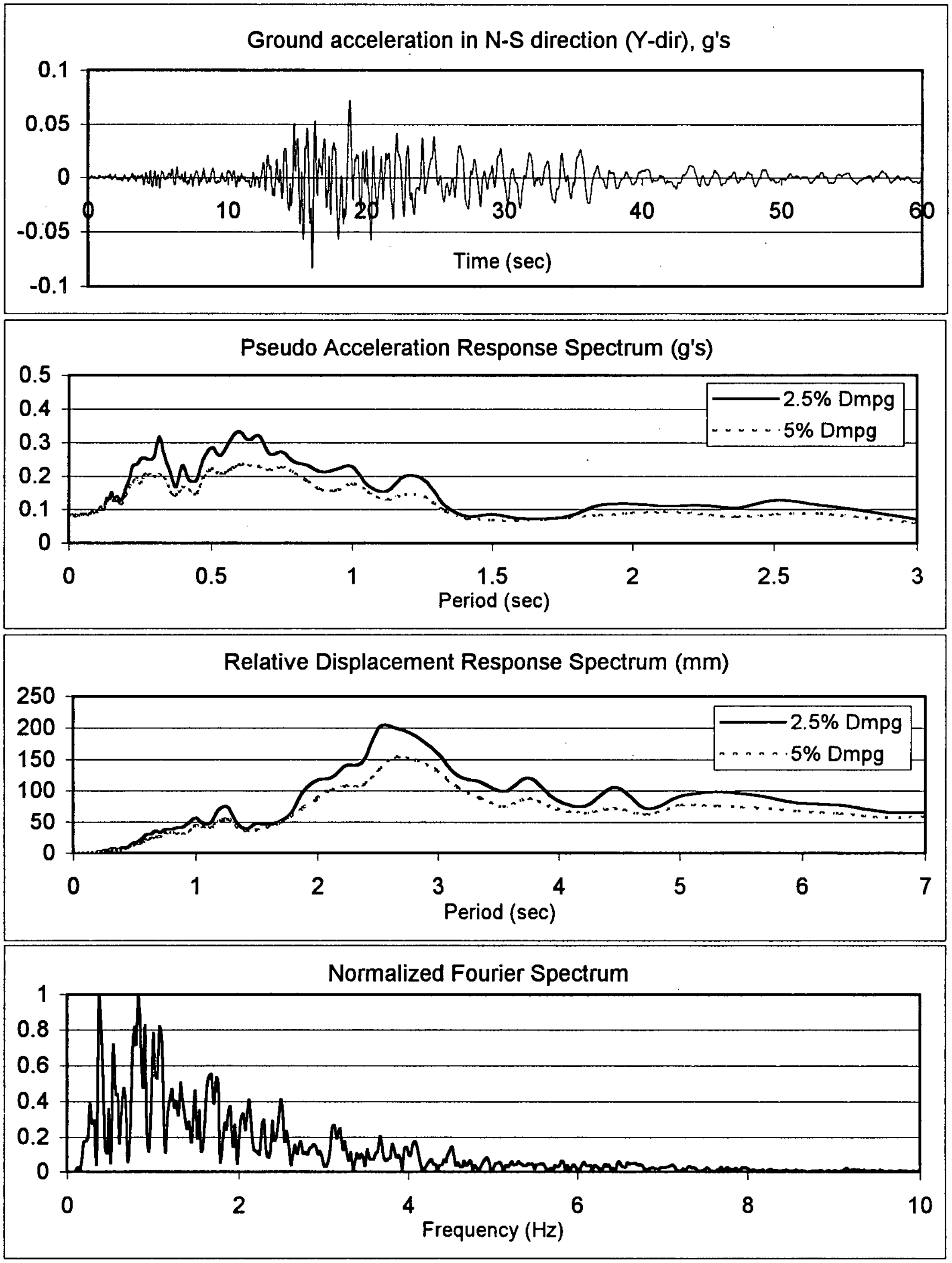

Figure 5.8.3 Time-history and spectral characteristics of N-S (Y) component of the ground motion recorded at the Richmond 3-story office building, during the 1989 Loma Prieta EQ.

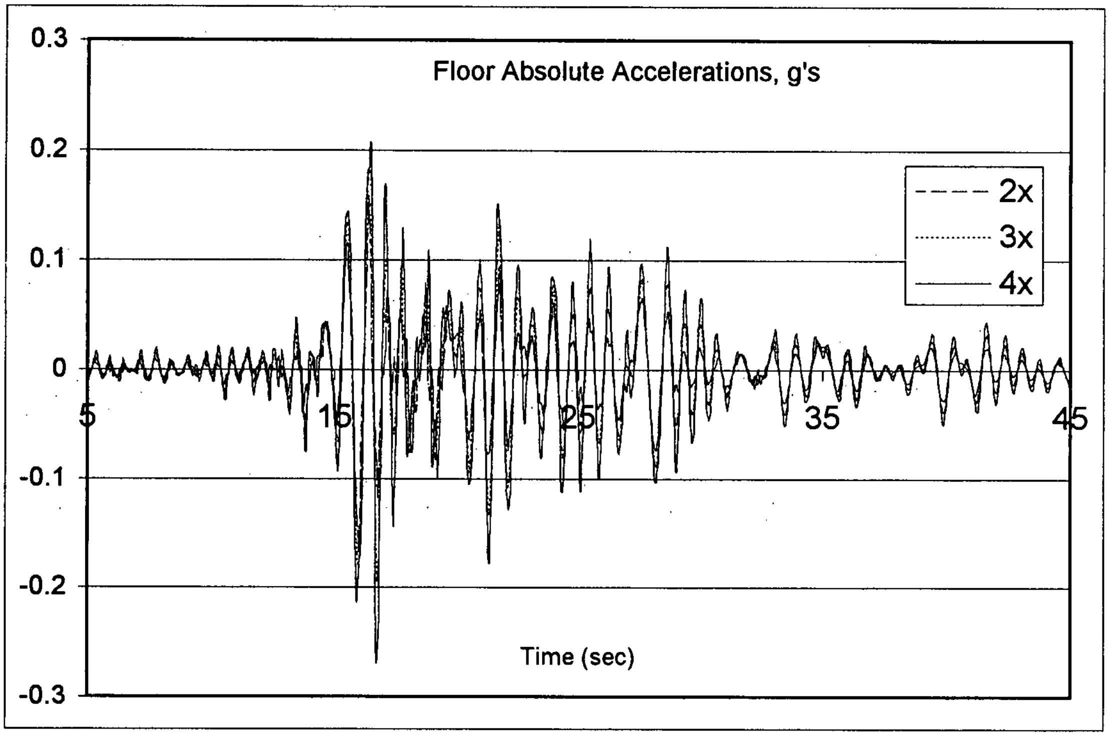

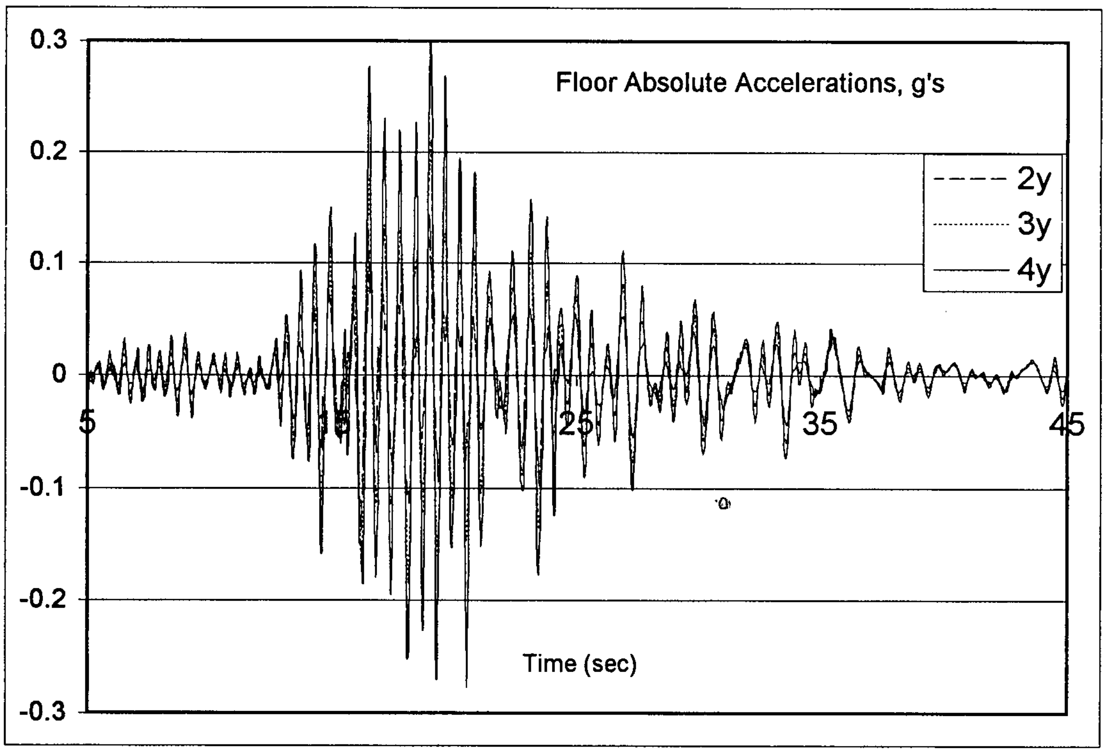

Figure 5.8.4 E-W (X-direction) & N-S (Y-direction) absolute accelerations of the upper floors of the Richmond 3-story office bldg., during the 1989 Loma Prieta EQ.

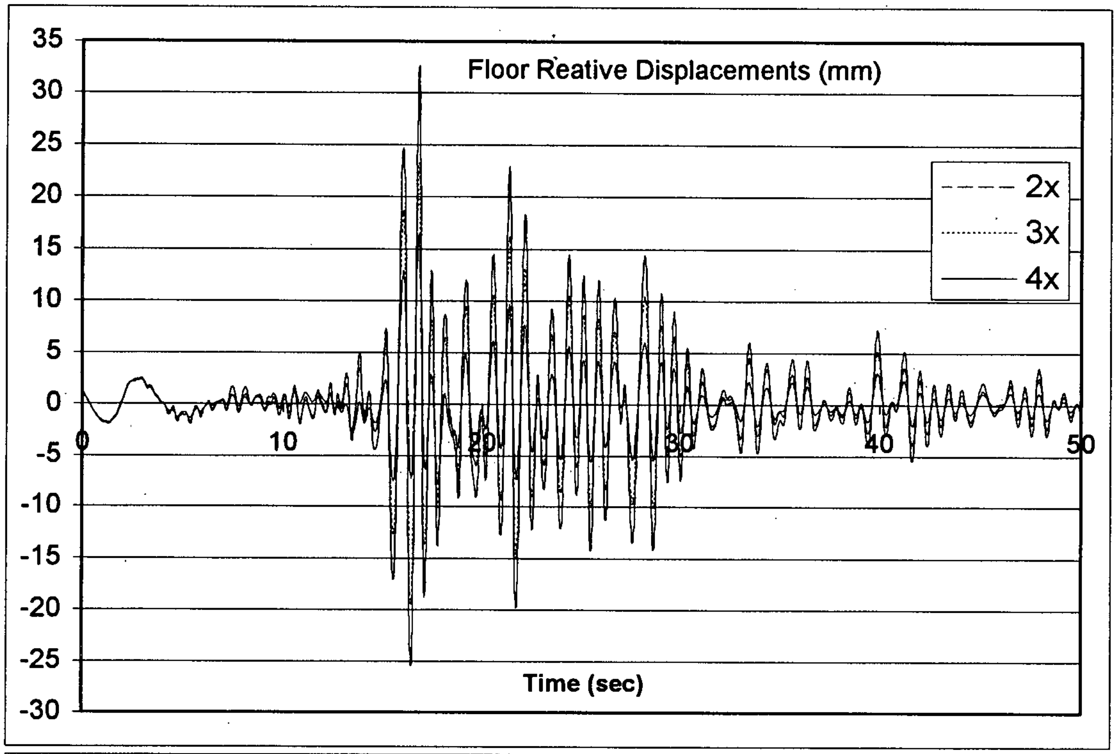

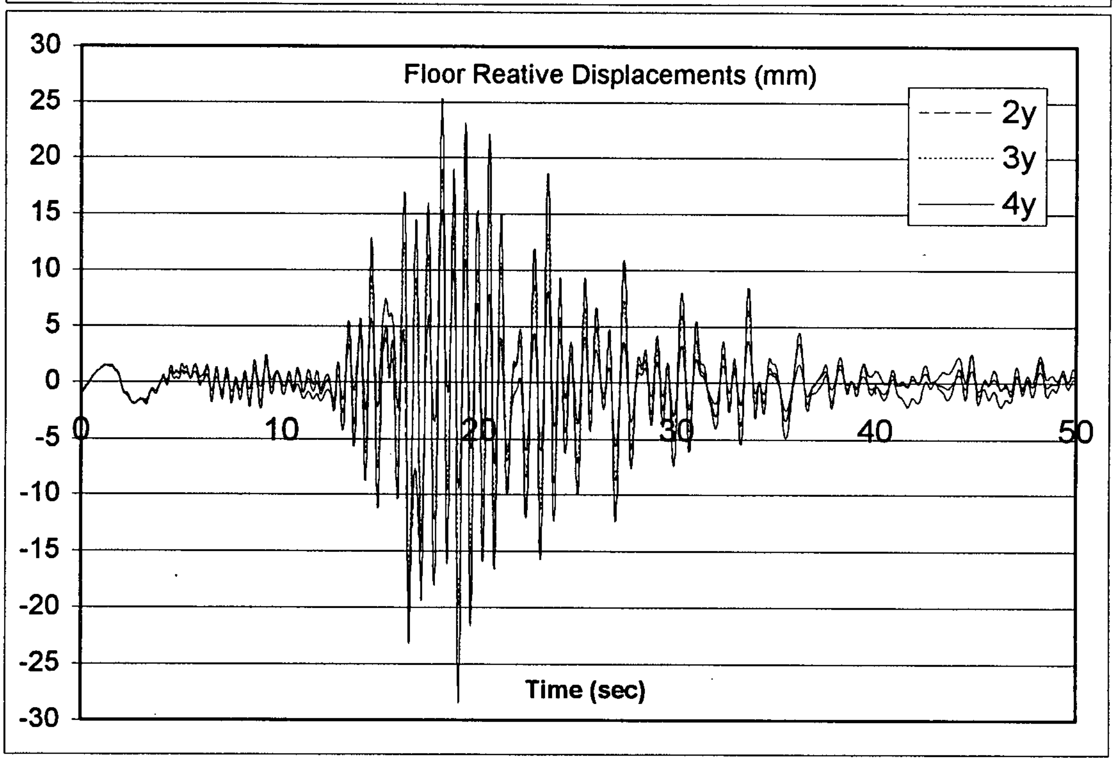

Figure 5.8.5 E-W (X-direction) & N-S (Y-direction) relative displacements of the upper floors of the Richmond 3-story office bldg., during the 1989 Loma Prieta EQ.

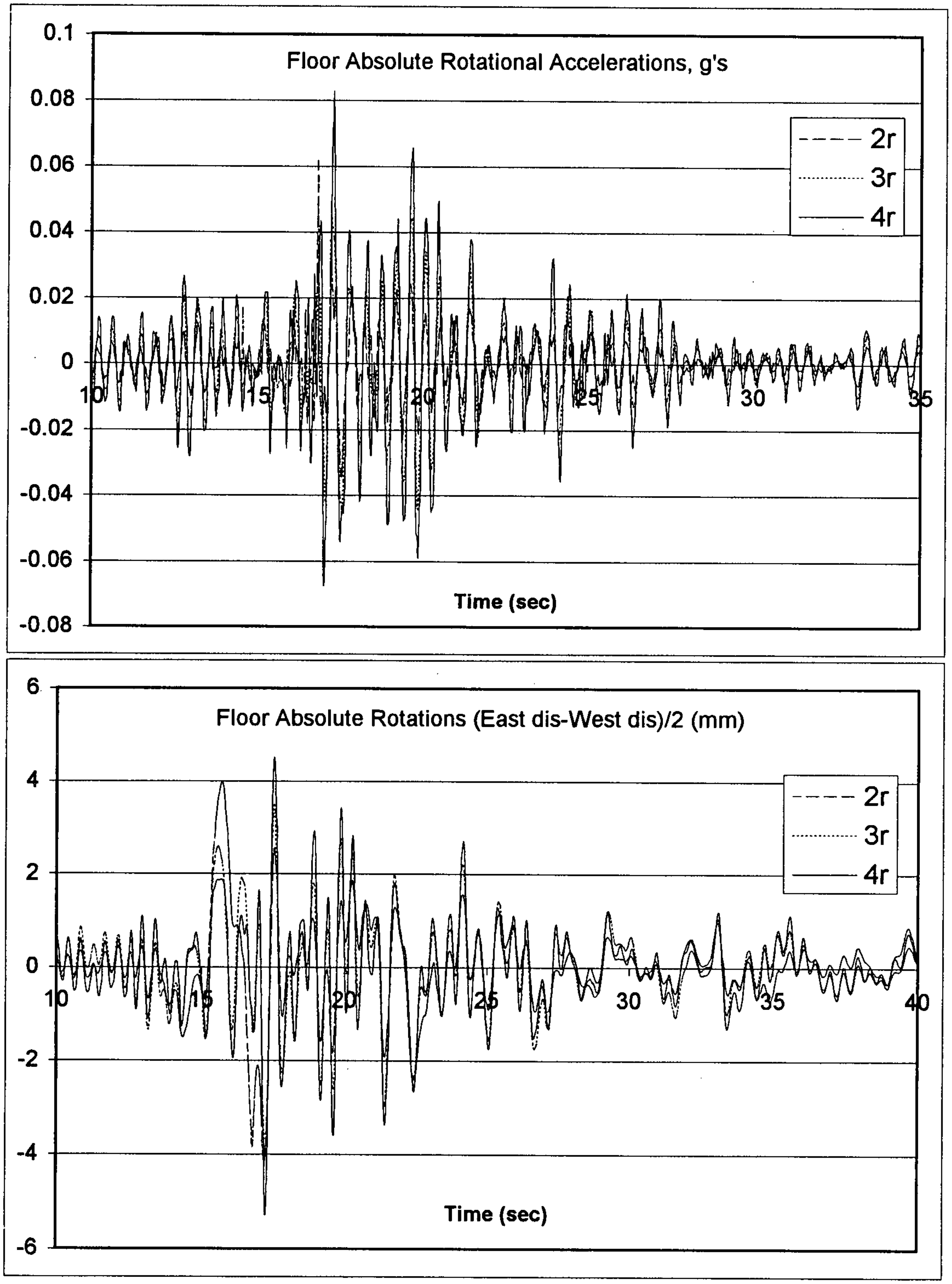

Figure 5.8.6 Torsional response of the Richmond 3-story office bldg., during the 1989 Loma Prieta EQ.

Absolute Displ. **Relative Displ.**

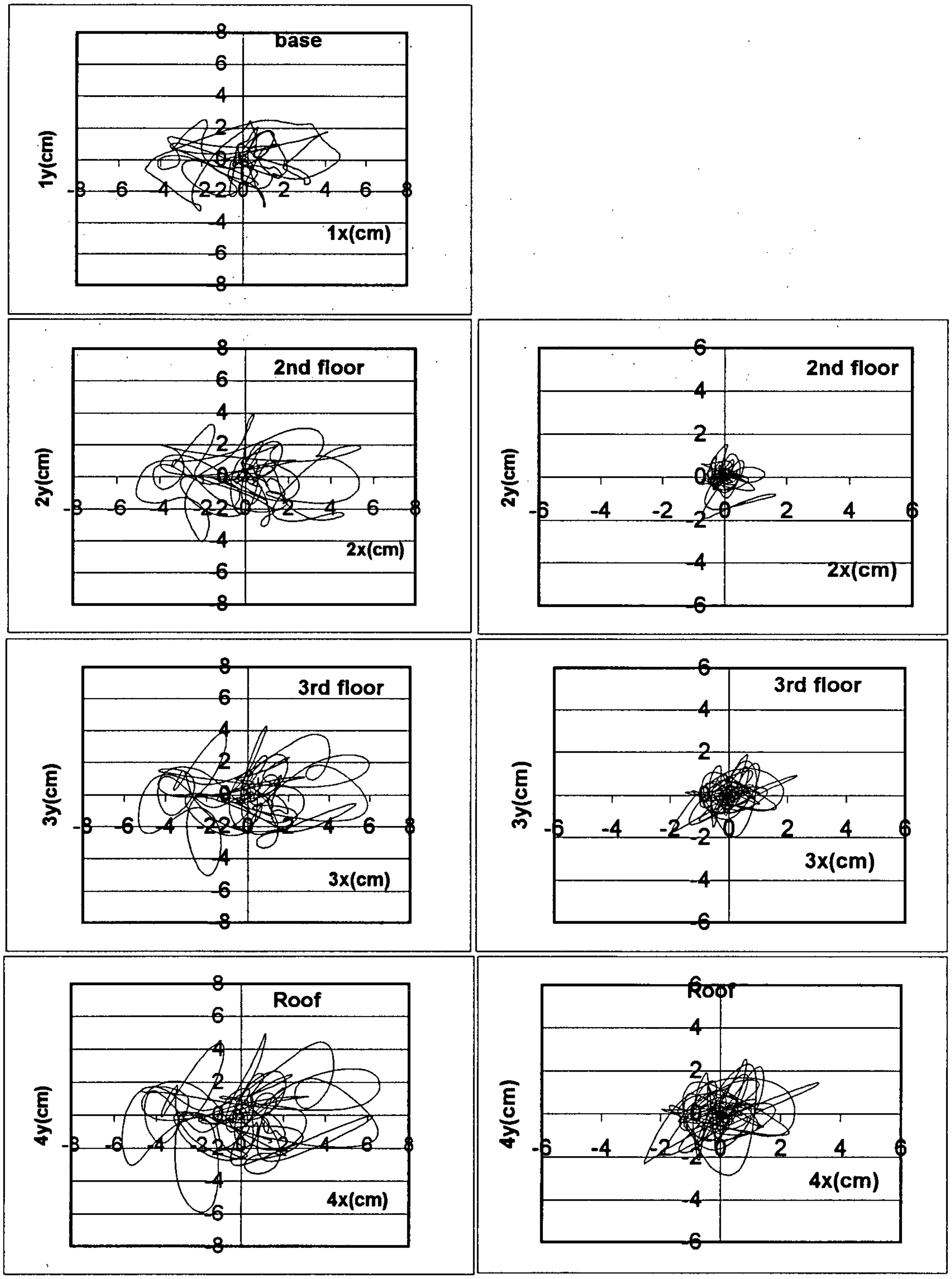

Figure 5.8.7 Orbital displacements at the center of the floors of the Richmond 3-story office bldg., during the 1989 Loma Prieta EQ.

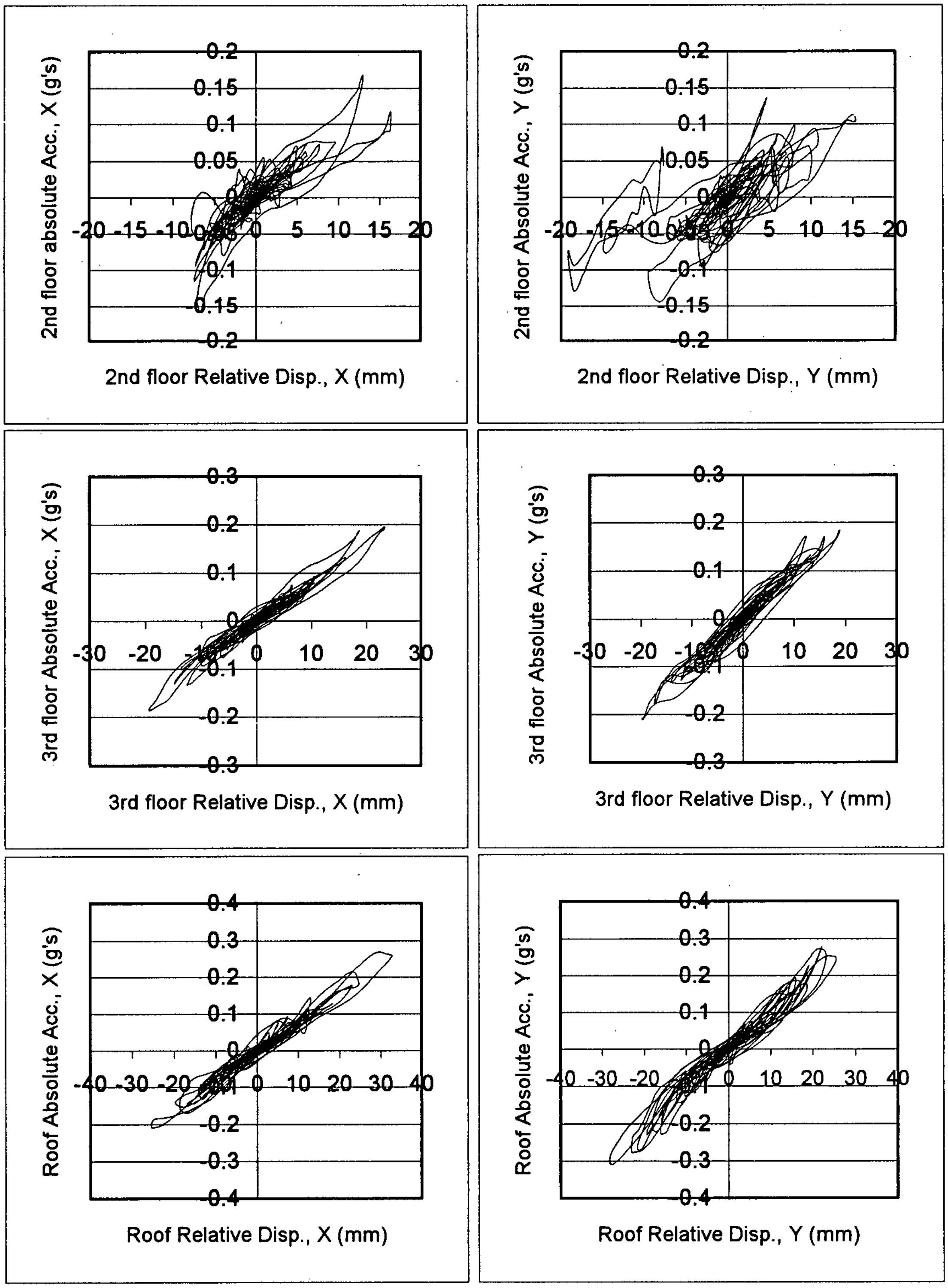

Figure 5.8.8 Representation of hysteretic behaviour at the instrumented floors of the Richmond 3-story office bldg., during the 1989 Loma Prieta EQ.

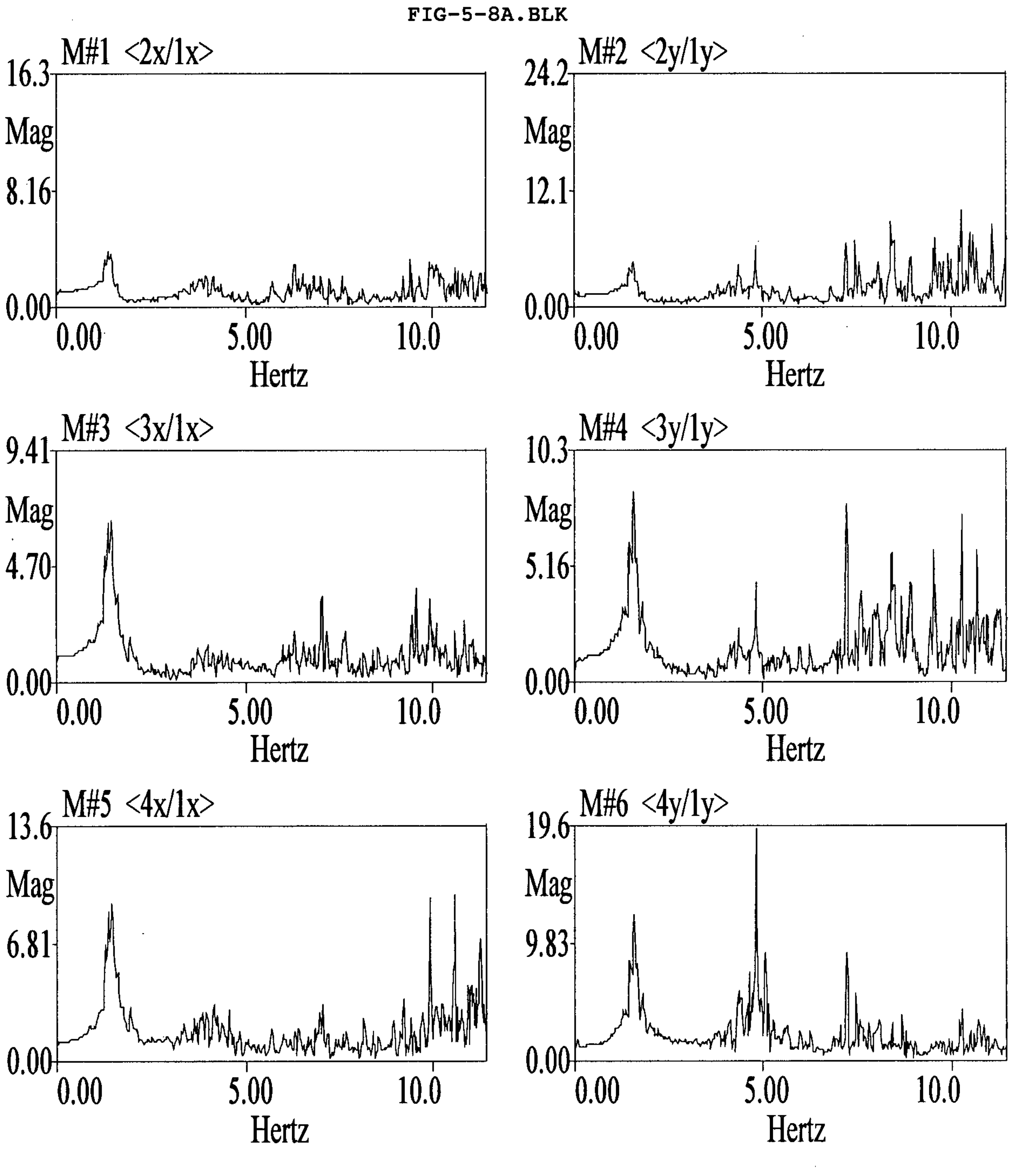

Figure 5.8.9 Frequency Response Functions of the instrumented floors of the Richmond 3-story office bldg., obtained from the 1989 Loma Prieta EQ records.

Note: The FRF's are computed by ME'scope using a Hanning window, a block size N=2048, 3 averages and 89% segment overlap.

FIG-5-8B.BLK

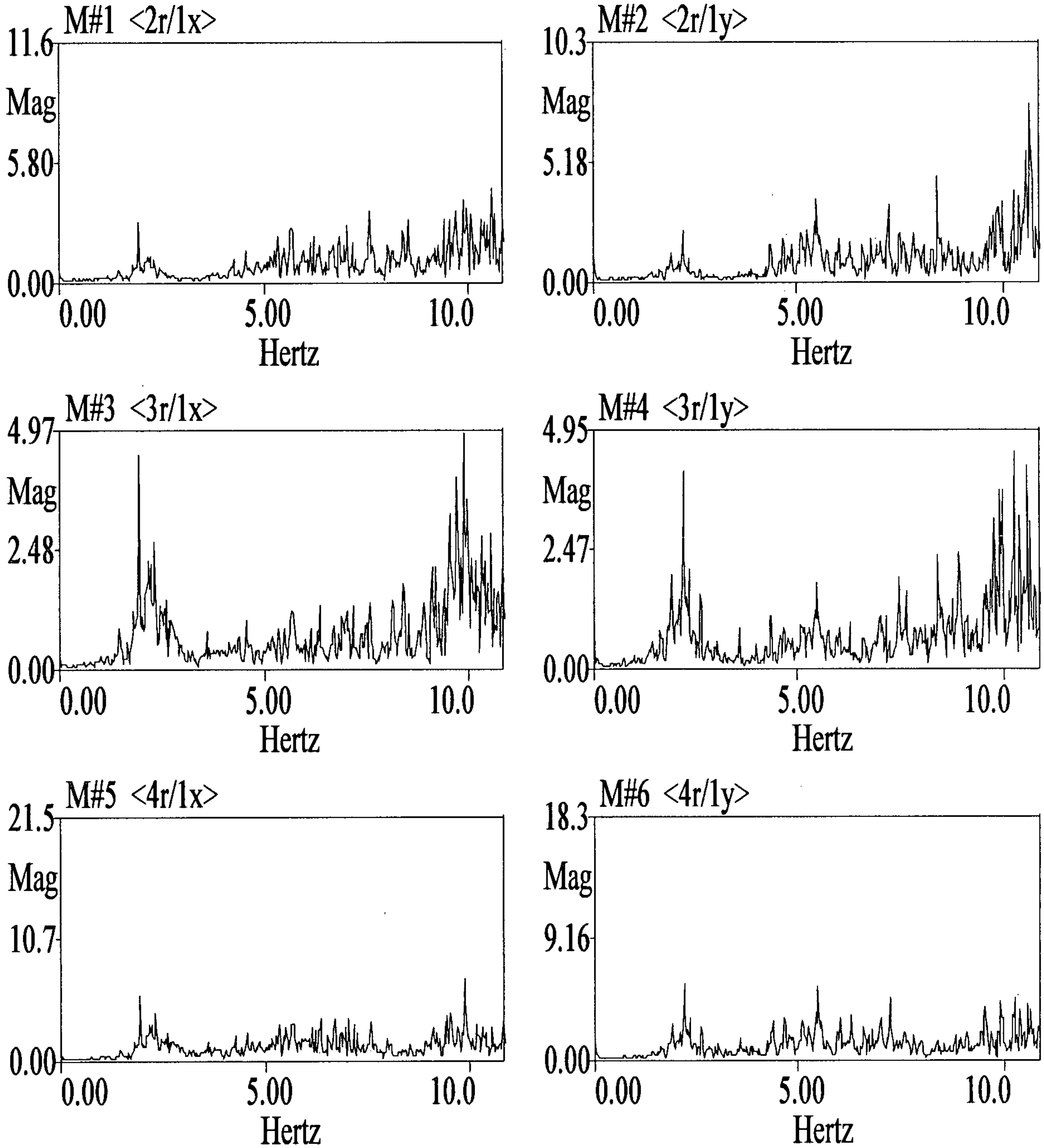

Figure 5.8.9 Cont'd

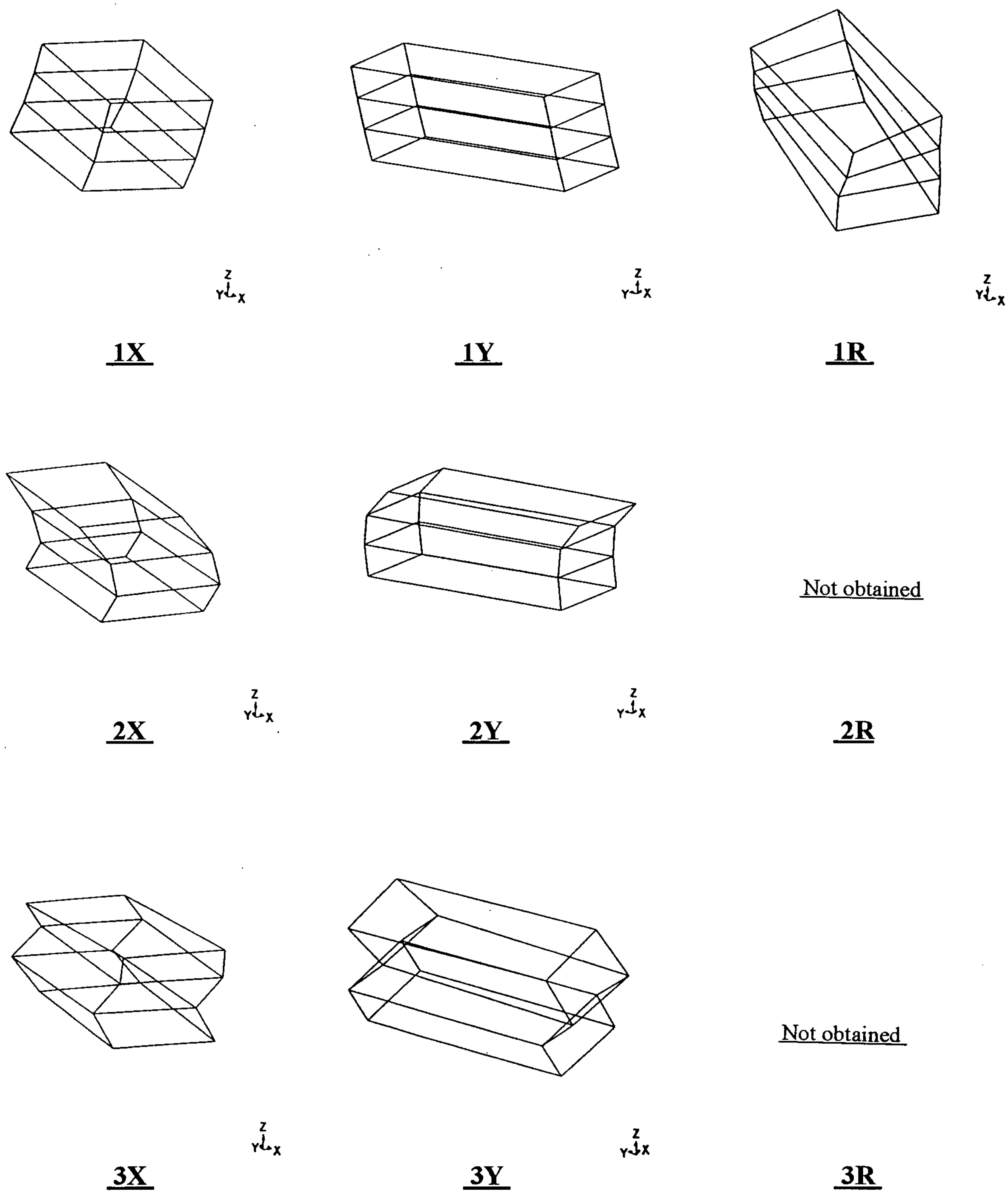

Figure 5.8.10 Mode shapes of the Richmond 3-story office bldg., obtained from the 1989 Loma Prieta EQ records.

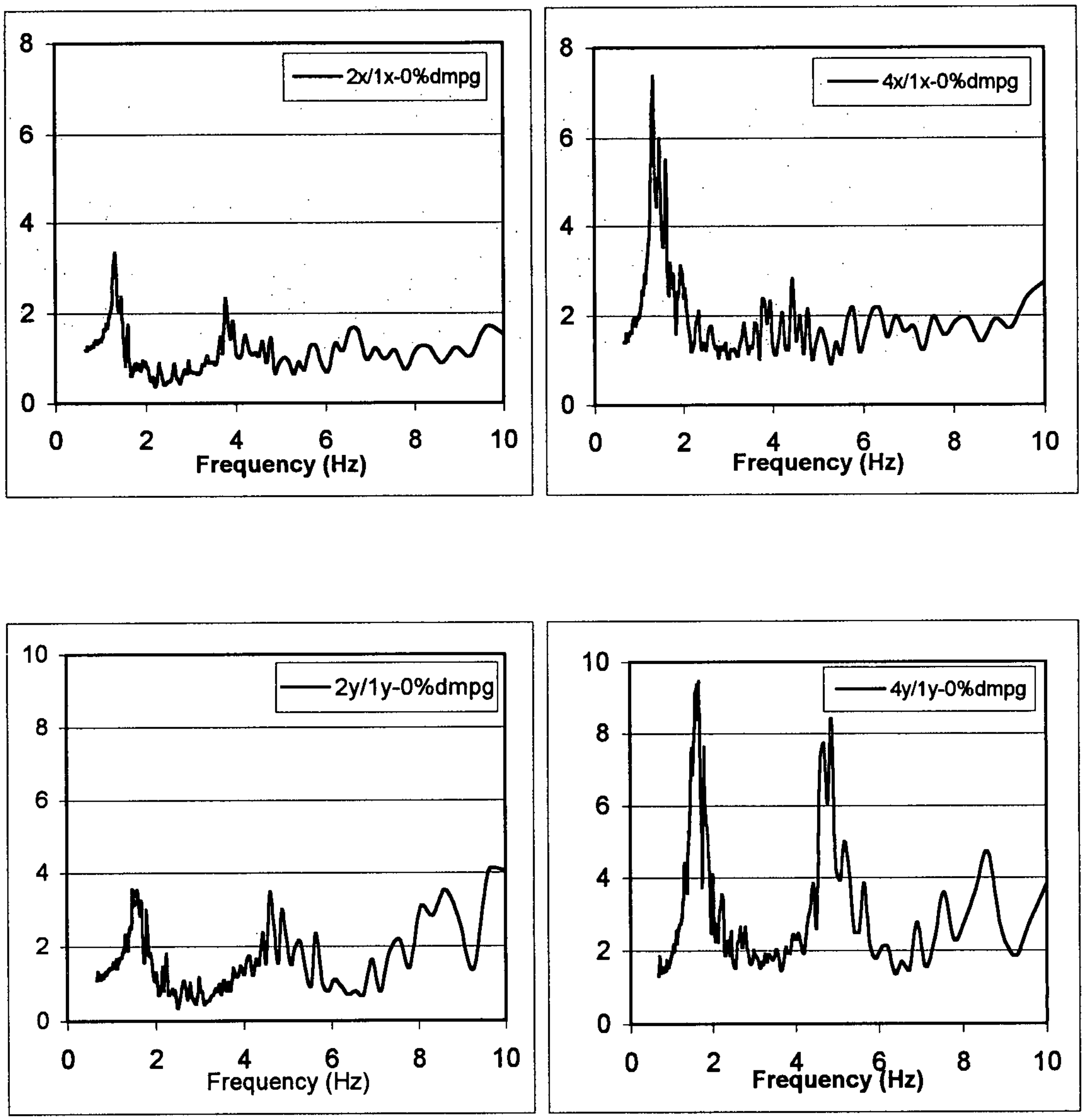

Figure 5.8.11 Spectral Response Functions of the Richmond 3-story office bldg., obtained from the 1989 Loma Prieta EQ records.

Table 5.8.1 Results of Frequency Response Functions for the Richmond 3-story office bldg., obtained from the 1989 Loma Prieta EQ records.

X-direction				
Potential Mode #	Frequency (Hz)	Amplification Factor (2X/1X)	Amplification Factor (3X/1X)	Amplification Factor (4X/1X)
1	1.42	3.72	6.62	9.24
2	4.13	2.18	1.17	3.28
3	7.00	2.10	3.45	3.24
Damping Ratio estimated by ME'scope for mode 1X: **4.55%**				
Y-direction				
Potential Mode #	Frequency (Hz)	Amplification Factor (2Y/1Y)	Amplification Factor (3Y/1Y)	Amplification Factor (4Y/1Y)
1	1.59	4.65	8.64	12.4
2	4.83	6.29	4.42	19.7
3	7.20	6.71	3.75	9.18
Damping Ratio estimated by ME'scope for mode 1Y: **2.40%**				

Table 5.8.2 Results of Spectral Response Functions for the Richmond 3-story office bldg., obtained from the 1989 Loma Prieta EQ records.

X-direction			
Potential Mode #	Frequency (Hz)	SRF 0% dmpg (2X/1X)	SRF 0% dmpg (4X/1X)
1	1.33	3.33	7.37
2a	3.76	2.32	2.38
2b	4.43	1.12	2.83
Y-direction			
Potential Mode #	Frequency (Hz)	SRF 0% dmpg (2Y/1Y)	SRF 0% dmpg (4Y/1Y)
1a	1.58	3.54	9.19
1b	1.67	3.27	9.49
2	4.87	3.00	8.40

Table 5.8.3 Estimated natural frequencies (and periods) of the Richmond 3-story office bldg. based on the results of FRF results, SRF results and visual inspection of the three dimensional mode shapes obtained from analysis of 1989 Loma Prieta EQ data.

LOMA PRIETA EARTHQUAKE DATA						
	X-Direction (E-W)		Y-Direction (E-W)		Rotation	
	Frequency (Hz)	Period (S)	Frequency (Hz)	Period (S)	Frequency (Hz)	Period (S)
Mode1	1.43	0.70	1.57	0.64	2.1	0.48
Mode 2	4.17	0.24	4.80	0.21	5.4	0.19
Mode 3	7.01	0.14	7.28	0.14	9.9	0.10

*** Spectral values at the natural periods in the ground motion response spectra and the response time-histories suggest that the 1st mode dominated the structural response.**

Fundamental Period according to **NBCC 1995**:

$\mathbf{T = 0.1\ N} \Longrightarrow \mathbf{T} = 0.30$ sec

$\mathbf{T = 0.085\ (h_n)^{3/4}} = 0.085\ (13.44\text{m})^{3/4} = 0.60$ sec

Fundamental Period according to **UBC 1997**:

$\mathbf{T = 0.035\ (h_n)^{3/4}} = 0.035\ (44.08\text{ ft})^{3/4} = 0.60$ sec

5.9 Redlands 7-Story Commercial Building

Properties of the Strong Motion Data:

Record Length: 60 sec

Time interval: 0.02 sec

No. of data points for each channel: 3000

Usable frequency range: 0.2 Hz to 23.0 Hz

Manipulating the data to obtain the motion of the center of the building in the 3 directions, E-W (or X-directions), N-S (or Y-directions) and rotation about vertical axis (or R-component):

1X = - Chan13 + {[(Chan9-Chan8)/2] .(93/140)}

1Y = - (Chan9+Chan8)/2 , 1R = (Chan9-Chan8)/2

3X = - Chan12 + {[(Chan7-Chan6)/2] .(93/140)}

3Y = - (Chan7+Chan6)/2 , 3R = (Chan7-Chan6)/2

5X = - Chan11 + {[(Chan5-Chan4)/2] .(93/140)}

5Y = - (Chan5+Chan4)/2 , 5R = (Chan5-Chan4)/2

8X = - Chan10 + {[(Chan3-Chan2)/2] .(93/140)}

8Y = - (Chan3+Chan2)/2 , 8R = (Chan3-Chan2)/2

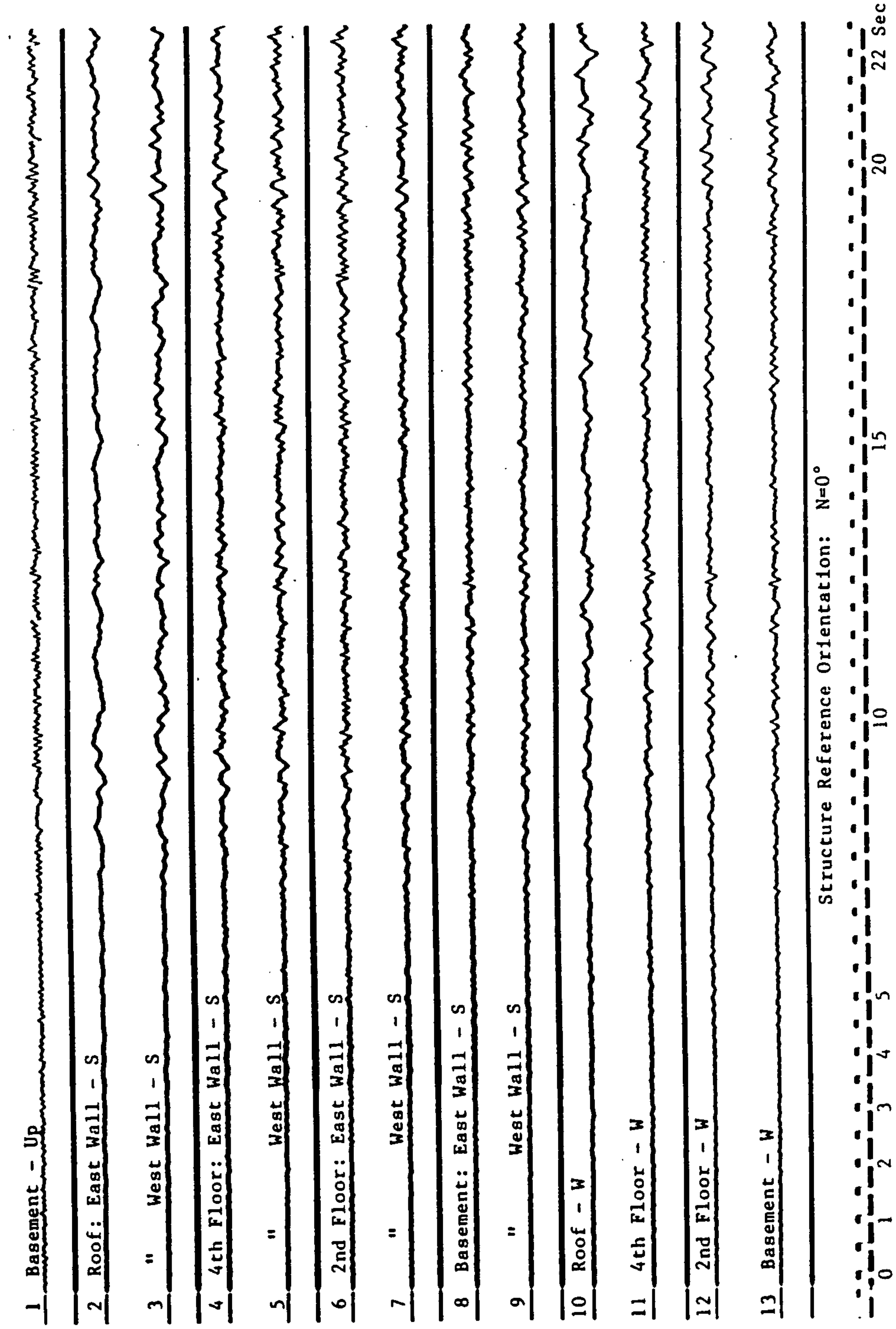

Figure 5.9.1 Accelerations recorded at the Redlands 7-story commercial bldg., during the 1992 Landers Earthquake (After Shakal, et al., 1992)

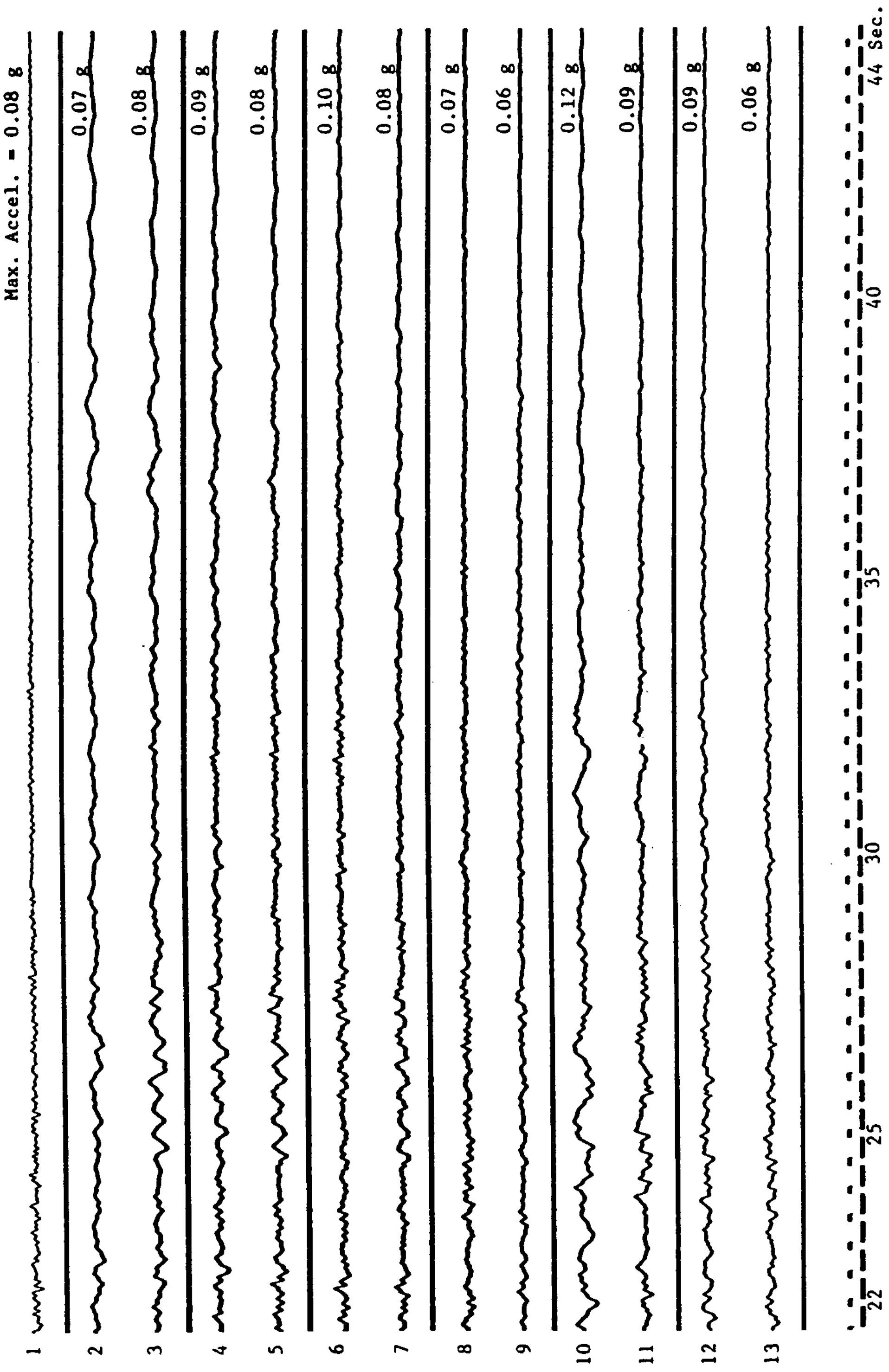

Figure 5.9.1 Continued

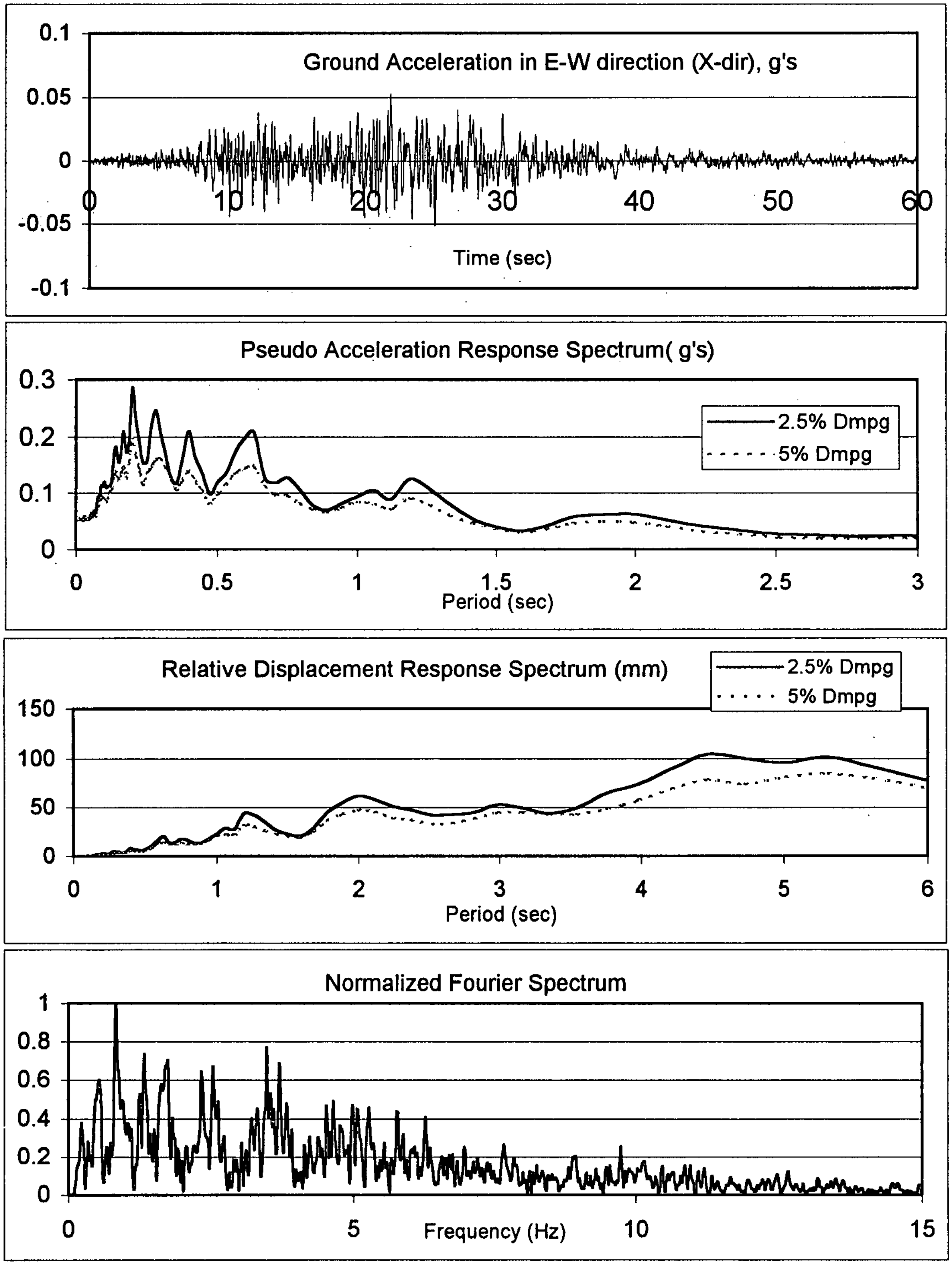

Figure 5.9.2 Time-history and spectral characteristics of E-W (X) component of the ground motion recorded at the Redlands 7-story commercial bldg., during the 1992 Landers EQ.

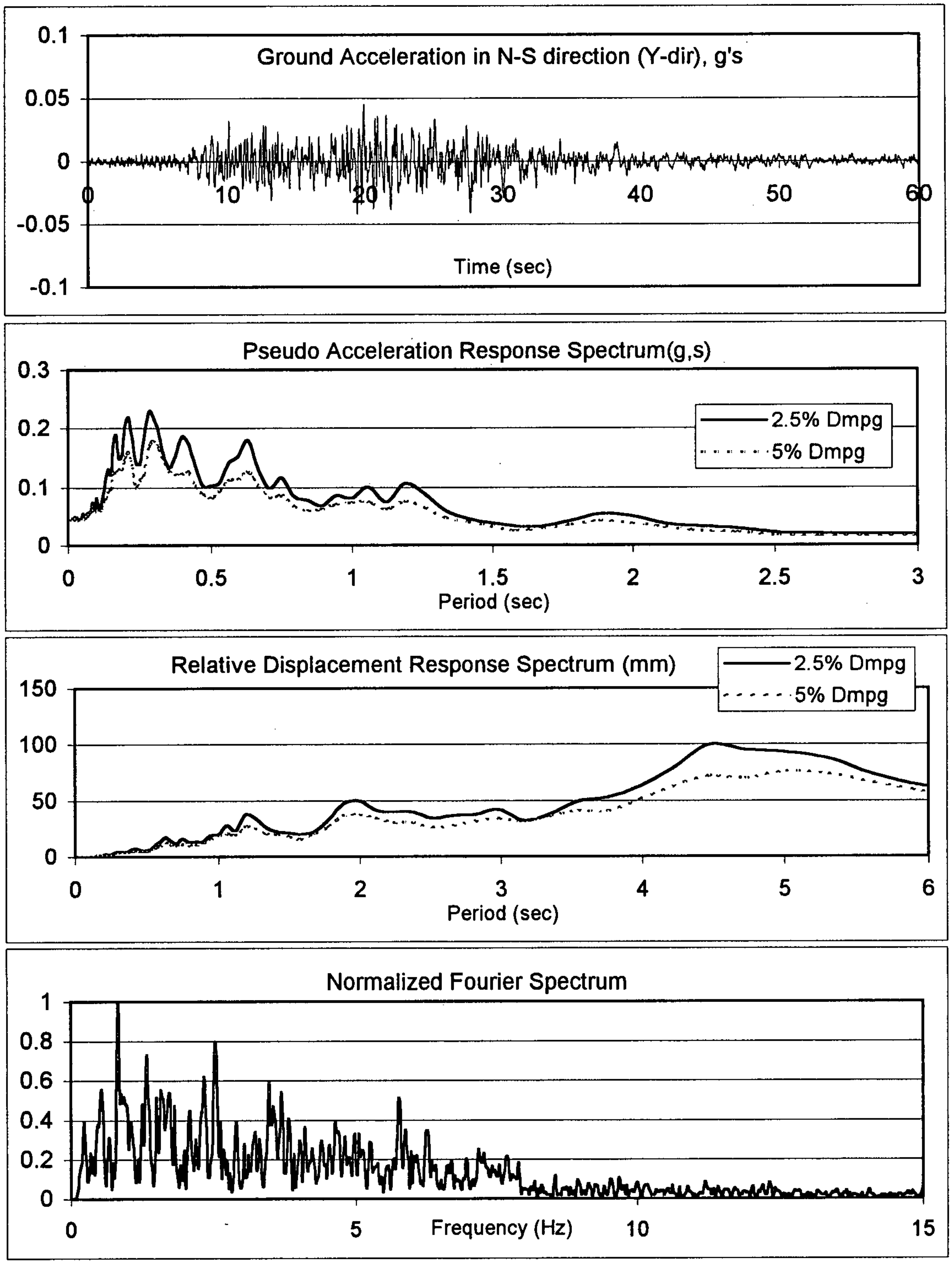

Figure 5.9.3 Time-history and spectral characteristics of N-S (Y) component of the ground motion recorded at the Redlands 7-story commercial bldg., during the 1992 Landers EQ.

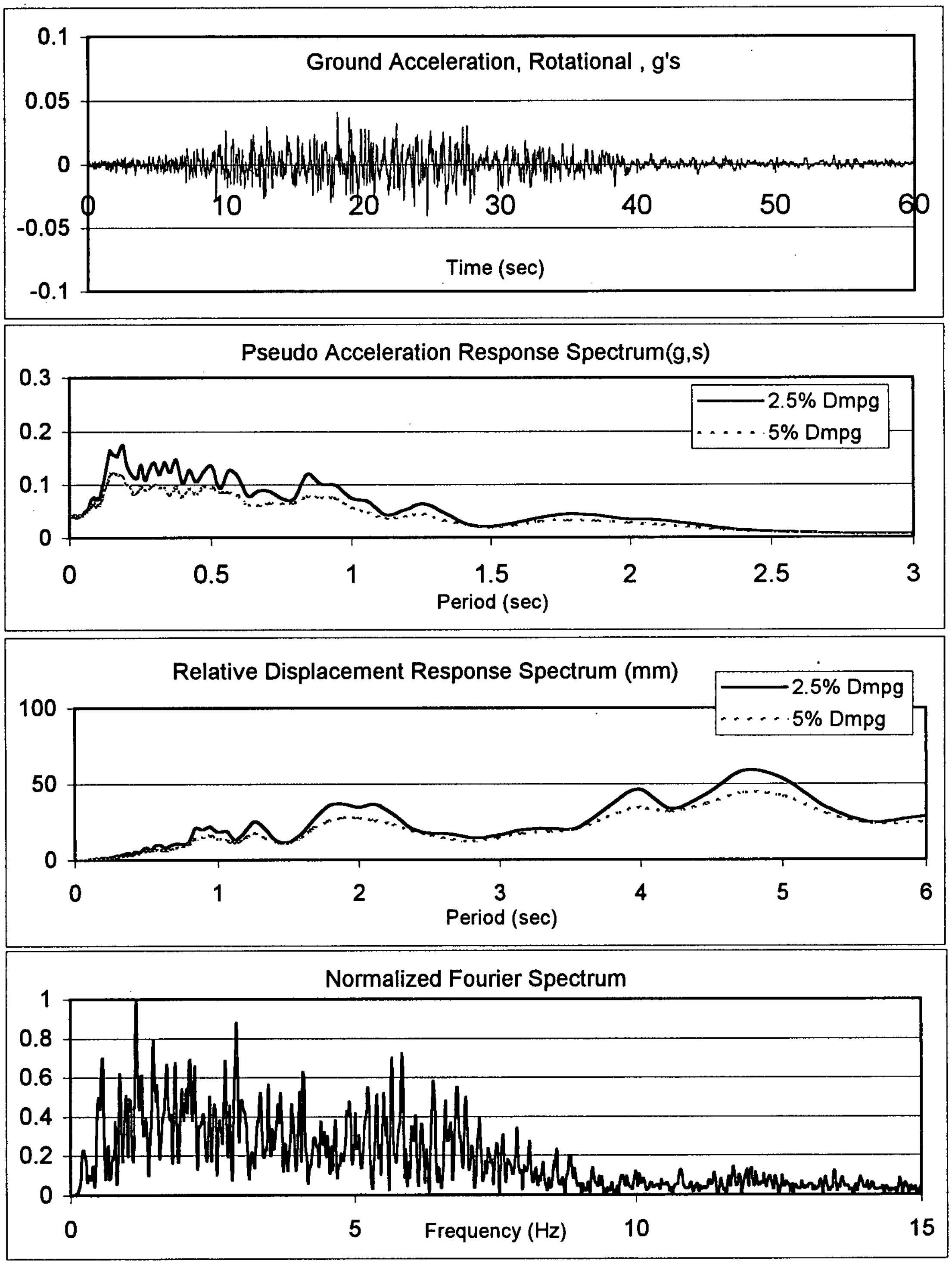

Figure 5.9.4 Time-history and spectral characteristics of rotational (R) component of the ground motion recorded at the Redlands 7-story commercial bldg., during the 1992 Landers EQ.

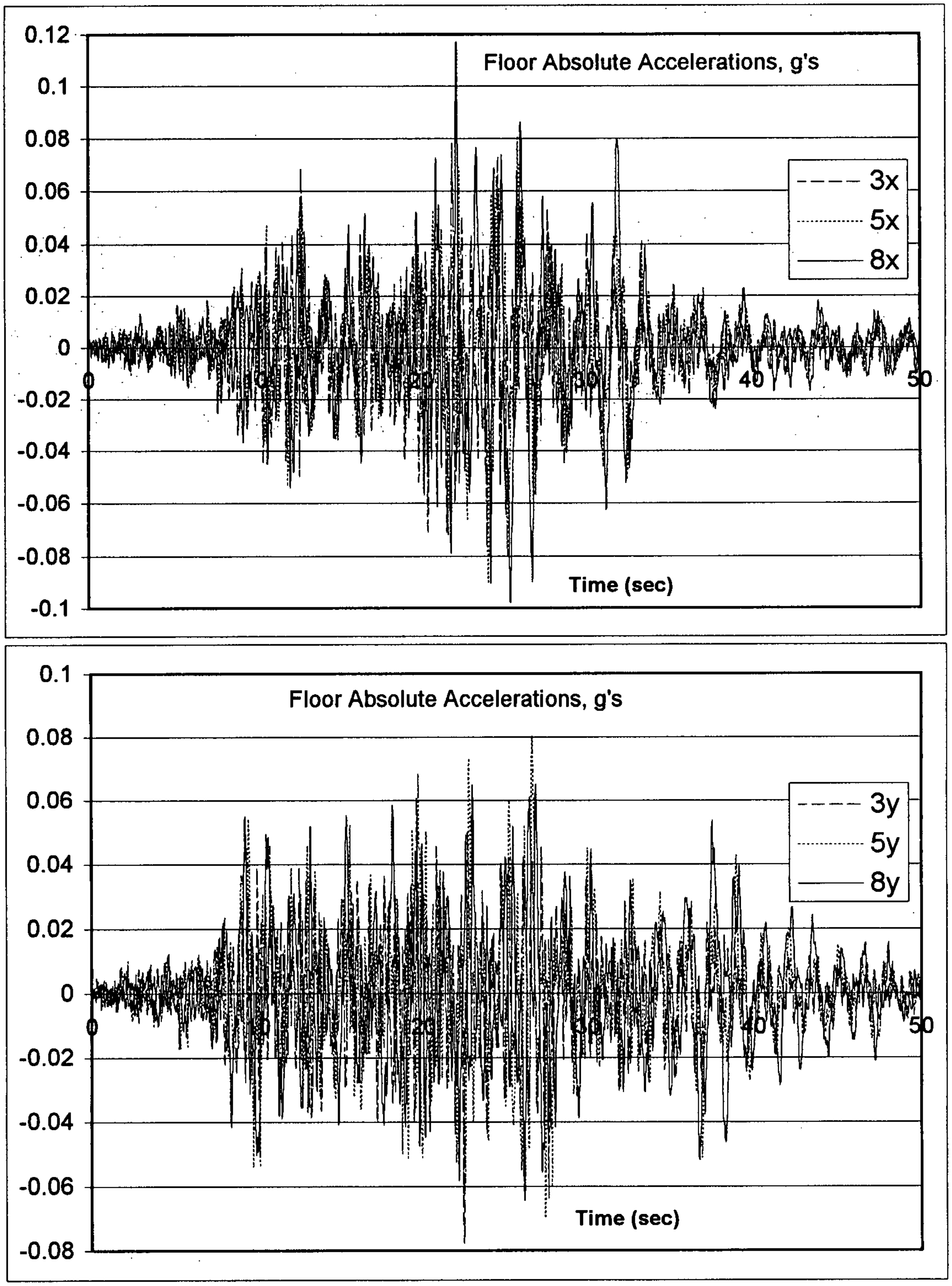

Figure 5.9.5 E-W (X-direction) & N-S (Y-direction) absolute accelerations of the instrumented upper floors of the Redlands 7-story commercial bldg., during the 1992 Landers EQ.

Note: See Appendix A for individual plots of the absolute accelerations.

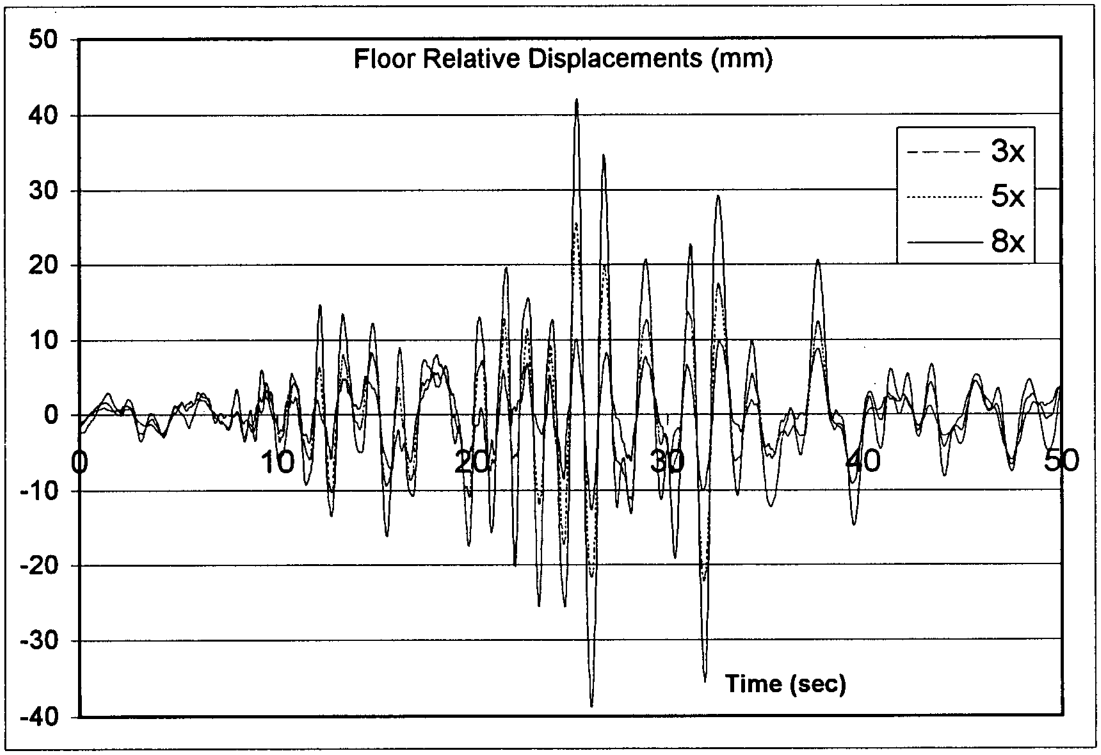

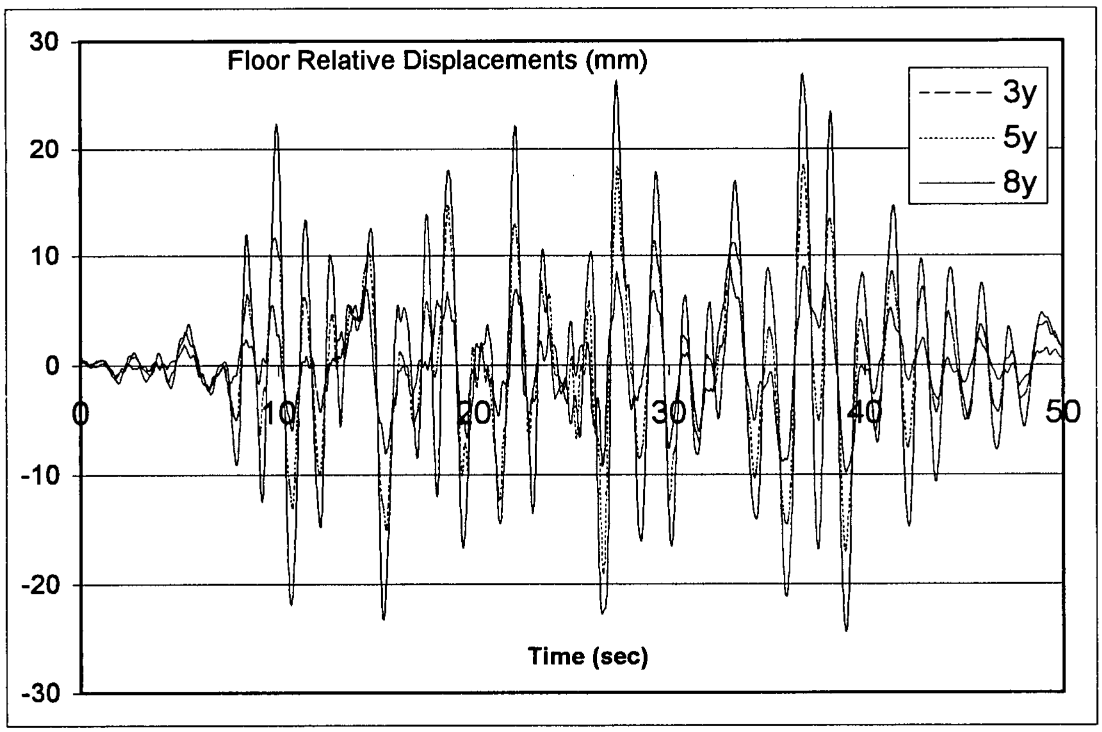

Figure 5.9.6 E-W (X-direction) & N-S (Y-direction) relative displacements of the instrumented upper floors of the Redlands 7-story commercial bldg., during the 1992 Landers EQ.

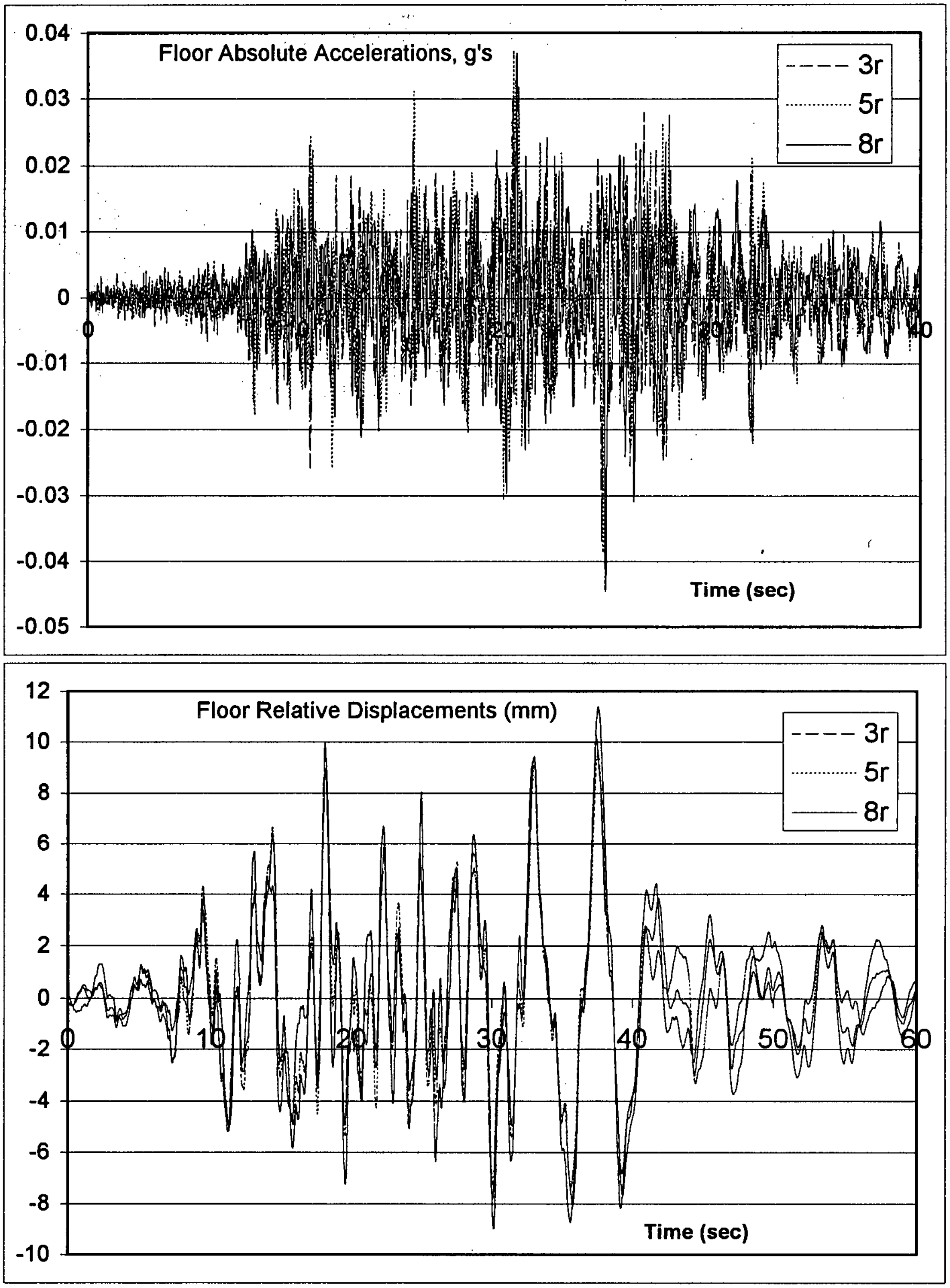

Figure 5.9.7 Torsional response of the instrumented upper floors of the Redlands 7-story commercial bldg., during the 1992 Landers EQ.

Absolute Displ. **Relative Displ.**

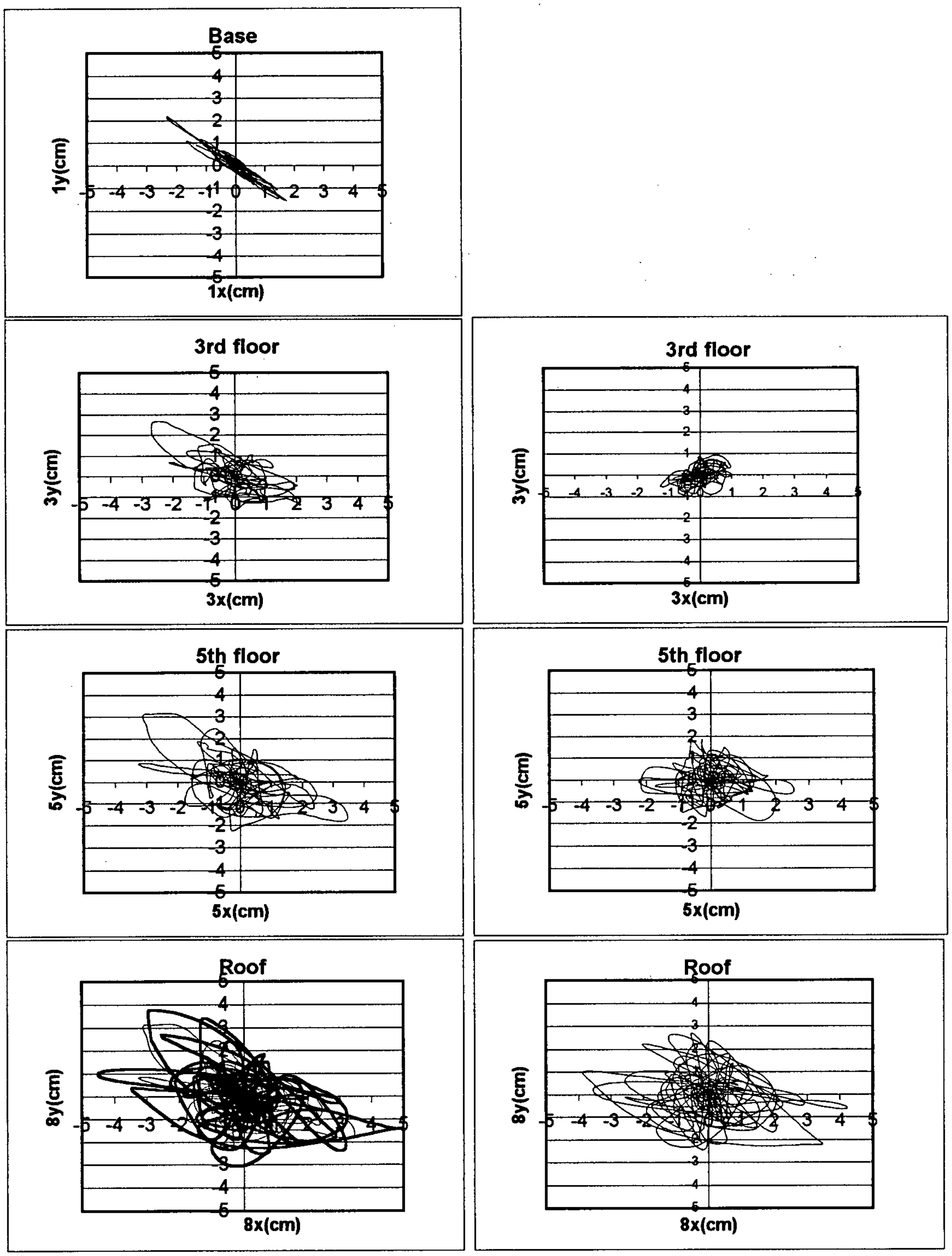

Figure 5.9.8 Orbital displacements at the center of the instrumented floors of the Redlands 7-story commercial bldg., during the 1992 Landers EQ.

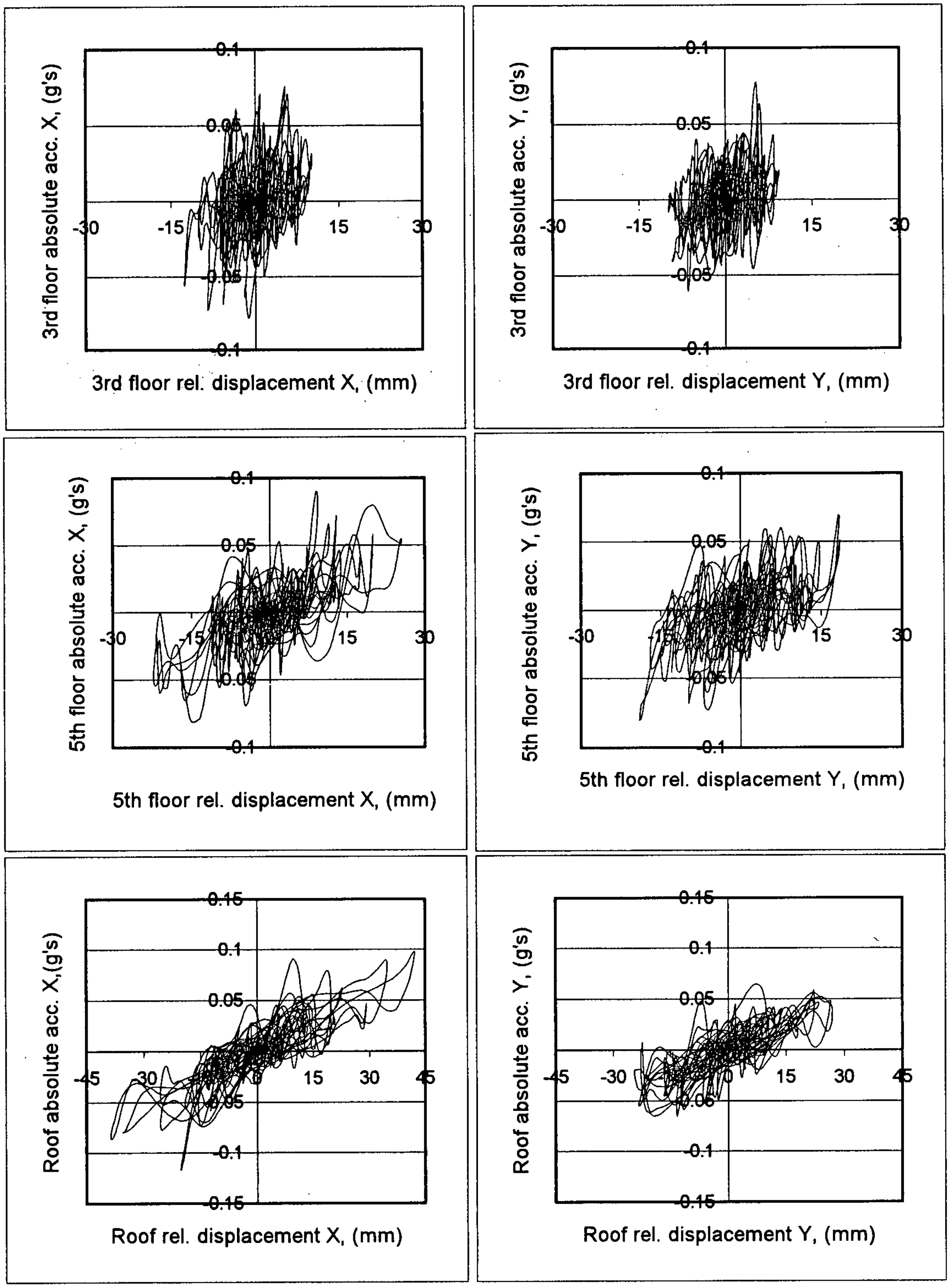

Figure 5.9.9 Representation of hysteretic behaviour at the instrumented floors of the Redlands 7-story commercial bldg., during the 1992 Landers EQ.

FIG5-9.BLK

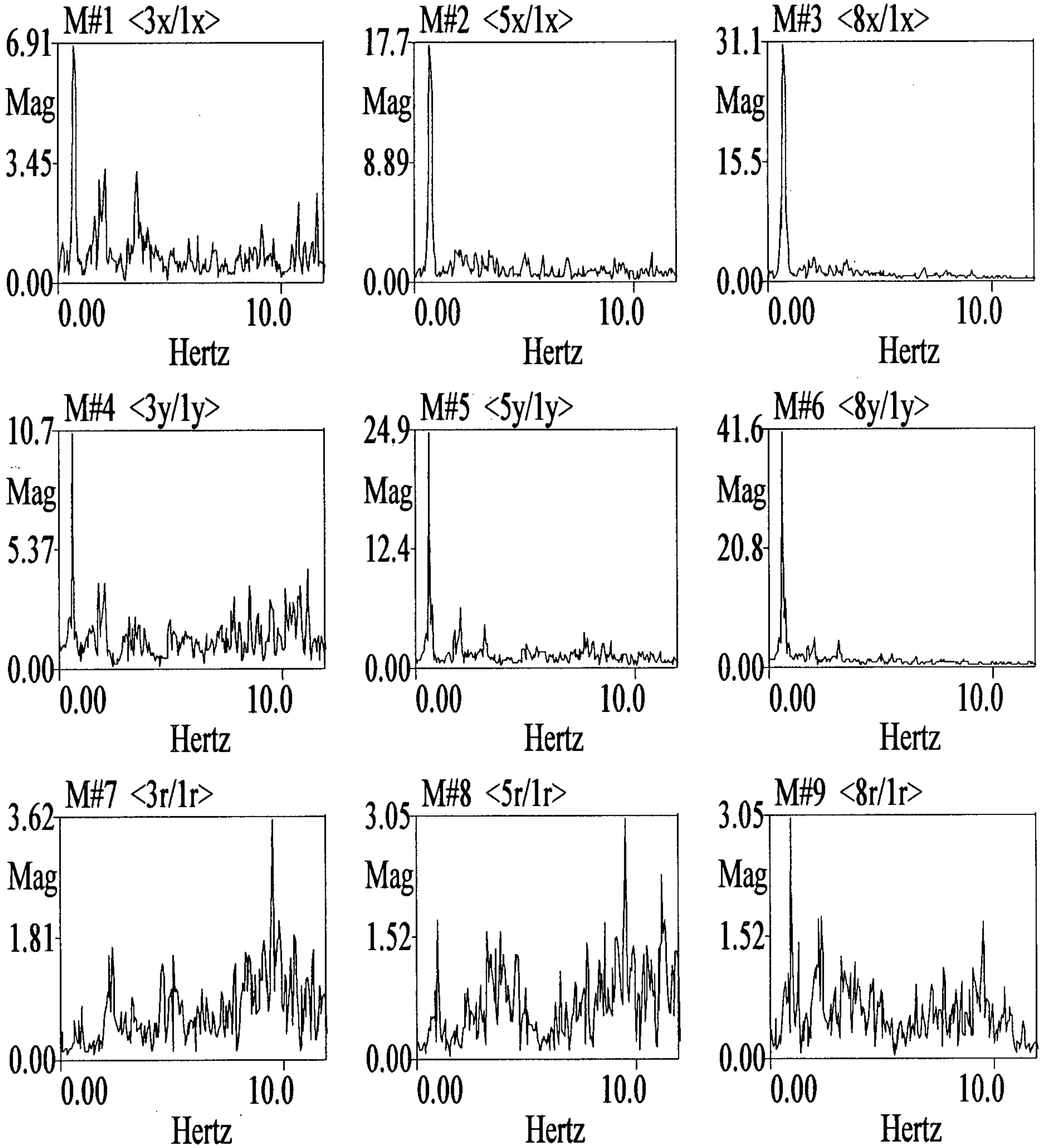

Figure 5.9.10 Frequency Response Functions of the instrumented floors of the Redlands 7-story commercial bldg., obtained from the 1992 Landers EQ records.

Note: The FRF's are computed by ME'scope using a Hanning window, a block size N=1024, 20 averages and 90% segment overlap.

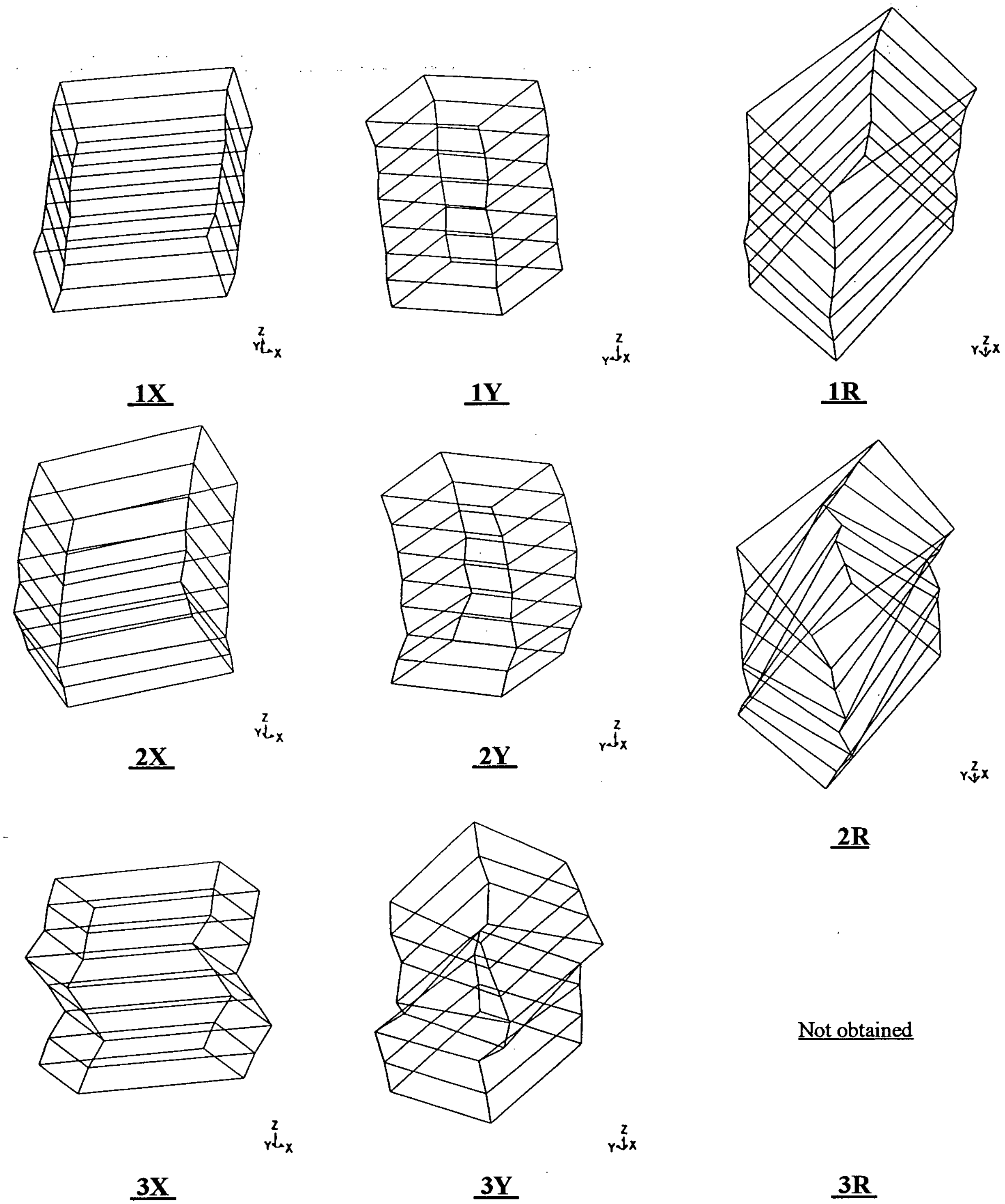

Figure 5.9.11 Mode shapes of the Redlands 7-story commercial bldg., obtained from the 1992 Landers EQ records.

Note: The displacements of levels 3, 5 and 8 (roof) are obtained from measured data. Displacements of the other floors are based on ME'scope's interpolation algorithm.

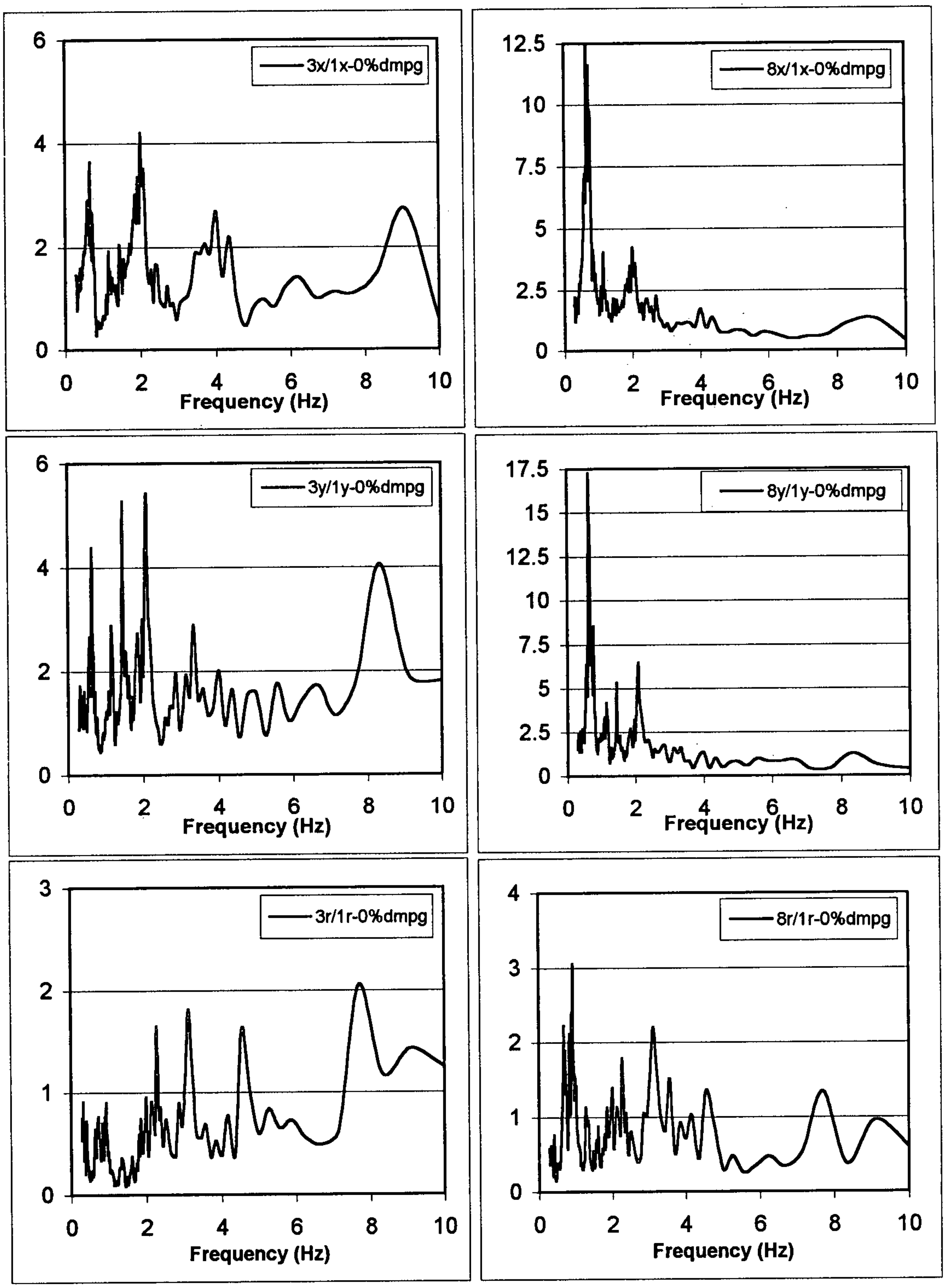

Figure 5.9.12 Spectral Response Functions of the Redlands 7-story commercial bldg., obtained from the 1992 Landers EQ records.

Table 5.9.1 Results of Frequency Response Functions for the Redlands 7-story commercial bldg., obtained from the 1992 Landers EQ records.

X-direction				
Potential Mode #	Frequency (Hz)	Amplification Factor (3X/1X)	Amplification Factor (5X/1X)	Amplification Factor (8X/1X)
1	0.73	6.40	16.4	29.1
2	2.10	3.27	2.35	3.00
3	5.52	3.24	1.84	2.53
Damping Ratio estimated by ME'scope for the first mode: **3.94%**				
Y-direction				
Potential Mode #	Frequency (Hz)	Amplification Factor (3Y/1Y)	Amplification Factor (5Y/1Y)	Amplification Factor (8Y/1Y)
1	0.59	10.8	24.9	41.7
2	1.76	3.81	3.75	3.51
Damping Ratio estimated by ME'scope for the first mode: **3.53%**				
R-direction				
Potential Mode #	Frequency (Hz)	Amplification Factor (3R/1R)	Amplification Factor (5R/1R)	Amplification Factor (8R/1R)
1	0.93	0.80	1.70	3.10
2	3.17	0.89	1.58	1.28
Damping Ratio estimated by ME'scope for the first mode: **4.18%**				

Table 5.9.2 Results of Spectral Response Functions for the Redlands 7-story commercial bldg., obtained from the 1992 Landers EQ records

Potential Mode #	Frequency (Hz)	SRF 0% dmpg (3rd floor/base)	SRF 0% dmpg (8th floor/base)
1X	0.66	3.55	12.4
1Y	0.63	4.37	17.2
1R	0.94	0.90	3.05

Table 5.9.3 Estimated natural frequencies (and periods) of the Redlands 7-story commercial bldg., based on the results of FRF results, SRF results and visual inspection of the three dimensional mode shapes obtained from analysis of 1992 Landers EQ data.

LANDERS EARTHQUAKE DATA						
	X-Direction (E-W)		Y-Direction (E-W)		Rotation	
	Frequency (Hz)	Period (S)	Frequency (Hz)	Period (S)	Frequency (Hz)	Period (S)
Model	0.73	1.37	0.63	1.59	0.95	1.05
Mode 2	2.10	0.48	1.90	0.53	3.30	0.30
Mode 3	3.50	0.29	-	-	-	-

*** Spectral values at the natural periods in the ground motion response spectra and the response time-histories suggest that the 2nd & 3rd modes had a significant contribution in the structural response.**

Fundamental Period according to **NBCC 1995**:

T = 0.1 N ==> T = 0.70 sec

$\mathbf{T = 0.085\,(h_n)^{3/4}} = 0.085\,(31.83m)^{3/4} = 1.14$ sec

Fundamental Period according to **UBC 1997**:

$\mathbf{T = 0.035\,(h_n)^{3/4}} = 0.035\,(104.42ft)^{3/4} = 1.14$ sec

5.10 San Bernardino 3-Story Office Building

Properties of the Strong Motion Data:

Record Length: 80 sec

Time interval: 0.02 sec

No. of data points for each channel: 4000

Usable frequency range: 0.16 Hz to 23.0 Hz

Manipulating the data to obtain the motion of the center of the building in the 3 directions, E-W (or X-directions), N-S (or Y-directions) and rotation about vertical axis (or R-component):

1X = -(Chan9), 1Y = (Chan13)

2X = -(Chan7 + Chan8)/2, 2Y = (Chan12), 2R = (Chan6-Chan4)/2

3X = -(Chan4 + 2 .Chan5 + Chan6)/4, 3Y = (Chan11), 3R = (Chan8-Chan7)/2

4X = -(Chan3 + Chan2)/2, 4Y = (Chan10), 4R = (Chan3-Chan2)/2

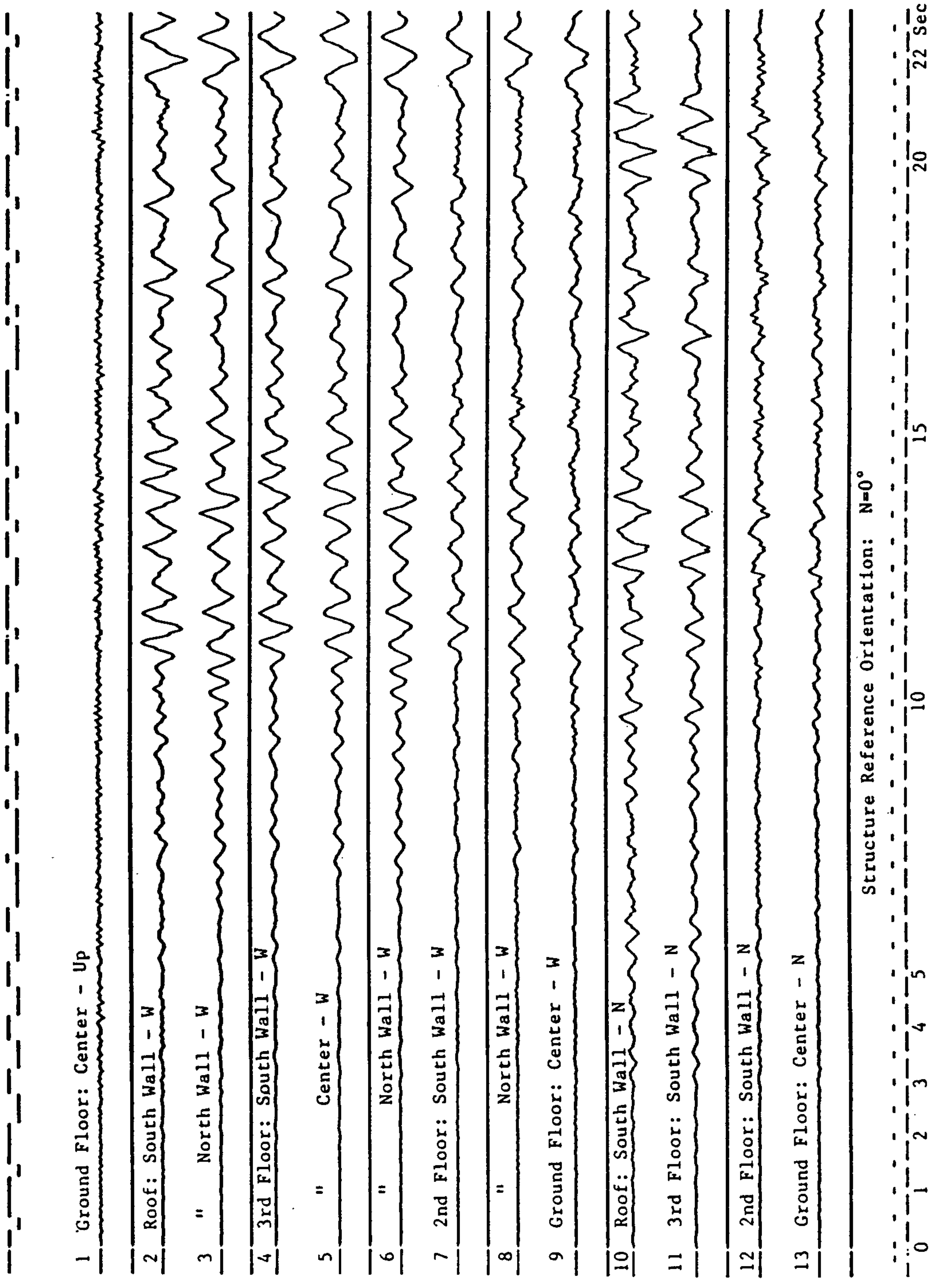

Figure 5.10.1 Accelerations recorded at the San Bernardino 3-story office bldg., during the 1992 Landers Earthquake (After Shakal, et al., 1992)

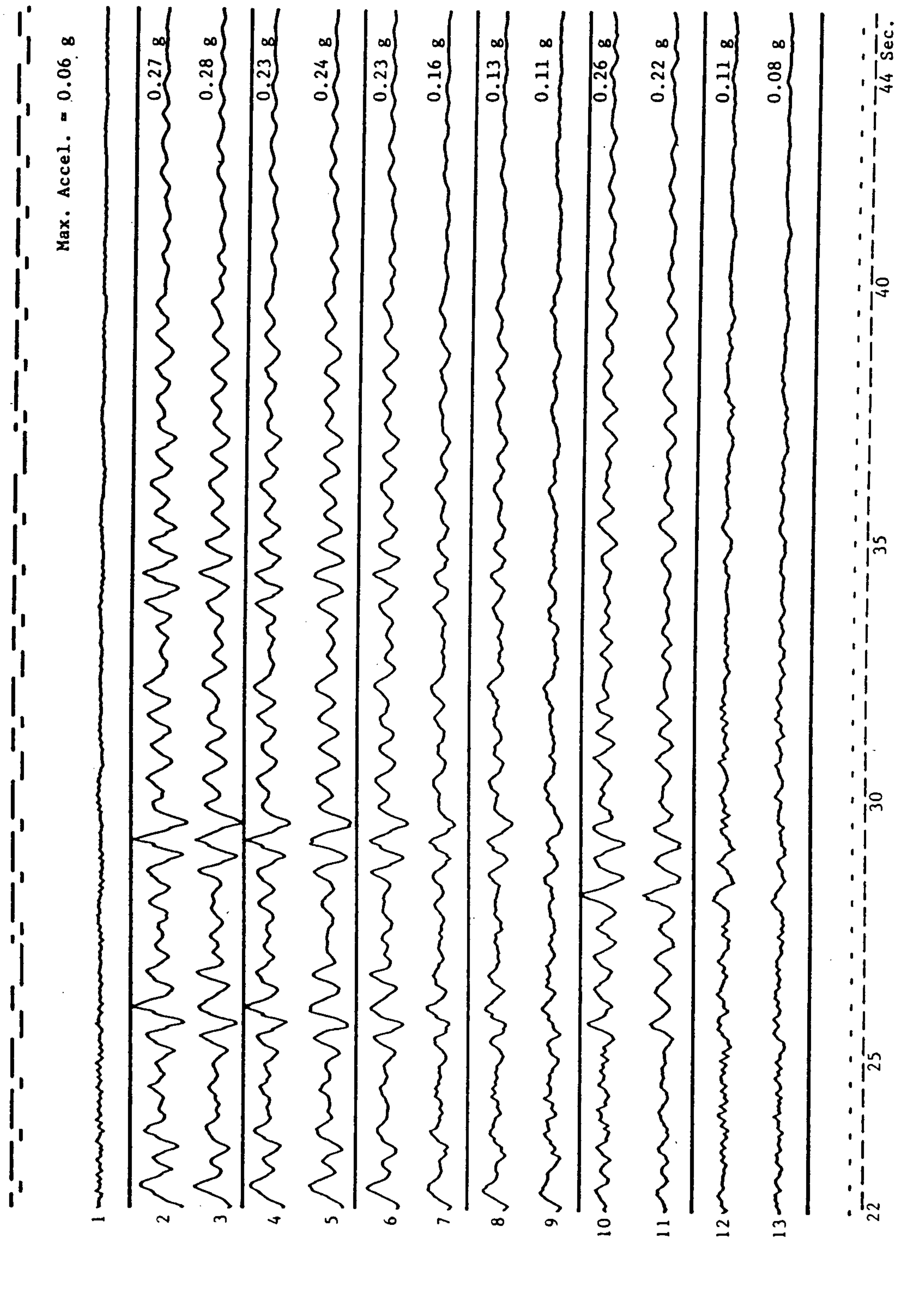

Figure 5.10.1 Continued

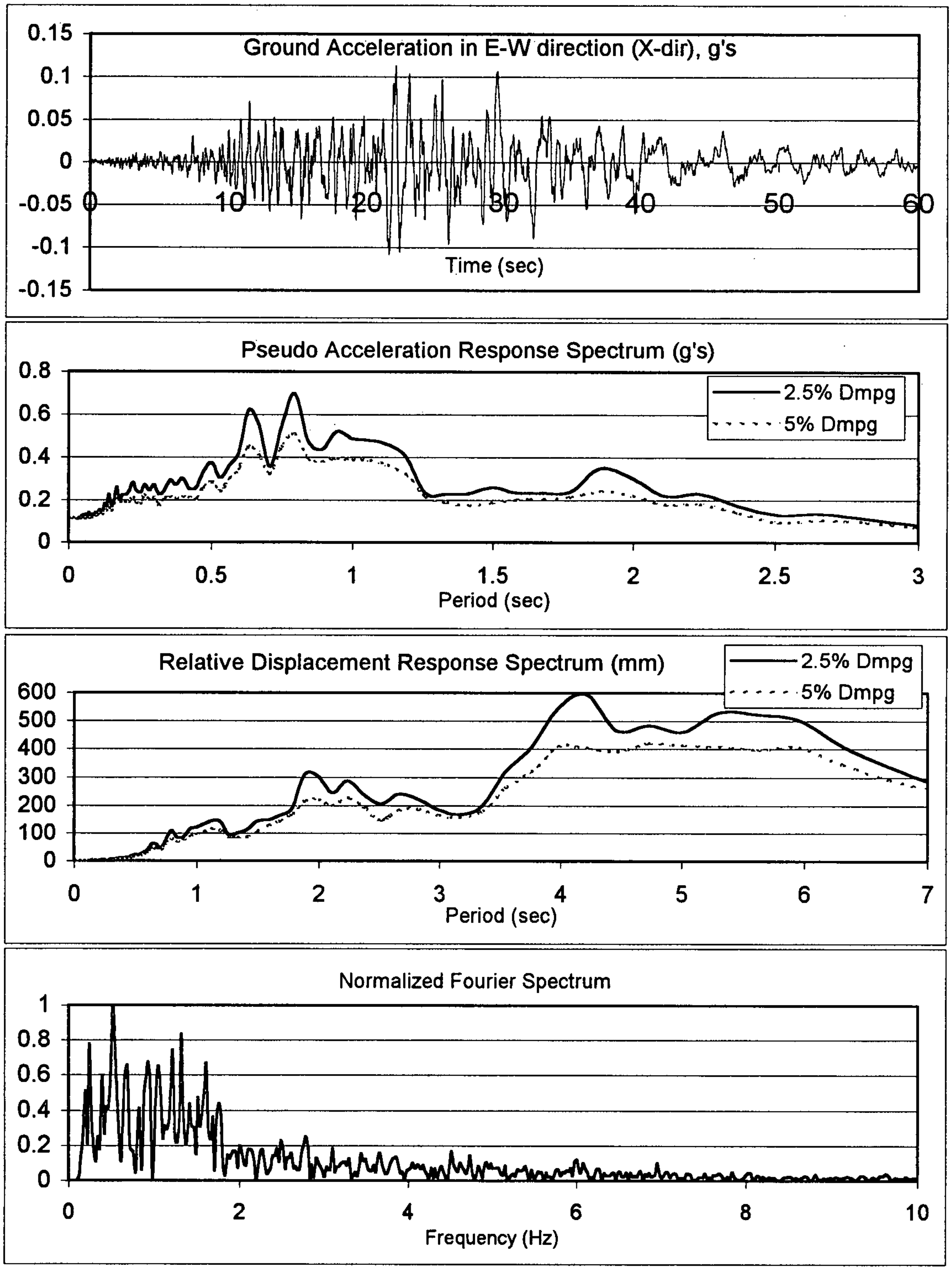

Figure 5.10.2 Time-history and spectral characteristics of E-W (X) component of the ground motion recorded at the San Bernardino 3-story office bldg., during the 1992 Landers EQ.

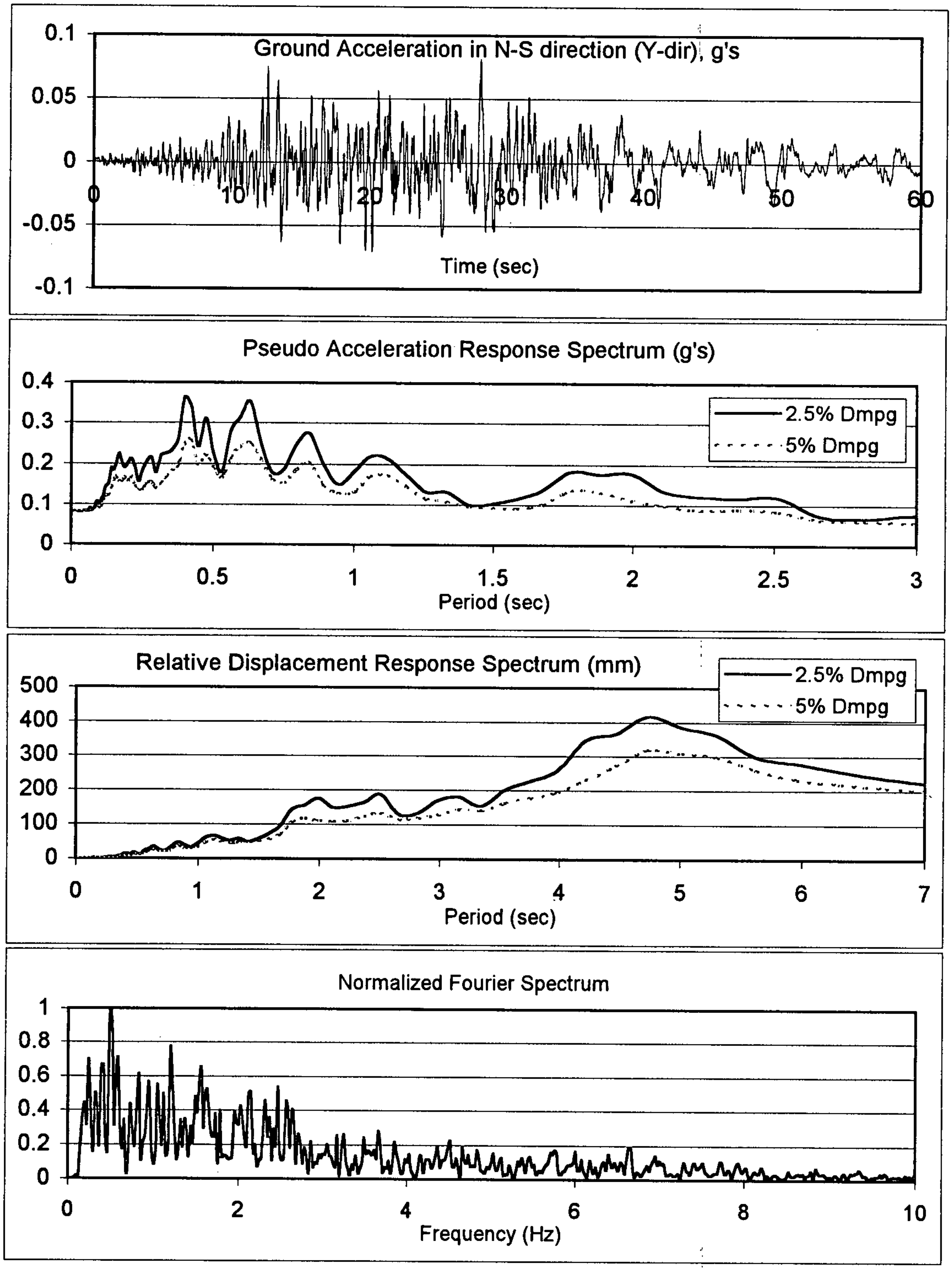

Figure 5.10.3 Time-history and spectral characteristics of N-S (Y) component of the ground motion recorded at the San Bernardino 3-story office bldg., during the 1992 Landers EQ.

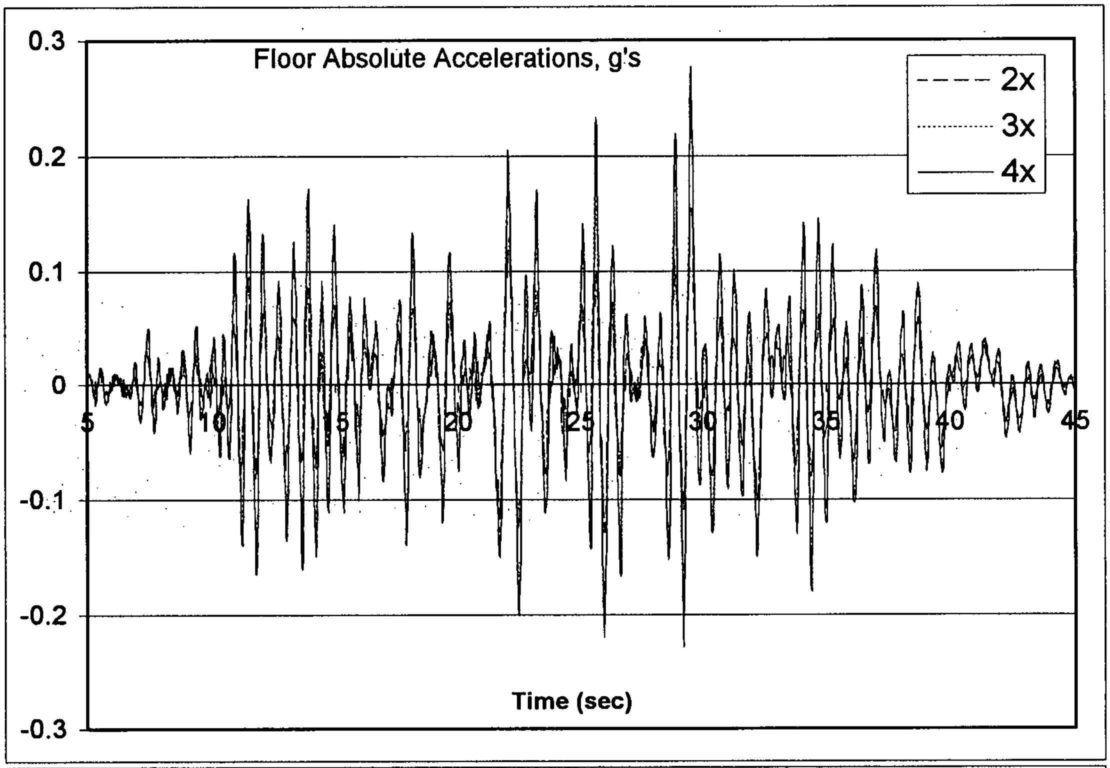

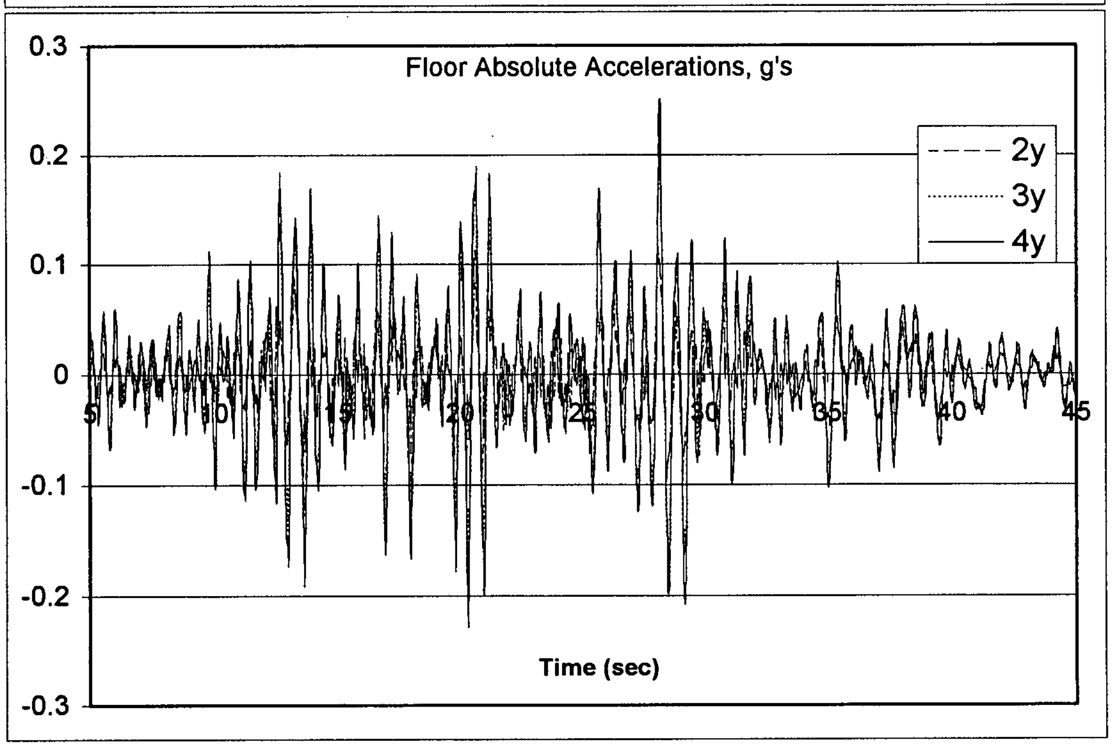

Figure 5.10.4 E-W (X-direction) & N-S (Y-direction) absolute accelerations of the upper floors of the San Bernardino 3-story office bldg., during the 1992 Landers EQ.

Note: See Appendix A for individual plots of the absolute accelerations.

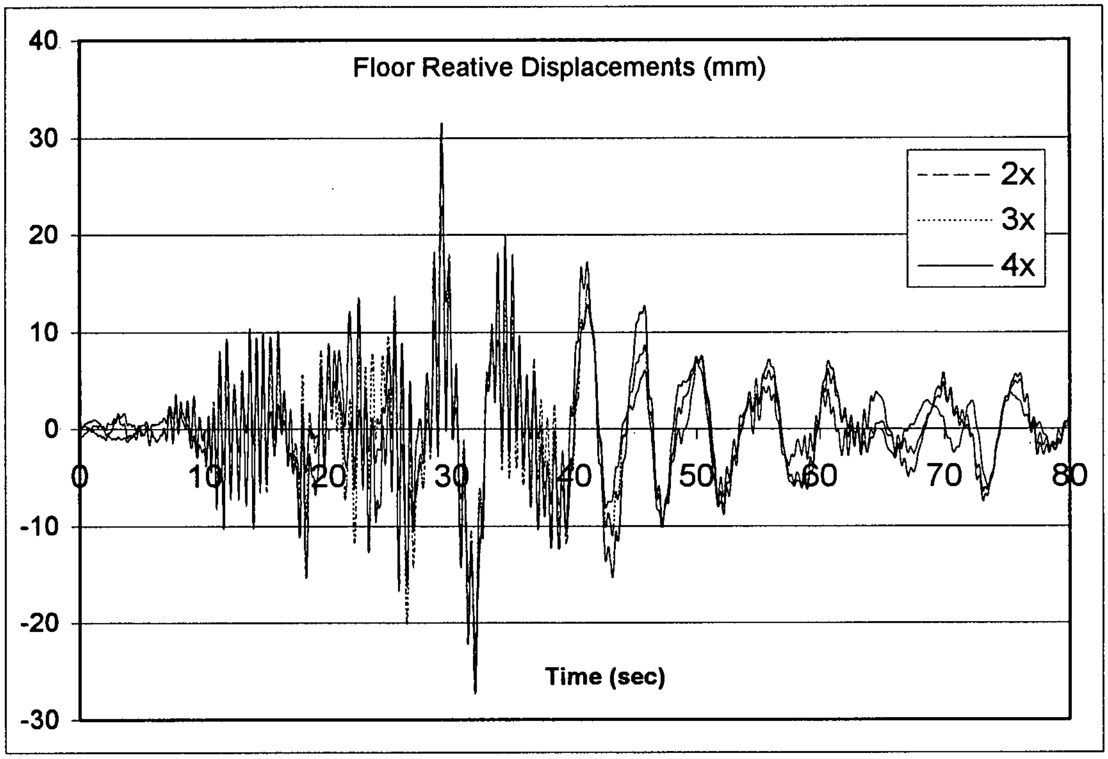

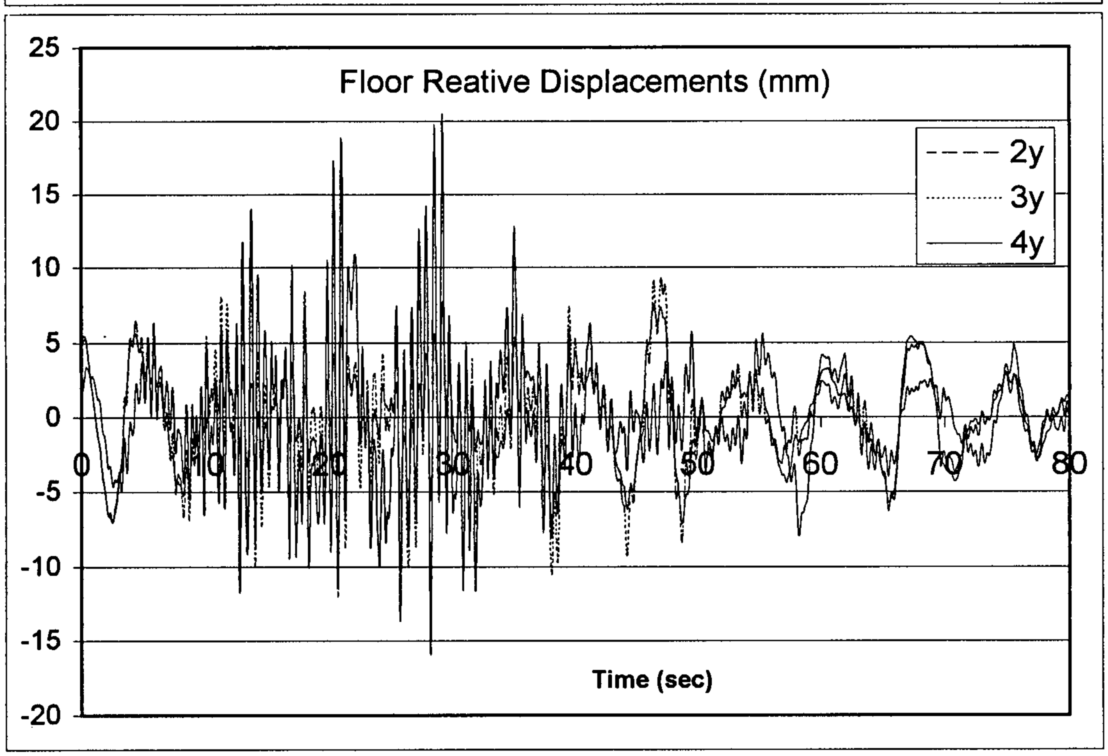

Figure 5.10.5 E-W (X-direction) & N-S (Y-direction) relative displacements of the upper floors of the San Bernardino 3-story office bldg., during the 1992 Landers EQ.

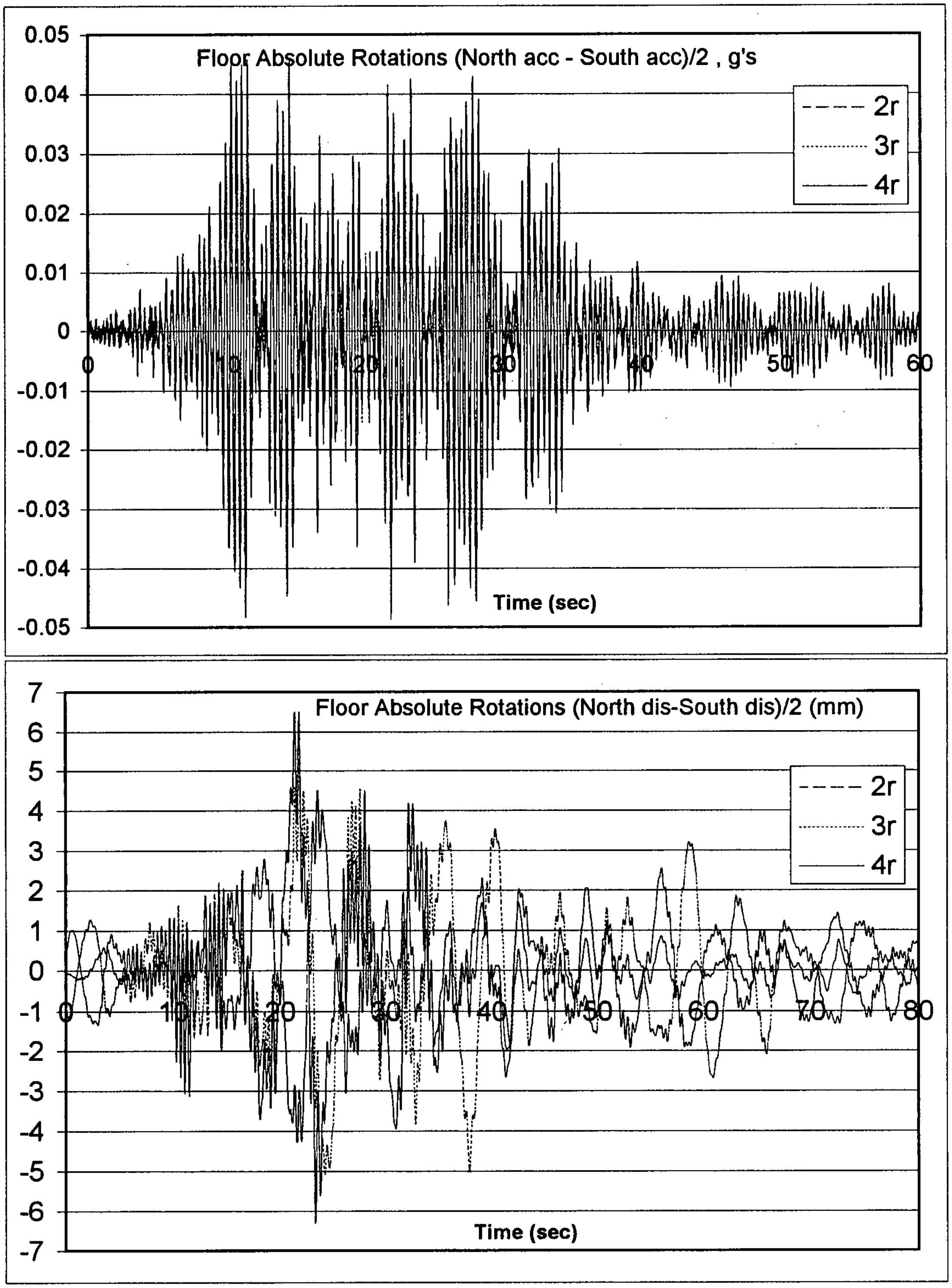

Figure 5.10.6 Torsional response of the upper floors of the San Bernardino 3-story office bldg., during the 1992 Landers EQ.

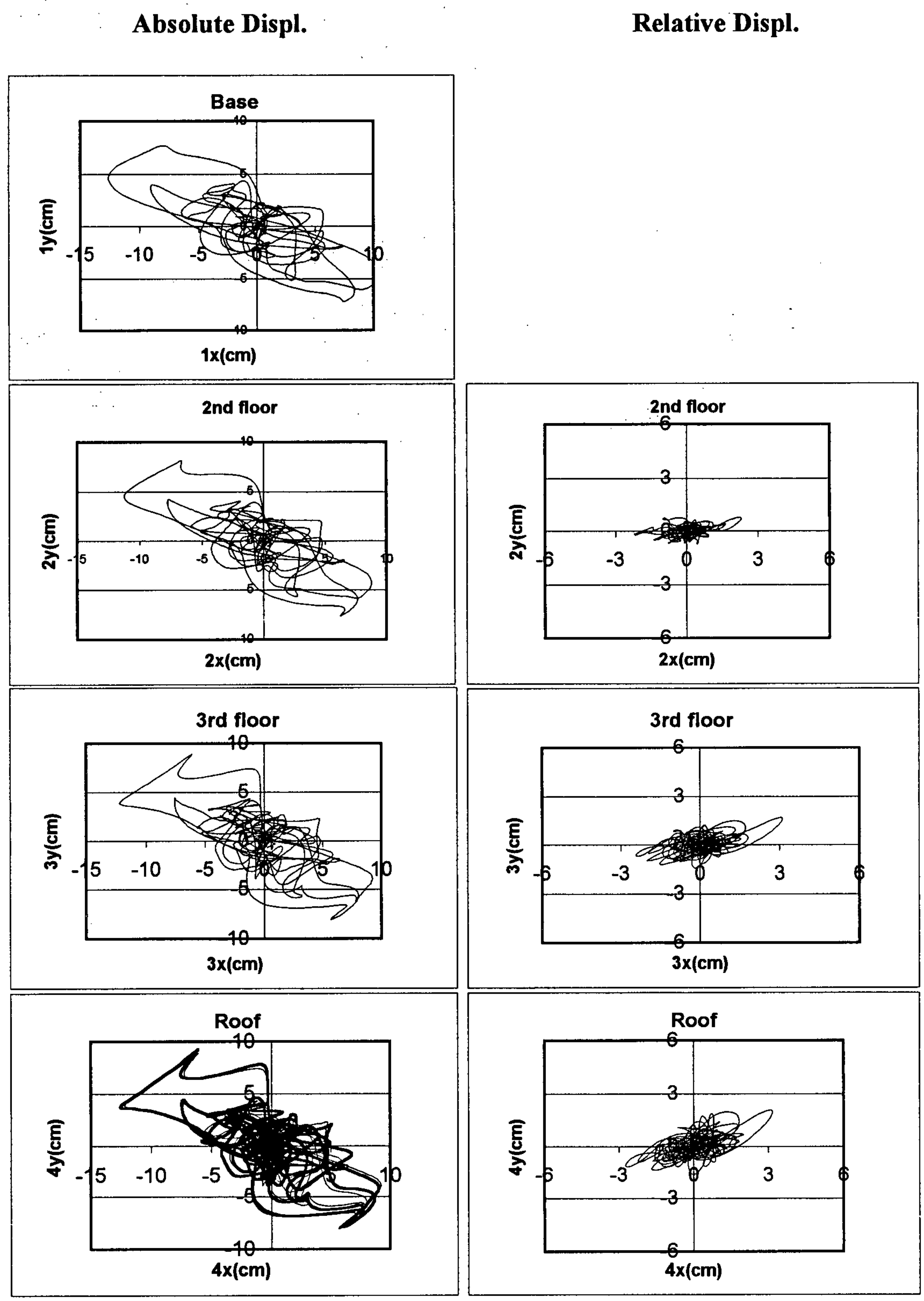

Figure 5.10.7 Orbital displacements at the center of the floors of the San Bernardino 3-story office bldg., during the 1992 Landers EQ.

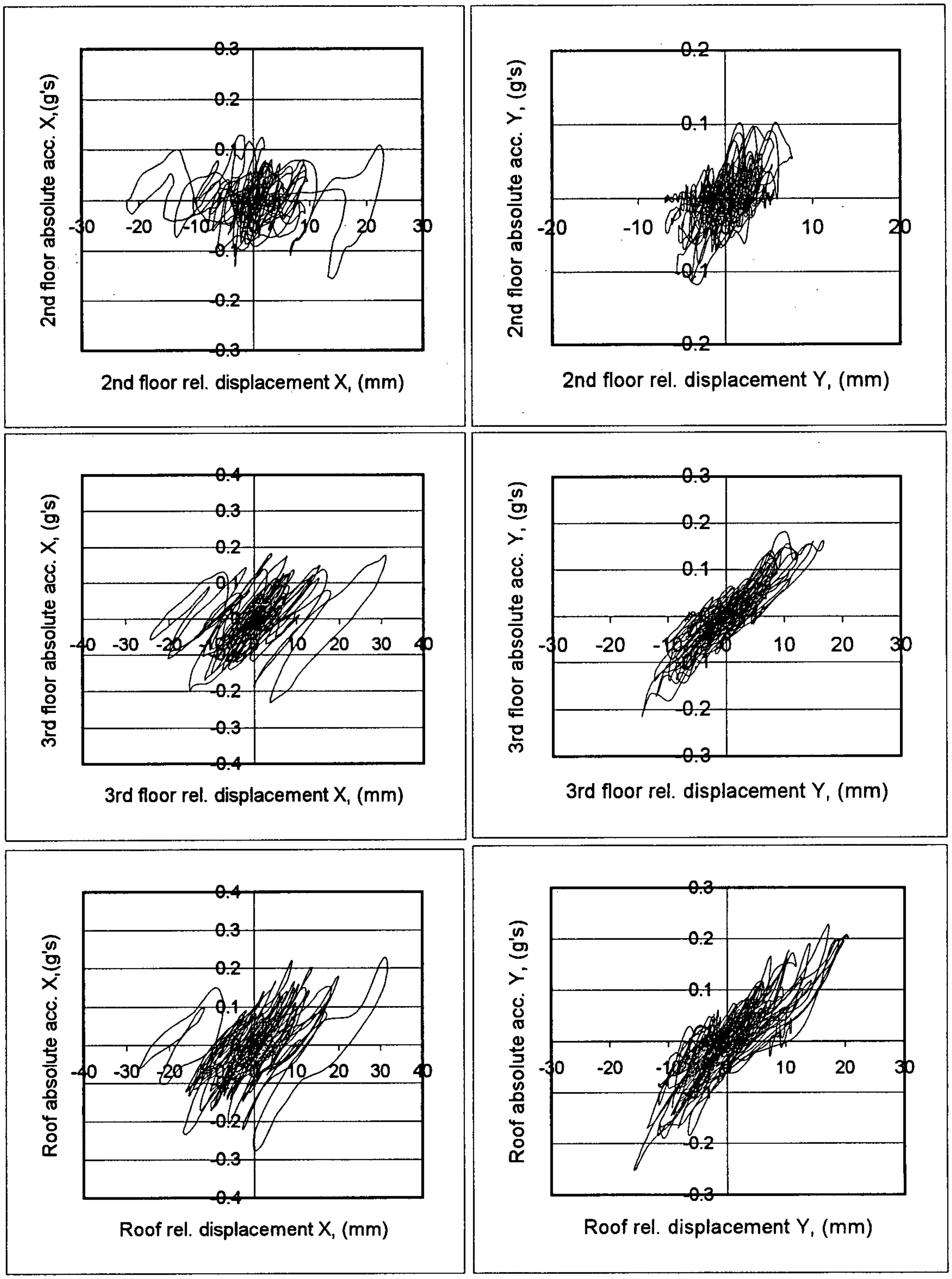

Figure 5.10.8 Representation of hysteretic behaviour of the San Bernardino 3-story office bldg., during the 1992 Landers EQ.

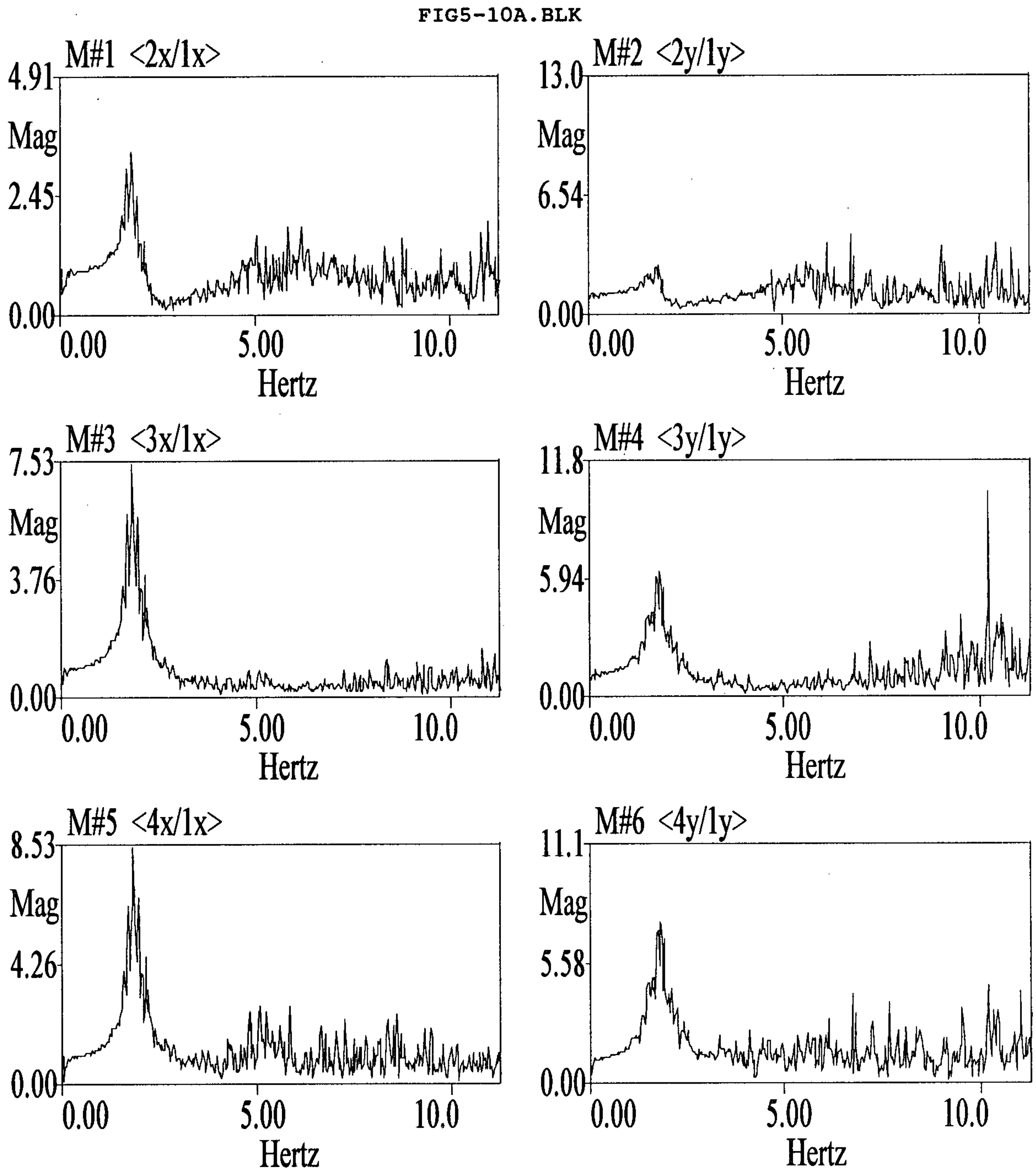

Figure 5.10.9 Frequency Response Functions of the San Bernardino 3-story office bldg., obtained from the 1992 Landers EQ records.

Note: The FRF's are computed by ME'scope using a Hanning window, a block size N=2048, 10 averages and 89% segment overlap.

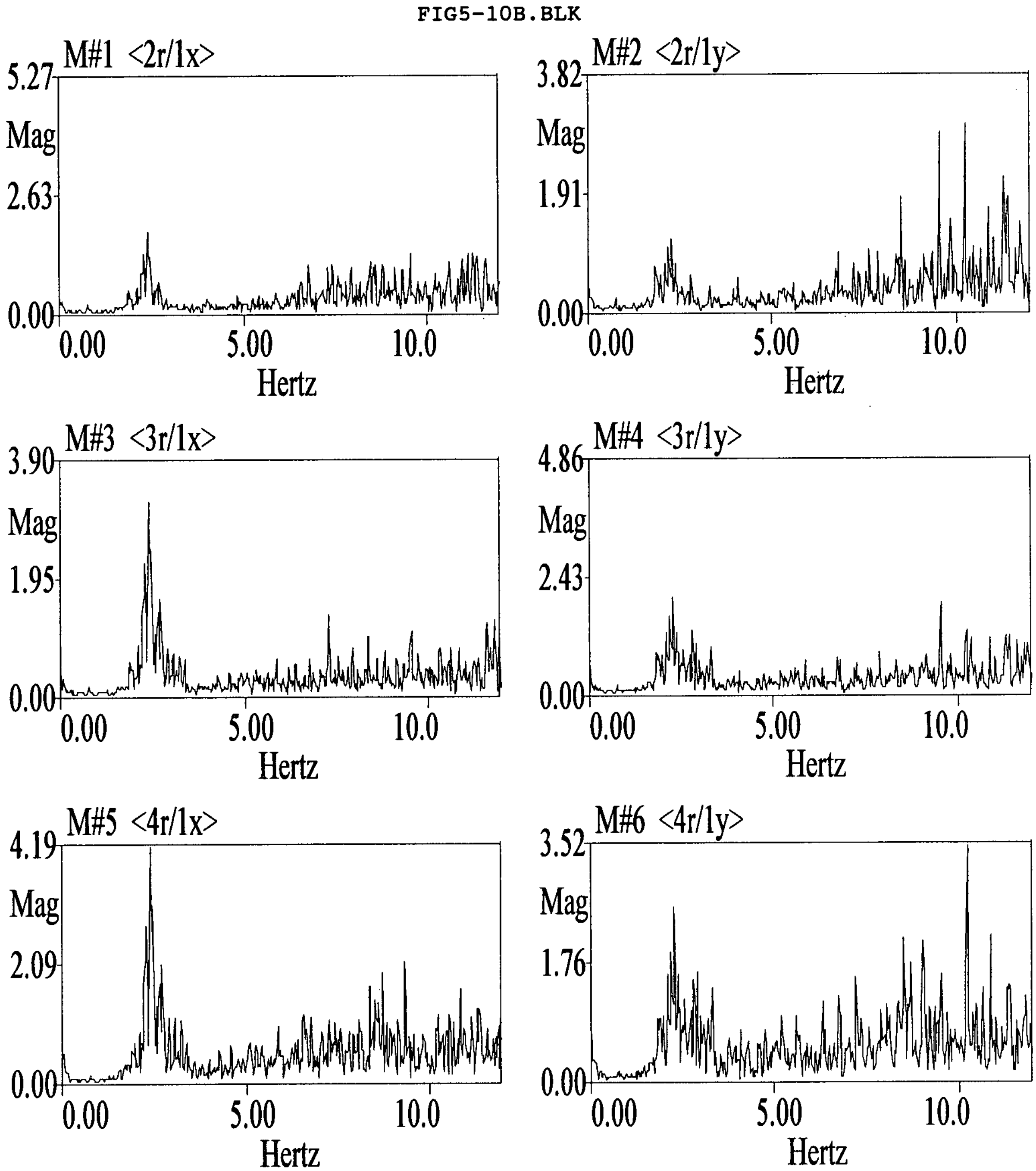

Figure 5.10.9 Cont'd

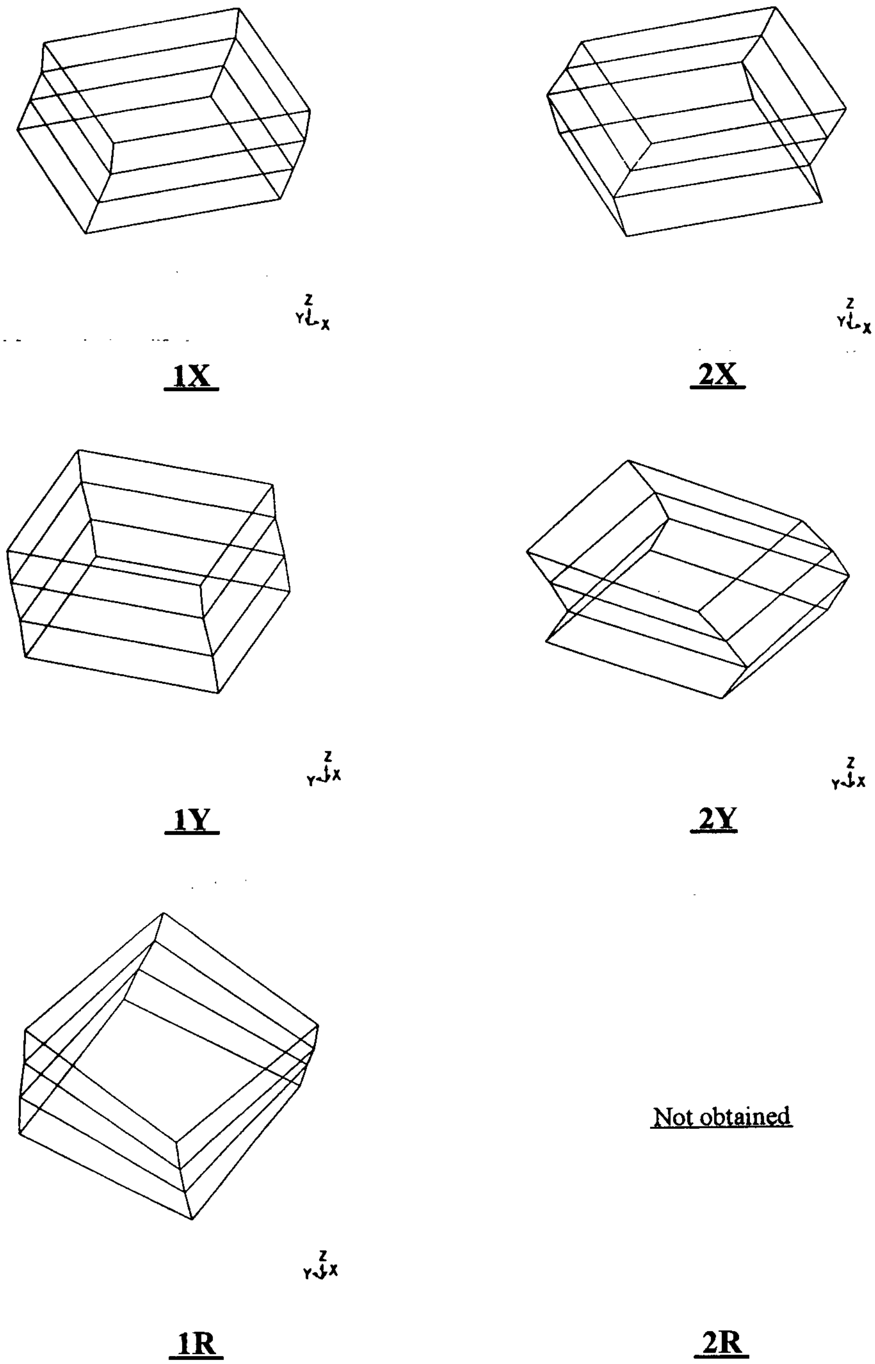

Figure 5.10.10 Mode shapes of the San Bernardino 3-story office bldg., obtained from the 1992 Landers EQ records.

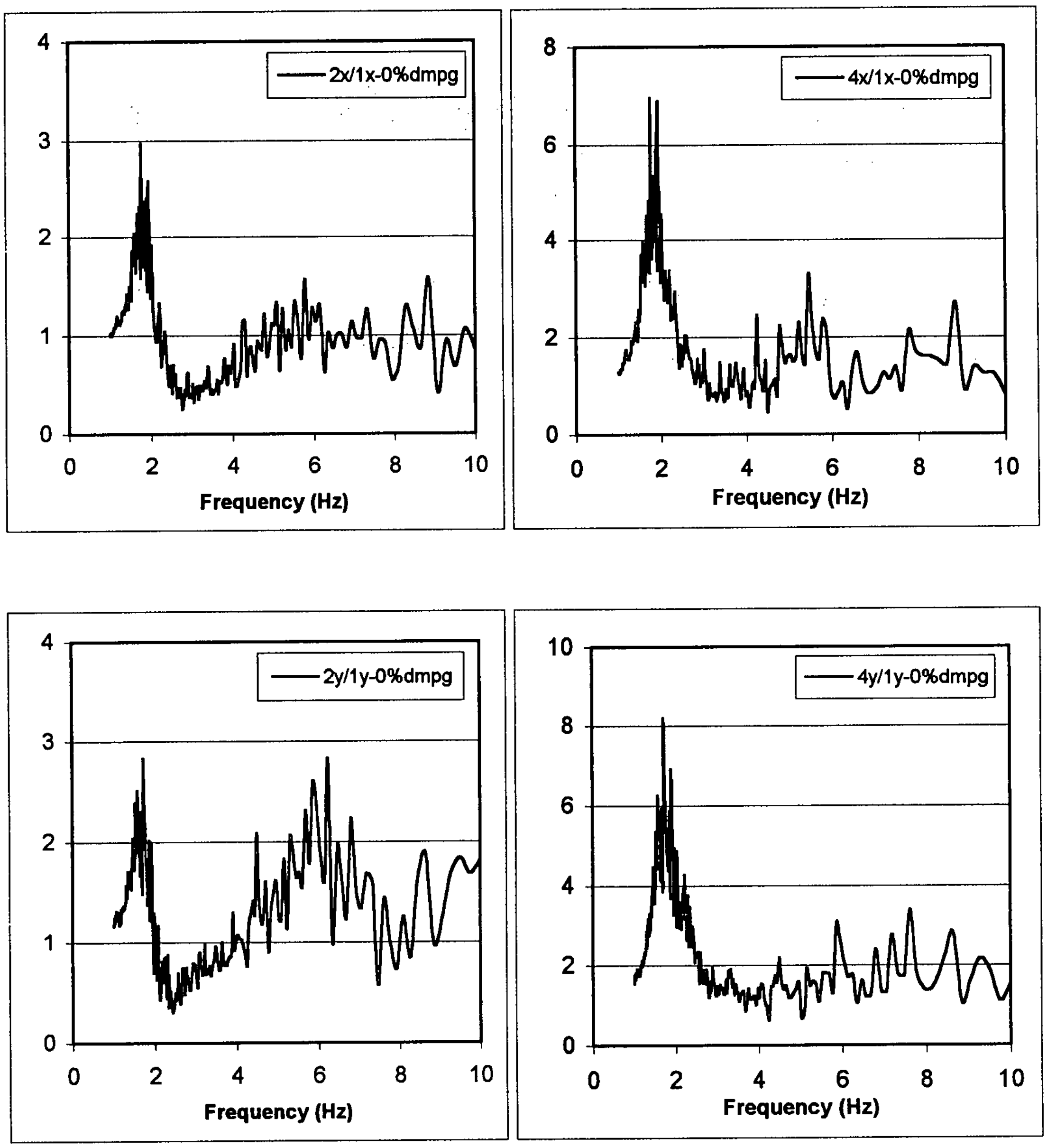

Figure 5.10.11 Spectral Response Functions of the San Bernardino 3-story office bldg., obtained from the 1992 Landers EQ records.

Table 5.10.1 Estimated natural frequencies (and periods) of the San Bernardino 3-story office bldg., based on the results of FRF results, SRF results and visual inspection of the three dimensional mode shapes obtained from analysis of 1992 Landers EQ data.

LANDERS EARTHQUAKE DATA						
	X-Direction (E-W)		Y-Direction (E-W)		Rotation	
	Frequency (Hz)	Period (S)	Frequency (Hz)	Period (S)	Frequency (Hz)	Period (S)
Model	1.83	0.55	1.77	0.56	2.4	0.42
Mode 2	5.9	0.17	5.9	0.17	-	-
Damping ratio of fundamental mode estimated by ME'scope: **7.7%**						

*** Spectral values at the natural periods in the ground motion response spectra and the response time-histories suggest that the 1st mode dominated the structural response.**

Fundamental Period according to **NBCC 1995**:

T = 0.1 N ==> **T** = 0.30 sec

$\mathbf{T = 0.085\ (h_n)^{3/4}} = 0.085\ (12.60\text{m})^{3/4} = 0.57$ sec

Fundamental Period according to **UBC 1997**:

$\mathbf{T = 0.035\ (h_n)^{3/4}} = 0.035\ (41.34\text{ft})^{3/4} = 0.57$ sec

5.11 Los Angeles 2-Story Fire Command Control Building

Properties of the Strong Motion Data:

Record Length: 60 sec

Time interval: 0.01 sec

No. of data points for each channel: 6001

Usable frequency range: 0.2 Hz to 46.0Hz

Manipulating the data to obtain the motion of the center of the building in the 3 directions, E-W (or X-directions) , N-S (or Y-directions) and rotation about vertical axis (or R-component):

FF = Free Field

Level 0 = Foundation (below isolators)

Level 1 = Base (above isolators)

$FF\text{-}X = [(FF90^{\circ}) * SIN(50^{\circ})] + [(FF180^{\circ}) * COS(50^{\circ})]$

$FF\text{-}Y = [(FF90^{\circ}) * COS(50^{\circ})] - [(FF180^{\circ}) * SIN(50^{\circ})]$

$0X = -(Chan7 + Chan6)/2$, $0Y = Chan5 - [(Chan7-Chan6) . (14/188)]$, $0R = (Chan7-Chan6)/2$

$1X = -(Chan11 + Chan9)/2$, $1Y = Chan8 - [(Chan11-Chan9).(14/188)]$, $1R = (Chan11-Chan9)/2$

$3X = -(Chan16 + Chan14)/2$, $3Y = Chan13 - [(Chan16-Chan14).(14/188)]$,

$3R = (Chan16 - Chan14)/2$

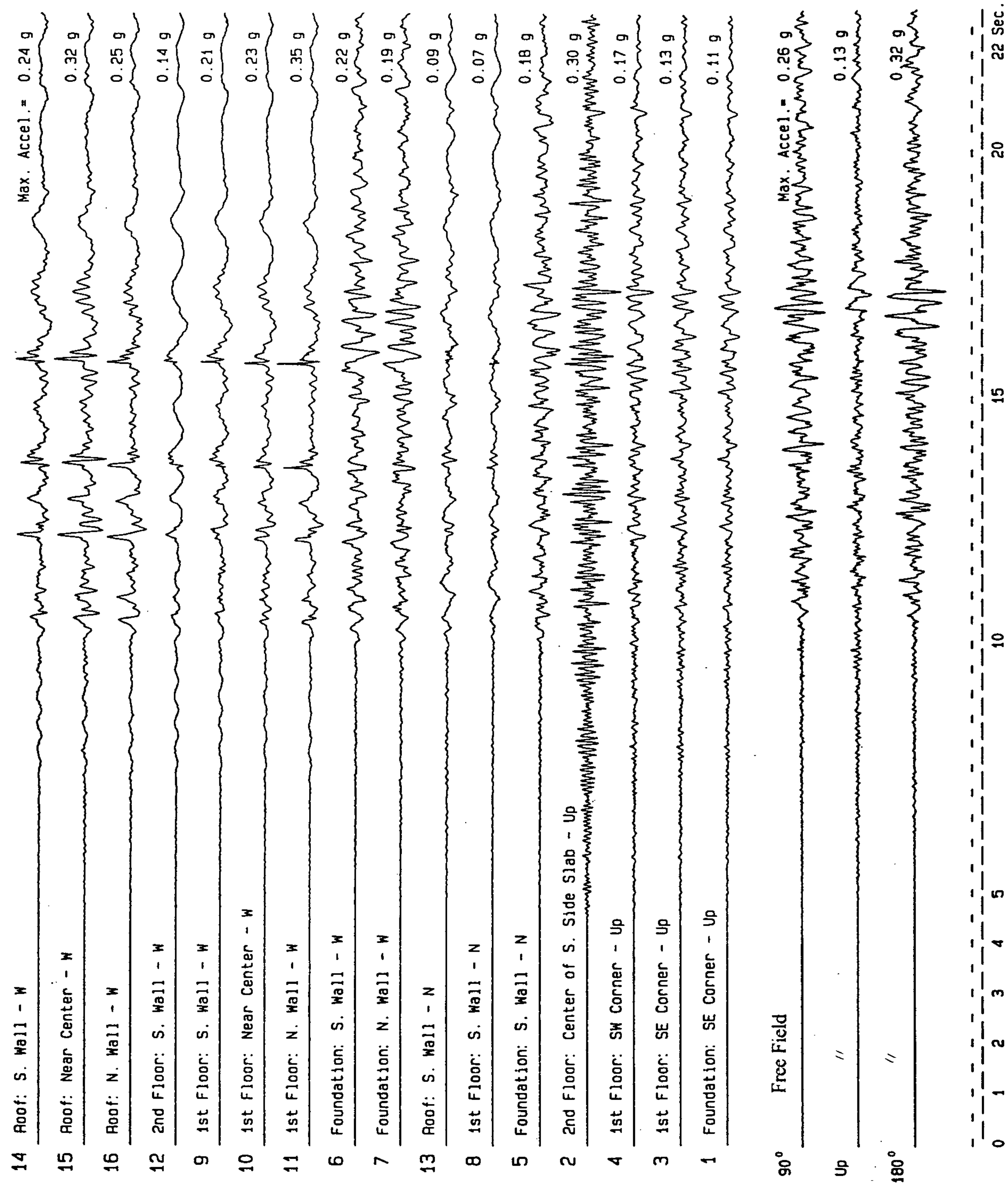

Figure 5.11.1 Accelerations recorded at the LA 2-story fire control bldg. during the 1994 Northridge EQ (After Shakal, et al., 1994)

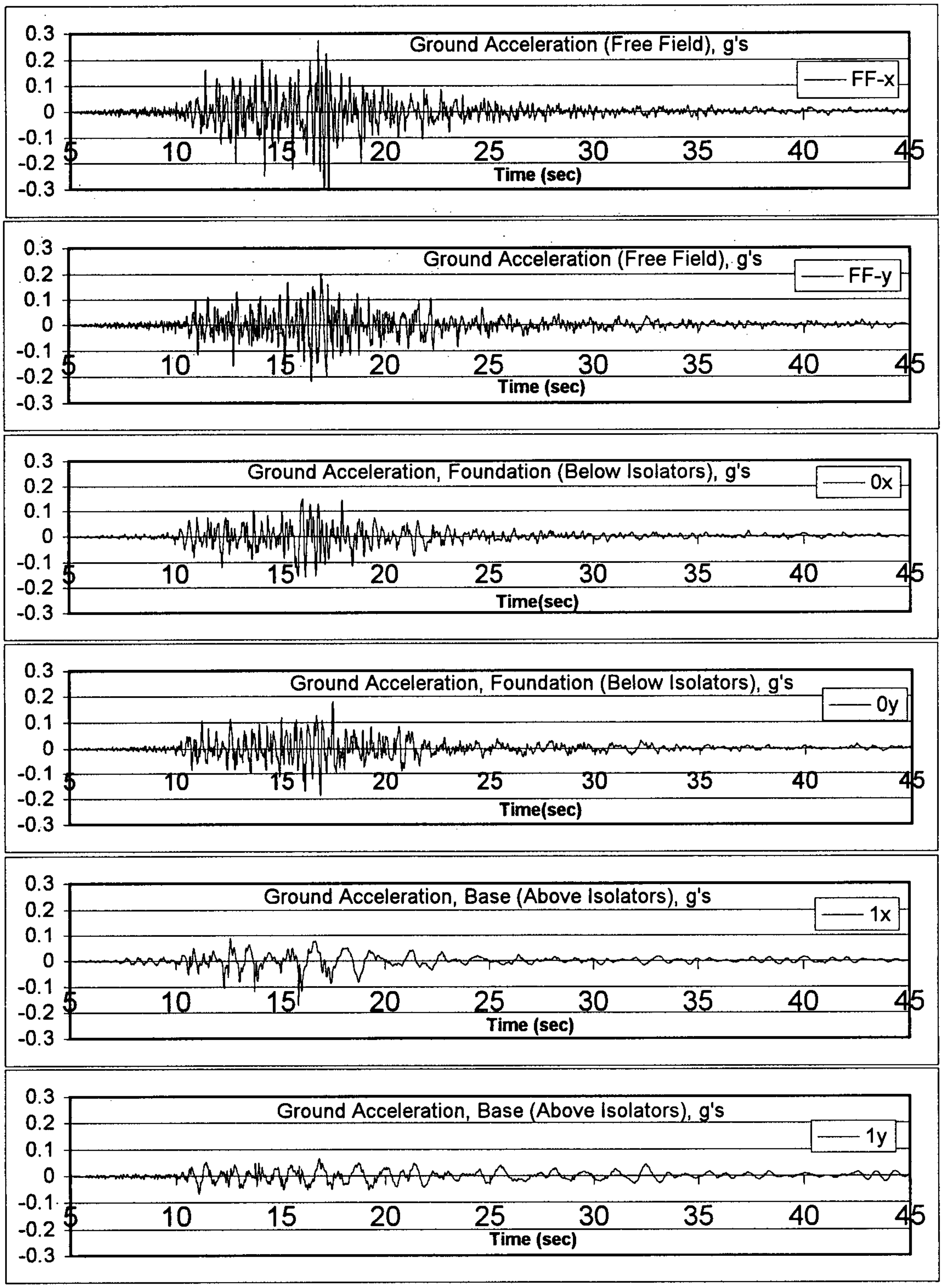

Figure 5.11.2 Acceleration time histories of free field, foundation (below isolators) and base (above isolators) at the LA 2-story fire control bldg., during the 1994 Northridge EQ.

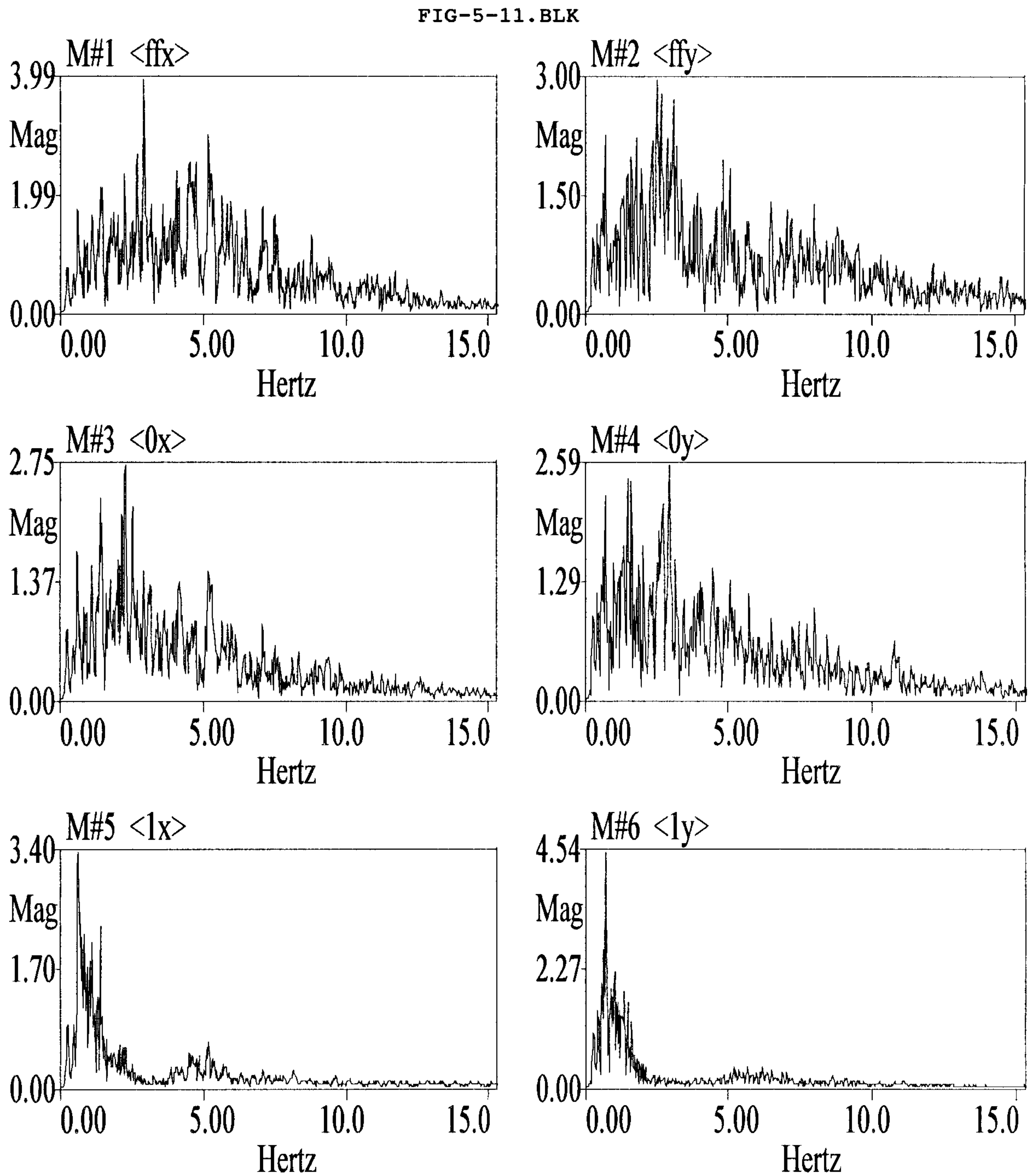

Figure 5.11.3 Normalized Fourier Spectrum of accelerations of free field, foundation (below isolators) and base (above isolators) at the LA 2-story fire control bldg., during the 1994 Northridge EQ.

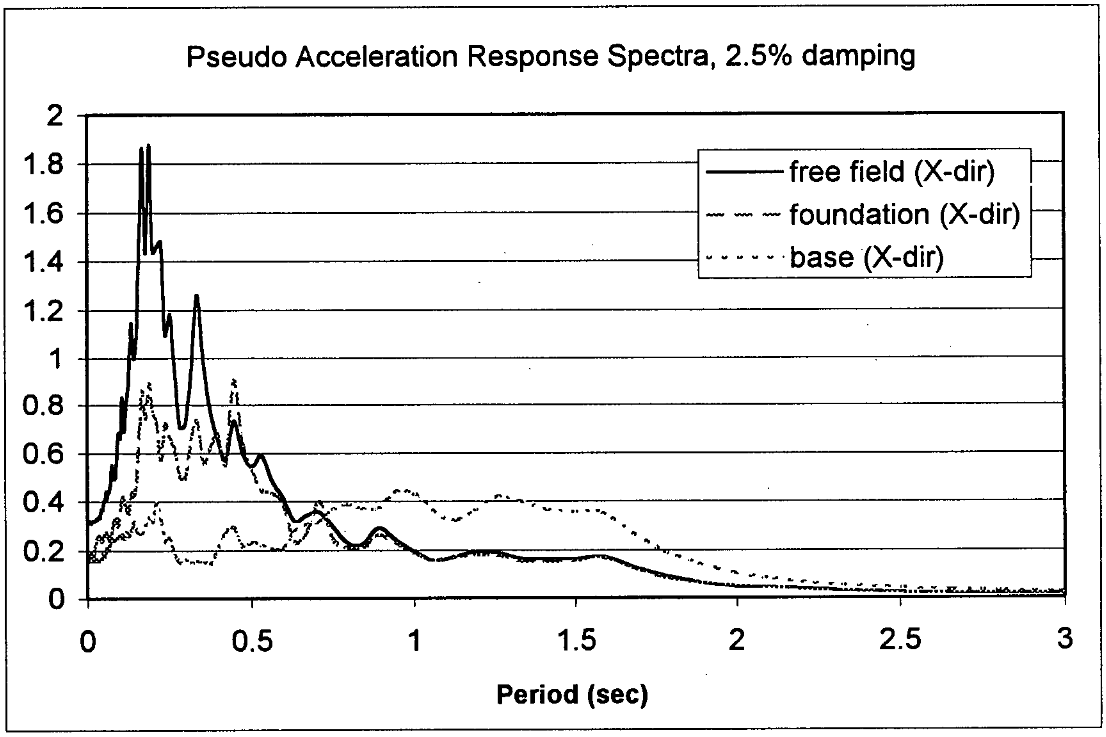

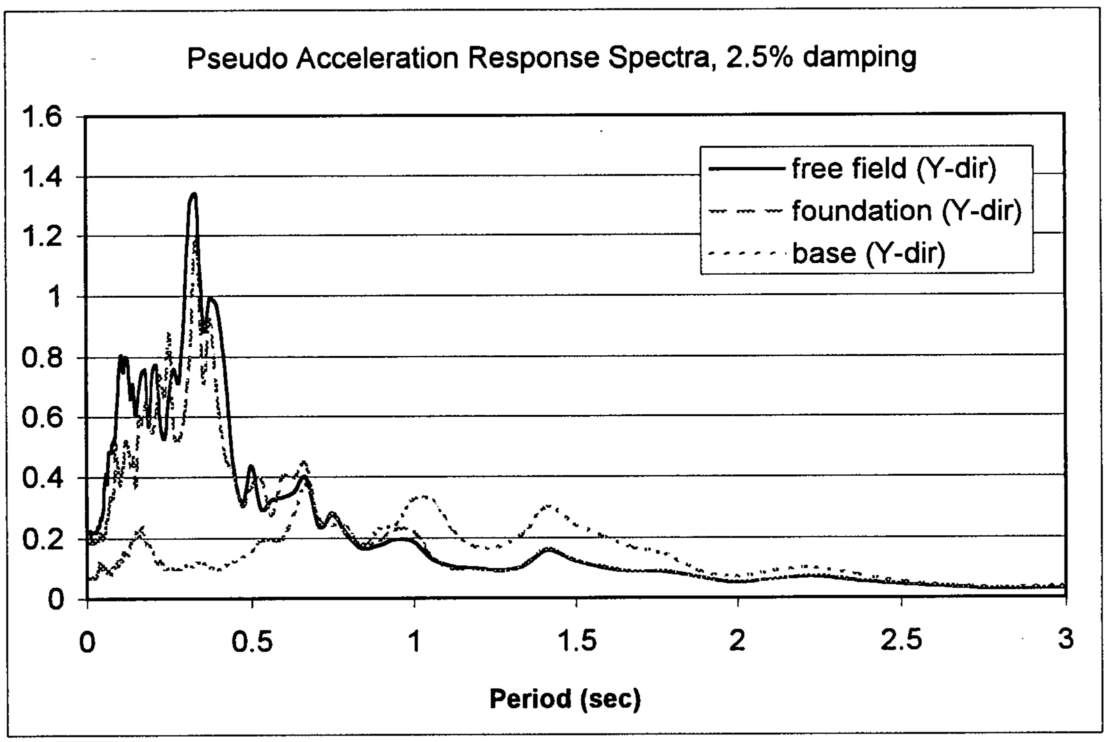

Figure 5.11.4 Pseudo acceleration response spectra of the motion of free field, foundation (below isolators) and base (above isolators) at the LA 2-story fire control bldg., during the 1994 Northridge EQ.

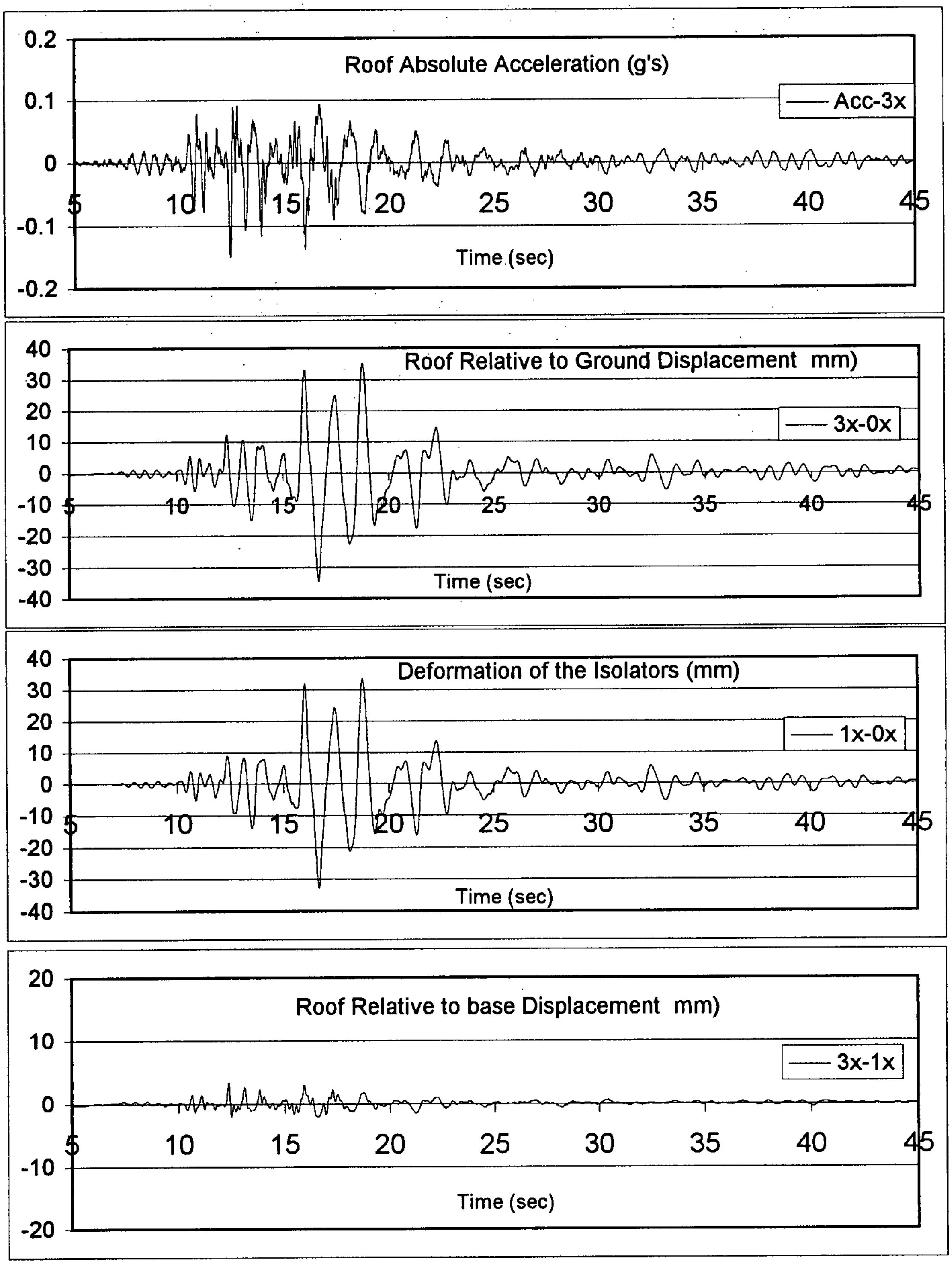

Figure 5.11.5 E-W (X) component of the response of the LA 2-story fire control bldg., during the 1994 Northridge EQ.

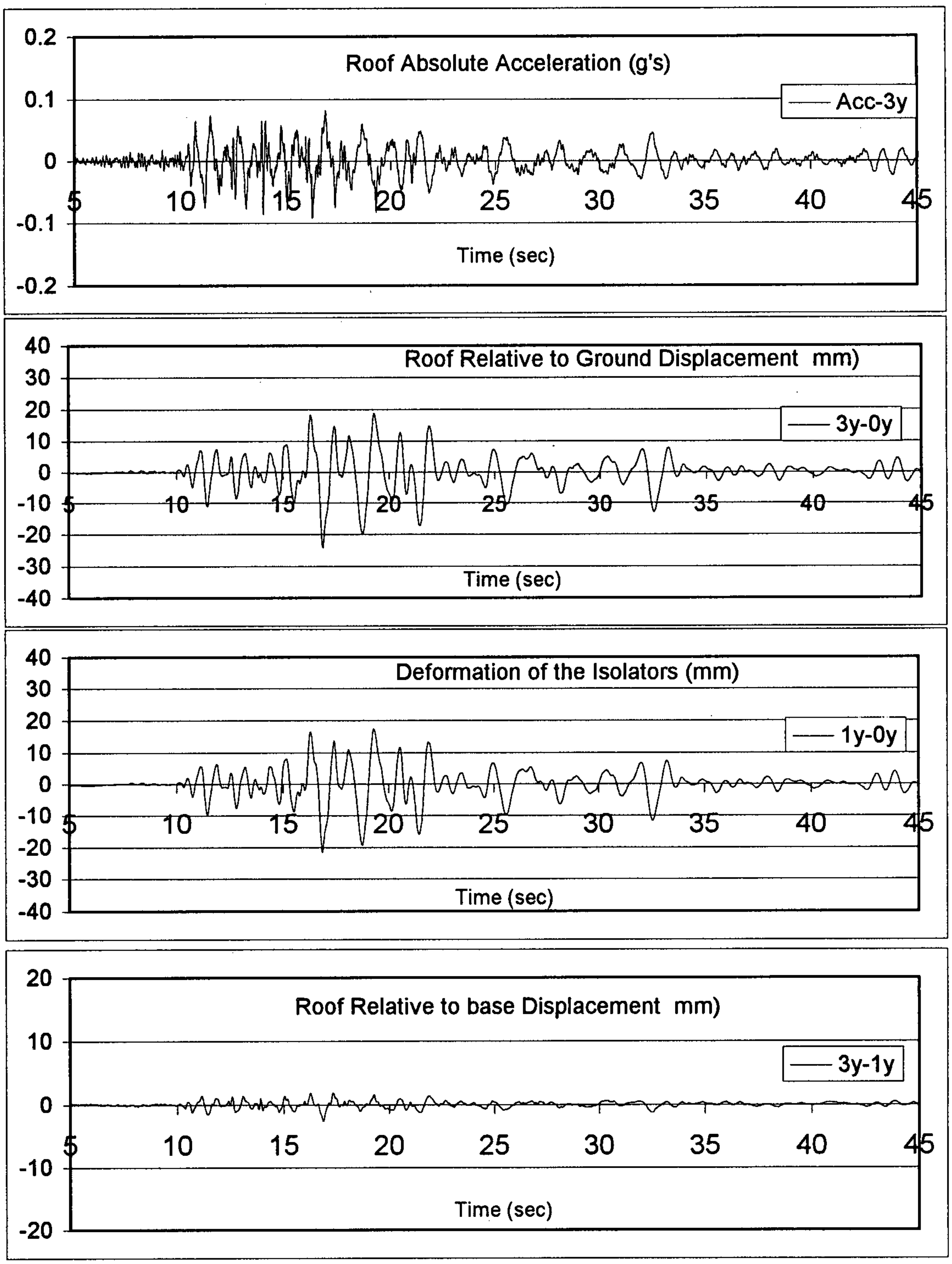

Figure 5.11.6 N-S (Y) component of the response of the LA 2-story fire control bldg., during the 1994 Northridge EQ.

Absolute Displ. **Relative Displ.**

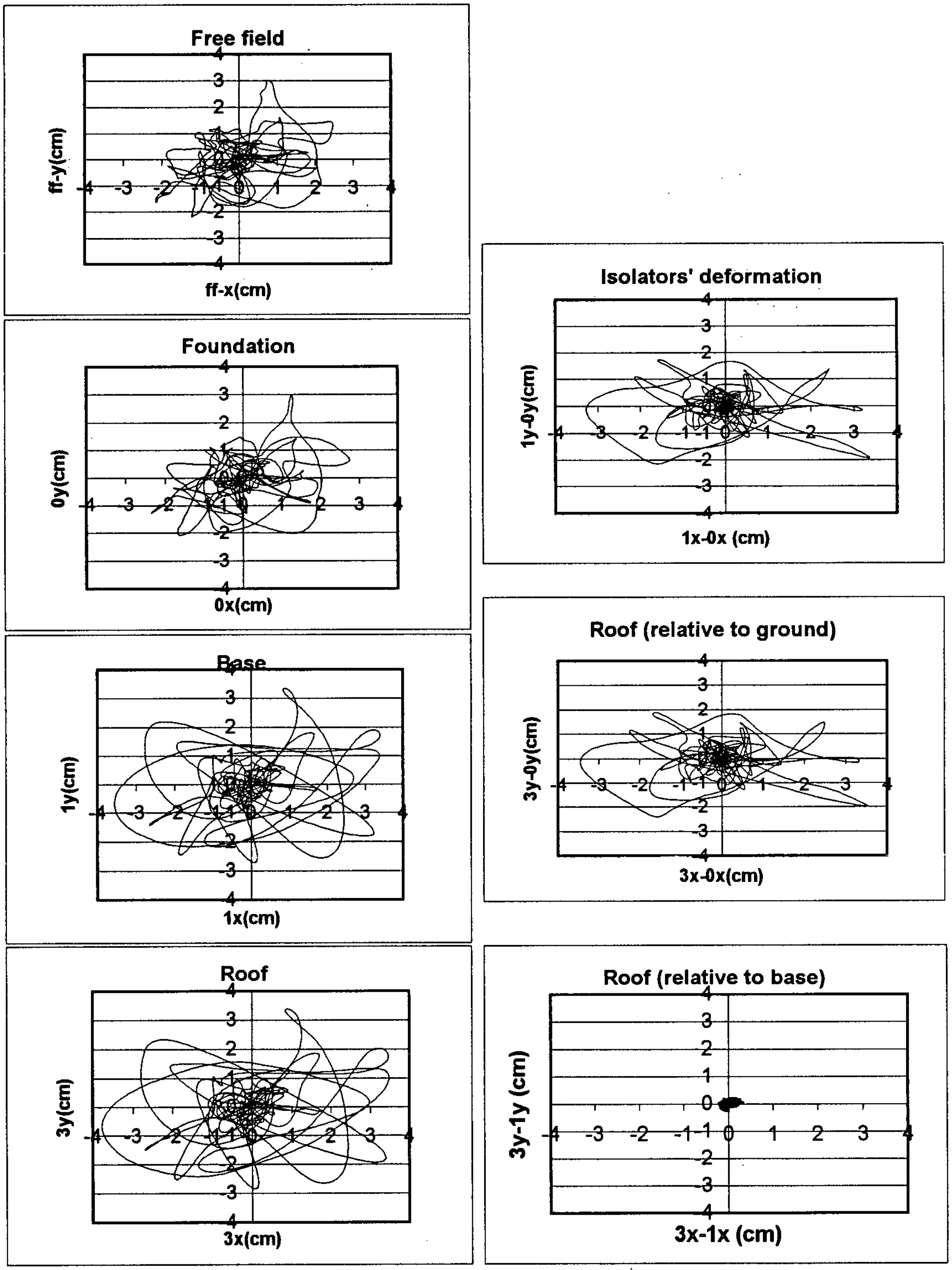

Figure 5.11.7 Orbital displacements at the center of the instrumented floors of the LA 2-story fire control bldg., during the 1994 Northridge EQ

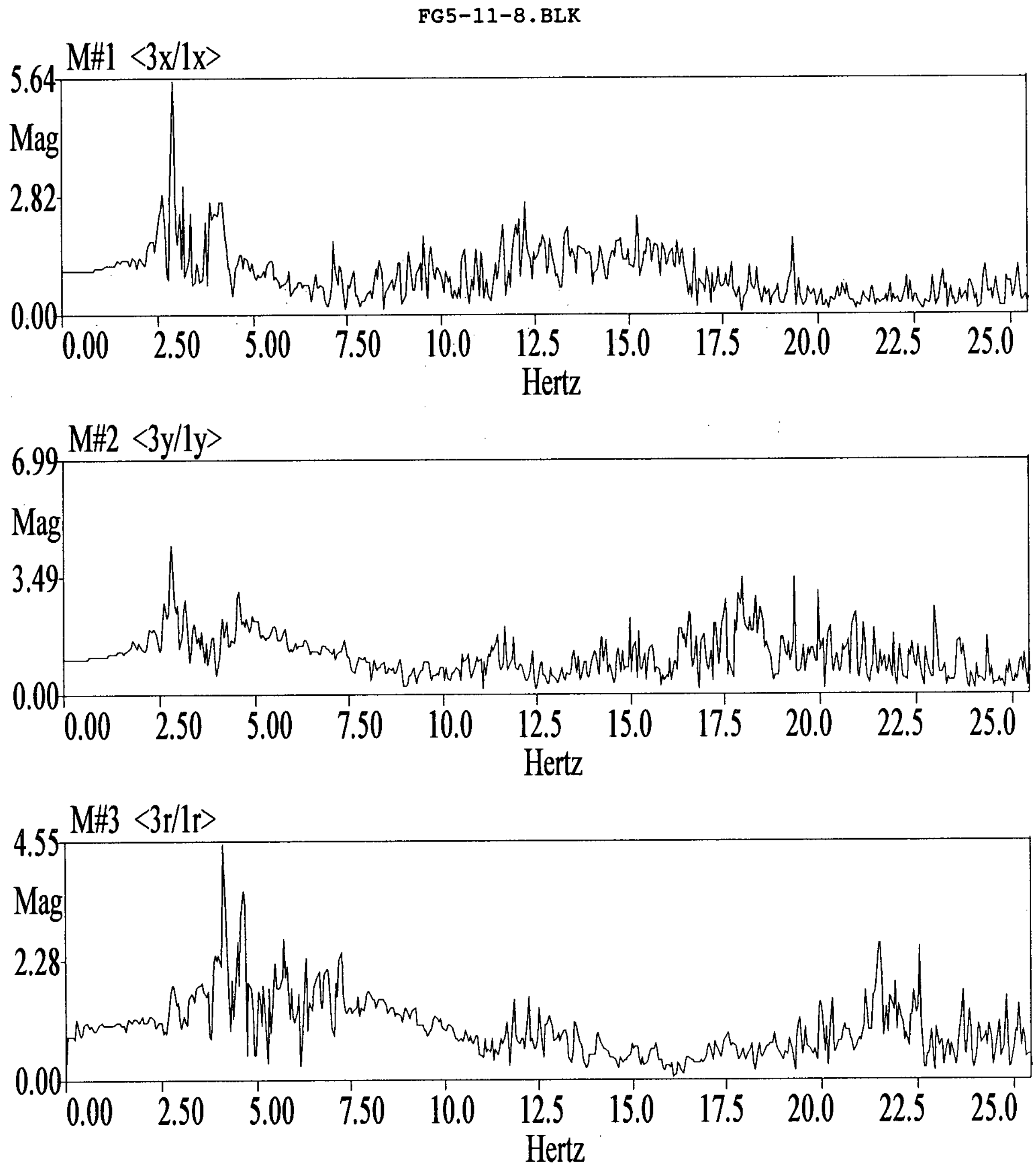

Figure 5.11.8 Frequency Response Functions of the roof with respect to first floor (above isolators) of the LA 2-story fire control bldg., obtained from the 1994 Northridge EQ records.

Note: The FRF's are computed by ME'scope using a Hanning window, a block size N=2048, 15 averages and 86% segment overlap.

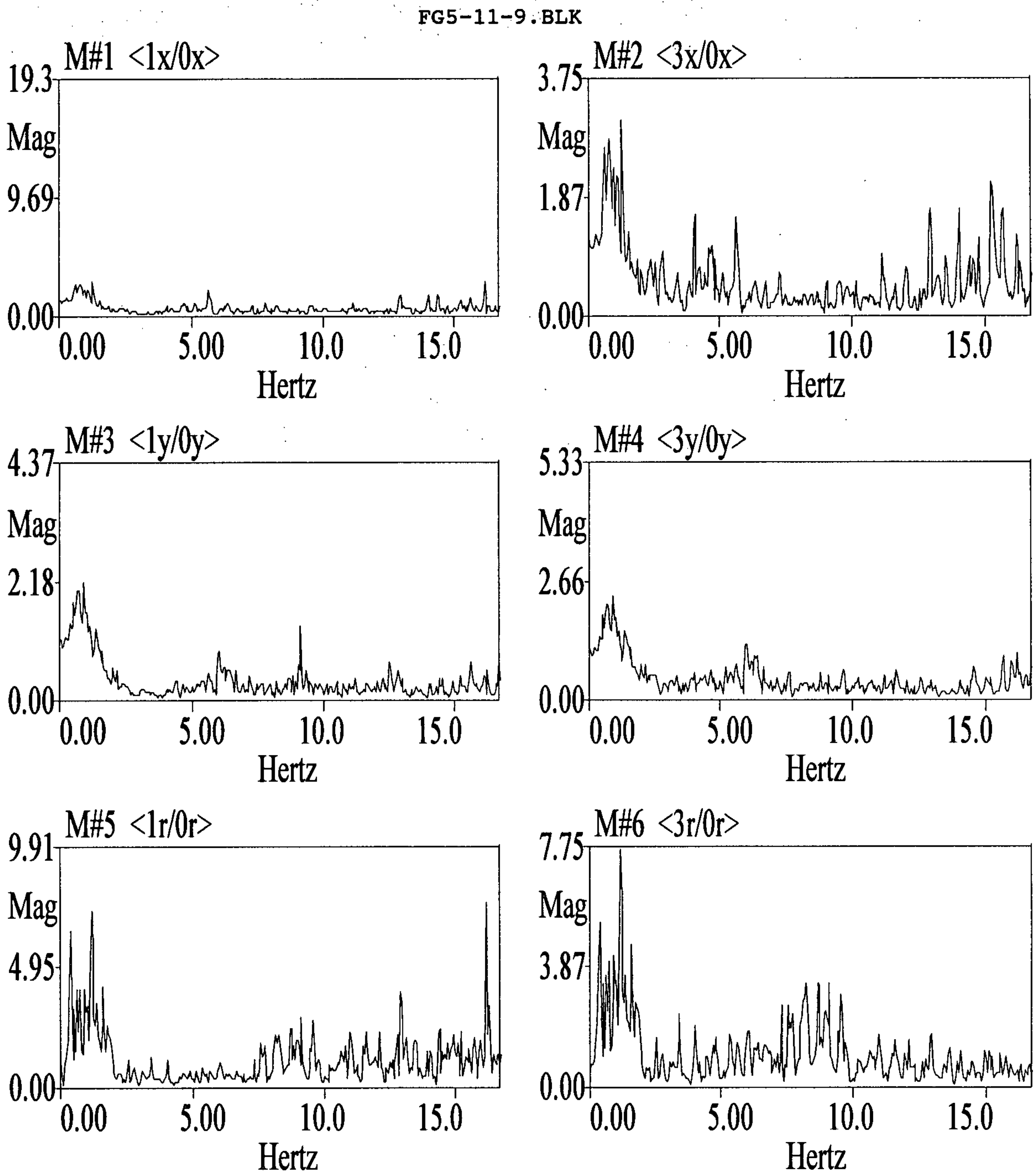

Figure 5.11.9 Frequency Response Functions of the roof and first floor with respect to the foundation (below isolators) of the LA 2-story fire control bldg., obtained from the 1994 Northridge EQ records.

Note: The FRF's were computed by ME'scope using the same parameters as noted for figure 5.11.8

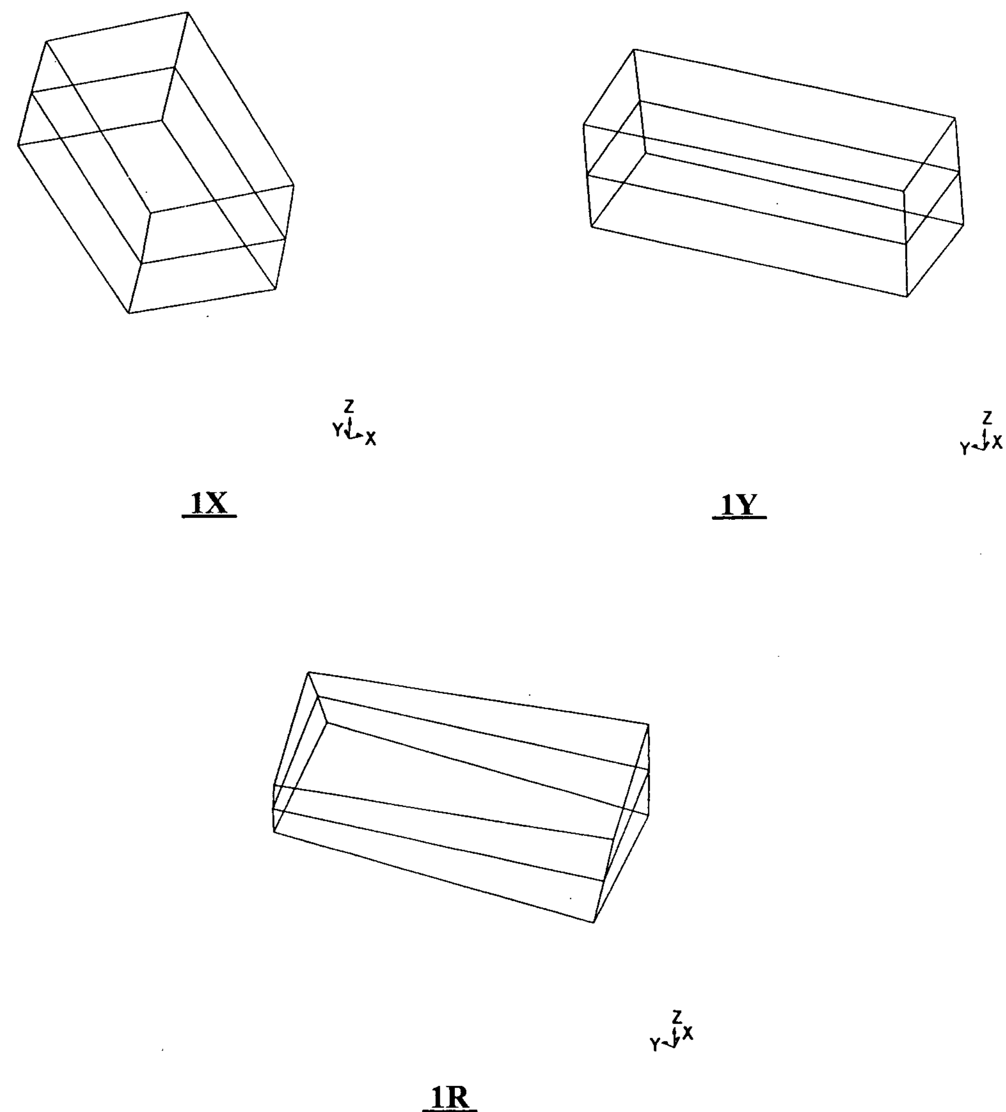

Figure 5.11.10 Mode shapes of the superstructure the LA 2-story fire control bldg. (without isolators), obtained from the 1994 Northridge records.

Note: The displacements of roof are obtained from measured data. Displacements of the 2nd floor are based on ME'scope's interpolation algorithm.

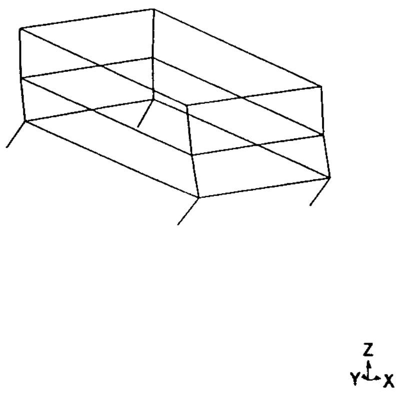

1X

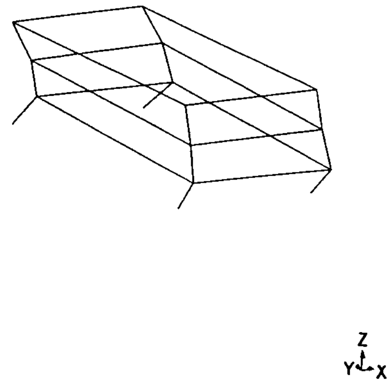

2X

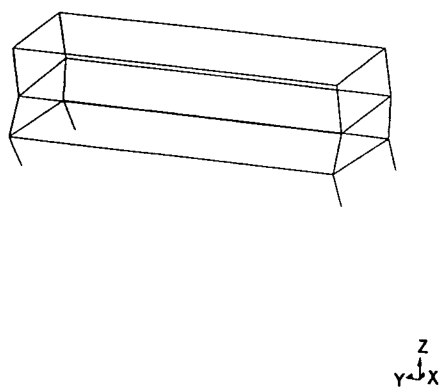

1Y

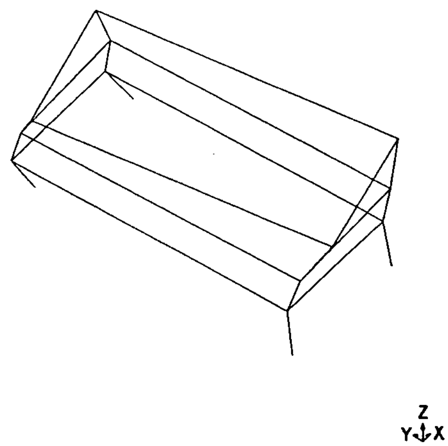

1R

Figure 5.11.11 Mode shapes of the LA 2-story fire control bldg. (with an extra story at the bottom representing the deformation of the isolators), obtained based on Northridge EQ Records.

Note: The displacements of 1st floor and roof are obtained from measured data. Displacements of the 2nd floor are based on ME'scope's interpolation algorithm.

Table 5.11.1 Estimated natural frequencies (and periods) of the LA 2-story fire control bldg., based on the FRF results and visual inspection of the three dimensional mode shapes obtained from analysis of 1994 Northridge EQ data.

SUPERSTRUCTURE (obtained from the FRF's of Figure 5.11.8)						
	X-Direction (E-W)		Y-Direction (E-W)		Rotation	
	Frequency (Hz)	Period (S)	Frequency (Hz)	Period (S)	Frequency (Hz)	Period (S)
Model	2.9	0.34	2.9	0.34	4.1	0.24
Mode 2	-	-	-	-	-	-
BASE-ISOLATED (obtained from the FRF's of Figure 5.11.9)						
	X-Direction (E-W)		Y-Direction (E-W)		Rotation	
	Frequency (Hz)	Period (S)	Frequency (Hz)	Period (S)	Frequency (Hz)	Period (S)
Mode 1	0.9	1.1	0.9	1.1	1.2	0.8
Mode 2	6.0	0.17	6.0	0.17	9.0	0.11

Fundamental Period of the building without Base Isolation:

a) NBCC 1995:

$\mathbf{T = 0.1\ N} \Longrightarrow \mathbf{T} = 0.20$ sec

$\mathbf{T = 0.09\ h_n / (D_s)^{1/2}} = 0.09\ (9.75\text{m}) / (25.6\text{m})^{1/2} = 0.17$

b) UBC 1997:

$\mathbf{T = 0.020\ (h_n)^{3/4}} = 0.020\ (32\text{ft})^{3/4} = 0.27$ sec

5.12 Los Angeles 7-Story University Hospital

Properties of the Strong Motion Data:

Record Length: 60 sec

Time interval: 0.01 sec

No. of data points for each channel: 6001

Usable frequency range: 0.2 Hz to 46.0 Hz

Manipulating the data to obtain the motion of the center of the building in the 3 directions, E-W (or X-directions) , N-S (or Y-directions) and rotation about vertical axis (or R-component):

FF = Free Field

Level 0 = Foundation (below isolators)

Level 1 = Base (above isolators)

FF-X = [(Chan27) * COS(5°)] - [(Chan25) * SIN(5°)]

FF-Y = [(Chan25) * COS(5°)] + [(Chan27) * SIN(5°)]

0X = Chan7 , 0Y = Chan5 , 0R = (Chan8 - Chan6)/2

1X = Chan11 , 1Y = Chan9 , 1R = (Chan12 - Chan10)/2

4X = Chan15 , 4Y = Chan13 , 4R = (Chan16 - Chan14)/2

6X = Chan19 , 6Y = Chan17 , 6R = (Chan20 - Chan18)/2

8X = Chan23 , 8Y = Chan21 , 8R = (Chan24 - Chan22)/2

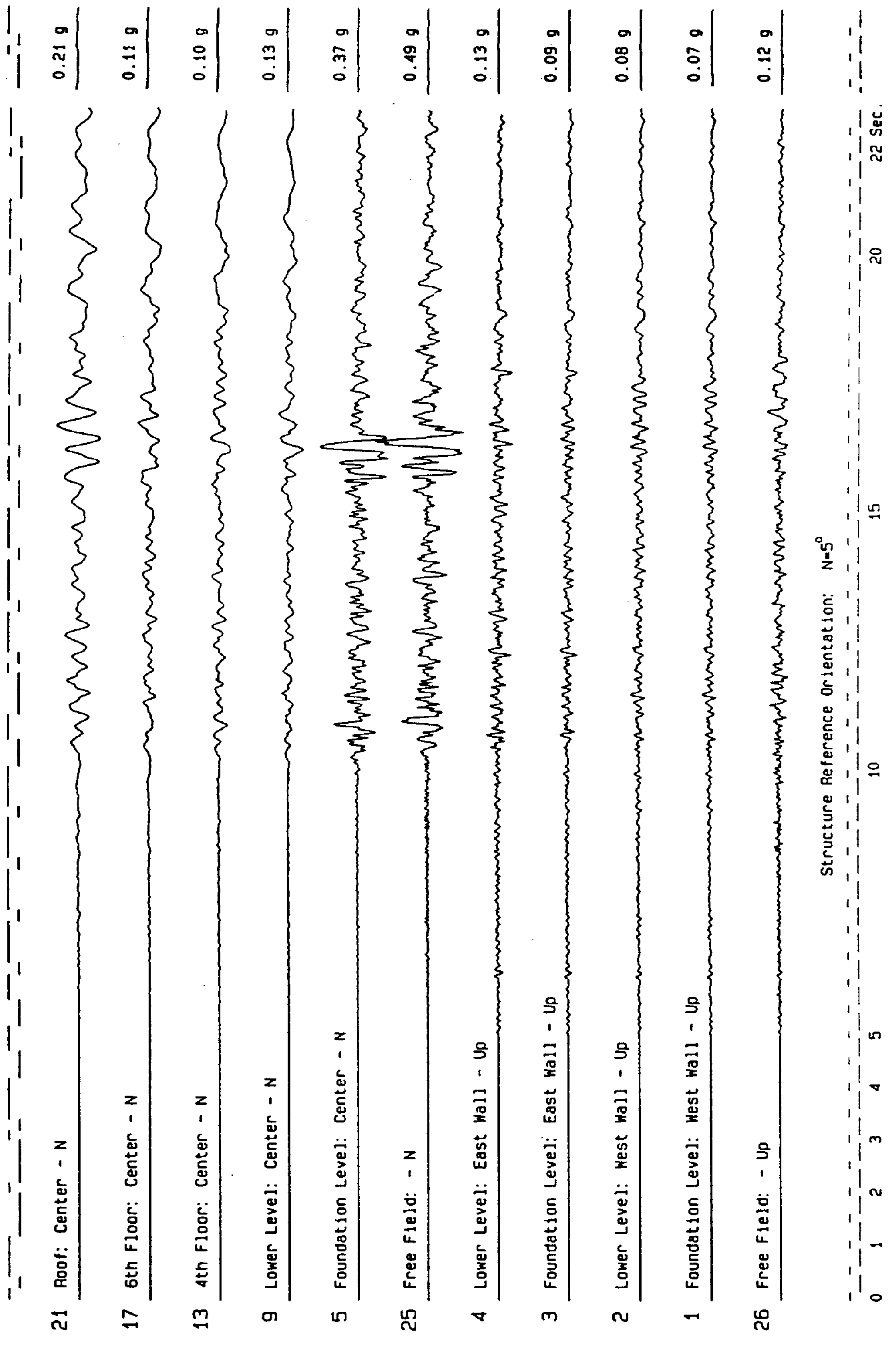

Figure 5.12.1 Accelerations recorded at LA 7-story university hospital, during the 1994 Northridge EQ. (After Shakal, et al., 1994)

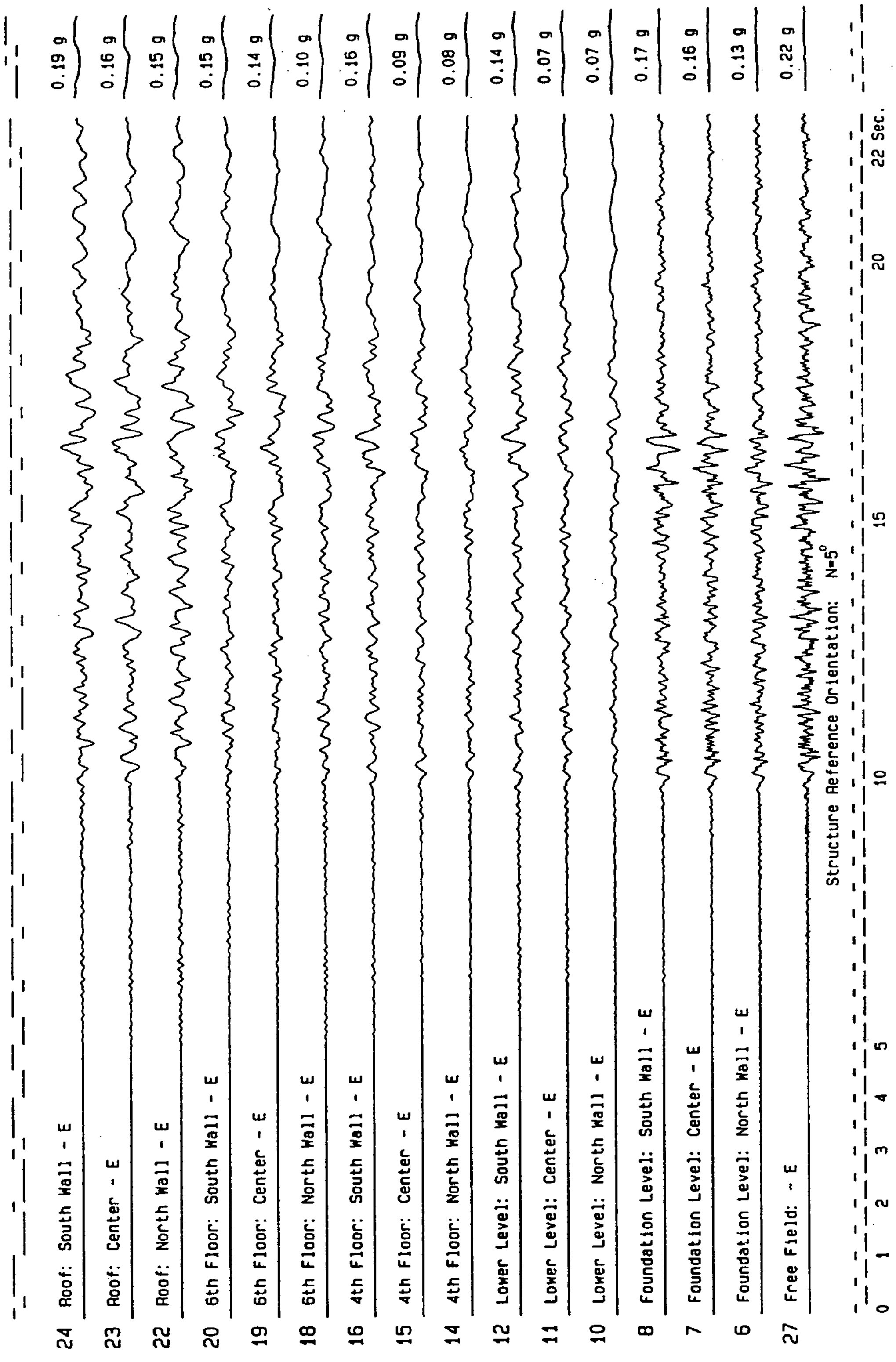

Figure 5.12.1 Continued

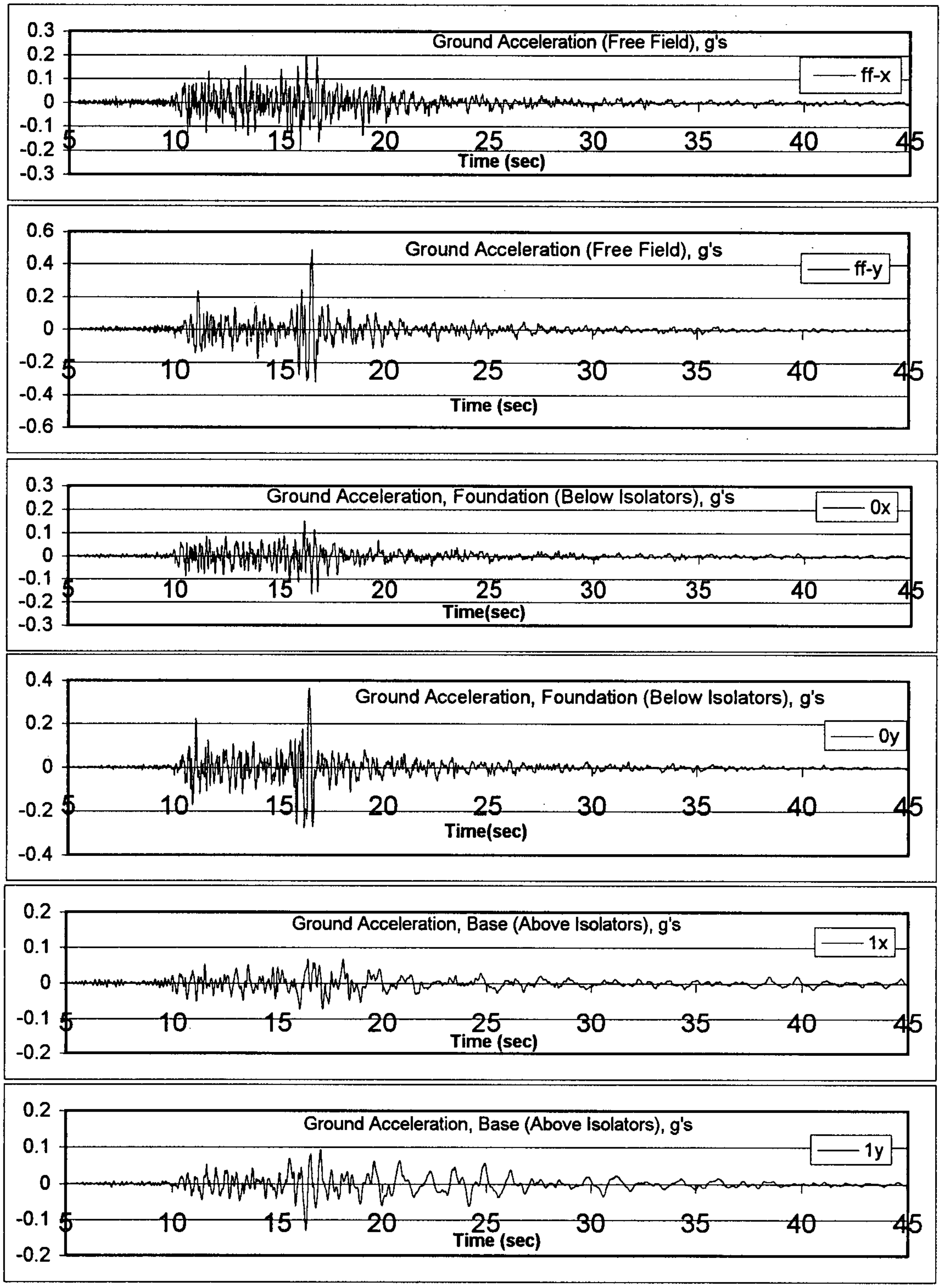

Figure 5.12.2 Acceleration time histories of free field, foundation (below isolators) and base (above isolators) at the LA 7-story university hospital, during the 1994 Northridge EQ.

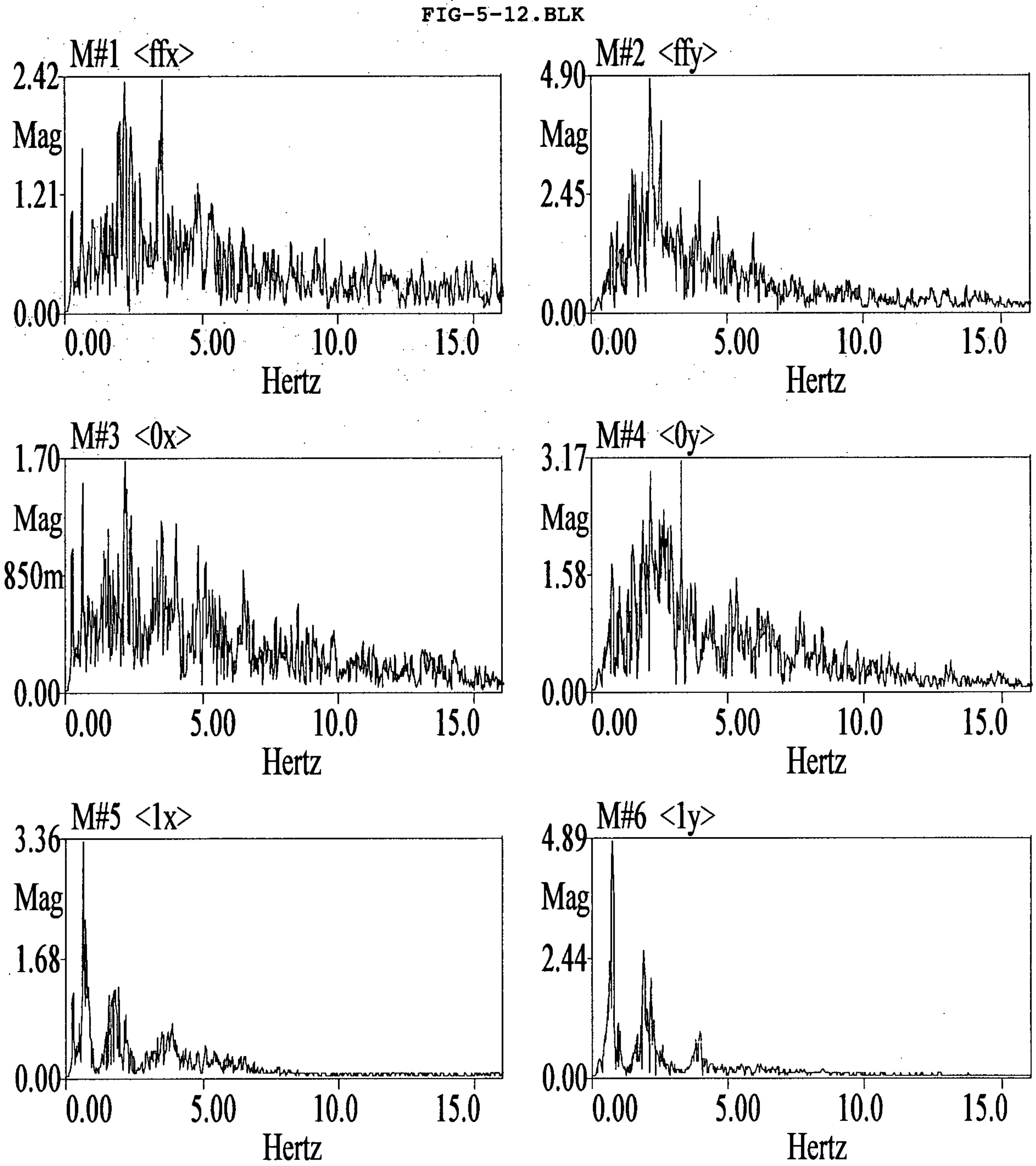

Figure 5.12.3 Normalized Fourier Spectrum of accelerations of free field, foundation (below isolators) and base (above isolators) at the LA 7-story university hospital, during the 1994 Northridge EQ.

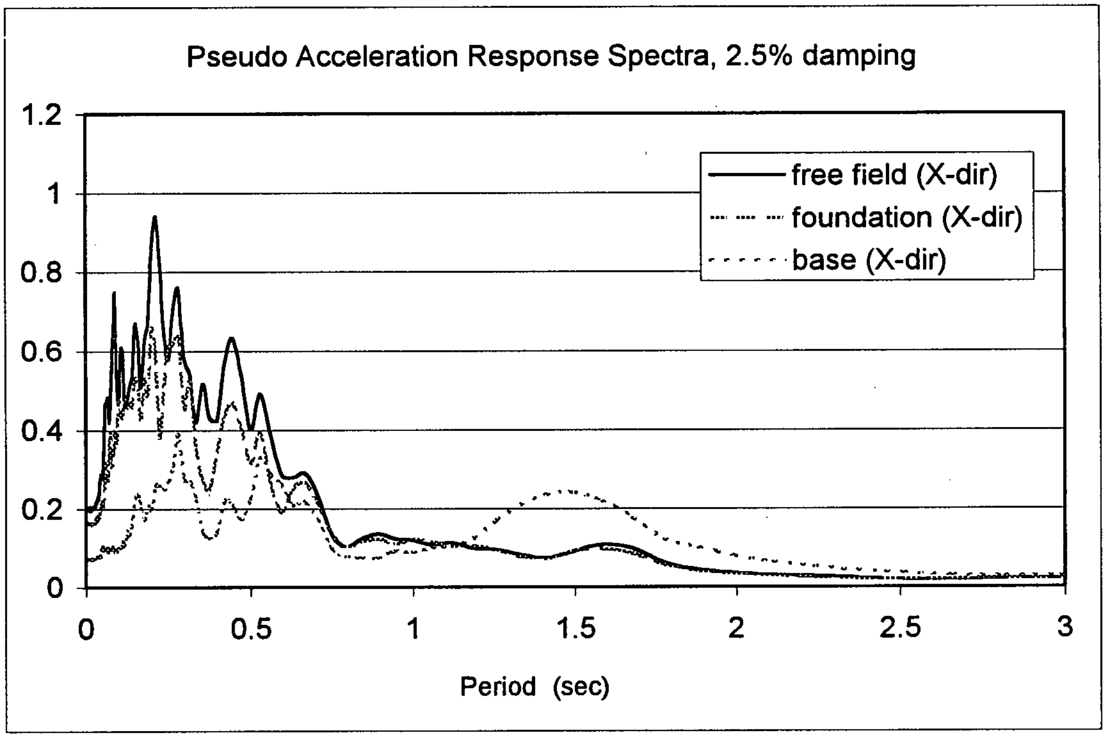

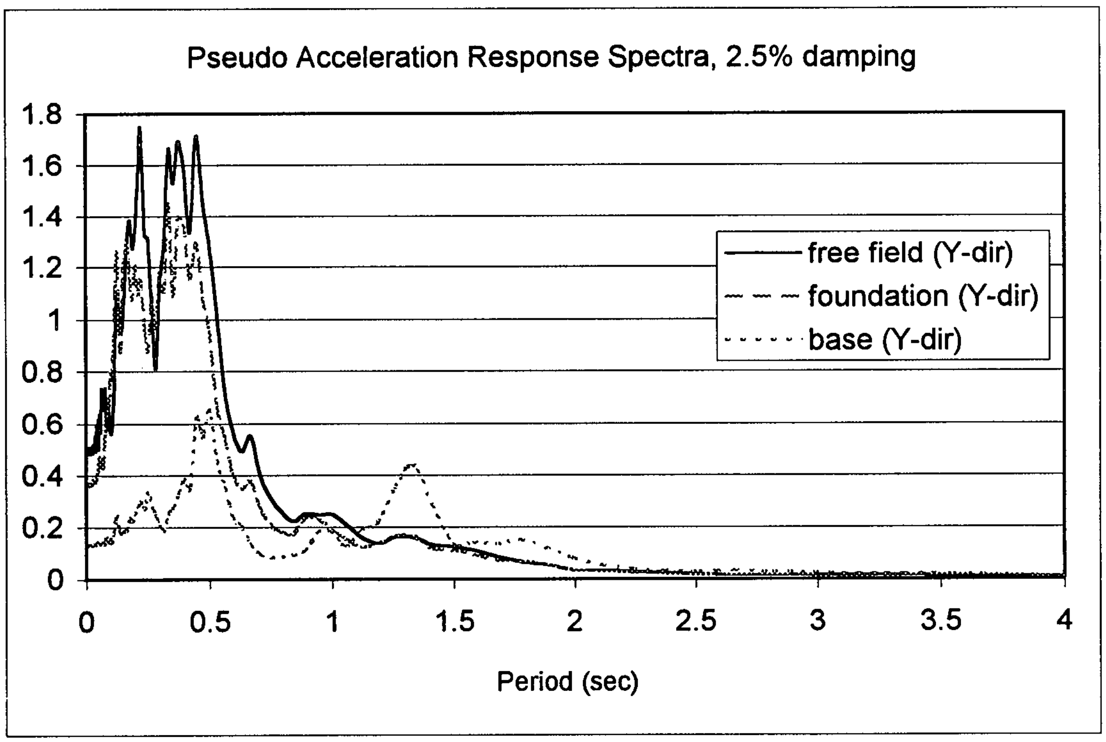

Figure 5.12.4 Pseudo acceleration response spectra of the motion of free field, foundation (below isolators) and base (above isolators) at the LA 7-story university hospital, during the 1994 Northridge EQ.

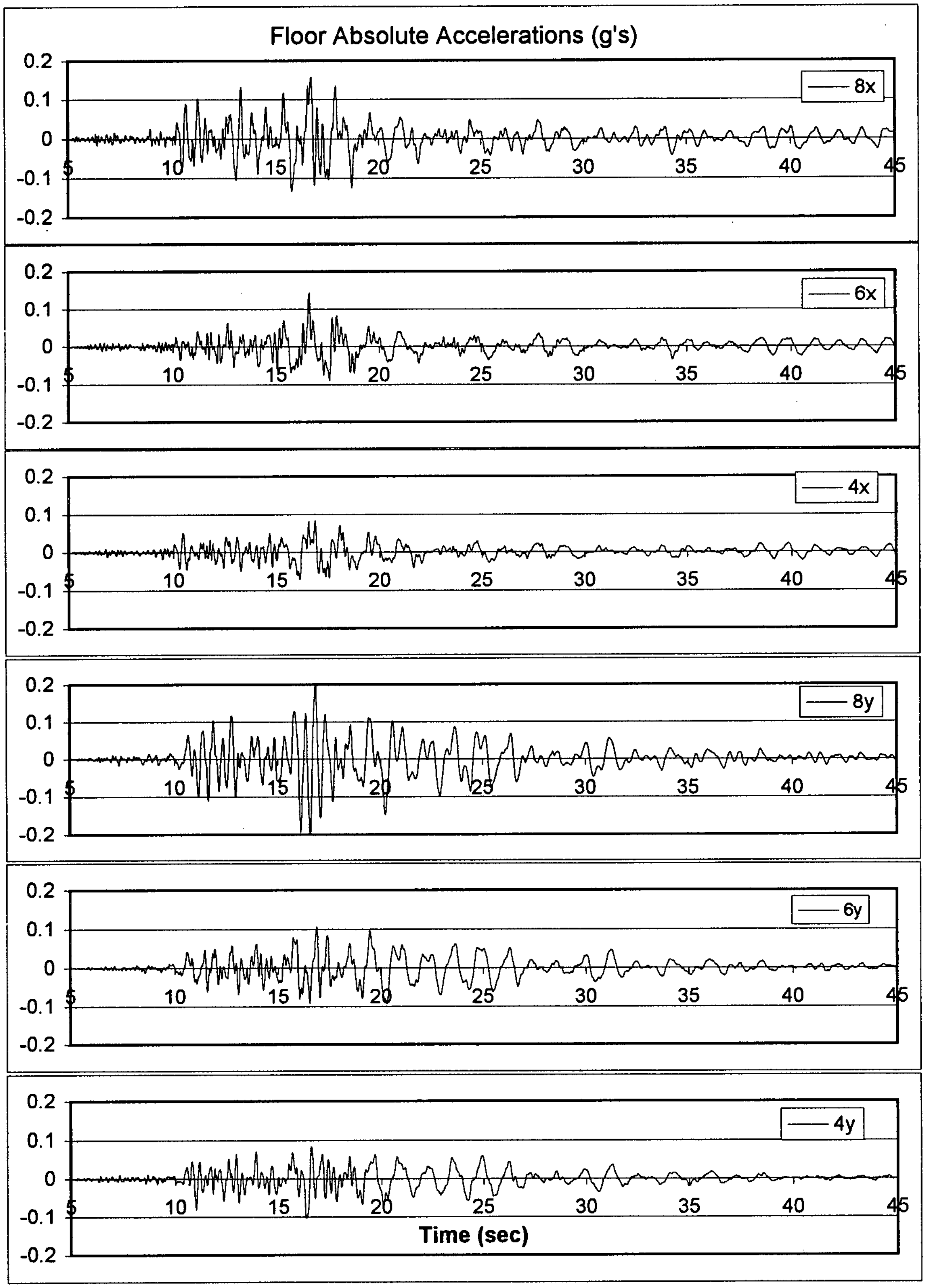

Figure 5.12.5 E-W (X-direction) & N-S (Y-direction) absolute accelerations of the instrumented upper floors of the LA 7-story university hospital, during the 1994 Northridge EQ.

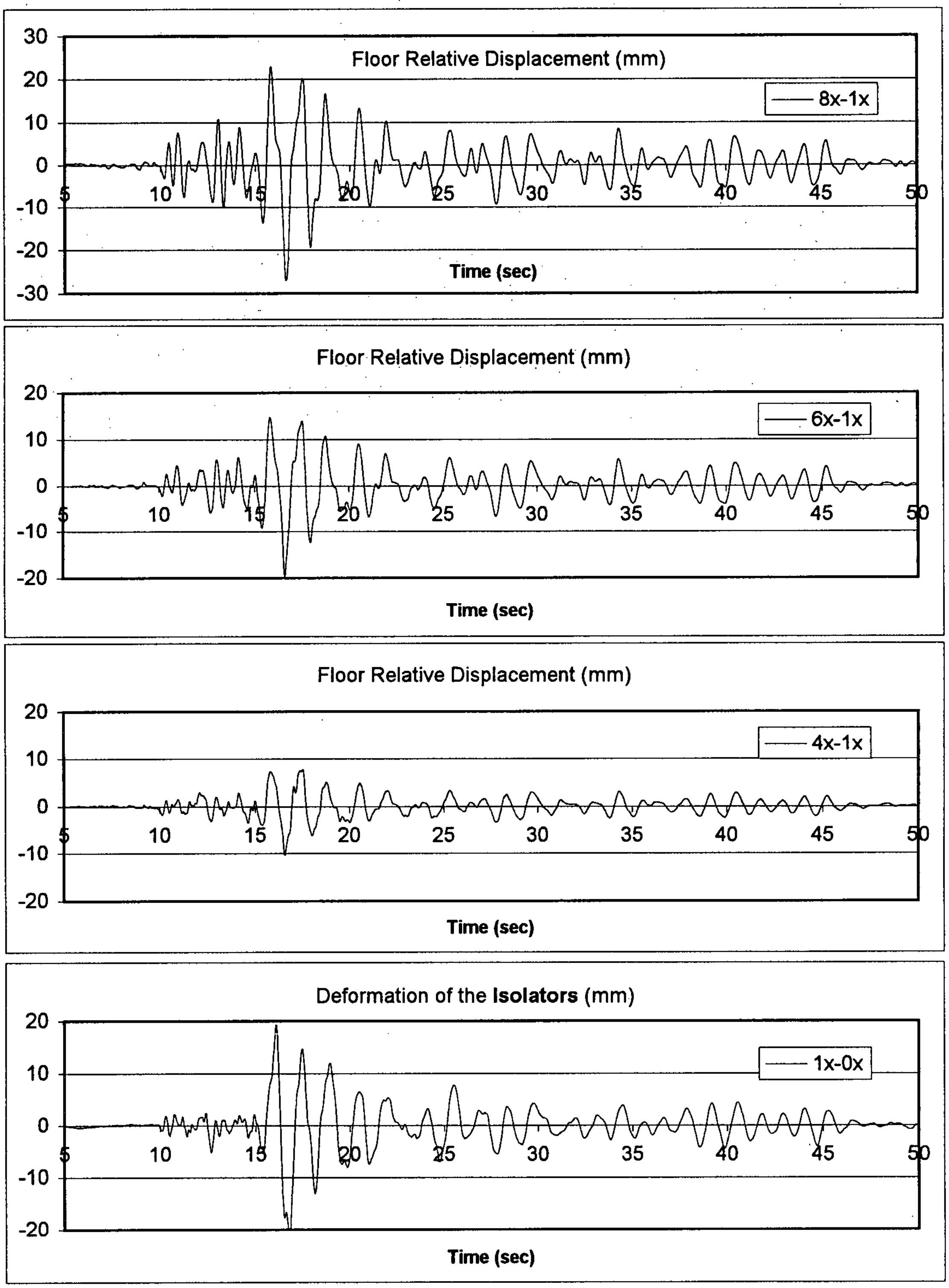

Figure 5.12.6 E-W (X-direction) relative displacements of the instrumented upper floors of the LA 7-story university hospital, during the 1994 Northridge EQ.

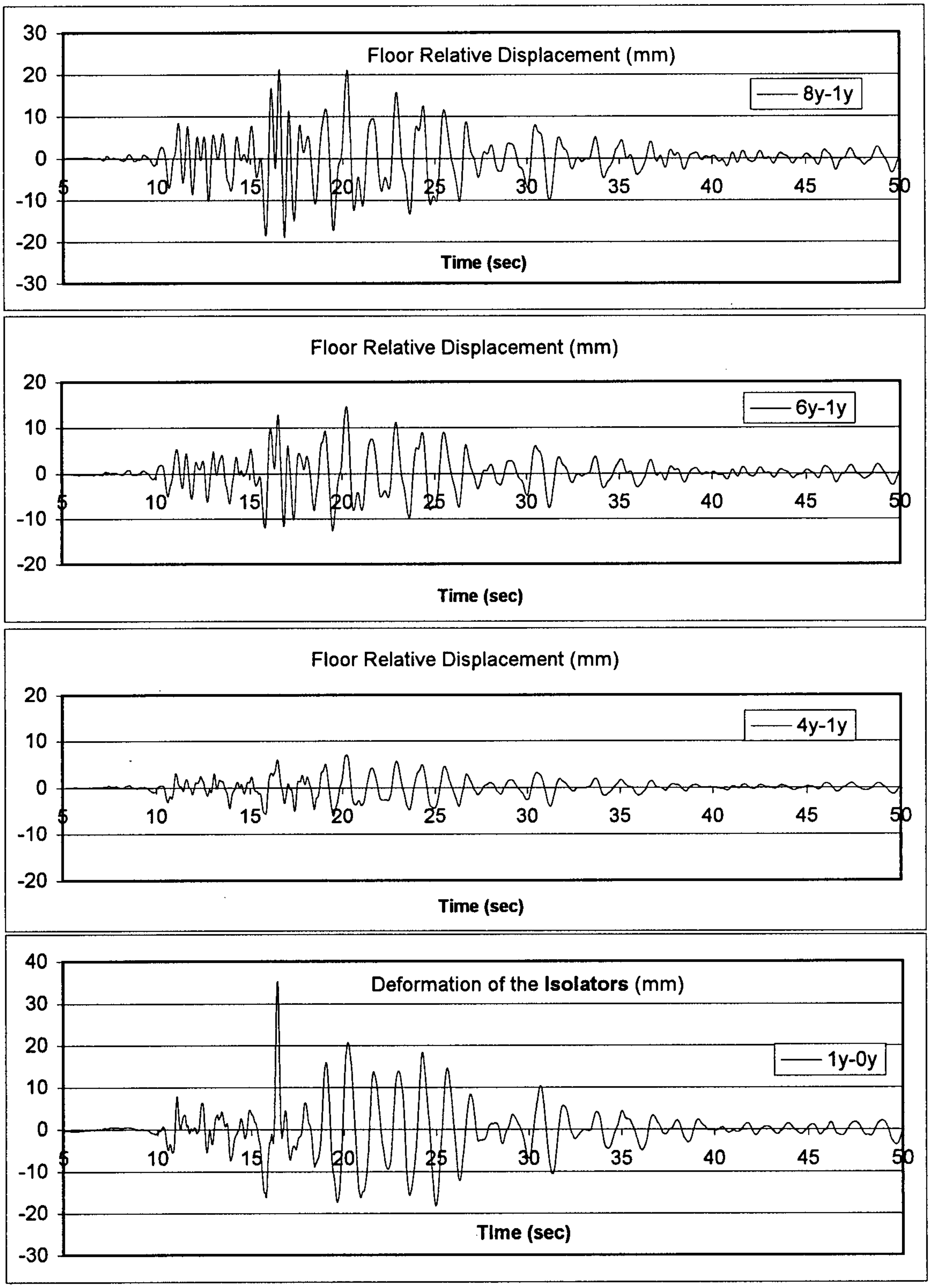

Figure 5.12.7 N-S (Y-direction) relative displacements of the instrumented upper floors of the LA 7-story university hospital, during the 1994 Northridge EQ.

Absolute Displacements

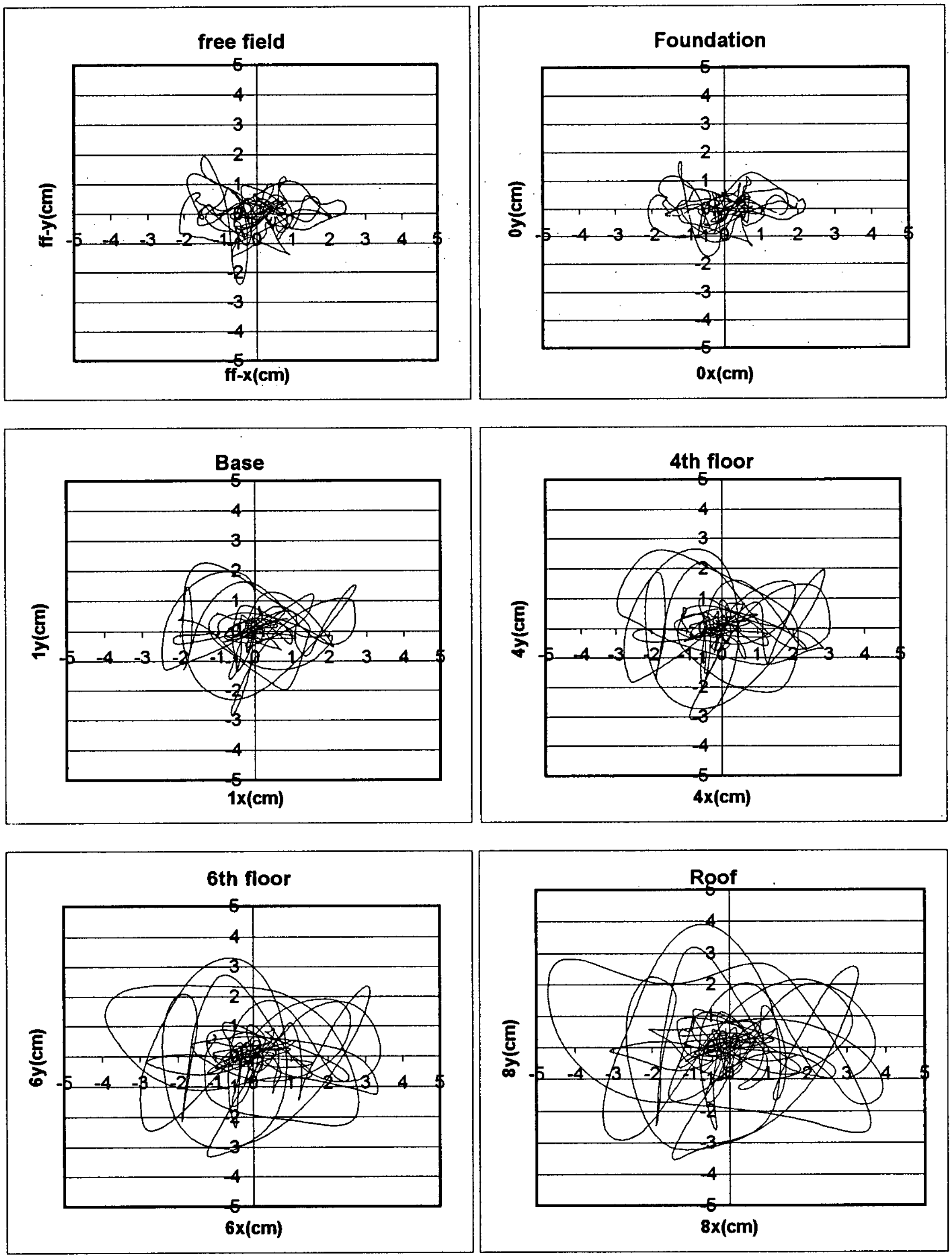

Figure 5.12.8 Orbital displacements (absolute displacements) at the center of the instrumented floors of the LA 7-story university hospital, during the 1994 Northridge EQ

Relative Displacements

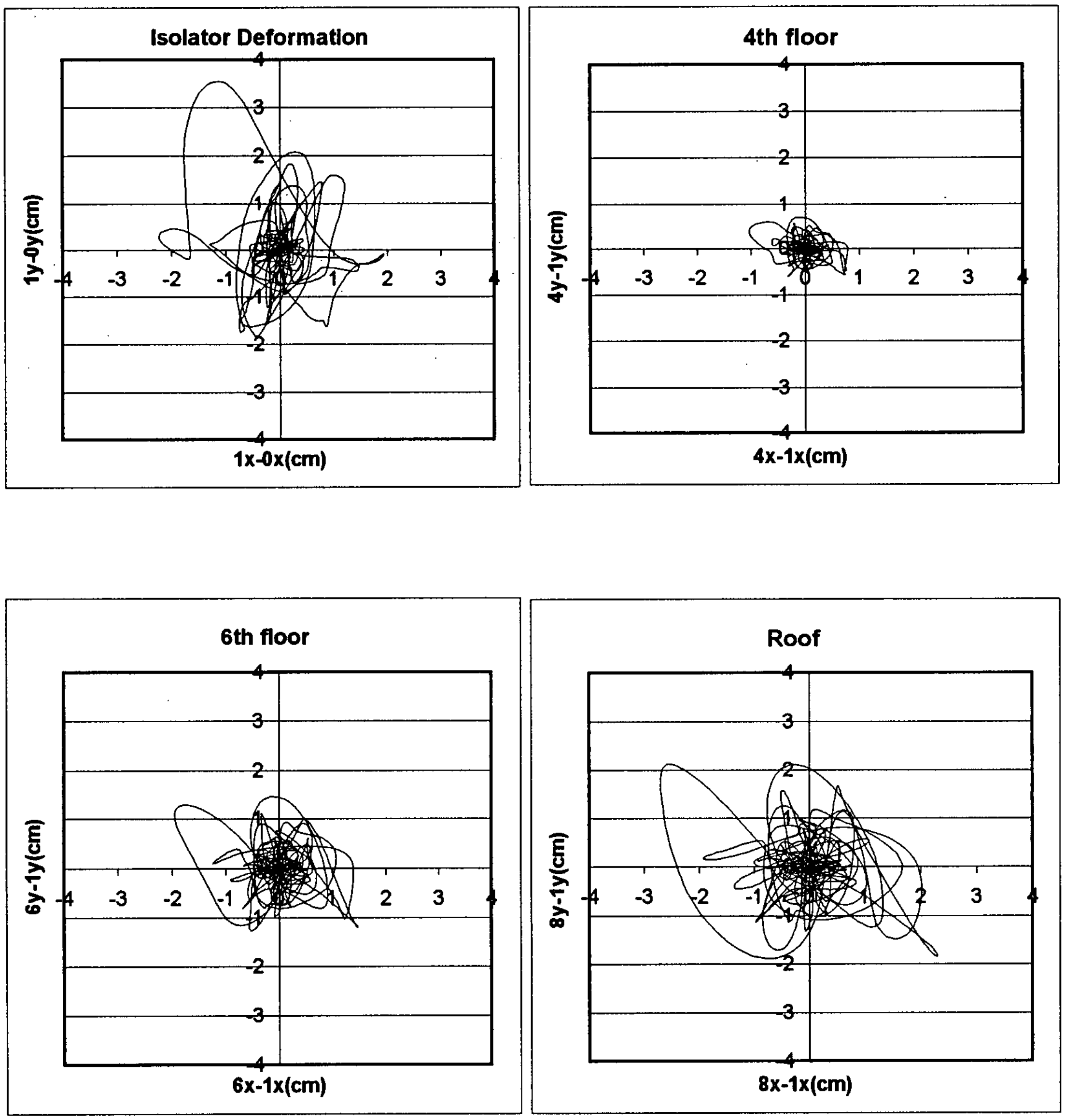

Figure 5.12.9 Orbital displacements (relative displacements) at the center of the instrumented floors of the LA 7-story university hospital, during the 1994 Northridge EQ

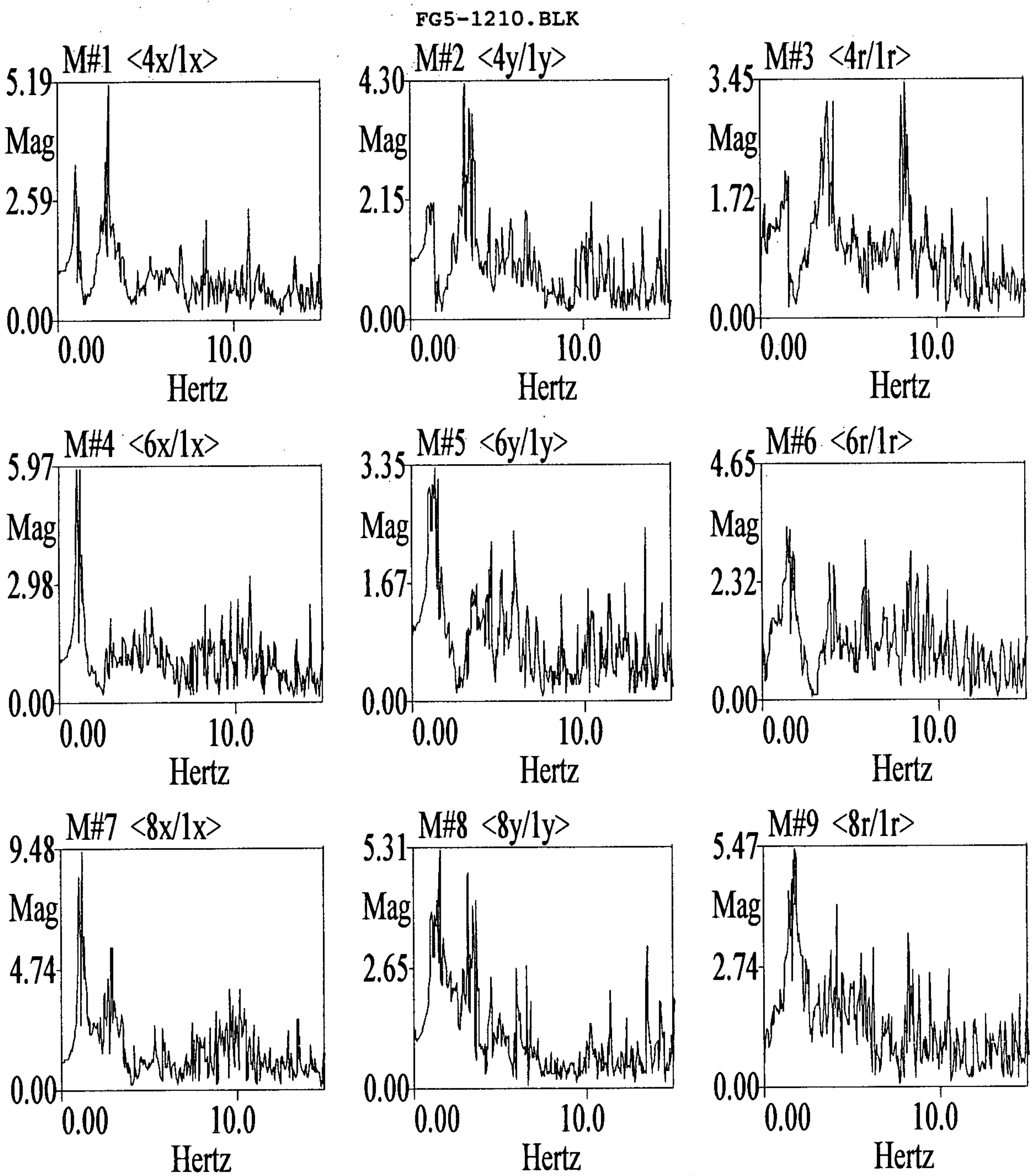

Figure 5.12.10 Frequency Response Functions of the instrumented upper floors with respect to the first floor (above isolators) of the LA 7-story university hospital, obtained from the 1994 Northridge EQ records.

Note: FRF's are computed using a Hanning window, a block size N=2048, 20 averages and 90% segment overlap.

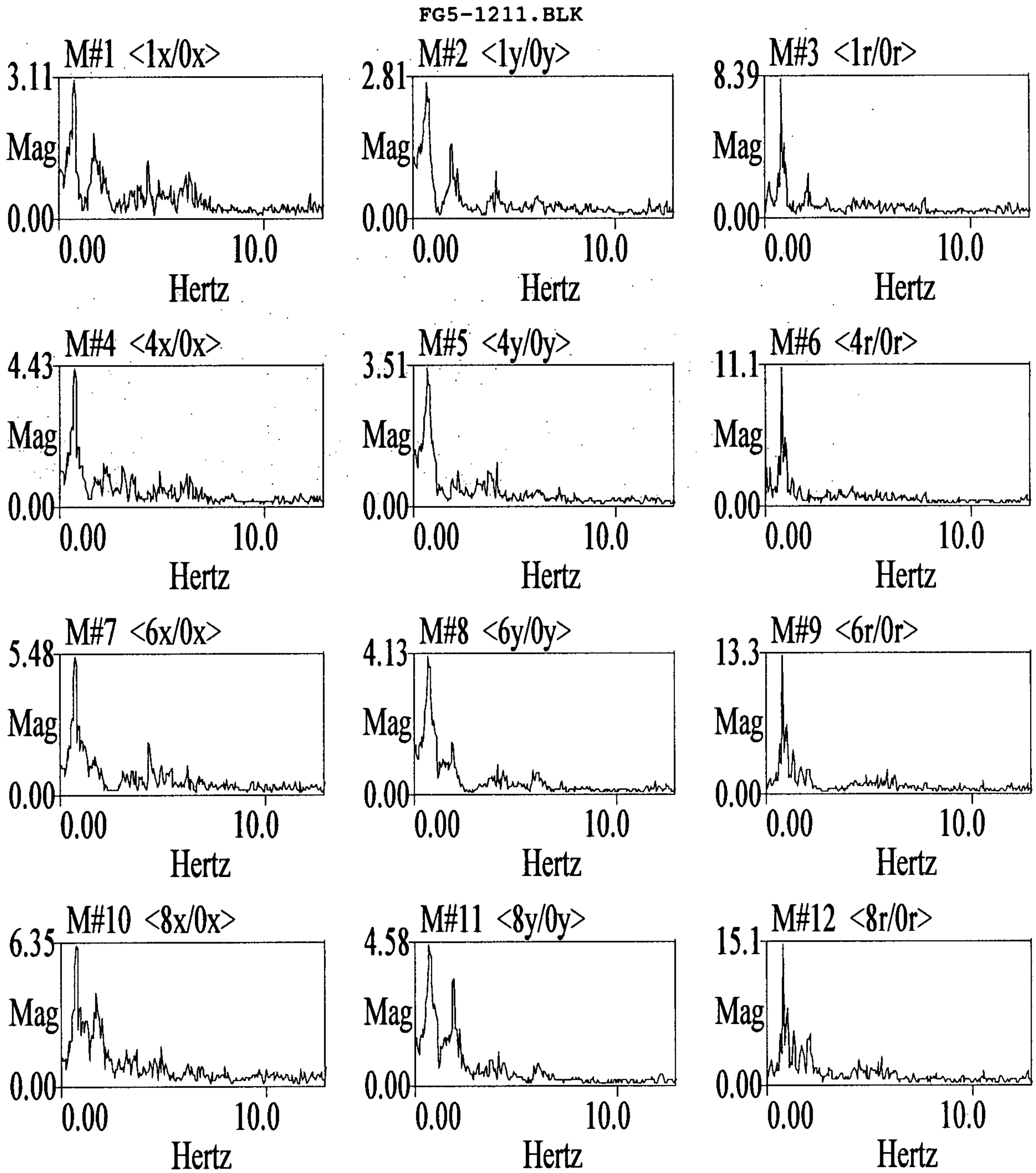

Figure 5.12.11 Frequency Response Functions of the instrumented floors (including the first floor) with respect to the foundation (below isolators) of the LA 7-story university hospital, obtained from the 1994 Northridge EQ records.

Note: FRF's are computed using a Hanning window, a block size N=2048, 20 averages and 90% segment overlap.

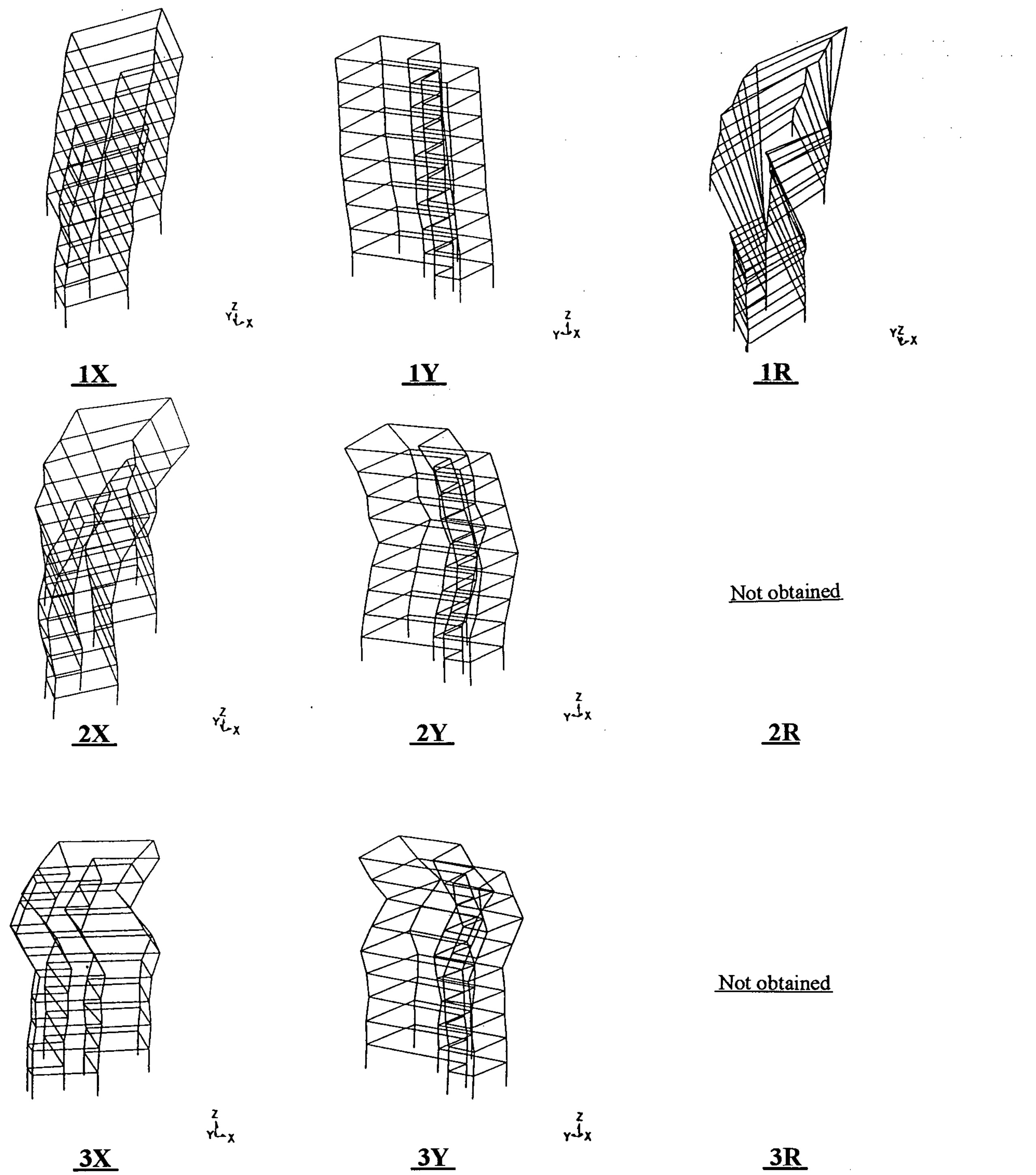

Figure 5.12.12 Mode shapes of the superstructure the LA 7-story university hospital (without isolators), obtained from the 1994 Northridge records.

Note: The displacements of 4th, 6th and 8th floors are obtained from measured data. Displacements of the other floors are based on ME'scope's interpolation algorithm.

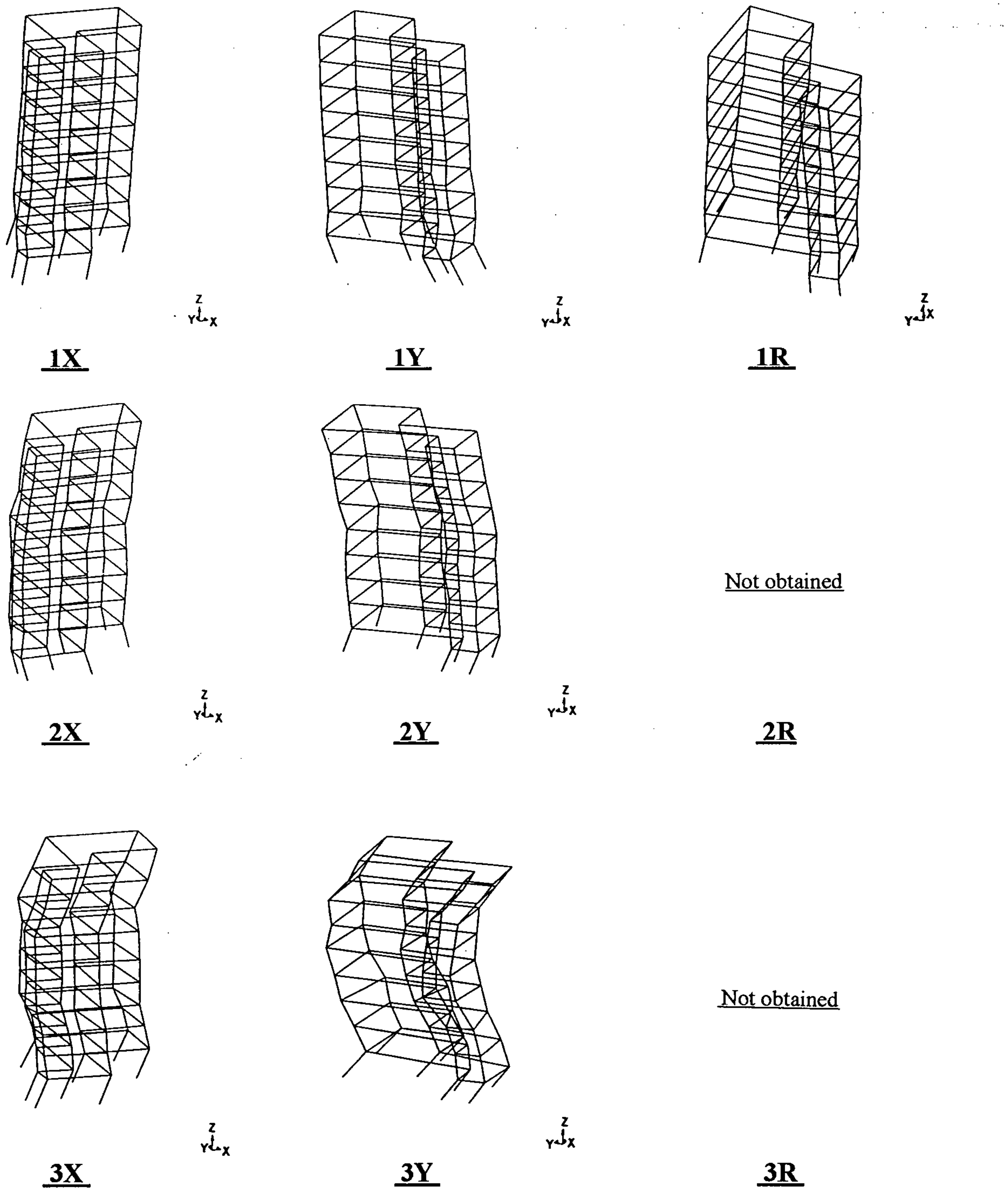

Figure 5.12.13 Mode shapes of the LA 7-story university hospital (with an extra story at the bottom representing the deformation of the isolators), obtained based on Northridge EQ Records. **Note:** The displacements of 1st, 4th, 6th and 8th floors are obtained from measured data. Displacements of the other floors are based on ME'scope's interpolation algorithm.

Table 5.12.1 Estimated natural frequencies (and periods) of the LA 7-story university hospital, based on the of FRF results and visual inspection of the three dimensional mode shapes obtained from analysis of 1994 Northridge EQ data.

SUPERSTRUCTURE (obtained from the FRF's of Figure 5.12.10)						
	X-Direction (E-W)		Y-Direction (E-W)		Rotation	
	Frequency (Hz)	Period (S)	Frequency (Hz)	Period (S)	Frequency (Hz)	Period (S)
Model	1.10	0.91	1.39	0.72	1.65	0.61
Mode 2	2.8	0.36	3.33	0.30	3.9	0.26
Mode 3	5.5	0.18	6.4	0.16	-	-
BASE-ISOLATED (obtained from the FRF's of Figure 5.12.11)						
	X-Direction (E-W)		Y-Direction (E-W)		Rotation	
	Frequency (Hz)	Period (S)	Frequency (Hz)	Period (S)	Frequency (Hz)	Period (S)
Mode 1	0.73	1.37	0.7	1.43	0.8	1.25
Mode 2	1.7	0.59	1.9	0.53	2.1	0.48

Fundamental Period of the building without Base Isolation:

a) NBCC 1995:

$\mathbf{T = 0.1\ N} \Longrightarrow \mathbf{T} = 0.80$ sec

$\mathbf{T_x = 0.09\ h_n / (D_{sx})^{1/2}} = 0.09\ (35.66\text{m}) / (77.11\text{m})^{1/2} = 0.37$

$\mathbf{T_y = 0.09\ h_n / (D_{sy})^{1/2}} = 0.09\ (35.66\text{m}) / (92.35.11\text{m})^{1/2} = 0.33$

b) UBC 1997:

$\mathbf{T = 0.020\ (h_n)^{3/4}} = 0.020\ (117\text{ft})^{3/4} = 0.71$ sec

Chapter 6 DISCUSSION OF THE INFORMATION OBTAINED FROM STRONG MOTION DATA

6.1 General

A detailed discussion of all the information presented in Chapter 5 is beyond the scope of this thesis due to time and space constraints. However, the following important observations could be made from the analyses performed.

6.2 Properties of the Ground Motions

The **time-history** plots of the ground motions indicated that, although the instruments recorded motions with durations of 40 to 100 seconds, the strong portion of the shaking in most cases started after 5 to 10 seconds with durations of 10 to 20 seconds.

The Normalized **Fourier Spectra** of the ground motions indicated that the frequency content of the records were mainly within the range of 0.5 to 15 Hz with peak values typically occurring in the range of 1.0 to 2.0 Hz.

The **Pseudo Acceleraton Response Spectra** provided the most critical information about the ground motions where seismic response of buildings is concerned. The peaks of the acceleraton response spectra in most cases were within a period range of 0.2 to 0.4 seconds and a significant drop was observed in the spectral values for periods greater than 1.0 second. This implies that the participation of the first mode in the response of buildings with a fundamental period of greater than 1.0 second will be relatively small under such seismic loading. There were also cases where the peaks of the acceleraton response spectra were within a period range of 0.5 to 1.0 seconds and the drop in the spectral value started after a period of 1.5 seconds.

The variation in the shape of the **Relative Displacement Response Spectra** was much greater than that of the acceleration response spectra. The periods corresponding to the peak displacement spectral values were always greater than those of the acceleration spectral values, ranging from 1.2 to 9.0 seconds.

6.3 Three-Dimensional Nature of the Ground Motion and the Response of the Buildings

In addition to the vertical motions recorded in the earthquakes, it can be observed from the orbital motion plots presented in Chapter 5 that the horizontal ground motion has a two dimensional nature and the X and Y components of the motion presented in the time history plots are not the two components of a unidirectional motion. The two translational components of the ground motion seem to be uncorrelated and their peaks do not occur simultaneously.

The response of the buildings has also a three dimensional nature. This is both due to the 3-D ground motions and the 3-D properties of the structure.

This issue becomes more critical when the structure is non-symmetrical and has mass eccentricity which results in coupling of the translational and torsional modes of vibrations of the structure.

6.4 Rotational Ground Motion

The ground motion time-history plots show that the portion of the ground accelerations at the ends of the buildings due to pure rotation were 10 to 35 percent of the magnitude of the translational accelerations at the center of the buildings. This affects the 3-D response of the structures. Further research has to be done to evaluate the significance of this effect and whether there is need for including a torsional seismic design load in addition to the torsion due to accidental mass eccentricity introduced by building codes.

De la Llera and Chopra (1991 and 1992) studied the response of three low-rise nominally symmetric buildings (including the Richmond 3-story office building and the San Jose 3-story office building) to evaluate the code accidental torsional provisions. The study showed that UBC accidental eccentricity (5 percent of the building dimension) seems to be satisfactory in representing the torsional motion of the Richmond 3-story office building during the 1989 Loma Prieta Earthquake. It was also concluded that accidental eccentricity may not be necessary in designing these three buildings. However, "extrapolating these observations to other situations is somewhat speculative" [De la Llera and Chopra, 1992].

6.5 Vertical Ground Motion

The ratio of vertical to horizontal peak ground accelerations **(PGA)** measured in the buildings is summarized in Table 6.1. This ratio is mainly within the range of 30% to 50%.

The response of the buildings to vertical ground motion depends on the vertical vibration properties of the structure. These properties, which are determined by the distribution of the mass and the stiffness of the vertical load resisting system, are independent from the lateral vibration properties and may vary for the different parts of the structure.

A plot of vertical to horizontal PGA ratio versus epicentral distance for the buildings under study does not show a clear relationship between these two parameters (Fig 6.1).

Table 6.1 Comparison of the peak ground accelerations of the buildings in various directions and their epicentral distances.

Building	EQ	Epicentral distance (km)	Peak Ground Acceleration (g's)				
			E-W	N-S	Absolute Horiz.	Vertical	Vertical to Hoz. Ratio
Burbank, 6-Story Office Building	Whittier	25	0.16	0.22	0.24	0.09	36%
	Northridge	22	0.30	0.26	0.31	0.12	40 %
San Bernardino 5-Story Hospital	Northridge	113	0.05	0.06	0.06	0.03	51%
Pasadena 6-Story Office Building	Northridge	37	0.10	0.15	0.15	0.07	45%
San Jose 3-Story Office Building	Loma Prieta	21	0.20	0.17	0.20	0.12	57%
San Francisco 4-Story Hospital	Loma Prieta	85	0.15	0.14	0.16	0.08	52%
Berkeley 2-Story Hospital	Loma Prieta	97	0.12	0.11	0.12	0.04	33%
Richmond 3-Story Office Building	Loma Prieta	112	0.11	0.08	0.12	0.04	35%
Redlands 7-Story Commercial Bldg.	Landers	72	0.05	0.05	0.07	0.06	95%
San Bernardino 3-Story Office Bldg.	Landers	83	0.11	0.10	0.11	0.06	53%
LA 2-Story Fire Control Building	Northridge	38	0.16	0.19	0.24	0.11	44%
LA 7-Story University Hospital	Northridge	36	0.16	0.37	0.37	0.07	18%

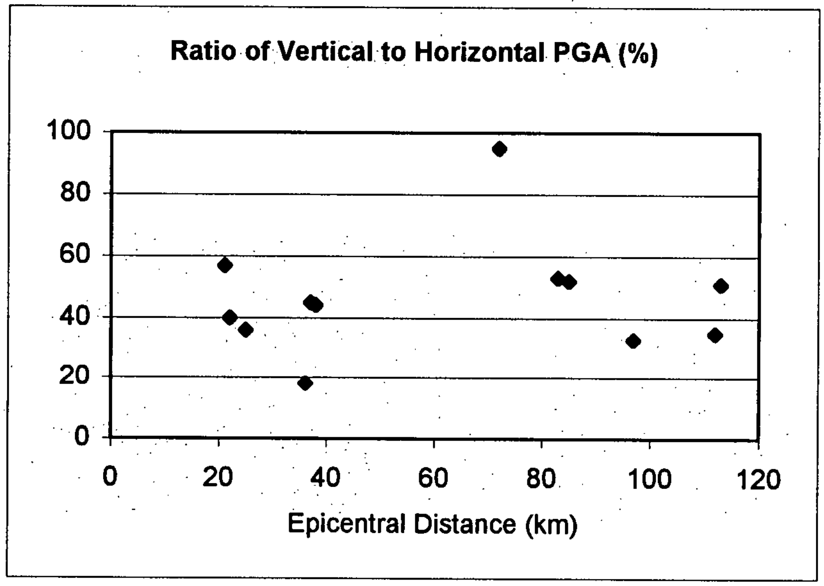

Figure 6.1 Vertical to horizontal PGA ratio versus epicentral distance

6.6 Amplification of the Motion

The time history plots show that peak accelerations were amplified in the upper floors in most cases. However, the variation in these results was significant. For example, the peak accelerations recorded at the roof level of the San Bernardino 5-story hospital during the Northridge earthquake were about three times the recorded PGA's, whereas the peak acceleration recorded at the roof level of the Pasadena 6-story office building in the N-S direction during the same earthquake was about 15 % less than the recorded PGA in that direction. This significant difference is mainly due to the large difference between the fundamental periods of these buildings (see Table 6.2).

In the Burbank 6-story office building during the Whittier earthquake an increase of approximately 30 % (with respect to the PGA) was observed in the roof peak acceleration in the N-S direction whereas no amplification was recorded in the E-W direction. During the Northridge earthquake, the results for this building were the opposite, i.e. there was about a 50 % increase in peak acceleration in the E-W direction and only approximately 10 % increase in N-S direction.

6.7 Comparison of Measured Periods to those Estimated by Code Empirical Formulae

The results of this study, which are summarized in Table 6.2 show that the fundamental period of buildings in most cases are 50% to 100% higher than the values estimated by empirical formulae.

The equation **T= 0.1N** significantly under-estimates the fundamental period for the type of buildings of this research, which are mainly office buildings and their floor to floor heights are usually greater than residential buildings. The height dependent formula for steel moment frame buildings, $\mathbf{T = 0.085\ (h_n)^{3/4}}$ shows a better agreement with the results of this research. Even though the latter formula provides a relatively better estimate of the fundamental period in many cases, it shows a significant error in some cases and the reliability of such empirical formulae in calculating the seismic base shear becomes questionable.

Another important observation is that the results of the Burbank 6-story office building indicate a higher period during the 1994 Northridge earthquake than the 1987 Whittier earthquake (which had a lower peak ground acceleration). This issue, which will be discussed in more detail in Chapters 8 & 9, indicates a non-linear behaviour of the building. The non-linearity can be due to yielding of the main structural and/or non-structural elements or nonlinear elastic behavior of the system (which results in lower global stiffness at higher levels of displacement).

Table 6.2 Comparison of the measured periods to those estimated by code empirical formulae.

Building	P.G.A.(g)		0.1N	$0.085 * (h_n)^{3/4}$	$0.09\ h_n / (D_s)^{1/2}$		Measured Period (sec)	
	E-W	N-S			E-W	N-S	E-W	N-S
Burbank 6-st bldg. (Whittier EQ records)	0.16	0.22	0.6	0.96	-	-	1.25	1.32
Burbank 6-st bldg. (Northridge EQ records)	0.30	0.26	0.6	0.96	-	-	1.41	1.41
San Bernardino 5-Story Hospital	0.05	0.06	0.5	0.84	-	-	0.50	0.48
Pasadena 6-Story Office Building	0.10	0.15	0.7	0.95	-	-	2.22	1.72
San Jose 3-Story Office Building	0.20	0.17	0.3	0.65	-	-	0.64	0.73
San Francisco 4-Story Hospital	0.15	0.14	0.4	0.68	-	-	0.67	0.70
Berkeley 2-Story Hospital	0.12	0.11	0.2	-	0.16	0.16	0.35	0.33
Richmond 3-Story Office Building	0.11	0.08	0.3	0.60	-	-	0.70	0.64
Redlands 7-Story Commercial Building	0.05	0.05	0.7	1.14	-	-	1.37	1.59
San Bernardino 3-Story Office Building	0.11	0.10	0.3	0.57	-	-	0.55	0.56
LA 2-Story Fire Control Building	0.16	0.19	0.2	-	0.17	0.17	0.34	0.34
LA 7-Story University Hospital	0.16	0.37	0.8	-	0.37	0.33	0.91	0.72

6.8 Periods Measured by Other Researchers.

A summary of the periods measured for low-rise steel structures by other researchers (extracted from the reports that were mentioned in Chapter 2) is included in this section for additional information and for comparison with the results of this thesis. These values are presented in Tables 6.3 to 6.8.

Table 6.3 Measured periods for steel moment frame buildings (after Goel and Chopra 1997).

Building Location[1]	ID Number[2]	Number of Stories	Height (m)	EQ Name	Measured Period (sec)	
					Longitudinal	Transverse
Burbank*	C24370	6	24.2	Northridge	1.36	1.38
				Whittier	1.32	1.30
Long Beach	C14323	7	27.7	Whittier	1.19	1.50
Los Angeles	U5208	6	31.7	Northridge	0.94	0.96
Norwalk	U5239	7	29.3	Whittier	1.54	1.54
Norwalk	U5239	7	29.9	Whittier	1.30	1.22
Palm Springs	C12299	4	15.7	Palm Springs	0.71	0.63
Pasadena*	C24541	6	28.1	Northridge	2.19	1.79
Richmond *	C58506	3	13.7	Loma Prieta	0.63	0.74
					0.60	0.76
San Bernardino*	C23516	3	12.6	Whittier	0.50	0.46
San Jose*	C57562	3	13.7	Loma Prieta	0.67	0.69
					0.69	0.69

Note 1: * Denotes that the building is the same as studied in this thesis.

Note 2: The letters C and U denote the **CSMIP** (California Strong Motion Instrumentation Plan) and **USGS** (United States Geological Survey) station numbers.

Table 6.4 Measured periods for the San Francisco 4-story hospital (after Fenves 1990).

Earthquake Name	Peak Ground Acceleration (g's)		Time Window	Measured Period (sec)	
	Longitudinal	Transverse		Longitudinal	Transverse
Morgan Hill	0.02	0.03	0-15 sec	0.54	0.54
			15-40 sec	0.56	0.57
Loma Prieta	0.14	0.16	0-9 sec	0.61	0.65
			9-26 sec	0.71	0.71

Table 6.5 Measured frequencies for the Richmond 3-story office building (after De la LLera and Chopra 1991).

Earthquake Name	Measured Frequency for the First Modes (Hz)		
	X-lateral	Y-lateral	Torsional
Loma Prieta	1.317	1.672	2.242

Table 6.6 Periods measured for the Richmond 3-story bldg. and the San Jose 3-story bldg. (after De la Llera and Chopra 1992).

	Earthquake Name	Measured Periods for the First Modes (sec)		
		X-lateral	Y-lateral	Torsional
Richmond 3-story office building	Loma Prieta	0.63	0.74	0.46
San Jose 3-story office building	Loma Prieta	0.67	0.69	0.65-0.69

Table 6.7 Measured periods from forced vibration measurements for a two story office bldg. (with no basement) in Oakland (after McClure, 1991).

Mode #	Measured Period (sec)
1	0.426
2	1.672
Building Dimensions: 49.7m x 46.6m , height : 8.5m	

Table 6.8 Measured periods for steel moment frame buildings (after Cole et al. 1992).

Building Location	CSMIP Station Number	Number of Stories	Height (m)	EQ Name	Measured Period (sec)	
					Transverse	Longitudinal
Burbank*	24370	6	24.2	Whittier	1.30	1.32
Long Beach	14323	7	27.7	Whittier	1.50	1.19
Palm Springs	12299	4	15.7	Palm Springs	0.63	0.71
Richmond*	58506	3	13.7	Loma Prieta	0.76	0.60
San Bernardino*	23516	3	12.6	Whittier	0.46	0.50
San Jose*	57562	3	15.1	Loma Prieta	0.69	0.69
San Francisco*	58261	4	16.0	Loma Prieta	0.71	0.71

Note: * Denotes that the building is the same as studied in this thesis.

6.9 Contribution of the Higher Modes

Contribution of the higher modes of vibration in the overall response of the buildings to ground motion mainly depends on the natural frequencies of the structure and the shape of ground motion response spectra. The first mode usually contains 70 % to 80 % of the effective mass of the structure. (The higher modal acceleration amplification factors for the first modes presented in the tables of Chapter 5 are due to this fact). However, the periods of the higher modes usually are in the region of higher amplitude in the ground motion response spectra.

In this study, the significance of the contribution of the higher modes in the structural response were evaluated by locating the natural periods of the buildings in the ground motion response spectra and investigating the out of phase accelerations and displacements on the time-history plots.

A fundamental period in the low amplitude range of the acceleration response spectra indicates a small contribution of the first mode in the seismic response of the building. It was observed that for the buildings with the above mentioned situation, time history plots showed out of phase accelerations and displacements for the various floors, indicating the significance of the effect of the higher modes in the overall response of these buildings.

The results of this study showed significant higher mode effects for the buildings with a fundamental period of greater than 1.0 second. In the buildings with a period of less than 0.5 seconds the first mode seemed to dominate the overall response.

It is important to note that the periods of some of the buildings in this study were significantly higher than what is usually expected for low-rise buildings, and their response was highly affected by the second and third modes. In other words, these buildings behaved more like typical high-rise buildings.

6.10 Error Due to Manipulation of the Data

At this point it is important to note that in order to identify the translational and rotational vibration properties of the buildings, the X, Y, and Rotational components of the ground motion and the structural response at the center of the buildings were calculated by manipulating the recorded data. This calculation, which was done based on the assumption of rigid floors and small displacements, may have introduced a measure of error to the analysis results. This error may be of larger magnitude for the time histories calculated for the center of the buildings at the foundation level of the buildings with spread footings (where there is no concrete diaphragm at that level). The rotational data, which are obtained by subtracting the two translational time-history data, have a smaller magnitude than the translational data whereas their random error and noise is of the same order of magnitude. This results in a significantly higher percentage of error for rotational data which should be considered when using those data.

6.11 Mode Shapes

The existing data and the techniques used to determine the mode shapes were not precise enough to clearly distinguish between the modes in the X and Y direction when their periods were very close to each other.

As a special case, the Burbank 6-story office building has almost identical structural properties in the X and Y directions with no mass eccentricity and no coupling between the modes. For such a structure, theoretically, there are no separate modes of vibration in the X and Y directions. The X and Y mode shapes are the same with the same period. In such cases any linear combination of the two mode shapes can also be a mode shape and will satisfy the properties of a mode shape in the dynamic equilibrium equations.

6.12 Base-Isolated Buildings

Two of the buildings considered in this study were base-isolated. The response of both buildings (Los Angeles 2-story fire control building and Los Angeles 7-story University hospital) has been studied in detail by Huang et al. (1993) and Nagarajaiah and Xiahong (1995). The parameters that control the response of this type of building are more complicated than for rigid base buildings. In particular, the use of a classical (Rayleigh's) damping matrix for structural analysis and the concept of equivalent linear damping has limited meaning for these structures. The effect of damping mechanisms on the response of base isolated buildings has been studied by Chang and Markis (1999). The theoretical basis of seismic isolation and energy dissipation has been studied by Kelly, (1997).

More detailed study of the behaviour of the base-isolated structures was not within the scope of work of this research. However, a brief review of the information obtained from the strong motion data (presented in Chapter 5) shows that base isolation mainly affects the seismic response of the buildings in the following two ways:

1) The fundamental period of the structure increases due to base isolation (a 50% increase was observed in the Los Angeles 7-story hospital and 200% in the Los Angeles 2-story fire control building). This places the fundamental period of the building in the low amplitude part of the ground motion response spectra and is very beneficial for low-rise buildings where their relatively low periods are usually in the high amplitude part of the ground motion response spectra.

2) A significant portion of the deformation of the building due to seismic loads happens in the isolators, which are capable of undergoing several circles of large deformations without significant damage. As a result, the elastic deformation of the rest of the building is significantly less than ordinary buildings.

6.13 Damping Ratios

The estimated damping ratios were mainly within the range of 2 to 5 %.

The data has undergone several stages of processing and curve fitting before estimating the damping values. The analysis results indicated that the method used in this project to estimate the damping values from the strong motion data does not always yield reliable results. Specifically, the results for higher modes did not seem to be reliable and were excluded from the final report. The damping values estimated for the first modes in each direction were included in the report for information. However, the accuracy of these results is questionable.

6.14 Modal Acceleration Amplification Factors

The modal acceleration amplification factors obtained from the FRF and SRF analyses (presented in Chapter 5) were mainly used for estimating the natural frequencies of the buildings. However, they can also represent the dynamic response properties of these buildings.

The amplification factors calculated for the fundamental modes were significantly higher than those of the higher modes. As noted in Section 6.9, this is due to the fact that for low-rise and mid-rise buildings, the first mode usually contains 70 % to 80 % of the effective dynamic mass of the system.

Chapter 7 COMPUTER MODELING OF THE BURBANK 6-STORY OFFICE BUILDING

7.1 Introduction

The Burbank 6-story office building was chosen for a detailed computer modeling and structural analysis. The building has a symmetrical plan with no irregularities. The motion of the building was recorded during the 1994 Northridge and the 1987 Whittier earthquakes. The building experienced a peak ground acceleration of 0.3g during the Northridge earthquake. These facts made the Burbank building a desirable choice for this part of the research, where investigating the accuracy of various analysis techniques was the main objective.

7.2 Structural System

General information on the Burbank 6-story office building is included in Chapter 4. In addition, the following information was also used in computer modeling of the building. The building does not have a basement and the 4 inch concrete slab on grade provides grounds for assumption of a rigid diaphragm at the first floor. This assumption was used to generate data for the ground accelerations at the center of the building. Typical floors consist of a 3 inch light-weight concrete slab over corrugated metal decks supported by steel girders, which transfer the floor loads to the columns. Shear studs, 19 mm (3/4 inch) in diameter and 114 mm (4.5 inch) in length, welded to the steel girders at 305 mm c/c (12 inch) provide composite action between the concrete slabs and the steel girders in the E-W direction.

The composite action of the beams in the E-W direction may be a reason for the higher stiffness (lower period) observed in the building during the 1987 Whittier earthquake. The friction between concrete and steel components of the composite beam may be one of the reasons for the higher damping values estimated for the building in this direction.

The columns are made of wide-flange, hot rolled structural steel sections, which are spliced at 3 feet above the third and fifth floors (where the column sections are reduced in size). The exterior columns, which form the moment-resisting frames, are welded to steel grade beams. These beams are encased in reinforced concrete and supported by 9.75 m (32 feet) long, 762 mm (30 inch) diameter reinforced concrete piles. A pair of piles under each column is expected to provide moment resisting supports at the base of the column in the plane of the perimeter frames (Figure 7.2.3). The flexibility of the steel grade beams, however, makes the assumption of fixed supports questionable (Shen and Astaneh, 1990). The interior columns are supported on base plates anchored to concrete grade beams. These columns are also supported on 30 inch diameter concrete piles with a length of 10.0 to12.2 meters (33 to 40 feet).

Two types of beam to column connections are used in the structural system. Pin connections are used for the interior beams and moment resisting connections for the perimeter beams. Figures 7.2.1 to 7.2.5 show the typical framing, rigid and pin connections, and column base connection details.

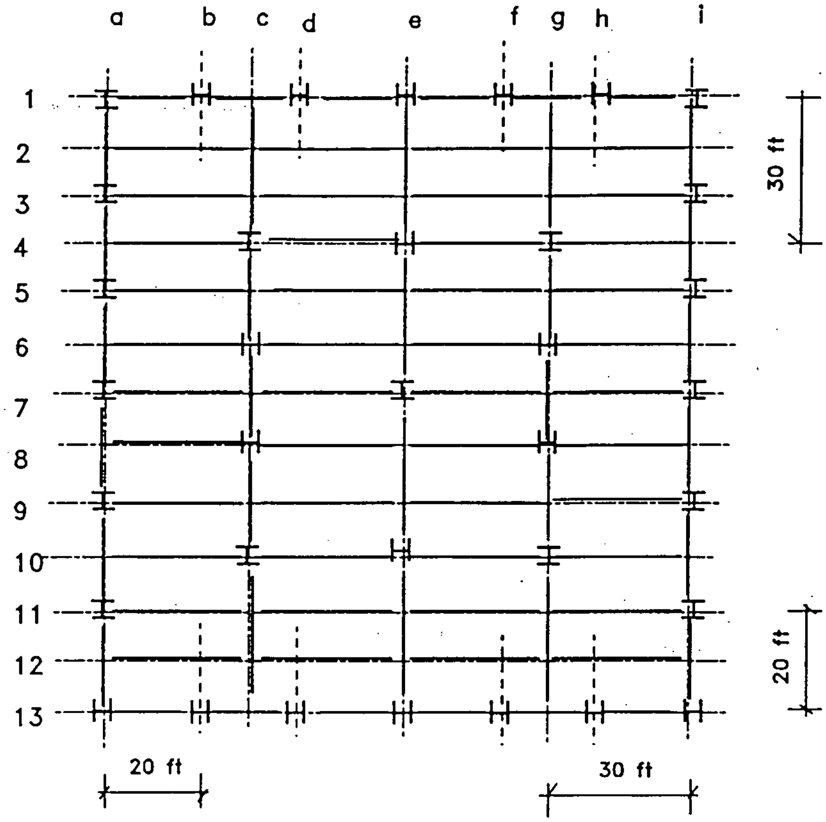

Figure 7.2.1 Typical floor framing plan of the Burbank 6-story bldg. (after Shen & Astaneh, 1990).

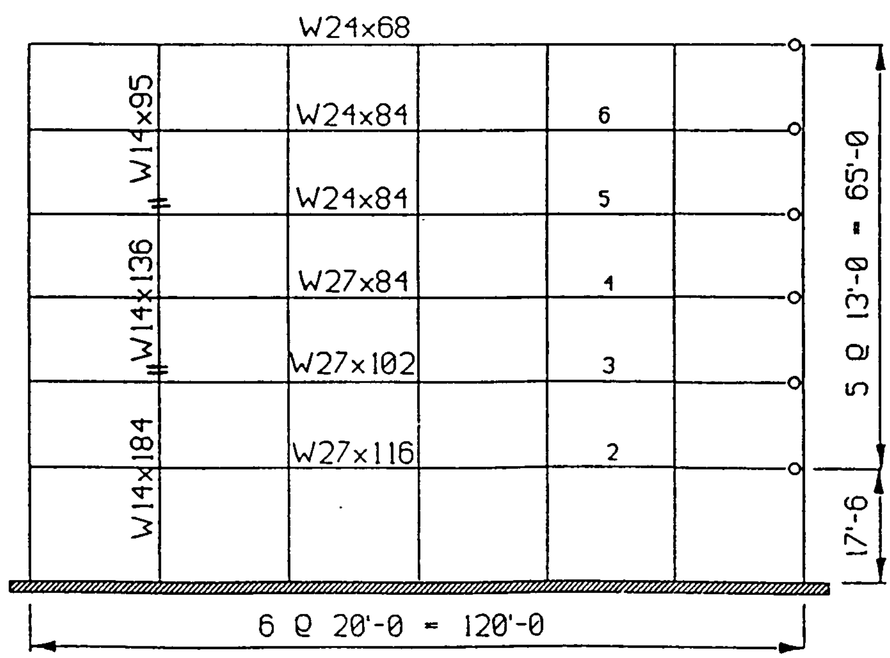

Figure 7.2.2 Typical perimeter moment resisting frame of the Burbank 6-story bldg.

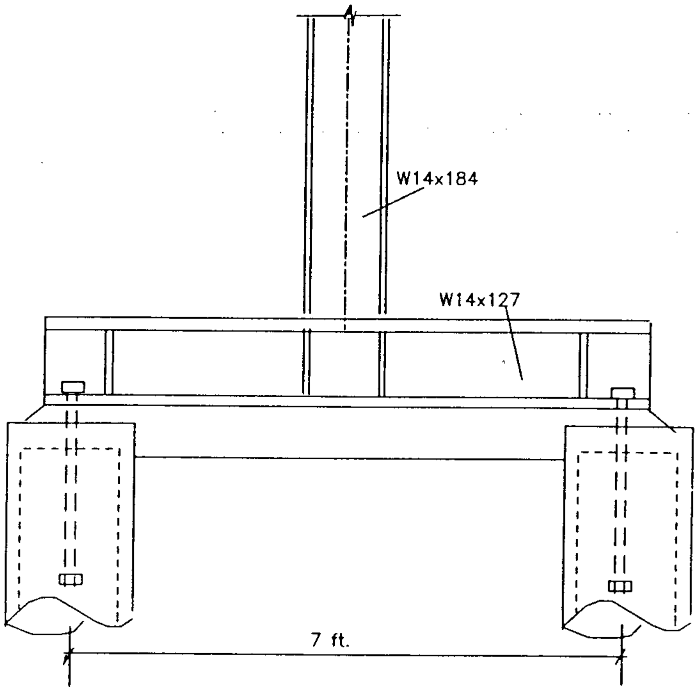

Figure 7.2.3 Typical perimeter column base connection detail of the Burbank 6-story bldg. (after Shen & Astaneh, 1990).

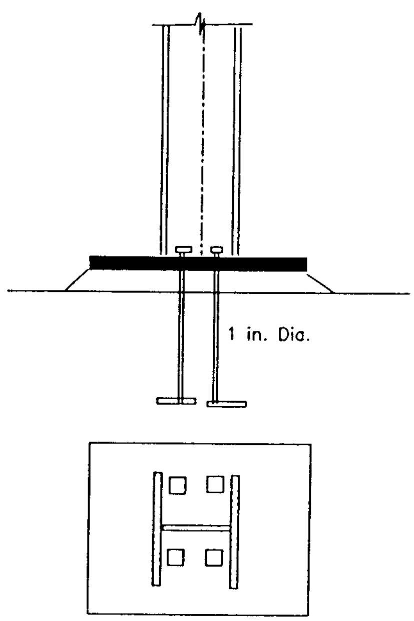

Figure 7.2.4 Typical interior column base connection detail of the Burbank 6-story bldg. (after Shen & Astaneh, 1990).

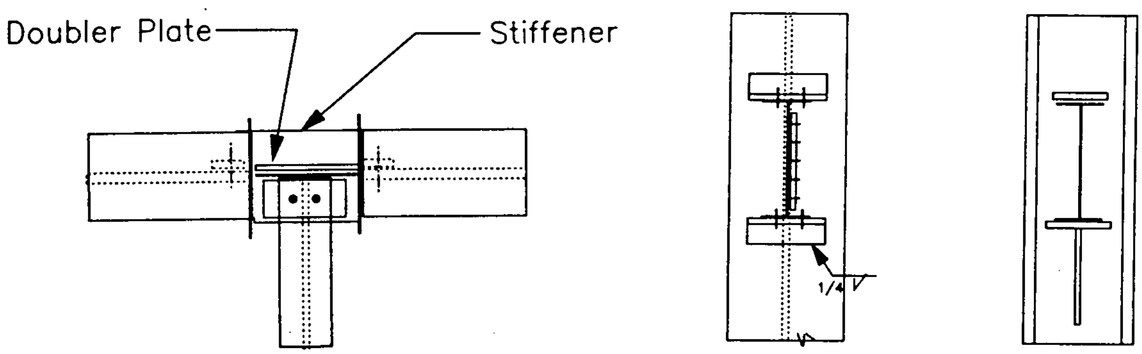

flange web

Moment Connection Shear Connection

Figure 7.2.5 Typical beam to column connection detail of the Burbank 6-story building (after Shen & Astaneh, 1990).

The building drawings indicate the following material properties of the structural elements:

- Structural steel: **ASTM A-36**
- Reinforcing Steel: **Grade 40 or 60**
- Lightweight Concrete: 17.3 kN/m^3 **(110 pcf)** with $\mathbf{f'_c}$ = 20.7 MPa **(3000 psi)** (for fill in metal decks)
- Normal weight Concrete: $\mathbf{f'_c}$ = 13.8 MPa **(2000 psi)** for slabs on grade, $\mathbf{f'_c}$ = 20.7 MPa **(3000 psi)** for all others.

7.3 Estimated Weight of the Building

The floor weights were calculated based on the information provided in the structural drawings and the following assumptions:

3 inch deep metal deck	3.0 psf
Concrete fill + 3.5 inch topping (light weight concrete, 110pcf)	44.0 psf
Steel beams and columns (2nd floor)	14.0 psf
Steel beams and columns (3rd floor)	12.0 psf
Steel beams and columns (typical floor)	10.0 psf
Steel beams and columns (roof)	8.0 psf
Partition walls	5.0 psf
Perimeter glass walls (wall area)	8.5psf(wall)
Ceiling + Mechanical	6.0 psf
Roofing	7.0 psf
Penthouse roof	30.0 psf
Elevator machine room, concrete slab & walls	150.0 pcf
Roof parapet (per unit length)	135.0 plf

With this information, the floor weights and corresponding rotational moments of inertia were calculated to be used in the dynamic analysis.

Table 7.2.1 shows the floor weights and the moments of inertia used in the computer models of the Burbank building.

Table 7.3.1 Estimated floor weights and rotational moments of inertia of Burbank 6-story building.

Floor	Dimensions **ft**	Total Floor Weight **kips (kN)**	Moment of Inertia **kips . ft^2 (KN . m^2)**
2nd	130 x 130	1367 (6085)	4352000 (1800000)
3rd	121.5 x 121.5	1115 (4965)	3022000 (1250000)
4th	121.5 x 121.5	1087 (4839)	2901000 (1200000)
5th	121.5 x 121.5	1082 (4817)	2780000 (1150000)
6th	121.5 x 121.5	1082 (4817)	2780000 (1150000)
Roof+P.H.	133 x 133	1477 (6577)	4594000 (1900000)
Total	-	7210 (32100)	-

7.4 Description of the Structural Model

The structure was modeled as 3-D frame structure with fully rigid connections for perimeter frames and all column bases. The interior beams were modeled in two ways. In the first model they were modeled with pin connections so that they would not contribute to the lateral stiffness of the structure. In the second model the interior beams were modeled as continuous beams with rigid connections to the columns. The objective was to account for the composite action of the beams in E-W (X-direction), the interaction of the concrete slabs and the columns, and partial fixity of the shear connections. The section properties of the interior beams in the second model were modified to provide the overall lateral stiffness such that the natural frequencies of the structural model matched those obtained from the Whittier earthquake data.

P-delta effects, rotational and vertical ground accelerations were considered.

All floors were assumed to be rigid diaphragms and the floor masses were lumped at the center of gravity of the diaphragms.

Since all the interior beams were pin connected to the other elements, the vertical loads on these beams would not affect the behaviour of the perimeter moment resisting frames. The gravity loads and vertical seismic loads were only applied to the perimeter frame members in the model. To apply the vertical seismic loads, the distributed loads on the perimeter beams were lumped in the mid-span and the two ends of each beam (2/3 of the total distributed load lumped as a concentrated load at mid-span so that it would result in the same fixed end moment as a uniformly distributed load).

In modeling the spliced columns, where the top 3/4 (approximately) of the length of the column had a smaller cross section, single elements with approximately equivalent section properties were used.

7.5 Description of the Structural Analysis Program CANNY-E

The program **CANNY-E** (CANNY-E User's Manual, 1996) was used for the nonlinear analyses in this study. CANNY-E is capable of performing 3-dimensional non-linear dynamic time-history structural analysis. The nonlinearity of CANNY-E's structural elements is based on a lumped plasticity model, which assumes that yielding only occurs at the two ends of the element. CANNY-E includes a library of various types of hysteresis models that can be assigned to each element based on its material and structural properties.

The program does not consider geometric nonlinearity (which is due to large deformations). However, P-delta effects can be considered in the analysis. The user has the option of including rotational and vertical ground accelerations. The lateral seismic loads are applied to the centroid of the rigid floor diaphragms according to the lumped masses assigned to each diaphragm. Vertical seismic loads can be applied to the structural model (locally) by assigning lumped masses to selected nodes.

7.6 Analysis Parameters used in the CANNY-E Model

The following parameters were used in the CANNY-E model of the structure.

1) Damping: The program CANNY-E uses a Rayleigh type damping, where the damping matrix is a linear combination of the mass and stiffness matrices. In this method the damping ratio of only two modes can be defined by the user. This did not allow assigning different damping values to various modes in the X and Y directions. Because of this limitation of the program, the analyses were performed with different damping values until the best match with the recorded data in two directions was obtained. The analyses showed that the damping value, which gave a better match with N-S (Y-direction) data was lower than that of the E-W (X-direction) data. However, a critical damping ratio of 3.0% assigned to the first two modes (which showed reasonable results for both directions) was used in the final model.

2) Time step method: CANNY-E has the option of using various time step integration techniques. The Newmark's method with a Beta value of 0.25 was used for the time step analysis in this project (see Chopra, 1995).

3) Hysteresis model: Bi-linear Degrading Elasto-Plastic hysteresis loops were used to model the bending stiffness properties of the beams and columns and axial stiffness of the columns. Figure 7.6.1 shows the CANNY-E hysteretic model used for the nonlinear analysis in this project.

The following parameters were used in defining the hysteretic models:

- Post yielding stiffness factor of 0.02 (with reference to SAC 95-04, 1995)
- Unloading stiffness degradation factor $\gamma = 0.3$
- Strength degradation factor $\lambda_n = 0.75$

The factor γ is used determine the unloading stiffness as following:

$$K_u = K_0 \cdot \left(\frac{d_y - d'_y}{d_{max} - d'_{max}} \right)^{\gamma}$$

Where K_u, K_o, d_y, d'_y, d_{max} and d'_{max}, are shown in Figure 7.5.1.

The factor λ_n is used to determine the reloading yield strength as follows (where d_m and d_y are shown in Figure 7.5.1, $u = d_m / d_y$ represents ductility and F_y represents the initial yield strength):

$$\overline{F_y} = F_y \cdot \left(1 - \lambda_u \cdot \left(1 - \frac{1}{u}\right)\right)$$

For example, $\lambda_n = 0.75$ will result in a 50% reduction in strength at ductility $u = 3$.

4) Material Strength: The expected yield stress of the structural steel was considered to be 1.05Fy = 260 MPa based on the recommendations of the Interim Guidelines (FEMA1995).

For plastic moment, $M_p = Z \, . \, F_y$ (where Z is the plastic modulus of the steel section) was used in the bi-linear Hysteretic models for beam & column bending properties.

5) Shear: Shear stiffness properties were modeled as linear elastic.

7.7 Modified Linear Elastic Model (ETABS Model)

The program CANNY-E does not include an option for performing a response spectrum analysis. Since spectral dynamic analysis is widely used in the seismic design of the structures, it was desirable to include in this study a comparison of results from time-history and response spectrum analyses. For this reason a simpler model of the building was prepared to be analyzed with the program ETABS (ETABS User's Manual, 1995).

The properties of the ETABS model, which was also 3-dimensional, were as follows:

- Linear elastic behaviour
- No interior beams (interior columns were laterally supported by the rigid diaphragms)
- Unidirectional input ground motion (only the E-W (X-dir) component of the ground motion recorded during the Northridge EQ) was applied to the model.
- The period of the first mode in the X direction was very close to that of model **A** (the CANNY-E model which matched the Northridge earthquake records, as described in the next chapter).

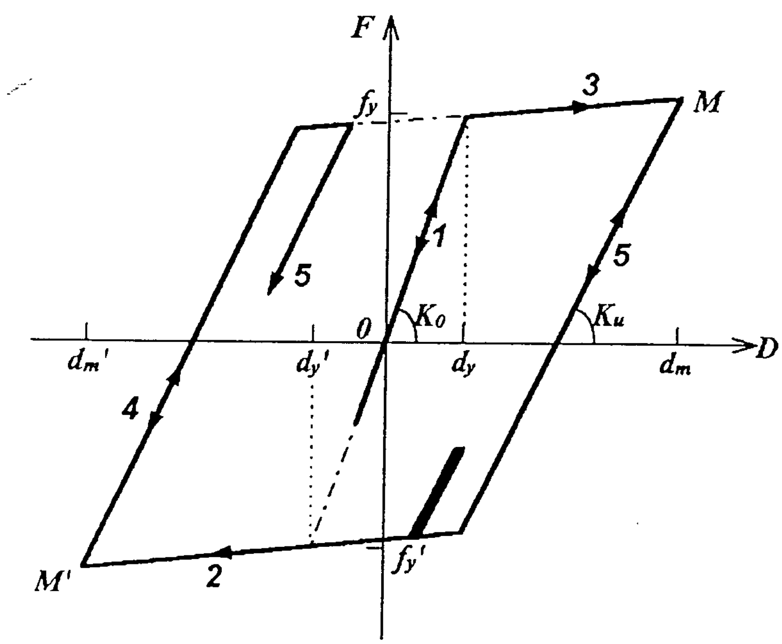

Figure 7.6.1 CANNY-E hysteretic model used in nonlinear analysis (CANNY-E User's manual, 1996).

Chapter 8 DYNAMIC ANALYSIS OF THE BURBANK 6-STORY OFFICE BUILDING

8.1 General

In this chapter, a summary of the results of the analyses performed on the structural models of the Burbank 6-story office building, and a comparison of the results of various analysis methods, will be presented in the format of tables and diagrams. A more detailed discussion of the results will be included in Chapter 9.

8.2 Definition of the Structural Models used for the Analyses

Three different structural models of the building were used in this study. These are:

Model A: CANNY-E non-linear model with pin connected interior beams, no composite action between beams and concrete slabs, fully fixed column bases and exterior beam-column connections. The floor weights were modified so that the model had the same natural frequencies as those obtained from the measurements during the Northridge earthquake. Time-history outputs of this model matched the Northridge earthquake Records. Model A was also used for the non-linear analyses with higher levels of input ground motion.

Model B: CANNY-E non-linear model with fixed end interior beams in the E-W (X) direction and increased stiffness properties for all the elements. The stiffness of this model was scaled so that its natural frequencies matched the higher frequencies obtained from measurements during the Whittier earthquake.

The additional stiffness in this model may be justified by partial fixity of the interior connections, interaction of concrete slabs with the steel beams and columns, and the stiffness of the non-structural elements.

Model C: ETABS linear elastic model (as described in Chapter 7) for comparison of the results from the following analysis methods:

1) Time-history analysis

2) Response spectrum analysis based on true response spectra of the recorded ground motion

3) Response spectrum analysis based on code defined response spectra

4) Equivalent Static analysis.

8.3 Results of Analysis Based on Whittier Earthquake Records

As explained in Section 8.2, the stiffness of Model **B** was scaled to match the Whittier EQ data. A dynamic time-history analysis was performed on this model, using the ground accelerations obtained from the Whittier earthquake records. This section includes a summary of the results of this analysis.

The natural frequencies and periods of Model B are listed in Table 8.3.1.

A comparison of the floor acceleration and displacement time-histories obtained from dynamic analysis of Model B with those obtained from the Whittier earthquake records is presented in Figures 8.3.1 and 8.3.2.

The maximum values of story shears, overturning moments, inter-story drift ratios, floor displacements and the forces in selected structural members, obtained from time-history analysis are presented in Tables 8.3.2 to 8.3.4.

Figure 8.3.3 includes plots of the envelopes of maximum story shears and overturning moments. Important results from this time-history analysis include:

- Max Base Shear in X direction: 2675 kN (= 0.0833 W)
- Max Base Shear in Y direction: 3567 kN (= 0.1111 W)
- Max Absolute Horizontal Base Shear : 3599 kN (= 0.1121 W)
- Max Ductility in beams : 0.48
- Max Ductility in columns : 0.43

Note: The analysis showed no yielding in the structure. (i.e. the response was within the <u>linear elastic</u> range.)

Table 8.3.1 Natural frequencies and periods of model **B**

	X-Direction (E-W)		Y-Direction (E-W)		Rotation	
	Frequency (Hz)	Period (S)	Frequency (Hz)	Period (S)	Frequency (Hz)	Period (S)
Mode # 1	0.808	1.238	0.774	1.292	1.192	0.834
Mode 2	2.267	0.441	2.182	0.458	3.257	0.307
Mode 3	4.037	0.248	3.909	0.256	5.790	0.173
Mode 4	6.075	0.165	5.935	0.169	8.711	0.115
Mode 5	8.532	0.117	8.403	0.119	12.136	0.082
Mode 6	11.377	0.088	11.325	0.088	15.823	0.063

A critical damping ratio of 3.5 % assigned to the first and the second modes results in a Rayleigh's damping matrix [C] = 0.0070 [K] + 0.1738 [M], in which [K] and [M] represent stiffness and mass matrices.

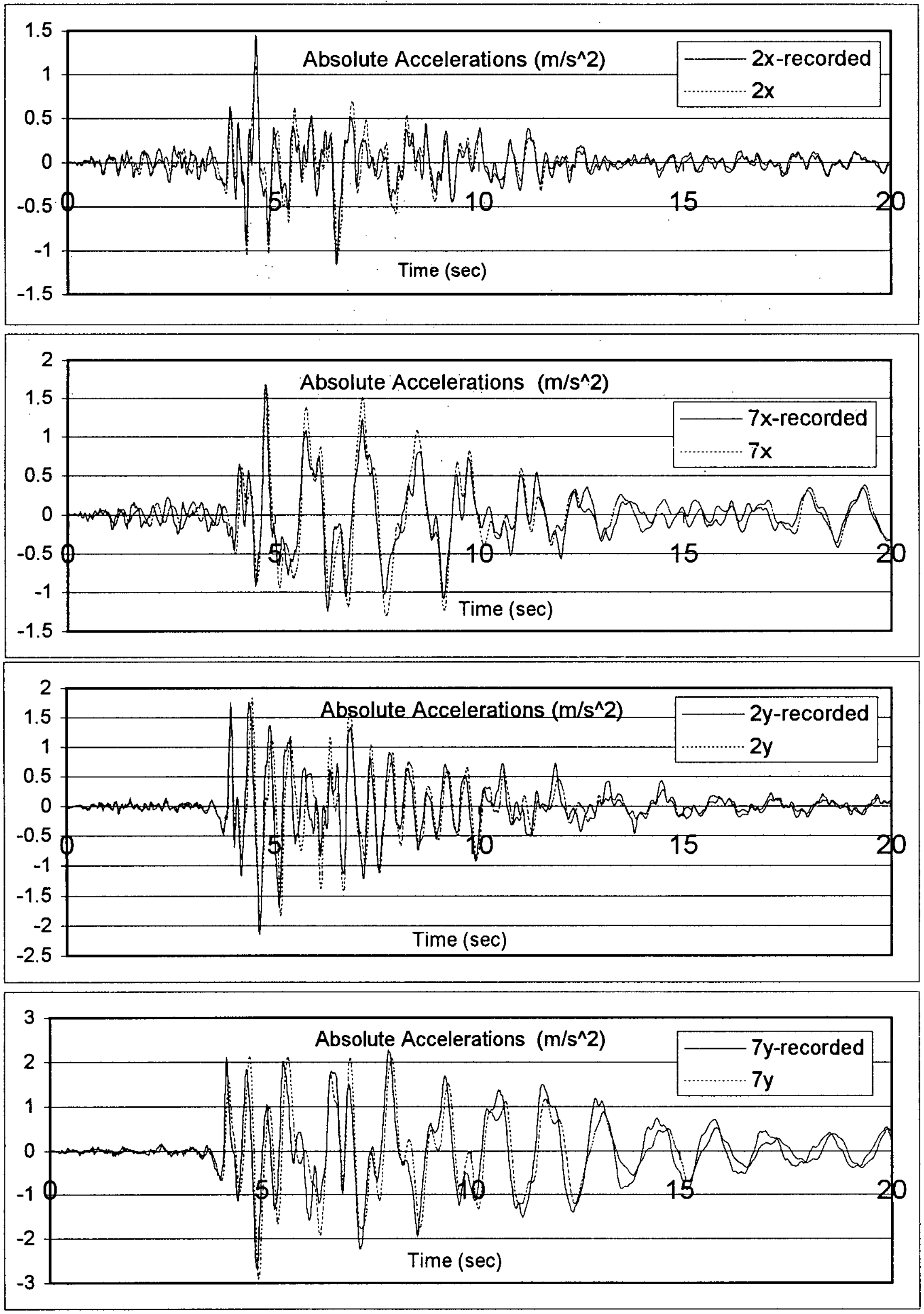

Figure 8.3.1 Comparison the absolute acceleration time-histories obtained from the analysis of Model **B** with the Whittier EQ records.

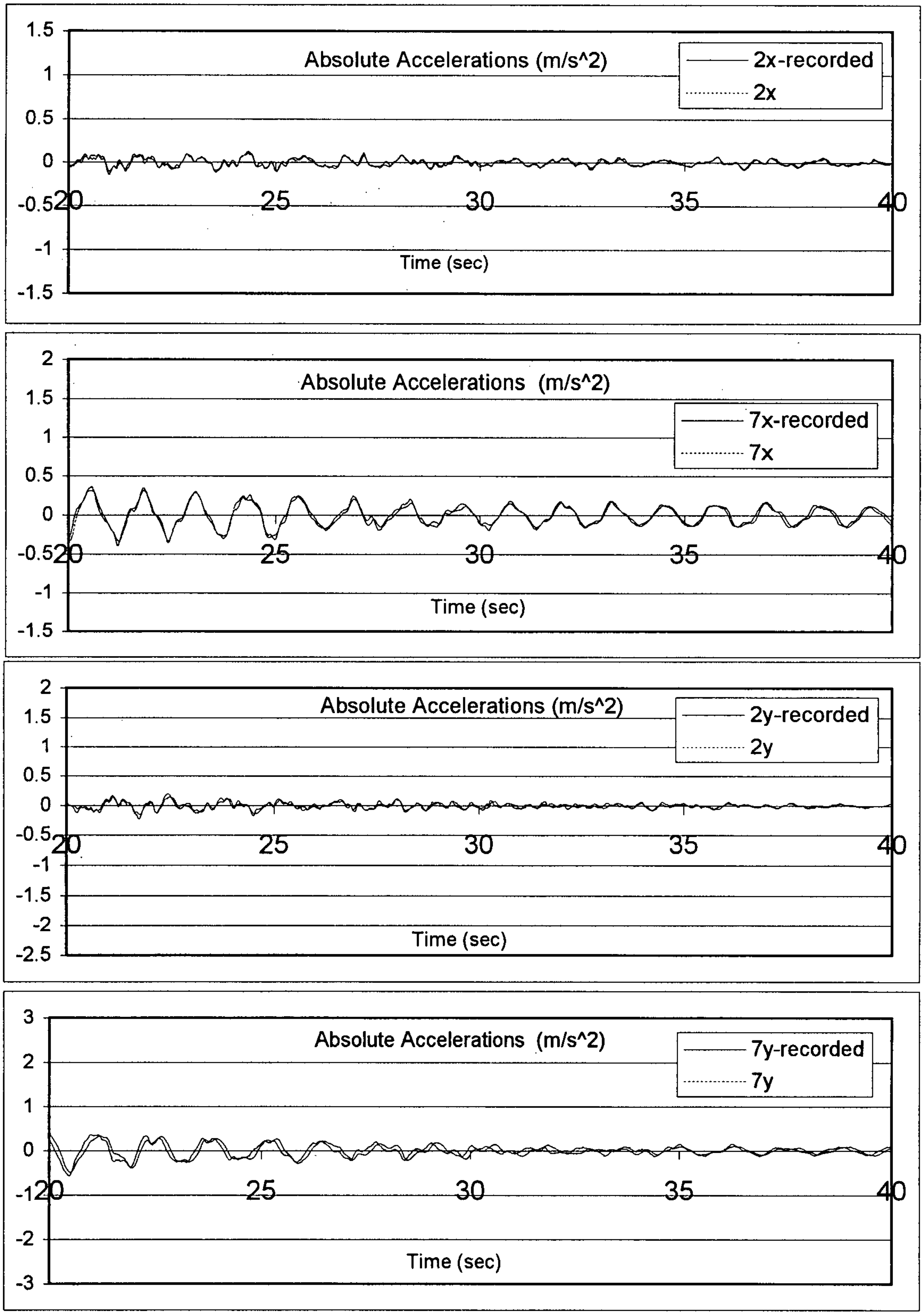

Figure 8.3.1 Cont'd

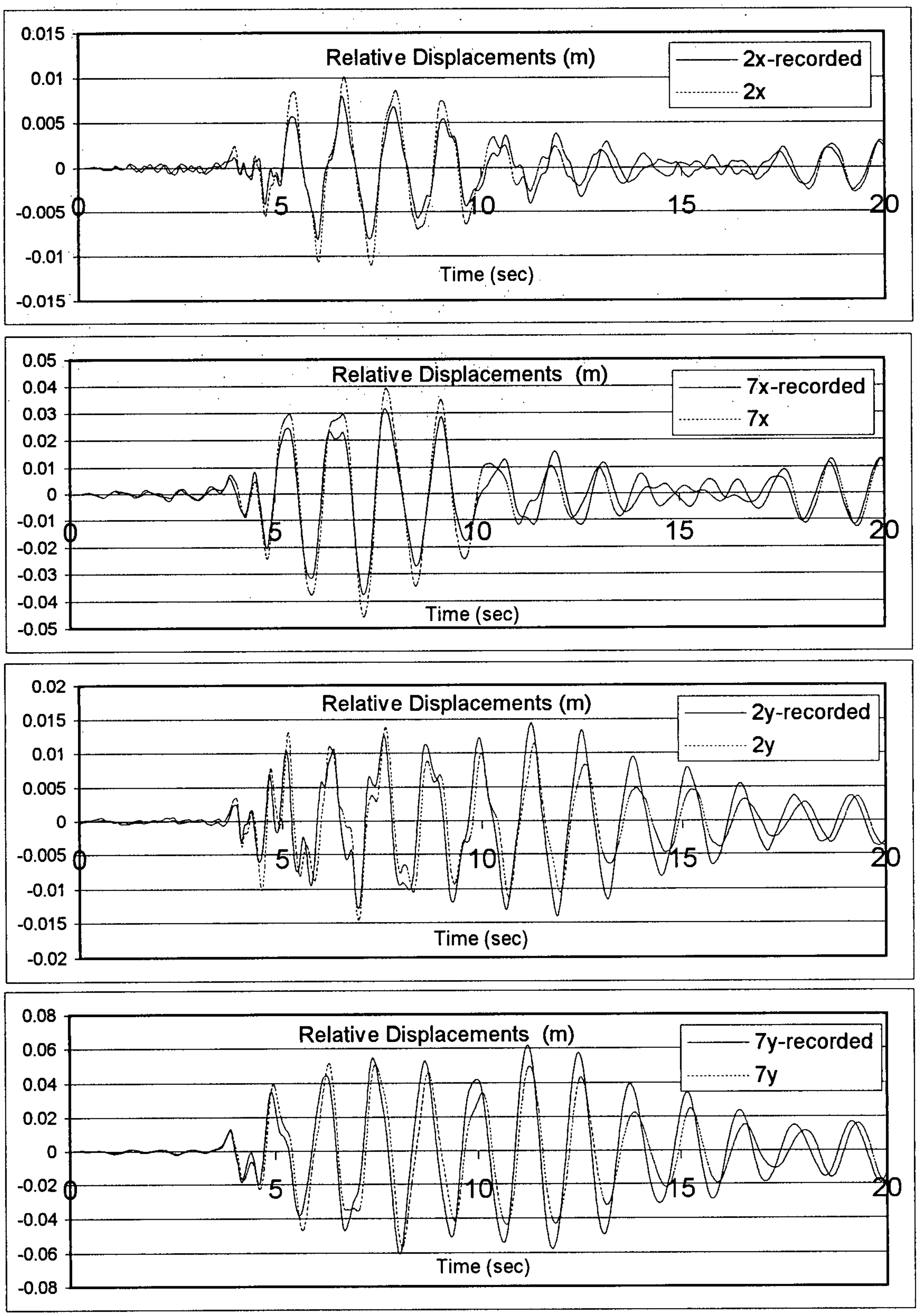

Figure 8.3.2 Comparison the relative displacement time-histories obtained from the analysis of Model **B** with the Whittier EQ records.

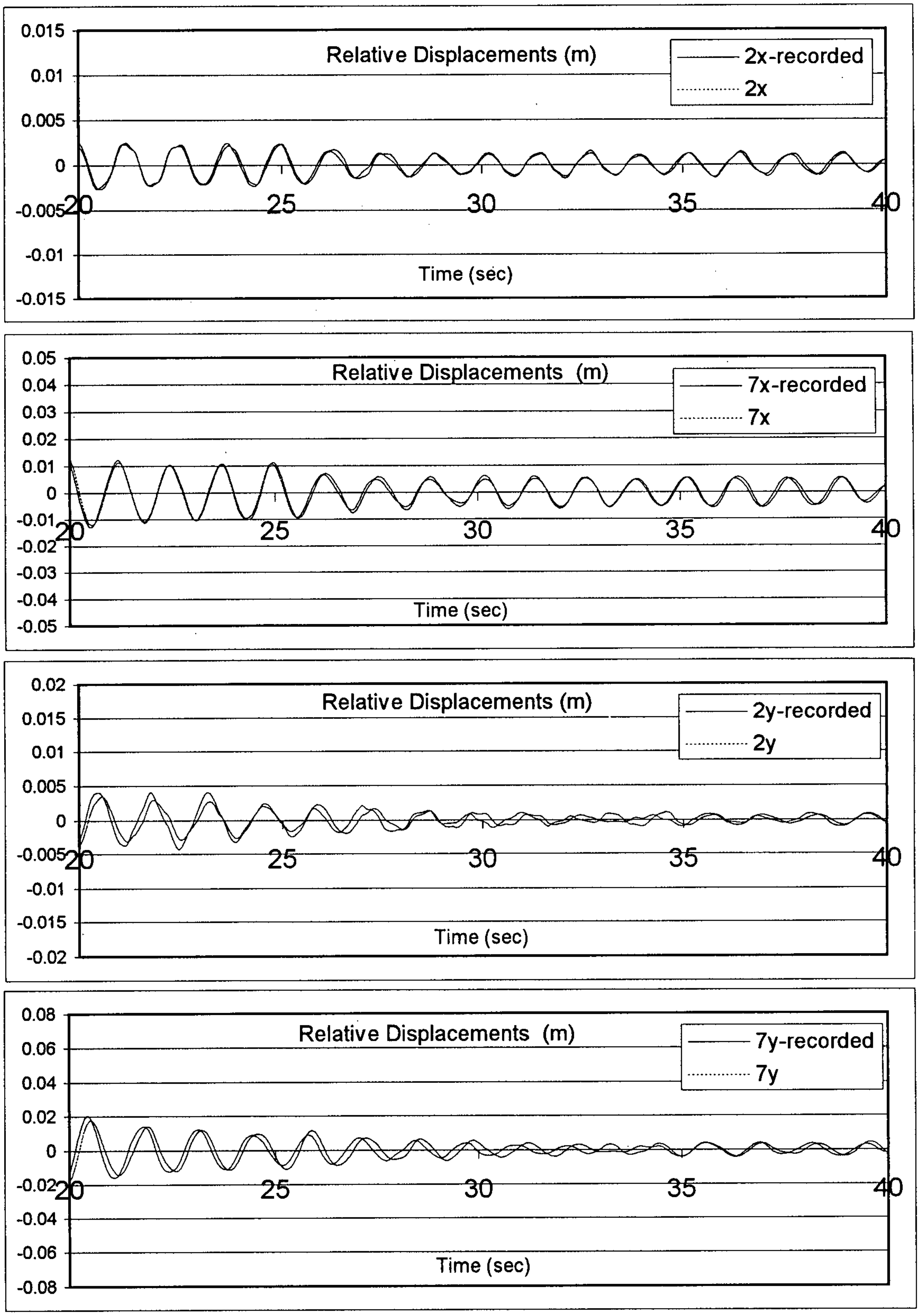

Figure 8.3.2 Cont'd

Table 8.3.2 Maximum story shears and overturning moments, time-history analysis of Model **B** with the ground accelerations obtained from the Whittier EQ records.

	Overturning Moment (N.m)		Story Shear (N)		M_{max} / V_{max} (m)	
	M_x(max)	M_y(max)	V_x(max)	V_y(max)	X	Y
6th story	4.28e6	7.65e6	1.080e6	1.931e6	3.96	3.96
5th story	9.91e6	16.63e6	1.506e6	2.277e6	6.58	7.30
4th story	16.88e6	23.94e6	1.782e6	2.352e6	9.74	10.18
3rd story	24.49e6	32.01e6	2.022e6	2.251e6	12.11	14.22
2nd story	32.84e6	39.51e6	2.371e6	2.715e6	13.85	14.55
Base	45.61e6	47.57e6	2.675e6	3.567e6	17.05	13.34

Note: The ratios of overturning moments to story shears at each floor represent an equivalent lever arm length indicating the hypothetical location where applying a static force equal to the maximum story shear would result in an overturning moment equal to the maximum overturning moment obtained from the time-history analysis at the corresponding floor.

Table 8.3.3 Maximum floor displacements and story drift ratios, time-history analysis of model **B** with the ground accelerations obtained from the Whittier EQ records.

	Floor Displacement (m)			Story drift ratio (%)	
	D_x(max)	D_y(max)		d_x(max)	d_y(max)
7th floor	0.046	0.057	6th story	0.15	0.29
6th floor	0.040	0.048	5th story	0.20	0.33
5th floor	0.034	0.037	4th story	0.20	0.30
4th floor	0.026	0.031	3rd story	0.20	0.24
3rd floor	0.019	0.024	2nd story	0.20	0.24
2nd floor	0.011	0.015	1st story	0.21	0.28

Table 8.3.4 Maximum Forces in the South-West corner column and the beams connected to it in E-W (X-dir), time-history analysis of Model **B** with the ground accelerations obtained from the Whittier EQ records.

Column forces				Beam forces		
	Moment (kN-m)	Shear (kN)	Axial (kN)		Moment (kN-m)	Shear (kN)
6th story	106.3	57.2	118.5	7th floor	112.9	57.8
5th story	118.8	70.0	263.8	6th floor	208.9	80.6
4th story	141.8	82.3	431.8	5th floor	274.5	102.6
3rd story	162.2	94.3	600.3	4th floor	306.3	113.1
2nd story	200.1	91.8	773.0	3rd floor	403.0	146.5
1st story	370.9	132.5	979.0	2nd floor	518.1	187.3

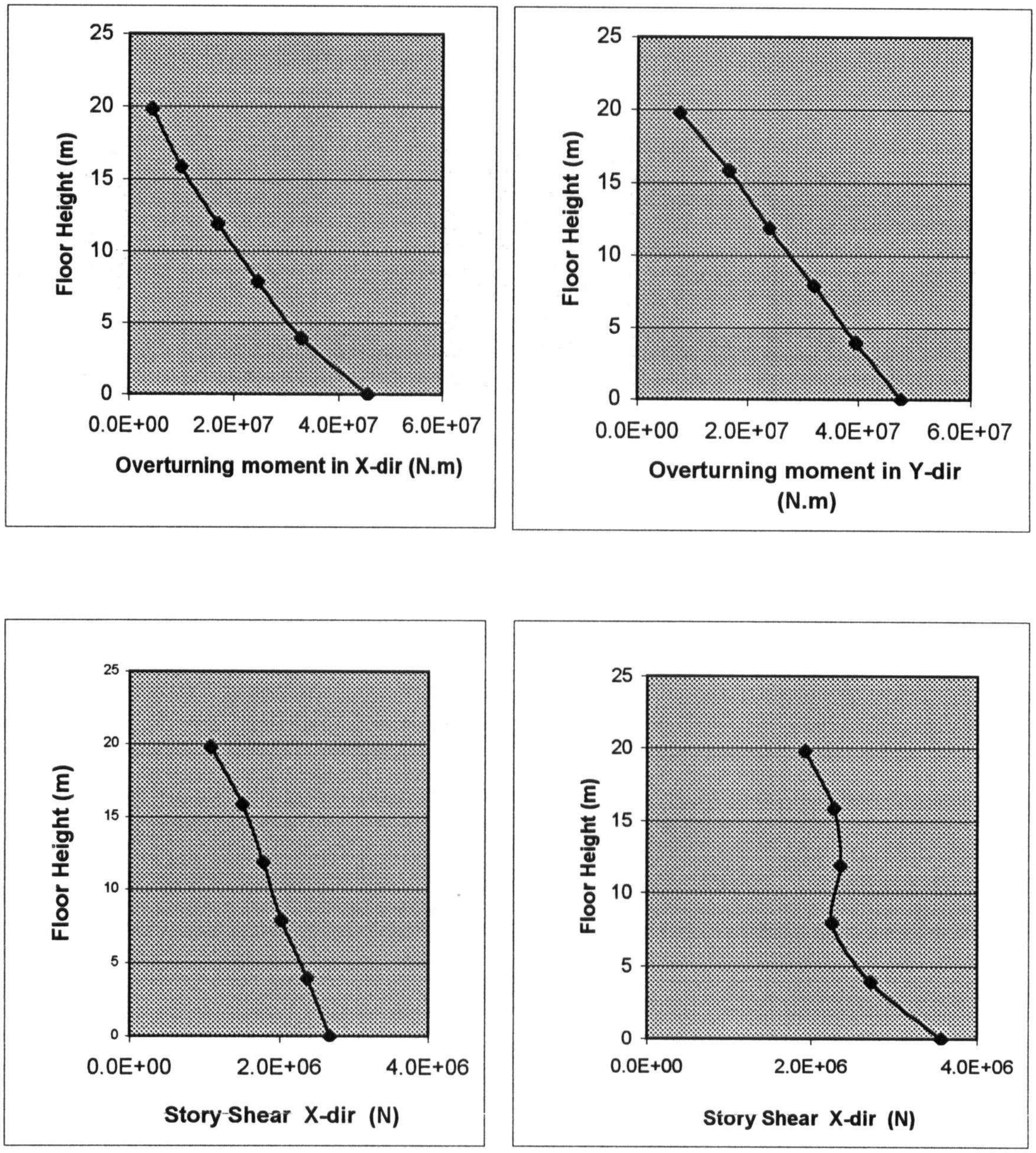

Figure 8.3.3 Envelope of maximum story shears and overturning moments obtained from the time-history analysis of Model **B** with the ground accelerations obtained from the Whittier EQ records.

8.4 Results of Analysis Based on Northridge Earthquake Records

The natural frequencies and periods of Model **A** matched those obtained from the Northridge earthquake records. This model was used for a dynamic time-history analysis with the ground motions obtained from the Northridge earthquake data. The results of this analysis are presented in this section.

The natural frequencies and periods of Model **A** are listed in Table 8.4.1.

A comparison of the floor acceleration and displacement time-histories obtained from the dynamic analysis of Model **A** with those obtained from the Northridge earthquake records is presented in Figures 8.4.1 and 8.4.2. Although the analysis of Model **B** with the Whittier earthquake ground motions showed good agreement with the recorded data, the results of the analysis of this model with the Northridge earthquake ground motions did not match the recorded data. The results of time-history analysis of Model **B** with Northridge earthquake ground motions are presented in Figures 8.4.3 and 8.4.4 for comparison.

The maximum values of story shears, overturning moments, inter-story drift ratios, floor displacements and the forces in selected structural members, obtained from time-history analysis of Model **A** with the ground motions obtained from the Northridge EQ data are presented in Tables 8.4.2 to 8.4.4.

Figure 8.4.5 includes plots of the envelopes of maximum story shears and overturning moments. In Figures 8.4.6 to 8.4.9 absolute accelerations and relative displacements of all upper floors (second to seventh floors) are presented in an overlaid format to observe the out-of-phase response of the various floors. This out-of-phase response, which is more noticeable in the acceleration plots, indicates the significance of the effect of the higher modes in the structural response.

Important results from this time-history analysis include:

- Maximum Base Shear in X direction: 4290 kN (= 0.1336 W)
- Maximum Base Shear in Y direction: 3509 kN (= 0.1093 W)
- Maximum Combined (X & Y) Base Shear : 4642 kN (= 0.1446 W)
- Maximum Ductility in beams : 0.71
- Maximum Ductility in columns : 0.78

Note: The analysis showed no yielding in the structure. (i.e. the response was within the linear elastic range.)

Table 8.4.1 Natural frequencies and periods of Model **A**.

	X-Direction (E-W)		Y-Direction (E-W)		Rotation	
	Frequency (Hz)	Period (S)	Frequency (Hz)	Period (S)	Frequency (Hz)	Period (S)
Mode1	0.723	1.383	0.725	1.379	1.133	0.882
Mode 2	2.041	0.490	2.049	0.488	3.110	0.322
Mode 3	3.678	0.272	3.691	0.271	5.543	0.180
Mode 4	5.634	0.178	5.653	0.177	8.382	0.119
Mode 5	8.110	0.123	8.124	0.123	11.779	0.085
Mode 6	11.025	0.091	11.038	0.091	15.480	0.065

A critical damping ratio of 3.5 % assigned to the first and the second modes results in a Rayleigh's damping matrix [C]=0.0077[K]+0.1593[M], in which [K] and [M] represent stiffness and mass matrices.

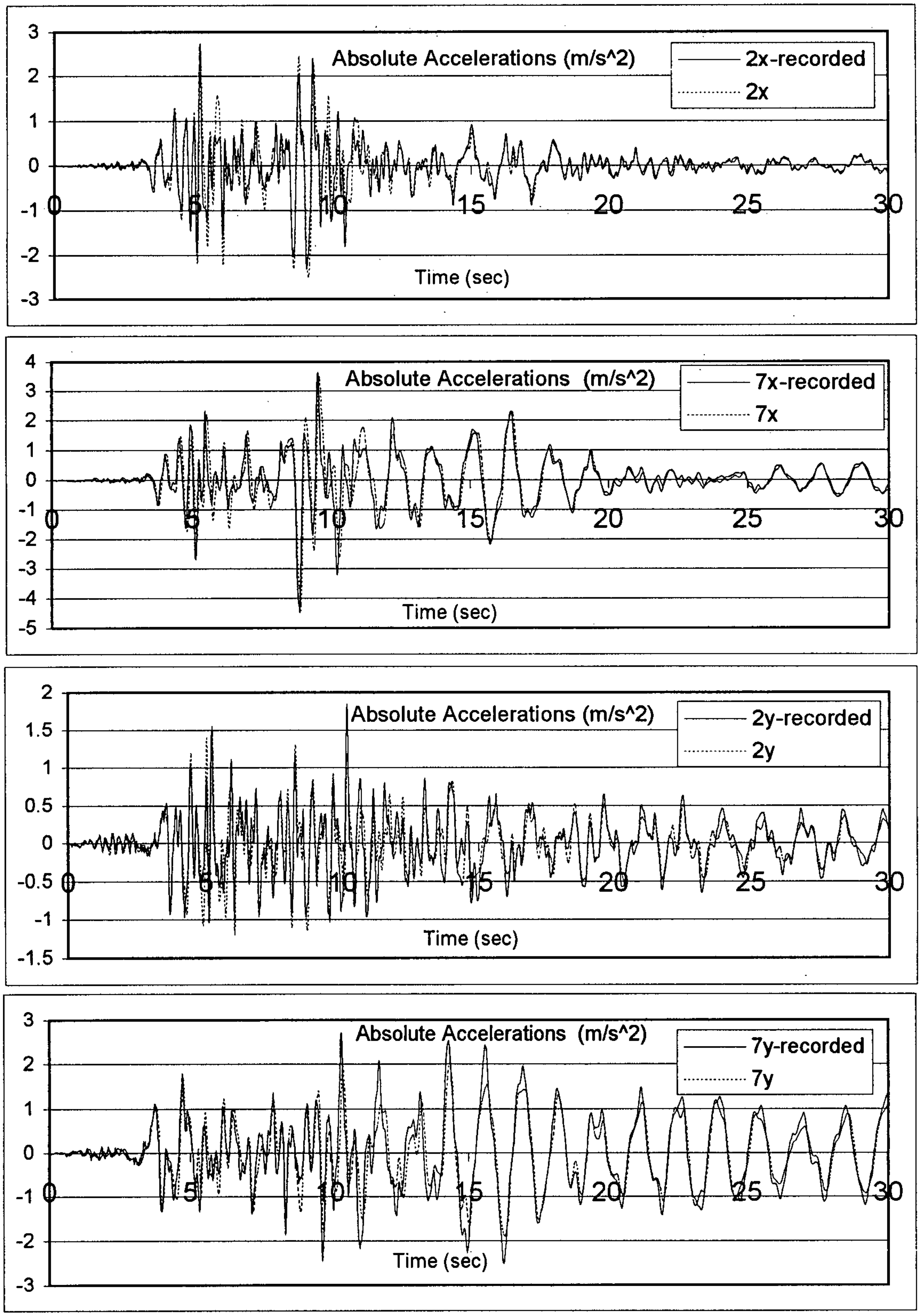

Figure 8.4.1 Comparison the absolute acceleration time-histories obtained from the analysis of Model **A** with the Northridge EQ records.

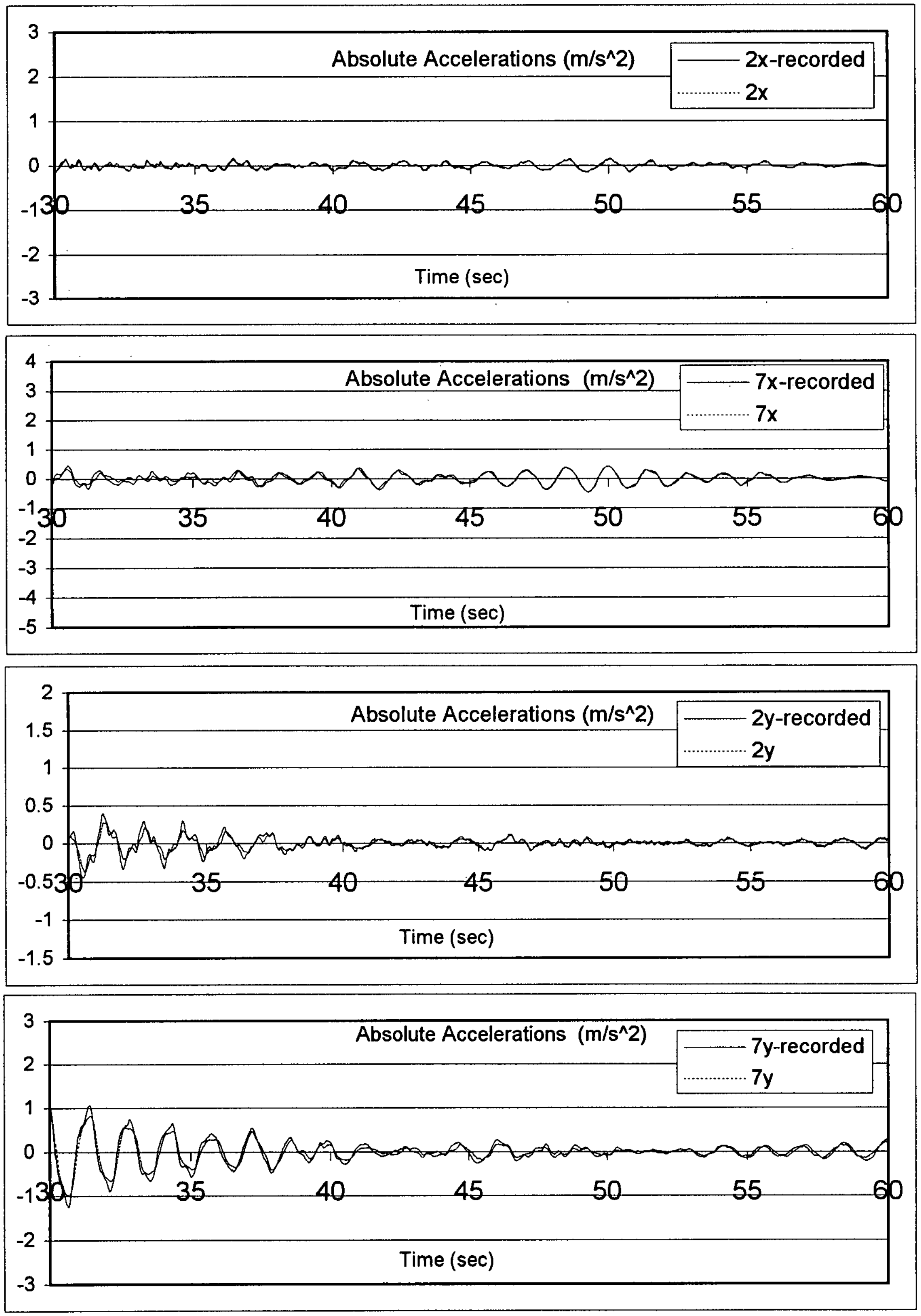

Figure 8.4.1 Cont'd

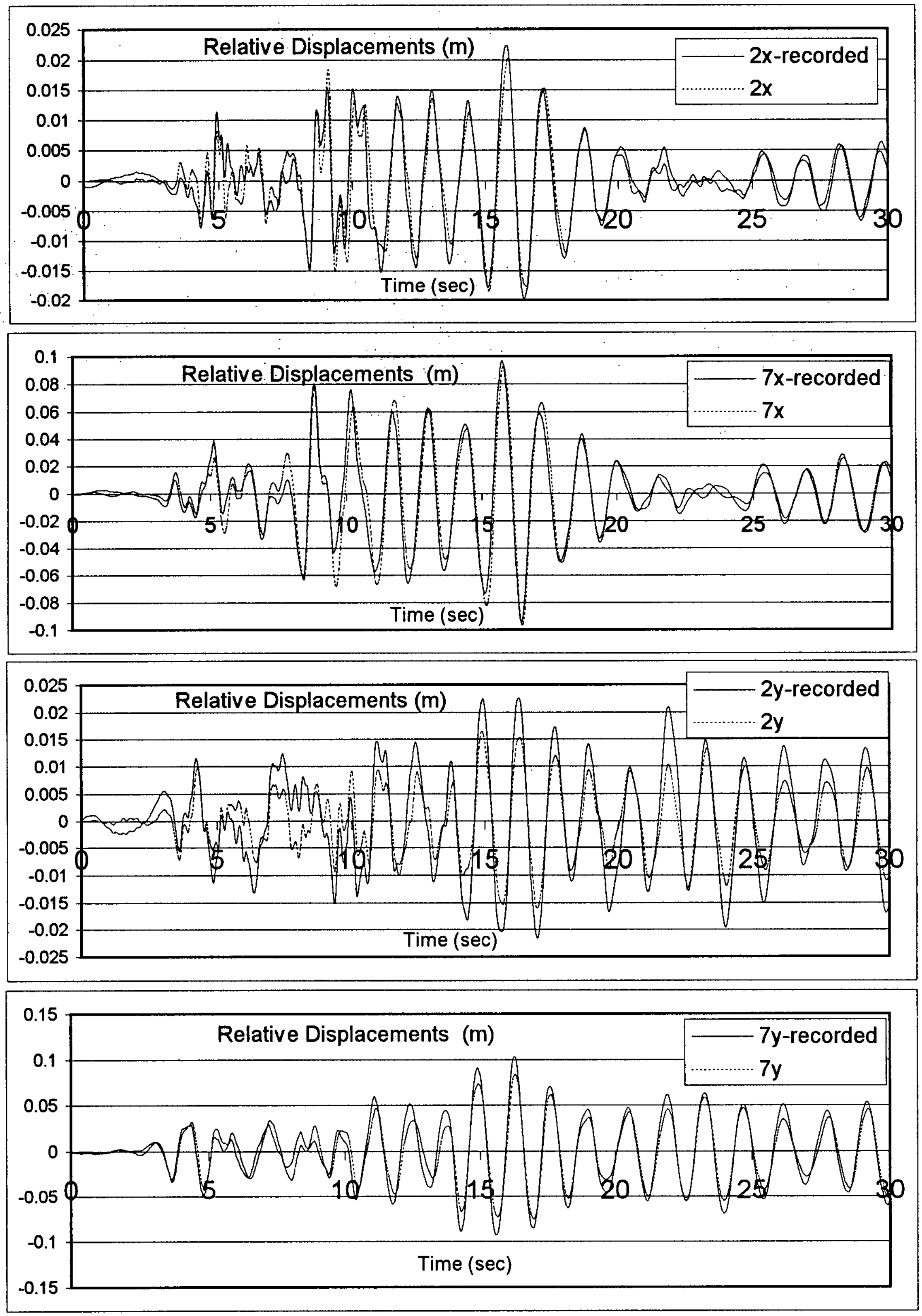

Figure 8.4.2 Comparison the relative displacement time-histories obtained from the analysis of Model **A** with the Northridge EQ records.

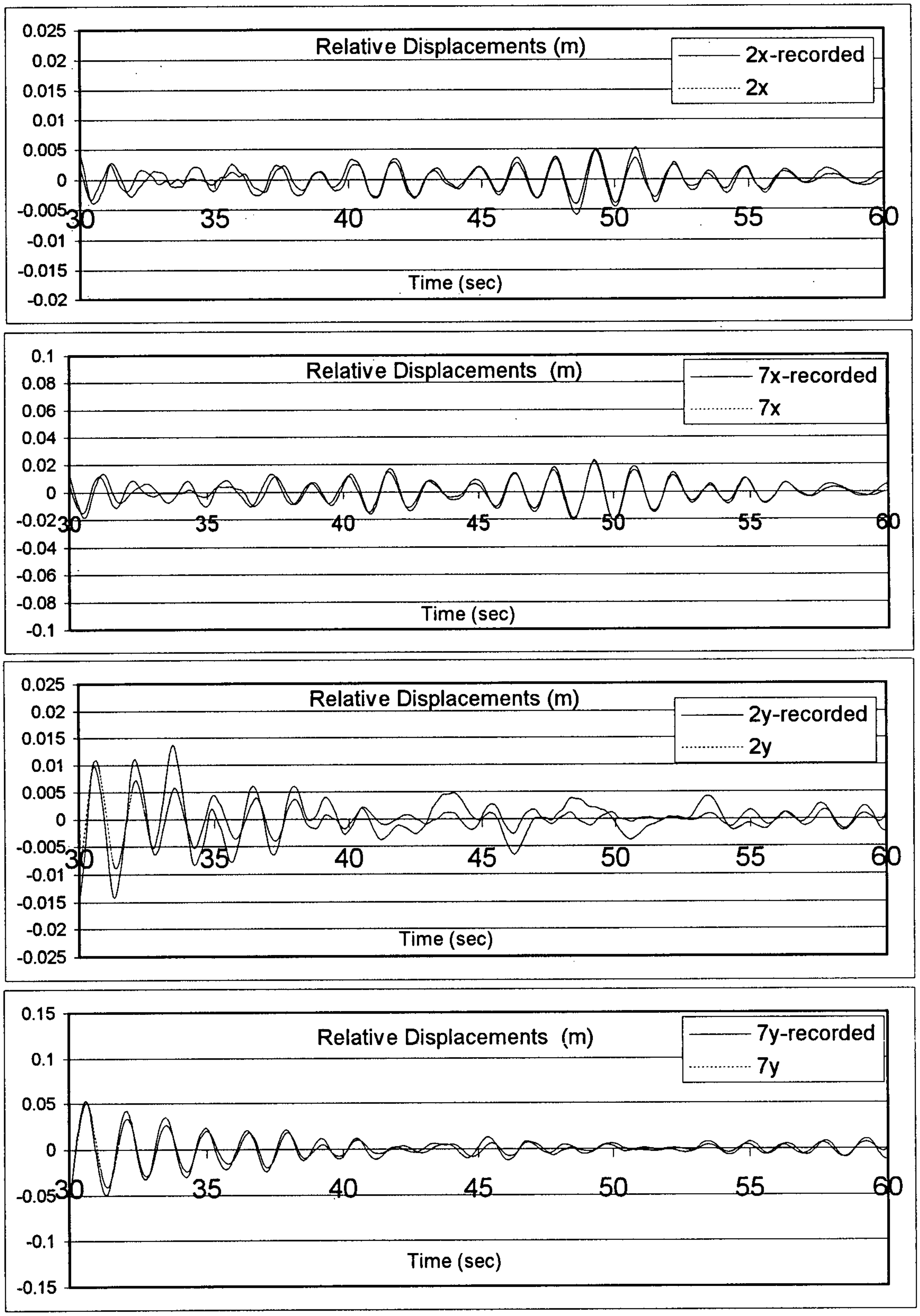

Figure 8.4.2 Cont'd

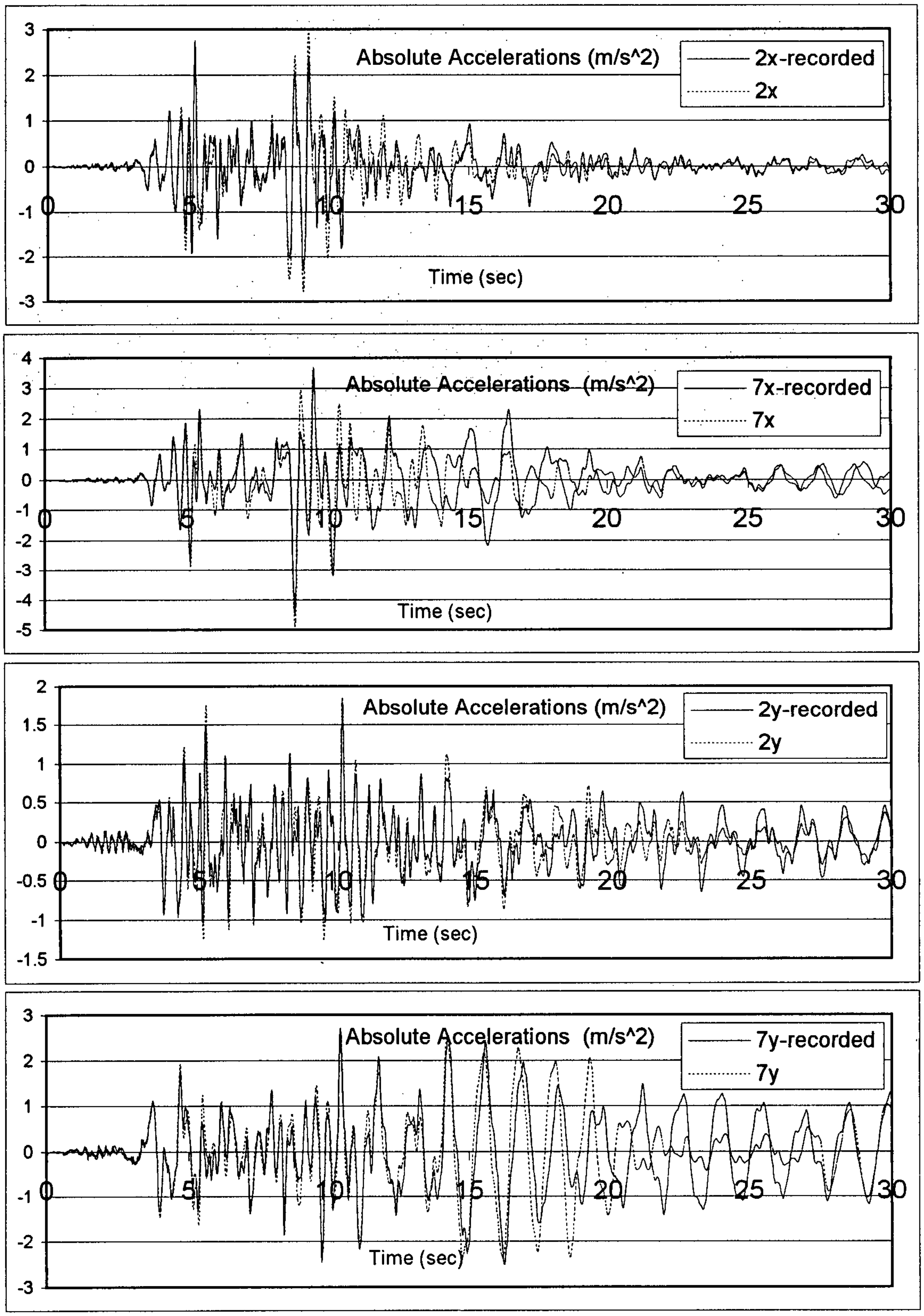

Figure 8.4.3 Comparison the absolute acceleration time-histories obtained from the analysis of Model **B** with the Northridge EQ records.

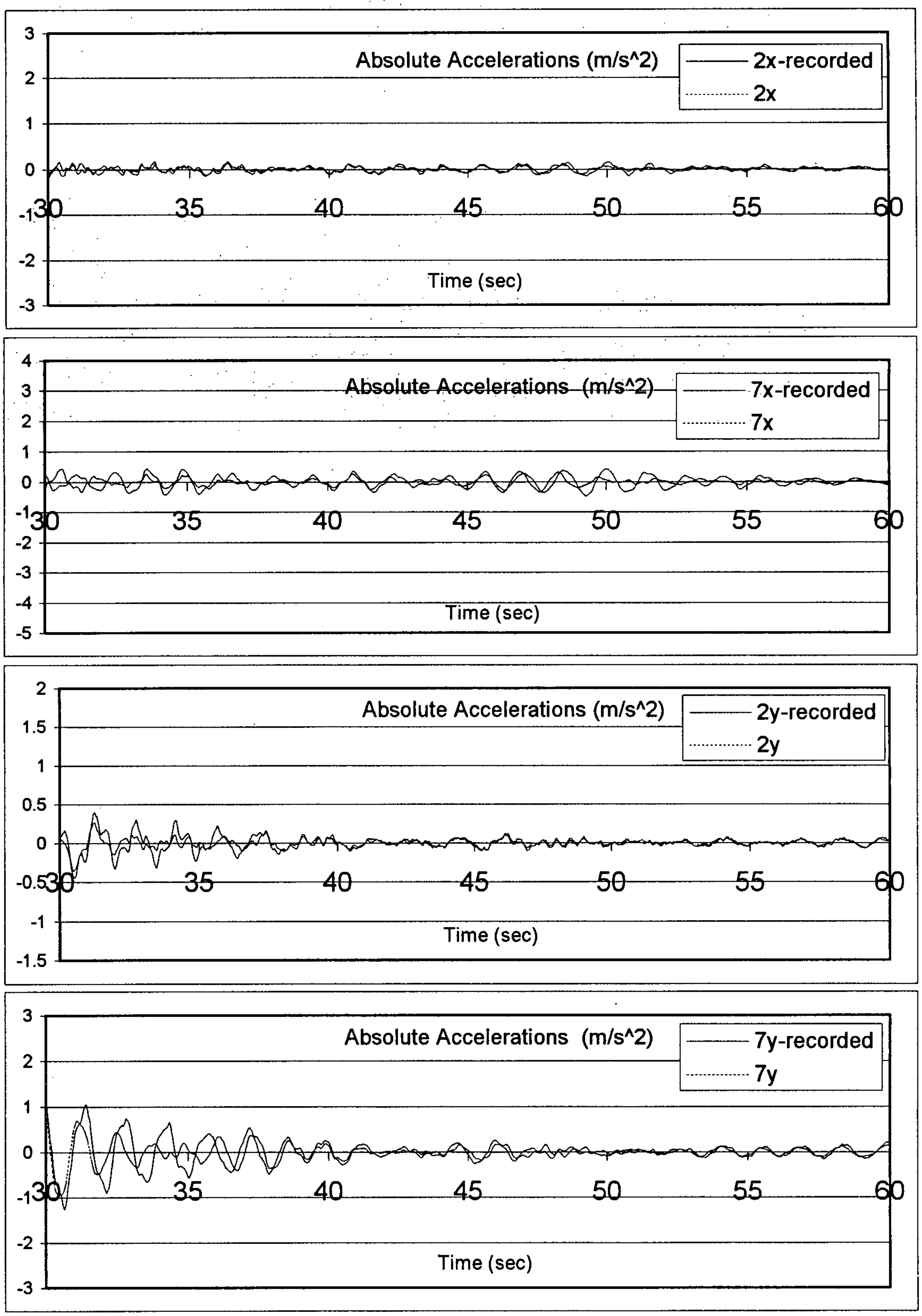

Figure 8.4.3 Cont'd

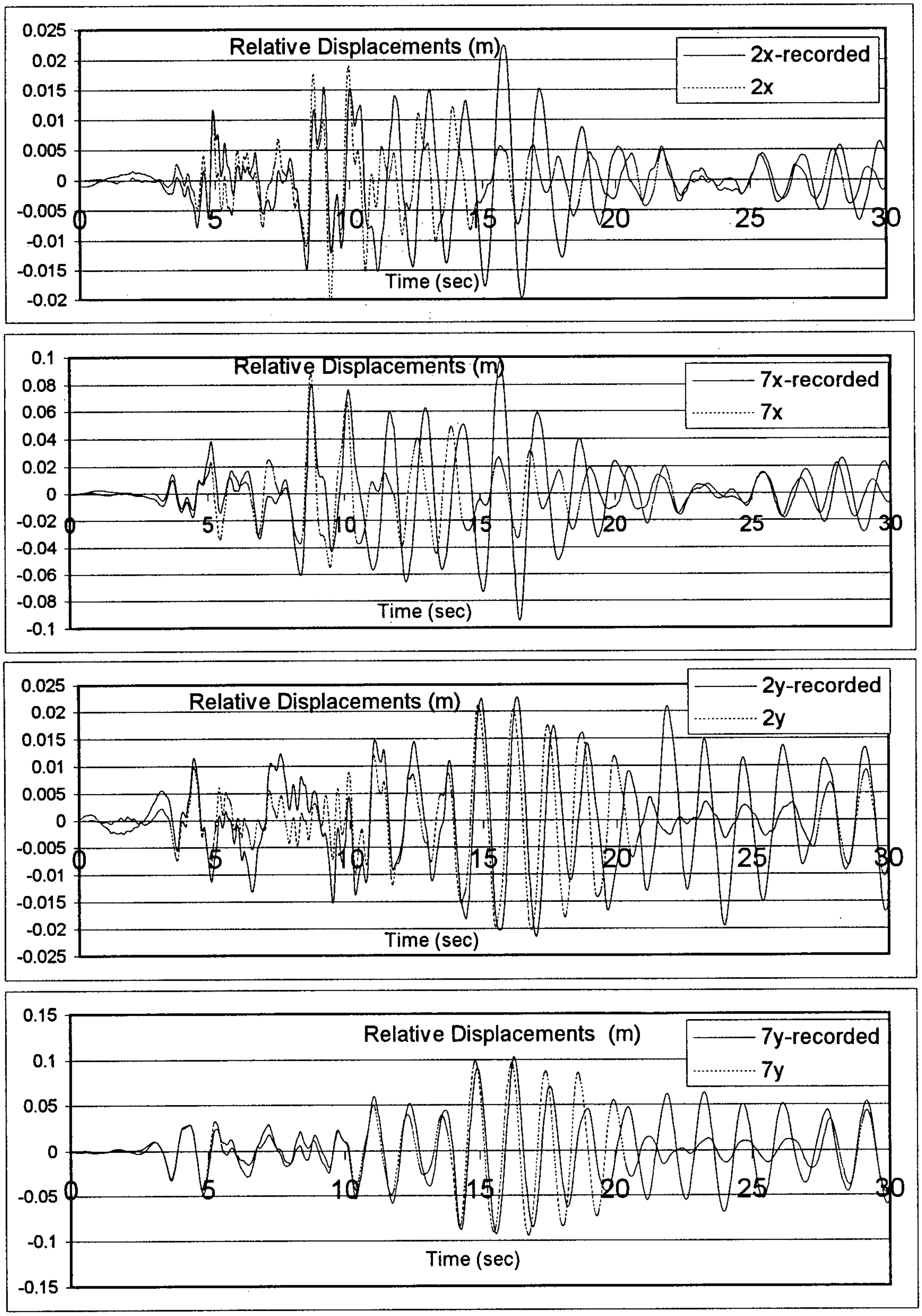

Figure 8.4.4 Comparison the relative displacement time-histories obtained from the analysis of Model **B** with the Northridge EQ records.

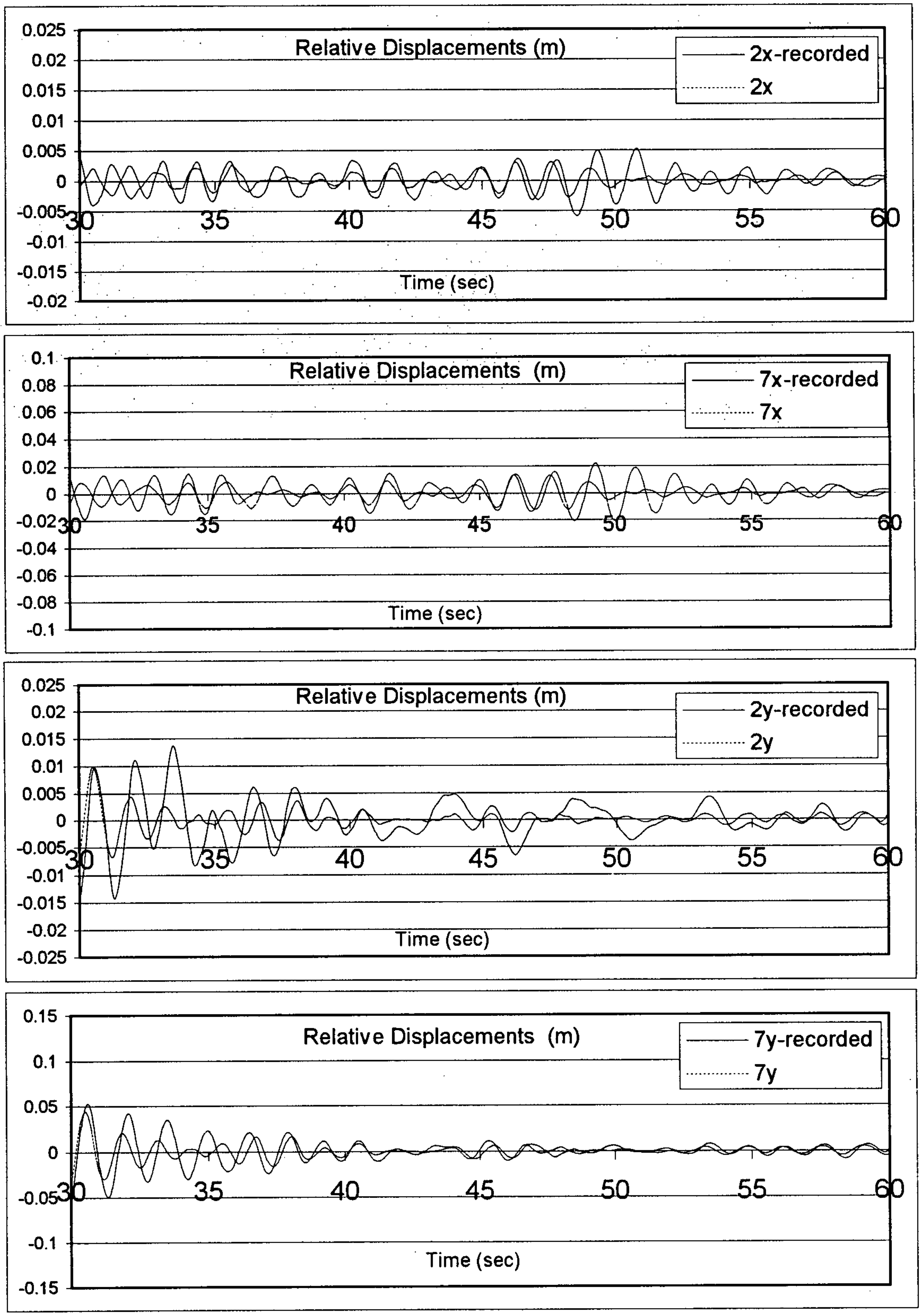

Figure 8.4.4 Cont'd

Table 8.4.2 Maximum story shears and overturning moments, time-history analysis of Model **A** with the ground accelerations obtained from the Northridge EQ data.

	Overturning Moment (N.m)		Story Shear (N)		M_{max} / V_{max} (m)	
	M_x(max)	M_y(max)	V_x(max)	V_y(max)	X	Y
6th story	11.90e6	5.45e6	3.002e6	1.375e6	3.96	3.96
5th story	26.53e6	13.75e6	3.751e6	2.106e6	7.07	6.53
4th story	38.94e6	24.16e6	3.347e6	2.731e6	11.63	8.85
3rd story	46.52e6	36.41e6	3.521e6	3.112e6	13.21	11.70
2nd story	56.45e6	49.06e6	3.804e6	3.239e6	14.84	15.15
Base	74.87e6	65.55e6	4.290e6	3.509e6	17.45	18.68

Note: The ratios of overturning moments to story shears at each floor represent an equivalent lever arm length indicating the hypothetical location where applying a static force equal to the maximum story shear would result in an overturning moment equal to the maximum overturning moment obtained from the time-history analysis at the corresponding floor.

Table 8.4.3 Maximum floor displacements and story drift ratios, time-history analysis of Model **A** with the ground accelerations obtained from the Northridge EQ data.

	Floor Displacement (m)			Story drift ratio (%)	
	D_x(max)	D_y(max)		d_x(max)	d_y(max)
7th floor	0.097	0.084	6th story	0.55	0.26
6th floor	0.085	0.074	5th story	0.62	0.37
5th floor	0.068	0.059	4th story	0.47	0.40
4th floor	0.052	0.043	3rd story	0.43	0.38
3rd floor	0.036	0.030	2nd story	0.40	0.33
2nd floor	0.020	0.017	1st story	0.39	0.32

Table 8.4.4 Maximum forces in the South-West corner column and the beams connected to it in E-W (X-dir), time-history analysis of Model **A** with the ground accelerations obtained from the Northridge EQ data.

Column forces				Beam forces		
	Moment (kN-m)	Shear (kN)	Axial (kN)		Moment (kN-m)	Shear (kN)
6th story	305.5	165.2	170.3	7th floor	339.9	106.8
5th story	376.4	209.0	400.7	6th floor	643.0	193.4
4th story	355.0	181.0	638.1	5th floor	674.5	206.9
3rd story	344.5	189.2	835.6	4th floor	651.4	226.8
2nd story	370.9	212.7	1010.0	3rd floor	747.7	261.0
1st story	646.1	222.7	1318.1	2nd floor	891.7	284.8

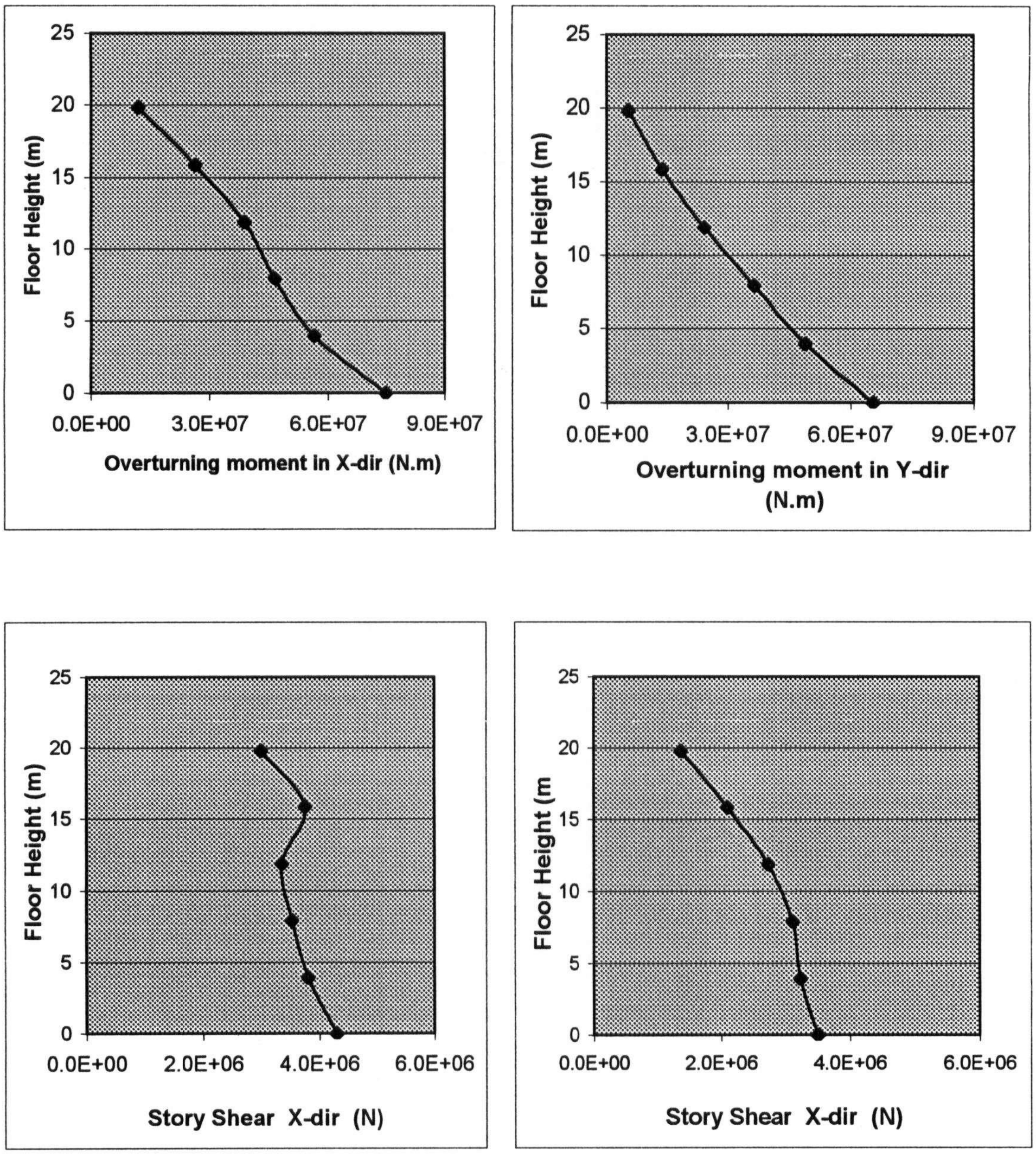

Figure 8.4.5 Envelope of maximum story shears and overturning moments, time-history analysis of Model **A** with the ground accelerations obtained from the Northridge EQ data.

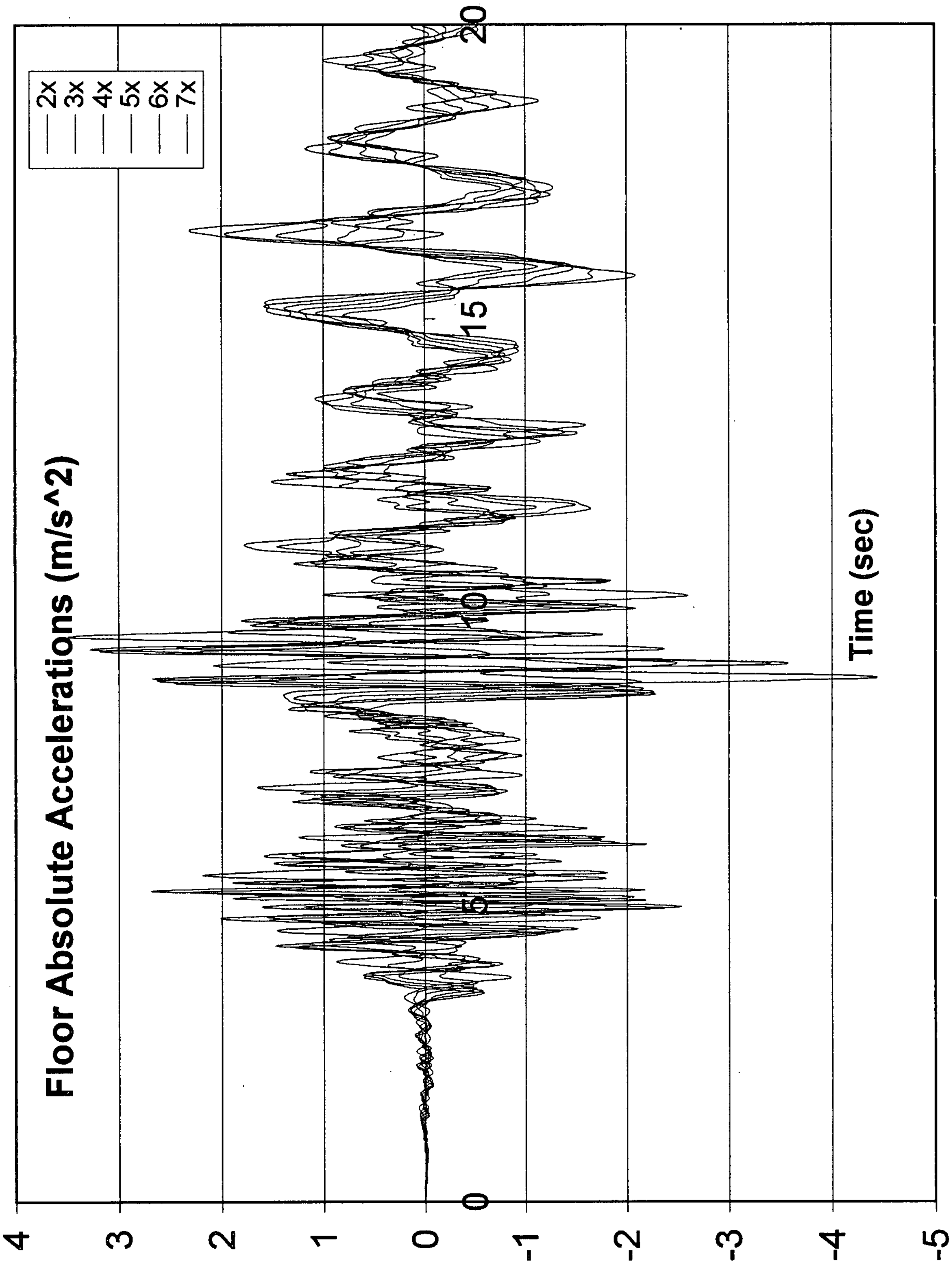

Figure 8.4.6 Overlaid plot of floor absolute accelerations of (X-dir), obtained from the time-history analysis of Model **A** with the ground accelerations obtained from the Northridge EQ data.

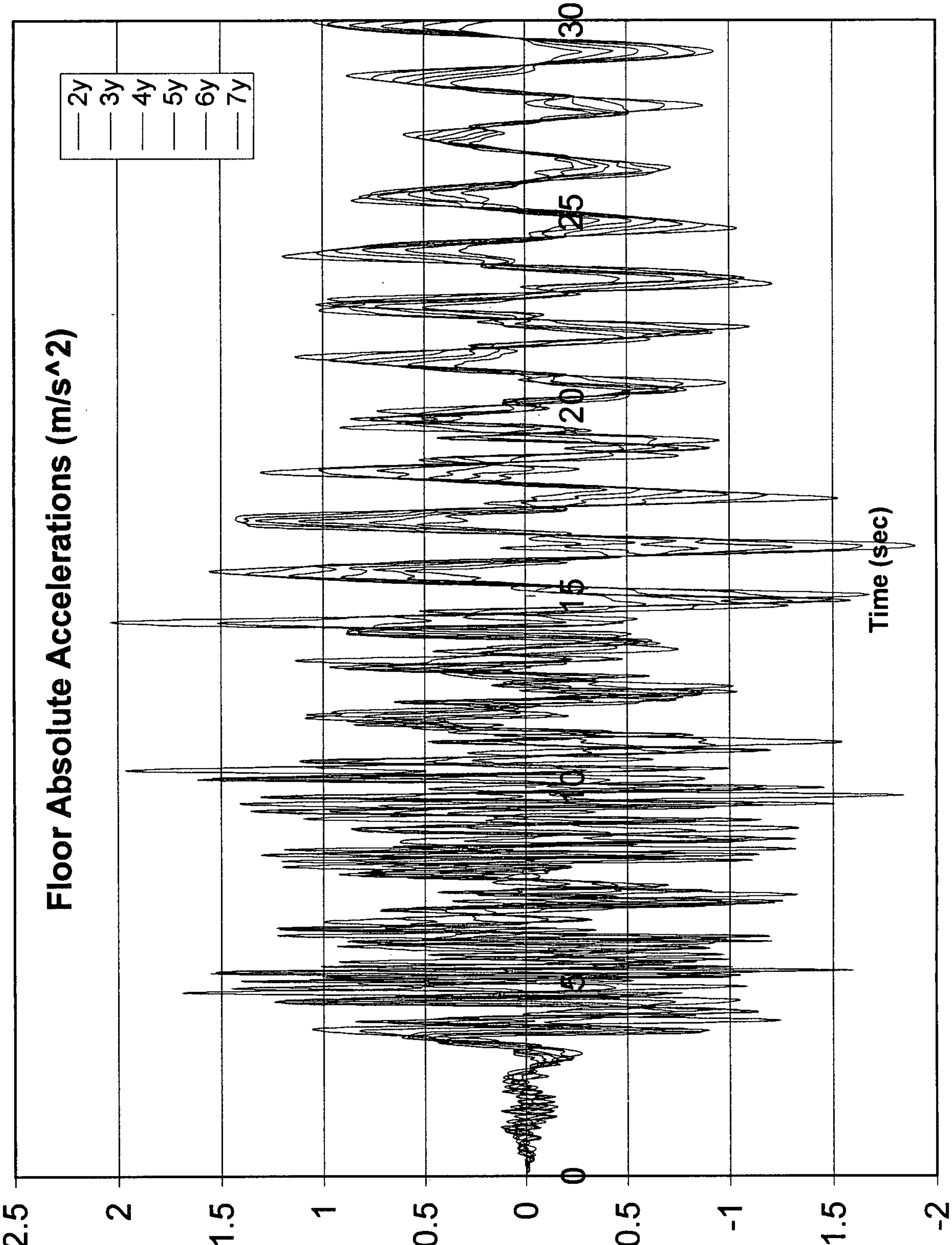

Figure 8.4.7 Floor absolute accelerations (Y-dir), obtained from the time-history analysis of Model **A** with the ground accelerations obtained from the Northridge EQ data.

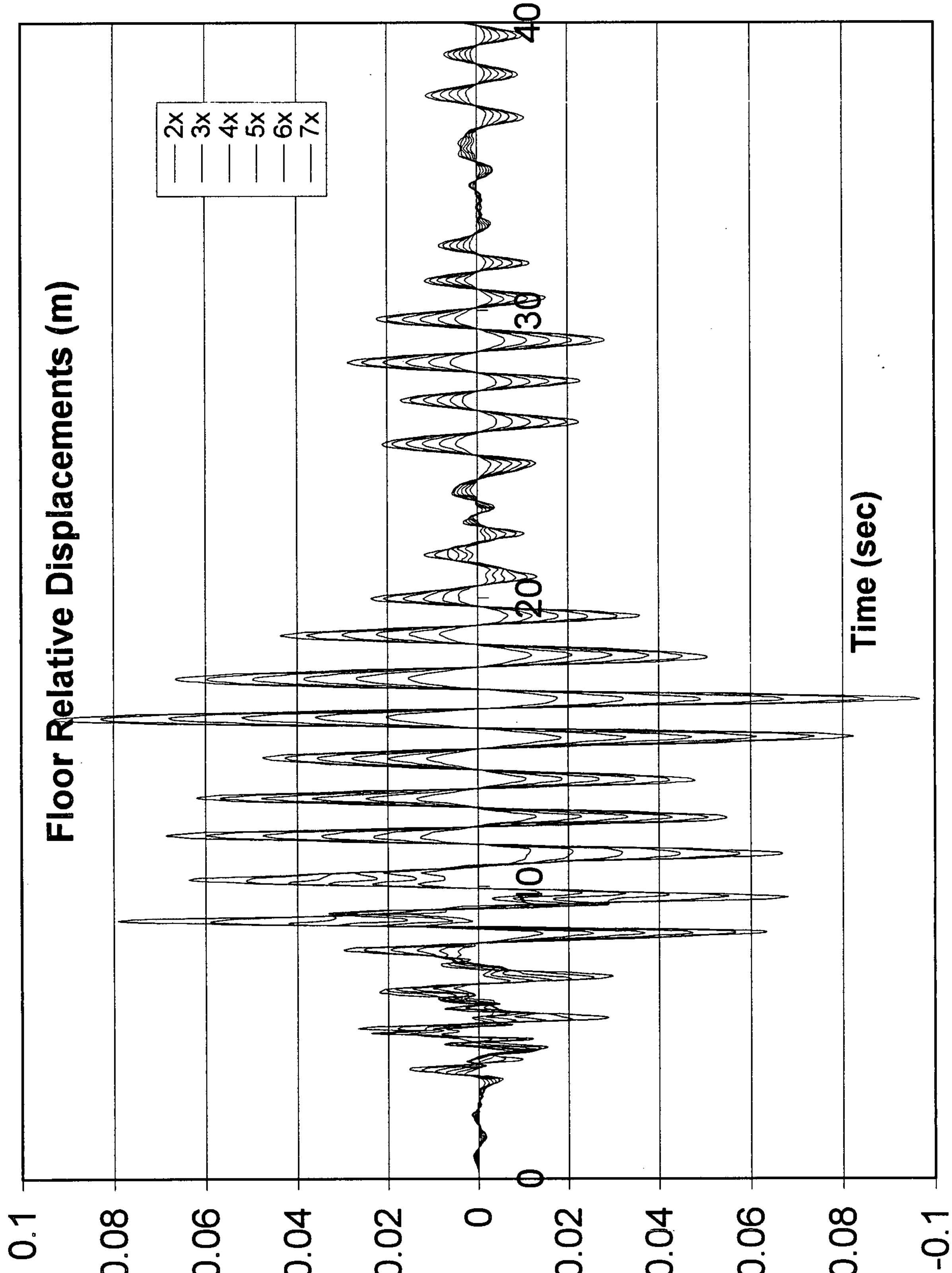

Figure 8.4.8 Floor relative displacements (X-dir), obtained from the time-history analysis of Model **A** with the ground accelerations obtained from the Northridge EQ data.

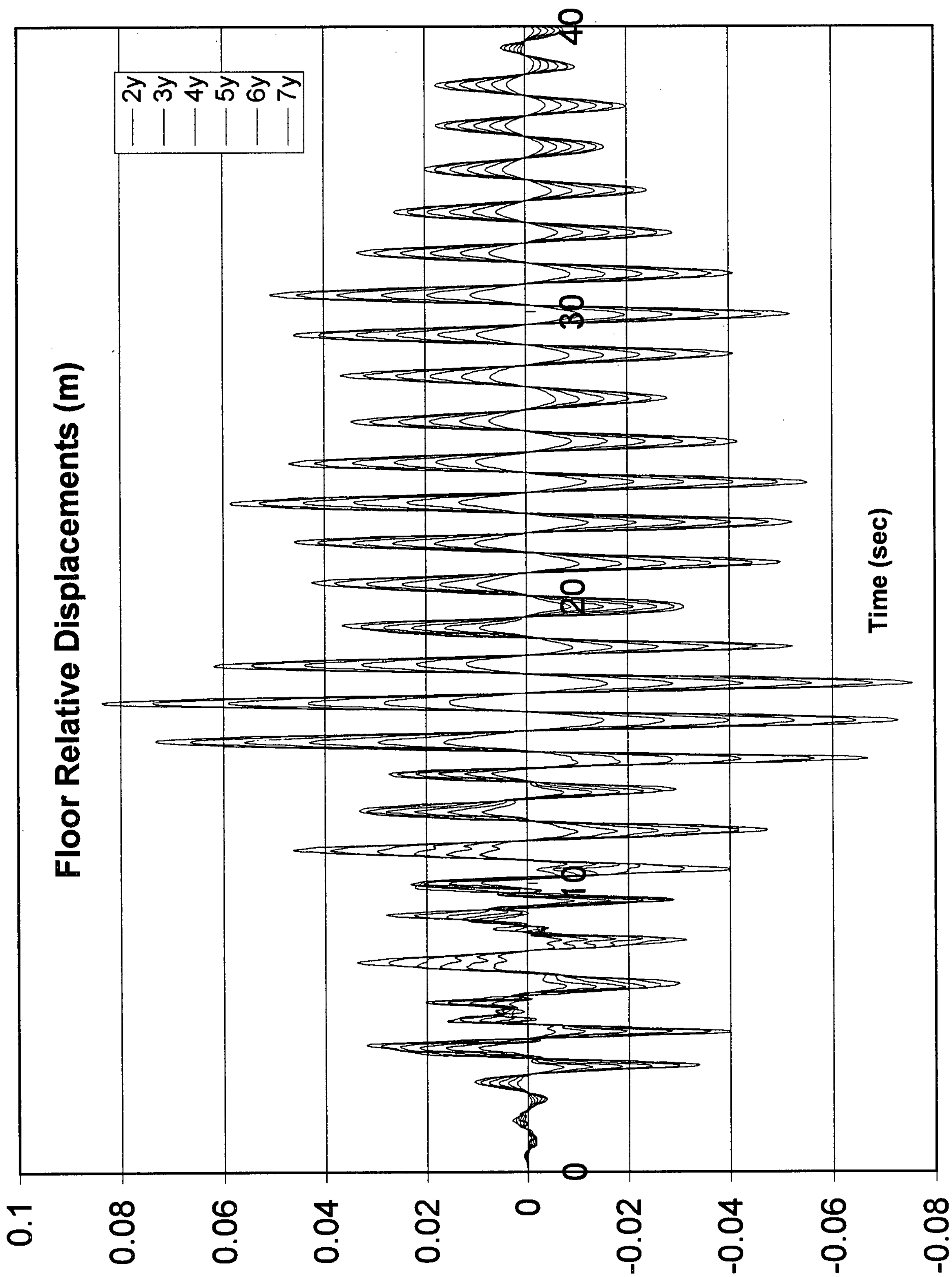

Figure 8.4.9 Floor relative displacements (Y-dir), obtained from the time-history analysis of Model **A** with the ground accelerations obtained from the Northridge EQ data.

8.5 Comparison of the Results of Various Linear-Elastic Analysis Methods

In this section, the linear elastic Model **C** (the ETABS explained in Chapter 7) was analyzed in six different ways:

- **C1**: Time-History Analysis (X-direction ground acceleration of Northridge EQ records)
- **C2**: Modal Spectral Analysis with true response spectrum calculated for the above record.
- **C3**: Similar to C2 but scaled to the base shear of C1.
- **C4**: Modal Spectral Analysis with UBC97 recommended design response spectrum, assuming soil profile type S_D (stiff soil), $_{\text{and}}$ scaled to the base shear of C1.
- **C5**: Similar to C4 but assuming soil profile type S_E (soft soil).
- **C6**: Static Analysis with base shear same as C1 and code recommended vertical distribution of lateral loads.

A **critical damping ratio of 3.5 %** was used for all modes of the models **C1** to **C5**.

Figure 8.5.1 shows a three dimensional view of Model **C.**

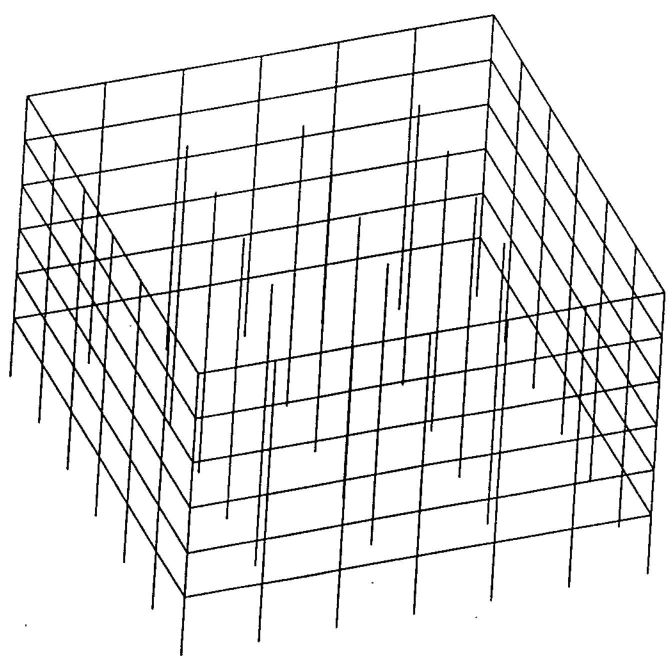

Figure 8.5.1 3-D view of Model C (ETABS Model)

The Response Spectra used for the analyses of Models **C4** and **C5** were calculated using UBC97 guidelines (See Figures 8.5.2 & 8.5.3), based on the following assumptions:

<u>Model **C4**</u>:

Seismic source distance > 10Km

$N_a = N_v = 1.0$

Soil Profile Type: S_D (Stiff Soil)

$Z = 0.4$

$Ca = 0.44\ Na = 0.44$

$Cv = 0.64Nv = 0.64$

$T_s = Cv / 2.5Ca = 0.582$ sec

$T_o = 0.2\ T_s = 0.116$ sec

<u>Model **C5**</u>:

Seismic source distance > 10Km

N_a, N_v, and Z, same as above

Soil Profile Type: S_D (Stiff Soil)

Soil profile type: S_E (Soft Soil)

$Ca = 0.36\ Na = 0.36$

$Cv = 0.96Nv = 0.96$

$T_s = Cv / 2.5Ca = 1.0667$ sec

$T_o = 0.2\ T_s = 0.2133$ sec

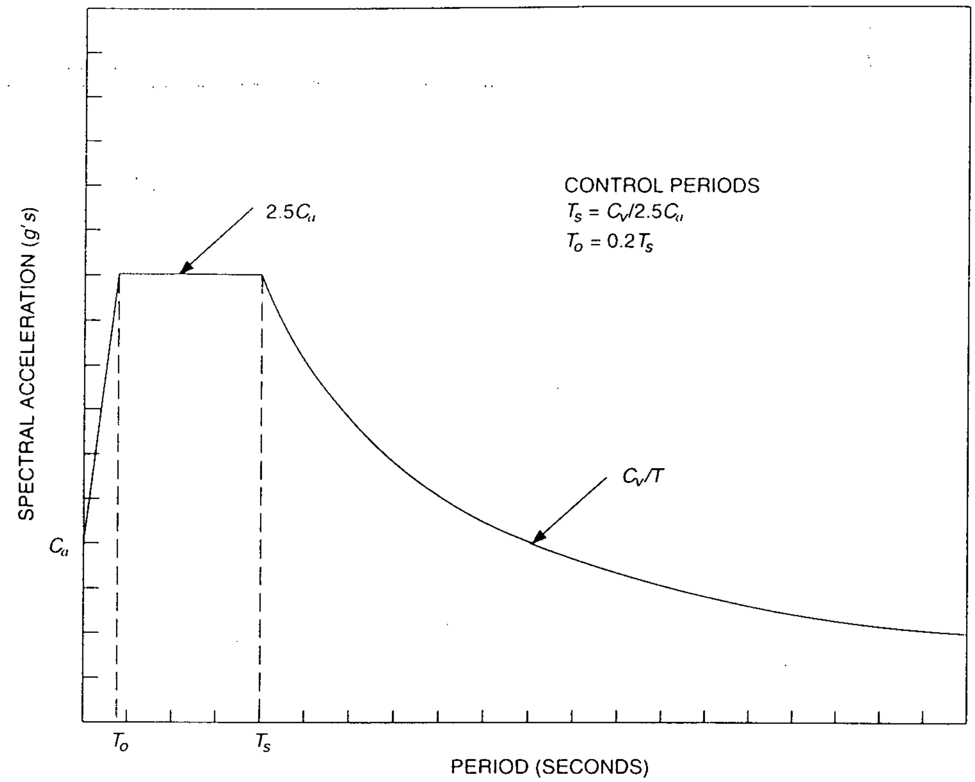

Figure 8.5.2 Design Response Spectra, Uniform Building Code (UBC1997)

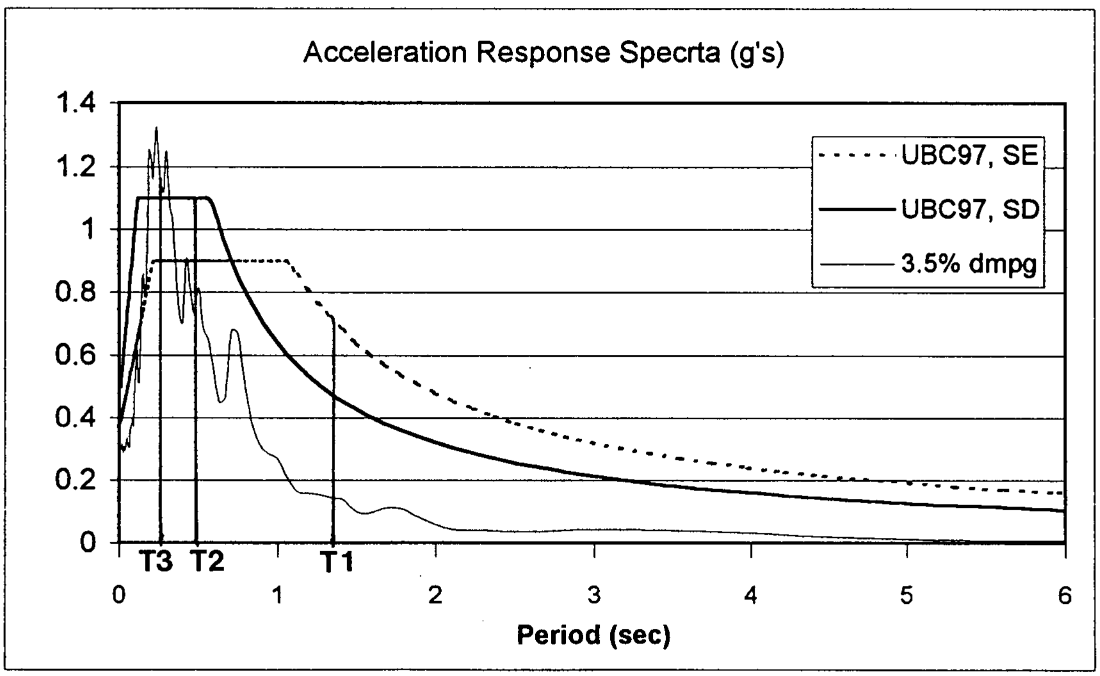

Figure 8.5.3 Response Spectra used in analyses of Models **C2** to **C5**.

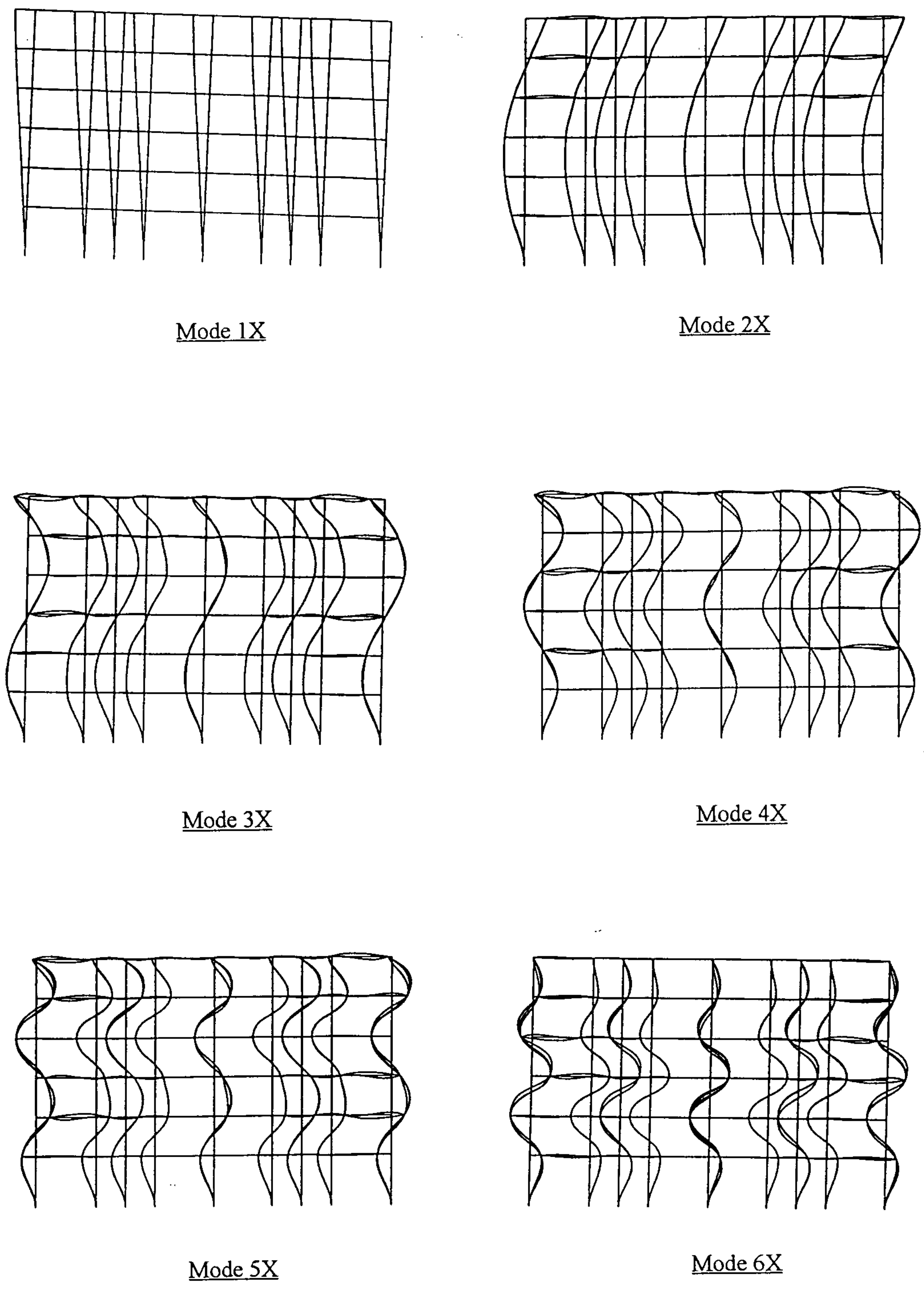

Figure 8.5.4 Two dimensional view of the mode shapes of Model C in X-direction.

In Model **C6**, the base shear obtained from the time history analysis of model **C1** was applied as static lateral loads, distributed in the height of the building based on code static analysis procedure. In this process, the extra concentrated load at top level, F_t (see UBC97 and/or NBCC95) was calculated based on a period obtained from the following empirical formula:

$\mathbf{T = 0.085\ (h_n)^{3/4}} = 0.085\ (25.15\text{m})^{3/4} = 0.955$ sec

==> Ft = 0.07 T V = 0.07 x 0.955 x 4256.85 = 284.57 kN

The calculations of the lateral static loads used in Model **C6** are summarized in Table 8.5.1.

Table 8.5.1 Vertical distribution of seismic loads for Static Analysis.

	Wi(kN)	hi(m)	Wi.hi	Wi.hi/ Sum	Ft	fi	Fi=fi+Ft	Fi . hi
7th floor	6577	25.000	164425	0.3366	284.57	1337.1	1621.7	40542
6th floor	4817	21.038	101338	0.2075	-	824.1	824.1	17337
5th floor	4817	17.075	82251	0.1684	-	668.9	668.9	11421
4th floor	4839	13.113	63452	0.1299	-	516.0	516.0	6766
3rd floor	4965	9.150	45432	0.0930	-	369.5	369.5	3381
2nd floor	6085	5.188	31569	0.0646	-	256.7	256.7	1332
Sum.	32100		488468	1			4256.9	80779

The dynamic properties of Model **C** are summarized in Tables 8.5.2 through 8.5.4.

The natural frequencies and periods of Model **C** are included in Table 8.5.2. A two dimensional view of the natural mode shapes of Model **C** in the X direction is presented in Figure 8.5.4.

In Table 8.5.3 effective masses of the individual modes of the structure are presented as a percentage of the total mass of the building. Participation of each mode in the total dynamic loads applied to the structure is determined as the product of the modal mass and the spectral value at the period corresponding to that mode. A comparison of the response spectrum base shears of the X direction modes of Models **C1** to **C5** is presented in Table 8.5.4

Table 8.5.2 Natural frequencies and periods of Model **C**

	X-Direction (E-W)		Y-Direction (E-W)		Rotation	
	Frequency (Hz)	Period (S)	Frequency (Hz)	Period (S)	Frequency (Hz)	Period (S)
Model	0.738	1.355	0.738	1.355	1.144	0.874
Mode 2	2.067	0.484	2.067	0.484	3.148	0.318
Mode 3	3.639	0.275	3.640	0.275	5.508	0.182
Mode 4	5.541	0.181	5.544	0.180	8.296	0.121
Mode 5	7.754	0.129	7.755	0.129	11.454	0.087
Mode 6	10.316	0.097	10.309	0.097	14.869	0.067

Table 8.5.3 Effective mass factors of Model **C**

	X-Direction (E-W)		Y-Direction (E-W)		Rotation	
	%-MASS	%-SUM	%-MASS	%-SUM	%-MASS	%-SUM
Model	81.14	81.1	81.11	81.1	80.82	80.8
Mode 2	13.17	94.3	13.17	94.3	14.33	95.2
Mode 3	3.82	98.1	3.83	98.1	3.46	98.6
Mode 4	1.24	99.4	1.20	99.4	0.89	99.6
Mode 5	0.45	99.8	0.46	99.8	0.27	99.9
Mode 6	0.18	100.0	0.18	100.0	0.09	100.0

As is shown in Table 8.5.3, the first mode in each direction includes 81% of the dynamic response factor of the structure. However, a look at the response spectra of Figure 8.5.3 shows that the higher modes are in the higher amplitude region of the spectra. Therefore, the participation of the first mode in the total response is less than 81% (Table 8.5.4). This issue becomes more significant in taller buildings with larger fundamental periods.

A comparison of the results of the different methods of analysis in terms of story shears, overturning moments, displacements, inter-story drift ratios and selected element forces is summarized in Tables 8.5.5 to 8.5.10. Plots of maximum story shears and floor overturning moments are presented in Figure 8.5.5 for a more clear comparison of the results.

Table 8.5.4 Dynamic response spectrum base shears of individual (X direction) modes of Models **C2** to **C5**.

	Modal Base Shears (kN)			
	C2	**C3**	**C4**	**C5**
Mode 1	3675	3077	3951	4157
Mode 2	3166	2651	1493	857
Mode 3	1364	1142	433	249
Mode 4	422	353	140	73
Mode 5	83	70	51	23
Mode 6	27	23	18	8
CQC	5084	4257	4257	4257

Table 8.5.5 Comparison of maximum story shears of Models **C1** to **C6**.

	Story Shear (kN)					
	C1	**C2**	**C3**	**C4**	**C5**	**C6**
6th story	3202.1	2749.4	2302.2	1632.1	1426.9	1621.7
5th story	3786.6	3202.1	2681.3	2406.9	2306.8	2445.8
4th story	3473.3	3250.3	2721.7	2926.5	2993.4	3114.7
3rd story	3200.3	3406.6	2852.5	3376.8	3531.1	3630.7
2nd story	3662.4	3937.3	3296.9	3817.6	3940.1	4000.1
Base	4256.9	5083.7	4256.9	4256.9	4256.9	4256.9

Table 8.5.6 Comparison of maximum floor overturning moments of Models **C1** to **C6**.

	Overturning Moment (kN-m)					
	C1	**C2**	**C3**	**C4**	**C5**	**C6**
6th floor	12700	10900	9120	6470	5650	6430
5th floor	27500	22800	19100	15800	14700	16100
4th floor	39700	33200	27800	26800	26400	28500
3rd floor	47900	42400	35500	39200	40000	42800
2nd floor	52200	51600	43200	52800	55200	58700
Base	71300	67700	56700	72700	76500	80800
	Base Overturning Moment Base Shear Ratio (M_b / V_b)					
	16.75	13.32	13.32	17.08	17.97	18.98

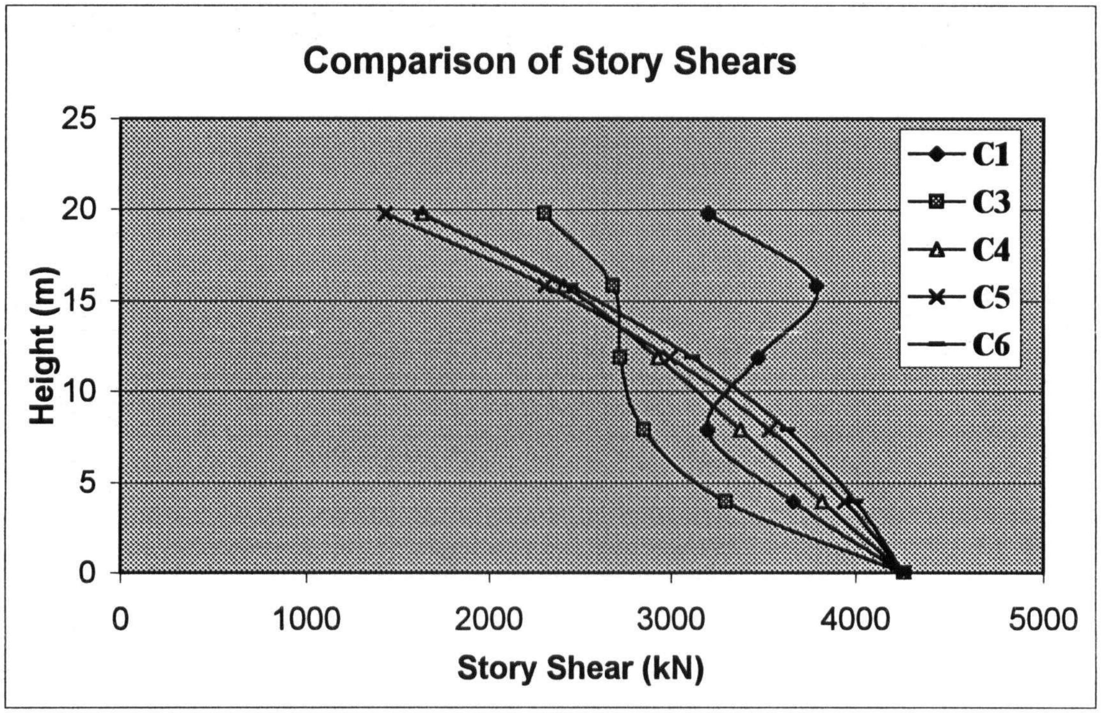

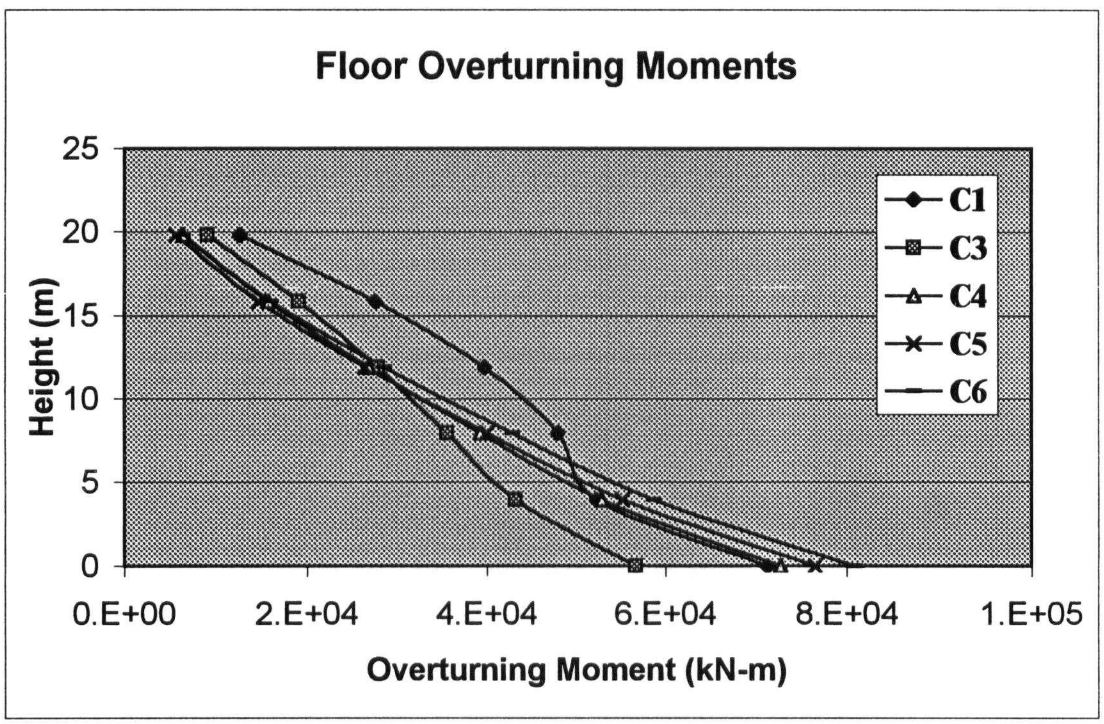

Figure 8.5.5 Comparison of maximum story shears and floor overturning moments of Models **C1** to **C6**.

Table 8.5.7 Comparison of maximum floor displacements of Models **C1** to **C6**.

	Floor Displacement (mm)					
	C1	**C2**	**C3**	**C4**	**C5**	**C6**
7th floor	95.8	89.5	74.9	94.1	98.6	105.2
6th floor	84.0	77.2	64.7	82.8	87.1	91.5
5th floor	67.3	64.2	53.7	67.9	71.2	73.7
4th floor	49.6	51.2	42.9	51.5	53.5	54.7
3rd floor	33.4	37.3	31.3	34.9	35.7	36.2
2nd floor	18.0	21.7	18.1	19.0	19.1	19.3

Table 8.5.8 Comparison of maximum inter-story drift ratios of Models **C1** to **C6**.

	Inter-Story Drift Ratio (% hi)					
	C1	**C2**	**C3**	**C4**	**C5**	**C6**
6th story	0.62	0.52	0.44	0.34	0.31	0.35
5th story	0.64	0.54	0.45	0.43	0.42	0.45
4th story	0.51	0.47	0.40	0.44	0.46	0.48
3rd story	0.45	042	0.35	0.43	0.45	0.47
2nd story	0.39	0.41	0.34	0.41	0.42	0.43
1st story	0.35	0.42	0.35	0.37	0.37	0.37

Table 8.5.9 Comparison of maximum forces in the South-West corner column, obtained from the analyses of Models **C1** to **C6**.

	Max. Moment (kN-m)					
	C1	**C2**	**C3**	**C4**	**C5**	**C6**
6th story	325	276	231	169	149	167
5th story	361	304	255	233	228	239
4th story	359	323	270	269	274	282
3rd story	327	326	273	309	321	331
2nd story	365	387	324	374	389	396
1st story	627	756	633	645	648	649
Max. Shear (kN)						
	C1	**C2**	**C3**	**C4**	**C5**	**C6**
6th story	183	158	133	91	77	88
5th story	207	176	147	130	124	131
4th story	189	177	148	158	162	168
3rd story	189	185	155	181	189	194
2nd story	210	229	192	220	226	229
1st story	239	285	239	238	238	234
Axial Force (kN)						
	C1	**C2**	**C3**	**C4**	**C5**	**C6**
6th story	127	109	91	64	55	62
5th story	345	288	241	191	175	193
4th story	551	456	382	351	340	369
3rd story	707	609	510	540	545	586
2nd story	804	759	636	760	790	843
1st story	1036	955	799	1019	1071	1135

Table 8.5.10 Comparison of Maximum Forces in the perimeter beams of the first span from West at the South edge of the building.

	Max. Moment (kN-m)					
	C1	**C2**	**C3**	**C4**	**C5**	**C6**
6th story	412	352	294	211	185	209
5th story	696	575	482	410	386	420
4th story	664	587	492	517	522	551
3rd story	655	624	523	624	652	677
2nd story	727	735	615	744	776	793
1st story	860	989	828	900	916	924
Max. Shear (kN)						
	C1	**C2**	**C3**	**C4**	**C5**	**C6**
6th story	130	111	93	67	58	65
5th story	225	186	156	133	125	136
4th story	218	193	161	169	171	181
3rd story	215	205	172	205	214	222
2nd story	240	242	203	245	256	261
1st story	275	316	265	288	293	295

8.6 Non-Linear Analysis Using Ground Motions Stronger than those Recorded during the Northridge Earthquake.

Since the time-history analysis of the non-linear model with recorded ground motions indicated no yielding in major structural elements, the analysis was repeated with higher levels of ground motions, which were obtained by amplifying those recorded in Northridge earthquake by factors of two and three. The objective was to compare the results of nonlinear and linear elastic dynamic time-history analyses and nonlinear static (push-over) analysis.

For this purpose the following analyses were performed:

BU-A-N: Model A, Time-History Analysis, Northridge EQ ground acc. (same as section 8.4).

BU-A-2N: Model A, Nonlinear, Time-History Analysis, 2 x (Northridge EQ ground acc.)

BU-A-3N: Model A, Nonlinear, Time-History Analysis, 3 x (Northridge EQ ground acc.)

EL-A-2N: Model A, Linear Elastic, Time-History Analysis, 2 x (Northridge EQ ground acc.)

EL-A-3N: Model A, Linear Elastic, Time-History Analysis, 3 x (Northridge EQ ground acc.)

PL-A-ST: Model A, Non-Linear Static (Push-Over) Analysis with roof maximum displacement set to be equal to that of time-history analysis of **BU-A-3N** & **EL-A-3N**.

A **critical damping ratio of 3.5 %** was assigned to the first two modes in all of the above mentioned dynamic analyses.

In non-linear analysis, in addition to the dissipation of energy due to damping, an extra amount of energy dissipates due to the plastic behavior. It is generally recommended to use smaller damping values for non-linear analysis to avoid under-estimating the displacements. However, in this study, the objective was to compare the results of various analysis methods. Therefore the same damping values were used for all analyses.

At the end, to visualize the impact of a smaller damping value, the analysis of model **BU-A-3N** was repeated with a damping value of 1.5%. The roof acceleration and displacement time-histories obtained from this analysis are presented in Figure 8.6.2 to be compared to the results analysis with 3.5% damping (presented in Figure 8.6.1).

Vertical distribution of the lateral loads for the nonlinear static (push-over) analysis was chosen to be the same as the code recommended distribution for static analysis (same as that of Model **C6** in Chapter 8). The load factors used to distribute the base shear along the height of the building in this analysis are shown in Table 8.6.4.

A comparison of the base shears, maximum floor displacements, and inter-story drift ratios obtained from the linear and nonlinear analyses of this section is included in Tables 8.6.1 and 8.6.2. In Table 8.6.3, maximum ductility factors of selected beams and columns obtained from the nonlinear analyses are compared.

The results of the push-over analysis (see Tables 8.6.1 to 8.6.3) are presented for the two cases where the structure is pushed until achieving roof displacements equal to the maximum roof displacements obtained from the analyses of **BU-A-3N** and **EL-A-3N**.

Plots of floor displacements versus base shear obtained from the push-over analysis with a maximum roof displacement of 2.00 meter is presented in Figure 8.6.3

Table 8.6.1 Comparison of maximum floor displacements and base shears of non-linear and linear models,

	Max. floor displacement in X-dir (mm)						
	BU-A-N	**BU-A-2N**	**BU-A-3N**	**EL-A-2N**	**EL-A-3N**	**PL-A-ST***	
7th floor	97	188	252	194	290	252	290
6th floor	85	165	217	169	254	227	264
5th floor	68	130	162	136	204	185	215
4th floor	52	96	111	104	156	137	158
3rd floor	36	66	77	72	108	88	101
2nd floor	20	37	42	41	61	46	51
Base Shear (kN)	4290	7842	8668	8576	12860	8709	8973

Table 8.6.2 Comparison of maximum inter-story drifts of non-linear and linear models.

	Inter-story drift in X-dir (% hi)						
	BU-A-N	**BU-A-2N**	**BU-A-3N**	**EL-A-2N**	**EL-A-3N**	**PL-A-ST***	
6th story	0.55	1.05	1.65	1.08	1.62	0.66	0.69
5th story	0.62	1.33	2.21	1.23	1.85	1.06	1.22
4th story	0.47	0.97	1.63	0.94	1.41	1.21	1.44
3rd story	0.43	0.77	0.99	0.86	1.30	1.21	1.44
2nd story	0.40	0.73	0.86	0.79	1.18	1.07	1.27
1st story	0.39	0.72	0.82	0.78	1.17	0.89	0.98

* The two columns include the results of analysis of **PL-A-ST** with the maximum roof displacements of equal to those obtained from the analyses of **BU-A-3N** and **EL-A-3N**.

Maximum beam ductility factor in the original analysis was observed at the first span from West on Southern edge of the building. Max Column ductility was observed in 3rd column from West on the same side of the building. In Table 8.5.4 ductility factors of columns and beams at the above mentioned location are compared.

Table 8.6.3 Comparison of ductility factors of dynamic and static analyses.

	Column Ductility Factor				
	BU-A-N	**BU-A-2N**	**BU-A-3N**	**PL-A-ST***	
6th story	0.78	1.94	3.66	0.89	0.93
5th story	**0.78**	**2.63**	**4.72**	**1.50**	**1.87**
4th story	0.58	1.17	2.06	1.02	1.21
3rd story	0.46	0.83	1.04	0.92	0.94
2nd story	0.48	0.86	0.94	1.50	1.95
1st story	0.51	0.93	1.04	1.27	1.48
	Beam Ductility Factor				
	BU-A-N	**BU-A-2N**	**BU-A-3N**	**PL-A-ST***	
7th floor	0.45	0.82	2.02	0.48	0.49
6th floor	0.67	2.69	6.26	0.88	0.95
5th floor	**0.71**	**2.92**	**6.95**	2.68	3.59
4th floor	0.63	1.45	3.28	**3.47**	**4.57**
3rd floor	0.58	1.11	1.96	3.20	4.28
2nd floor	0.55	1.10	1.65	2.70	3.54

* The two columns include the results of analysis of **PL-A-ST** with the maximum roof displacements of equal to those obtained from the analyses of **BU-A-3N** and **EL-A-3N**.

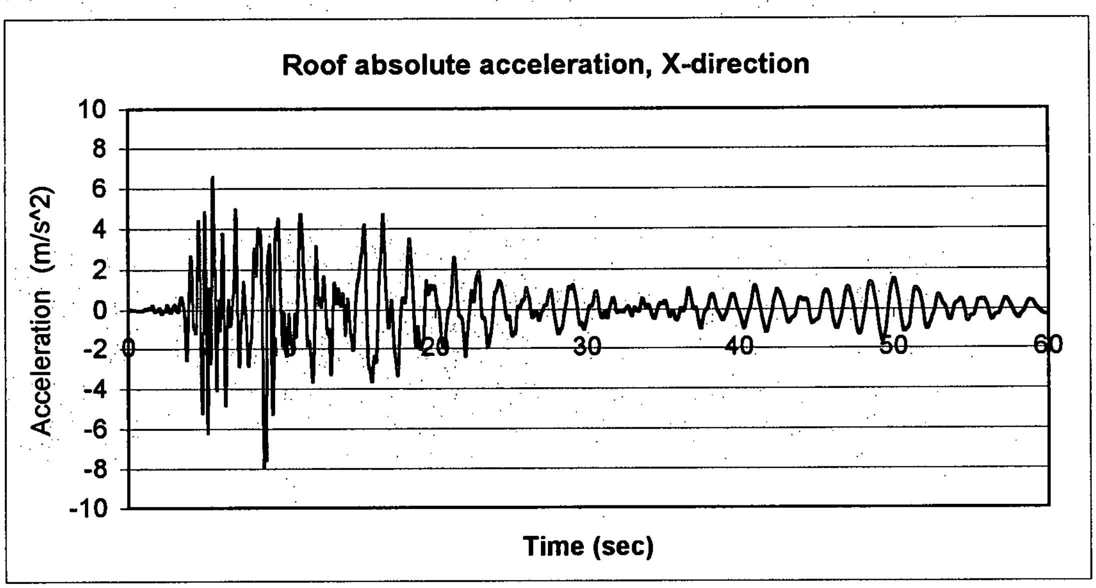

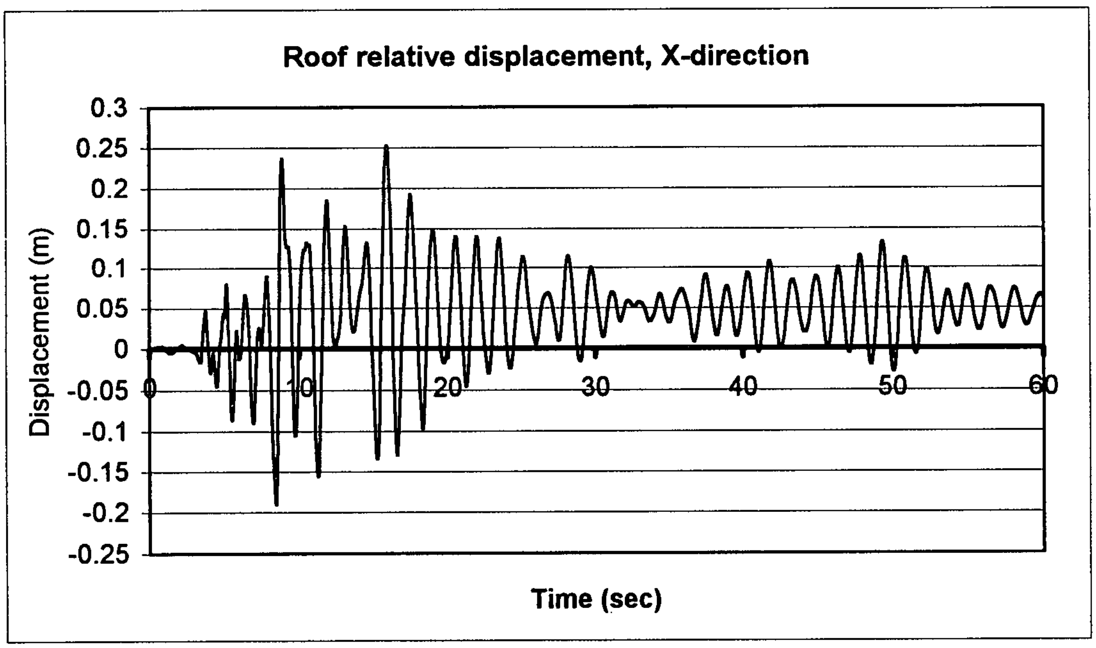

Figure 8.6.1 Roof absolute acceleration and relative displacement time-histories obtained from the nonlinear analysis of model **BU-A-3N** (3.5% damping).

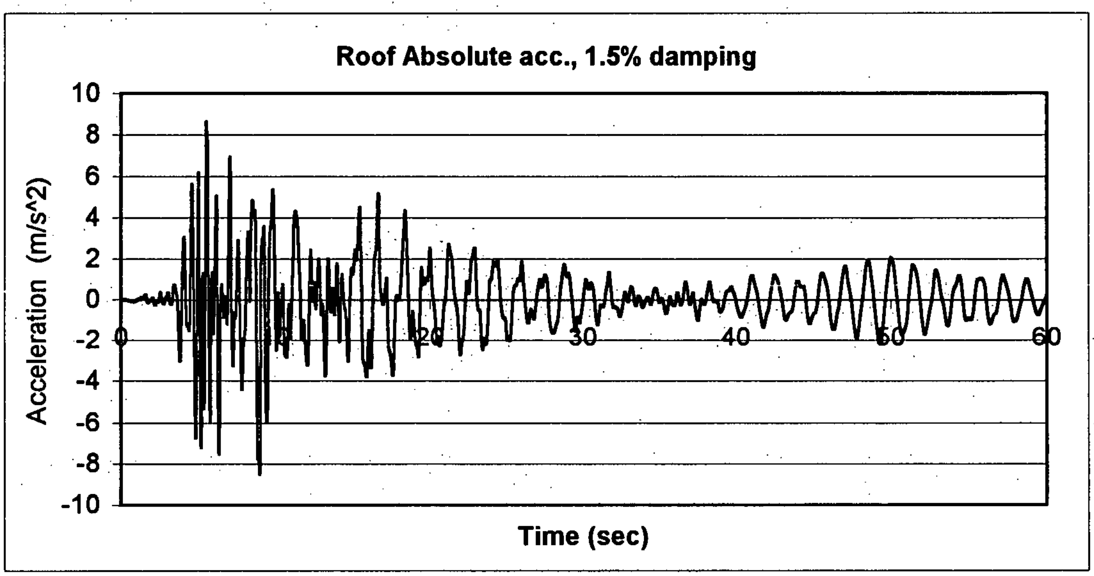

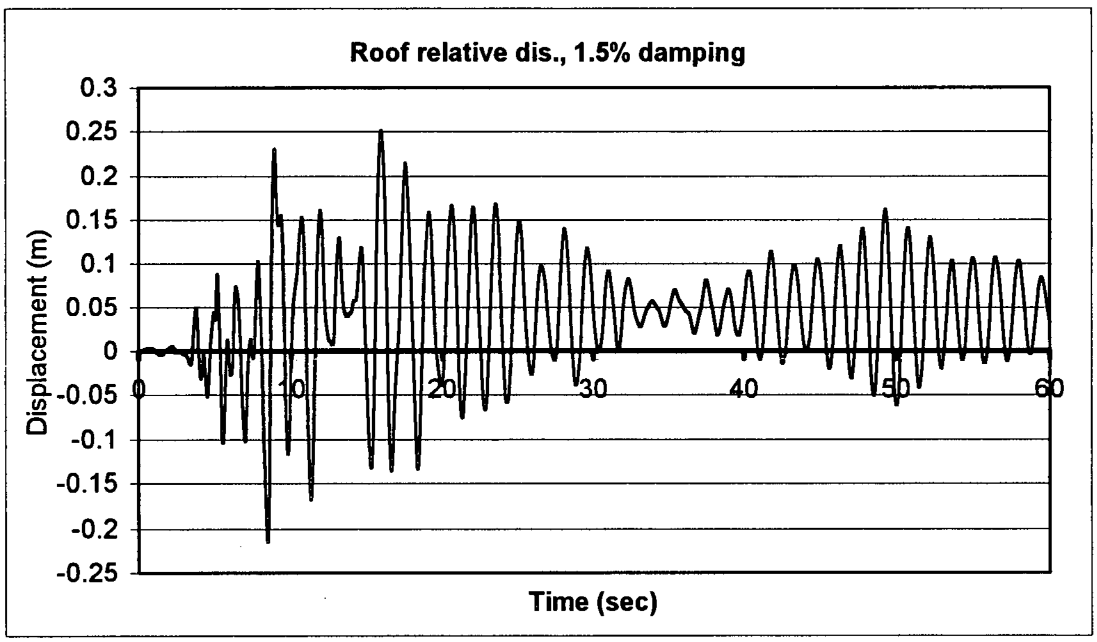

Figure 8.6.2 Roof absolute acceleration and relative displacement time-histories obtained from the nonlinear analysis of model **BU-A-3N** (1.5% damping).

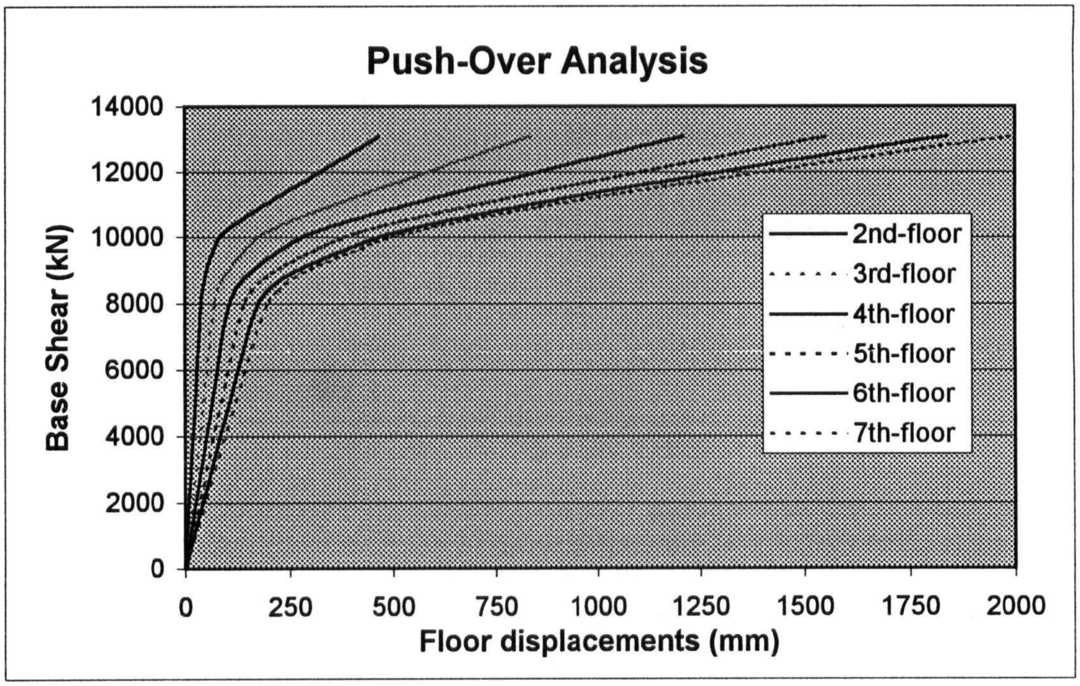

Figure 8.6.3 Force-displacement relationship obtained from push-over analysis.

Table 8.6.4 The vertical distribution factors of the lateral loads, used for nonlinear static (Push-Over) analysis of model **PL-A-ST**.

	load distribution factors					
Floor Level	2nd Floor	3rd Floor	4th Floor	5th Floor	6th Floor	Roof
Lateral Load Factor	0.060	0.087	0.121	0.157	0.194	0.381

Chapter 9 DISCUSSION OF THE RESULTS OF THE ANALYSES OF THE BURBANK 6-STORY OFFICE BUILDING

9.1 General Remarks

The acceleration and displacement time histories obtained from the dynamic analyses of the Burbank 6-story office building matched closely with those obtained from the strong motion data. As a result, it can be concluded that the results of the analyses performed on the mathematical models of the building (presented in Chapter 8), are reasonable representations of the behaviour of this building under seismic loading. In general, the results of the type of the analyses presented in the previous chapter, can be used for the following purposes:

1) studying the behaviour of the building in actual earthquakes,

2) predicting the behaviour under higher levels of shaking,

3) comparing the results of various analysis techniques with the actual response of the building.

Sections 9.2 to 9.6 include some conclusions inferred from reviewing the results of the analyses of the Burbank 6-story office building. The analysis showed that during the Northridge earthquake, although the building experienced a peak ground acceleration of 0.3 g and a peak acceleration of 0.45 g at roof level, the maximum base shear was only 14% of the weight of the building. The maximum inter-story drift ratios (which was observed in the fifth story) was 0.6% of the story height, which is only 30 % of the maximum allowable drift ratio according to the building codes.

9.2 Possible Structural Damage during the Northridge Earthquake

The strong motion data indicate a higher natural period for the building in the Northridge earthquake which had a higher peak ground acceleration than the Whittier earthquake. The results of the time-history analysis of Model **B** (which was scaled to have the same natural frequencies as measured in the Whittier earthquake) matched the recorded data. However, analyzing the same model with the Northridge earthquake ground accelerations showed good agreement with only the first 10 seconds of the recorded response. Time history analysis of model **A,** which had smaller natural frequencies, matched the Northridge earthquake data very well. This may indicate that the stiffness of the building has dropped due to some damage in the building (which may have occurred during the first 10 seconds of the Whittier earthquake). Since the low-stiffness model's (Model A) results matched the small displacement part at the end of the Northridge records, it may be concluded that the drop in frequency is due to permanent decrease in the stiffness of the system (i.e. some damage in the building) and not because of nonlinear elastic behavior due to higher displacements. The nonlinear analysis did not show any yielding in the main structural elements. Therefore, damage may have occurred in one of the following areas:

1. Bond between concrete and steel in composite action of the beams and interaction of concrete slabs and steel columns.

2. Interior beam to column connections which provide partial fixity in spite of being considered pin connections.

3. Connections of rigid frame elements.

Further investigation is required to confirm the existence of any damage of above mentioned types.

9.3 Effect of the Higher Modes on the Response

The fundamental period of 1.4 seconds is significantly higher than what is usually expected for a six story building. This is partly due to relatively high floor to floor height (17ft high 1st story and 13ft high upper stories). The period of 1.4 seconds places the first mode of the building in the low amplitude part of the response spectrum (See Figure 8.4.4). As a result, the contribution of the 2nd and 3rd modes become significant. The out of phase response of the middle floors (see figures 8.4.7 and 8.4.8), and the small decrease in the level of the forces in the upper floors of the building (Tables 8.3.2, 8.3.4, 8.4.2, & 8.4.4), also confirm the significance of the higher mode effects. In this respect, it can be concluded that the building behaved in a way that is usually expected from taller buildings.

9.4 Response Spectrum Analysis versus Time-history Analysis

The analysis using a response spectrum calculated by the program Nonlin for the recorded ground motion over-estimated the base shear and under-estimated the base moment by approximately 20% (Table 8.5.5 and 8.5.6).

9.5 Spectral Analysis with Code Design Response Spectra

Spectral Analysis with code design response spectra showed a more rapid drop in the forces at the upper stories and a higher base overturning moment to base shear ratio (See Table 8.4.6). This is due to a higher contribution of the first mode in the response which results from the relatively high amplitude of the code response spectra in the period range of approximately 0.7 seconds and higher (See Figure 8.4.4).

It may be concluded that conducting a spectral dynamic analysis using code design response spectra and scaling the results to a designated base shear (which is commonly done in practice), may result in unrealistic distribution of the lateral loads throughout the structure and in particular, it may under-estimate the forces at the upper levels of such structures.

9.6 Non-Linear Time-History Analysis

Since the structural model did not reach the nonlinear range when the recorded ground motions were applied, it was not possible to evaluate the accuracy of this type of analysis (which is very sensitive to the parameters used for defining the hysteretic behavior of the structural material). Non-linear time-history analysis for ground motions of two and three times those recorded in Northridge earthquake resulted in 3% and 13% smaller maximum roof displacements than the linear elastic time-history analyses results. The close results of the linear and nonlinear analyses agree with the equal displacement assumption which is usually used for estimating the ductility demand. However, the analysis shows a higher element ductility demand than the global ductility of the structure. As an example, comparing the results of the analysis of model **BU-A-3N** to those of model **BU-A-N** (see Tables 8.6.2 and 8.6.4) showed that an increase in roof maximum displacement by a factor of 2.35 coincided with an increase in the maximum ductility of the columns by a factor of 4.7 and maximum beam ductility by a factor of 7.0.

9.7 Effect of Damping Value

Repeating the nonlinear analysis of model **BU-A-3N** with a damping value of 1.5% instead of 3.5% resulted in a small increase in the roof maximum displacement. However, the increase in the amplitude of the response (due to the lower damping value) became more significant after T=20sec, where the response was mainly in the linear elastic range. See Figures 8.6.1 and 8.6.2. It can be concluded that the results of nonlinear analysis are less sensitive to the damping value than those of linear elastic analysis.

9.8 Non-Linear Static (Push-over) Analysis

Non-Linear Static (Push-over) Analysis with code defined lateral distribution of equivalent static loads under-estimated the element ductility demands (see Table 8.6.4). This is mainly due to the fact that the effect of the higher modes, (which results in higher levels of inter-story drifts for the same levels of roof maximum displacement), is not considered in this type of analysis.

Chapter 10 CONCLUSIONS

10.1 Behaviour of the Buildings

The objective of the first part of this research was to extract as much information as possible from the recorded motions of the selected low-rise steel frame buildings. The following conclusions can be made from the results of this part:

1. The measured fundamental periods in most cases were 50 to 100% higher than those estimated by empirical formulae. In the case of the San Bernardino 5-story hospital, however, the measured period was significantly less than the value suggested by the height dependent period formula for steel frame buildings. Since the response of the low-rise buildings is very sensitive to their fundamental period, using empirical period formulae in seismic design of these buildings may result in unrealistic estimates of the seismic behavior of these buildings.

2. Significant higher mode effects were detected in three of the buildings (which had fundamental periods greater than 1.0 second).

3. The analysis of the recorded data indicated that both ground motion and structural response have a 3-dimensional nature including translational and rotational components.

4. Detailed structural analysis of a computer model of the Burbank 6-story Building (calibrated to match the recorded data), did not show yielding in the major lateral load resisting elements. The building was subjected to a peak ground acceleration of 0.3g.

5. The records from two earthquakes (the 1987 Whittier and the 1994 Northridge earthquakes) were studied for the Burbank building. A drop in the natural frequency of this building was observed during the Northridge earthquake. Further investigation is required to verify any damage to the secondary elements or connections.

6. The Base-Isolated buildings considered in this study showed a significant increase in the natural period of the structure due to the relatively soft isolators, resulting in a smaller seismic loading. The isolators absorbed the major portion of the seismic induced displacements.

7. The information extracted from the strong motion data obtained from the selected low-rise steel frame buildings in earthquakes was presented in this thesis as a series of diagrams and tables in order to gain a better understanding and elucidate significant features of the seismic behavior of this type of buildings.

10.2 Analysis Techniques

In the second part of this research the objective was to investigate the accuracy and efficiency of various analysis methods. The following conclusions were made by comparing the results obtained from the various methods used for analyzing the computer models of the Burbank 6-story building and comparing the results of the time-history analyses with the recorded data:

1. The time-history analysis results showed that a linear dynamic time-history analysis using proper values for the mass and stiffness of the structure can accurately predict the behaviour of the structures in earthquakes (provided their response is within the elastic range).

2. Since the structural model did not enter the non-linear range, it was not possible to investigate the accuracy of this type of analysis, which is very sensitive to the parameters used in defining the hysteretic behaviour of the structural material.

3. The response spectrum analysis using the response spectrum obtained from the recorded ground motions, resulted in a reasonable approximation of the response of the building. The results, however, were not as accurate as those of time-history analysis.

4. The response spectrum analyses with code recommended design response spectra, under-estimated the effect of the higher modes. In view of this, it is recommended to conduct spectral dynamic analyses with at least two different spectral shapes: one with high amplitude in the high period region, which gives higher first mode effects, resulting in conservative results for the base overturning moment and the displacements in the upper floors; the second response spectrum with higher amplitude in the low period region and lower amplitude in the high period region (similar to code recommended spectra for very stiff soil). This results in a larger "higher mode effects" and gives a conservative distribution of the loads in the upper levels of the structure.

5. Nonlinear time history analysis indicated that the level of ductility demand for the individual elements can be significantly higher than the global ductility demand for the structure.

6. The nonlinear static (push-over) analysis performed in this research underestimated the element ductility demands. This was mainly due to not including the effect of the higher modes in the seismic response.

In closing it is recommended to perform a dynamic analysis in seismic design of all types of multi-story structures to:

- Obtain a more realistic estimate of the natural periods of the buildings,
- Capture the 3-D behavior and coupling between translational and torsional modes,
- Include the effects of higher modes in the response.

Nonlinear static (push-over) analysis is not recommended for evaluating the seismic behavior of the multi-story buildings, where the effect of the higher modes and the coupling between the modes cannot be captured by a static analysis.

REFERENCES

Beauchamp, K.G., 1979, "Digital Methods for Signal Analysis", George Allen & Unwin Ltd. London. (Chapters 1, 3, 4 & 6).

Bendat, J.S. and Piersol, A.G., 1993, "Engineering Applications of Correlation and Spectral Analysis", John Wiley & Sons, Inc., Toronto. (Chapters 1, 4, 5, 8, & 11).

CANNY-E Users' Manual, Li, K.N, CANNY Consultants Pte. Ltd., Singapore, November, 1996.

Chang, S. and Markis, N., "Effects of Damping Mechanisms on the Seismic Response of Isolated Structures", Proceedings of the 17th International Modal Analysis Conference (IMAC) Kissimmee, Florida, 1999, Volume I, pp. 146-152.

Chopra, A.K., 1995, "Dynamics of Structures: Theory and Applications to Earthquake Engineering", Prentice Hall, Upper Saddle River, N.J.

Clough, R.W. and Penzien, J., 1993, "Dynamics of Structures", McGraw-Hill, London

Cole, E. E., Tokas, C. V. and Meehan, J. F., "Analysis of Recorded Building Data to Verify or Improve 1991 Uniform Building Code (UBC) Period of Vibration Formulas", Proceedings of SMIP92 (Strong Motion Instrumentation plan) Seminar on Seismological and Engineering Implications of Recent Strong Motion Data, Sacramento California, May 21, 1992.

De la LLera, J. C. and Chopra, A. K., "Evaluation of Code Accidental Torsional Provisions Using Strong Motion Records from Regular Buildings", Proceedings of SMIP91 (Strong Motion Instrumentation plan) Seminar on Seismological and Engineering Implications of Recent Strong Motion Data, Sacramento California, May 30, 1991.

De la Llera, J. C. and Chopra, A. K., "Evaluation of Code-Accidental Torsional Provisions Using Strong Motion Records from Three Nominally Symmetric Buildings", Proceedings of SMIP92 (Strong Motion Instrumentation plan) Seminar on Seismological and Engineering Implications of Recent Strong Motion Data, Sacramento California, May 21, 1992.

De la Llera, J. C. and Chopra, A. K., "Evaluation of Seismic Code Provisions Using Strong-Motion Records from the 1994 Northridge Earthquake", Proceedings of SMIP95 (Strong Motion Instrumentation plan) Seminar on Seismological and Engineering Implications of Recent Strong Motion Data, Sacramento California, May 16, 1995.

Ding, Y. 1999, "A Study on the Seismic Behaviour of a 52-Story Steel Frame Building", M.A.Sc. Thesis

ETABS User's Manual (Version 6.2), Ashraf Habibullah, Computers & Structures Inc., Berkeley, California, May, 1997.

Federal Emergency Management Agency, "Interim Guidelines: Evaluation, Repair, Modification and Design of Welded Steel Moment Frame Structures", FEMA 267 August 1995.

Federal Emergency Management Agency, "Interim Guidelines Advisory No.1", FEMA 267A March 1997.

Fenves, G. L., "Evaluation of Lateral Force Procedures for Buildings", Proceedings of SMIP90 (Strong Motion Instrumentation plan) Seminar on Seismological and Engineering Implications of Recent Strong Motion Data, Sacramento California, June 8, 1990.

Goel, R. K. and Chopra, A. K., "Period Formulas for Moment-Resisting Frame Buildings", Journal of Structural Engineering, November 1997, pp. 1454-1461.

Goel, R. K. and Chopra, A. K., "Vibration properties of buildings during earthquakes", Earthquake Engineering Research Center, University of California at Berkeley, Report No. UCB/EERC-97/14, December 1997.

Handbook of Steel Construction, 1985, Canadian Institute of Steel Construction, Willowdale, Ontario.

Huang, M. J., Malhotra, P. K. and Shakal, A. F., "Analysis of Records from four Base-Isolated Buildings during the 1992 Landers Earthquake", Proceedings of SMIP93 (Strong Motion Instrumentation plan) Seminar on Seismological and Engineering Implications of Recent Strong Motion Data, Sacramento California, May 20, 1993.

Kelly, J., "Earthquake resistant design with rubber", Springer, N.Y., 1997

Manual of Steel Construction, American Institute of Steel Construction Inc., 1973.

McClure, F. E., "Analysis of a Two Story Oakland Office Building During the Loma Prieta Earthquake", Proceedings of SMIP91 (Strong Motion Instrumentation plan) Seminar on Seismological and Engineering Implications of Recent Strong Motion Data, Sacramento California, May 30, 1991.

"The ME'Scope", 1998, Operating Manual Version 4.0, Vibrant Technology, Jamestown, CA.

Naeim, F., "Performance of 20 Extensively-Instrumented Buildings during the 1994 Northridge Earthquake", Proceedings of SMIP96 (Strong Motion Instrumentation plan) Seminar on Seismological and Engineering Implications of Recent Strong Motion Data, Sacramento California, May 14, 1996.

Nagarajaiah, S. and Xiahong, S., "Response of Base-Isolated Buildings during the 1994 Northridge Earthquake", Proceedings of SMIP95 (Strong Motion Instrumentation plan) Seminar on Seismological and Engineering Implications of Recent Strong Motion Data, Sacramento California, May 16, 1995.

Nagarajaiah, S., "System Identification of Base-Isolated USC Hospital Building from Recorded Response", Proceedings of the 17th International Modal Analysis Conference (IMAC) Kissimmee, Florida, 1999, Volume I, pp. 159-165.

National Building Code of Canada (**NBCC1995**), National Research Council of Canada, Ottawa, 1995

Pardoen, G., "Building Vibration Characteristics from Recorded Data", Proceedings of SMIP89 (Strong Motion Instrumentation plan) Seminar on Seismological and Engineering Implications of Recent Strong Motion Data, Sacramento California, May 9, 1989.

SAC 95-04, 1995, "Analytical and Field Investigations of Buildings Affected by the Northridge Earthquake of January 17, 1994".

SAC 95-05, 1995, "Parametric Analytical investigations of Ground Motion and Structural Response, Northridge Earthquake of January 17, 1994".

SAP90 Users Manual, Wilson, A. and Habibullah, A., Computers & Structures Inc., Berkeley, California, 1989.

Shakal, A., Huang, M., Darragah, R., Cao, T., Sherburne, R., Malhotra, P., Cramer, C., Sydnor, R., Grazier, R., Maldonado, G., and Petersen, C., Wampole, J., 1994, "CSMIP Strong-Motion Records from the Northridge, California Earthquake of January 17, 1994," Calif. Dept. of Conservation, Division of Mines and Geology, Office of Strong Motion Studies, Report OSMS 94-07, Sacramento, CA, 308 p.

Shakal, A. F., Huang, M. J. and Darragah, R., "Some Implications of Strong Motion records from the 1994 Northridge Earthquake", Proceedings SMIP94 (Strong Motion Instrumentation plan) Seminar on Seismological and Engineering Implications of Recent Strong Motion Data, Sacramento California, May 26, 1994.

Shakal, A. F., Huang, M. J., Cao, T. Q., Sherburne, R. W., Sydnor, R., Fung, P., Malhotra, P., Cramer, C., Su, F., Darragh, R.,Wampole, J., "CSMIP STRONG-MOTION RECORDS from the Landers, California Earthquake Of June 28, 1992", California Department of Conservation, Division of Mines and Geology, Office of Strong Motion Studies, Report OSMS 92-09

Shakal, A. F., Huang, M. J., Reichle, M., Ventura, C. E., Cao, T. Q., Sherburne, R. W., Savage, M., Darragh, R., Peterson, C., "CSMIP Strong-motion Records from the SANTA CRUZ mountains (Loma Prieta), California Earthquake Of 17 October 1989", California Department of Conservation, Division of Mines and Geology, Office of Strong Motion Studies, Report OSMS 89-06

Shakal, A. F., Huang, M. J., Ventura, C. E., Parke, D. L., Cao, T. Q., Sherburne, R. W., Blazquez, R., "CSMIP Strong-motion Records from the Whittier, California Earthquake Of 1 October 1987", California Department of Conservation, Division of Mines and Geology, Office of Strong Motion Studies, Report OSMS 87-05

Shen, J., Astaneh, A., “Seismic Response Evaluation of an Instrumented Six-story Steel Building”, Earthquake Engineering Research Center, University of California at Berkeley, Report No. UCB/EERC-90/20, December 1990

Uniform Building Code (UBC), 1997, International Conf. of Building Officials, Whittier, CA.

APPENDIX A

Separated floor accelerations of selected buildings.

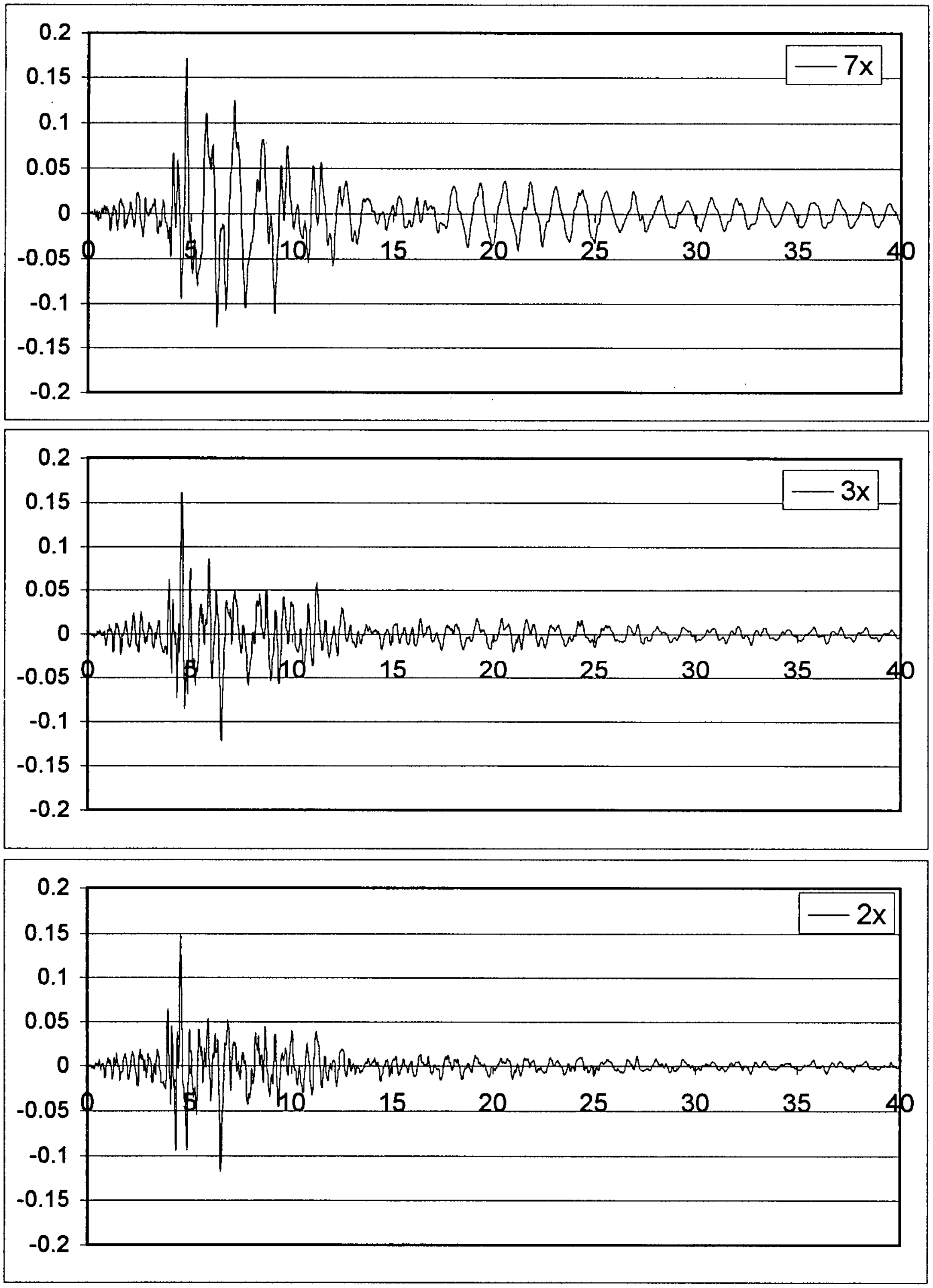

Figure A1 Absolute accelerations of the upper floors of the Burbank 6-story office bldg. in the E-W (X) direction, obtained from the 1987 Whittier EQ records.

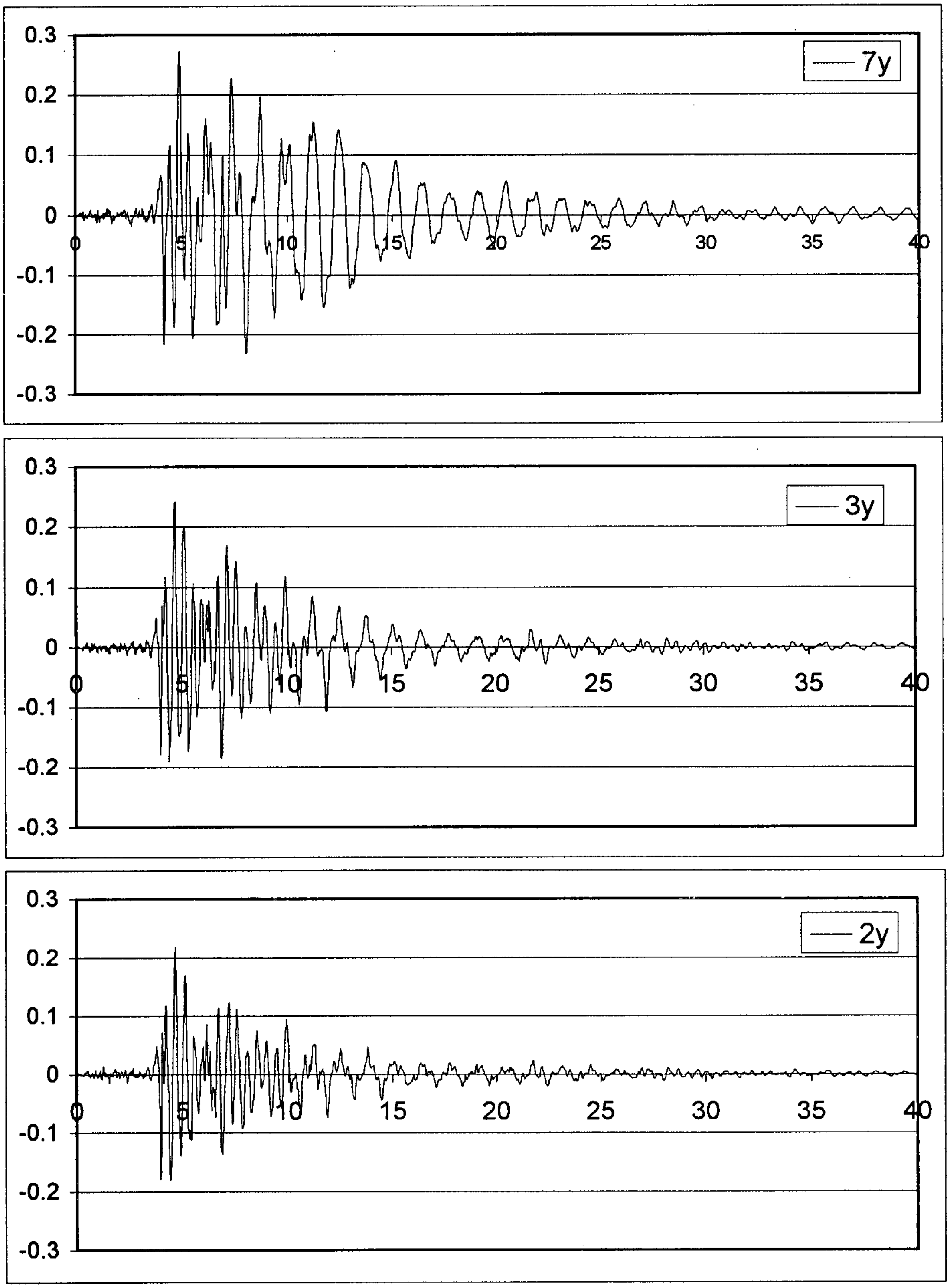

Figure A2 Absolute accelerations of the upper floors of the Burbank 6-story office bldg. in the N-S (Y) direction, obtained from the 1987 Whittier EQ records.

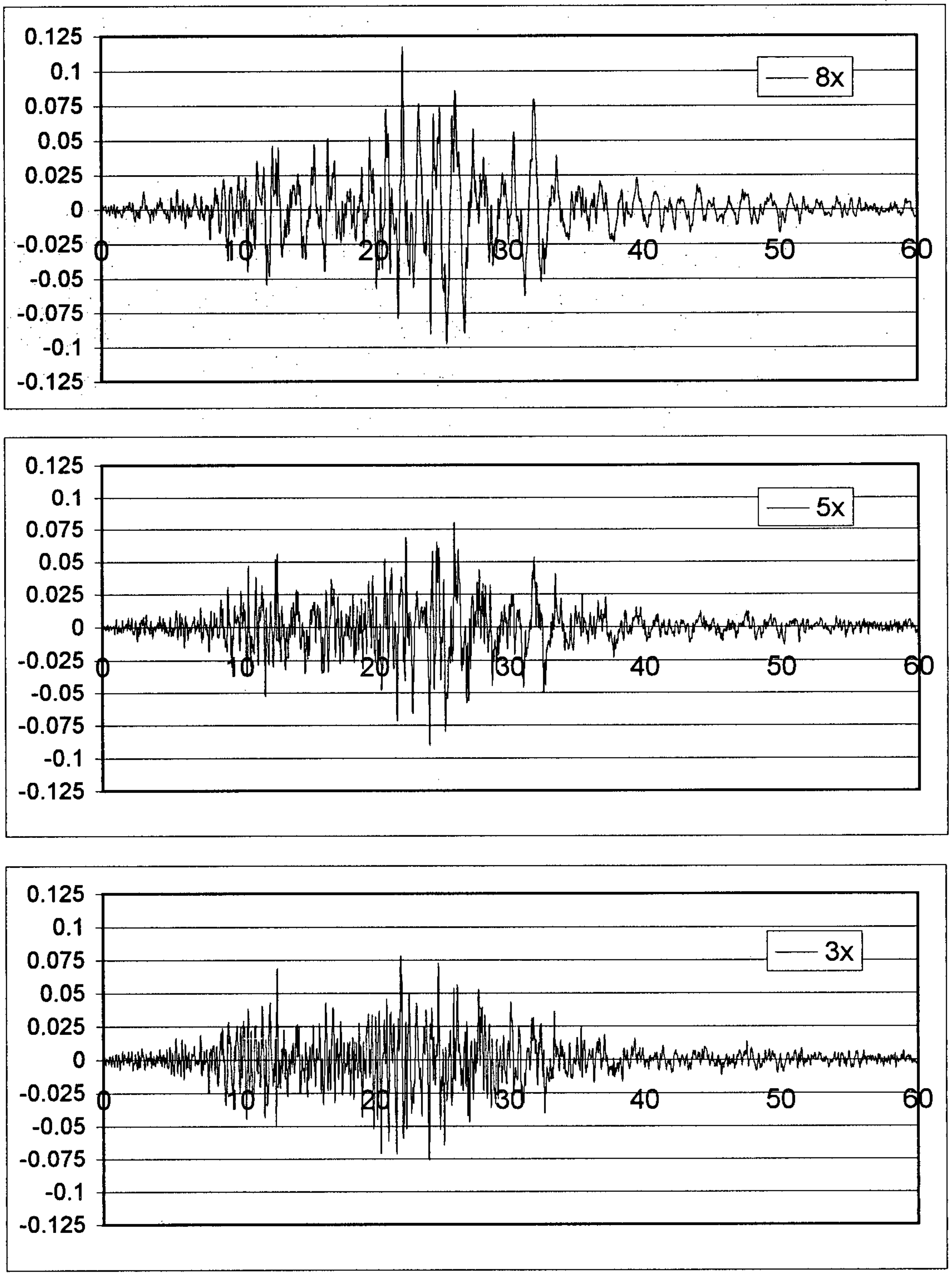

Figure A3 Absolute accelerations of the upper floors of the Redlands 7-story commercial bldg. in the E-W (X) direction, obtained from the 1992 Landers EQ records.

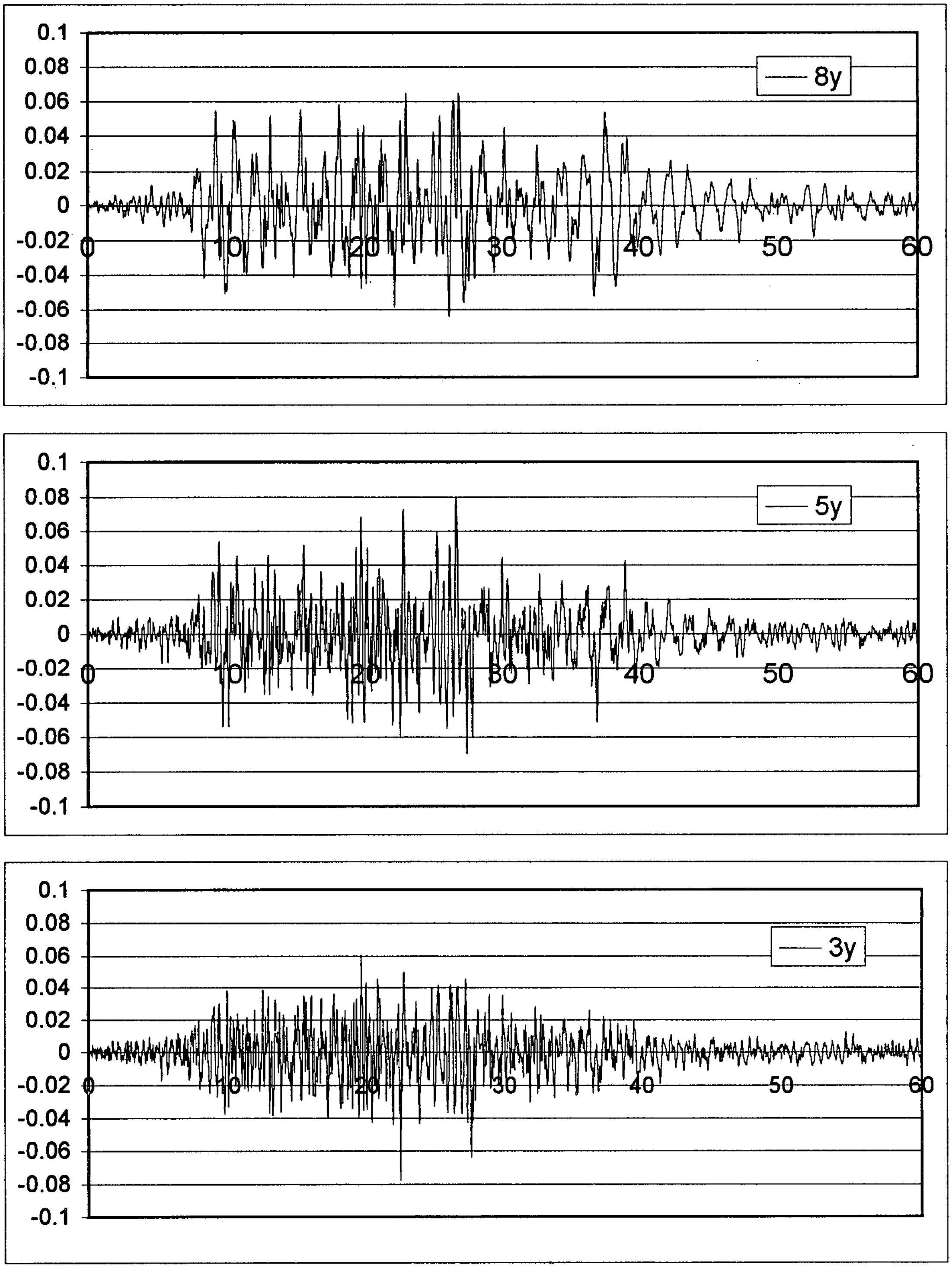

Figure A4 Absolute accelerations of the upper floors of the Redlands 7-story commercial bldg. in the N-S (Y) direction, obtained from the 1992 Landers EQ records.

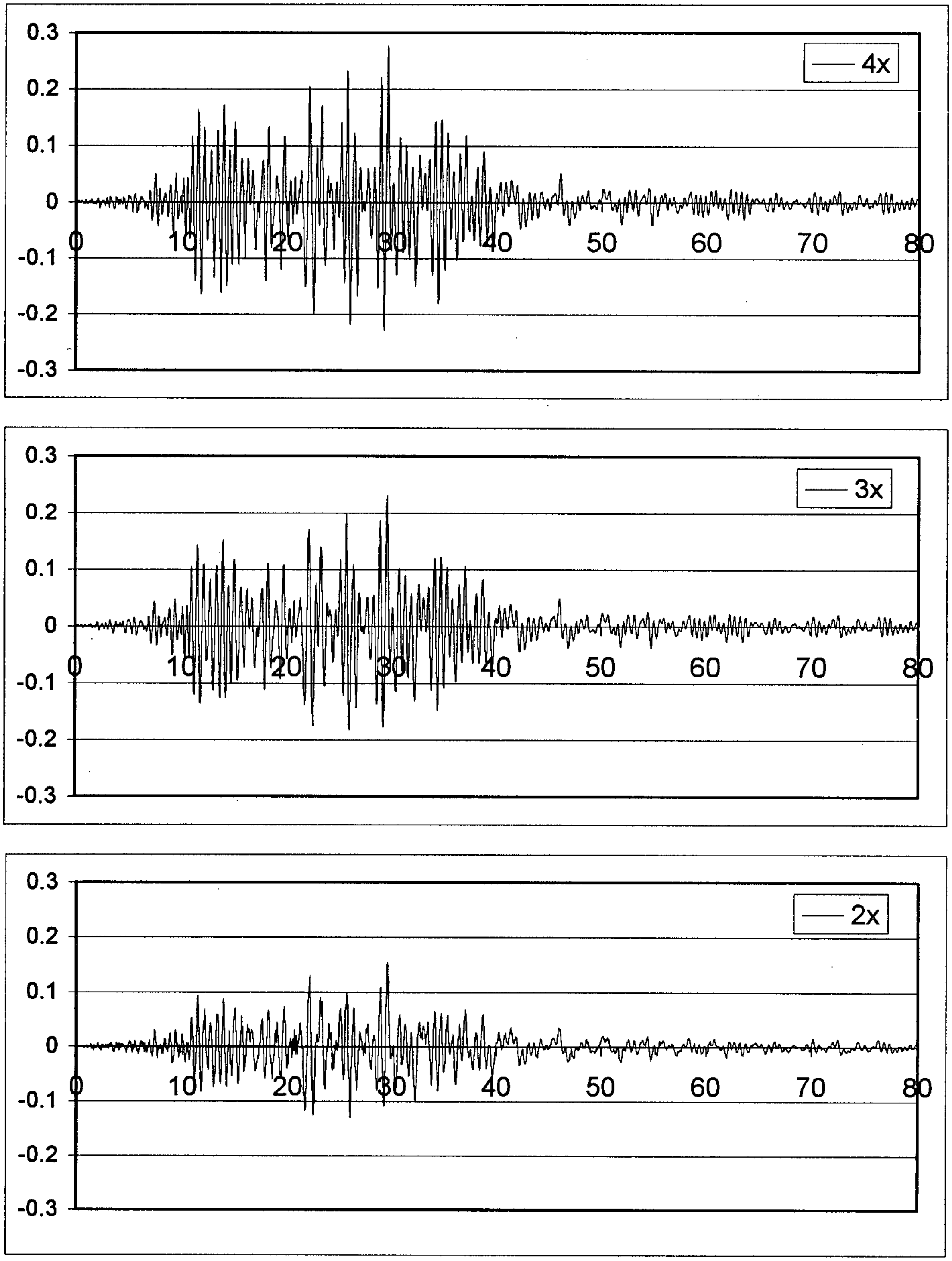

Figure A5 Absolute accelerations of the upper floors of the San Bernardino 3-story office bldg. in the E-W (X) direction, obtained from the 1992 Landers EQ records.

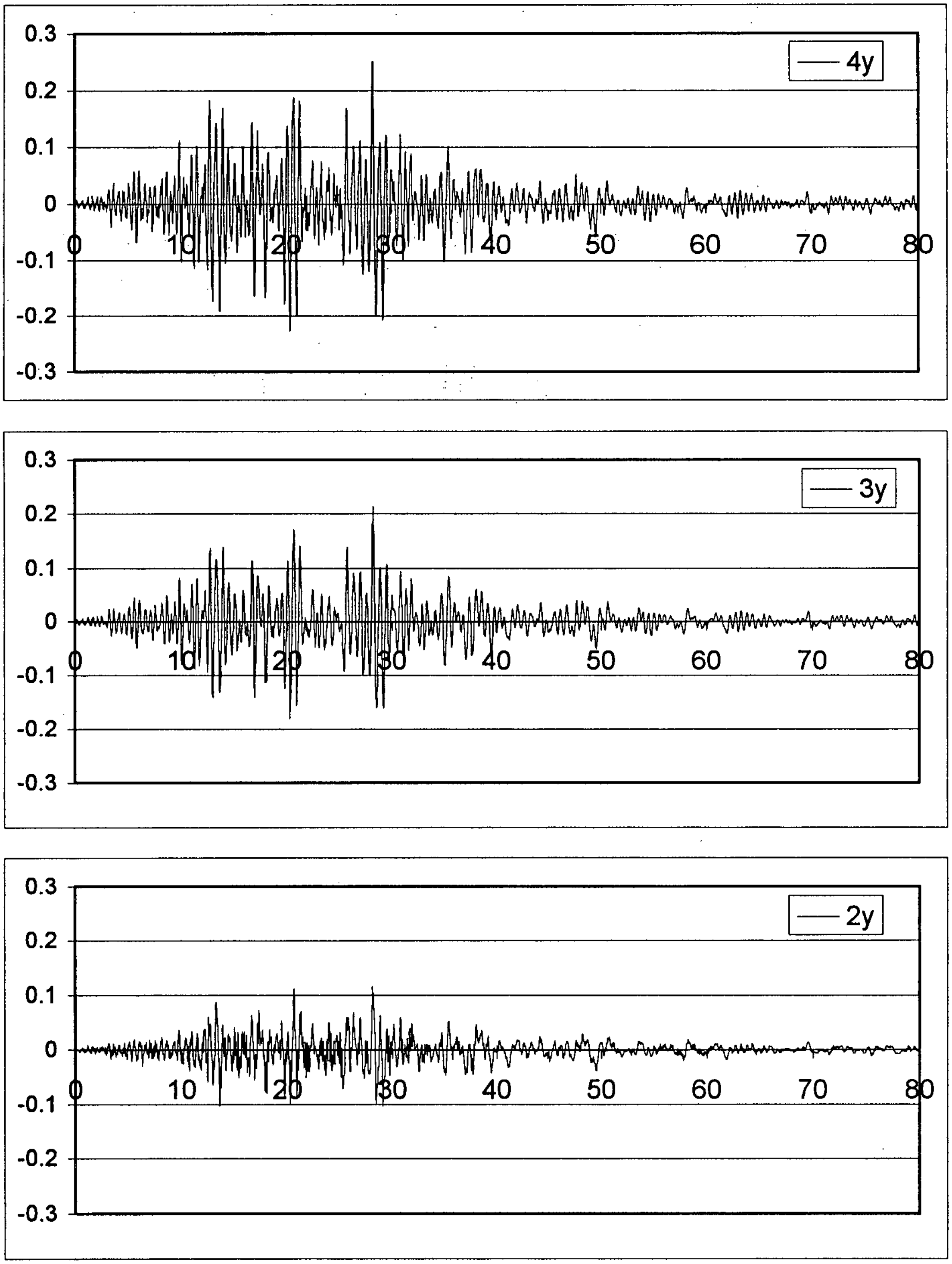

Figure A6 Absolute accelerations of the upper floors of the San Bernardino 3-story office bldg. in the N-S (Y) direction, obtained from the 1992 Landers EQ records.

APPENDIX B

Samples of ME'scope outputs.

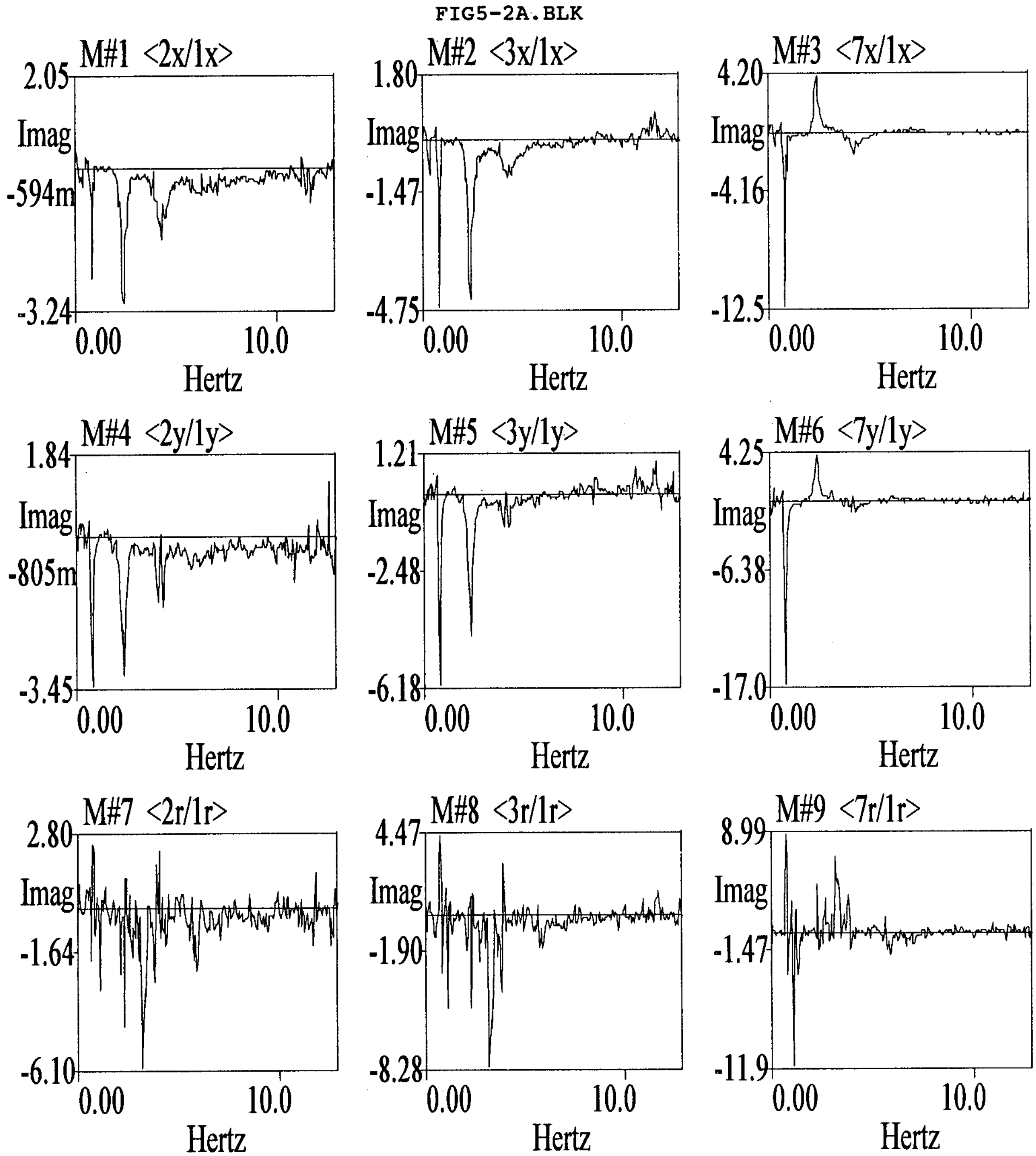

Figure B1 Frequency Response Functions of the instrumented floors of the Burbank 6-Story Bldg., obtained from the 1987 Whittier EQ records. (Plots of the Imaginary part of the complex values)

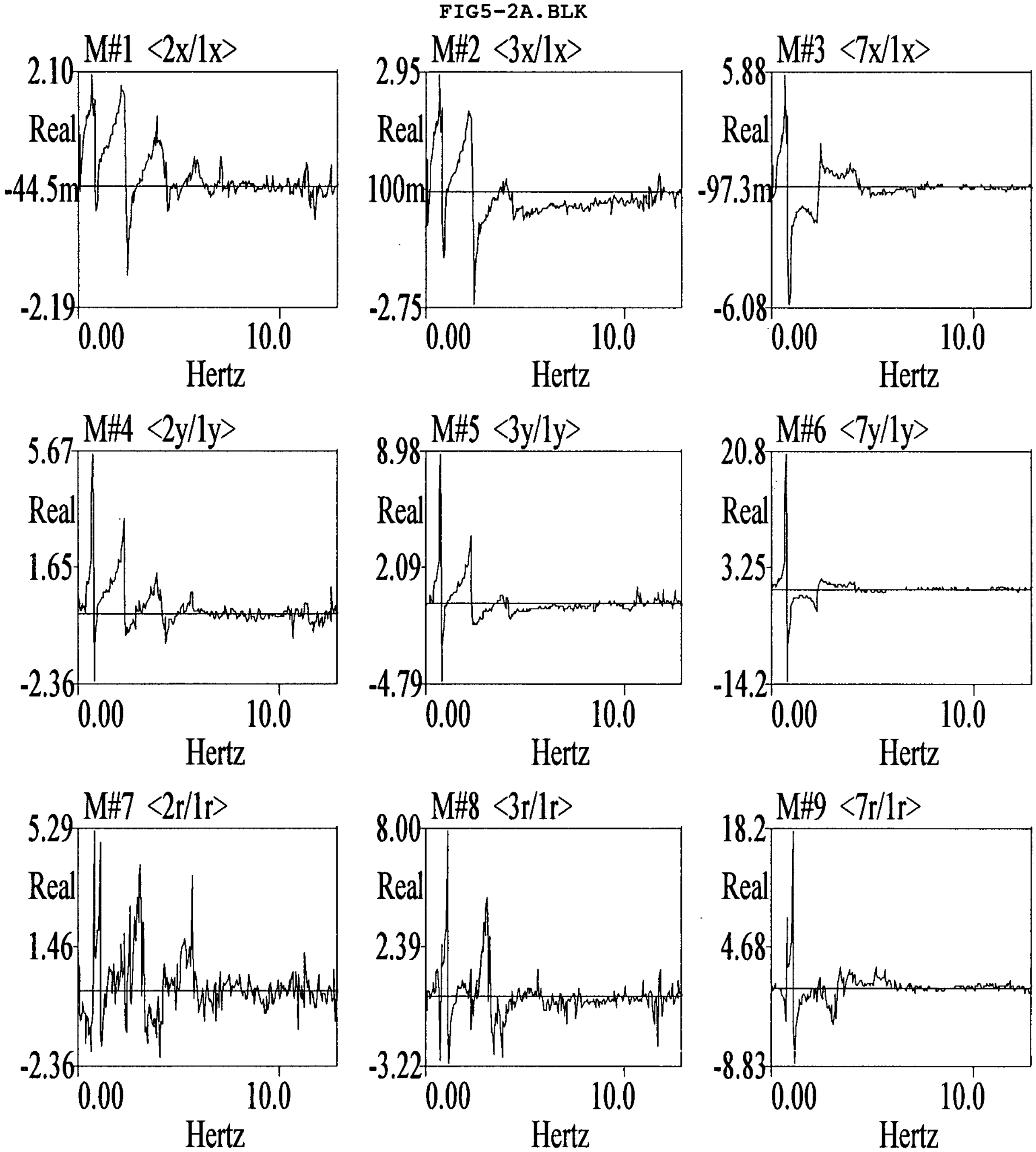

Figure B2 Frequency Response Functions of the instrumented floors of the Burbank 6-Story Bldg., obtained from the 1987 Whittier EQ records. (Plot of the Real part of the complex values)

FIG5-2A.BLK

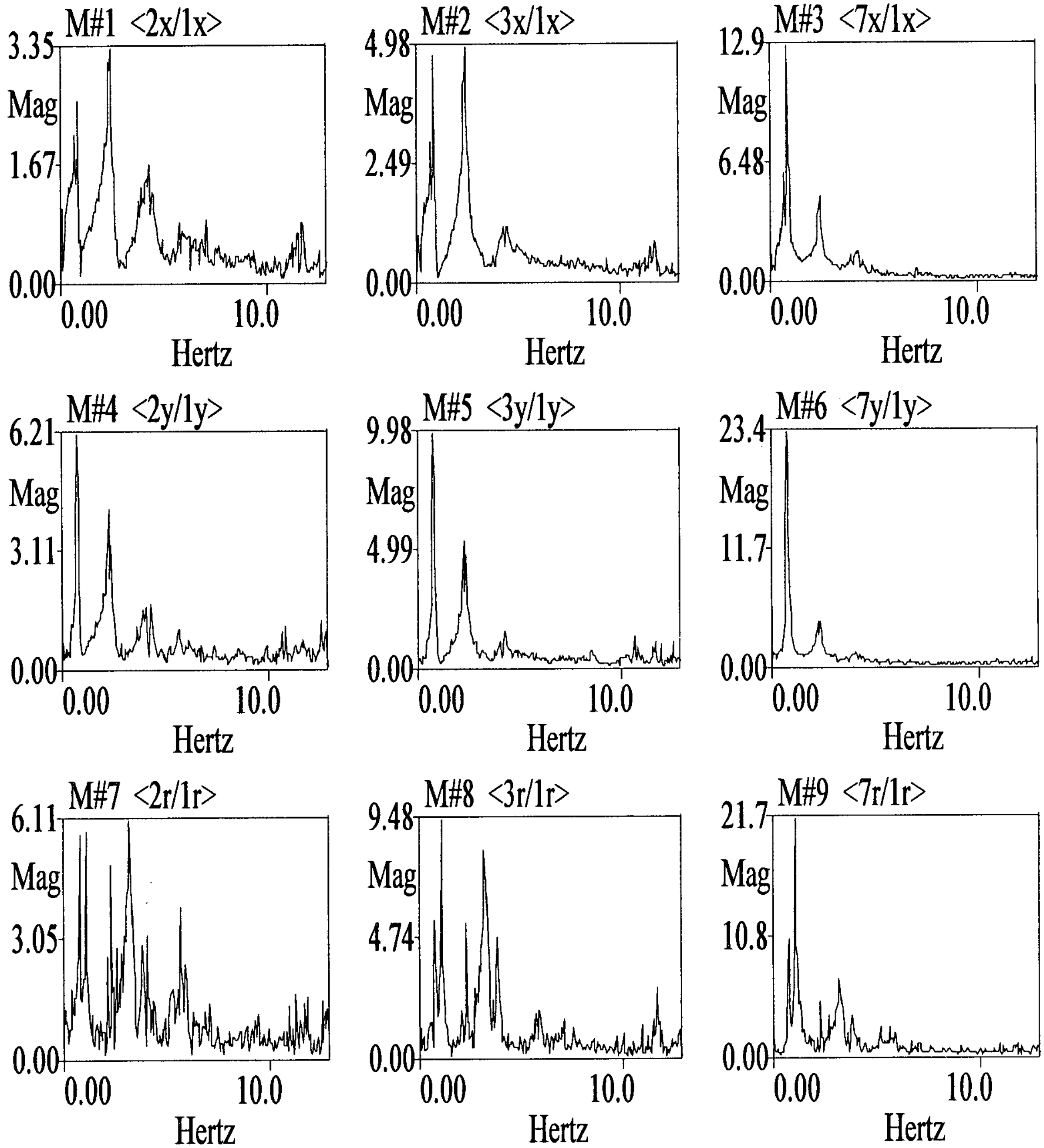

Figure B3 Frequency Response Functions of the instrumented floors of the Burbank 6-Story Bldg., obtained from the 1987 Whittier EQ records. (Plot of the Magnitude of the complex values)

FIG5-2A.BLK

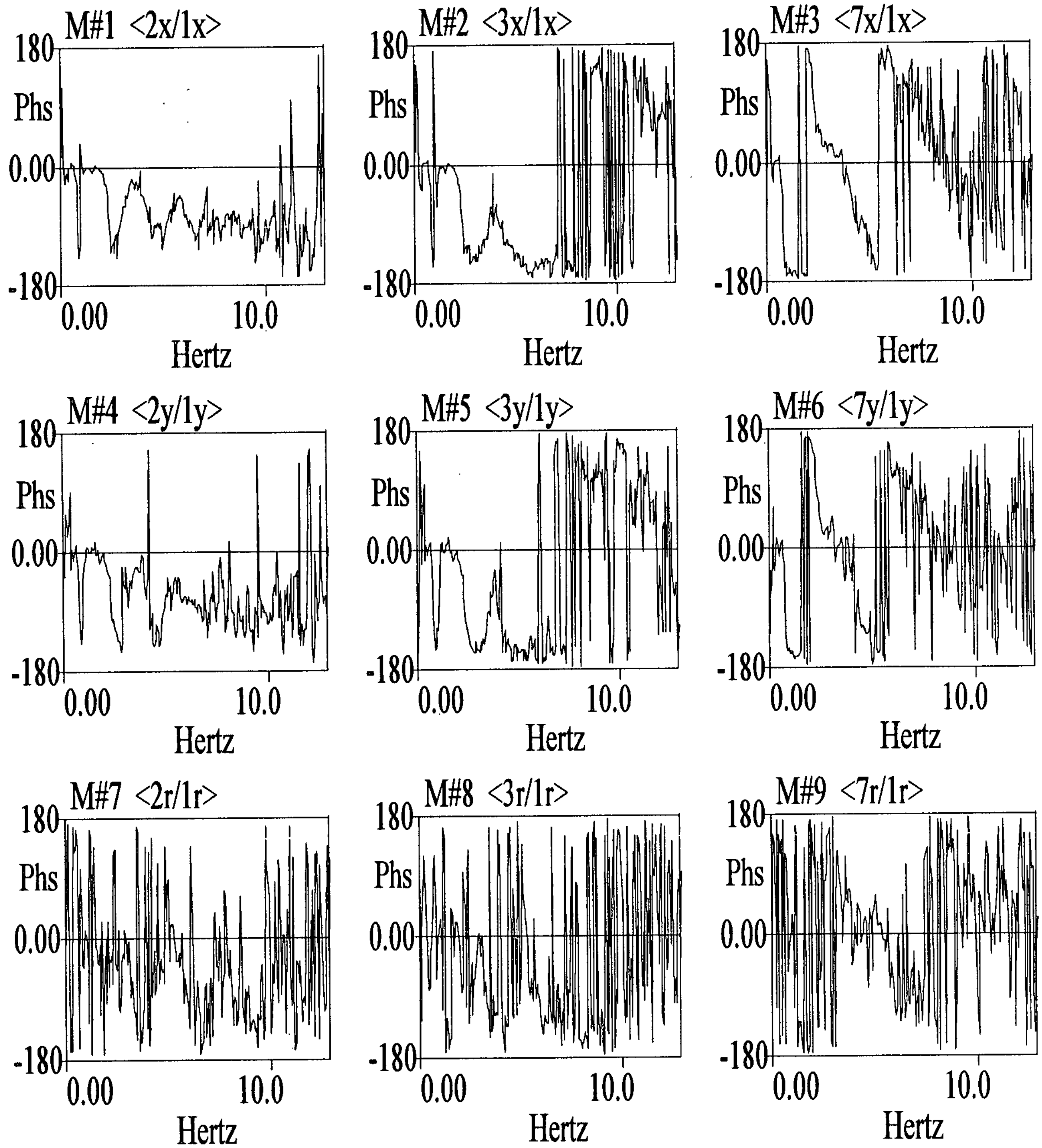

Figure B4 Frequency Response Functions of the instrumented floors of the Burbank 6-Story Bldg., obtained from the 1987 Whittier EQ records. (Plots of the Phase angle)

BURBA-N.STR

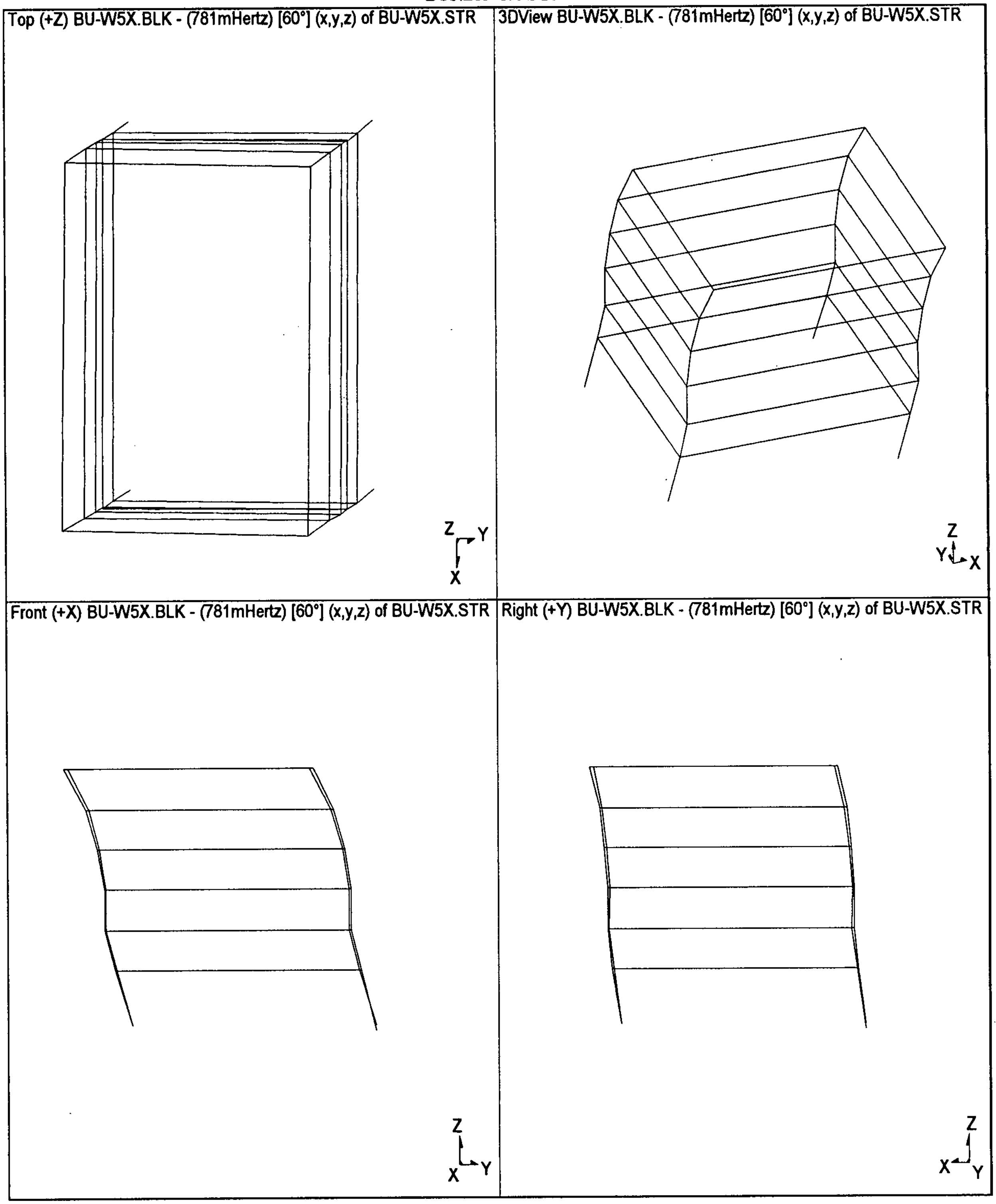

Figure B5 1st translational mode shape of the Burbank 6-story bldg., obtained from the 1987 Whittier EQ records.

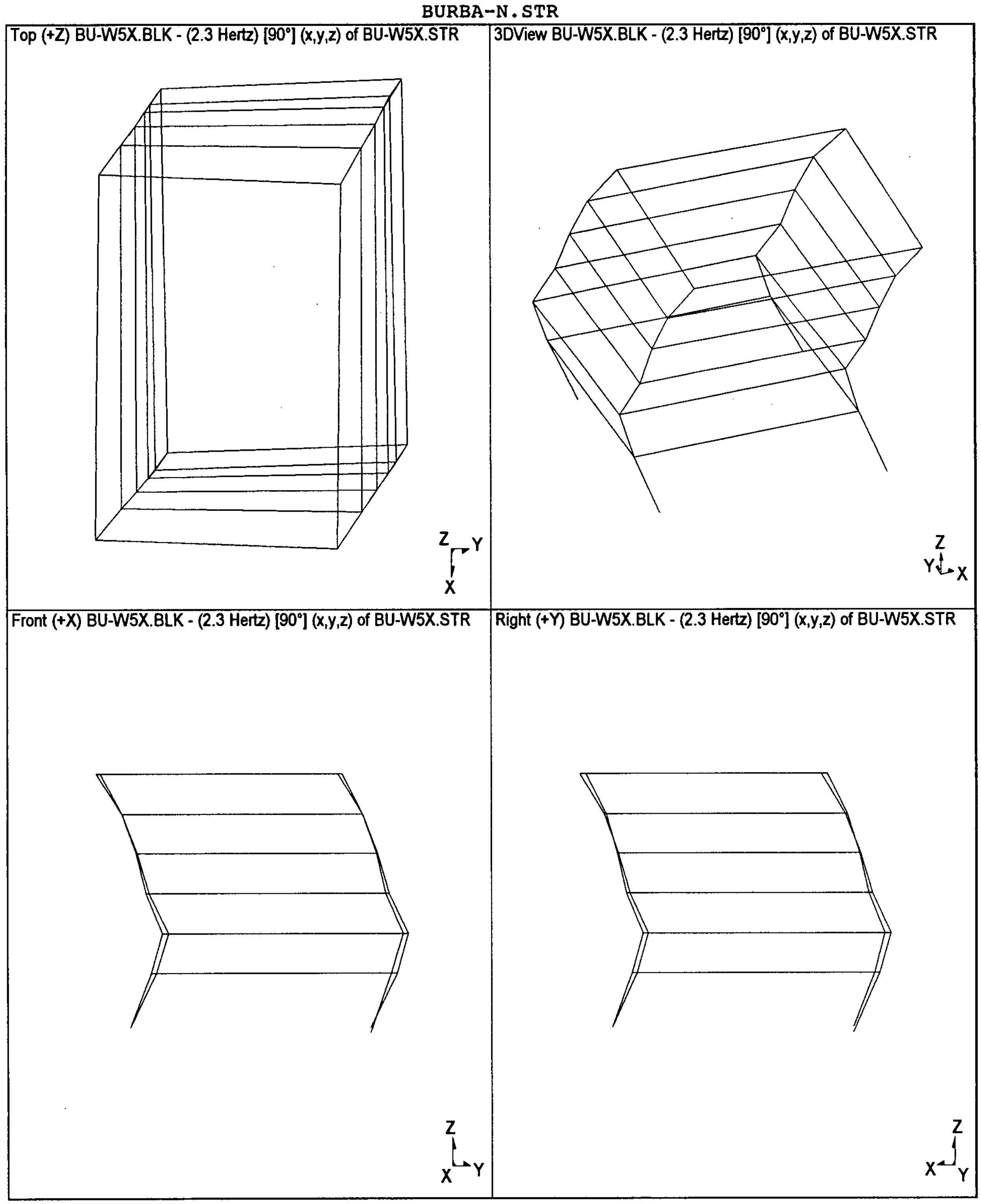

Figure B6 2nd translational mode shape of the Burbank 6-story bldg., obtained from the 1987 Whittier EQ records.

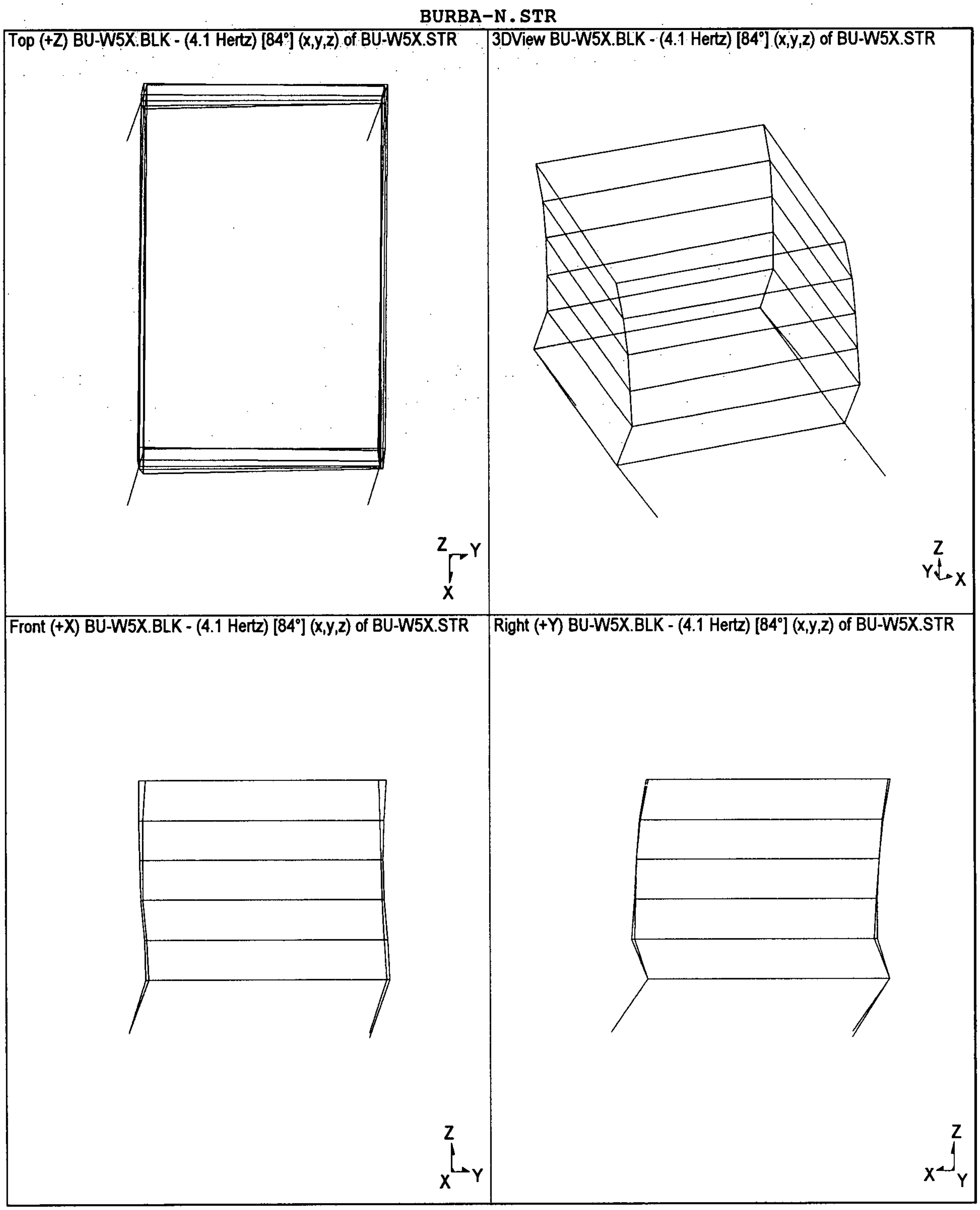

Figure B7 3rd translational mode shape of the Burbank 6-story bldg., obtained from the 1987 Whittier EQ records.

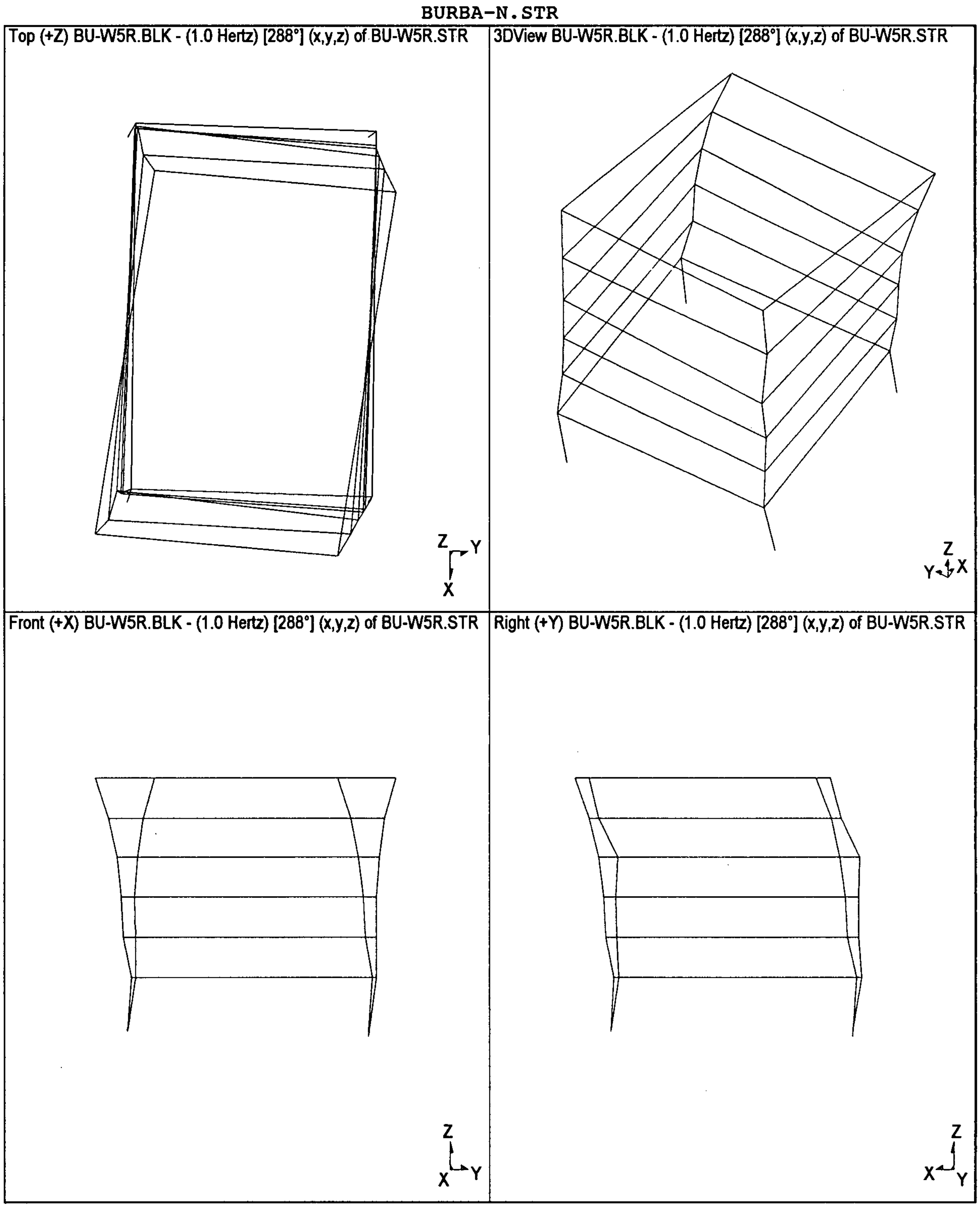

Figure B8 1st torsional mode shape of the Burbank 6-story bldg., obtained from the 1987 Whittier EQ records.

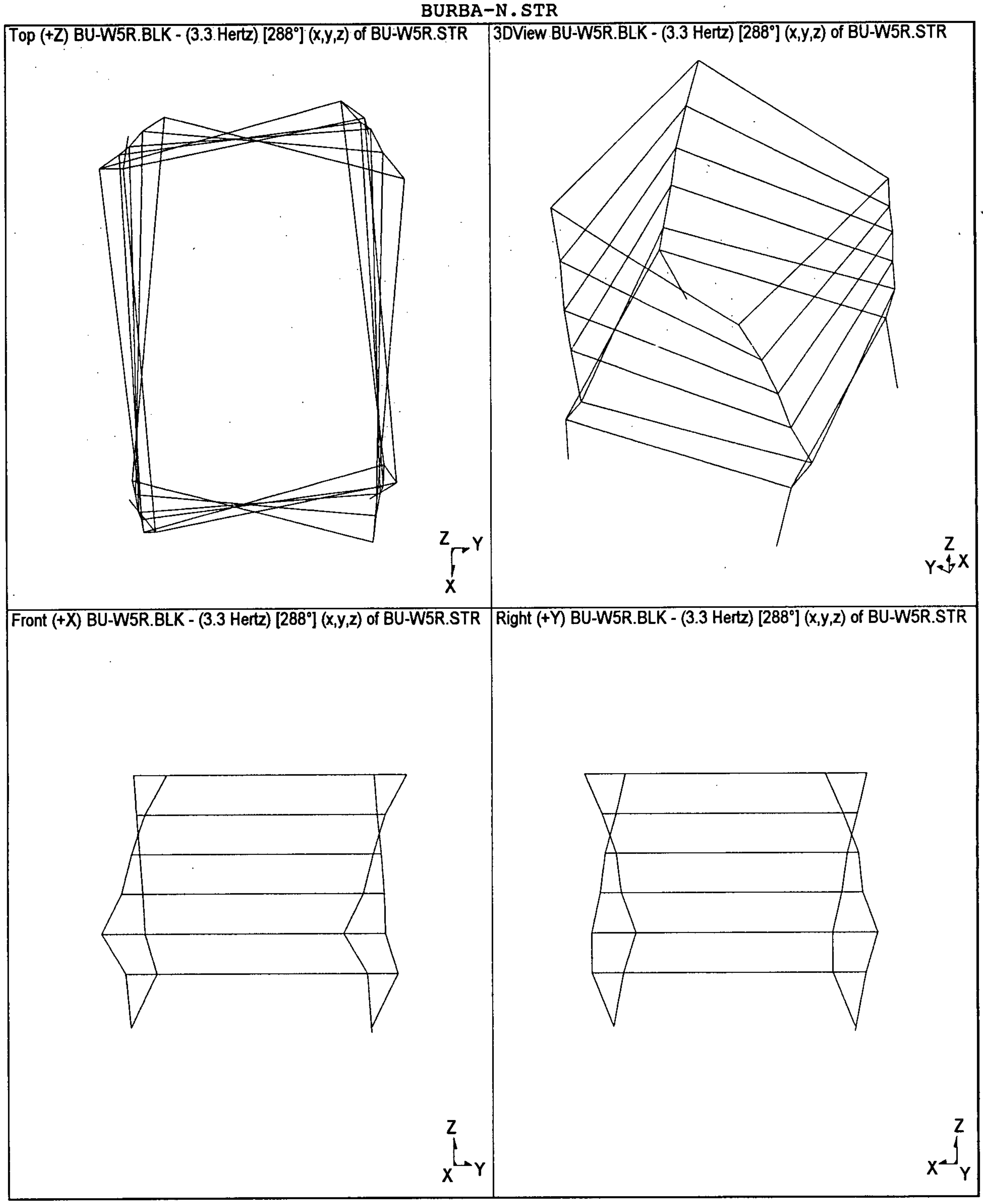

Figure B9 2nd torsional mode shape of the Burbank 6-story bldg., obtained from the 1987 Whittier EQ records.

APPENDIX C

Selected parts of the CANNY-E input file for Model A

```
Nonlinier dynamic analysis of Burbank Federal Savings Bldg.

* Ground motion recorded in Northridge EQ
* Including Vertical & rotational ground motion
* P-D effects included
* No Soil Structure Interaction
* 3.50% damping

// analysis assumptions and output options

title :  Burbank,#1, Nonlinear, 3.50% damping
force unit = N
length unit = m
time unit = sec

P-Delta
floor rotation
gravity acceleration is 9.807
output of overall response at floor levels
output of nodal displacement, velocity and acceleration
output all of beams, column results
output of extreme responses

// control data of static analysis
loading direction in 0 degree (from X-axis)
master DOFs for analysis control : X-translation at 7F
displacement limit 5.0
binary format output of analysis results at every 1-step
destination base shear factor 1.0 by increment 0.01
/*destination displacement 0.3 by increment 0.002
/*destination displacement 0.4 by increment 0.005
//

// control data of dynamic response
master DOFs for analysis control : X-translation at 7F
integration 1-step for one acceleration data
integration time interval 0.02
start time 0.0, end time  60.0
check peak displacement 0.02
response limit 5.0
master DOFs for analysis control : 7F X-translation
binary format output of response results at every 1-step
Newmark method using Beta-value 0.25
damping constant 0.0350 to first mode
damping constant 0.0350 to second mode
/*damping in time-varying frequency
scale factor 1 to X-EQ file = c:\canny\burbank\burb-n.ew
scale factor 1 to Y-EQ file = c:\canny\burbank\burb-n.ns
scale factor 1 to R-EQ file = c:\canny\burbank\burb-n.rt
scale factor 1 to Z-EQ file = c:\canny\burbank\burb-n.up

// ----------- node locations ------------------
X1 , Y1,  1F
X3 , Y1,  1F
X5 , Y1,  1F
X7 , Y1,  1F
X9 , Y1,  1F
X11, Y1,  1F
X13, Y1,  1F
X1 , Y3,  1F
X13, Y3,  1F
X4 , Y4,  1F
X7 , Y4,  1F
X10, Y4,  1F
X1 , Y5,  1F
X13, Y5,  1F
X4 , Y6,  1F
X7 , Y6,  1F
X10, Y6,  1F
X1 , Y7,  1F
X13, Y7,  1F
```

```
X4 , Y8,  1F
X7 , Y8,  1F
X10, Y8,  1F
X1 , Y9,  1F
X13, Y9,  1F
X4 , Y10, 1F
X7 , Y10, 1F
X10, Y10, 1F
X1 , Y11, 1F
X13, Y11, 1F
X1 , Y13, 1F
X3 , Y13, 1F
X5 , Y13, 1F
X7 , Y13, 1F
X9 , Y13, 1F
X11, Y13, 1F
X13, Y13, 1F
X1~X13, Y1~Y13,   2F~7F
//
// ------------ node degrees of freedom -------------------
general DOFs: all components
node X1 , Y1,  1F  eliminate all components
node X3 , Y1,  1F  eliminate all components
node X5 , Y1,  1F  eliminate all components
node X7 , Y1,  1F  eliminate all components
node X9 , Y1,  1F  eliminate all components
node X11, Y1,  1F  eliminate all components
node X13, Y1,  1F  eliminate all components
node X1 , Y3,  1F  eliminate all components
node X13, Y3,  1F  eliminate all components
node X4 , Y4,  1F  eliminate all components
node X7 , Y4,  1F  eliminate all components
node X10, Y4,  1F  eliminate all components
node X1 , Y5,  1F  eliminate all components
node X13, Y5,  1F  eliminate all components
node X4 , Y6,  1F  eliminate all components
node X7 , Y6,  1F  eliminate all components
node X10, Y6,  1F  eliminate all components
node X1 , Y7,  1F  eliminate all components
node X13, Y7,  1F  eliminate all components
node X4 , Y8,  1F  eliminate all components
node X7 , Y8,  1F  eliminate all components
node X10, Y8,  1F  eliminate all components
node X1 , Y9,  1F  eliminate all components
node X13, Y9,  1F  eliminate all components
node X4 , Y10, 1F  eliminate all components
node X7 , Y10, 1F  eliminate all components
node X10, Y10, 1F  eliminate all components
node X1 , Y11, 1F  eliminate all components
node X13, Y11, 1F  eliminate all components
node X1 , Y13, 1F  eliminate all components
node X3 , Y13, 1F  eliminate all components
node X5 , Y13, 1F  eliminate all components
node X7 , Y13, 1F  eliminate all components
node X9 , Y13, 1F  eliminate all components
node X11, Y13, 1F  eliminate all components
node X13, Y13, 1F  eliminate all components
//
// node weight
node   X1 , Y1,  2F        w = 0
node   X2 , Y1,  2F        w = 52150
node   X3 , Y1,  2F        w = 26100
node   X4 , Y1,  2F        w = 192400
node   X5 , Y1,  2F        w = 26100
node   X6 , Y1,  2F        w = 52150
node   X7 , Y1,  2F        w = 192400
node   X8 , Y1,  2F        w = 52150
node   X9 , Y1,  2F        w = 26100
node   X10, Y1,  2F        w = 192400
node   X11, Y1,  2F        w = 26100
node   X12, Y1,  2F        w = 52150
```

```
node   X13, Y1,  2F        w = 0
node   X1 , Y13, 2F       w = 0
node   X2 , Y13, 2F       w = 52150
node   X3 , Y13, 2F       w = 26100
node   X4 , Y13, 2F       w = 192400
node   X5 , Y13, 2F       w = 26100
node   X6 , Y13, 2F       w = 52150
node   X7 , Y13, 2F       w = 192400
node   X8 , Y13, 2F       w = 52150
node   X9 , Y13, 2F       w = 26100
node   X10, Y13, 2F       w = 192400
node   X11, Y13, 2F       w = 26100
node   X12, Y13, 2F       w = 52150
node   X13, Y13, 2F       w = 0
node   X1 , Y2 , 2F        w = 89600
node   X1 , Y3 , 2F        w = 44800
node   X1 , Y4 , 2F        w = 89600
node   X1 , Y5 , 2F        w = 44800
node   X1 , Y6 , 2F        w = 89600
node   X1 , Y7 , 2F        w = 44800
node   X1 , Y8 , 2F        w = 89600
node   X1 , Y9 , 2F        w = 44800
node   X1 , Y10, 2F        w = 89600
node   X1 , Y11, 2F        w = 44800
node   X1 , Y12, 2F        w = 89600
node   X13, Y2 , 2F       w = 89600
node   X13, Y3 , 2F       w = 44800
node   X13, Y4 , 2F       w = 89600
node   X13, Y5 , 2F       w = 44800
node   X13, Y6 , 2F       w = 89600
node   X13, Y7 , 2F       w = 44800
node   X13, Y8 , 2F       w = 89600
node   X13, Y9 , 2F       w = 44800
node   X13, Y10, 2F       w = 89600
node   X13, Y11, 2F       w = 44800
node   X13, Y12, 2F       w = 89600

node   X1 , Y1,  3F        w = 0
node   X2 , Y1,  3F        w = 31300
node   X3 , Y1,  3F        w = 15600
node   X4 , Y1,  3F        w = 124800
node   X5 , Y1,  3F        w = 15600
..........................................................

..........................................................
node   X13, Y10, 7F       w = 89600
node   X13, Y11, 7F       w = 44800
node   X13, Y12, 7F       w = 89600
//

// ----------- floor level -----------
7F(rigid) Z=24.994 G(18.660,18.300), W=6577000  Rj=1900000000
6F(rigid) Z=21.031 G(18.288,18.288), W=4817000  Rj=1150000000
5F(rigid) Z=17.069 G(18.288,18.288), W=4817000  Rj=1150000000
4F(rigid) Z=13.106 G(18.288,18.288), W=4839000  Rj=1200000000
3F(rigid) Z=9.144  G(18.288,18.288), W=4965000  Rj=1250000000
2F(rigid) Z=5.182  G(18.288,18.288), W=6085000  Rj=1800000000
1F(fixed) Z=0
//
// frame locations
X1: 0
X2: 3.048
X3: 6.096
X4: 9.144
X5: 12.192
X6: 15.24
X7: 18.288
X8: 21.336
X9: 24.384
X10: 27.432
X11: 30.48
```

```
X12: 33.528
X13: 36.576
Y1: 0
Y2: 3.048
Y3: 6.096
Y4: 9.144
Y5: 12.192
Y6: 15.24
Y7: 18.288
Y8: 21.336
Y9: 24.384
Y10: 27.432
Y11: 30.48
Y12: 33.528
Y13: 36.576
//
// element data : beam
/* 2nd floor perimeter beams
frame Y1, X1-X2,      2F LU100 RU100 SU200 r(0.19 0.00  /* w30x116
frame Y1, X2-X3,      2F LU100 RU100 SU200 r(0.00 0.19  /* w30x116
frame Y1, X3-X4,      2F LU100 RU100 SU200 r(0.19 0.00  /* w30x116
frame Y1, X4-X5,      2F LU100 RU100 SU200 r(0.00 0.19  /* w30x116
frame Y1, X5-X6,      2F LU100 RU100 SU200 r(0.19 0.00  /* w30x116
frame Y1, X6-X7,      2F LU100 RU100 SU200 r(0.00 0.19  /* w30x116
frame Y1, X7-X8,      2F LU100 RU100 SU200 r(0.19 0.00  /* w30x116
frame Y1, X8-X9,      2F LU100 RU100 SU200 r(0.00 0.19  /* w30x116
frame Y1, X9-X10,     2F LU100 RU100 SU200 r(0.19 0.00  /* w30x116
frame Y1, X10-X11,    2F LU100 RU100 SU200 r(0.00 0.19  /* w30x116
frame Y1, X11-X12,    2F LU100 RU100 SU200 r(0.19 0.00  /* w30x116
frame Y1, X12-X13,    2F LU100       SU200 r(0.00 0.00  /* w30x116

frame Y13, X1-X2,     2F       RU100 SU200 r(0.00 0.00  /* w30x116
frame Y13, X2-X3,     2F LU100 RU100 SU200 r(0.00 0.19  /* w30x116
frame Y13, X3-X4,     2F LU100 RU100 SU200 r(0.19 0.00  /* w30x116
frame Y13, X4-X5,     2F LU100 RU100 SU200 r(0.00 0.19  /* w30x116
frame Y13, X5-X6,     2F LU100 RU100 SU200 r(0.19 0.00  /* w30x116
frame Y13, X6-X7,     2F LU100 RU100 SU200 r(0.00 0.19  /* w30x116
frame Y13, X7-X8,     2F LU100 RU100 SU200 r(0.19 0.00  /* w30x116
frame Y13, X8-X9,     2F LU100 RU100 SU200 r(0.00 0.19  /* w30x116
frame Y13, X9-X10,    2F LU100 RU100 SU200 r(0.19 0.00  /* w30x116
frame Y13, X10-X11,   2F LU100 RU100 SU200 r(0.00 0.19  /* w30x116
frame Y13, X11-X12,   2F LU100 RU100 SU200 r(0.19 0.00  /* w30x116
frame Y13, X12-X13,   2F LU100 RU100 SU200 r(0.00 0.19  /* w30x116

frame X1, Y1-Y2,      2F       RU100 SU200 r(0.00 0.00  /* w30x116
frame X1, Y2-Y3,      2F LU100 RU100 SU200 r(0.00 0.19  /* w30x116
frame X1, Y3-Y4,      2F LU100 RU100 SU200 r(0.19 0.00  /* w30x116
frame X1, Y4-Y5,      2F LU100 RU100 SU200 r(0.00 0.19  /* w30x116
frame X1, Y5-Y6,      2F LU100 RU100 SU200 r(0.19 0.00  /* w30x116
frame X1, Y6-Y7,      2F LU100 RU100 SU200 r(0.00 0.19  /* w30x116
frame X1, Y7-Y8,      2F LU100 RU100 SU200 r(0.19 0.00  /* w30x116
frame X1, Y8-Y9,      2F LU100 RU100 SU200 r(0.00 0.19  /* w30x116
frame X1, Y9-Y10,     2F LU100 RU100 SU200 r(0.19 0.00  /* w30x116
frame X1, Y10-Y11,    2F LU100 RU100 SU200 r(0.00 0.19  /* w30x116
frame X1, Y11-Y12,    2F LU100 RU100 SU200 r(0.19 0.00  /* w30x116
frame X1, Y12-Y13,    2F LU100 RU100 SU200 r(0.00 0.19  /* w30x116

frame X13, Y1-Y2,     2F LU100 RU100 SU200 r(0.19 0.00  /* w30x116
frame X13, Y2-Y3,     2F LU100 RU100 SU200 r(0.00 0.19  /* w30x116
frame X13, Y3-Y4,     2F LU100 RU100 SU200 r(0.19 0.00  /* w30x116
frame X13, Y4-Y5,     2F LU100 RU100 SU200 r(0.00 0.19  /* w30x116
frame X13, Y5-Y6,     2F LU100 RU100 SU200 r(0.19 0.00  /* w30x116
frame X13, Y6-Y7,     2F LU100 RU100 SU200 r(0.00 0.19  /* w30x116
frame X13, Y7-Y8,     2F LU100 RU100 SU200 r(0.19 0.00  /* w30x116
frame X13, Y8-Y9,     2F LU100 RU100 SU200 r(0.00 0.19  /* w30x116
frame X13, Y9-Y10,    2F LU100 RU100 SU200 r(0.19 0.00  /* w30x116
frame X13, Y10-Y11,   2F LU100 RU100 SU200 r(0.00 0.19  /* w30x116
frame X13, Y11-Y12,   2F LU100 RU100 SU200 r(0.19 0.00  /* w30x116
frame X13, Y12-Y13,   2F LU100       SU200 r(0.00 0.00  /* w30x116

/* 2nd floor interior beams
```

```
frame Y2, X1-X2,     2F     LU101 RU101 SU201               /* w16x26
frame Y2, X2-X3,     2F     LU101 RU101 SU201               /* w16x26
frame Y2, X3-X4,     2F     LU101 RU101 SU201               /* w16x26
frame Y2, X4-X5,     2F           RU102 SU202               /* w16x31
frame Y2, X5-X6,     2F     LU102 RU102 SU202               /* w16x31
frame Y2, X6-X7,     2F     LU102 RU102 SU202               /* w16x31
frame Y2, X7-X8,     2F           RU101 SU201               /* w16x26
frame X12, Y4-Y5,     7F     LU999 RU999 SU201              /* ??  ??
frame X12, Y5-Y6,     7F     LU999 RU999 SU201              /* ??  ??
frame X12, Y6-Y7,     7F     LU999 RU999 SU201              /* ??  ??
frame X12, Y7-Y8,     7F     LU999 RU999 SU201              /* ??  ??
frame X12, Y8-Y9,     7F     LU999 RU999 SU201              /* ??  ??
frame X12, Y9-Y10,    7F     LU999 RU999 SU201              /* ??  ??
frame X12, Y10-Y11,   7F     LU999 RU999 SU201              /* ??  ??
frame X12, Y11-Y12,   7F     LU999 RU999 SU201              /* ??  ??
frame X12, Y12-Y13,   7F     LU999 RU999 SU201              /* ??  ??
.............................................................

.............................................................


// element data : column
/*
/* 1st story columns
/*
X1  Y1  1-2F BX301 BY301 TX301 TY301 SX401 SY401 AU501 r(0.00 0.38 /* w14x184 H
X3  Y1  1-2F BX301 BY301 TX301 TY301 SX401 SY401 AU501 r(0.00 0.38 /* w14x184 H
X5  Y1  1-2F BX301 BY301 TX301 TY301 SX401 SY401 AU501 r(0.00 0.38 /* w14x184 H
X7  Y1  1-2F BX301 BY301 TX301 TY301 SX401 SY401 AU501 r(0.00 0.38 /* w14x184 H
X9  Y1  1-2F BX301 BY301 TX301 TY301 SX401 SY401 AU501 r(0.00 0.38 /* w14x184 H
X11 Y1  1-2F BX301 BY301 TX301 TY301 SX401 SY401 AU501 r(0.00 0.38 /* w14x184 H
X13 Y1  1-2F BX302 BY302 TX302 TY302 SX402 SY402 AU502 r(0.00 0.38 /* w14x184 I
X1  Y3  1-2F BX302 BY302 TX302 TY302 SX402 SY402 AU502 r(0.00 0.38 /* w14x184 I
X13 Y3  1-2F BX302 BY302 TX302 TY302 SX402 SY402 AU502 r(0.00 0.38 /* w14x184 I
X4  Y4  1-2F BX304 BY304 TX304 TY304 SX404 SY404 AU504             /* w14x87  I
X7  Y4  1-2F BX303 BY303 TX303 TY303 SX403 SY403 AU503             /* w14x87  H
X10 Y4  1-2F BX304 BY304 TX304 TY304 SX404 SY404 AU504             /* w14x87  I
X1  Y5  1-2F BX302 BY302 TX302 TY302 SX402 SY402 AU502 r(0.00 0.38 /* w14x184 I
X13 Y5  1-2F BX302 BY302 TX302 TY302 SX402 SY402 AU502 r(0.00 0.38 /* w14x184 I
X4  Y6  1-2F BX303 BY303 TX303 TY303 SX403 SY403 AU503             /* w14x87  H
X7  Y6  1-2F BX305 BY305 TX305 TY305 SX405 SY405 AU505   /* w14x111 I  longer
X10 Y6  1-2F BX306 BY306 TX306 TY306 SX406 SY406 AU506             /* w14x95  H
X1  Y7  1-2F BX302 BY302 TX302 TY302 SX402 SY402 AU502 r(0.00 0.38 /* w14x184 I
X13 Y7  1-2F BX302 BY302 TX302 TY302 SX402 SY402 AU502 r(0.00 0.38 /* w14x184 I
X4  Y8  1-2F BX303 BY303 TX303 TY303 SX403 SY403 AU503             /* w14x87  H
X7  Y8  1-2F BX307 BY307 TX307 TY307 SX407 SY407 AU507             /* w14x95  I
X10 Y8  1-2F BX306 BY306 TX306 TY306 SX406 SY406 AU506             /* w14x95  H
X1  Y9  1-2F BX302 BY302 TX302 TY302 SX402 SY402 AU502 r(0.00 0.38 /* w14x184 I
X13 Y9  1-2F BX302 BY302 TX302 TY302 SX402 SY402 AU502 r(0.00 0.38 /* w14x184 I
X4  Y10 1-2F BX304 BY304 TX304 TY304 SX404 SY404 AU504             /* w14x87  I
X7  Y10 1-2F BX306 BY306 TX306 TY306 SX406 SY406 AU506             /* w14x95  H
X10 Y10 1-2F BX307 BY307 TX307 TY307 SX407 SY407 AU507             /* w14x95  I
X1  Y11 1-2F BX302 BY302 TX302 TY302 SX402 SY402 AU502 r(0.00 0.38 /* w14x184 I
X13 Y11 1-2F BX302 BY302 TX302 TY302 SX402 SY402 AU502 r(0.00 0.38 /* w14x184 I
X1  Y13 1-2F BX302 BY302 TX302 TY302 SX402 SY402 AU502 r(0.00 0.38 /* w14x184 I
X3  Y13 1-2F BX301 BY301 TX301 TY301 SX401 SY401 AU501 r(0.00 0.38 /* w14x184 H
X5  Y13 1-2F BX301 BY301 TX301 TY301 SX401 SY401 AU501 r(0.00 0.38 /* w14x184 H
X7  Y13 1-2F BX301 BY301 TX301 TY301 SX401 SY401 AU501 r(0.00 0.38 /* w14x184 H
X9  Y13 1-2F BX301 BY301 TX301 TY301 SX401 SY401 AU501 r(0.00 0.38 /* w14x184 H
X11 Y13 1-2F BX301 BY301 TX301 TY301 SX401 SY401 AU501 r(0.00 0.38 /* w14x184 H
X13 Y13 1-2F BX301 BY301 TX301 TY301 SX401 SY401 AU501 r(0.00 0.38 /* w14x184 H
/*
/*  2nd story columns
/*
X1  Y1  2-3F BX301 BY301 TX301 TY301 SX401 SY401 AU501 r(0.38 0.34 /* w14x184 H
X3  Y1  2-3F BX301 BY301 TX301 TY301 SX401 SY401 AU501 r(0.38 0.34 /* w14x184 H
X5  Y1  2-3F BX301 BY301 TX301 TY301 SX401 SY401 AU501 r(0.38 0.34 /* w14x184 H
X7  Y1  2-3F BX301 BY301 TX301 TY301 SX401 SY401 AU501 r(0.38 0.34 /* w14x184 H
X9  Y1  2-3F BX301 BY301 TX301 TY301 SX401 SY401 AU501 r(0.38 0.34 /* w14x184 H
X11 Y1  2-3F BX301 BY301 TX301 TY301 SX401 SY401 AU501 r(0.38 0.34 /* w14x184 H
```

```
X13 Y1  2-3F BX302 BY302 TX302 TY302 SX402 SY402 AU502 r(0.38 0.34 /* w14x184 I
.........................................................

.........................................................

//

// stiffness and hysteresis parameters
/*
/* Beams  Bending section properties
/*
U100 CA3 2.0e+11  2060e-6 C(1614.6e3,1614.6e3) Y(1615e3,1615e3) A(1,1) B(0.02,0.02) P(0.3 0.75) /*
w30x116
U101 CA3 2.0e+11   127e-6 C(0189.8e3,0189.8e3) Y(0190e3,0190e3) A(1,1) B(0.02,0.02) P(0.3 0.75) /*
w16x26
U102 CA3 2.0e+11   156e-6 C(0230.1e3,0230.1e3) Y(0231e3,0231e3) A(1,1) B(0.02,0.02) P(0.3 0.75) /*
w16x31
U103 CA3 2.0e+11   985e-6 C(0954.2e3,0954.2e3) Y(0955e3,0955e3) A(1,1) B(0.02,0.02) P(0.3 0.75) /*
w24x84
U104 CA3 2.0e+11   370e-6 C(0475.8e3,0475.8e3) Y(0476e3,0476e3) A(1,1) B(0.02,0.02) P(0.3 0.75) /*
w18x55
U105 CA3 2.0e+11   186e-6 C(0273.0e3,0273.0e3) Y(0274e3,0274e3) A(1,1) B(0.02,0.02) P(0.3 0.75) /*
w16x36
U106 CA3 2.0e+11  1510e-6 C(1300.0e3,1300.0e3) Y(1301e3,1301e3) A(1,1) B(0.02,0.02) P(0.3 0.75) /*
w27x102
U107 CA3 2.0e+11  1190e-6 C(1042.6e3,1042.6e3) Y(1043e3,1043e3) A(1,1) B(0.02,0.02) P(0.3 0.75) /*
w27x84
U108 CA3 2.0e+11   764e-6 C(0754.0e3,0754.0e3) Y(0755e3,0755e3) A(1,1) B(0.02,0.02) P(0.3 0.75) /*
w24x68
U109 CA3 2.0e+11   246e-6 C(0353.6e3,0353.6e3) Y(0354e3,0354e3) A(1,1) B(0.02,0.02) P(0.3 0.75) /*
w16x45
U110 CA3 2.0e+11  1120e-6 C(1079.0e3,1079.0e3) Y(1080e3,1080e3) A(1,1) B(0.02,0.02) P(0.3 0.75) /*
w24x94
U111 CA3 2.0e+11   437e-6 C(0562.4e3,0562.4e3) Y(0563e3,0563e3) A(1,1) B(0.02,0.02) P(0.3 0.75) /*
w18x64
U112 CA3 2.0e+11   127e-6 C(0189.8e3,0189.8e3) Y(0190e3,0190e3) A(1,1) B(0.02,0.02) P(0.3 0.75) /*
w16x26
U113 CA3 2.0e+11   156e-6 C(0230.1e3,0230.1e3) Y(0231e3,0231e3) A(1,1) B(0.02,0.02) P(0.3 0.75) /*
w16x31
U114 CA3 2.0e+11   186e-6 C(0273.0e3,0273.0e3) Y(0274e3,0274e3) A(1,1) B(0.02,0.02) P(0.3 0.75) /*
w16x36
U115 CA3 2.0e+11   246e-6 C(0353.6e3,0353.6e3) Y(0354e3,0354e3) A(1,1) B(0.02,0.02) P(0.3 0.75) /*
w16x45
U116 CA3 2.0e+11   216e-6 C(0311.0e3,0311.0e3) Y(0312e3,0312e3) A(1,1) B(0.02,0.02) P(0.3 0.75) /*
w16x40
U117 CA3 2.0e+11   600e-6 C(0758.0e3,0758.0e3) Y(0760e3,0760e3) A(1,1) B(0.02,0.02) P(0.3 0.75) /*
w18x85
U118 CA3 2.0e+11   216e-6 C(0311.0e3,0311.0e3) Y(0312e3,0312e3) A(1,1) B(0.02,0.02) P(0.3 0.75) /*
w16x40
U119 CA3 2.0e+11   874e-6 C(0856.0e3,0856.0e3) Y(0857e3,0857e3) A(1,1) B(0.02,0.02) P(0.3 0.75) /*
w24x76
U999 EL1 2.0e+1   1000e-6
/* Beams  Shear section properties
/*
U200 EL1 0.77e+11  10820e-6    /* w30x116
U201 EL1 0.77e+11   2474e-6    /* w16x26
U202 EL1 0.77e+11   2821e-6    /* w16x31
U203 EL1 0.77e+11   7313e-6    /* w24x84
U204 EL1 0.77e+11   4577e-6    /* w18x55
U205 EL1 0.77e+11   3123e-6    /* w16x36
U206 EL1 0.77e+11   8978e-6    /* w27x102
U207 EL1 0.77e+11   8034e-6    /* w27x84
U208 EL1 0.77e+11   6181e-6    /* w24x68
U209 EL1 0.77e+11   3649e-6    /* w16x45
U210 EL1 0.77e+11   8052e-6    /* w24x94
U211 EL1 0.77e+11   4325e-6    /* w18x64
U212 EL1 0.77e+11   2474e-6    /* w16x26
U213 EL1 0.77e+11   2821e-6    /* w16x31
U214 EL1 0.77e+11   3123e-6    /* w16x36
U215 EL1 0.77e+11   3649e-6    /* w16x45
U216 EL1 0.77e+11   2337e-6    /* w16x40
```

```
U217 EL1 0.77e+11   6217e-6    /* w18x85
U218 EL1 0.77e+11   2337e-6    /* w16x40
U219 EL1 0.77e+11   6787e-6    /* w24x76
/*
/* Column Bending section properties
/*
X301 CA3 2.0e+11  944.8e-6 C(1440.1e3,1440.1e3) Y(1441e3,1441e3) A(1,1) B(0.02,0.02) P(0.3 0.75) /*
W14x184 (H)
Y301 CA3 2.0e+11  367.5e-6 C(0728.6e3,0728.6e3) Y(0729e3,0729e3) A(1,1) B(0.02,0.02) P(0.3 0.75)
X302 CA3 2.0e+11  367.5e-6 C(0728.6e3,0728.6e3) Y(0729e3,0729e3) A(1,1) B(0.02,0.02) P(0.3 0.75) /*
W14x184 (I)
Y302 CA3 2.0e+11  944.8e-6 C(1440.1e3,1440.1e3) Y(1441e3,1441e3) A(1,1) B(0.02,0.02) P(0.3 0.75)
X303 CA3 2.0e+11  402.5e-6 C(0721.4e3,0721.4e3) Y(0722e3,0722e3) A(1,1) B(0.02,0.02) P(0.3 0.75) /*
W14x87  (H)
Y303 CA3 2.0e+11  145.6e-6 C(0311.0e3,0311.0e3) Y(0312e3,0312e3) A(1,1) B(0.02,0.02) P(0.3 0.75)
X304 CA3 2.0e+11  145.6e-6 C(0311.0e3,0311.0e3) Y(0312e3,0312e3) A(1,1) B(0.02,0.02) P(0.3 0.75) /*
W14x87  (I)
Y304 CA3 2.0e+11  402.5e-6 C(0721.4e3,0721.4e3) Y(0722e3,0722e3) A(1,1) B(0.02,0.02) P(0.3 0.75)
X305 CA3 2.0e+11  189.4e-6 C(0323.8e3,0323.8e3) Y(0324e3,0324e3) A(1,1) B(0.02,0.02) P(0.3 0.75) /*
W14x111 (I)
Y305 CA3 2.0e+11  528.6e-6 C(0835.1e3,0835.1e3) Y(0836e3,0836e3) A(1,1) B(0.02,0.02) P(0.3 0.75)
X306 CA3 2.0e+11  441.2e-6 C(0707.4e3,0707.4e3) Y(0708e3,0708e3) A(1,1) B(0.02,0.02) P(0.3 0.75) /*
W14x95  (H)
Y306 CA3 2.0e+11  159.8e-6 C(0340.4e3,0340.4e3) Y(0341e3,0341e3) A(1,1) B(0.02,0.02) P(0.3 0.75)
X307 CA3 2.0e+11  159.8e-6 C(0340.4e3,0340.4e3) Y(0341e3,0341e3) A(1,1) B(0.02,0.02) P(0.3 0.75) /*
W14x95  (I)
Y307 CA3 2.0e+11  441.2e-6 C(0707.4e3,0707.4e3) Y(0708e3,0708e3) A(1,1) B(0.02,0.02) P(0.3 0.75)
X308 CA3 2.0e+11  661.8e-6 C(1035.3e3,1035.3e3) Y(1036e3,1036e3) A(1,1) B(0.02,0.02) P(0.3 0.75) /*
W14x136 (H)
Y308 CA3 2.0e+11  236.4e-6 C(0498.5e3,0498.5e3) Y(0499e3,0499e3) A(1,1) B(0.02,0.02) P(0.3 0.75)
X309 CA3 2.0e+11  236.4e-6 C(0498.5e3,0498.5e3) Y(0499e3,0499e3) A(1,1) B(0.02,0.02) P(0.3 0.75) /*
W14x136 (I)
Y309 CA3 2.0e+11  661.8e-6 C(1035.3e3,1035.3e3) Y(1036e3,1036e3) A(1,1) B(0.02,0.02) P(0.3 0.75)
X310 CA3 2.0e+11  266.8e-6 C(0434.6e3,0434.6e3) Y(0435e3,0435e3) A(1,1) B(0.02,0.02) P(0.3 0.75) /*
W14x61  (H)
Y310 CA3 2.0e+11   44.5e-6 C(0139.3e3,0139.3e3) Y(0140e3,0140e3) A(1,1) B(0.02,0.02) P(0.3 0.75)
X311 CA3 2.0e+11   44.5e-6 C(0139.3e3,0139.3e3) Y(0140e3,0140e3) A(1,1) B(0.02,0.02) P(0.3 0.75) /*
W14x61  (I)
Y311 CA3 2.0e+11  266.8e-6 C(0434.6e3,0434.6e3) Y(0435e3,0435e3) A(1,1) B(0.02,0.02) P(0.3 0.75)
X312 CA3 2.0e+11   93.7e-6 C(0242.9e3,0242.9e3) Y(0243e3,0243e3) A(1,1) B(0.02,0.02) P(0.3 0.75) /*
W14x84  (I)
Y312 CA3 2.0e+11  386.3e-6 C(0617.8e3,0617.8e3) Y(0618e3,0618e3) A(1,1) B(0.02,0.02) P(0.3 0.75)
X313 CA3 2.0e+11  407.5e-6 C(0536.8e3,0536.8e3) Y(0537e3,0537e3) A(1,1) B(0.02,0.02) P(0.3 0.75) /*
W14x74  (H)
Y313 CA3 2.0e+11   55.4e-6 C(0172.6e3,0172.6e3) Y(0173e3,0173e3) A(1,1) B(0.02,0.02) P(0.3 0.75)
X314 CA3 2.0e+11   55.4e-6 C(0172.6e3,0172.6e3) Y(0173e3,0173e3) A(1,1) B(0.02,0.02) P(0.3 0.75) /*
W14x74  (I)
Y314 CA3 2.0e+11  407.5e-6 C(0536.8e3,0536.8e3) Y(0537e3,0537e3) A(1,1) B(0.02,0.02) P(0.3 0.75)
X315 CA3 2.0e+11  178.6e-6 C(0296.9e3,0296.9e3) Y(0297e3,0297e3) A(1,1) B(0.02,0.02) P(0.3 0.75) /*
W14x43  (H)
Y315 CA3 2.0e+11   18.8e-6 C(0073.7e3,0073.7e3) Y(0074e3,0074e3) A(1,1) B(0.02,0.02) P(0.3 0.75)
X316 CA3 2.0e+11   18.8e-6 C(0073.7e3,0073.7e3) Y(0074e3,0074e3) A(1,1) B(0.02,0.02) P(0.3 0.75) /*
W14x43  (I)
Y316 CA3 2.0e+11  178.6e-6 C(0296.9e3,0296.9e3) Y(0297e3,0297e3) A(1,1) B(0.02,0.02) P(0.3 0.75)
X317 CA3 2.0e+11   50.4e-6 C(0156.8e3,0156.8e3) Y(0157e3,0157e3) A(1,1) B(0.02,0.02) P(0.3 0.75) /*
W14x68  (I)
Y317 CA3 2.0e+11  301.4e-6 C(0490.0e3,0490.0e3) Y(0491e3,0491e3) A(1,1) B(0.02,0.02) P(0.3 0.75)
X318 CA3 2.0e+11  225.6e-6 C(0371.1e3,0371.1e3) Y(0372e3,0372e3) A(1,1) B(0.02,0.02) P(0.3 0.75) /*
W14x53  (H)
Y318 CA3 2.0e+11  023.9e-6 C(0093.3e3,0093.3e3) Y(0094e3,0094e3) A(1,1) B(0.02,0.02) P(0.3 0.75)
X319 CA3 2.0e+11  023.9e-6 C(0093.3e3,0093.3e3) Y(0094e3,0094e3) A(1,1) B(0.02,0.02) P(0.3 0.75) /*
W14x53  (I)
Y319 CA3 2.0e+11  225.6e-6 C(0371.1e3,0371.1e3) Y(0372e3,0372e3) A(1,1) B(0.02,0.02) P(0.3 0.75)
X801 CA3 2.0e+11  803.3e-6 C(1440.1e3,1440.1e3) Y(1441e3,1441e3) A(1,1) B(0.02,0.02) P(0.3 0.75) /*
W14x184 (H)
Y801 CA3 2.0e+11  302.0e-6 C(0728.6e3,0728.6e3) Y(0729e3,0729e3) A(1,1) B(0.02,0.02) P(0.3 0.75)
X802 CA3 2.0e+11  302.0e-6 C(0728.6e3,0728.6e3) Y(0729e3,0729e3) A(1,1) B(0.02,0.02) P(0.3 0.75) /*
W14x184 (I)
Y802 CA3 2.0e+11  803.3e-6 C(1440.1e3,1440.1e3) Y(1441e3,1441e3) A(1,1) B(0.02,0.02) P(0.3 0.75)
X803 CA3 2.0e+11  334.7e-6 C(0721.4e3,0721.4e3) Y(0722e3,0722e3) A(1,1) B(0.02,0.02) P(0.3 0.75) /*
W14x87  (H)
```

```
Y803 CA3 2.0e+11    95.1e-6 C(0311.0e3,0311.0e3) Y(0312e3,0312e3) A(1,1) B(0.02,0.02) P(0.3 0.75)
X804 CA3 2.0e+11    95.1e-6 C(0311.0e3,0311.0e3) Y(0312e3,0312e3) A(1,1) B(0.02,0.02) P(0.3 0.75) /*
W14x87  (I)
Y804 CA3 2.0e+11  334.7e-6 C(0721.4e3,0721.4e3) Y(0722e3,0722e3) A(1,1) B(0.02,0.02) P(0.3 0.75)
X805 CA3 2.0e+11  141.5e-6 C(0323.8e3,0323.8e3) Y(0324e3,0324e3) A(1,1) B(0.02,0.02) P(0.3 0.75) /*
W14x111 (I)
Y805 CA3 2.0e+11  457.4e-6 C(0835.1e3,0835.1e3) Y(0836e3,0836e3) A(1,1) B(0.02,0.02) P(0.3 0.75)
X806 CA3 2.0e+11  424.3e-6 C(0707.4e3,0707.4e3) Y(0708e3,0708e3) A(1,1) B(0.02,0.02) P(0.3 0.75) /*
W14x95  (H)
Y806 CA3 2.0e+11  107.6e-6 C(0340.4e3,0340.4e3) Y(0341e3,0341e3) A(1,1) B(0.02,0.02) P(0.3 0.75)
X807 CA3 2.0e+11  107.6e-6 C(0340.4e3,0340.4e3) Y(0341e3,0341e3) A(1,1) B(0.02,0.02) P(0.3 0.75) /*
W14x95  (I)
Y807 CA3 2.0e+11  424.3e-6 C(0707.4e3,0707.4e3) Y(0708e3,0708e3) A(1,1) B(0.02,0.02) P(0.3 0.75)
X808 CA3 2.0e+11  551.5e-6 C(1035.3e3,1035.3e3) Y(1036e3,1036e3) A(1,1) B(0.02,0.02) P(0.3 0.75) /*
W14x136 (H)
Y808 CA3 2.0e+11  198.1e-6 C(0498.5e3,0498.5e3) Y(0499e3,0499e3) A(1,1) B(0.02,0.02) P(0.3 0.75)
X809 CA3 2.0e+11  198.1e-6 C(0498.5e3,0498.5e3) Y(0499e3,0499e3) A(1,1) B(0.02,0.02) P(0.3 0.75) /*
W14x136 (I)
Y809 CA3 2.0e+11  551.6e-6 C(1035.3e3,1035.3e3) Y(1036e3,1036e3) A(1,1) B(0.02,0.02) P(0.3 0.75)
X810 CA3 2.0e+11  222.7e-6 C(0434.6e3,0434.6e3) Y(0435e3,0435e3) A(1,1) B(0.02,0.02) P(0.3 0.75) /*
W14x61  (H)
Y810 CA3 2.0e+11    31.7e-6 C(0139.3e3,0139.3e3) Y(0140e3,0140e3) A(1,1) B(0.02,0.02) P(0.3 0.75)
X811 CA3 2.0e+11    31.7e-6 C(0139.3e3,0139.3e3) Y(0140e3,0140e3) A(1,1) B(0.02,0.02) P(0.3 0.75) /*
W14x61  (I)
Y811 CA3 2.0e+11  222.7e-6 C(0434.6e3,0434.6e3) Y(0435e3,0435e3) A(1,1) B(0.02,0.02) P(0.3 0.75)
X812 CA3 2.0e+11    72.0e-6 C(0242.9e3,0242.9e3) Y(0243e3,0243e3) A(1,1) B(0.02,0.02) P(0.3 0.75) /*
W14x84  (I)
Y812 CA3 2.0e+11  343.8e-6 C(0617.8e3,0617.8e3) Y(0618e3,0618e3) A(1,1) B(0.02,0.02) P(0.3 0.75)
X813 CA3 2.0e+11  316.5e-6 C(0536.8e3,0536.8e3) Y(0537e3,0537e3) A(1,1) B(0.02,0.02) P(0.3 0.75) /*
W14x74  (H)
Y813 CA3 2.0e+11    39.6e-6 C(0172.6e3,0172.6e3) Y(0173e3,0173e3) A(1,1) B(0.02,0.02) P(0.3 0.75)
X814 CA3 2.0e+11    39.6e-6 C(0172.6e3,0172.6e3) Y(0173e3,0173e3) A(1,1) B(0.02,0.02) P(0.3 0.75) /*
W14x74  (I)
Y814 CA3 2.0e+11  316.5e-6 C(0536.8e3,0536.8e3) Y(0537e3,0537e3) A(1,1) B(0.02,0.02) P(0.3 0.75)
/*
/* Column Shear section properties
/*
X401 EL1 0.77e+11  8335e-6   /* W14x184 (H)
Y401 EL1 0.77e+11 27844e-6
X402 EL1 0.77e+11 27844e-6   /* W14x184 (I)
Y402 EL1 0.77e+11  8335e-6
X403 EL1 0.77e+11  3951e-6   /* W14x87  (H)
Y403 EL1 0.77e+11 12862e-6
X404 EL1 0.77e+11 12862e-6   /* W14x87  (I)
Y404 EL1 0.77e+11  3951e-6
X405 EL1 0.77e+11 16513e-6   /* W14x111 (I)
Y405 EL1 0.77e+11  5217e-6
X406 EL1 0.77e+11  3989e-6   /* W14x95  (H)
Y406 EL1 0.77e+11 14032e-6
X407 EL1 0.77e+11 14032e-6   /* W14x95  (I)
Y407 EL1 0.77e+11  3989e-6
X408 EL1 0.77e+11  6542e-6   /* W14x136 (H)
Y408 EL1 0.77e+11 20222e-6
X409 EL1 0.77e+11 20222e-6   /* W14x136 (I)
Y409 EL1 0.77e+11  6542e-6
X410 EL1 0.77e+11  3356e-6   /* W14x61  (H)
Y410 EL1 0.77e+11  8065e-6
X411 EL1 0.77e+11  8065e-6   /* W14x61  (I)
Y411 EL1 0.77e+11  3356e-6
X412 EL1 0.77e+11 11613e-6   /* W14x84  (I)
Y412 EL1 0.77e+11  3989e-6
X413 EL1 0.77e+11  4022e-6   /* W14x74  (H)
Y413 EL1 0.77e+11 10615e-6
X414 EL1 0.77e+11 10615e-6   /* W14x74  (I)
Y414 EL1 0.77e+11  4022e-6
X415 EL1 0.77e+11  2747e-6   /* W14x43  (H)
Y415 EL1 0.77e+11  5161e-6
X416 EL1 0.77e+11  5161e-6   /* W14x43  (I)
Y416 EL1 0.77e+11  2747e-6
X417 EL1 0.77e+11  8871e-6   /* W14x68  (I)
Y417 EL1 0.77e+11  3952e-6
```

```
X418 EL1 0.77e+11  3387e-6   /* W14x53  (H)
Y418 EL1 0.77e+11  7097e-6
X419 EL1 0.77e+11  7097e-6   /* W14x53  (I)
Y419 EL1 0.77e+11  3387e-6
X601 EL1 0.77e+11  6990e-6   /* Average (H)
Y601 EL1 0.77e+11 22127e-6
X602 EL1 0.77e+11 22127e-6   /* Average (I)
Y602 EL1 0.77e+11  6990e-6
X603 EL1 0.77e+11  3505e-6   /* Average (H)
Y603 EL1 0.77e+11  9264e-6
X604 EL1 0.77e+11  9264e-6   /* Average (I)
Y604 EL1 0.77e+11  3505e-6
X605 EL1 0.77e+11 12838e-6   /* Average (I)
Y605 EL1 0.77e+11  4294e-6
X606 EL1 0.77e+11  4013e-6   /* Average (H)
Y606 EL1 0.77e+11 11469e-6
X607 EL1 0.77e+11 11469e-6   /* Average (I)
Y607 EL1 0.77e+11  4013e-6
X608 EL1 0.77e+11  4626e-6   /* Average (H)
Y608 EL1 0.77e+11 15580e-6
X609 EL1 0.77e+11 15580e-6   /* Average (I)
Y609 EL1 0.77e+11  4626e-6
X610 EL1 0.77e+11  2899e-6   /* Average (H)
Y610 EL1 0.77e+11  5887e-6
X611 EL1 0.77e+11  5887e-6   /* Average (I)
Y611 EL1 0.77e+11  2899e-6
X612 EL1 0.77e+11  9556e-6   /* Average (I)
Y612 EL1 0.77e+11  3960e-6
X613 EL1 0.77e+11  3546e-6   /* Average (H)
Y613 EL1 0.77e+11  7976e-6
X614 EL1 0.77e+11  7976e-6   /* Average (I)
Y614 EL1 0.77e+11  3546e-6
/*
/* Column Axial section properties
/*
U501 CA3 2.0e+11  34903e-6 C(9074.8e3,9074.8e3) Y(9075e3,9075e3) A(1,1) B(0.02,0.02) P(0.3 0.75) /*
W14x184 (H)
U502 CA3 2.0e+11  34903e-6 C(9074.8e3,9074.8e3) Y(9075e3,9075e3) A(1,1) B(0.02,0.02) P(0.3 0.75) /*
W14x184 (I)
U503 CA3 2.0e+11  16516e-6 C(4293.5e3,4293.5e3) Y(4294e3,4294e3) A(1,1) B(0.02,0.02) P(0.3 0.75) /*
W14x87  (H)
U504 CA3 2.0e+11  16516e-6 C(4293.5e3,4293.5e3) Y(4294e3,4294e3) A(1,1) B(0.02,0.02) P(0.3 0.75) /*
W14x87  (I)
U505 CA3 2.0e+11  21097e-6 C(5484.0e3,5484.0e3) Y(5485e3,5485e3) A(1,1) B(0.02,0.02) P(0.3 0.75) /*
W14x111 (I)
U506 CA3 2.0e+11  18000e-6 C(4679.0e3,4679.0e3) Y(4680e3,4680e3) A(1,1) B(0.02,0.02) P(0.3 0.75) /*
W14x95  (H)
U507 CA3 2.0e+11  18000e-6 C(4679.0e3,4679.0e3) Y(4680e3,4680e3) A(1,1) B(0.02,0.02) P(0.3 0.75) /*
W14x95  (I)
U508 CA3 2.0e+11  25806e-6 C(6709.6e3,6709.6e3) Y(6710e3,6710e3) A(1,1) B(0.02,0.02) P(0.3 0.75) /*
W14x136 (H)
U509 CA3 2.0e+11  25806e-6 C(6709.6e3,6709.6e3) Y(6710e3,6710e3) A(1,1) B(0.02,0.02) P(0.3 0.75) /*
W14x136 (I)
U510 CA3 2.0e+11  11548e-6 C(3002.5e3,3002.5e3) Y(3003e3,3003e3) A(1,1) B(0.02,0.02) P(0.3 0.75) /*
W14x61  (H)
U511 CA3 2.0e+11  11548e-6 C(3002.5e3,3002.5e3) Y(3003e3,3003e3) A(1,1) B(0.02,0.02) P(0.3 0.75) /*
W14x61  (I)
U512 CA3 2.0e+11  15936e-6 C(4143.3e3,4143.3e3) Y(4144e3,4144e3) A(1,1) B(0.02,0.02) P(0.3 0.75) /*
W14x84  (I)
U513 CA3 2.0e+11  14064e-6 C(3656.5e3,3656.5e3) Y(3657e3,3657e3) A(1,1) B(0.02,0.02) P(0.3 0.75) /*
W14x74  (H)
U514 CA3 2.0e+11  14064e-6 C(3656.5e3,3656.5e3) Y(3657e3,3657e3) A(1,1) B(0.02,0.02) P(0.3 0.75) /*
W14x74  (I)
U515 CA3 2.0e+11   8129e-6 C(2113.5e3,2113.5e3) Y(2114e3,2114e3) A(1,1) B(0.02,0.02) P(0.3 0.75) /*
W14x43  (H)
U516 CA3 2.0e+11   8129e-6 C(2113.5e3,2113.5e3) Y(2114e3,2114e3) A(1,1) B(0.02,0.02) P(0.3 0.75) /*
W14x43  (I)
U517 CA3 2.0e+11  12903e-6 C(3354.5e3,3354.5e3) Y(3355e3,3355e3) A(1,1) B(0.02,0.02) P(0.3 0.75) /*
W14x68  (I)
U518 CA3 2.0e+11  10064e-6 C(2616.2e3,2616.2e3) Y(2617e3,2617e3) A(1,1) B(0.02,0.02) P(0.3 0.75) /*
W14x53  (H)
```

```
U519 CA3 2.0e+11  10064e-6 C(2616.2e3,2616.2e3) Y(2617e3,2617e3) A(1,1) B(0.02,0.02) P(0.3 0.75) /*
W14x53  (I)

U701 CA3 2.0e+11  28081e-6 C(6709.6e3,6709.6e3) Y(6710e3,6710e3) A(1,1) B(0.02,0.02) P(0.3 0.75) /*
Average (H)
U702 CA3 2.0e+11  28081e-6 C(6709.6e3,6709.6e3) Y(6710e3,6710e3) A(1,1) B(0.02,0.02) P(0.3 0.75) /*
Average (I)
U703 CA3 2.0e+11  12790e-6 C(3002.5e3,3002.5e3) Y(3003e3,3003e3) A(1,1) B(0.02,0.02) P(0.3 0.75) /*
Average (H)
U704 CA3 2.0e+11  12790e-6 C(3002.5e3,3002.5e3) Y(3003e3,3003e3) A(1,1) B(0.02,0.02) P(0.3 0.75) /*
Average (I)
U705 CA3 2.0e+11  17226e-6 C(4143.3e3,4143.3e3) Y(4144e3,4144e3) A(1,1) B(0.02,0.02) P(0.3 0.75) /*
Average (I)
U706 CA3 2.0e+11  15048e-6 C(3656.5e3,3656.5e3) Y(3657e3,3657e3) A(1,1) B(0.02,0.02) P(0.3 0.75) /*
Average (H)
U707 CA3 2.0e+11  15048e-6 C(3656.5e3,3656.5e3) Y(3657e3,3657e3) A(1,1) B(0.02,0.02) P(0.3 0.75) /*
Average (I)
U708 CA3 2.0e+11  19952e-6 C(6709.6e3,6709.6e3) Y(6710e3,6710e3) A(1,1) B(0.02,0.02) P(0.3 0.75) /*
Average (H)
U709 CA3 2.0e+11  19952e-6 C(6709.6e3,6709.6e3) Y(6710e3,6710e3) A(1,1) B(0.02,0.02) P(0.3 0.75) /*
Average (I)
U710 CA3 2.0e+11   8984e-6 C(2113.5e3,2113.5e3) Y(2114e3,2114e3) A(1,1) B(0.02,0.02) P(0.3 0.75) /*
Average (H)
U711 CA3 2.0e+11   8984e-6 C(2113.5e3,2113.5e3) Y(2114e3,2114e3) A(1,1) B(0.02,0.02) P(0.3 0.75) /*
Average (I)
U712 CA3 2.0e+11  13661e-6 C(3354.5e3,3354.5e3) Y(3355e3,3355e3) A(1,1) B(0.02,0.02) P(0.3 0.75) /*
Average (I)
U713 CA3 2.0e+11  11065e-6 C(2616.2e3,2616.2e3) Y(2617e3,2617e3) A(1,1) B(0.02,0.02) P(0.3 0.75) /*
Average (H)
U714 CA3 2.0e+11  11065e-6 C(2616.2e3,2616.2e3) Y(2617e3,2617e3) A(1,1) B(0.02,0.02) P(0.3 0.75) /*
Average (I)
//

// initial load data
beam Y1   X1~X13  2F     (loade 12800)
beam Y13 X1~X13  2F     (loade 12800)
beam X1   Y1~Y13  2F     (loade 22000)
beam X13 Y1~Y13  2F     (loade 22000)
node Y1   X4      2F     (Pz =  140240)
node Y1   X7      2F     (Pz =  140240)
node Y1   X10     2F     (Pz =  140240)
node Y13 X4      2F     (Pz =  140240)
node Y13 X7      2F     (Pz =  140240)
node Y13 X10     2F     (Pz =  140240)

beam Y1   X1~X13  3F     (loade 7700)
beam Y13 X1~X13  3F     (loade 7700)
beam X1   Y1~Y13  3F     (loade 16900)
beam X13 Y1~Y13  3F     (loade 16900)
node Y1   X4      3F     (Pz =   93500)
node Y1   X7      3F     (Pz =   93500)
node Y1   X10     3F     (Pz =   93500)
node Y13 X4      3F     (Pz =   93500)
node Y13 X7      3F     (Pz =   93500)
node Y13 X10     3F     (Pz =   93500)

beam Y1   X1~X13  4F~6F  (loade 7440)
beam Y13 X1~X13  4F~6F  (loade 7440)
beam X1   Y1~Y13  4F~6F  (loade 16640)
beam X13 Y1~Y13  4F~6F  (loade 16640)
node Y1   X4      4F~6F  (Pz =   93500)
node Y1   X7      4F~6F  (Pz =   93500)
node Y1   X10     4F~6F  (Pz =   93500)
node Y13 X4      4F~6F  (Pz =   93500)
node Y13 X7      4F~6F  (Pz =   93500)
node Y13 X10     4F~6F  (Pz =   93500)

beam Y1   X1~X13  7F     (loade 12800)
beam Y13 X1~X13  7F     (loade 12800)
beam X1   Y1~Y13  7F     (loade 22000)
beam X13 Y1~Y13  7F     (loade 22000)
```

```
node Y1   X4        7F      (Pz =   140240)
node Y1   X7        7F      (Pz =   140240)
node Y1   X10       7F      (Pz =   140240)
node Y13  X4        7F      (Pz =   140240)
node Y13  X7        7F      (Pz =   140240)
node Y13  X10       7F      (Pz =   140240)
//
```